

# **The Effect of MGN3 on In Vitro Models of Diabetic Impaired Wound Healing**

A thesis submitted in partial fulfilment of the requirements  
of Manchester Metropolitan University for the degree of  
Doctor of Philosophy

**Mohammed Subhan Asif**

Department of Life Sciences

Manchester Metropolitan University

2025

## Table of contents

<b>List of Abbreviations</b> .....	<b>xi</b>
<b>List of Figures</b> .....	<b>xiii</b>
<b>List of Tables</b> .....	<b>xvii</b>
<b>Abstract</b> .....	<b>xviii</b>
<b>Declaration and Copyright Statements</b> .....	<b>xx</b>
<b>About the Author</b> .....	<b>xxi</b>
<b>Acknowledgements</b> .....	<b>xxii</b>
<b>Dedication</b> .....	<b>xxii</b>
<b>Chapter 1 – Introduction</b> .....	<b>1</b>
<b>1.1 Diabetes</b> .....	<b>2</b>
1.1.1 The Effects of DM on the Innate Immune System .....	3
<b>1.2 The Immune System</b> .....	<b>4</b>
<b>1.3 Wound Healing</b> .....	<b>6</b>
1.3.1 Haemostasis .....	8
1.3.2 Inflammation .....	10
1.3.2.1 Chronic Inflammation .....	12
1.3.3 Proliferation .....	13
1.3.4 Maturation .....	14
<b>1.4 Impaired Wound Healing in Diabetes Mellitus</b> .....	<b>15</b>
<b>1.5 Bacterial Biofilms</b> .....	<b>15</b>
1.5.1 Biofilms in Chronic Wounds .....	17
1.5.2 Biofilm Treatments .....	18
<b>1.6 Dietary Fibres</b> .....	<b>20</b>
1.6.1 Biobran (MGN3) .....	20
<b>1.7 The Effects of MGN3 on Wound Healing</b> .....	<b>21</b>
<b>1.8 Aim and Objectives:</b> .....	<b>22</b>
<b>Chapter 2 – Materials and Methods</b> .....	<b>24</b>

<b>2.1 Materials</b> .....	<b>25</b>
<b>2.2 Methods</b> .....	<b>28</b>
2.2.1 Media .....	28
2.2.2 Cell Culture.....	28
2.2.3 U937 Monocyte Differentiation into M0 Macrophages.....	29
2.2.4 CD11b Analysis.....	29
2.2.5 M0 Macrophages Differentiation into M1 Macrophages .....	30
2.2.6 CD197 Analysis.....	30
2.2.7 Bacteria Preparation .....	31
2.2.8 Host-pathogen Interaction (HPI) Assay .....	32
2.2.9 Wound Healing (Cell Exclusion) Assay .....	32
2.2.10 Seahorse Technology Analysis.....	33
2.2.11 Glucose Utilisation .....	34
2.2.12 MTT Assay .....	35
2.2.13 Visualising Mediators of Wound Healing.....	36
2.2.13.1 Fluorescence microscopy .....	36
2.2.13.2 Enzyme Linked Immunosorbent Assays.....	37
2.2.13.3 Lysozyme Assay .....	39
2.2.14 Mechanistic Investigations.....	39
2.2.14.1 Cathelicidin Assay.....	39
2.2.14.2 Beta-2 Defensin (BD2) Assay.....	40
2.2.14.3 Keratinocyte Growth Factor (KGF) Assay .....	41
2.2.14.4 Fibroblast Growth Factor 2 (FGF2) Assay.....	41
2.2.14.5 Epidermal Growth Factor (EGF) Assay .....	42
2.2.14.6 Monocyte Chemoattractant Protein-1 (MCP-1) Assay.....	42
2.2.14.7 Nuclear Factor Erythroid-2 Related Factor 2 (NRF2) Assay.....	43
2.2.15 Data Analysis .....	44
<b>Chapter 3: The Impact of Chronic Hyperglycaemia on Cell Function</b> .....	<b>45</b>
<b>3.1 Introduction</b> .....	<b>46</b>
3.1.1 Glucose Metabolism .....	46

3.1.1.1 Glucose.....	46
3.1.1.2 Insulin Signalling Pathway.....	46
3.1.1.3 ATP Production.....	47
3.1.2 The Effect of Hyperglycaemia on Macrophage Function.....	50
3.1.3 The Effect of Hyperglycaemia on Fibroblast Function.....	50
3.1.4 The Effect of Hyperglycaemia on Keratinocyte Function.....	51
<b>3.2 Aims and Objectives.....</b>	<b>52</b>
3.2.1 Aim.....	52
3.2.2 Objectives.....	52
<b>3.3 Methods.....</b>	<b>53</b>
3.3.1 Generation of M1 macrophages.....	53
3.3.2 CD11b/ CD197 analysis.....	53
3.3.3 Glucose Evaluation.....	53
3.3.4 Seahorse Analysis.....	53
<b>3.4 Results.....</b>	<b>54</b>
3.4.1 Differentiation of U937 Monocytes to M0 Macrophages.....	54
3.4.2 Differentiation of U937 Monocytes to M1 Macrophages.....	56
3.4.3 The Effect of Glucose on Cell Viability.....	58
3.4.4 Cellular Glucose Uptake.....	60
3.4.4.1 Monocyte Glucose Uptake.....	60
3.4.4.1.1 Glucose Degradation in RPMI Medium.....	60
3.4.4.1.2 Monocyte-Mediated Change in Medium Glucose Levels.....	61
3.4.4.1.3 Monocyte Glucose Utilisation.....	62
3.4.4.1.4 Effect of Glucose on Monocyte Count.....	63
3.4.4.1.5 Effect of Glucose on Monocyte Appearance.....	64
3.4.4.2 M1 Macrophage Glucose Uptake.....	65
3.4.4.2.1 Macrophage-Mediated Change in Medium Glucose Levels.....	65
3.4.4.2.2 Macrophage Glucose Utilisation.....	66
3.4.4.2.3 Effect of Glucose on Macrophage Count.....	67
3.4.4.2.4 Effect of Glucose on Macrophage Appearance.....	68

3.4.4.3 Fibroblasts glucose evaluation .....	69
3.4.4.3.1 Glucose Degradation in DMEM Medium .....	69
3.4.4.3.2 Fibroblast-Mediated Change in Medium Glucose Levels .....	70
3.4.4.3.3 Fibroblast Glucose Utilisation .....	71
3.4.4.3.4 Effect of Glucose on Fibroblast Count.....	72
3.4.4.3.5 Effect of Glucose on Fibroblast Appearance .....	73
3.4.4.4 Keratinocytes Glucose Evaluation .....	74
3.4.4.4.1 Keratinocyte-Mediated Change in Medium Glucose Levels .....	74
3.4.4.4.3 Effect of Glucose on Keratinocyte Count .....	76
3.4.4.4.4 Effect of Glucose on Keratinocyte Appearance.....	77
3.4.5 Effect of Glucose on Cellular Metabolism .....	78
3.4.5.1 Fibroblast Metabolism .....	78
3.4.5.2 Keratinocyte Metabolism.....	81
<b>3.5 Discussion .....</b>	<b>84</b>
<b>Chapter 4: The Effect of MGN3 on Monocyte/Macrophage Function .....</b>	<b>89</b>
<b>4.1 Introduction .....</b>	<b>90</b>
4.1.1 <i>Staphylococcus aureus</i> .....	90
4.1.2 <i>Pseudomonas aeruginosa</i> .....	90
4.1.2.1 Lipopolysaccharides .....	91
4.1.3 Bacterial Biofilms Evade the Immune System.....	92
4.1.4 Macrophages and Immune Cell Signalling.....	92
4.1.5 The Importance of Toll-like Receptors in the Innate Immune System.....	94
4.1.6 Hyperglycaemic Effects on Macrophage Cell Signalling.....	95
4.1.7 Reversing the Hyperglycaemic Effect on Macrophage Cell Signalling .....	96
<b>4.2 Aims and Objectives .....</b>	<b>97</b>
4.2.1 Aim .....	97
4.2.2 Objectives.....	97
<b>4.3 Methods .....</b>	<b>98</b>
4.3.1 Generation of M1 macrophages .....	98
4.3.2 Biofilm Generation .....	98

4.3.3 Host-Pathogen Assay.....	98
4.3.4 ELISAs .....	98
4.3.5 Chemotaxis Assay.....	99
4.3.6 Cathelicidin (LL37) Assay .....	99
<b>4.4 Results .....</b>	<b>100</b>
4.4.1 The Direct Effect of MGN3 on MRSA and PA01 Growth .....	100
4.4.2 The Effect of Glucose on MRSA and PA01 Growth.....	101
4.4.3 The Effect of MGN3 on Phagocytosis of MRSA Biofilms .....	102
4.4.4 The Effect of MGN3 on Phagocytosis of PA01 Biofilms.....	103
4.4.5 The Contribution of TLR Signalling to MGN3-Mediated Phagocytosis of MRSA Biofilms.....	104
4.4.6 The Contribution of TLR Signalling to MGN3-Mediated Phagocytosis of PA Biofilms.....	105
4.4.7 Effect of MGN3 on Growth Factor, Chemokine, Antimicrobial Peptide and Antimicrobial Enzyme Production.....	107
4.4.7.1 Secretion of Epidermal Growth Factor (EGF) by M1 macrophages .....	107
4.4.7.2 Secretion of Fibroblast Growth Factor 2 (FGF2) by M1 macrophages.....	109
4.4.7.3 Secretion of Monocyte Chemoattractant Protein-1 (MCP-1) by M1 macrophages.....	110
4.4.7.4 Intracellular Cathelicidin (LL37) Levels in M1 Macrophages .....	111
4.4.7.5 Intracellular Lysozyme Levels in M1 Macrophages.....	112
4.4.8 Chemotaxis Activity of U937 Monocytes in Response to Macrophage, Keratinocyte and Fibroblast-Derived Supernatant .....	113
4.4.9 Antimicrobial Activity of Cathelicidin (LL37) from M1 Cell Lysates.....	116
4.4.9.1 The Antibacterial Effect of Cathelicidin (LL37) from M1 Cell Lysates against MRSA.....	116
4.4.9.2 The Antibacterial Effect of Cathelicidin (LL37) from M1 Cell Lysates Against PA.....	118
<b>4.5 Discussion .....</b>	<b>119</b>
<b>Chapter 5: The Effect of MGN3 on Fibroblast and Keratinocyte-Mediated Wound Repair under Hyperglycaemic Conditions .....</b>	<b>135</b>
<b>5.1 Introduction .....</b>	<b>136</b>

5.1.1 The Importance of Fibroblasts and Keratinocytes in Wound Healing .....	136
5.1.2 The Effect of Glucose on Fibroblast and Keratinocyte Function .....	136
5.1.3 The Effect of MGN3 on Fibroblast and Keratinocyte Function .....	137
<b>5.2 Aims and Objectives .....</b>	<b>138</b>
5.2.1 Aim .....	138
5.2.2 Objectives.....	138
<b>5.3 Methods .....</b>	<b>139</b>
5.3.1 Cell Culture.....	139
5.3.2 Wound Healing Assay.....	139
<b>5.4 Results .....</b>	<b>140</b>
5.4.1 Effect of Glucose on Fibroblast ‘Wound’ Closure.....	140
5.4.2 Effect of MGN3 on Fibroblast ‘Wound’ Closure.....	141
5.4.3 Effect of TLR inhibition on MGN3-Mediated Fibroblast ‘Wound’ Closure .....	144
5.4.3.1 Effect of TLR inhibition on MGN3_Mediated Fibroblast ‘Wound’ Closure at Pre-diabetic (11mM Glucose) Culture Conditions .....	144
5.4.3.2 Effect of TLR inhibition on MGN3-Mediated Fibroblast ‘Wound’ Closure under Hyperglycaemic (20mM Glucose) Culture Conditions .....	146
5.4.3.3 Effect of TLR inhibition on MGN3-Mediated Fibroblast ‘Wound’ Closure under Hyperglycaemic (30mM Glucose) Culture Conditions .....	148
5.4.4 Contribution of Cell Proliferation and Migration on MGN3-Mediated Fibroblast ‘Wound’ Closure.....	150
5.4.4.1 The Effect Mitomycin C on Fibroblast Proliferation .....	150
5.4.4.2 The Effect of Mitomycin C on Fibroblast ‘Wound’ Closure at 11mM Glucose.....	153
5.4.4.3 The Effect of Cytochalasin D on Fibroblast ‘Wound’ Closure at 11mM ...	155
.....	156
5.4.4.4 The Effect of Mitomycin C on Fibroblast ‘Wound’ Closure at 20mM glucose .....	157
.....	157
5.4.4.5 The Effect of Cytochalasin D on Fibroblast ‘Wound’ Closure at 20mM ...	159
5.4.4.6 The Effect of Mitomycin C on Fibroblast ‘Wound’ Closure at 30mM glucose .....	161
.....	161
5.4.4.7 The Effect of Cytochalasin D on Fibroblast ‘Wound’ Closure at 30mM ...	163

5.4.8 The Effect of Glucose on Keratinocyte ‘Wound’ Closure .....	165
5.4.9 Effect of MGN3 on Keratinocyte ‘Wound’ Closure.....	166
5.4.10 Effect of TLR inhibition on MGN3-Mediated Fibroblast ‘Wound’ Closure....	168
5.4.10.1 The Effect of MGN3 with TLR inhibition on Keratinocyte ‘Wound’ Closure at 11mM glucose.....	168
5.4.10.2 The Effect of MGN3 with TLR inhibition on Fibroblast ‘Wound’ Closure at 20mM glucose.....	170
5.4.10.3 The Effect of MGN3 with TLR inhibition on Keratinocyte ‘Wound’ Closure at 30mM glucose.....	172
5.4.11 Contribution of Cell Proliferation and Migration on MGN3-Mediated Keratinocyte ‘Wound’ Closure .....	174
5.4.11.1 The Effect Mitomycin on Cell Proliferation .....	174
5.4.11.2 The Effect of Mitomycin C on Keratinocyte ‘Wound’ Closure at 11mM glucose .....	175
5.4.11.3 The Effect of Cytochalasin D on Keratinocyte ‘Wound’ Closure at 11mM .....	177
5.4.11.4 The Effect of Mitomycin C on Keratinocyte ‘Wound’ Closure at 20mM glucose .....	179
5.4.11.5 The Effect of Cytochalasin D on Keratinocyte ‘Wound’ Closure at 20mM .....	181
5.4.11.6 The Effect of Mitomycin C on Keratinocyte ‘Wound’ Closure at 30mM glucose .....	183
5.4.11.7 The Effect of Cytochalasin D on Keratinocyte ‘Wound’ Closure at 30mM .....	185
<b>5.5 Discussion .....</b>	<b>187</b>
<b>Chapter 6: The Effect of MGN3 on Fibroblast and Keratinocyte Cell Function .....</b>	<b>191</b>
<b>6.1 Introduction .....</b>	<b>192</b>
6.1.1 Immune Cell Signalling with Fibroblasts and Keratinocytes .....	192
6.1.2 The Hyperglycaemic Effects on Fibroblasts and Keratinocytes.....	193
6.1.3 Reversing the Hyperglycaemic Effect on Fibroblasts and Keratinocytes .....	194
<b>6.2 Aims and Objectives .....</b>	<b>195</b>
6.2.1 Aim .....	195
6.2.2 Objectives.....	195

<b>6.3 Methods</b> .....	<b>196</b>
6.3.1 MTT Assay .....	196
6.3.2 Seahorse Analysis.....	196
6.3.3 ELISAs .....	196
6.3.4 Thunder Microscopy .....	197
6.3.5 Functional Protein Assays .....	197
6.3.6 Antimicrobial Peptide Assays .....	197
6.3.7 NRF2 Assay.....	197
<b>6.4 Results</b> .....	<b>198</b>
6.4.1 The Effect of MGN3 on HDF Cell Viability and Proliferation .....	198
6.4.2 The Effect of MGN3 on Fibroblast Cellular Metabolism .....	200
6.4.2.1 Fibroblast Metabolism at Low Glucose Following TLR inhibition .....	200
6.4.2.2 Fibroblast Metabolism at High Glucose Following TLR Inhibition .....	203
6.4.3 Effect of MGN3 on Matrix, Growth Factor and Inflammatory Cytokine Secretion by Human Dermal Fibroblasts (HDFs).....	205
6.4.3.1 Secretion of Collagen-1 levels from HDFs .....	205
6.4.3.2 Secretion of Epidermal Growth Factor from HDFs .....	206
6.4.3.3 Fibroblast Growth Factor-2 Secretion from HDFs.....	207
6.4.3.4 Monocyte Chemoattractant Protein-1 Secretion from HDFs.....	208
6.4.3.5 Matrix Metalloprotenase-1 Secretion from HDFs.....	209
6.4.3.6 Transforming Growth Factor beta 1 Secretion from HDFs.....	210
6.4.3.7 Keratinocyte Growth Factor Secretion from HDFs.....	211
6.4.4 Effect of MGN3 on Matrix, Growth Factor and Inflammatory Cytokine Protein Expression in Human Dermal Fibroblasts (HDFs).....	212
6.4.4.1 COL-1 Protein Expression in HDFs.....	212
6.4.4.2 TGF $\beta$ 1 Protein Expression in HDFs .....	214
6.4.5 Influence of MGN3-Induced M1 Macrophage-, Keratinocyte- and Fibroblast- Derived EGF and FGF2 Secretion on Fibroblast Proliferation .....	216
6.4.5.1 Influence of MGN3-Induced EGF Secretion on Fibroblast Proliferation ..	216
6.4.5.2 Influence of MGN3-Induced FGF2 Secretion on Fibroblast Proliferation	219
6.4.6 The Effect of MGN3 on HACAT Cell Viability and Proliferation .....	222

6.4.7 The Effect of MGN3 on Keratinocyte Cellular Metabolism .....	224
6.4.7.1 Keratinocyte Metabolism at Low Glucose Following TLR Inhibition.....	224
6.4.7.2 Keratinocyte Metabolism at High Glucose Following TLR Inhibition .....	227
6.4.8 Effect of MGN3 on Growth Factor, Transcription Factor and Antimicrobial Peptide Production by HACAT Cells .....	230
6.4.8.1 Secretion of Epidermal Growth Factor from HACATs.....	230
6.4.8.2 Secretion of Fibroblast Growth Factor 2 by HACATs .....	231
6.4.8.3 Secretion of Transforming Growth Factor Beta 1 by HACATs.....	232
6.4.8.4 Secretion of Nuclear Factor Erythroid 2–related Factor 2 by HACATs .....	233
6.4.8.5 Intracellular Nuclear Factor Erythroid 2–related Factor 2 Protein Expression in HACATs .....	234
6.4.8.6 Intracellular Cathelicidin Peptide Expression in HACATs.....	235
6.4.8.7 Intracellular Beta Defensin 2 Peptide Expression in HACATs .....	236
6.4.9 Effect of MGN3 on Intracellular TGFβ1 Protein and Cathelicidin Peptide Expression in HACAT Cells .....	237
6.4.9.1 Intracellular TGFβ1 Expression in HACATs.....	237
6.4.9.2 Cathelicidin (LL37) Expression in HACATs.....	239
6.4.10 Influence of MGN3-Induced Keratinocyte-, Fibroblast- and M1 Macrophage- Derived EGF and FGF2 Secretion on Keratinocyte Proliferation .....	241
6.4.10.1 Influence of MGN3-Induced EGF Secretion on Keratinocyte Proliferation .....	241
6.4.10.2 Influence of MGN3-Induced FGF2 Secretion on Keratinocyte Proliferation .....	245
6.4.11 Effect of Keratinocyte-Derived Antimicrobial Peptides on Bactericidal Activity .....	248
6.4.11.1 Effect of Keratinocyte-Derived BD2 Peptide on MRSA and PA01 Killing	248
6.4.11.2 Effect of Keratinocyte-Derived LL37 Peptide on MRSA and PA01 Killing .....	249
6.4.12 Effect of MGN3 on NRF2 Protein Expression in HACATs .....	250
6.4.12.1 NRF2 Expression in Keratinocytes.....	250
6.4.12.2 Secretion of MCP-1 from Keratinocytes after NRF2 Inhibition .....	251
<b>6.5 Discussion .....</b>	<b>252</b>

<b>Chapter 7: Discussion and Future Work .....</b>	<b>264</b>
<b>7.1 Discussion .....</b>	<b>265</b>
<b>7.2 Future Work .....</b>	<b>284</b>
<b>7.3 Conclusion .....</b>	<b>285</b>
<b>Chapter 8: References.....</b>	<b>288</b>

## List of Abbreviations

<b>AB-</b>	Antibiotic free
<b>ATP</b>	Adenosine triphosphate
<b>BD2</b>	Beta defensin-2
<b>BSA</b>	Bovine Serum Albumin
<b>CD11b</b>	Cluster of differentiation 11b
<b>CD14</b>	Cluster of differentiation 14
<b>CD197</b>	Cluster of differentiation 197
<b>CFU</b>	Colony Forming Units
<b>CM</b>	Complete Media
<b>COL-1</b>	Collagen-1
<b>CytoD</b>	Cytochalasin D
<b>DFU</b>	Diabetic Foot Ulcer
<b>DM</b>	Diabetes Mellitus
<b>DMEM</b>	Dulbecco Modified Eagle Medium
<b>DPBS</b>	Dulbecco Phosphate Buffered Saline
<b>ECAR</b>	Extracellular Acidification Rate
<b>ECM</b>	Extracellular matrix
<b>EGF</b>	Epidermal growth factor
<b>ELISA</b>	Enzyme-linked immunosorbent assays
<b>FBS</b>	Foetal Bovine Serum
<b>FGF2</b>	Fibroblast growth factor 2
<b>FITC</b>	Fluorescein isothiocyanate
<b>GlycoATP</b>	Glycolytic ATP production
<b>HACAT</b>	Human Epidermal Keratinocytes
<b>HDF</b>	Human Dermal Fibroblasts

<b>HPI</b>	Host Pathogen Interaction
<b>IFN<math>\gamma</math></b>	Interferon gamma
<b>KGF</b>	Keratinocyte growth factor
<b>LL37</b>	Cathelicidin
<b>LPS</b>	Lipopolysaccharides
<b>MCP-1</b>	Monocyte chemoattractant protein-1
<b>MFI</b>	Mean Fluorescence Intensity
<b>MGN3</b>	Dietary fibre derived from rice bran
<b>MITO</b>	Mitomycin C
<b>MitoATP</b>	Mitochondrial ATP production
<b>mM</b>	Millimolar
<b>MMP-1</b>	Matrix Metalloproteinase-1
<b>MRSA</b>	Methicillin Resistant <i>Staphylococcus aureus</i>
<b>NF-<math>\kappa</math>B</b>	Nuclear factor kappa-B
<b>NRF2</b>	Nuclear factor erythroid 2-related factor 2
<b>OCR</b>	Oxygen Consumption Rate
<b>PA01</b>	<i>Pseudomonas aeruginosa</i> strain 1
<b>PFA</b>	Paraformaldehyde
<b>PMA</b>	Phorbol 12-Myristate 13-Acetate
<b>RPMI</b>	Roswell Park Memorial Institute
<b>RS</b>	Rice Starch
<b>TGF<math>\beta</math>1</b>	Transforming growth factor beta 1
<b>TLR2</b>	Toll-like Receptor 2
<b>TLR4</b>	Toll-like Receptor 4
<b>TLRi</b>	Toll-like Receptor Inhibitor
<b>TNF<math>\alpha</math></b>	Tumour Necrosis Factor alpha

## List of Figures

<i>Figure 1. 1: Schematic Illustration of the Immune System.....</i>	<i>6</i>
<i>Figure 1. 2: Schematic Illustration of the Wound Healing Process. ....</i>	<i>8</i>
<i>Figure 1. 3: Schematic Illustration of the Haemostasis Stage of Wound Healing. ....</i>	<i>10</i>
<i>Figure 1. 4: Schematic illustration of the Inflammatory Stage of Wound Healing. ....</i>	<i>12</i>
<i>Figure 1. 5: Schematic Illustration of the Proliferation Stage of Wound Healing. ....</i>	<i>13</i>
<i>Figure 1. 6: The chemical structure of the arabinoxylan hemicellulose component of MGN3.....</i>	<i>21</i>
<i>Figure 3. 1: Insulin triggers a cascade which allows glucose to enter a cell. ....</i>	<i>47</i>
<i>Figure 3. 2: Glucose is used in the production of ATP. ....</i>	<i>48</i>
<i>Figure 3. 3: Differentiation of U937 Monocytes into M0 macrophages. ....</i>	<i>55</i>
<i>Figure 3. 4: Differentiation of U937 monocytes into M1 macrophages. ....</i>	<i>57</i>
<i>Figure 3. 5: Effect of Glucose on Cell Viability. ....</i>	<i>59</i>
<i>Figure 3. 6: Glucose Depletion in RPMI Medium.....</i>	<i>60</i>
<i>Figure 3. 7: Monocyte-Mediated Change in Medium Glucose Levels. ....</i>	<i>61</i>
<i>Figure 3. 8: U937 Monocyte Glucose Utilisation.....</i>	<i>62</i>
<i>Figure 3. 9: Effect of Glucose on U937 Monocyte Cell Count. ....</i>	<i>63</i>
<i>Figure 3. 10: Effect of Glucose on Monocyte Appearance. ....</i>	<i>64</i>
<i>Figure 3. 11: Macrophage-Mediated Change in Medium Glucose Levels. ....</i>	<i>65</i>
<i>Figure 3. 12: Macrophage Glucose Utilisation.....</i>	<i>66</i>
<i>Figure 3. 13: Effect of Glucose on Macrophage Count.....</i>	<i>67</i>
<i>Figure 3. 14: Effect of Glucose on Macrophage Appearance.....</i>	<i>68</i>
<i>Figure 3. 15: Glucose Depletion in DMEM Medium.....</i>	<i>69</i>
<i>Figure 3. 16: Fibroblast-Mediated Change in Medium Glucose Levels. ....</i>	<i>70</i>
<i>Figure 3. 17: Fibroblast Glucose Utilisation. ....</i>	<i>71</i>
<i>Figure 3. 18: Effect of Glucose on Fibroblast Count. ....</i>	<i>72</i>
<i>Figure 3. 19: Effect of Glucose on Fibroblast Appearance. ....</i>	<i>73</i>
<i>Figure 3. 20: Keratinocyte-Mediated Change in Medium Glucose Levels.....</i>	<i>74</i>
<i>Figure 3. 21: Keratinocyte Glucose Utilisation.....</i>	<i>75</i>
<i>Figure 3. 22: Effect of Glucose on Keratinocyte Count.....</i>	<i>76</i>
<i>Figure 3. 23: Effect of Glucose on Keratinocyte Appearance.....</i>	<i>77</i>
<i>Figure 3. 24: Fibroblast Cellular Metabolism.....</i>	<i>80</i>
<i>Figure 3. 25: Keratinocyte Cellular Metabolism.....</i>	<i>83</i>
<i>Figure 4. 1: Schematic illustration of LPS and LOS structure. ....</i>	<i>91</i>
<i>Figure 4. 2: Macrophage Cell Interactions in the Wound Healing Process.....</i>	<i>93</i>
<i>Figure 4. 3: The signalling pathways of TLR2 and TLR4.....</i>	<i>95</i>
<i>Figure 4. 4: Direct Effect of MGN3 on MRSA and PA01 Growth.....</i>	<i>100</i>
<i>Figure 4. 5: The Effect of Glucose on MRSA and PA01 Growth.....</i>	<i>101</i>

<i>Figure 4. 6: The Effect of MGN3 on the phagocytosis of MRSA Biofilms. ....</i>	<i>102</i>
<i>Figure 4. 7: The Effect of MGN3 on the phagocytosis of PA01 biofilms. ....</i>	<i>103</i>
<i>Figure 4. 8: Contribution of TLR Signalling to MGN3-Mediated Phagocytosis of MRSA Biofilms Under Pre-diabetic and Hyperglycaemic Conditions. ....</i>	<i>104</i>
<i>Figure 4. 9: Contribution of TLR Signalling to MGN3-Mediated Phagocytosis of PA Biofilms Under Pre-diabetic and Hyperglycaemic Conditions. ....</i>	<i>106</i>
<i>Figure 4. 10: Secretion of Epidermal Growth Factor (EGF) by M1 macrophages. ....</i>	<i>108</i>
<i>Figure 4. 11: Secretion of Fibroblast Growth Factor 2 (FGF2) by M1 Macrophages. ....</i>	<i>109</i>
<i>Figure 4. 12: Secretion of Monocyte Chemoattractant Protein-1 (MCP-1) by M1 Macrophages. ....</i>	<i>110</i>
<i>Figure 4. 13: Secretion of Cathelicidin (LL37) by M1 Macrophages Lysates. ....</i>	<i>111</i>
<i>Figure 4. 14: Intracellular levels of Lysozymes in M1 Macrophages. ....</i>	<i>112</i>
<i>Figure 4. 15: The Effect of Macrophage, Keratinocyte and Fibroblast Supernatant on U937 Monocyte Chemotaxis. ....</i>	<i>114</i>
<i>Figure 4. 16: The Antibacterial Effect of Cathelicidin (LL37) from M1 Cell Lysates against MRSA. ....</i>	<i>117</i>
<i>Figure 4. 17: The Antibacterial Effect of Cathelicidin (LL37) from M1 Cell Lysates Against PA01. ....</i>	<i>118</i>
<i>Figure 5. 1: Effect of Glucose on % Fibroblast ‘Wound’ Closure. ....</i>	<i>140</i>
<i>Figure 5. 2: Effect of MGN3 on % Fibroblast ‘Wound’ Closure. ....</i>	<i>141</i>
<i>Figure 5. 3: The Effect of MGN3 on Fibroblast ‘Wound’ Closure at Different Glucose Levels. ....</i>	<i>143</i>
<i>Figure 5. 4: Effect of TLR inhibition on MGN3-Mediated Fibroblast ‘Wound’ Closure under 11mM Culture Conditions. ....</i>	<i>144</i>
<i>Figure 5. 5: The Effect of MGN3 on Fibroblast ‘Wound’ Closure at 11mM Glucose after TLR2 and TLR4 Inhibition. ....</i>	<i>145</i>
<i>Figure 5. 6: Effect of TLR inhibition on MGN3-Mediated Fibroblast ‘Wound’ Closure under 20mM Culture Conditions. ....</i>	<i>146</i>
<i>Figure 5. 7: The Effect of MGN3 on Fibroblast ‘Wound’ Closure at 20mM Glucose after TLR2 and TLR4 Inhibition. ....</i>	<i>147</i>
<i>Figure 5. 8: Effect of TLR inhibition on MGN3-Mediated Fibroblast ‘Wound’ Closure under 30mM Culture Conditions. ....</i>	<i>148</i>
<i>Figure 5. 9: The Effect of MGN3 on Fibroblast ‘Wound’ Closure at 30mM Glucose after TLR2 and TLR4 Inhibition. ....</i>	<i>149</i>
<i>Figure 5. 10: Evaluation of Fibroblast proliferation inhibition following mitomycin C treatment. ....</i>	<i>151</i>
<i>Figure 5. 11: % ‘Wound’ Closure in HDFs at 11mM glucose after MGN3 treatment and mitomycin C treatment. ....</i>	<i>153</i>

<i>Figure 5. 12: The Effect of Mitomycin C on Fibroblast ‘Wound’ Closure at 11mM Glucose.</i>	154
<i>Figure 5. 13: % ‘Wound’ closure in HDFs at 11mM glucose after MGN3 and Cytochalasin D treatment.</i>	155
<i>Figure 5. 14: The Effect of Cytochalasin D on Fibroblast ‘Wound’ Closure after at 11mM Glucose.</i>	156
<i>Figure 5. 15: % ‘Wound’ closure in HDFs at 20mM glucose after MGN3 treatment and mitomycin C treatment.</i>	157
<i>Figure 5. 16: The Effect of MGN3 on Fibroblast ‘Wound’ Closure after Mitomycin C treatment at 20mM Glucose.</i>	158
<i>Figure 5. 17: % ‘Wound’ closure in HDFs at 20mM glucose after MGN3 and Cytochalasin D treatment.</i>	159
<i>Figure 5. 18: The Effect of Cytochalasin D on Fibroblast ‘Wound’ Closure after at 11mM Glucose.</i>	160
<i>Figure 5. 19: % ‘Wound’ Closure in HDFs at 30mM glucose after MGN3 treatment and Mitomycin C treatment.</i>	161
<i>Figure 5. 20: The Effect of MGN3 on Fibroblast ‘Wound’ Closure after Mitomycin C treatment at 30mM Glucose.</i>	162
<i>Figure 5. 21: % ‘Wound’ closure in HDFs at 30mM glucose after MGN3 and CytoD treatment.</i>	163
<i>Figure 5. 22: The Effect of Cytochalasin D on Fibroblast ‘Wound’ Closure after at 30mM Glucose.</i>	164
<i>Figure 5. 23: The Effect of glucose on Keratinocyte % ‘Wound’ closure.</i>	165
<i>Figure 5. 24: Effect of MGN3 on Keratinocyte % ‘Wound’ Closure.</i>	166
<i>Figure 5. 25: The Effect of MGN3 on Keratinocyte ‘Wound’ Closure at Different Glucose Levels.</i>	167
<i>Figure 5. 26: Effect of TLR inhibition on MGN3-Mediated Keratinocyte ‘Wound’ Closure under 11mM Culture Conditions.</i>	168
<i>Figure 5. 27: The Effect of MGN3 on Keratinocyte ‘Wound’ Closure at 11mM Glucose after TLR2 and TLR4 Inhibition.</i>	169
<i>Figure 5. 28: Effect of TLR inhibition on MGN3-Mediated Keratinocyte ‘Wound’ Closure under 20mM Culture Conditions.</i>	170
<i>Figure 5. 29: The Effect of MGN3 on Keratinocyte ‘Wound’ Closure at 20mM Glucose after TLR2 and TLR4 Inhibition.</i>	171
<i>Figure 5. 30: Effect of TLR inhibition on MGN3-Mediated Keratinocyte ‘Wound’ Closure under 30mM Culture Conditions.</i>	172
<i>Figure 5. 31: The Effect of MGN3 on Keratinocyte ‘Wound’ Closure at 30mM Glucose after TLR2 and TLR4 Inhibition.</i>	173

<i>Figure 5. 32: Evaluation of keratinocyte proliferation following mitomycin C treatment.</i>	174
<i>Figure 5. 33: % 'Wound' Closure in HACATs at 11mM glucose after MGN3 treatment and mitomycin C treatment.</i>	175
<i>Figure 5. 34: The Effect of Mitomycin C on Keratinocyte 'Wound' Closure at 11mM Glucose.</i>	176
<i>Figure 5. 35: % 'Wound' closure in HACATs at 11mM glucose after MGN3 and CytoD treatment.</i>	177
<i>Figure 5. 36: The Effect of Cytochalasin D on Keratinocyte 'Wound' Closure after at 11mM Glucose.</i>	178
<i>Figure 5. 37: % 'Wound' closure in HACATs at 20mM glucose after MGN3 treatment and Mitomycin C treatment.</i>	179
<i>Figure 5. 38: The Effect of Mitomycin C on Keratinocyte 'Wound' Closure at 20mM Glucose.</i>	180
<i>Figure 5. 39: % 'Wound' closure in HDFs at 20mM glucose after MGN3 and CytoD treatment.</i>	181
<i>Figure 5. 40: The Effect of Cytochalasin D on Keratinocyte 'Wound' Closure after at 20mM Glucose.</i>	182
<i>Figure 5. 41: % 'Wound' Closure in HACATs at 30mM glucose after MGN3 treatment and mitomycin C treatment.</i>	183
<i>Figure 5. 42: The Effect of Mitomycin C on Keratinocyte 'Wound' Closure at 30mM Glucose.</i>	184
<i>Figure 5. 43: % 'Wound' closure in HACATs at 30mM glucose after MGN3 and CytoD treatment.</i>	185
<i>Figure 5. 44: The Effect of Cytochalasin D on Keratinocyte 'Wound' Closure after at 30mM Glucose.</i>	186
<i>Figure 6. 1 Fibroblast and Keratinocyte Cell Interactions Involved in Wound Healing</i>	193
<i>Figure 6. 2: The Effect of MGN3 on HDF Proliferation.</i>	199
<i>Figure 6. 3: Fibroblast Cellular Metabolism at Low Glucose Following TLR Inhibition.</i>	202
<i>Figure 6. 4: Fibroblast Cellular Metabolism at High Glucose following TLR inhibition</i>	204
<i>Figure 6. 5: Secretion of Collagen-1 (COL-1) by Fibroblasts</i>	205
<i>Figure 6. 6: Secretion of Epidermal Growth Factor (EGF) by Fibroblasts.</i>	206
<i>Figure 6. 7: Secretion of Fibroblast Growth Factor 2 (FGF2) by Fibroblasts.</i>	207
<i>Figure 6. 8: Secretion of Monocyte Chemoattractant Protein-1 (MCP-1) by Fibroblasts.</i>	208
<i>Figure 6. 9: Secretion of Matrix Metalloproteinase-1 (MMP-1) by Fibroblasts.</i>	209
<i>Figure 6. 10: Secretion of Transforming Growth Factor beta 1 (TGFβ1) by Fibroblasts</i>	210
<i>Figure 6. 11: Secretion of Keratinocyte Growth Factor (KGF) by Fibroblasts.</i>	211
<i>Figure 6. 12: COL-1 Protein Expression in HDFs at Low and High Glucose.</i>	213
<i>Figure 6. 13: TGFβ1 Expression in HDFs at Low and High Glucose.</i>	215

<i>Figure 6. 14: Influence of MGN3-Induced EGF Secretion on Fibroblast Proliferation. ....</i>	<i>218</i>
<i>Figure 6. 15: Influence of MGN3-Induced FGF2 Secretion on Fibroblast Proliferation....</i>	<i>221</i>
<i>Figure 6. 16: The Effect of MGN3 on HACAT Proliferation. ....</i>	<i>223</i>
<i>Figure 6. 17: Keratinocyte Cellular Metabolism at Low Glucose Following TLR Inhibition. ....</i>	<i>226</i>
<i>Figure 6. 18: Keratinocyte Cellular Metabolism at High Glucose Following TLR Inhibition. ....</i>	<i>229</i>
<i>Figure 6. 19: Secretion of Epidermal Growth Factor (EGF) by Keratinocytes. ....</i>	<i>230</i>
<i>Figure 6. 20: Secretion of Fibroblast Growth Factor 2 (FGF2) by Keratinocytes. ....</i>	<i>231</i>
<i>Figure 6. 21: Secretion of Transforming Growth Factor beta 1 (TGFβ1) by Keratinocytes. ....</i>	<i>232</i>
<i>Figure 6. 22: Secretion of Nuclear factor erythroid 2-related factor 2 (NRF2) by Keratinocytes.....</i>	<i>233</i>
<i>Figure 6. 23: Intracellular Nuclear Factor Erythroid 2–related Factor 2 Protein Expression in HACATs.....</i>	<i>234</i>
<i>Figure 6. 24: Intracellular Cathelicidin Peptide Expression in HACATs. ....</i>	<i>235</i>
<i>Figure 6. 25: Intracellular Beta Defensin 2 Peptide Expression in HACATs. ....</i>	<i>236</i>
<i>Figure 6. 26 TGFβ1 Expression in HACATs at Low and High Glucose. ....</i>	<i>238</i>
<i>Figure 6. 27: LL37 Expression in HACATs at Low and High Glucose. ....</i>	<i>240</i>
<i>Figure 6. 28: : Influence of MGN3-Induced EGF Secretion on Keratinocyte Proliferation. ....</i>	<i>244</i>
<i>Figure 6. 29: Influence of MGN3-Induced FGF2 Secretion on Keratinocyte Proliferation. ....</i>	<i>247</i>
<i>Figure 6. 30: Effect of Keratinocyte-Derived BD2 Peptide on MRSA and PA01 Killing. ....</i>	<i>248</i>
<i>Figure 6. 31: Effect of Keratinocyte-Derived LL37 Peptide on MRSA and PA01 Killing.....</i>	<i>249</i>
<i>Figure 6. 32: The Effect of MGN3 on NRF2 Expression in Keratinocytes. ....</i>	<i>250</i>
<i>Figure 6. 33: Secretion of MCP-1 from Keratinocytes after NRF2 Inhibition. ....</i>	<i>251</i>
<i>Figure 7. 1: The Effects of MGN3 on different cell types involved in wound healing.....</i>	<i>287</i>

## List of Tables

<i>Table 2. 1: A list of antibodies used for Thunder microscopy staining. ....</i>	<i>36</i>
--	-----------

## Abstract

Chronic elevation of blood glucose levels have profound negative impacts on wound healing in diabetic patients, often leading to the development of diabetic foot ulcers (DFUs) which can become colonised by bacteria. Clinical wound infections, the major cause of lower extremity amputations in DFU patients, occur when bacterial growth is not kept in check by the patient's immune system. Dietary fibres such as MGN3 (Biobran) show promise in counteracting the damaging effects of hyperglycaemia by reducing inflammation and enhancing immune responses such as phagocytosis. However, little is known about the broader impacts of MGN3 on wound repair processes under hyperglycaemic conditions. Thus, this study examined the effect of MGN3 on key wound-healing activities in monocytes, macrophages, fibroblasts and keratinocytes cultured under chronic hyperglycaemic conditions.

Wound healing (cell exclusion) assays (n = 12) using hyperglycaemia-exposed keratinocytes (HACATs) and human dermal fibroblasts (HDFs) assessed the *in vitro* effect of MGN3 on wound closure. Cell proliferation (n = 4) and propidium iodide (PI) flow cytometry (n = 5) assessments were used to evaluate the influence of MGN3 on cell growth and cytotoxicity following hyperglycaemia. Metabolic effects in fibroblasts and keratinocytes were analysed via Seahorse metabolic analysis (n = 3). Flow cytometry (n = 5) examined the effect of MGN3 on U937 monocyte differentiation and M1 macrophage polarisation under hyperglycaemic conditions. Host-pathogen assays (n = 18) were used to determine the effect of MGN3 on M1 macrophage-mediated clearance of *Staphylococcus aureus* and *Pseudomonas aeruginosa* biofilms. Chemotaxis assays (n = 8) assessed the effect of MGN3 on monocyte chemoattractant protein 1 (MCP-1) production and its subsequent effect on monocyte chemotaxis. Mechanistic investigations were incorporated within cell-based assays to determine key receptors and cellular pathways through which MGN3 acts in different cell types. Nuclear factor erythroid 2-related factor 2 (NRF2) expression in keratinocytes (n = 10) was measured by flow cytometry. Thunder microscopy (n = 5) and enzyme-linked immunosorbent assays (ELISAs) (n = 6-15) were used

to visualise/quantify ECM components, secreted growth factors, chemokine secretion, transcription factor expression and antimicrobial mediator production.

This study showed that MGN3 promoted wound closure under hyperglycaemic conditions primarily by enhancing keratinocyte and fibroblast migration rather than proliferation. MGN3 improved metabolism in fibroblasts and keratinocytes by stimulating mitochondrial respiration, particularly under hyperglycaemic conditions. MGN3 increased collagen-1 (COL-1) secretion in fibroblasts, cell proliferation (fibroblasts and keratinocytes), and growth factors (epidermal growth factor (EGF), fibroblast growth factor 2 (FGF2)) secretion in macrophages, fibroblasts and keratinocytes. MGN3 elevated MCP-1 levels whilst reducing excessive hyperglycaemia-induced transforming growth factor beta-1 (TGF $\beta$ 1) secretion from keratinocytes. Additionally, MGN3 enhanced macrophage-mediated phagocytosis of MRSA and PA biofilms and stimulated antimicrobial mediator production of lysozyme, cathelicidin (LL37) and beta-defensin 2 (BD2). MGN3 also upregulated NRF2 protein expression at pre-diabetic conditions and activated NRF2 at both pre-diabetic and hyperglycaemic conditions. Mechanistic investigation confirmed the effects of MGN3 on wound healing processes were partly mediated via toll-like receptor (TLR) proteins, TLR2 and TLR4.

In conclusion, MGN3 showed largely positive effects on a range of cell activities and processes involved in skin regeneration, reversing the detrimental impact of hyperglycaemia on cellular function. These findings provide an initial body of evidence suggesting the incorporation of MGN3 into hydrogel-based wound dressings might be a potential novel therapeutic strategy for non-infected and infected DFUs that warrants further investigation.

# Declaration and Copyright Statements

## Declaration:

No portion of the work referred to in this thesis has been submitted in support of an application for another degree or qualification of this or any other university or institute of learning.



Signed: ..... (Candidate)      Date: 03/01/2025

## Statement 1:

This thesis is being submitted in partial fulfilment of the requirements for the degree of PhD



Signed: ..... (Candidate)      Date: 03/01/2025

## Statement 2:

This thesis is the result of my own independent work/investigations, except where otherwise stated. Other sources are acknowledged by explicit references.



Signed: ..... (Candidate)      Date: 03/01/2025

## Statement 3:

I hereby give consent for my thesis, if accepted, to be available for photocopying and interlibrary loan, and for the title and summary to be made available to outside organisations.



Signed: ..... (Candidate)      Date: 03/01/2025

## About the Author

The author attended the 2023 Phagocytes Gordon Research Conference and Seminar in New Hampshire, USA and presented poster titled: “The Effects of Dietary Fibres on Inflammatory Processes under Hyperglycaemic Conditions” and “Biobran (MGN-3) Concurrently Reverses Lipopolysaccharide-Induced Elevation of CD14 and Impairment of Macrophage-Mediated Bacterial Clearance in a Model of Diabetic Wound Biofilms.”

## Acknowledgements

I would like to give a huge thank you to Dr Jason Ashworth for his continued support over the last couple of years. Our journey goes all the way back to undergraduate level where we first worked together, then during my Master's and all the way to now. It has been an honour and privilege to have been part of the Ashworth lab. Thank you for believing in me, motivating me and giving me the opportunity to be part of an amazing group of scientists.

I want to thank the other members of the Ashworth lab; Sana, Amina and Mohammed. Especially Mohammed, who I first got the chance to work with at undergraduate and then masters level. Thank you for your support and being a great friend inside and outside the lab. We all had many great moments together which I will cherish for a longtime. I wish you all the very best for the future.

I also want to thank my lab mates Jiandong and Razan you both always provided a great atmosphere in lab and always managed to brighten my day.

I want to give a special shout out to my parents and siblings; Mera, Shan and Mobs for your ongoing support throughout my highs and lows in life. Also, thanks for listening to me going on and on about my research (even though sometimes you can get bored of hearing about it!)

I want to thank Almighty God for pathing such a beautiful path for me and guiding me through patience to where I am today. Alhamdulillah.

Lastly, I want to thank whoever is reading this right now. Thank you taking the time to read what I have been over the last few years. It really means a lot!

## Dedication

I want to dedicate my thesis to my beloved father. I appreciate all your hard work and struggles in life to give your family the best opportunities in life. I hope you are proud of your son.

This thesis is for you ....

# Chapter 1 – Introduction

## 1.1 Diabetes

Diabetes mellitus (DM) is a common chronic disease categorised by elevated blood glucose levels, hyperglycaemia (Chait and Bornfeldt, 2009; Shaw *et al*, 2010). DM is becoming a growing problem with estimates showing up to 550 million people could suffer from the disease by 2030 (Alam *et al*, 2014). It thought the driving forces behind this increase is an ageing population and poor lifestyle habits resulting in other illnesses such as obesity (Kaul *et al*, 2013).

There are two common types of DM; type 1 and type 2. It is estimated type 1 DM makes up around 5-10% of all diabetes cases (Atkinson *et al*, 2014) and type 2 DM accounts for ~90% of all cases (Alam *et al*, 2014). Type 1 DM is an autoimmune disease due to the destruction of pancreatic  $\beta$  cells by self-antibodies resulting in very low insulin production (Alam *et al*, 2014; Ozougwu *et al*, 2013). This type of DM usually occurs during early child development to early adolescence and scientists are yet to understand exactly why this occurs (Ozougwu *et al*, 2013). Patients who suffer from this form of DM can suffer from cognitive dysfunction and visual impairments due to the chronic hyperglycaemia (McCrimmon *et al*, 2012). The most common form of diabetes, type 2 DM, results from insulin resistance (Alam *et al*, 2014). This disease is usually the direct result of poor lifestyle choices resulting in illnesses such as obesity (McCrimmon *et al*, 2012; Kaul *et al*, 2013). Patients who suffer from type 2 DM have elevated free fatty acids (FFAs) in the blood, allowing FFAs to be used as biomarkers for early diagnosis of the disease (Sobczak *et al*, 2019). FFAs under normal circumstances are stored as triglycerides within adipose tissue and can be used as an alternative energy source instead of glucose. Insulin regulates lipolysis which leads to the release of these triglycerides (Hussain *et al*, 2010; Campbell *et al*, 2006).

Type 2 diabetes mellitus (DM) can often be managed by lifestyle changes such as an improved diet and increasing exercise, but such strategies may not always be effective (Tay *et al*, 2014; El-Kader, 2014). The alternative typically involves drug treatments such as sulfonylureas. However, these medicines can sometimes lead to lactic acidosis and hypoglycaemia (Bodmer *et al*, 2008; Van Dalem *et al*, 2016). The dietary fibre MGN3 has shown to have a positive impact on the immune system, ranging from activation of

different immune cell types (Ghoneum and Agrawal, 2011) to reducing Immunosenescence (Elsaid *et al*, 2018).

### **1.1.1 The Effects of DM on the Innate Immune System**

The immune system plays a critical role in the protection and maintenance of the human body. Phagocytosis is a defence mechanism used by the innate immune system in response to invading pathogens (Hooper *et al*, 2012). In DM the immune response is increased because of elevated CD14 expression from inflammatory cells (Fernández-Real *et al*, 2011; Anas *et al*, 2010). According to studies, macrophages release high amounts of CD14 over long durations of chronic inflammation, resulting in elevated levels of proinflammatory markers (Fernández-Real *et al*, 2011; Anas *et al*, 2010). Type 2 diabetes is widely accepted to be linked to obesity, which is linked to chronic inflammation (McCrimmon *et al*, 2012). The link between insulin resistance causing chronic inflammation in adipose tissue and obesity was illustrated in a murine study carried out by Xu *et al* (2003). Chronic inflammation causes an overabundance of pro-inflammatory cytokines and damaging mediators (Segura-Egea *et al*, 2012). Chronic inflammation does not resolve, resulting in an uncontrollable flow of leukocytes to the infection/trauma site and subsequent tissue damage (Buckley *et al*, 2001). Chronic inflammation can develop in type 2 diabetes because of increased apoptosis and tissue damage (Donath and Shoelson, 2011).

It has been shown that hyperglycaemic conditions reduce the effectiveness of immune responses carried out by immune cells (Alasady *et al*, 2014). Diabetic patients have a reduced chemotaxis and phagocytic activity by their monocytes (Waltenberger *et al*, 2000). Similarly, less responsive polymorphonuclear leukocytes have been reported (Daniel *et al*, 2012; Lin *et al*, 2006) including reduced bactericidal activity, phagocytosis impairment, decreased release of lysosomal enzymes, and reduced generation of reactive oxygen species by diabetic neutrophils (Alba-Loureiro *et al*, 2007).

## 1.2 The Immune System

The critical function of the immune system is to protect the host from external pathogens which may have the potential to cause disease (Janeway, 2001). This is done via a combination of specific and non-specific responses which occur on a cellular level (Bouman *et al*, 2004). The immune system branches into two main pathways (see Figure 1. 1) including the initial response, known as innate immunity and the secondary response known as adaptive immunity (Chaplin, 2010). In some cases, the steps from the innate may be skipped and the adaptive response may be triggered resulting in a faster long-lasting response (Cooper and Alder, 2006).

The innate immune system has many ways in preventing external pathogens from bypassing the host defences in the form of physical and chemical barriers (Chaplin, 2010; Purnamasari and Hidayat, 2023; Sperandio *et al*, 2015). The largest organ on the body, the skin along with mucous lined membranes such as the nasal cavity provides an excellent physical barrier in the protection of external pathogens (Chaplin, 2010; Purnamasari and Hidayat, 2023; Sperandio *et al*, 2015). If pathogens were to enter via the mouth, they would be unable to survive the harsh acidic conditions of the stomach (Chaplin, 2010; Purnamasari and Hidayat, 2023; Sperandio *et al*, 2015). Under some circumstances pathogens may overcome the hosts' physical and chemical barriers in the form of a wound or infection. In this situation the inflammatory response would be triggered by the release of histamines from mast cells, where a combination of specialized leukocytes which work together producing inflammatory cytokines such as TNF $\alpha$  and IFN $\gamma$  to aid in the repair of wounds and fight infection (Thangam *et al*, 2018; Wojdasiewicz *et al*, 2014; Cavalcanti *et al*, 2012; Kin *et al*, 2008).

The adaptive immune system is a specific response where subtypes of lymphocytes kill pathogens by external secretions and or engulfing pathogens via phagocytosis (Jutras and Desjardins, 2005). In the presence of a pathogen some cells can undergo phagocytosis (Nagl *et al*, 2002). Examples of phagocytes are neutrophils, macrophages and dendritic cells (Dale *et al*, 2008; Nagl *et al*, 2002; Savina and Amigoren. 2007). Pathogens such as bacteria release chemo-attractants which are recognized by G-protein coupled receptors

(GPCRs) on phagocytes (Meena and Kimmel, 2017; Pan *et al*, 2016). Phagocytes engulf the bacteria and store them in a vacuole called a phagosome (Botelho and Grinstein, 2011). Hydrolytic enzymes called lysosomes are secreted by phagocyte into the phagosome to break up the pathogen (Botelho and Grinstein, 2011).

Pathogens have unique surface markers called antigens which help to identify them (Deutsch *et al*, 2009). The pathogen antigens are then displayed on the surface of the phagocyte using specialized proteins called major histocompatibility complex 2 (MHCII) (Neefjes *et al*, 2011; Unanue *et al*, 2016). The phagocyte can now be referred to as an antigen presenting cell (APC). Lymphocytes produce the thymus gland; T lymphocytes are stimulated into T helper cells which detect the APC (Miller, 2002). The T helper cells detect the APC and attach to the MHCII on the APC using surface marker proteins on the T helper called CD4+ (Saalmüller *et al*, 2002; König and Zhou, 2004). The T helper cell then proliferates into multiple T helper cells to detect other APCs and secretes cytokines to trigger the humoral response (Rezende *et al*, 2018). The cytokines secreted by the T helper cells would result in B lymphocytes migrate to the site of the T cells (Antsiferova *et al*, 2005). B lymphocytes are specialized cells produced in bone marrow (Paramithiotis and Cooper, 1997). The B lymphocytes then can differentiate into plasma cells which will produce antibodies specific to the antigen detected (LeBien and Tedder, 2008). The antibodies will attach to the antigens on the pathogen immobilizing them (LeBien and Tedder, 2008). Some of the plasma cells will remain in the blood should a future infection re-occur ie memory B cells (Paramithiotis and Cooper, 1997). Some healthy cells may have been infected by the pathogens and will display proteins on their surface via the major histocompatibility complex 1 (MHCI) (Croft *et al*, 2019). This would again be noticed by the T helper cells which can signal for cell mediated response by the stimulation of cytotoxic t cells (Broere and van Eden, 2019). Cytotoxic T cells bind to MHC I molecules via CD8+ proteins and release cytolytic enzymes into infected cells, inducing lysis and apoptosis (Saalmüller *et al*, 2002; Raskov *et al*, 2021). Some cytotoxic T cells may remain within the blood in the form of memory T cells, should the infection arise again (Löhning *et al*, 2002).

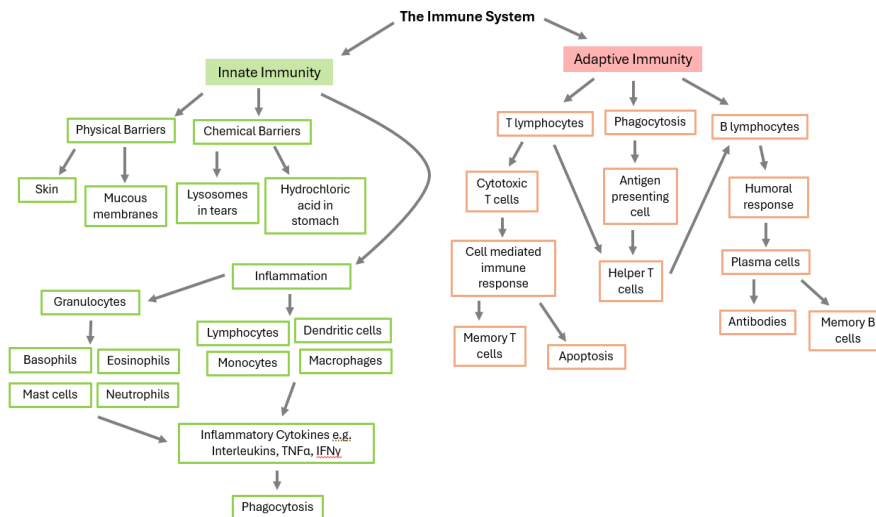


**Figure 1. 1: Schematic Illustration of the Immune System.** The immune system branches into two pathways the innate immune response or the adaptive immune response. Figure based on information from Chaplin (2010), Thangam et al (2018), Wojdasiewicz et al (2014), Rezende et al (2018) and Broere and van Eden, (2019).

### 1.3 Wound Healing

Wound healing refers to the process of tissue repair (Velnar, *et al*, 2009) and can be categorised into acute or chronic (Velnar, *et al*, 2009; Martin and Nunan, 2015). Acute wounds can heal without or with limited medical intervention, within a period of 5-30 days depending on the size of the wound (Velnar, *et al*, 2009; Martin and Nunan, 2015; Percival, *et al*, 2012). Chronic wounds however, struggle to heal even after 2-3 months (Percival, *et al*, 2012; Velnar, *et al*, 2009). It thought this is due to elevated inflammatory markers and the wound healing process struggling to overcome the inflammatory phase (Frykberg and Banks, 2015; Martin and Nunan, 2015). Repeated tissue injury of chronic wounds (such as in the case of diabetic foot ulcers) leads to the constant stimulation of proinflammatory markers as well elevating protease levels which in turn damages the extracellular matrix thus leading to more inflammatory cells migrating to the wounds (Frykberg and Banks, 2015; Velnar, *et al*, 2009). Some other factors resulting to chronic wounds failing to heal include infection, tissue hypoxia and necrotic tissue (Velnar, *et al*, 2009). One of the main obstacles in the way of wound healing is bacterial biofilms. Both acute and chronic wounds are susceptible to biofilm formation (Percival, *et al*, 2012). If the wounds are left untreated,

they can become infected with bacteria leading to biofilm formation (Westgate and Cutting, 2011). Biofilms are difficult to treat as they have a high resistance to conventional antibiotics (Wu *et al*, 2014; Simoes *et al*, 2009; Percival, *et al*, 2012). Biofilms found in chronic wounds seem to be densely packed with an extracellular outer layer unlike those found in acute wounds (James, *et al*, 2008).

The wound healing process is dependent on the regenerative ability of the tissue (Giannoudis and Pountos, 2005; Nauta *et al*, 2011). It is important to note, human tissue consists of different cell types which have their own unique functions (Giannoudis and Pountos, 2005; Julier *et al*, 2017), due to this fact some tissues have better healing abilities than others (Ferreira *et al*, 2012; Krafts, 2010). The process of wound healing can be categorised into four groups (shown in Figure 1.2); Haemostasis, Inflammation, Proliferation and Maturation (Akbik, *et al*, 2014; Wang, *et al*, 2019; Wilkinson, *et al*, 2020). The wound healing process is a complex process which requires multiple specialised cell types working together to heal a wound over a span of 10-12 days (Akbik, *et al*, 2014; Wang, *et al*, 2019; Wilkinson, *et al*, 2020). The main cell types involved in wound healing include monocytes, macrophages, fibroblasts, keratinocytes and endothelial cells, as well as others.

The first stage of wound healing is coagulation and haemostasis. In some literature the coagulation and inflammation stages are combined (Wild *et al*, 2010). The coagulation phase occurs immediately after injury and involves platelet aggregation and blood clotting (Wild *et al*, 2010; Velner *et al*, 2009). The inflammation phase also occurs at this time and involves the migration of inflammatory cells to the site of injury, vasodilation and phagocytosis (Wild *et al*, 2010; Velner *et al*, 2009). These initial phases typically last a few days depending on the severity of the injury. The proliferation phase includes re-epithelialisation to restore the epidermis, the migration of fibroblasts to the injury site to form matrix proteins (fibronectin and collagen) and angiogenesis (promotion of new capillaries) in the dermis (Enoch and Leaper, 2008; Wild *et al*, 2010; Velner *et al*, 2009). The final phase, remodelling, is where the collagen laid down by fibroblasts is continually turned over to form the mature scar tissue (Wild *et al*, 2010; Velner *et al*, 2009; Enoch and

Leaper, 2008). The wound healing process is complete once the dead or damaged tissues are replaced with new tissues (Buckley *et al*, 2001).

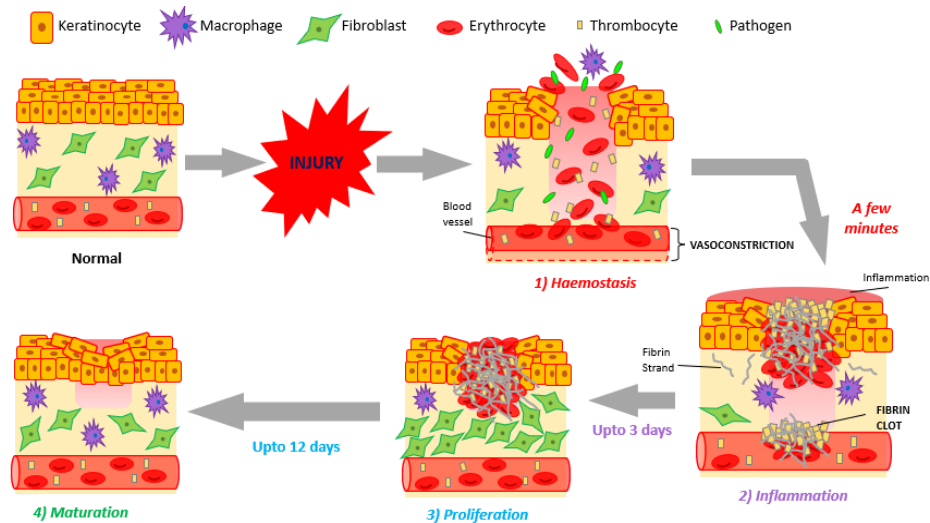


**Figure 1. 2: Schematic Illustration of the Wound Healing Process.** Following injury, the wound healing process is triggered in multiple stages, inflammation, proliferation and maturation. Figure based on information from Akbik, *et al* (2014), Wang, *et al* (2019) and Wilkinson, *et al* (2020).

### 1.3.1 Haemostasis

Haemostasis is the first process which occurs in the event of vascular injury to prevent bleeding (Batty and Smith, 2010). The word haemostasis is derived from the Greek words "haem" which means "blood" and "stasis" which means "halt." (Palta, *et al*, 2014). There are four stages involved in haemostasis: vasoconstriction, the platelet plug, activation of the coagulation cascade and the fibrin plug formation.

After an injury is sustained, some capillaries may be damaged. This would result in blood to pool around the site of the wound. After an injury the most important step is ensuring the blood flow at the site of the wound is stopped to prevent excess blood loss and starting the healing process. The blood is made up of many components; erythrocytes, thrombocytes, leukocytes among others which all play their own important role in the healing process (Garraud and Tissot; 2018; Palta, *et al*, 2014).

The blood vessels around the site of injury initially will constrict or narrow, this process is known as vasoconstriction and results in the reduction of blood flow to the injury

(Periayah *et al*, 2017; Minors, 2007; Rodrigues *et al*, 2019). This process also helps to avoid heat loss from the internal blood particularly in the case of a severe injury (Charkoudian, 2010; Alba *et al*, 2019). The process of vasoconstriction is followed by the process of vasodilation. Vasodilation increases vascular permeability and is the result of histamine release by damaged mast cells (Rodrigues *et al*, 2019; Ebeigbe and Talabi, 2014; Romero *et al*, 2017) along with other inflammatory mediators such as nitric oxide and endothelial derived hyperpolarizing factors (EDHF) (Ozkor and Quayumi, 2011).

The next stage of haemostasis is the activation of the coagulation cascade (see Figure 1.3). This process is triggered by the release of inflammatory cytokines like TNF $\alpha$ , released from around the site of injury (Schoenmakers *et al*, 2005; Witkowski *et al*, 2016). At the beginning of the coagulation cascade a change in vascular blood flow is detected by the glycoprotein von Willebrand factor which in turn connects platelet glycoproteins to damaged collagen fibres in effect to form a clot, this is known as a platelet plug. The clumped platelets then release signals such as platelet-derived growth factor (PDGF) which is found with the platelet granules (Krafts, 2010). This in turn act alongside other glycoproteins to trigger the coagulation cascade (Yun *et al*, 2016; Swieringa *et al*, 2018; Bye *et al*, 2016). The coagulation cascade is made of three pathways: Intrinsic, Extrinsic and Common (Schoenmakers *et al*, 2005, Minors, 2007). There are a group of 12 proteins involved in the coagulation cascade which are referred to as “factors”. The factors (F) are referred to using the roman numerical system and the activated versions of the factors are indicated using “a”, for example FIIa (Palta *et al*, 2014). The Intrinsic pathway is triggered when the skin surface is damaged and features FXII (Hageman factor), FXI (plasma thromboplastin antecedent), FIX (Christmas factor) and FVIII (antihemophilic factor) (Chaudhry *et al*, 2018; Roghani *et al*, 2014). The Extrinsic pathway is triggered from trauma or inflammation and features Tissue factor (TF), also known as FIII, and FVII (Proconvertin) (Roghani *et al*, 2014). These two factors can combine to make a TF-FVII complex that can activate FX (Stuart-power factor). This is done when the TF-FVII complex combines with FVIII which in turn activates the common pathway via FX activation. Activated FX allows the protease prothrombin (FII) activation resulting in thrombin. The glycoprotein fibrinogen undergoes an enzymatic reaction involving thrombin resulting in fibrin strands

(Smith *et al*, 2015). The fibrin is then used in combination with platelets and erythrocytes to form a fibrin plug (Smith *et al*, 2015).

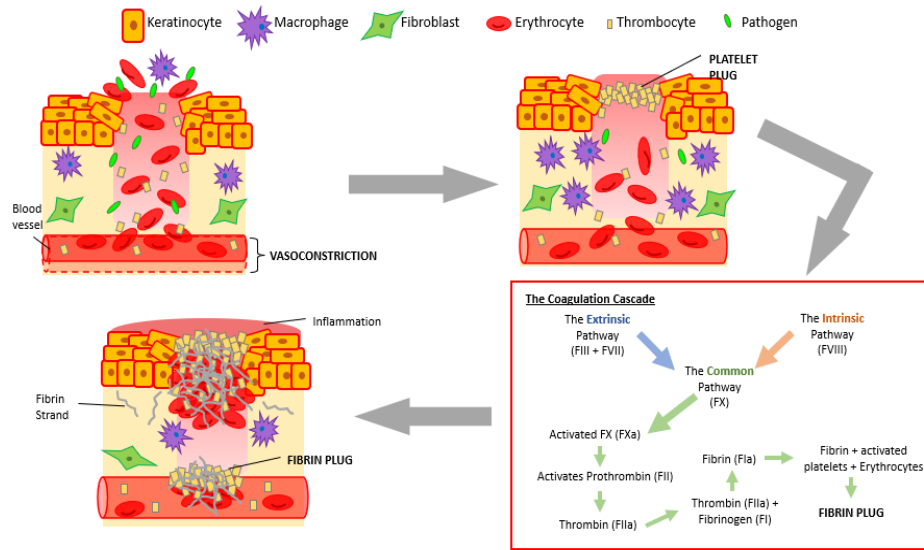


**Figure 1. 3: Schematic Illustration of the Haemostasis Stage of Wound Healing.** Following injury, Haemostasis is the initial stage of restricting blood flow by vasoconstriction and the activation of the coagulation cascade. Figure based on information from; Bye *et al* (2016), Rodrigues *et al* (2019), Roghani *et al* (2014), Periyah *et al* (2017), Schoenmakers *et al* (2005), Smith *et al* (2015), Swieringa *et al* (2018) and Yun *et al* (2016).

### 1.3.2 Inflammation

Inflammation is the result of inflammatory stimuli such as pathogens, triggering the synthesis of inflammatory mediators (Chen *et al*, 2018; Martin and Leibovich, 2005). Through interactions with cell surface receptors called Toll like receptors (TLRs) (El-Zayat *et al*, 2019). The activation of these receptors along with other receptors from the class of interleukins mediate the inflammation process and trigger other important intracellular signalling pathways (Chen *et al*, 2018; Kaminska, 2005). Examples of these additional signalling pathways include the Janus kinase (JAK)-signal transducer and activator of transcription (STAT) pathway, nuclear factor kappa-B (NF- $\kappa$ B), and mitogen-activated protein kinase (MAPK) (Chen *et al*, 2018; Henríquez-Olguín *et al*, 2015).

Inflammation can be triggered inflammatory mediators such as PDGF and transforming growth factor beta (TGF $\beta$ ) released from platelets around a wound (Martin and Leibovich, 2005). The elevated cytokine and inflammatory mediators cause blood vessels around the

wound to dilate (vasodilation) increasing blood flow to the wound and in turn recruiting more immune cells to wound area (Rodrigues *et al*, 2019).

Under normal conditions, endothelial cells lining the blood vessels are tightly packed together. However, during inflammation, as more immune cells are recruited, gaps begin to form between the endothelial cells, allowing immune cells to exit the bloodstream. This is known as increased vascular permeability (Curry and Adamson, 2010 and Claesson-Welsh, 2010). The endothelial cells are activated during proinflammatory cytokines such as IL-1 $\beta$ , tissue necrosis factor alpha (TNF $\alpha$ ) and Interferon gamma (IFN  $\gamma$ ) (Eming *et al*, 2007). The activated endothelial cells then express cell surface markers known as cell adhesion molecules (CAMs). The molecules are detected by integrins on the surface of neutrophils some examples being CD11 and CD18 (Eming *et al*, 2007) (Figure 1. 4). Chemoattractants, such as interleukin-8 (IL-8) induce the circulating neutrophils in the blood to move out of the blood vessel into the wound area (Geering *et al*, 2013). Neutrophils are granulocytic polymorphonuclear leukocytes arrive at the wound area with a few minutes after an injury, making them among the first immune cell to arrive at the site of injury (Eming *et al*, 2007). The majority of cellular activity is undertaken by the neutrophils for the initial 24-48 hours after injury. They remove pathogens via phagocytosis and release of reactive oxygen species (ROS) (Sadik *et al*, 2011; Eming *et al*, 2007). Monocytes from the blood differentiate into macrophages in the presence of chemoattractants such as macrophage chemoattractant protein 1 and macrophage inflammatory protein (Dipietro *et al*, 2001 and Maurer and Von Stebut, 2004). These macrophages then carry out phagocytosis of any remaining pathogens and apoptotic neutrophils (Rodero and Khosrotehrani, 2010).

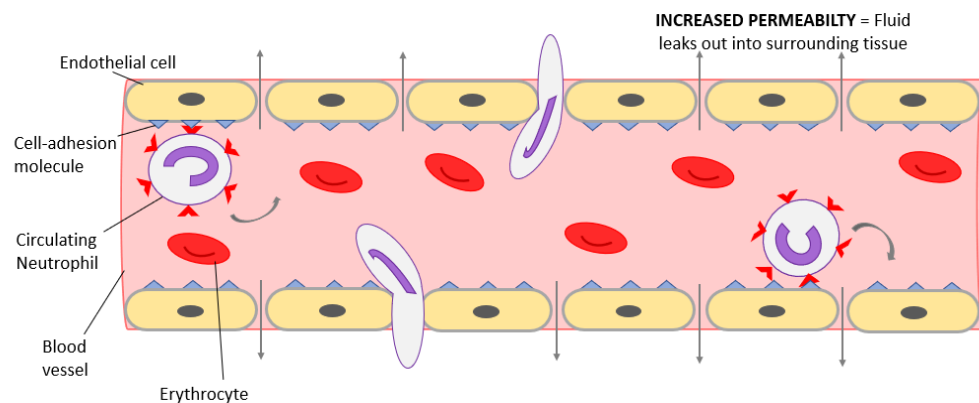


**Figure 1. 4: Schematic illustration of the Inflammatory Stage of Wound Healing.** During Inflammation increased inflammatory cytokine levels result in increased vascular permeability. Figure based on information from Martin and Leibovich (2005) and Eming *et al* (2007).

### 1.3.2.1 Chronic Inflammation

Under normal circumstances during the acute inflammatory phase several factors are involved to halt inflammation (Zhang and An, 2007). Inflammatory cytokines levels IL-1 $\beta$ , IL-6 and TNF $\alpha$  reduce when there are no longer any inflammatory stimuli detected, this will in turn stop cell recruitment to the site of injury (Zhang and An, 2007). This is further assisted by the releasing anti-inflammatory cytokines such as IL-10 by T helper cells, macrophages and dendritic cells (Iyer and Cheng, 2012). IL-10 assists in the activation the cell mediated response (Iyer and Cheng, 2012; Shibata *et al*, 1998). IL-10 has also shown to suppress several inflammatory cytokines, mainly, TNF- $\alpha$ , IL-6 and IL-1 (Zhang and An, 2007).

Chronic inflammation can be categorized by two major factors: constant tissue damage and the presence of fibrous tissue (Medzhitov, 2008; Ueha *et al*, 2012). There are many causes of chronic inflammation, these include persistent infections, hypersensitive reactions and autoimmune diseases (Medzhitov, 2008; Furman *et al*, 2019; Uzzaman and Cho, 2012). Some bacteria such as mycobacterium tuberculosis are difficult to remove by the body resulting implications due to the chronic disease tuberculosis (Amaral *et al*, 2021; Zumla *et al*, 2015). Chronic inflammation can arise due to hypersensitive reactions such as bronchial asthma where the subject is deficient in IgE antibodies resulting in allergies toward things which normally don't result in a severe reaction such as house dust mites

(Ukena *et al*, 2008; Uzzaman and Cho, 2012). Autoimmune diseases such as DM can result to chronic inflammation due to constant high levels of glucose in the blood damaging surrounding tissue, causing the release of inflammatory cytokines and triggering the NF- $\kappa$ B, MAPK, and JAK-STAT pathways (Chen *et al*, 2017; Lukens *et al*, 2011).

Chronic inflammation is a problem because it lasts longer than normal acute inflammation ranging from a few weeks to years (Feghali and Wright, 1997). During this period there is constant cellular chemotaxis resulting in elevated levels of inflammatory cytokines (Feghali and Wright, 1997; Ptaschinski and Lukacs, 2018) These cytokines would then damage healthy tissue around the wound and lead to fibrosis (Ueha *et al*, 2012). Fibrous tissue is a major problem because it can reduce tissue function in the long-term resulting in chronic diseases such as DM (Ueha *et al*, 2012, Kingber *et al*, 2013).

### 1.3.3 Proliferation

The proliferative stage (see Figure 1. 5) can be summarized by multiple steps; Angiogenesis, formation of the extracellular matrix (ECM) and restoration of the epithelium (re-epithelialisation) (Eming *et al*, 2007).

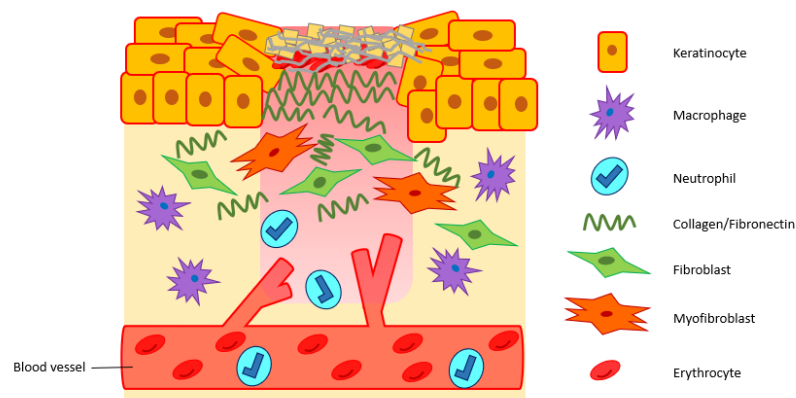


**Figure 1. 5: Schematic Illustration of the Proliferation Stage of Wound Healing.** During the proliferate stage new blood vessels form via angiogenesis due to the presence of TGF $\beta$ , FGF, PDGF and VEGF. These growth factors along with others promote fibroblasts to secrete proteins such as collagen and fibronectin which are necessary in the formation of granular tissue. Figure based on information from Eming *et al* (2007) and Greaves *et al* (2013).

Angiogenesis is the formation of new blood vessels by the migration and proliferation of endothelial cells (Eming *et al*, 2007). Transforming growth factor beta (TGF $\beta$ ), basic

fibroblast growth factor (bFGF), PDGF and vascular endothelial growth factor (VEGF) are all growth factors which help to promote angiogenesis (Eming *et al*, 2007). The presence of growth factors such as bFGF stimulates the migration and proliferation of endothelial cells by specialised cell surface receptors on the endothelial cells known as ligands, such as, alphavbeta3 (avb3) (Tonnesen *et al*, 2000; Greaves *et al*, 2013; Sahni and Francis, 2004). Endothelial cells form tube-like structures which branch into the wound area re-establishing an oxygen and nutrient supply to the surrounding cells (Greaves *et al*, 2013).

During proliferation, fibroblasts are attracted in the wound area by macrophage derived growth factors released by macrophages; PDGF, insulin-like growth factor 1 (IGF-1), VEGF and TGF- $\beta$ 1 (Krzyszczuk *et al*, 2018; Murray *et al*, 2011; Vannella *et al*, 2017; Wynn *et al*, 2016). Fibroblasts play an important role in the formation of granular tissue because they synthesize proteins such as collagen, fibronectin and elastin (Halper and Kjaer, 2014). During this stage fibroblasts differentiate in the presence of TGF- $\beta$ , into an activated fibrotic phenotype known as myofibroblasts (Plikus *et al*, 2021; Kendall and Feghali-Bostwick, 2014). It has also been shown that myofibroblasts can be derived from other cell types such as endothelial and mononuclear cells (Watsky *et al*, 2010). Myofibroblasts play an important role in the production of the ECM and collagen (Hinz, 2016; Petrov *et al*, 2002). The ECM is a glycoprotein made from proteins and carbohydrates, which binds to the collagen strands to form the granulation tissue in the wound area (Yue, 2014). The proteins produced by the fibroblasts combines with the ECM to form a type of connective tissue known as granulation tissue via fibroplasia (Greaves *et al*, 2013). This granulation tissue allows keratinocytes to migrate over the tissue and assist in closing the wound (Krzyszczuk *et al*, 2018). As the granulation tissue is forming a process called fibrinolysis occurs. This is where plasmin, a by-product of plasminogen breaks down fibrin strands within the fibrin plug (Chapin and Hajjar, 2015).

#### **1.3.4 Maturation**

The final stage of wound healing is the maturation stage. During this stage the granulation tissue turns into scar tissue (Harper *et al*, 2008). Fibroblasts interact with the surrounding ECM for wound contraction to occur (Enoch and Leaper, 2008). This influenced by several

cytokines, including TGF- $\beta$ , PDGF and bFGF (Enoch and Leaper, 2008). Granulation tissue is broken down by specific enzymes, metalloproteinases produced by fibroblast and macrophages present within the wound (Enoch and Leaper, 2008). Over time the vascularity of the scar tissue will decrease resulting in an altered appearance, as well as structural changes due to the replacement of type 1 collagen with type 3 collagen (Harper *et al*, 2008).

#### **1.4 Impaired Wound Healing in Diabetes Mellitus**

There are several factors which can result in impaired or ineffective wound healing. These factors can be categorized into two main groups; local, which is easy to solve and systemic, which is difficult to solve (Gao and Di Pietro, 2010; Enoch and Leaper, 2008). Examples of local factors include poor blood circulation, infection and presence of foreign bodies. Systemic factors include poor diet/obesity, inflammatory diseases (e.g. diabetes mellitus or rheumatoid arthritis) and age/gender (Gao and Di Pietro, 2010; Enoch and Leaper, 2008).

DM is a chronic disease because of hyperglycaemia (Chait and Bornfeldt, 2009). It is thought the hyperglycaemic conditions occur due to ineffectiveness or insignificant insulin production (McCrimmon *et al*, 2012). DM leads to chronic inflammation and over production of pro-inflammatory cytokines, which in turn leads to ineffective bacterial clearance and poor wound healing (McCrimmon *et al*, 2012; Idriss and Naismith, 2000; Anas *et al*, 2010). Diabetic foot ulcers (DFUs) are chronic wounds that result from peripheral ischaemic neuropathy due to hyperglycaemia-induced microvascular damage (Falanga, 2005). DFUs often become infected with bacteria in the wound environment preventing key immune processes such as phagocytosis and chemotaxis (Falanga, 2005; Brem and Tomic-Canic, 2007).

#### **1.5 Bacterial Biofilms**

Bacterial cells combine to form multi-cellular colonies, increasing their chances of survival from antibiotics as well as the hosts immune defences (e.g. phagocytosis) (Hassan *et al*,

2011; O'Toole *et al*, 2000; Whitchurch *et al*, 2002). These bacterial colonies encase themselves in a polysaccharide layer to form a biofilm, making up ~90% of the biofilm biomass (Kostakioti *et al*, 2013). The first record of biofilms dates to the 1670s when the Dutch scientist Antonie van Leuwenhoek observed biofilms taken from a human tooth (Garrett *et al*, 2008). Today it is common knowledge that a biofilm is an extracellular matrix made up of many components including extracellular polymeric substances, binding proteins, bacterial pili, flagella and extracellular DNA (Kostakioti *et al*, 2013; Tielker *et al*, 2005; Ariciola *et al*, 2012; Yang *et al*, 2007; Whitchurch *et al*, 2002). Biofilms can adapt to fit their surrounding environment. Under normal conditions essential nutrients are stored within the biofilm but should these nutrients become scarce the bacteria secrete enzymes altering the biofilm composition. This allows the bacteria to migrate to new locations (Kostakioti *et al*, 2013; Sauer *et al*, 2004; Gjermansen *et al*, 2005).

Bacteria can use a variety of mechanisms to form biofilms, these are often dependant on bacterial strain characteristics along with environmental factors (Lopez *et al*, 2010). Biofilm formation can be categorised into multiple stages; attachment, accumulation, maturation and detachment (Ariciola *et al*, 2012). The attachment of bacteria to surfaces depends on a multitude of factors including atomic interactions (e.g., Van der Waals forces) and the bacterium cell surface properties (Ariciola *et al*, 2012; Donlan, 2002). Bacteria have fimbriae and pili which contain hydrophobic proteins, meaning they are repelled by water (Donlan, 2002). This contributes towards the cell surface hydrophobicity and plays a key role in the attachment phase (Krasowska and Sigler, 2014). The next stages of the biofilm formation, accumulation and maturation, involve the bacteria sticking together forming multiple layers and changes in gene expression needed to form the extracellular matrix (Kostakioti *et al*, 2013; Ariciola *et al*, 2012). Cells within the biofilm communicate by gene expression using a system called quorum sensing (Subramani and Jayaprakashvel, 2019; Ariciola *et al*, 2012). The quorum sensing system consists of three components: a gene component (LuxI synthase homolog), signal molecules (acyl-homoserine-lactone (AHL)), and a receptor (LuxR receptor homolog) (Brackman *et al*, 2011; Dang *et al*, 2017). The final stage of biofilms, detachment, is when the bacterial cells disperse from the biofilm and migrate to a new location (Ariciola *et al*, 2012; Donlan, 2002). This could be due to particles

colliding within the biofilm or constant disturbance of the biofilm by removal small sections (Donlan, 2002).

There are a variety of different bacteria which form biofilms, two well studied examples include opportunistic bacteria *Staphylococcus aureus* (SA) and *Pseudomonas aeruginosa* (PA) (Lopez *et al*, 2010; Rezzoagli *et al*, 2020). Biofilms can pose a threat to human health both internally and externally. This is a problem found in hospitals as methicillin-resistant *Staphylococcus aureus* (MRSA) biofilms are commonly found on surgical equipment and medical implants (Garrett *et al*, 2008; Ariciola *et al*, 2012). Both MRSA and PA biofilms can be found within acute and chronic wounds infections (e.g. diabetic foot ulcers) and are difficult to treat as they are resistant to multiple antibiotics (Garrett *et al*, 2008; Kirker *et al*, 2012; Vestby *et al*, 2020). It is thought that bacterial biofilms such as those caused by PA grow at the site of wounds due to impaired wound healing and release surfactants, known as rhamnolipids, which leads to chronic inflammation (Vestby *et al*, 2020; Percival *et al*, 2012; Klockgether and Tümmeler, 2017).

### **1.5.1 Biofilms in Chronic Wounds**

Chronic wounds arise due to impaired wound healing, often because of implications during the inflammatory phase of healing (Frykberg and Banks, 2015). An example of chronic wounds is diabetic foot ulcers (DFUs). This is the result of diabetic neuropathy; whereby diabetic patients do not feel the initial trauma on the foot and if the physical pressure is sustained several factors such as tissue ischemia, necrosis and inflammation can quickly lead to DFUs (Doupis *et al*, 2009; Boulton *et al*, 2020). DFUs are characterized by pronounced inflammation and prolonged tissue ischaemia (Alavi *et al*, 2014). DFUs typically get colonized by several opportunistic bacteria and can become infected if left untreated (Ogba *et al*, 2019; Percival *et al*, 2018; Piri *et al*, 2013).

Biofilms play a crucial part within chronic wounds because they are said to be main reason behind the continuous inflammation with an estimate of <90% of chronic wounds containing some degree of biofilm formation (Attinger and Wolcott, 2012). Convectional antimicrobial therapies are said be significantly less effective against biofilms than they

are against planktonic bacteria, further hindering the recovery of chronic wounds (Omar, *et al*, 2017). In DFUs a combination of hyperglycaemia and restricted oxygen supply leads to large amounts of necrotic tissue resulting in biofilms usually consisting of both aerobic and anaerobic bacteria (Pouget *et al*, 2020; Dowd *et al*, 2008; Oates *et al*, 2012) further complicating the use of convectional antimicrobial therapies.

In a study conducted by Thurlow *et al*, 2011, it was shown that SA biofilms can evade bacterial recognition pathways as well the innate immune system. A murine model was used in which a biofilm infection was simulated using a catheter. In this study the activity of TLR2 and TLR9 was evaluated. The findings showed neither of the TLRs seemed to be affected by the presence of bacteria or inflammatory mediators along with low levels of cytokine levels; TNF- $\alpha$ , IL-1 $\beta$ .

Bacterial colonies can produce extracellular polysaccharides matrix structures, called biofilms, protecting them as they stay attached to surfaces and share resources within their colony (Donlan, 2001; O'toole *et al*, 2000; Vu *et al*, 2009). Biofilms can occur on various surfaces in the human body; including medical implants, teeth in the form of dental plaques and chronic wounds in the form of diabetic foot ulcers (DFUs) (Frank *et al*, 2007; Donlan, 2001; Fine *et al*, 2001). Biofilms can cause serious health problems if left untreated; for example, in dental plaques they can result in gum diseases (Fine *et al*, 2001). Moreover, biofilms are a major problem in DFUs. It is already understood that diabetic patients have impaired wound healing abilities due to weakened immune cells, resulting in a high susceptibility to wound infections like DFUs. This provides the ideal condition for biofilms to form within the wounds (Davies *et al*, 2006; Dowd *et al*, 2008). Bacteria inside biofilms have a greater likelihood of developing resistance to antimicrobial agents compared planktonic bacteria (Donlan, 2001; Frank *et al*, 2007).

### **1.5.2 Biofilm Treatments**

*Staphylococcus aureus* (SA) and *Pseudomonas aeruginosa* (PA) infections can typically be treated with conventional antibiotics; however, biofilm-associated infections are significantly more difficult to eradicate. This is because antibiotics primarily target

bacterial colonies on the outer layers of the biofilm, while deeper-seated colonies remain protected within the biofilm matrix (Singh *et al.*, 2010). Biofilms are typically large in structure,  $\approx 35 - 55\mu\text{m}$  (Odegaard *et al.*, 2000) compared to phagocytic immune cells, such as macrophages  $\approx 21\mu\text{m}$  (Fuchs *et al.*, 2016). This means that normal immune defence mechanisms, such as phagocytosis, cannot occur.

Once a biofilm is established it is extremely difficult to treat them with conventional antibiotics due to increased bacterial antibiotic resistance (Wu *et al.*, 2014; Simoes *et al.*, 2009) and the treatment is limited to surgical removal (Zimmerli *et al.*, 2012). Biofilms don't usually become symptomatic until the quorum sensing system is formed during the maturation stage (Aparna and Yadav, 2008). At this stage it is already too late for treatment as the biofilm has already formed. As a result, the chance of deep tissue infections (e.g. diabetic foot ulcers) is largely increased.

It has been suggested that disrupting the social interactions of bacteria within biofilms could potentially stop biofilms forming. This could be done by targeting biofilm virulence factors, by encourage bacterial strains to mix as a result they would compete for shared molecule and thus virulence would be reduced (Rezzoagli *et al.*, 2020; Zimmerli *et al.*, 2012). However, the obvious problem with this is that one strain would outcompete with the other and form its own biofilm. Another way of disrupting the social interactions is using quorum sensing inhibitors. If the quorum sensing system was disrupted it would allow antibiotics to target the bacteria (Rezzoagli *et al.*, 2020; Brackman *et al.*, 2011). Another strategy is to target the external and the internal structure of biofilms. Bacteria specific viruses have been used to form bacteriophages to disrupt exopolysaccharides (Sharma *et al.*, 2014; Morello *et al.*, 2011; Alemayehu *et al.*, 2012) and antimicrobial peptides have been used to disrupt protein synthesis within PA biofilms (Sharma *et al.*, 2014; Kapoor *et al.*, 2011).

The problem with these treatment methods is that the bacterial biofilms would need to be treated during the early stages of their development i.e., during the maturation stage before or whilst the quorum sensing system is being formed. This may be difficult in the

case of diabetic patients as the elevated blood glucose would cause vascular damage leading to peripheral neuropathy.

## **1.6 Dietary Fibres**

Dietary fibres are natural plant-derived polymers, in the form of oligosaccharides or polysaccharides (Elleuch *et al*, 2011). Dietary fibres have been suggested as a therapeutic alternative to modern antibiotics for the treatment of DFU infections. The reasons for this include the potential effects of dietary fibres on stimulating wound healing (Al-Ghazzewi *et al*, 2015), reducing inflammatory markers (Weickert *et al*, 2008) and increasing phagocytosis (Schley and Field, 2002).

There are two types of dietary fibres,  $\beta$ -glucans and celluloses. The  $\beta$ -glucans are frequently derived from oat and barley grains (El Khoury *et al*, 2012) and celluloses are typically derived from plant cell walls (Scheller and Ulyskov, 2010). When consumed as part of the diet,  $\beta$ -glucans have been found to increase immunological activity in both human and animal models (Tzianabos, 2000; Volman *et al*, 2008).

Xylans are hemicellulose polymers found within plant cell walls typically made up of 1,4-linked  $\beta$ -D-xylopyranosyl backbone (Hsieh and Harris, 2019). The structure of xylans can be altered; for example, if arabinose sugars are attached to xylans they become arabinoxylans (Scheller and Ulyskov, 2010). Arabinoxylans are cereal derived fibres which have demonstrated a positive impact on both the innate and adaptive immune systems (Zhang *et al*, 2015). A commonly studied example of an arabinoxylan is biobran, otherwise known as MGN3.

### **1.6.1 Biobran (MGN3)**

MGN3 is an abbreviation of the surnames of the scientists who developed this dietary fibre; Maeda, Ghoneum and Ninomiya. It was the third polymer they developed; hence the fibre was designated with the number 3 (Masood *et al*, 2013). MGN3 is an arabinoxylan polymer derived from rice bran which is hydrolysed using enzymes from

shitake mushrooms (Figure 1. 6) (Ooi *et al*, 2018). MGN3 has shown to have many positive effects on the immune system. These include activation of immune cells such as T cells and monocytes (Ghoneum and Agrawal, 2011), increased dendritic cell activation (Ghoneum and Agrawal, 2011) and reduced immunosenescence of natural killer (NK) cells (Elsaid *et al*, 2018).

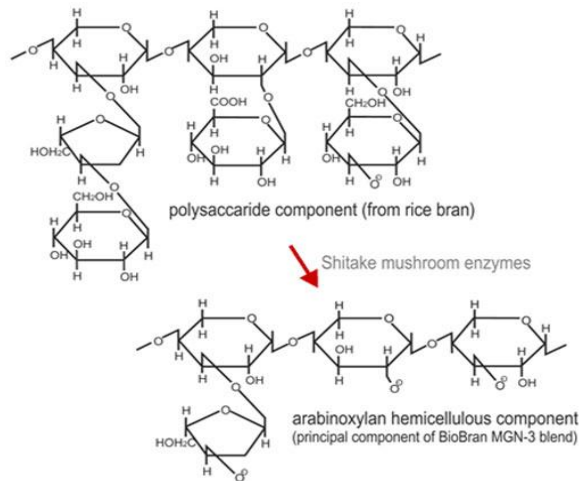


**Figure 1. 6: The chemical structure of the arabinoxylan hemicellulose component of MGN3.** Polysaccharide taken from rice bran, broken down using shitake mushrooms enzymes to obtain the arabinoxylan molecule named Biobran, also known as MGN3 (Biobran, 2022).

## 1.7 The Effects of MGN3 on Wound Healing

Clinical trials involving MGN3 have shown it can stimulate NK cell activity (Elsaid *et al*, 2018) and cognitive functions in the older population (Elsaid *et al*, 2020). It has also been shown that MGN3 can stimulate peripheral lymphocytes to increase their interleukin-2 (IL-2) production (Giese *et al*, 2008) as well as reducing proinflammatory cytokine levels (Ali *et al*, 2012). This is further supported by *in vivo* models where MGN3 has been shown to improve the phagocytic function of M0 macrophages (Asif, 2020; Tan, 2018). Asif (2020) showed that MGN3 promoted bacterial clearance *in vitro*. MGN3 also significantly ( $P < 0.05$ ) reversed the impaired phagocytic function induced by elevated glucose concentrations. In an earlier study done by Tan, 2018, it was shown that MGN3 increased macrophage-induced phagocytosis of MRSA by acting on TLR-4 and dectin-1 receptors. MGN3 increased the phagocytosis of yeast by murine macrophages (Ghoneum and

Matsuura, 2004) and the phagocytosis of *Escherichia coli* by human monocytes and neutrophils (Ghoneum *et al*, 2008).

MGN3 has several characteristics that indicate it could be used as a successful topical treatment for wound management. MGN3 is already ingested as a common dietary supplement (Elsaid *et al*, 2018) and has a safe toxicology record (Ghoneum *et al*, 2013). Moreover, MGN3 is known to be highly soluble in water (Kamiya *et al*, 2014), making it easy to add to hydrogels typically utilized in aqueous topical wound dressings (Uraloğlu *et al*, 2014). However, to date the use of MGN3 as a potential topical treatment to promote healing and/or clear bacterial infections in chronic wounds has not been evaluated, highlighting the urgent need to carry out such investigations.

### **1.8 Aim and Objectives:**

The overarching aim of the project was to investigate the potential use of MGN3 to enhance tissue repair processes and host immune responses to biofilm infections under hyperglycaemic conditions using *in vitro* models of human wound healing.

The objectives include:

- Determining the effect of MGN3 on the cellular activities of different skin cell types (including cell viability, proliferation, migration, chemotaxis, differentiation, phagocytosis and inflammatory marker expression) under hyperglycaemic conditions.
- Determining the effect of MGN3 on wound closure under hyperglycaemic conditions using *in vitro* cell exclusion assays.
- Performing host-pathogen interaction assays using biofilm models of typical diabetic wound infections to determine the effect of MGN3 on bacterial clearance under hyperglycaemic conditions.
- Visualising host-pathogen interactions by confocal/thunder microscopy.
- Investigating the effect of MGN3 on cell metabolism of dermal cell types (keratinocytes and fibroblasts) under hyperglycaemic conditions using Seahorse

technology (cytosolic calcium and adenosine triphosphate (ATP) production assessments).

- Performing receptor-binding investigations using pharmacological inhibitors and/or neutralising antibodies to determine the key receptors and cellular pathways through which MGN3 acts in different cell types.
- Perform flow cytometry and enzyme-linked immunosorbent assays (ELISAs) to assess downstream mediators of MGN3 activated pathways at pre-diabetic and hyperglycaemic conditions.

## **Chapter 2 – Materials and Methods**

## 2.1 Materials

Alexa Fluor 488 Anti-NRF2 monoclonal antibody (Abcam, UK)

Anti-beta 2 defensin (BD2) antibody (Ab9871) (Abcam, UK)

Antigen Affinity-purified Polyclonal Goat IgG Human EGF antibody (R&D systems, USA)

Anti-Human KGF/FGF-7 Antibody (R&D systems, USA)

Anti-mouse Alexa Fluor 488 secondary antibody (Thermofisher, UK)

Anti-mouse Alexa Fluor 568 secondary antibody (Thermofisher, UK)

Anti-rabbit Alexa Fluor 647 secondary antibody (Thermofisher, UK)

Beta-defensin 2 (BD2) human peptide (Hycult Biotech, Netherlands)

Bovine Serum Albumin (BSA) (Sigma-aldrich, UK)

Cathelicidin (LL37) monoclonal mouse antibody (Thermofisher, UK)

Collagen 1 monoclonal mouse antibody (COL-1) (Thermofisher, UK)

Cytochalasin D (Sigma-aldrich, UK)

D (+) Glucose (Sigma-aldrich, UK)

Dulbecco Modified Eagle Medium (DMEM) (thermofisher, UK)

Dulbecco phosphate buffered saline (DPBS) (Sigma-aldrich, UK)

EnzChek Lysozyme Assay Kit (Thermofisher, UK)

Ethanol (Fisher Scientific, UK)

Fluorescein isothiocyanate (FITC)-conjugated anti-human CD11b antibody (BioLegend, UK)

Fluorescein isothiocyanate (FITC)-conjugated anti-human CD197 (CCR7) antibody (BioLegend, UK)

Foetal Bovine serum (FBS) (Lonza, UK)

HACAT human keratinocyte cell line

Halt protease and phosphatase inhibitor cocktail (100x) (Thermofisher, UK)

Human BD-2 Standard ABTS ELISA Development Kit (Peprotech/ thermofisher, UK)

Human CCL2/MCP-1 ELISA kit DY279 (R&D systems, USA)

Human Dermal Fibroblasts (HDF) cell line

Human EGF ELISA kit DY236 (R&D systems, USA)

Human FGF basic/FGF2/bFGF ELISA kit DY233-05 (R&D systems, USA)

Human KGF/FGF-7 ELISA kit DY251 (R&D systems, USA)

Human LL-37 ELISA kit HK321 (Hycult Biotech, Netherlands)

Human NRF2 ELISA kit ab277397 (Abcam, UK)

Human Pro-collagen I  $\alpha$  1 ELISA kit DY6220-05 (R&D systems, USA)

Human TGF beta 1 ELISA Kit ab100647 (Abcam, UK)

Human TGF beta 1 ELISA Kit DY240-05 (R&D systems, USA)

Human total MMP-1 ELISA kit DY901B-05 (R&D systems, USA)

In Vitro Toxicology Assay Kit – MTT Based (Sigma, USA)

Lipopolysaccharide (LPS) from the membrane of Escherichia coli (Sigma-Aldrich, UK)

LL37 (Cathelicidin) protein (Biotechnne-R&D systems, USA)

LL37/CAP-18 human monoclonal antibody (Hycult Biotech, Netherlands)

Methicillin Resistant *Staphylococcus aureus* strain 11 (Hospital isolates, Manchester, UK)

MGN3/Biobran (Revital, UK)

Mitomycin C (Sigma-aldrich, UK)

ML 385 NRF2 Inhibitor (R&D systems, USA)

M-PER Mammalian protein extraction reagent (Thermofisher, UK)

Nutrient agar (Oxoid, UK)

Recombinant Anti-Nrf2 (phospho S40) antibody [EP1809Y] (ab76026) (Abcam, UK)

Seahorse XF glucose (Agilent Technologies, USA)

Seahorse XF L-Glutamine (Agilent Technologies, USA)

Seahorse XF Pyruvate (Agilent Technologies, USA)

Seahorse XF Real-Time ATP Rate Assay Kit – contains Oligomycin and Rotenone + Antimycin A mix (Agilent Technologies, USA)

Seahorse XF RPMI medium (Agilent Technologies, USA)

Seahorse XFp FluxPak – containing 12 XFp sensor cartridges, 12 XFp cell culture miniplates and Seahorse calibrant solution (Agilent Technologies, USA)

Sodium nitrate (Sigma-Aldrich, UK)

TGF Beta-1 Monoclonal mouse antibody (TB21) (Thermofisher, UK)

Trypsin-versene mixture (Lonza, UK)

## 2.2 Methods

### 2.2.1 Media

Complete RPMI medium (RPMI CM): RPMI-1640 media with L-Glutamine, and 25mM HEPES, supplemented with 10% FBS and 2% penicillin-streptomycin.

Antibiotic-free (AB-) medium: RPMI-1640 media with L-Glutamine, 25mM HEPES, supplemented with 10% FBS.

Complete DMEM medium (DMEM CM): DMEM media with 1g glucose, L-glutamine, and sodium pyruvate, supplemented with 10% FBS and 2% (v/v) penicillin-streptomycin.

Glucose-supplemented RPMI media: D-(+)-glucose dissolved in RPMI CM, or AB-medium to give a final concentration of 461.1mM and then used to prepare additional glucose-supplemented media with final glucose concentrations of 15, 20 or 30mM by serial dilution.

Glucose-supplemented DMEM media: D-(+)-glucose dissolved in DMEM CM medium to give a final concentration of 455.55mM (DMEM) and then used to prepare additional glucose-supplemented media with final glucose concentrations of 11, 20 or 30mM by serial dilution.

MGN-3 supplemented medium: MGN-3 dissolved in RPMI CM/ DMEM CM or AB-free medium to a concentration of 2mg/ml.

Seahorse medium: XF RPMI Medium (w/o Phenol Red) + Seahorse XF Glucose (1M) + Seahorse XF Pyruvate (100mM) + Seahorse XF L-Glutamine (200mM)

### 2.2.2 Cell Culture

U937 monocytes were cultured at  $0.5 \times 10^6$  viable cells/ml in RPMI CM at 37°C and 5% CO<sub>2</sub>. Cell viability checks and media changes were performed every 2 days on a Biorad 27 TC10 automated cell counter using the trypan blue staining method (Crowley *et al*, 2016).

HDF fibroblasts and HACAT keratinocytes were cultured until 80% confluency was reached with medium changes every 2 days. When 80% confluency was reached, cell

viability was checked using a biorad 27 TC10 automated cell counter via the trypan blue method. The cells were detached from their flasks with the use of trypsin-versene mixture (2ml), incubated for 10 minutes at 37°C and 5% CO<sub>2</sub> and then the trypsin was neutralised by adding DMEM CM (2ml) to the flask.

A hyperglycaemic model was simulated by increasing glucose concentrations in an incremental manner. In the case of U937 monocytes, the glucose was increased in subsets from 11mM to 15mM, to 20mM, to 30mM after 7-day intervals. This process allowed for 4 sets of U937 cells to be generated simultaneously. A similar process was used for HDF and HACAT cells, generating 3 sets of cells cultured under 11, 20 and 30mM glucose. In all cases the cells were allowed to grow in the appropriate glucose concentrations for 2 weeks and reaching cell viabilities of 85% or higher before starting experiments.

### **2.2.3 U937 Monocyte Differentiation into M0 Macrophages**

U937 monocytes were re-suspended in RPMI CM (11, 15, 20, or 30mM glucose) media at a density of 1x10<sup>6</sup> cells/ml. PMA (50ng/mL) was administered to the U937 monocytes to induce differentiation into adherent U937 M0 macrophages. The monocytes were incubated at 37°C and 5% CO<sub>2</sub> for 24 hour and replaced with glucose supplemented medium for a further 48hours allowing the M0 macrophages to rest. PMA is routinely utilised in this methodology because it induces differentiation of monocytic cells into macrophage-like cells through the activation of protein kinase receptors and changes cell gene expression transcription factors such as activator protein-1 (Song *et al*, 2015).

### **2.2.4 CD11b Analysis**

M0 macrophage differentiation was confirmed by assessing CD11b cell marker expression using flow cytometry. U937 were treated with or without PMA (undifferentiated negative control; NC). After differentiation (see section 2.2.3), the cells were washed with DPBS and trypsin EDTA was added to each well for 5 minutes at 37°C and 5% CO<sub>2</sub>. The trypsin was then neutralised by adding 50µl of RPMI media. The cells were then centrifuged at 500g for 5 minutes and the cell pellet washed in DPBS. After centrifugation, cells were fixed with 200µl of 4% paraformaldehyde at room temperature for 10 minutes. The cells were centrifuged, washed and re-suspended triton x-100 (0.1%)

in DPBS for 5 minutes. The cells were centrifuged, washed and re-suspended in blocking buffer (3% BSA in DPBS) for 1 hour at room temperature. The cells were washed and FITC-conjugated CD11b antibody diluted 1:5 with wash buffer [1:10 FBS in DPBS] was added. The cells incubated in the fridge for 24 hours. The cells were washed a final time with DPBS and analysed on a BD Accuri C6F1 flow cytometer to determine the expression of the CD11b cell surface marker. The cytometer analysed 10,000 individual cell events using BD Accuri C6 Software in the FSC and FL1-A. The data collected were displayed as the mean fluorescence intensity (MFI) compared to the NC (undifferentiated U937 monocytes).

### **2.2.5 M0 Macrophages Differentiation into M1 Macrophages**

U937 monocytes were differentiated in M0 macrophages (see section 2.2.3). The M0 macrophages were treated with a combination of LPS (100ng/mL) and IFN  $\gamma$  (20ng/mL) in glucose supplemented media for 24hours to generate classically activated M1 macrophages (Orecchioni *et al*, 2019). After 24 hours the media was removed and replaced with glucose supplemented medium and the cells were incubated for a further 96 hours, with the media changed again after 48 hours. LPS is routinely used in this methodology because it activates macrophages by acting through the TLR4 receptor, which then triggers a cascade of signaling events that enhances the production of inflammatory mediators (Fang *et al*, 2004). IFN- $\gamma$  is routinely used because it assists in macrophage activation by priming macrophages to be less responsive anti-inflammatory cytokines such as type I IFNs and IL-10, and more responsive to pro-inflammatory STAT1-dominated cytokines (Hu *et al*, 2008).

### **2.2.6 CD197 Analysis**

M1 macrophage differentiation was confirmed by assessing CD197 cell marker expression using flow cytometry. U937 were differentiated into M0 macrophages (see section 2.2.3) and then polarized into M1 macrophages (see section 2.2.5). M1 macrophages were then washed with DPBS and detached from wells using 50 $\mu$ l trypsin EDTA incubation for 5 minutes at 37°C and 5% CO<sub>2</sub>. The trypsin was then neutralised by adding 50 $\mu$ l of RPMI media and cells were centrifuged at 500g for 5 minutes prior to washing the cell pellet in DPBS. After centrifugation, cells were fixed with 200 $\mu$ l of 4%

paraformaldehyde at room temperature for 10 minutes. The macrophages were centrifuged, washed in DPBS and re-suspended triton x-100 (0.1%) in DPBS for 5 minutes. The cells were centrifuged, washed in DPBS, and re-suspended in blocking buffer (3% BSA in DPBS) for 1 hour at room temperature. Following washing in DPBS, macrophages were incubated with FITC-conjugated CD197 antibody diluted 1:5 with wash buffer [1:10 FBS in DPBS] at room temperature for 1 hour in the dark. The cells were washed a final time in DPBS and analysed on a BD Accuri C6F1 flow cytometer to determine the expression of the CD197 cell surface marker. The cytometer analysed 10,000 individual cell events using BD Accuri C6 Software in the FSC and FL1-A. The data collected were displayed as the mean fluorescence intensity (MFI) compared with the NC (undifferentiated U937 monocytes) and M0 macrophages.

### **2.2.7 Bacteria Preparation**

This project utilised methicillin-resistant MRSA strain II and PA strain I (PA01). Both bacterial strains were defrosted from frozen stores (at -80°C) and cultured separately in nutrient broth (NB) for 3 days at 37°C before a small quantity (1mL) of broth was spread on nutrient agar (NA) and incubated for a further 24 hours. After 24 hours, a streak plate was prepared to allow for bacterial colony isolation. The streak plates were stored at 4°C and replaced every 4-6 weeks.

When the bacteria were required for experiments, bacterial colonies were taken from the streak plate and incubated in fresh NB at 37°C for 24 hours. The bacterial broths were centrifuged at 3500rpm for 10 minutes and the bacterial was washed and resuspended in saline. This was repeated twice before performing serial dilutions. Serial dilutions (ten-fold) were performed in saline and aliquots (100ul) were spread on duplicate NA plates, which were then incubated for 24 hours at 37°C. After the incubation the colony forming units (CFU) were counted and bacterial densities (CFU/mL) were calculated. The bacterial density of  $2 \times 10^4$  CFU/mL was used for experimentation and bacteria was aliquoted on membranes and incubated at 37 °C and 5% CO<sub>2</sub> for 24 hours to allow bacterial biofilms to form.

### **2.2.8 Host-pathogen Interaction (HPI) Assay**

M1 macrophages were generated from U937 monocytes (see section 2.2.5) on polycarbonate membranes (n=6) in 24 well plates (at  $1 \times 10^6$  cells/mL). The macrophages were grown on membranes so that they could be easily transferred and interact with bacterial biofilms. The medium was removed, and macrophages treated with AB-medium (UC) (11, 15, 20 or 30mM), RS in AB-medium (2mg/mL), LPS in AB-medium (5mg/ml) and MGN3 in AB-medium (0.5, 1 and 2mg/mL). Multiple plates were created for the different glucose concentrations (11, 15, 20 and 30mM). The plates were then incubated at 37 °C and 5% CO<sub>2</sub> for 24 hours. Following removal of treatments and washing in DPBS, macrophage-bound membranes were exposed to membranes containing bacterial biofilms (MRSA or PAO1) and incubated in AB-media at 37 °C and 5% CO<sub>2</sub> for 1 hour. The supernatant was collected and diluted 1:1000 before plating on NA and incubated at 37 °C and 5% CO<sub>2</sub> for 24 hours. The bacterial recovery from the NA plates was collected the following day.

This was repeated with and without (w/o) TLR receptor inhibitors (TLR2 and TLR4) for the highest (30mM) and lowest (11mM) glucose concentrations to determine the pathways through which MGN3 may act. As separate controls, the direct effect of glucose (11, 15, 20 and 30mM) and the direct effect of MGN3 on MRSA and PAO1 bacterial biofilm growth was evaluated using the HPI method performed in the absence of macrophages.

### **2.2.9 Wound Healing (Cell Exclusion) Assay**

HDF fibroblasts and keratinocytes ( $5 \times 10^4$  cells/mL) were cultured in cell exclusion inserts within 24-well plates at glucose concentrations of 11, 20, and 30mM. Fibroblasts were incubated for 4 days, and keratinocytes for 3 days, at 37 °C with 5% CO<sub>2</sub>.

This allowed for the formation of an empty fixed cell exclusion zone (gap width 500µm) within the lawn of cultured fibroblasts and keratinocytes in each well through which the cells could later migrate and proliferate into following removal of the inserts. After incubation the cell-exclusion inserts were removed, creating a defined 500µm-wide gap ('wound') in the monolayer. Fibroblasts were washed twice with DPBS before treatment (n=3) with or without LPS (5µg/mL) or MGN3 (2mg/mL), then placed on the Phase

Holographic Imaging (Phiab) Holomonitor live-cell imaging system, housed in a standard 5% CO<sub>2</sub> incubator at 37 °C for 60 hours. Images across the wound (n=12) were captured every hour and individually analysed using the Holomonitor software to generate percentage wound closure graphs and perform data analysis. The same procedure was applied to keratinocytes after treatments and the keratinocytes were imaged using the Holomonitor system under identical incubator conditions for 24 hours. Images (n=12) were captured every 45 minutes and analysed to assess wound closure over time.

Additional treatments (n=3) were prepared in the presence/absence of 200um TLR2 (TL2-C29 InvivoGen) or TLR4 (TLR4-IN-C34 InvivoGen) inhibitor, along with/without an inhibitor for cell migration (10ug/ml cytochalasin D; C8273 Sigma-Aldrich) following a 2 hour pre-treatment incubation with/without an inhibitor of cell proliferation (20ug/ml mitomycin C; 50-07-7 Sigma-Aldrich).

To optimise mitomycin C (MC) concentration for effective inhibition of cell proliferation prior to migration assays, fibroblasts and keratinocytes were seeded in 24-well plates at  $5 \times 10^4$  cells/mL and incubated at 37 °C with 5% CO<sub>2</sub> until ~50% confluency. The supernatant was discarded, and cells were treated with or without MC at varying concentrations (2, 5, 10, 20µg/mL) for 2 hours. After treatment, cells were washed with DMEM CM, and initial cell counts (n=3) were taken using the trypan blue exclusion method (see Section 2.2.2). Fibroblasts were further incubated for 72 hours, with cell counts recorded at 24, 48, and 72 hours, while keratinocytes were incubated for 24 hours only. The % inhibition of cell proliferation in MC-treated fibroblasts/keratinocytes (+MC) compared to the negative untreated controls (NC) lacking MC exposure was calculated at each time point for all MC concentrations using the equation:

$$\% \text{ Inhibition of Cell Proliferation} = (CP_{NC} - CP_{+MC}) / CP_{NC} * 100$$

.....where Cell Proliferation (CP) = Cell Count [at time T] - Initial Cell Count

### **2.2.10 Seahorse Technology Analysis**

Fibroblasts and keratinocytes were seeded at  $1 \times 10^5$  cells/ml in low and glucose and incubated at 37°C and 5% CO<sub>2</sub> for 24 hours. The fibroblasts were then treated (n=3) with/without LPS (5ug/ml) or MGN3 (2mg/ml) for 24 hours at 37°C and 5% CO<sub>2</sub>. Further

replicates were generated that had the presence of TLR2 or TLR4 inhibitors (200ng/ml) added to fibroblasts for 1 hour before adding LPS/MGN3 treatments. A sensor cartridge (Agilent Seahorse XFp FluxPak) was prepared one day before starting the seahorse analysis. This preparation consisted of taking an empty sensor cartridge adding seahorse calibrant in the outer wells (400µl), main wells (200µl) and incubating the cartridge overnight at 37°C without CO<sub>2</sub>. On the day of the analysis the seahorse assay medium was prepared under sterile conditions (9.7ml XF RPMI Medium (w/o Phenol Red) + 100ul Seahorse XF Glucose (1M Solution) + 100ul Seahorse XF Pyruvate (100mM solution) + 100ul Seahorse XF L-Glutamine (200mM)). The seahorse analysis antibiotics: Oligomycin and Rotenone+Antimycin A were prepared. Oligomycin (O) (1.5µM) and Rotenone+Antimycin A (RA) (0.5µM) dilutions were prepared in seahorse assay medium (300ul). The media was removed from the first cell culture plate and the fibroblasts were washed with seahorse assay medium (100ul), fresh seahorse assay medium was added to the fibroblasts (100ul) and they were incubated at 37°C without CO<sub>2</sub> for 30 minutes. Whilst the fibroblasts were in the incubator, the sensor cartridge was prepared for calibration. This was done by adding 20ul of O to all A ports and 22ul of RA to all B ports and the cartridge was placed into an Agilent seahorse analyser for calibration which lasted for 15-20 minutes. this preloaded the analyser with O and RA for the analysis. After the calibration the cell culture plate was removed from the incubator and the media in the wells was replaced with fresh seahorse assay medium (180ul) and the fibroblasts were analysed on an Agilent seahorse analyser to measure their oxygen consumption rate (OCR), extracellular acidification rate (ECAR) and real time ATP production. The assay lasted approximately 55 minutes, and the antibiotics were automatically added by the analyser at predesignated times (O was added after 15 minutes and RA was added after 35 minutes). After the cell counts were taken for data normalisation.

### **2.2.11 Glucose Utilisation**

Medium-supplemented glucose utilisation was evaluated for each cell type (U937-derived M1 macrophages, HDF and HACAT cells) to determine its effect on cell growth and viability.

U937 monocytes ( $2.5 \times 10^5$  cells/mL) were grown in RPMI CM at different glucose concentrations (11, 15, 20 and 30mM). Whilst cells were cultured for 8 days without medium changes, the glucose concentration in the RPMI CM medium were measured using a glucose monitor on days 0, 2, 5 and 8, alongside corresponding cell counts.

A separate set of U937 cells were grown in RPMI CM and differentiated to M1 macrophages (see section 2.2.5). The glucose concentration was recorded on day 0, together with glucose levels before and after PMA treatment during the M0 differentiation process. Medium levels of glucose concentration were then measured over 14 days, and M1 macrophage cell counts were determined on the final day (day 14).

Two sets of HDF and HACAT ( $1 \times 10^5$  cells/mL) were grown in DMEM CM at multiple glucose concentrations (11, 20 and 30mM). One set was grown for 7 days and the other for 14 days, with the medium changed on day 7. Glucose readings were recorded on days 0, 2, 4, 7, 10, 12 and 14. Corresponding cell counts were taken from the first set of cells on day 7 and the second set on day 14.

### **2.2.12 MTT Assay**

The MTT test was used to determine any cytotoxic effects of MGN3 treatment on HDF and HACAT growth and viability. The MTT assay is used to measure cellular metabolic activity in the form of cell viability, proliferation, and cytotoxicity (Borra *et al*, 2009). MTT (3-(4,5-dimethylthiazol-2-yl)-2,5-diphenyl-2H-tetrazolium bromide) is a positively charged salt which can pass through the inner mitochondrial membranes, where it is then reduced to a violet-coloured molecule, called formazan (Ghasemi *et al*, 2021; Van meerloo *et al*, 2011). These formazan crystals can then be dissolved and analysed to determine the cytotoxic effects of treatments, as well cellular activity such as proliferation (Van meerloo *et al*, 2011).

Both HDF and HACAT cells were seeded at  $1 \times 10^5$  cells/mL in 96 well plates in DMEM CM at multiple glucose concentrations (11, 15, 20 and 30mM) and incubated for 24 hours at 37°C and 5% CO<sub>2</sub>. The next day the cells were treated with LPS (5µg/mL) or MGN3 (0.5, 1.0 and 2.0 mg/mL) for another 24 hours. An untreated control (UC) group was also prepared where the cells were grown in DMEM CM. After incubation the medium was

removed from wells and MTT solution (5%) was added to each well. The plate was incubated for 3 hours at 37°C with 5% CO<sub>2</sub> prior to incubation with MTT solvent on an orbital shaker for 10 minutes. Absorbance readings of each well were then taken at 590nm.

## 2.2.13 Visualising Mediators of Wound Healing

### 2.2.13.1 Fluorescence microscopy

Cell mediators were observed in macrophages, HDF and HACAT by fluorescence microscopy and the assistance of thunder technology. The cell mediators investigated included collagen 1 and TGFβ1 in HDFs, and TGFβ1, LL37 and TGFβ1 in HACATs. All antibodies used for this microscopy work were fluorescently tagged monoclonal antibodies (Table 2.1).

**Table 2. 1: A list of antibodies used for Thunder microscopy staining.** The table lists the antibodies which were used for thunder microscopy in HDFs (COL-1 and TGFβ1) and HACATs

CELL TYPE	PRIMARY ANTIBODY	SECONDARY ANTIBODY
HDF	Collagen 1 Monoclonal mouse antibody (Thermofisher, UK)	anti-mouse ALEXA FLUOR 568 (Thermofisher, UK)
	TGF Beta-1 Monoclonal mouse antibody (Thermofisher, UK)	anti-mouse ALEXA FLUOR 488 (Thermofisher, UK)
HACAT	Cathelicidin monoclonal mouse antibody (Thermofisher, UK)	anti-mouse ALEXA FLUOR 568 (Thermofisher, UK)
	TGF Beta-1 Monoclonal mouse antibody (Thermofisher, UK)	anti-mouse ALEXA FLUOR 488 (Thermofisher, UK)

HDF and HACAT cells (5x10<sup>4</sup> HDF/ml and 1x10<sup>5</sup> HACAT/ml) were grown on coverslips at 11, 20 and 30mM glucose for 24 hours at 37°C with 5% CO<sub>2</sub>. The cells were then treated with LPS (5ug/ml) and MGN3 (2mg/ml) for 24 hours. The next day the cell supernatants were stored for ELISAs, and the cells were fixed with PFA (4%) for 10 minutes. The cells were washed with DPBS and treated with triton x-100 (0.05%) for 5 minutes. The cells were washed with DPBS and then incubated in blocking buffer (BB) 4% goat serum in DPBS) at room temperature for 45 minutes. The cells were washed with DPBS and primary antibody (1:100 in BB) was added to half of the wells (n = 12), whilst BB was added to the other half (unstained control). Plates were incubated overnight at 4°C, washed with DBPS and a secondary antibody (1:400) (see Table 2.1 for details) was added to all wells. Cells were incubated in the dark at room temperature for 1 hour, washed with DPBS, and phalloidin (1:800) added to all the wells for 45 minutes. The cells were washed and DAPI stain was added (1:800) for 10 minutes. The cells were washed with DPBS, and coverslips were attached to microscopes with vector shield mounting

medium. The coverslips were allowed to dry prior to observation by fluorescence microscopy. The microscope used was a Leica model equipped with Thunder Imaging capabilities, capturing five images per treatment at a 60x magnification.

### **2.2.13.2 Enzyme Linked Immunosorbent Assays**

Multiple sandwich ELISAs were completed for each cell type. Fibroblast supernatant was used to measure transforming growth factor beta 1 (TGF $\beta$ 1) (ab100647 TGF beta 1 Human ELISA Kit, Abcam) collagen 1 (COL-1) (Human Pro-collagen I  $\alpha$  1 ELISA kit DY6220-05, R&D systems), matrix metalloproteinase 1 (MMP-1) (Human total MMP-1 ELISA kit DY901B-05 R&D systems), Keratinocyte growth factor (KGF) (Human KGF/FGF-7 ELISA kit DY251, R&D systems), epidermal growth factor (EGF) (Human EGF ELISA kit DY236, R&D systems), fibroblast growth factor 2 (FGF2) (Human FGF basic/FGF2/bFGF ELISA kit DY233-05, R&D systems) and monocyte chemoattractant protein 1 (MCP-1) (Human CCL2/MCP-1 ELISA kit DY279, R&D systems). Keratinocyte supernatant was used to measure TGF $\beta$ 1 (Human TGF beta 1 ELISA Kit DY240-05, R&D systems), MCP-1 (Human CCL2/MCP-1 ELISA kit DY279, R&D systems), EGF (Human EGF ELISA kit DY236, R&D systems), FGF2 (Human FGF basic/FGF2/bFGF ELISA kit DY233-05, R&D systems) and nuclear factor erythroid-2 related factor 2 (NRF2) (ab277397 Human Nrf2 ELISA Kit, Abcam). Keratinocyte cell lysates were used to measure beta 2 defensin (BD2) (Human BD-2 Standard ABTS ELISA Development Kit, Peprotech) and cathelicidin (LL37) (Human LL-37 HK321, Hycult Biotech). Macrophage supernatant was used to measure FGF2 (Human FGF basic/FGF2/bFGF ELISA kit DY233-05, R&D systems), EGF (Human EGF ELISA kit DY236, R&D systems) and MCP-1 (Human CCL2/MCP-1 ELISA kit DY279, R&D systems). Macrophage cell lysates were used to measure LL37 (Human LL-37 HK321, Hycult Biotech).

Fibroblasts were seeded at  $5 \times 10^4$  cells/ml and keratinocytes and M1 macrophages at  $1 \times 10^5$  cells/ml in low or high glucose DMEM CM for 48 hours at 37°C and 5% CO<sub>2</sub>. After the incubation, fibroblasts were treated (n=6) with/without LPS (5ug/ml) or MGN3 (2mg/ml) in the presence/absence TLR2/TLR4 (200um) for 24 hours at 37°C and 5% CO<sub>2</sub>.

Each ELISA was carried out according to the manufacturer's instructions. The general ELISA protocol briefly involved coating a 96 well plate with a carrier protein overnight at room temperature. The next day the carrier protein was removed, and the plate was

washed with wash buffer (0.05% tween 20 in DPBS). Blocking buffer (1% BSA in DPBS) was added to the plate for 1 hour. The plate is washed again before adding samples and standards to the plate. The plate was incubated at room temperature for 1-2 hours, washed and detection antibody was added to the plate for 1-2 hours. The plate was washed again and streptavidin-HRP was added for 20 minutes prior to incubation at room temperature in the dark. The plate was washed and substrate solution (1:1 H<sub>2</sub>O<sub>2</sub> and Tetramethylbenzidine) added for 20 minutes at room temperature in the dark. Stop solution was added and the plate absorbance readings were taken at 450nm with background correction at 570nm in all cases in accordance with the ELISAs protocol manuals, except for the BD2 ELISA kit which recommended initial absorbance readings to be taken at 405nm with background correction at 650nm.

In some cases, cell lysates were used for ELISA analysis. There were two lysis reagents used, RIPA buffer and MPER protein extraction buffer. In the case of RIPA buffer lysis, cells were washed with DPBS (200ul) and detached using trypsin (50ul) incubation at 37°C with 5% CO<sub>2</sub> for 10 minutes. An equal volume of medium was added (50ul) to neutralise the trypsin and the cells were centrifuged at 500g for 5 minutes. The supernatant was removed, and RIPA buffer solution was added to the cell pellet (200ul). The RIPA buffer solution consisted of 10ul phosphatase inhibitor and 10ul of protease inhibitor for every 1ml of RIPA buffer. The cells were then stored at -80°C for 30 minutes and centrifuged again at 12000g for 5 minutes after defrosting. The cell lysates were plated on to a 96 well plate to analyse the protein concentration per sample using a BCA protein assay kit (Thermofisher, UK) according to the manufacturer's instructions. Briefly, a working solution consisting of sodium bicinchoninate (reagent A) and cupric sulphate (reagent B) (1:50) was added to wells (200ul), along with BSA standards to generate a standard curve. The plate was then incubated at 37°C with 5% CO<sub>2</sub> for 30 minutes before reading the absorbance at 562nm. M-PER protein extraction buffer (M-PER) was used as an alternative to RIPA buffer in some cases because it is less likely to cause denaturation of membrane-bound protein receptors (Arya *et al*, 2023). In the M-PER buffer lysis, cells were washed with DPBS (200ul), detached with trypsin (50ul) and the trypsin neutralised by adding an equal volume of medium (50ul). M-PER was added to cells (100ul), in addition with protease and phosphatase inhibitors (1:100), and the plate was placed on a rocker for 15 minutes. The samples were then centrifuged at 12000g for 5 minutes and

the supernatant was stored. The protein concentration was again determined using the BCA kit as described above.

### **2.2.13.3 Lysozyme Assay**

Macrophage cell lysates were prepared (see section 2.2.13.2) to measure the lysozyme concentrations. Lysozyme substrate was prepared in DPBS (1ml) containing sodium azide (2mM). When needed, 40ul of reconstituted lysozyme substrate was added to 760ul of 1x reaction buffer. Samples were added to a 96 well plate (50ul) along with the lysozyme substrate (50ul) to all wells. A lysozyme stock solution was also prepared (1000U/ml) to act as standards, ranging from 500U/ml down to 0U/ml. The plate was incubated at 37°C with 5% CO<sub>2</sub> for 30 minutes. The fluorescence intensity was then measured at 495nm and background at 520nm.

### **2.2.14 Mechanistic Investigations**

#### **2.2.14.1 Cathelicidin Assay**

The antibacterial cathelicidin (LL37) activity of MGN3-treated HACAT cells and M1 macrophages (M1) were tested against MRSA and PA01.

HACAT ( $2 \times 10^5$  cells/ml) and M1 macrophages ( $2 \times 10^6$  cells/ml) were cultured in 11/30mM DMEM CM and 11/30mM RPMI respectively. Multiple 24-well plates were prepared for both cell types (3x HACAT and 4x M1 macrophages) and incubated at 37°C with 5% CO<sub>2</sub> for 24 hours. MRSA and PA01 bacterial broths were prepared (see section 2.2.7). The next day M1 macrophages (n = 24) were treated with LPS (5ug/ml), MGN3 (2mg/ml) or RS (2mg/ml) for 24 hours. Both cell lines also had a set number (n = 24) of untreated control cells that were also incubated for 24 hours. Bacterial dilutions were also carried out on the same day (see section 2.2.7). Supernatant was collected and stored for later ELISA use and 4 wells from each plate were used to obtain cell counts, whilst the remaining cells were lysed in their wells using M-PER protein extraction buffer (see section 2.2.13.2). After the lysis process half of the wells (n = 10) on each plate were treated with 2ug/ml LL37/CAP-18 blocking antibody (Hycult Biontech) made up in dilution buffer (1% BSA in PBS), and the remaining 10 wells were treated with dilution buffer. An extra control plate containing no M1 cells was prepared with 12 negative control wells containing 50ul DPBS, and the remaining 12 positive controls wells (PC)

containing 10ug/ml LL37 recombinant protein (Biotechne). Subsequently, 2ug/ml LL37/CAP-18 blocking antibody (50ul) was added to half the NC wells (n = 6) and half the PC wells (n=6). Dilution buffer (50ul) was added to the 6 remaining NC and 6 remaining PC wells. All the plates were incubated at 37°C with 5% CO<sub>2</sub> for 2 hours to allow antibody binding. After the incubation period, 100ul MRSA (2x10<sup>4</sup> cells/ml) were added to half (n = 5) the wells containing the LL37/CAP-18 blocking antibody and half (n = 5) of all the wells lacking the blocking antibody. This was repeated with PA01 (2x10<sup>4</sup> cells/ml), adding 100ul PA01 to half (n = 5) the wells containing blocking antibody and half (n = 5) the wells lacking the blocking antibody. The 24-well plates were incubated for a further 3 hours at 37°C with 5% CO<sub>2</sub>. Well contents were diluted 1:100 and plated onto duplicate NA plates incubated at 37°C for 24 hours to determine bacterial recovery based on colony counts.

#### **2.2.14.2 Beta-2 Defensin (BD2) Assay**

The antibacterial beta-2 defensin (BD2) activity of MGN3-treated HACAT cells was evaluated against MRSA and PA01.

HACAT cells (2x10<sup>5</sup> cells/ml) were cultured in 11 and 30mM DMEM CM in 24-well plates for 24 hours at 37°C with 5% CO<sub>2</sub> for 24 hours. MRSA and PA01 bacterial broths were also prepared (see section 2.2.7). Cells were then treated (n = 24) with LPS (5ug/ml), MGN3 (2mg/ml) or DMEM CM (untreated control) for 24 hours at 37°C with 5% CO<sub>2</sub>. The supernatant was collected and stored for later ELISA use, 4 wells from each plate were used to obtain cell counts and the remaining cells were lysed (see section 2.2.13.2). Following cell lysis, half the remaining wells (n = 10) on each plate were treated with the 10ug/ml anti-BD2 antibody (ab9871, Abcam) and the rest were treated with dilution buffer. An additional control plate lacking HACAT cells was set up containing DPBS (50ul) to half of the plate (n = 12, NC) and 100ng/ml BD2 peptide (ab9872, Abcam) to the other half (n = 12, PC). Then anti-BD2 antibody was added (50ul) to half (n = 6) the NC and half (n=6) the PC wells. Dilution buffer (50ul) was added to the remaining NC and PC wells prior to incubation of all plates at 37°C with 5% CO<sub>2</sub> for 2 hours to allow antibody binding. After the incubation period 100ul MRSA (2x10<sup>4</sup> cells/ml) was added to half (n = 5) of all the wells containing the blocking antibody and half (n = 5) of all the wells lacking the blocking antibody. This was repeated with PA01 (2x10<sup>4</sup> cells/ml), adding 100ul PA01 to half (n = 5) of all the wells containing the blocking antibody and half (n = 5) of the

wells lacking the blocking antibody. The 24-well plates were incubated for a further 3 hours at 37°C with 5% CO<sub>2</sub>. Well contents were diluted 1:100 and plated onto duplicate NA plates incubated at 37°C for 24 hours to determine bacterial recovery based on colony counts.

#### **2.2.14.3 Keratinocyte Growth Factor (KGF) Assay**

This assay was used to investigate the influence of MGN3-induced production of HDF-derived keratinocyte growth factor (KGF) on HACAT proliferation, with mechanistic confirmation via neutralisation of secreted KGF activity, with or without TLR inhibition.

HDF cells ( $5 \times 10^4$  cells/ml) were cultured seeded in 24-wells plates in low (11mM) or high (30mM) DMEM CM (n = 12) and incubated for 24 hours at 37°C with 5% CO<sub>2</sub>. The HDFs were then treated (n=4) with/without LPS (5ug/ml) or MGN3 (2mg/ml) in the presence/absence of 200mM TLR inhibitors (TLRi), TLR2i or TLR4i. Plates were incubated for 1 hour at 37°C with 5% CO<sub>2</sub> to allow inhibitor binding. On the same day, HACAT cells ( $1 \times 10^5$  cells/ml) were seeded in 24-well plates in 11mM or 30mM DMEM CM (n = 12) and incubated for 24 hours at 37°C with 5% CO<sub>2</sub>.

The HACAT supernatant was removed and replaced with corresponding HDF supernatant, adding 10ug/ml anti-human KGF antibody to half the wells receiving each corresponding HDF-derived cell supernatant. The HACAT cells were then incubated for for 1 hour at 37°C with 5% CO<sub>2</sub> to allow antibody binding, prior to taking cell counts and performing the MTT assay to assess cell proliferation. The MTT assay was conducted by resuspending the HACAT cells in serum-free glucose-supplemented DMEM CM, adding MTT reagent (0.263mg/ml) to all the wells and incubating for 3 hours at 37°C with 5% CO<sub>2</sub>. After the incubation the supernatant was removed from the wells, and MTT solubilization solution was added (50ul) to each well to dissolve the formazan crystals, placing the plate on a rocker to ensure complete solubilization. The absorbance was then measured on a FLUOstar Omega microplate reader at 570nm with subtraction of background readings at 690nm.

#### **2.2.14.4 Fibroblast Growth Factor 2 (FGF2) Assay**

This assay was used to investigate the influence of MGN3-induced production of M1-, HDF- and HACAT-derived fibroblast growth factor 2 (FGF2) on HDF and HACAT

proliferation, with mechanistic confirmation via neutralisation of secreted FGF2 activity and TLR inhibition.

M1 ( $5 \times 10^5$  cells/ml), HDF ( $5 \times 10^4$  cells/ml) and HACAT ( $1 \times 10^5$  cells/ml) were cultured in 24-well plates using 11/30mM RPMI and DMEM CM and then treated with/without LPS or MGN3 ( $n = 3$ ) in the presence/absence (+/-) of TLR2i/TLR4i (see section 2.2.14.1). On the same day, untreated HDF ( $5 \times 10^4$  cells/ml) and HACAT ( $1 \times 10^5$  cells/ml) were cultured onto 24-well plates for 24 hours at 37°C with 5% CO<sub>2</sub> prior to removal of medium and replacement with supernatant collected from treated M1, HACAT or HDF cells. Anti-FGF2 antibody (0.6ug/ml) made up in appropriate glucose supplemented DMEM CM was added to half the wells receiving each corresponding M1/HDF/HACAT-derived cell supernatant. Plates were incubated for another 24 hours at 24 hours at 37°C with 5% CO<sub>2</sub> prior to taking cell counts and performing the MTT assay to assess cell proliferation. The MTT assay was conducted by resuspending the HDF/HACAT cells in serum-free glucose-supplemented DMEM CM, adding MTT reagent (0.263mg/ml) to all the wells and incubating for 3 hours at 37°C with 5% CO<sub>2</sub>. After the incubation the supernatant was removed from the wells, and MTT solubilization solution was added to each well to dissolve the formazan crystals, placing the plate on a rocker to ensure complete solubilization. The absorbance was then measured on a FLUOstar Omega microplate reader at 570nm with subtraction of background readings at 690nm.

#### **2.2.14.5 Epidermal Growth Factor (EGF) Assay**

This assay was used to investigate the influence of MGN3-induced production of M1-, HDF- and HACAT-derived epidermal growth factor (EGF) on subsequent HDF and HACAT proliferation, with mechanistic confirmation via neutralisation of secreted EGF activity and TLR inhibition.

The process was the same as the KGF assay (see section 2.2.14.4) but involved the use of anti-EGF antibody (0.6ug/ml).

#### **2.2.14.6 Monocyte Chemoattractant Protein-1 (MCP-1) Assay**

A chemotaxis assay was used to evaluate the influence of M1-, HDF- and HACAT-derived monocyte chemoattractant protein-1 (MCP-1) on U937-derived monocyte chemotaxis

following treatment of M1, HDF or HACAT cells with MGN3, with mechanistic confirmation via neutralisation of secreted MCP-1 activity.

M1 ( $5 \times 10^5$  cells/ml), HDF ( $5 \times 10^4$  cells/ml) and HACAT ( $1 \times 10^5$  cells/ml) were cultured in 24-well plates using 11/30mM RPMI and DMEM CM. M1, HDF and HACAT supernatants were collected following treatment with/without LPS or MGN3 ( $n = 3$ ) in the presence/absence of TLR inhibition (TLR2i/TLR4i) for 24 hours at 37°C with 5% CO<sub>2</sub> (see section 2.2.14.4). Suspension U937 monocytes were cultured ( $1 \times 10^6$  cells/ml) at 11 and 30mM RPMI CM and seeded onto the upper chambers of 96-well chemotaxis plates and then set aside. Appropriate lower chambers of the 96-well chemotaxis plates were loaded with 100ul recombinant MCP-1 protein (60ng/ml) or 100ul collected supernatant from each treatment. A further 50ul anti-MCP-1 blocking antibody (1ug/ml) made up in RPMI CM was added to half the lower chambers corresponding to each treatment, and the remaining chambers received 50ul RPMI CM. The plate lids were replaced, and lower chambers of chemotaxis plates were incubated for 1 hour to allow for antibody binding. The cultured U937 monocytes in the upper chambers of the chemotaxis plates were then returned and lids replaced. The plates were incubated for 4 hours at 37°C with 5% CO<sub>2</sub> to allow chemotaxis to take place. After incubation monocyte cell counts were taken in the lower chamber wells and the lower chamber was centrifuged at 500g for 5 minutes to pellet the monocytes. The supernatants were removed and MTT solution (50ul) was added to all lower chamber wells. The plates were incubated for 3 hours and then MTT solubilization (50ul) solution was added. Absorbance readings were taken at 570nm on a FLUOstar Omega microplate reader, subtracting background readings at 690nm.

#### **2.2.14.7 Nuclear Factor Erythroid-2 Related Factor 2 (NRF2) Assay**

This assay was used to assess the contribution of HACAT-derived nuclear factor erythroid-2 related factor 2 (NRF2) on HACAT synthesis of nitric oxide (NO) and monocyte-chemoattractant protein-1 (MCP-1) following treatment with MGN3.

HACAT cells ( $1 \times 10^5$  cells/ml) were cultured in 24 well plates using 11/30mM DMEM CM for 24 hours at 37°C with 5% CO<sub>2</sub>. The supernatant from each well was collected following subsequent treatment with/without 5ug/ml LPS or 2mg/ml MGN3 ( $n=4$ ), with/without 5uM NRF2 inhibitor (NRF2i) for 24 hours at 37°C with 5% CO<sub>2</sub>. Cell lysates

were also obtained from each well using MPER protein extraction buffer (see section 2.2.13.2).

Supernatants and cell lysates were used to measure NO levels using the Griess method and MCP-1 levels by ELISA (see section 2.2.13.2). Sodium nitrate standards were prepared for the Griess assay, ranging from 0 to 120uM. An equal volume of Griess reagent was added to all standards and supernatant/cell lysate samples. Following incubation in the dark for 20 minutes, the absorbance at 540nm was then measured on a FLUOstar Omega microplate reader.

Activated (phosphorylated) NRF2 was also measured via flow cytometry, along with cells counts, following treatments. Cells were washed with 250ul DMEM CM and detached via trypsinization (see section 2.2.2). Cells were resuspended in DMEM CM and cell counts performed by the trypan blue method (see section 2.2.2). The cells were pelleted by centrifugation at 500g for 5 minutes and fixed via incubation in 4% paraformaldehyde (PFA) for 10 minutes. Cells were then washed three times in DPBS, and 0.1% triton X-100 added for 10 minutes and then washed three times in DPBS. Blocking buffer (3% BSA in DPBS) was added for 1 hour and supernatant discarded following centrifugation at 500g for 5 minutes. Cells were then stained for 24 hours in the fridge with and without recombinant anti-NRF2 (phospho S40) antibody diluted 1:80 in wash buffer (10% FBS in DPBS). Following two steps of pelleting and washing in DPBS, cells were resuspended in anti-rabbit Alexa Fluor 647 secondary antibody for 2 hours in the dark. Samples were then centrifuged at 500g for 5 minutes, washed and resuspended twice in DPBS before analysis by flow cytometry (see section 2.2.4).

### **2.2.15 Data Analysis**

The data collected from the experiments was normalised against the cell counts and analysed (depending on the number of means) using IBM SPSS software for one-way ANOVAs and/or independent t-tests.

# **Chapter 3: The Impact of Chronic Hyperglycaemia on Cell Function**

## 3.1 Introduction

### 3.1.1 Glucose Metabolism

#### 3.1.1.1 Glucose

Glucose can be referred to as a simple carbohydrate known as a monosaccharide and can be classified as aldehydes or ketones with two or more hydroxyl groups (Wang *et al*, 2024; Genova *et al*, 2007). Glucose levels for random tests of <11.1mM are said to be within the normal range and >11.1mM is classed as hyperglycaemia as defined by Diabetes UK and the National Institute of Health and Care Excellence (Seery, 2022; NICE, 2024). Chronic hyperglycaemia can result in type 2 diabetes and usually is due to insulin resistance (Petersen and Shulman, 2018; Laville and Nazare, 2009). Insulin resistance can occur when there is not enough insulin produced, or the insulin is no longer effective (Petersen and Shulman, 2018).

#### 3.1.1.2 Insulin Signalling Pathway

Blood glucose levels are maintained by insulin. Insulin is a hormone which is released by  $\beta$  cells in the islet of Langerhans within the pancreas (Eliasson *et al*, 2008; Omar-Hmeadi and Idevall-Hagren, 2021; Rorsman and Ascroft, 2018). High glucose levels result in elevated  $\text{Ca}^{2+}$  (Smogorzewski *et al*, 1998), this increase in intracellular  $\text{Ca}^{2+}$  within  $\beta$  cells triggers the release of insulin (Rorsman and Ascroft, 2018; Eliasson *et al*, 2008).

Insulin binds to its receptor on the cell surface, initiating a signalling cascade that enables glucose uptake (Figure 3.1). This activates insulin receptor substrate (IRS), which recruits phosphatidylinositol 3-kinase (PI3K), leading to the activation of protein kinase B (PKB/AKT) (Arneth *et al*, 2019; Han *et al*, 2016; Lankatillake *et al*, 2019). AKT promotes the translocation of glucose transporter type 4 (GLUT4) to the cell membrane, facilitating glucose entry (Cong *et al*, 1997; Manna and Jian, 2013). AKT also phosphorylates and inhibits glycogen synthase kinase 3-beta (GSK-3 $\beta$ ), relieving its suppression of glycogen synthase, which converts UDP-glucose to glycogen (Andeva-Andany *et al*, 2016). Additionally, insulin-stimulated protein kinase (ISPK) activates protein phosphatase 1 (PP1/PP1G), enhancing glycogen synthase activity and preventing glycogen breakdown (Suzuki *et al*, 2001; Hansen *et al*, 1999). Thus, glucose is either used for ATP production

or stored as glycogen. It is understood that type 2 diabetes can result in insulin resistance, but the question is why this happens. It has been reported in diabetic patients who have insulin resistance also display signs of defective IRS proteins, in particular IRS-1 (Sesti *et al*, 2001). Hyperglycaemia has also shown to alter the function of pancreatic  $\beta$  cells which can lead to part or full inhibition of insulin release (Toschi *et al*, 2002).

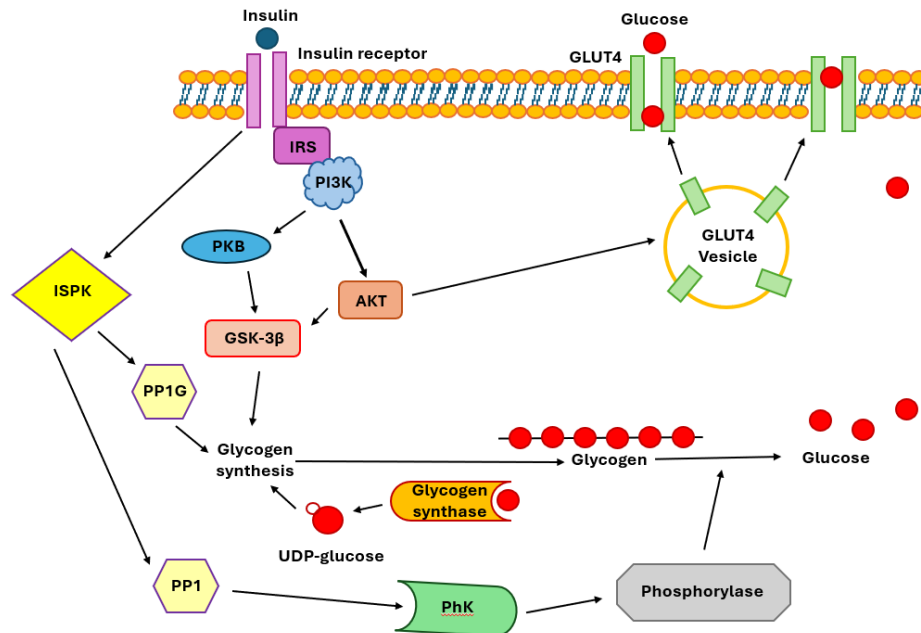


**Figure 3. 1: Insulin triggers a cascade which allows glucose to enter a cell.** Extracellular glucose triggers insulin release which binds to IRS. PI3K binds to the IRS activating PKB and AKT. The PKB/AKT pathway allows for the translocation of GLUT4 to cell surface to allow the uptake of glucose within the cell. PKB allows GSK-3 $\beta$  with the addition of ISPK to undergo glycogen synthesis. Schematic based on information from, Arneth *et al*, 2019; Han *et al*, 2016; Lankatillake *et al*, 2019; Hansen *et al*, 1999

### 3.1.1.3 ATP Production

Once glucose is taken up or stored in the cells it can be used to produce adenosine triphosphate (ATP) which is the main energy source for the cell (Patergnani *et al*, 2014). ATP is made up of a nitrogenous base called an adenine attached to a ribose sugar and three phosphate groups (Mahoney *et al*, 2018). ATP production follows two pathways, an anaerobic route known as glycolysis and an aerobic route known as mitochondrial respiration (Shen *et al*, 2024) (see Figure 3.2).

Glycolysis generates a net gain of two ATP molecules per glucose (TeSlaa & Teitell, 2014). Upon entering the cell, glucose is phosphorylated by hexokinase (HK) to form glucose-6-phosphate (G-6-P), using one ATP (Tan & Miyamoto, 2015). G-6-P is isomerized to fructose-6-phosphate (F-6-P) by glucose-6-phosphate isomerase (GPI) (Wu *et al*, 2005),

then phosphorylated by phosphofructokinase (PFK) to fructose-1,6-bisphosphate (F-1,6-BP), consuming another ATP (Wu *et al*, 2005). F-1,6-BP is split by aldolase into dihydroxyacetone phosphate (DHAP) and glyceraldehyde-3-phosphate (G-3-P), which can interconvert via triose phosphate isomerase (TPI) (Luo *et al*, 2022; Wang *et al*, 2024). G-3-P is oxidized by glyceraldehyde-3-phosphate dehydrogenase (GAPDH) to 1,3-bisphosphoglycerate (1,3-BPG), producing NADH from NAD<sup>+</sup> (Dan'shina *et al*, 2003; Xiaio *et al*, 2018). 1,3-BPG donates a phosphate to ADP via phosphoglycerate kinase (PGK), forming 3-phosphoglycerate (PGA) and ATP (Wang *et al*, 2024). PGA is converted to 2-phosphoglycerate (2PG) by phosphoglycerate mutase-1 (PGAM1), then to phosphoenolpyruvate (PEP) by enolase (Fukushi *et al*, 2022). Finally, pyruvate kinase (PK) catalyzes the conversion of PEP to pyruvate, generating two ATP (Ricci, 2000). Pyruvate may then be reduced to lactate or enter mitochondria for the Krebs cycle (Korla *et al*, 2015).

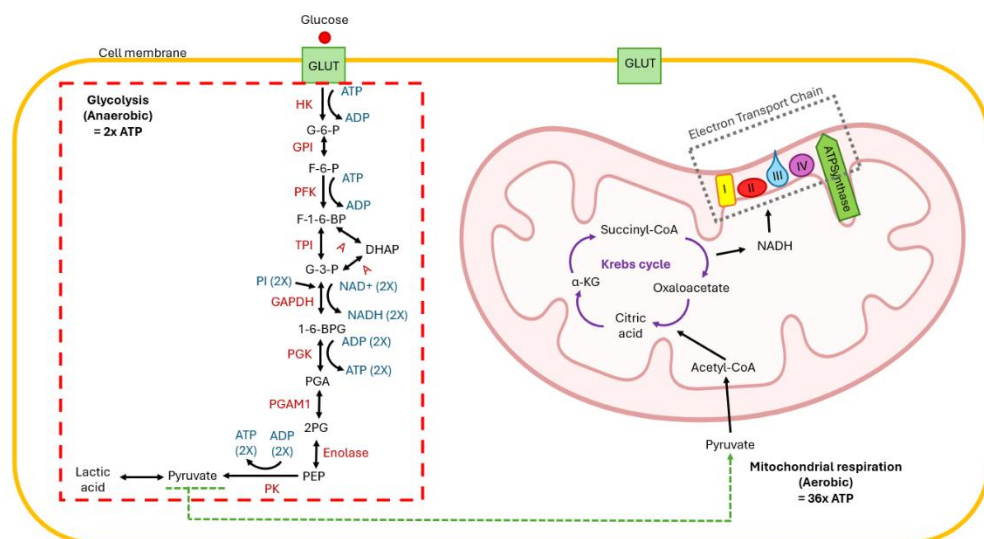


**Figure 3. 2: Glucose is used in the production of ATP.** After glucose enters the cell, it is used to produce ATP anaerobically via glycolysis and/ or aerobically via mitochondrial respiration. Both pathways result in a combined total of 38 ATP molecules produced. Schematic based on information from, Wu *et al*, 2005; Wang *et al*, 2024; Fukushi *et al*, 2022; Korla *et al*, 2015; Lushchak *et al*, 2014; Gasmı *et al*, 2021

Pyruvate from glycolysis is oxidized to acetyl-CoA, initiating the Krebs cycle (Figure 3.2). Also known as the citric acid or tricarboxylic acid (TCA) cycle, this mitochondrial process oxidizes acetyl-CoA to generate ATP (Gasmı *et al*, 2021). Acetyl-CoA combines with oxaloacetate to form citrate via citrate synthase (Lacobazzi & Infantino, 2014), which is then reversibly converted to isocitrate by aconitase (Lushchak *et al*, 2014). Isocitrate is oxidatively decarboxylated by isocitrate dehydrogenase to produce  $\alpha$ -ketoglutarate ( $\alpha$ -

KG), yielding NADH (Gasmi *et al*, 2021).  $\alpha$ -KG is further converted to succinyl-CoA by  $\alpha$ -KG dehydrogenase, also producing NADH (Ryan & O'Neil, 2020). Each glucose molecule yields 10 NADH and 2 FADH<sub>2</sub> through glycolysis and the Krebs cycle, which feed into the electron transport chain (ETC) for ATP production.

The ETC also known as oxidative phosphorylation, uses NADH and FADH<sub>2</sub> to drive a series of redox reactions, creating an electron gradient for ATP production (Kennett & Kuchel, 2003; Davies *et al*, 2011). Located in the inner mitochondrial membrane, the ETC includes complexes I–IV and ATP synthase (Davies *et al.*, 2011). Complex I oxidizes NADH, releasing electrons and protons (H<sup>+</sup>), and pumps H<sup>+</sup> into the intermembrane space (Titov *et al*, 2016; Sazanov, 2015). To minimize oxidative stress, electrons are transferred to coenzyme Q10 (CoQ10), which also receives electrons from FADH<sub>2</sub> via complex II, producing FAD and H<sup>+</sup> (Duberley *et al*, 2014; Gnaiger, 2023). CoQ10 then delivers electrons to complex III, enabling further H<sup>+</sup> pumping, followed by transfer to cytochrome c (CytoC), which carries them to complex IV (Musatov & Robinson, 2012). Complex IV continues proton pumping and transfers electrons to oxygen, forming water as a by-product (Chen *et al*, 2004). The resulting proton gradient drives ATP synthase to convert ADP and phosphate into ATP (Chen *et al*, 2004).

In diabetes, hyperglycaemia disrupts ATP production through multiple mechanisms. Mitochondrial transcription factor A (TFAM) regulates mitochondrial DNA (mtDNA) expression (Larsson *et al*, 1998), and its deletion induces a diabetic phenotype in mice (Silva *et al*, 2000). High glucose levels can cause mtDNA deletions, leading to instability in mtDNA-encoded proteins, including those in the electron transport chain (ETC) (Maechler & Wollheim, 2001). Type 2 diabetes involves both insulin resistance and impaired insulin secretion (Polonsky *et al*, 1996). ETC-derived ATP production is reduced by 50% in diabetic skeletal muscle (Maechler & Wollheim, 2001), and mtDNA levels in peripheral blood are decreased by 35% in type 2 diabetics (Lee *et al*, 1998). Accelerated tissue aging in diabetes is linked to mtDNA mutations (Michikawa *et al*, 1999). Mitochondria produce reactive oxygen species (ROS) due to inefficient electron transport, which is worsened by age-related increases in ROS and mtDNA damage (Beckman & Ames, 1998). Aging also reduces antioxidant enzymes like catalase, especially in  $\beta$  cells, heightening oxidative stress (Tiedge *et al.*, 1997; Maechler *et al*, 1999). This contributes to impaired insulin secretion in type 2 diabetes (Coordt *et al*,

1995). Dysfunctional  $\beta$  cell metabolism is a key driver of disease progression, as shown in diabetic patient  $\beta$  cells (Segerstolpe *et al*, 2016), human  $\beta$  cells exposed to high glucose (Brun *et al.*, 2015), and murine models displaying glycogen (Brereton *et al*, 2016) and stearoyl carnitine accumulation (Adam *et al.*, 2017), both of which impair insulin production.

### **3.1.2 The Effect of Hyperglycaemia on Macrophage Function**

Macrophages originate from blood monocytes and can differentiate into various phenotypes: inactive (M0), pro-inflammatory (M1), and anti-inflammatory (M2) (Epelman *et al*, 2014; Orekhov *et al*, 2019). M0 macrophages are highly plastic and respond to stimuli—IFN- $\gamma$ /LPS induces M1 differentiation, while IL-4/IL-13 promotes M2 activation (Tarique *et al*, 2015; Wager & Wormley, 2014). M1 macrophages secrete pro-inflammatory cytokines (TNF $\alpha$ , IL-1/6, NO) and express markers CD197 and CD86 (Magatti *et al*, 2017; McWhorter *et al*, 2015; Kadomoto *et al*, 2021). In contrast, M2 macrophages reduce inflammation via IL-10 and TGF $\beta$  and express CD163 and CD206 (Magatti *et al*, 2017; Tarique *et al*, 2015).

At pre-diabetic conditions, M1 macrophages produce proinflammatory cytokines and clear pathogens via phagocytosis (Savina & Amigorena, 2007). However, hyperglycaemia impairs macrophage function. Diabetic patients show reduced phagocytic activity compared to non-diabetics (Lecube *et al*, 2011), and macrophages exposed to high glucose (22mM) demonstrate decreased mycobacterial phagocytosis compared to low glucose (5mM) conditions (Vance *et al*, 2019). High glucose also downregulates surface markers such as CX3CR1 and CD169 (Vance *et al*, 2019). Additionally, hyperglycaemia alters cytokine profiles, increasing levels of GM-CSF, KC, TNF- $\alpha$ , and MCP-1 in diabetic mice (Awad *et al.*, 2015; Koulmanda *et al*, 2012). It also promotes macrophage polarization, with elevated CD11c expression observed under high glucose (15mM) conditions (Torres-Castro *et al*, 2016).

### **3.1.3 The Effect of Hyperglycaemia on Fibroblast Function**

Fibroblasts are spindle-shaped cells that produce ECM components like collagen and fibronectin (McAnulty, 2007; Younesi *et al*, 2024). When activated by TNF $\alpha$ , ILs, and

PDGF, fibroblasts transform into myofibroblasts, which have a stellate shape due to an enlarged Golgi and extensive endoplasmic reticulum for ECM production (McAnulty, 2007; Iwaisako *et al*, 2012). Fibroblasts primarily produce collagen type I (COL-1), which makes up 90% of the body's collagen (Hwang *et al*, 2021). Human dermal fibroblasts (HDFs) are crucial for wound healing, migrating to injury sites, becoming activated, and secreting actin bundles (Singer & Clark, 1999; Pilkus *et al*, 2021). HDF motility relies on cytokines and growth factors such as FGF, TGF $\beta$ 1, EGF, and PDGF (Singer & Clark, 1999; Park *et al*, 2000).

Diabetic patients usually present with impaired wound healing resulting in chronic wounds (e.g. DFUs). These chronic wounds have been linked to reduced ECM and fibronectin production in fibroblasts (Stoffels *et al*, 2013; Hamed *et al*, 2011). It has been shown diabetic wounds 5 days after injury, tend to have very low levels of fibrosis genes such as, COL1 and MMP2 (Haas *et al*, 2021). It was also shown there were low levels of spinocerebellar ataxia type 1 (SCA1) and high levels of CD29 in the wounds indicating impaired myofibroblasts function (Haas *et al*, 2021).

#### **3.1.4 The Effect of Hyperglycaemia on Keratinocyte Function**

Keratinocytes are the primary cellular constituents of the epidermis (Pastar *et al*, 2008; Pipponen *et al*, 2020) and play a key role in the inflammatory and maturation stages of wound healing (Wojtowicz *et al*, 2014; Pipponen *et al*, 2020). Keratinocytes are important in wound healing because they express multiple TLRs for example TLR4 which with the help of CD14 recognises LPS (Pipponen *et al*, 2020). HACAT cells are immortalised human keratinocytes which contain keratins commonly found in the epidermis making them useful for *in vivo* trials (Seo *et al*, 2012).

Impaired keratinocyte migration due to hyperglycaemia is thought to play a major role in defective diabetic wound healing (Li *et al*, 2019). Hyperglycaemia has shown to significantly reduce keratinocyte cell viability and cell migration *in vitro* (Kruse *et al*, 2016). It has been shown chronic hyperglycaemia results in the downregulation of the P38/MAPK pathway as the inactivation of autophagy which in turn restricts keratinocyte migration (Li *et al*, 2019; Jiang *et al*, 2014). It has also been suggested impaired wound healing in diabetes maybe caused due an increase and/or prolonged IL-6 expression by keratinocytes (Lee *et al*, 2019).

## 3.2 Aims and Objectives

### 3.2.1 Aim

To investigate the impact of chronic hyperglycaemia on the cellular function of U937 macrophages, fibroblasts and keratinocytes.

### 3.2.2 Objectives

- To assess the impact of hyperglycaemia on macrophage differentiation through the evaluation of cell surface marker expression
- To monitor glucose uptake by assessing glucose depletion, usage and change in U937 macrophages, fibroblasts and keratinocytes
- To evaluate the effect of hyperglycaemia on cellular metabolism in fibroblasts and keratinocytes

## 3.3 Methods

### 3.3.1 Generation of M1 Macrophages

U937 monocytes were cultured at different glucose concentrations (11, 15, 20 and 30mM) for over a minimum of 2 weeks prior to experimental use (see section 2.2.5). U937 monocytes were differentiated into M0 and M1 macrophages as shown in sections 2.2.3 and 2.2.5.

### 3.3.2 CD11b/ CD197 Analysis

M0 macrophages and M1 macrophages were prepared at different glucose concentrations (see sections 2.2.3 and 2.2.5) and the expression of CD11b in M0 macrophages and CD197 in M1 macrophages was confirmed using flow cytometry as shown in sections 2.2.4 and 2.2.6

### 3.3.3 Glucose Evaluation

Monocytes and macrophages were cultured at varying glucose concentrations, with glucose depletion monitored using a blood sugar monitor over 8 days. Fibroblasts and keratinocytes were cultured similarly for 14 days (see section 2.2.11).

The glucose usage/utilisation was calculated as follows:

Change in glucose concentration *{in presence of cells}* – Change in glucose concentration *{in absence of cells\*}*

\* i.e. just medium alone placed inside incubator without any cells

Whereby change in glucose concentration = glucose level measured at start (i.e. day zero; d0) – glucose level measured at end point (e.g. day; d14)

### 3.3.4 Seahorse Analysis

Fibroblasts (HDFs) and keratinocytes (HACATs) were analysed to measure the oxygen consumption rate (OCR), extracellular acidification rate (ECAR) and real-time ATP production (see section 2.2.10)

## 3.4 Results

### 3.4.1 Differentiation of U937 Monocytes to M0 Macrophages

U937 monocytes were cultured at different glucose concentrations and then differentiated into M0 macrophages (see section 2.2.3). After differentiation, the macrophages were assessed for CD11b cell marker expression using flow cytometry (Figure 3.3).

The flow cytometry results confirmed that the differentiation of U937 monocytes to M0 macrophages indicated by the increased expression in CD11b<sup>+</sup> macrophages relative to CD11b<sup>+</sup> monocytes for all glucose concentrations. Figure 3.3A and 3.3B illustrate that as glucose increased there was a small shift between the histogram peaks. There was a difference of 52.1% in CD11b expression in CD11b<sup>+</sup> monocytes as compared to CD11b<sup>+</sup> M0 macrophages for the 11mM data. As compared to 38.9%, 29.6% and 23.8% for 15, 20 and 30mM glucose respectively. This indicates that as glucose concentration is increased there was a decrease in CD11b expression.

Statistical analysis by t-tests, illustrated by the mean relative fluorescence (MRF) in Figure 3.3C, showed there was a significant increase in all cases ( $P < 0.01$ ) for CD11b expression in M0 macrophages relative to the corresponding undifferentiated (NC) monocytes cultured at the same glucose concentration. The analysis also showed a significant decrease ( $P < 0.01$ ) in all cases as the glucose concentration increased, indicating that elevated glucose has an inhibitory effect on the differentiation of U937 monocytes into M0 macrophages.

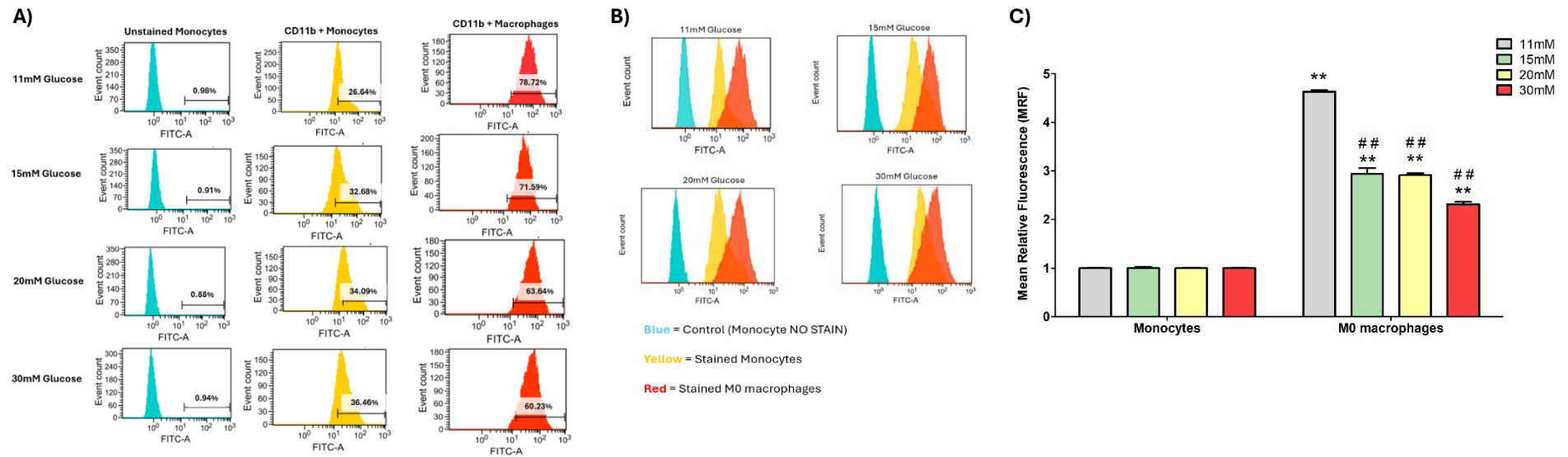


**Figure 3. 3: Differentiation of U937 Monocytes into M0 macrophages.** Flow cytometry charts showed the percentage of CD11b positive cells increases in PMA-differentiated M0 macrophages compared to monocytes in all glucose concentrations (A). As the glucose concentration increased the CD11b expression decreased in M0 macrophages compared to monocytes illustrated by a smaller shift in the holograph peaks (B). As glucose concentration increased there was a significant decrease (\*\*  $P < 0.01$  determined by t-tests;  $n = 5$ ) in CD11b expression as the glucose concentration increased, but a significant increase (##  $P < 0.01$  determined by t-tests;  $n = 5$ ) in CD11b expression relative to CD11b+ monocytes (B). The MRF values are relative to levels detected in CD11b+ monocytes (MRF =1). Columns and error bars indicate the MRF  $\pm$  standard error of the mean (SEM) in all cases.

### 3.4.2 Differentiation of U937 Monocytes to M1 Macrophages

U937 monocytes were cultured at different glucose concentrations and then differentiated into M1 macrophages (see section 3.3.1). After differentiation, the macrophages were assessed for CD197 cell marker expression using flow cytometry (Figure 3.4).

The flow cytometry results confirmed the differentiation of U937 monocytes to M1 macrophages for all glucose concentrations. Figure 3.4A and 3.4B illustrate that as glucose increased there was a large shift between the holograph peaks. There were increases of 23.8%, 23.3%, 15.4% and 15.3% in CD197+ M0 macrophages cultured at 11, 15, 20 and 30mM glucose respectively when compared to corresponding CD197+ monocytes cultured at the same glucose concentration. There were further increases of 23.5%, 31.2%, 42.7% and 60.1% in CD197+ M1 macrophages compared to corresponding CD197+ M0 macrophages cultured at the same glucose concentration.

Statistical analysis by t-tests showed a significant increase ( $P < 0.01$  for 11, 15 and 20mM and  $P = 0.042$  for 30mM) in MRF (Figure 3.4C) of CD197 expression in M0 macrophages relative to corresponding untreated (NC) monocytes cultured at the same glucose concentration. Similarly, there was a significant increase ( $P < 0.01$  in all cases) in CD197 in M1 macrophages relative to corresponding untreated (NC) monocytes and M0 macrophages cultured at the same glucose concentration. Moreover, compared to M0 macrophages cultured at 11mM glucose, there was a significant stepwise decrease in CD197 MRF in M0 macrophages cultured at 15mM ( $P = 0.01$ ), 20mM ( $P < 0.01$ ) and 30mM ( $P = 0.038$ ) glucose. However, an alternative picture was seen for M1 macrophages, with a stepwise significant increase ( $P < 0.01$ ) in CD197 MRF between M1 macrophages cultured at 15, 20 and 30mM glucose when compared to M1 macrophages cultured at 11mM.

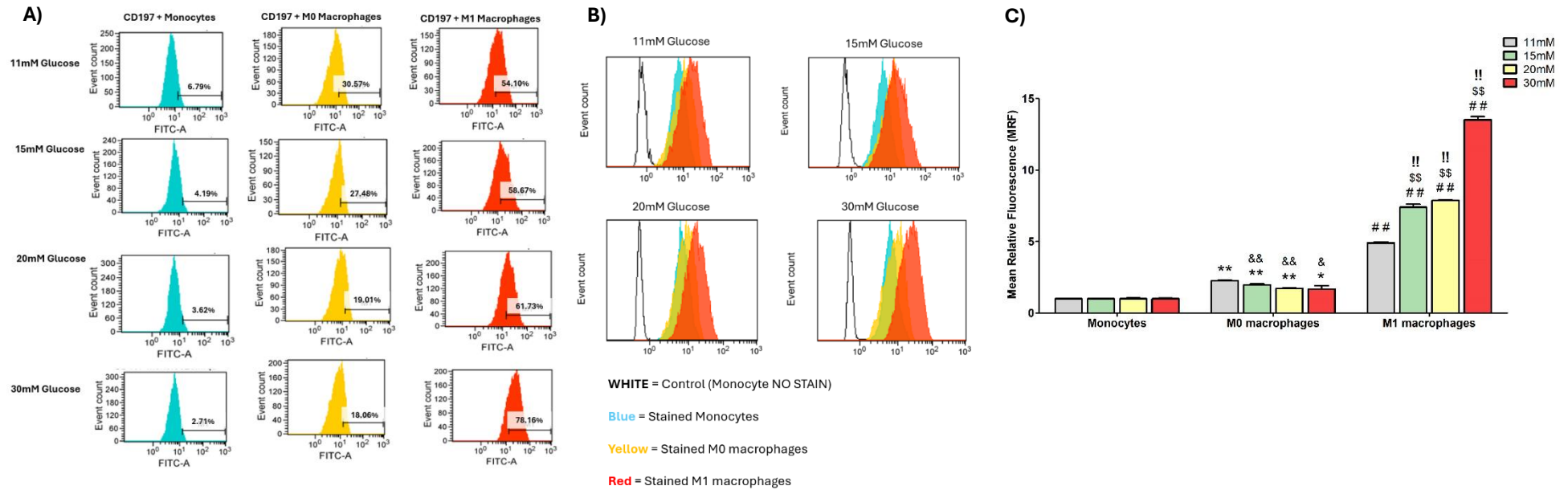


**Figure 3. 4: Differentiation of U937 monocytes into M1 macrophages.** Flow cytometry charts showed the percentage of CD197 positive cells increases in PMA-differentiated M0 and M1 macrophages compared to monocytes in all glucose concentrations (A and B). As the glucose concentration increased there was a significant increase (\*  $P < 0.05$  and \*\*  $P < 0.01$  determined by t-tests;  $n = 5$ ) in CD197 expression in CD197+ M0 macrophages and M1 macrophages (##  $P < 0.01$  determined by t-tests;  $n = 5$ ) relative to the corresponding monocytes. There was also a significant increase (\$\$  $P < 0.01$  determined by t-tests;  $n = 5$ ) in CD197+ M1 macrophages compared to the corresponding CD197+ M0 macrophages in all cases. Significant decreases were seen (&  $P < 0.05$  and &&  $P < 0.01$  determined by t-tests;  $n = 5$ ) between the M0 macrophage group when compared to the 11mM M0 and a significant increase (!!  $P < 0.01$  determined by t-tests;  $n = 5$ ) between the M1 macrophage group when compared to 11mM M1 macrophages. The MRF values are relative to levels detected in CD197+ monocytes (MRF =1). Columns and error bars indicate the MRF  $\pm$  standard error of the mean (SEM) in all cases.

### 3.4.3 The Effect of Glucose on Cell Viability

U937 monocytes were differentiated into M1 macrophages at 11 and 30mM glucose and then propidium iodide (PI) was added to assess cell viability (Figure 3.5) by flow cytometry. PI is used for the detection of dead or damaged cells because of its ability to bind cellular DNA (Rosenberg *et al*, 2019).

Flow cytometry analysis (Figure 3.5A) showed there was a higher level of dead or damaged cells (PI) present at high glucose (30mM) compared to low glucose (11mM). Mean fluorescence intensity (MFI) of PI expression (Figure 3.5B) was significantly ( $P < 0.01$ ) higher in M1 macrophages at 30mM glucose (79.8) compared to M1 macrophages at 11mM glucose (56.1), indicating chronic hyperglycaemia results in higher rates of cell death.

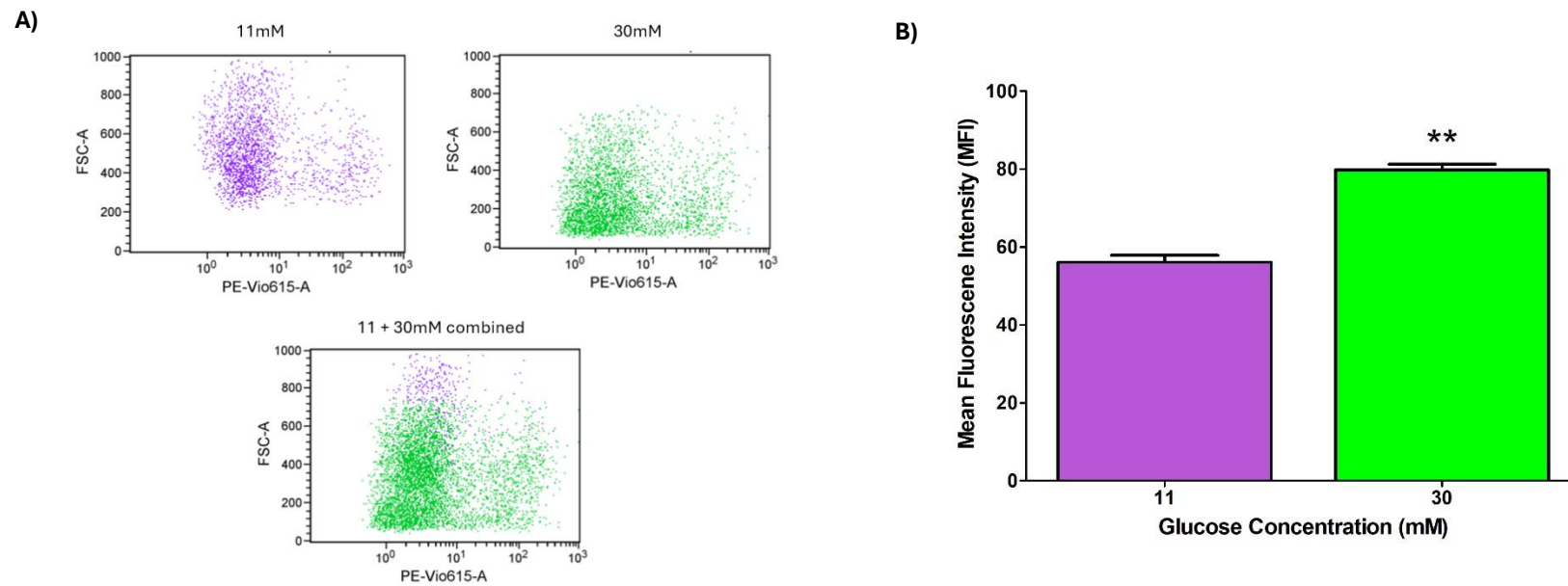


**Figure 3. 5: Effect of Glucose on Cell Viability.** Increased glucose concentration resulted in higher propidium iodide (PI) expression in M1 Macrophages (A). A significant increase (\*\*  $P < 0.01$  determined by t-tests;  $n = 5$ ) in Mean fluorescence intensity (MFI) of PI was observed in 30mM M1 macrophages compared to 11mM M1 macrophages (B), with data representing the mean MFI  $\pm$  standard error of the mean (SEM).

### 3.4.4 Cellular Glucose Uptake

#### 3.4.4.1 Monocyte Glucose Uptake

U937 monocytes were seeded at  $2.5 \times 10^5$  cells/ml in glucose-supplemented (11, 15, 20 or 30mM) RPMI medium and then incubated at 37°C and 5% CO<sub>2</sub> for a total of 8 days without changing the medium to monitor glucose uptake by monocytes. Glucose levels remaining in the media was measured to monitor glucose utilisation as well as the effect of glucose on monocyte cell counts and appearance.

##### 3.4.4.1.1 Glucose Degradation in RPMI Medium

RPMI medium at different glucose concentrations (11, 15, 20 and 30mM) was incubated at 37 °C and 5% CO<sub>2</sub> for 14 days. The data showed a gradual decrease in glucose in all media, with a significant glucose depletion detected from day 4 onwards compared to the starting glucose concentrations on day 0. (Figure 3.6).

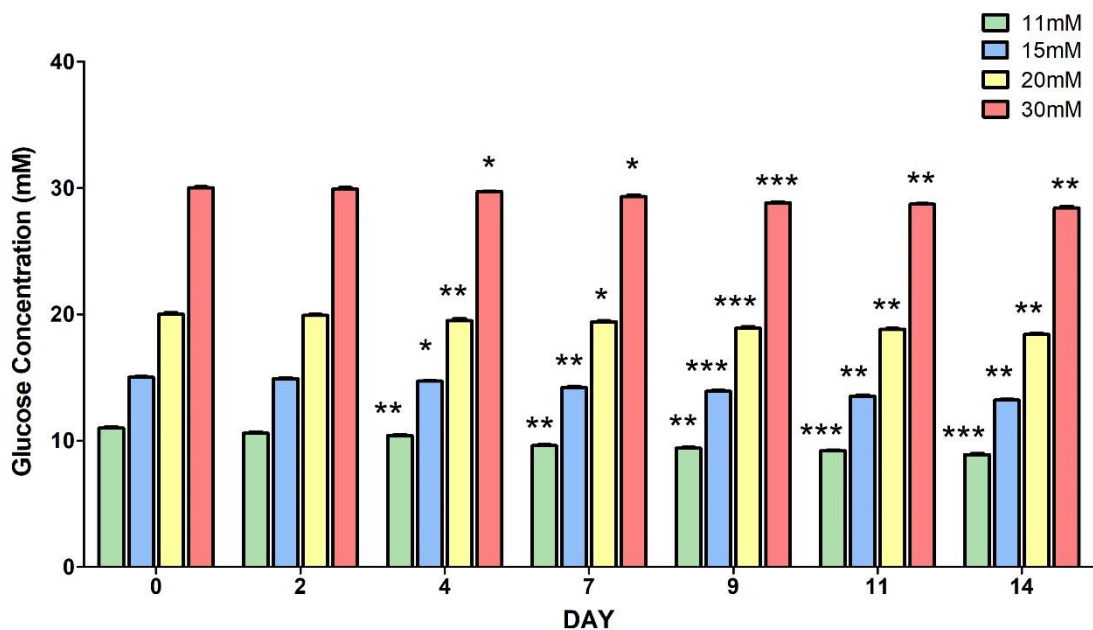


**Figure 3. 6: Glucose Depletion in RPMI Medium.** Glucose supplemented medium (11, 20, 15 and 30mM) was incubated for a span of 14 days to monitor the rate of glucose degradation in RPMI medium. A significant decrease (\*  $P < 0.05$ , \*\*  $P < 0.01$  and \*\*\*  $P < 0.001$  determined by t-tests;  $n = 3$ ) in glucose concentration was seen from day 4 onwards in all cases compared to day 0. Columns and error bars indicate the glucose concentration (mM)  $\pm$  the standard error of the mean (SEM) in all cases.

There were no significant differences detected on day 2 ( $P = 0.051$  for 11mM;  $P = 0.055$  for 15mM and  $P = 0.211$  for 20 and 30mM) when compared to day 0. Significant differences were seen on day 4 ( $P = 0.001$  for 11mM;  $P = 0.029$  for 15mM,  $P = 0.003$  for

20mM and  $P = 0.027$  for 30mM), day 7 ( $P = 0.002$  for 11mM;  $P = 0.001$  for 15mM,  $P = 0.030$  for 20mM and  $P = 0.024$  for 30mM), day 9 ( $P = 0.001$  for 11mM;  $P < 0.001$  for 15mM,  $P = 0.001$  for 20 and 30mM), day 11 ( $P < 0.001$  for 11mM;  $P = 0.001$  for 15, 20 and 30mM) and day 14 ( $P < 0.001$  for 11mM;  $P = 0.001$  for 15mM,  $P = 0.002$  for 20mM and  $P = 0.005$  for 30mM) when compared to initial glucose concentrations on day 0.

### 3.4.4.1.2 Monocyte-Mediated Change in Medium Glucose Levels

Data showed a gradual decrease in glucose in all glucose-supplemented medium from day 0 to day 8 (Figure 3.7).

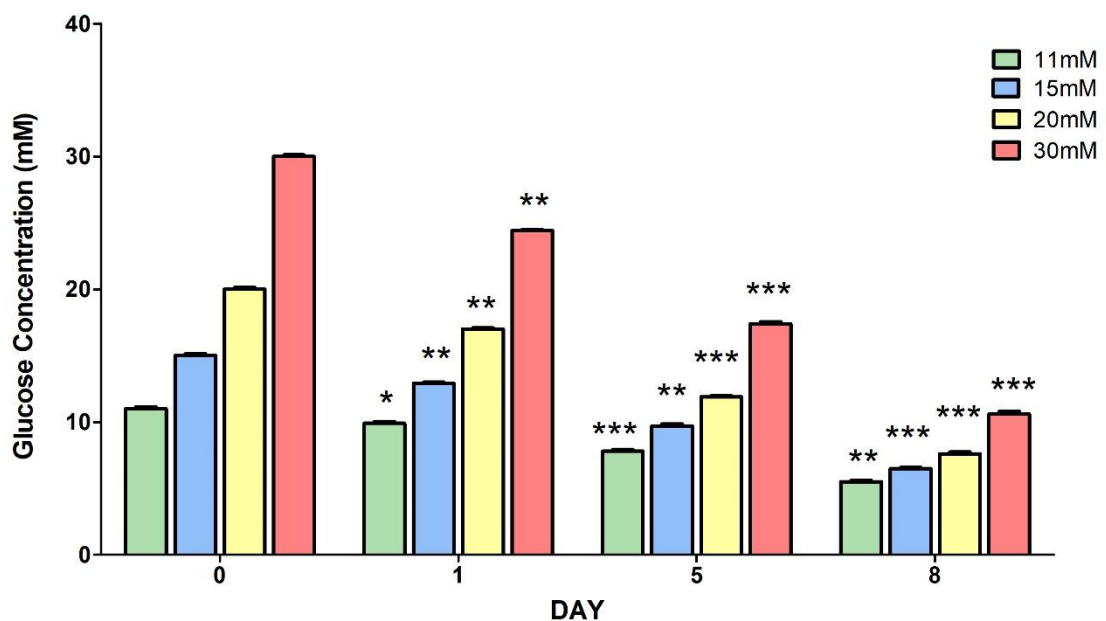


**Figure 3. 7: Monocyte-Mediated Change in Medium Glucose Levels.** Glucose usage was monitored in glucose-supplemented (11, 20, 15 and 30mM) RPMI medium containing U937 monocytes for a span of 8 days. Significant decreases ( $* P < 0.05$ ,  $** P < 0.01$  and  $*** P < 0.001$  determined by t-tests;  $n = 3$ ) in glucose concentration was observed in all groups from day 1 onwards compared to day 0. Columns and error bars indicate the glucose concentration (mM)  $\pm$  the standard error of the mean (SEM) in all cases.

There was a significant ( $P < 0.05$ ) glucose depletion in all glucose concentrations occurring from day 1 onwards compared to day 0. Over the span of 8 days of monocyte culture the total glucose decreased by 5.5, 8.5, 12. and 19.4mM in RPMI medium supplemented with 11, 15, 20 and 30mM glucose respectively. Medium levels of glucose significantly decreased on day 1 ( $P = 0.018$  for 11mM;  $P = 0.004$  for 15mM, 0.002 for 20mM and  $P = 0.001$  for 30mM), day 5 ( $P < 0.001$  for 11mM;  $P = 0.001$  for 15mM,  $P < 0.001$  for 20 and 30mM) and day 8 ( $P = 0.001$  for 11mM;  $P < 0.001$  for 15, 20 and 30mM) (Figure 3.7).

### 3.4.4.1.3 Monocyte Glucose Utilisation

As the glucose concentration of the RPMI medium increased there was a corresponding increase in glucose utilisation by monocytes (Figure 3.8).

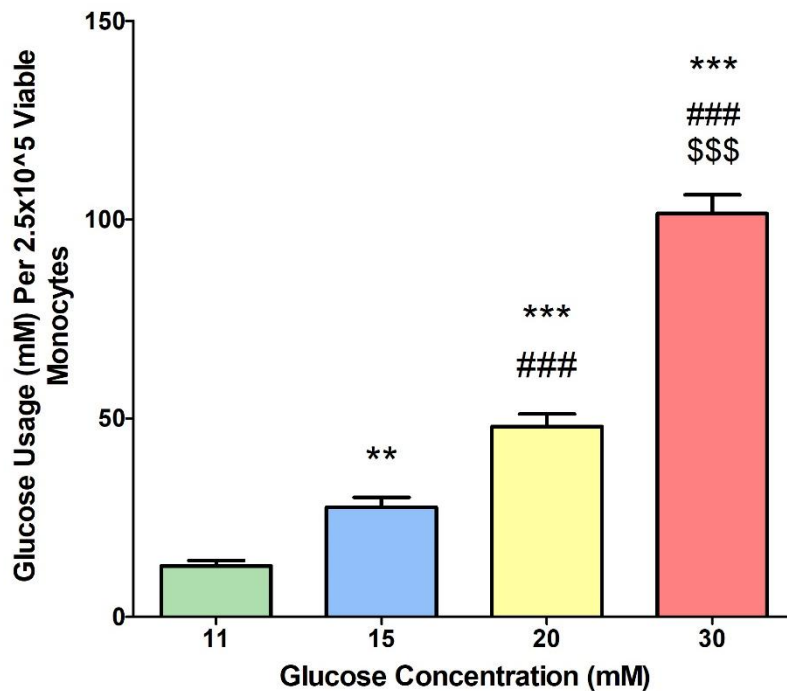


**Figure 3. 8: U937 Monocyte Glucose Utilisation.** The glucose uptake was monitored in RPMI medium containing U937 monocytes cultured at different glucose concentration (11, 20, 15 and 30mM) for a span of 8 days. There was a significant increase (\*\*  $P < 0.01$  and \*\*\*  $P < 0.001$  determined by t-tests;  $n = 3$ ) in glucose usage by monocytes as the glucose concentration increased. There was a significant increase (###  $P < 0.001$  determined by t-tests;  $n = 3$ ) in glucose usage by monocytes cultured in 20 and 30mM media compared to those cultured in 15mM, as well as an increase (\$\$\$  $P < 0.001$  determined by t-tests;  $n = 3$ ) in glucose usage by monocytes cultured at 30mM when compared to those cultured 20mM. Columns and error bars indicate the glucose usage (mM) per  $2.5 \times 10^5$  viable monocytes  $\pm$  the standard error

There was an increase in glucose usage (101.5mM) by monocytes cultured in 30mM RPMI after 8 days compared to those cultured in all other glucose-supplemented RPMI media (12.8mM for 11mM RPMI, 27.5mM for 15mM RPMI and 47.9mM for 20mM RPMI). Compared to monocyte cultured in 11mM RPMI medium, there was a significant increase in glucose utilisation by monocytes cultured in all other RPMI media ( $P = 0.001$  for 15mM RPMI and  $P < 0.001$  for 20 and 30mM RPMI). There was also a significant ( $P < 0.001$ ) increase in glucose usage by monocytes cultured in 20 and 30mM RPMI media compared to those cultured in 15mM RPMI medium, and by monocytes cultured in 30mM RPMI medium compared to those cultured in 20mM RPMI medium.

### 3.4.4.1.4 Effect of Glucose on Monocyte Count

There was a small increase in monocyte cell counts in all glucose concentrations on day 3 compared to starting monocyte cell counts on day 0 however, the cell counts decreased on days 5 and 8 with the largest decreases seen in at the highest glucose concentrations (Figure 3.9).

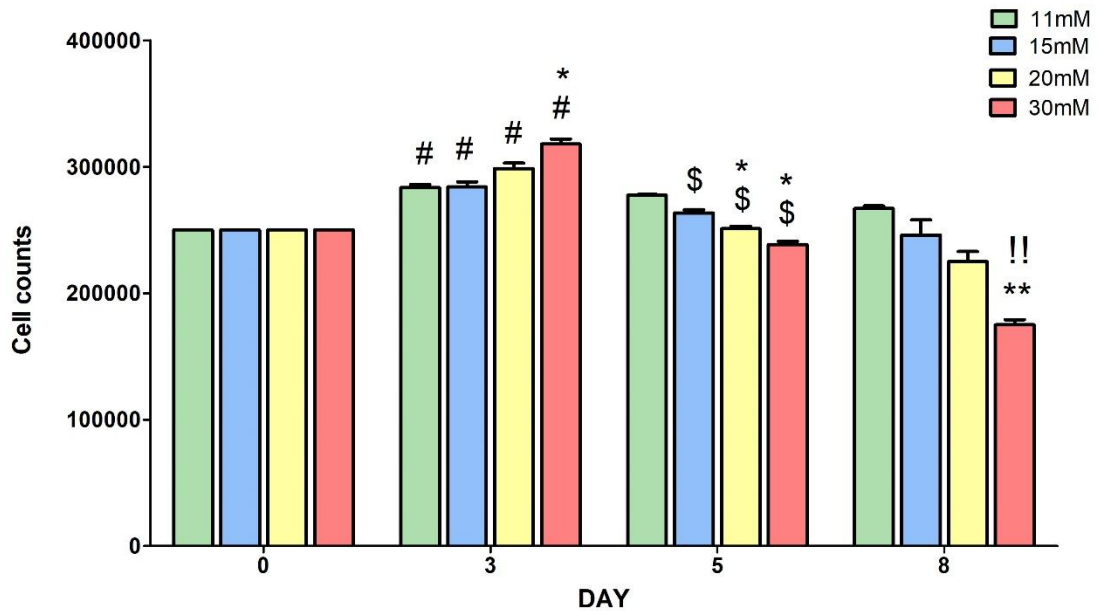


**Figure 3. 9: Effect of Glucose on U937 Monocyte Cell Count.** Cell counts were conducted on monocytes cultured in RPMI medium supplemented with different glucose concentrations (11, 20, 15 or 30mM) for a span of 8 days. There were significant differences when comparisons were made between the 11mM on Day 0 (\* $P < 0.05$  and \*\* $P < 0.01$  determined by t-tests;  $n = 3$ ), corresponding glucose concentrations on day 3 compared to day 0 (# $P < 0.05$  determined by t-tests;  $n = 3$ ), corresponding glucose concentrations on day 5 compared to day 3 (\$ $P < 0.05$  determined by t-tests;  $n = 3$ ) and corresponding glucose concentrations on day 8 compared to day 5 (!! $P < 0.01$  determined by t-tests;  $n = 3$ ). Columns and error bars indicate monocyte cell counts  $\pm$  the standard error of the mean (SEM) in all cases.

The monocyte counts significantly increased in all glucose-supplemented media on day 3 compared with day 0 ( $P = 0.024$  for 11mM RPMI;  $P = 0.037$  for 15mM RPMI;  $P = 0.029$  for 20mM RPMI;  $P = 0.019$  for 30mM RPMI), with the largest increase seen in monocytes cultured in 30mM RPMI. Also, on day 3 there was a significant increase in monocyte counts when cultured in 30mM RPMI ( $P = 0.014$ ) compared to monocytes grown in 11mM RPMI. On day 5 however, there was an overall fall in cell counts with significant decreases seen in monocytes cultured in RPMI supplemented with the higher glucose concentrations ( $P = 0.019$  for 20mM RPMI and  $P = 0.017$  for 30mM RPMI when compared with those cultured in 11mM RPMI). On day 8 a similar trend was observed again compared to day 5, with a significant ( $P = 0.005$ ) decrease in cell counts observed for those monocytes cultured in 30mM RPMI.

### 3.4.4.1.5 Effect of Glucose on Monocyte Appearance

Images were taken of monocytes at 11mM and 30mM glucose with a Leica microscope (40x magnification) on days 0 and 8 (Figure 3.10).

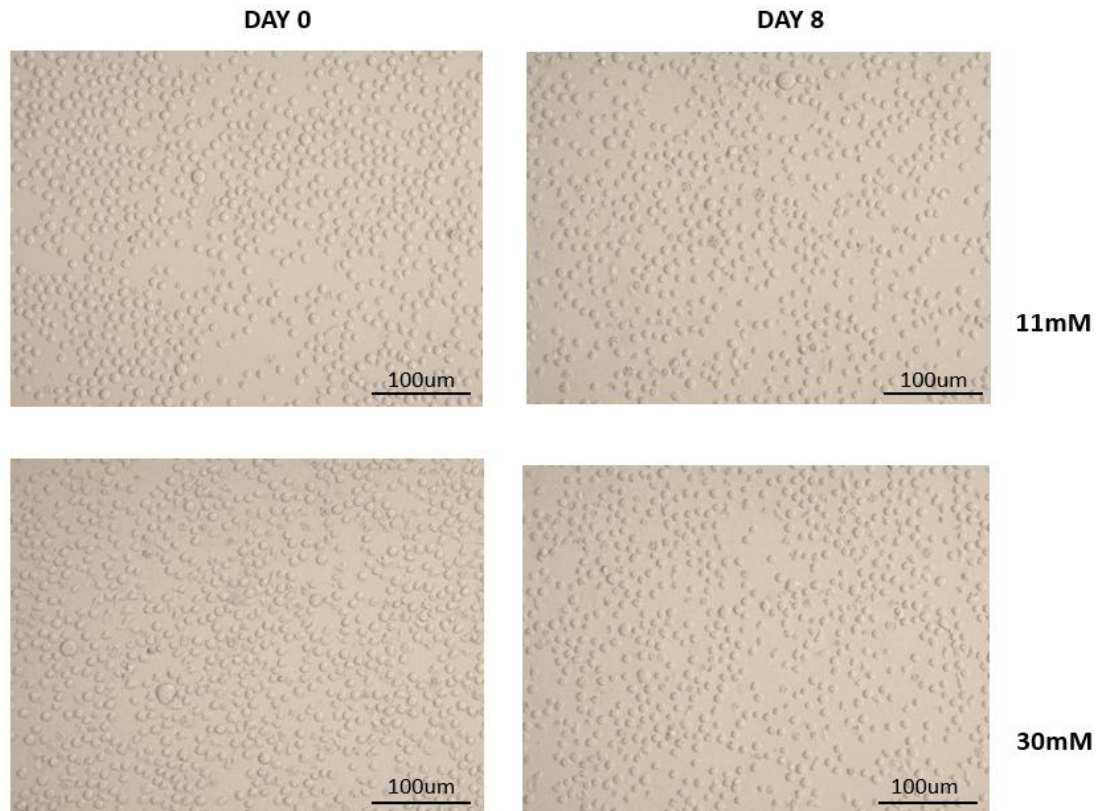


**Figure 3. 10: Effect of Glucose on Monocyte Appearance.** U937 monocytes were cultured in RPMI at 11 and 30mM and incubated for 8 days without medium changes. Pictures were captured on day 0 and day 8 at 40x magnification. On day 0 monocytes grown at 11mM glucose were consistent in size and symmetrical in shape whereas those cultured at 30mM had irregular sizes and shapes. On day 8, both sets of monocytes had visibly reduced cell viability, with those cultured at 30mM showing the greatest reduction in viability when stained with trypan blue.

On day 0, both sets had a cell viability of 95%. The monocytes cultured in 11mM RPMI were morphologically similar in size and symmetrical in shape. In contrast, monocytes cultured in 30mM RPMI had varied morphologies, ranging in shape and size.

On day 8, both groups had visibly reduced viability, with trypan blue confirming a percentage viability of 45% for monocytes cultured in 11mM RPMI and 25% viability for those grown in 30mM RPMI. There was a significant ( $P = 0.037$ ) increase in day 8 cell counts for monocytes cultured in 11mM RPMI compared to day 0 and significant ( $P = 0.034$ ) decrease in day 8 cell counts for monocytes cultured in 30mM RPMI compared to day 0.

### 3.4.4.2 M1 Macrophage Glucose Uptake

U937 monocytes were differentiated to M1 macrophages in glucose-supplemented (11, 15, 20 and 30mM) RPMI medium and then incubated at 37°C and 5% CO<sub>2</sub> for a total of 8 days without changing the medium. Glucose levels remaining in the media was measured to monitor glucose utilisation as well as the effect of glucose on macrophage cell counts and appearance.

#### 3.4.4.2.1 Macrophage-Mediated Change in Medium Glucose Levels

There was a gradual decrease in glucose concentration in all groups over the span of 8 days compared to the starting glucose concentrations on day 0 (Figure 3.11).

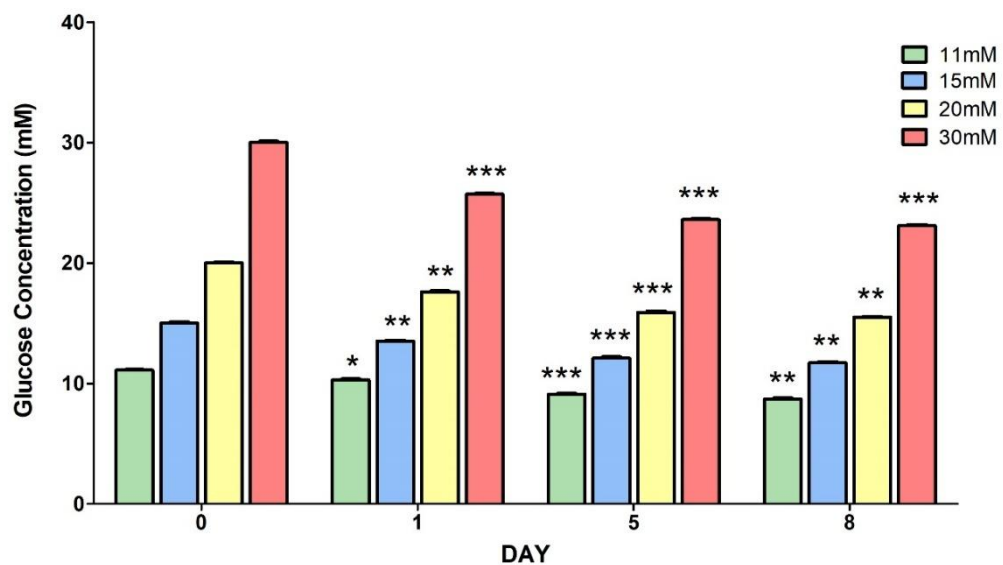


**Figure 3. 11: Macrophage-Mediated Change in Medium Glucose Levels.** The glucose uptake was monitored in RPMI medium containing M1 macrophages cultured at different glucose concentration (11, 20, 15 and 30mM) for a span of 8 days. Significant decreases (\*  $P < 0.05$ , \*\*  $P < 0.01$  and \*\*\*  $P < 0.001$  determined by t-tests;  $n = 3$ ) in glucose concentration were observed in all groups from day 1 onwards compared to day 0. Columns and error bars indicate the glucose concentration (mM)  $\pm$  the standard error of the mean (SEM) in all cases.

There was a significant ( $P < 0.05$ ) glucose depletion occurring from day 1 onwards. Over the span of 8 days the total glucose decreased by 2.3, 3.3, 4.5, and 6.9mM in RPMI medium supplemented with 11, 15, 20 and 30mM glucose respectively. Medium levels of glucose significantly decreased on day 1 ( $P = 0.012$  for 11mM;  $P = 0.002$  for 15mM, 0.002 for 20mM and  $P = 0.000$  for 30mM), day 5 ( $P < 0.01$  for all groups) and day 8 ( $P = 0.001$  for 11mM; for 15mM, for 20mM and  $P = 0.000$  30mM) when compared when median glucose levels on day 0.

### 3.4.4.2.2 Macrophage Glucose Utilisation

As the glucose concentration increased there was an increase in glucose usage (18.7mM) by macrophages cultured in 30mM RPMI after 8 days compared to those cultured in all other glucose-supplemented RPMI media (1mM for 11mM RPMI, 6.7mM for 15mM RPMI and 11.3mM for 20mM RPMI) (Figure 3.12).

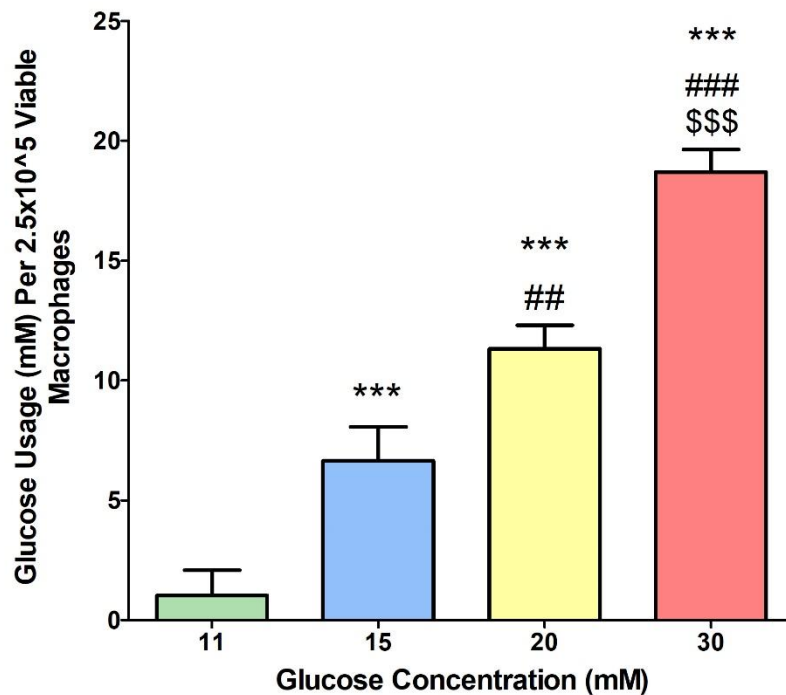


**Figure 3. 12: Macrophage Glucose Utilisation.** The glucose uptake was monitored in RPMI medium containing M1 macrophages cultured at different glucose concentrations (11, 20, 15 and 30mM) for a span of 8 days. There was a significant increase (\*\*  $P < 0.01$  and \*\*\*  $P < 0.001$  determined by t-tests;  $n = 3$ ) in usage as the glucose concentration increased. There was a significant increase (###  $P < 0.001$  determined by t-tests;  $n = 3$ ) in glucose usage in macrophages cultured at 20 and 30mM compared to those cultured at 15mM, as well as an increase (\$\$\$  $P < 0.001$  determined by t-tests;  $n = 3$ ) in macrophages cultured at 30mM when compared to 20mM. Columns and error bars indicate the glucose usage (mM) per  $2.5 \times 10^5$  viable monocytes  $\pm$  the standard error of the mean (SEM) in all cases.

Compared to macrophages cultured in 11mM RPMI medium, there was a significant increase in glucose utilisation by macrophages cultured in all other RPMI media ( $P = 0.000$  for all cases). There was also a significant ( $P < 0.001$ ) increase in glucose usage by macrophages cultured in 20 and 30mM RPMI media compared to those cultured in 15mM RPMI medium, and by macrophages cultured in 30mM RPMI medium compared to those cultured in 20mM RPMI medium.

### 3.4.4.2.3 Effect of Glucose on Macrophage Count

Macrophages were seeded at  $1 \times 10^5$  cells/ml in glucose-supplemented (11, 15, 20 or 30mM) RPMI medium and then incubated at 37°C and 5% CO<sub>2</sub> for a total of 8 days without changing the medium. Cell counts were taken over the 8 days (Figure 3.13).

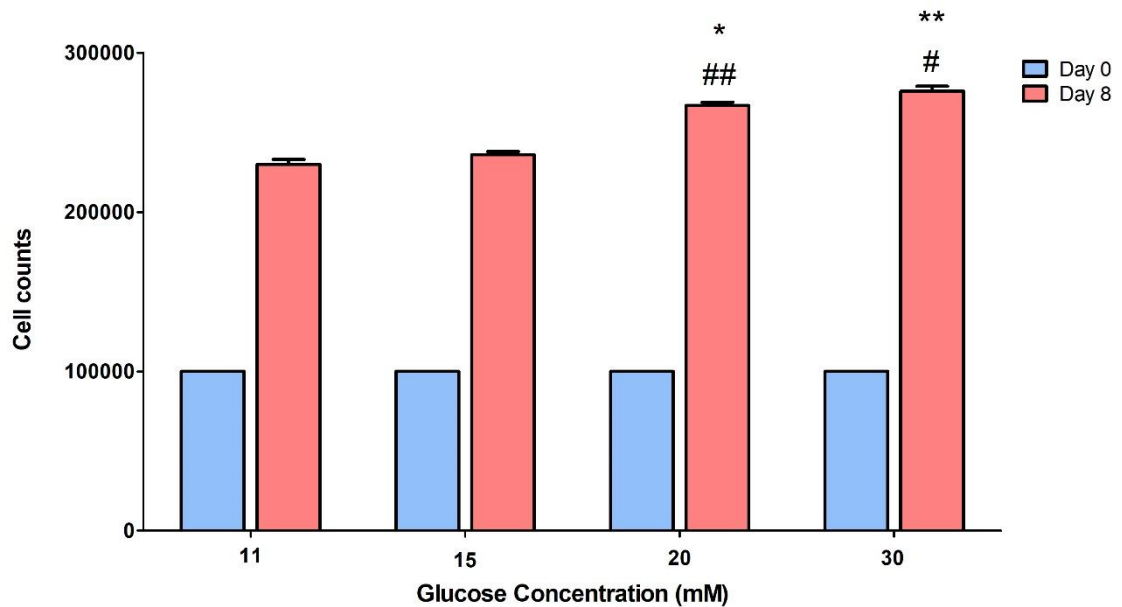


**Figure 3. 13: Effect of Glucose on Macrophage Count.** Macrophage counts were monitored when cultured at multiple glucose concentrations (11, 20, 15 and 30mM) for a span of 8 days. There were significant increases in macrophage counts (\* $P < 0.05$  determined by t-tests;  $n = 3$ ) when cultured in 20 and 30mM (\*\* $P < 0.01$  determined by t-tests;  $n = 3$ ) glucose on day 8 when compared to those cultured in 11mM RPMI, as well as significant increases in macrophage counts when grown in 20 or 30mM RPMI (#  $P < 0.05$  and ##  $P < 0.01$  determined by t-tests;  $n = 3$ ) when compared to 15mM RPMI. Columns and error bars indicate macrophage counts  $\pm$  the standard error of the mean (SEM) in all cases.

The macrophage counts significantly increased in glucose-supplemented media on day 8 compared with 11mM ( $P = 0.015$  for 20mM RPMI;  $P = 0.008$  for 30mM RPMI), with the largest increase seen in macrophage cultured in 30mM RPMI. Also, on day 8 there was a significant increase in macrophage counts when cultured in 20mM RPMI ( $P = 0.008$ ) and 30mM ( $P = 0.013$ ) compared to 15mM.

#### 3.4.4.2.4 Effect of Glucose on Macrophage Appearance

Images were taken of M1 macrophages at 11mM and 30mM glucose with a Leica microscope (40x magnification) on days 0 and 8 (Figure 3.14).

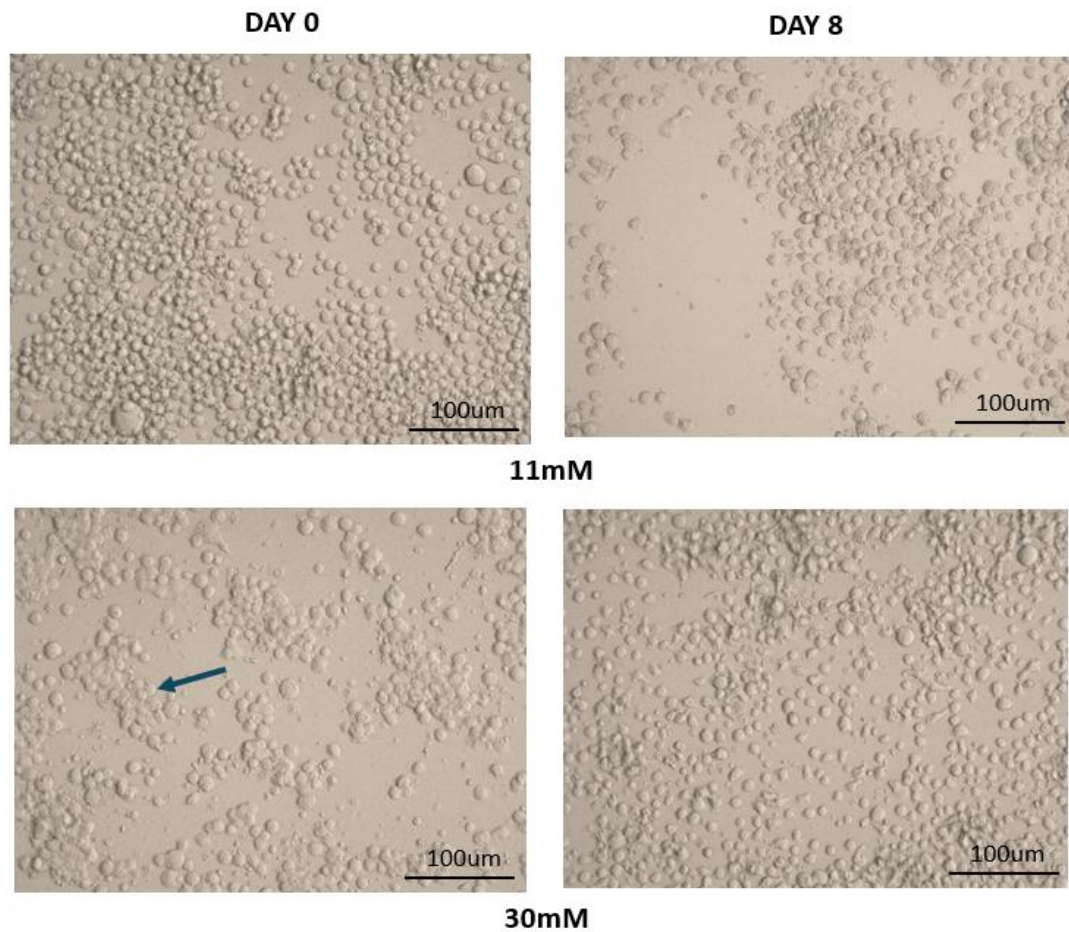


**Figure 3. 14: Effect of Glucose on Macrophage Appearance.** M1 macrophages were cultured at 11 and 30mM and incubated for 8 days. Pictures were captured on day 0 and day 8 at 40x magnification. On day 0 macrophages grown in 11mM RPMI formed large monolayer clusters whereas macrophages cultured at 30mM formed smaller clusters and cells appeared to grow at multiple layers. On day 8 there was a visible reduction in clusters in both groups.

On day 0 M1 macrophages cultured in 11mM RPMI formed multiple larger monolayer clusters adjacent to one another using the whole surface of the plate whereas macrophages cultured in 30mM RPMI accumulated in small multilayer clusters (illustrated by the blue arrow in figure 15). On day 8 there was reduction in cluster sizes in both cases however 11mM RPMI macrophages appeared to stay around the areas where the clusters had originally formed whereas 30mM RPMI macrophages appeared to be more scattered. There was a significant increase ( $P = 0.008$ ) in 30mM RPMI cell counts when compared to the 11mM RPMI.

### 3.4.4.3 Fibroblasts glucose evaluation

HDF fibroblasts were seeded at  $1 \times 10^5$  cells/ml in glucose-supplemented (11, 20 and 30mM) DMEM medium and then incubated at 37°C and 5% CO<sub>2</sub> for a total of 14 days without changing the medium. Glucose levels remaining in the media was measured to monitor glucose utilisation as well as the effect of glucose on fibroblast cell counts and appearance.

#### 3.4.4.3.1 Glucose Degradation in DMEM Medium

DMEM medium was incubated at 37 °C and 5% CO<sub>2</sub> in glucose supplemented medium (11, 20 and 30mM) for 14 days. Glucose levels remaining in the media were measured glucose degradation from different starting glucose concentrations. The data showed a gradual decrease in glucose at all media with significant glucose depletion from day 2 onwards (Figure 3.15).

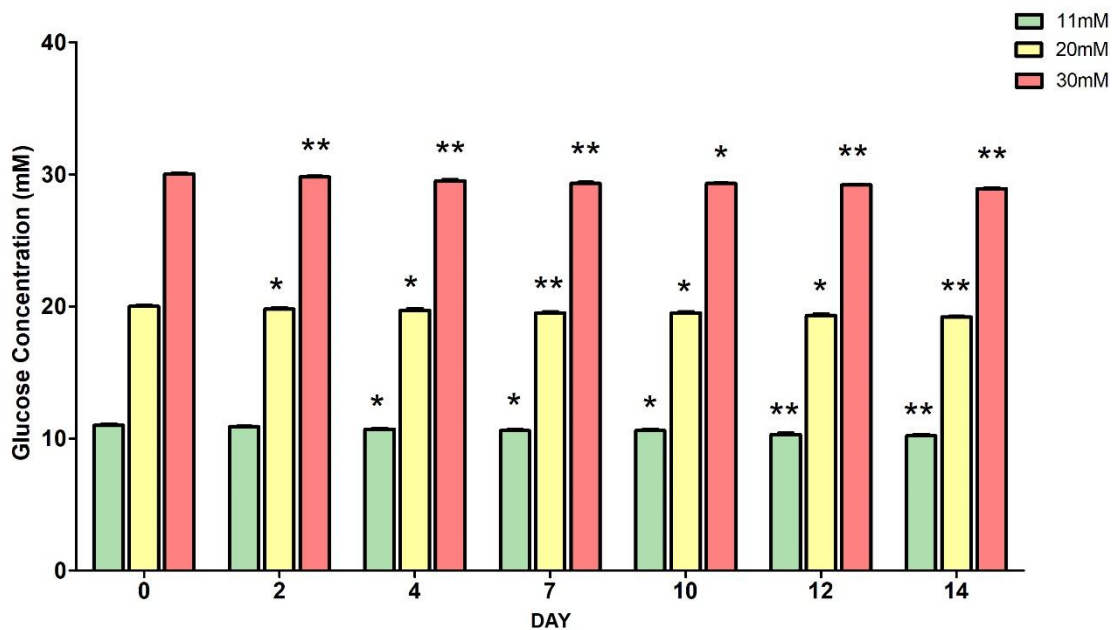


**Figure 3. 15: Glucose Depletion in DMEM Medium.** Glucose supplemented medium (11, 20 and 30mM) was incubated for a span of 14 days to monitor the rate of glucose degradation in DMEM medium. A significant decrease (\*  $P < 0.05$  and \*\*  $P < 0.01$  determined by t-tests;  $n = 3$ ) in glucose concentration for all cases was seen from day 2 onwards compared to day 0. Columns and error bars indicate the glucose concentration (mM)  $\pm$  the standard error of the mean (SEM) in all cases.

Significant differences were seen from day 2 in the 20 and 30mM groups ( $P = 0.037$ ,  $P = 0.01$ ) but no significance was seen in the 11mM group ( $P = 0.065$ ) and on day 4 there was significant decrease in glucose in all groups ( $P = 0.019$  11mM;  $P = 0.016$  20mM and

$P = 0.007$  30mM) compared to day 0. There was also a significant decrease seen on day 7 ( $P = 0.035$  11mM,  $P = 0.008$  20mM and  $P = 0.003$  30mM), day 10 ( $P = 0.036$  11mM,  $P = 0.038$  20mM and  $P = 0.013$  30mM), day 12 ( $P = 0.001$  11mM,  $P = 0.022$  20mM and  $P = 0.003$  30mM), and day 14 ( $P = 0.001$  11mM,  $P = 0.003$  20mM and  $P = 0.001$  30mM) compared to day 0.

### 3.4.4.3.2 Fibroblast-Mediated Change in Medium Glucose Levels

Data showed a gradual decrease in glucose in all glucose supplemented media over a span of 14 days. (Figure 3.16).

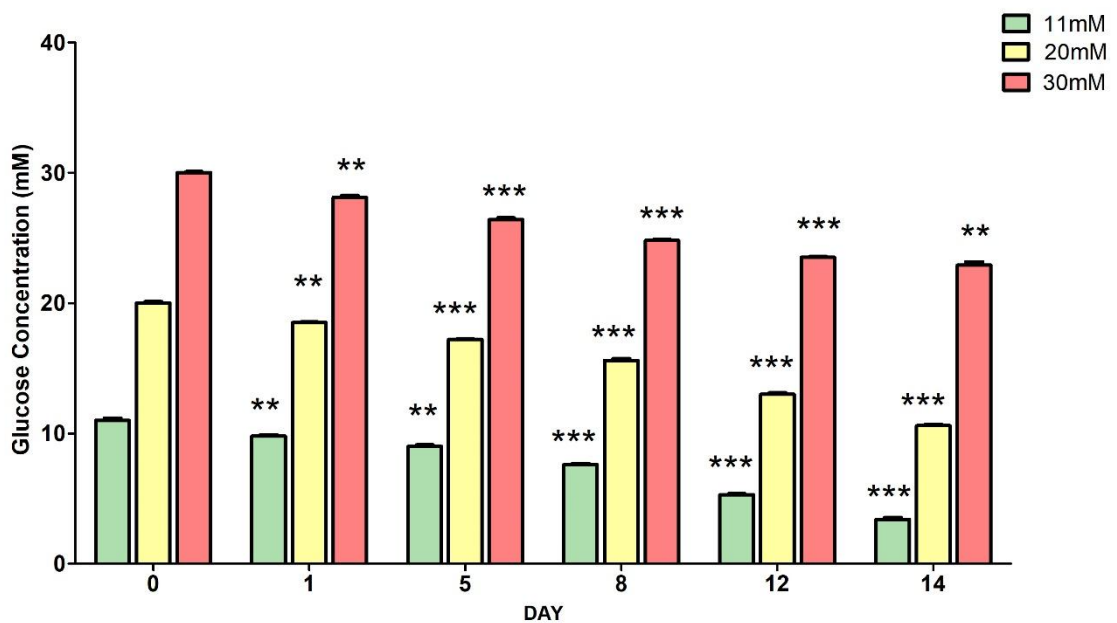


**Figure 3. 16: Fibroblast-Mediated Change in Medium Glucose Levels.** The glucose uptake was monitored in DMEM medium containing HDFs cultured at different glucose concentration (11, 20 and 30mM) for a span of 14 days. Significant decreases ( $* P < 0.05$ ,  $** P < 0.01$  and  $*** P < 0.001$  determined by t-tests ;  $n = 3$ ) in glucose concentration were observed in all groups from day 1 onwards compared to day 0. Columns and error bars indicate the glucose concentration (mM)  $\pm$  the standard error of the mean (SEM) in all cases.

There was a significant ( $P < 0.01$ ) glucose depletion in all glucose concentrations from day 1 onwards compared to day 0. Over the span of 14 days of fibroblast culture the total glucose decreased by 7.6, 9.4 and 7.1mM in DMEM medium supplemented with 11, 20 and 30mM glucose respectively. Medium levels of glucose significantly decreased on day 1 ( $P < 0.01$  for all cases), day 5 ( $P = 0.002$  for 11mM;  $P = 0.000$  for 20mM and  $P = 0.001$  for 30mM), day 8 ( $P < 0.01$  for all cases) and day 14 ( $P = 0.000$  for 11mM;  $P = 0.000$  for 20 and  $P = 0.001$  for 30mM) when compared to day 0.

### 3.4.4.3.3 Fibroblast Glucose Utilisation

As the glucose concentration of the DMEM medium increased there was a corresponding increase in glucose utilisation by fibroblasts (Figure 3.17).

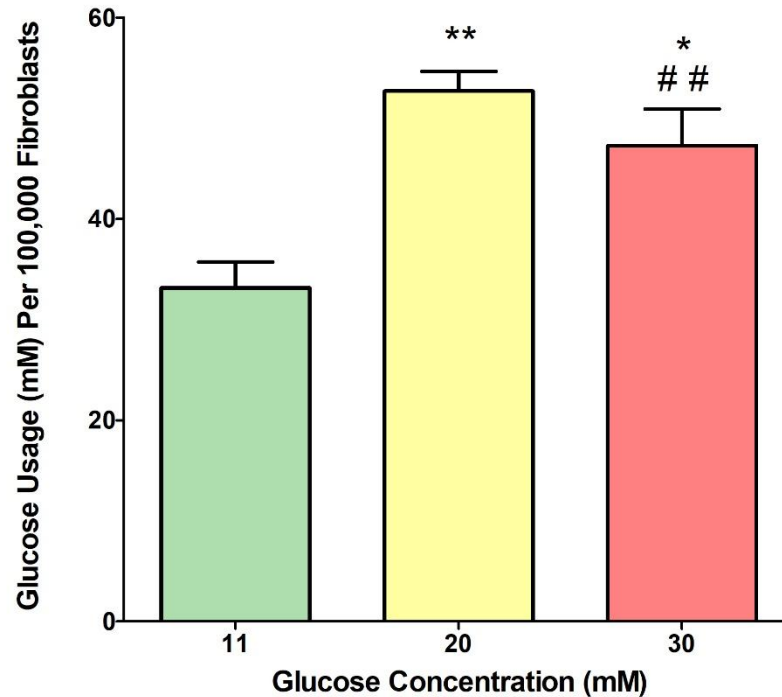


**Figure 3. 17: Fibroblast Glucose Utilisation.** The glucose uptake was monitored in DMEM medium containing HDFs cultured at different glucose concentration (11, 20 and 30mM) for a span of 14 days. There was a significant increase (\*\*  $P < 0.01$  determined by t-tests;  $n = 3$ ) in glucose usage in fibroblasts cultured in 20mM and 30mM DMEM (\*  $P < 0.05$  determined by t-tests;  $n = 3$ ) compared to fibroblasts cultured in 11mM DMEM. There was also a significant decrease (##  $P < 0.01$  determined by t-tests;  $n = 3$ ) in glucose usage in fibroblasts cultured in 30mM DMEM compared to fibroblasts cultured in 20mM DMEM. Columns and error bars indicate the glucose usage (mM) per  $1 \times 10^5$  fibroblasts  $\pm$  the standard error of the mean (SEM) in all cases.

There was an increase in glucose usage by fibroblasts cultured in 20mM (52.7mM) and 30mM (47.3mM) DMEM after 14 days compared to those cultured in all 11mM (33.1mM). Compared to fibroblasts cultured in 11mM DMEM medium, there was a significant increase in glucose utilisation by monocytes cultured in all other DMEM media ( $P = 0.003$  for 20mM DMEM and  $P = 0.015$  for 30mM DMEM).

### 3.4.4.3.4 Effect of Glucose on Fibroblast Count

Over the span of 14 days there was a decrease in fibroblast cell counts with the largest decrease seen at the highest glucose concentrations (Figure 3.18).

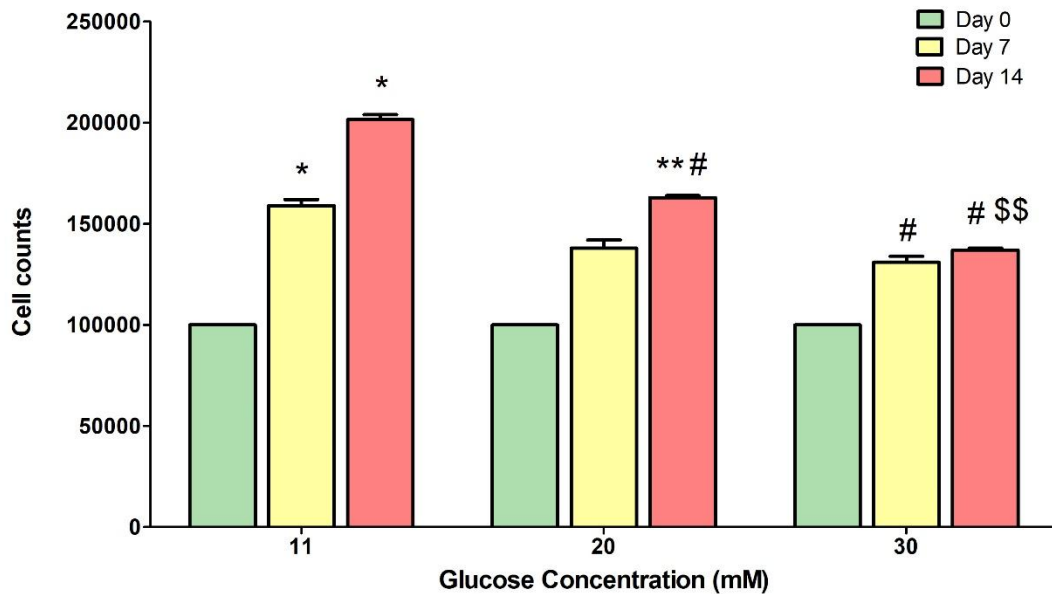


**Figure 3. 18: Effect of Glucose on Fibroblast Count.** Fibroblast cell counts were monitored when cultured at multiple glucose concentrations (11, 20 and 30mM) for a span of 14 days. There were significant increases in fibroblast counts at day 7 and/or 14 when compared to the corresponding day 0 counts of fibroblasts cultured at 11mM (\*:  $P < 0.05$ ; \*\*:  $P < 0.01$  determined by t-tests;  $n = 3$ ), 20mM (#:  $P < 0.05$  determined by t-tests;  $n = 3$ ) or 30mM (\$\$:  $P < 0.01$  determined by t-tests;  $n = 3$ ). Columns and error bars indicate fibroblast counts  $\pm$  the standard error of the mean (SEM) in all cases.

The fibroblast counts significantly increased in fibroblasts cultured at 11mM DMEM ( $P = 0.032$ ) on day 7 and day 14 ( $P = 0.016$  11mM,  $P = 0.01$  20mM and  $P = 0.017$  30mM) when compared to day 0. There were significant decreases in 20mM DMEM ( $P = 0.021$ ) on day 14 and decrease in 30mM DMEM on days 7 ( $P = 0.022$ ) and day 14 ( $P = 0.011$ ) when compared to the 11mM DMEM. There was also a significant decrease seen in 30mM DMEM on day 14 ( $P = 0.003$ ) when compared to the 20mM DMEM.

### 3.4.4.3.5 Effect of Glucose on Fibroblast Appearance

Images of fibroblasts at 11mM and 30mM glucose were taken with a Leica microscope (40x magnification) on day 14 (Figure 3.19).

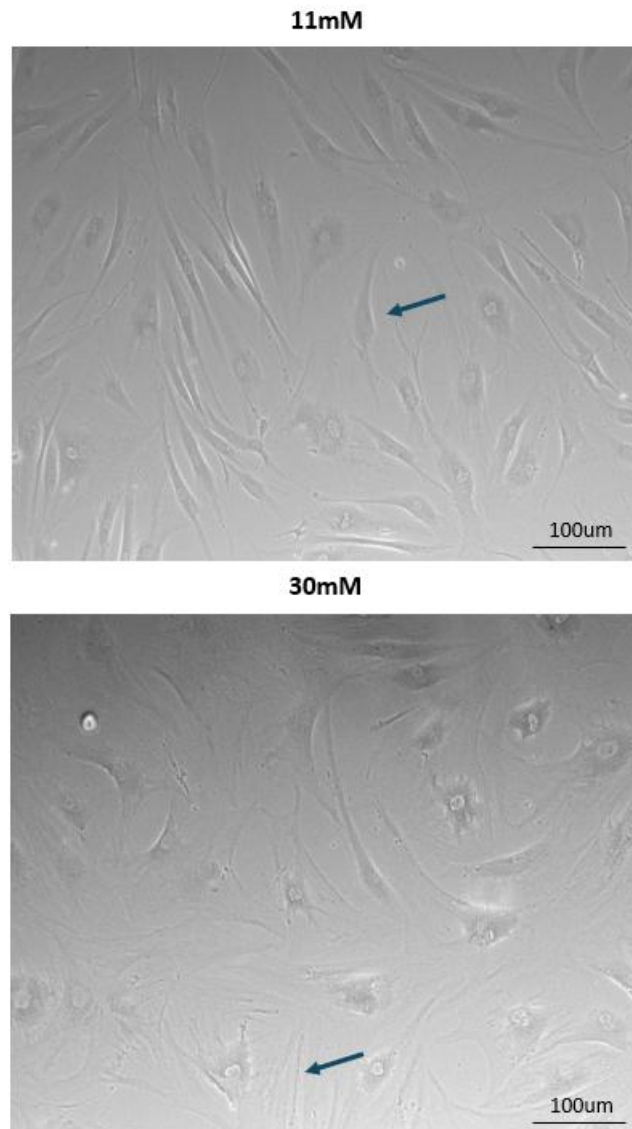


**Figure 3. 19: Effect of Glucose on Fibroblast Appearance.** HDFs were cultured at 11 and 30mM and incubated for 14 days. Pictures were captured on day 14 at 40x magnification. HDFs cultured at 11mM had long spindle-like shapes with a few stellate shapes whereas those cultured at 30mM group were very tightly packed with large stellate and very few spindle structures.

The fibroblasts grown at 11mM appeared as long thin spindle structure (shown by arrow in figure 20, 11mM panel) with a few stellate shapes and little to no sign of stress. The fibroblasts grown at 30mM appeared as larger tightly packed stellate shapes indicating the cells were undergoing a stress response (shown by arrow in figure 20, 30mM panel).

#### 3.4.4.4 Keratinocytes Glucose Evaluation

Keratinocytes (HACAT) were seeded at  $1 \times 10^5$ /ml in glucose-supplemented (11, 20 and 30mM) DMEM medium and then incubated at 37°C and 5% CO<sub>2</sub> for a total of 14 days without changing the medium. Glucose levels remaining in the media was measured to monitor glucose utilisation as well as the effect of glucose on keratinocyte cell counts and appearance.

##### 3.4.4.4.1 Keratinocyte-Mediated Change in Medium Glucose Levels

Data showed a gradual decrease in glucose in all glucose supplemented media over a span of 14 days. (Figure 3.20).

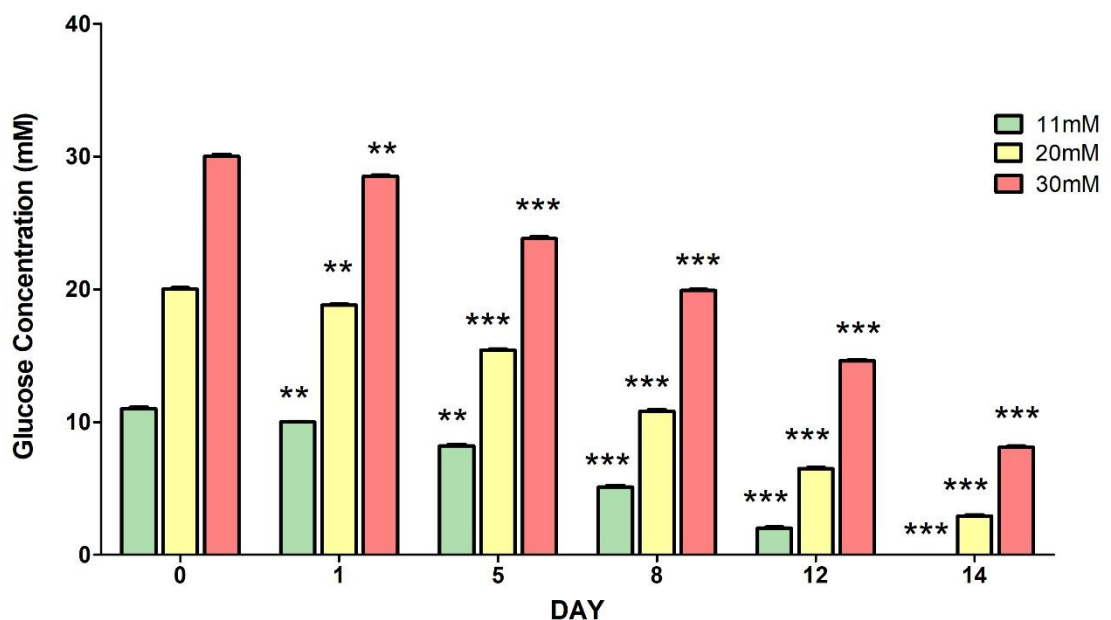


**Figure 3. 20: Keratinocyte-Mediated Change in Medium Glucose Levels.** The glucose uptake was monitored in DMEM medium containing HACATs at different glucose concentration (11, 20 and 30mM) for a span of 14 days. Significant decreases (\*\*  $P < 0.01$  and \*\*\*  $P < 0.001$  determined by t-tests;  $n = 3$ ) in glucose concentration was observed in all groups from day 1 onwards compared to day 0. Columns and error bars indicate the glucose concentration (mM)  $\pm$  the standard error of the mean (SEM) in all cases.

There was a significant ( $P < 0.05$ ) glucose depletion from day 1 onwards compared to day 0. Over the span of 14 days of keratinocyte culture the total glucose decreased by 11, 17.1, and 21.9mM in DMEM medium supplemented with 11, 20 and 30mM glucose respectively. Medium levels of glucose significantly decreased on day 1 ( $P = 0.002$  for 11mM;  $P = 0.002$  for 20mM and  $P = 0.004$  for 30mM), day 5 ( $P = 0.001$  for 11mM;  $P =$

0.000 for 20 and  $P = 0.000$  for 30mM) and days 8, 12 and 14 ( $P < 0.001$  in all cases) when comparisons were made against day 0.

#### 3.4.4.4.2 Keratinocyte Glucose Utilisation

As the glucose concentration of the DMEM medium increased there was a corresponding increase in glucose utilisation by keratinocytes (Figure 3.21).

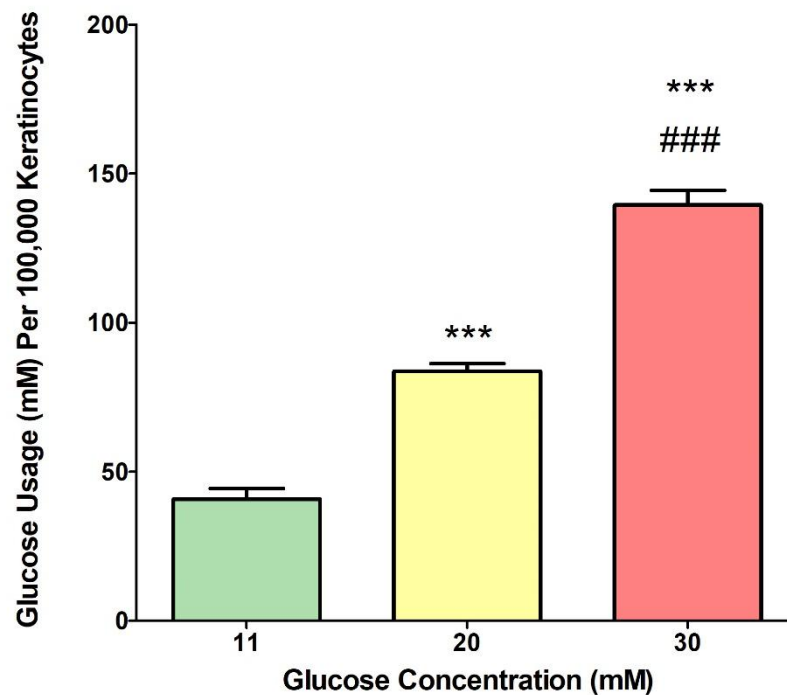


**Figure 3. 21: Keratinocyte Glucose Utilisation.** The glucose uptake was monitored in DMEM medium containing HACATs at different glucose concentration (11, 20 and 30mM) for a span of 14 days. There was a significant increase (\*\*\*)  $P < 0.001$  determined by t-tests;  $n = 3$ ) in glucose usage as the glucose concentrations increased. There was also a significant increase (###  $P < 0.001$  determined by t-tests;  $n = 3$ ) in the 30mM when compared to the 20mM group. Columns and error bars indicate the glucose usage (mM) per 100000 keratinocytes  $\pm$  the standard error of the mean (SEM) in all cases.

There was an increase in glucose usage (98.7mM) by keratinocytes cultured in 30mM DMEM after 14 days compared to those cultured in all other glucose-supplemented DMEM media (40.8mM for 11mM DMEM and 42.9mM for 20mM DMEM). Compared to keratinocytes cultured in 11mM RPMI medium, there was a significant increase in glucose utilisation by keratinocytes cultured in all other DMEM media ( $P = 0.000$  for 20 and 30mM DMEM). There was also a significant ( $P < 0.01$ ) increase in glucose usage by keratinocytes cultured in 30mM DMEM media compared to those cultured in 20mM DMEM medium.

### 3.4.4.4.3 Effect of Glucose on Keratinocyte Count

Over the span of 14 days there was a decrease in keratinocyte cell counts with the largest decrease seen at the highest glucose concentrations (Figure 3.22).

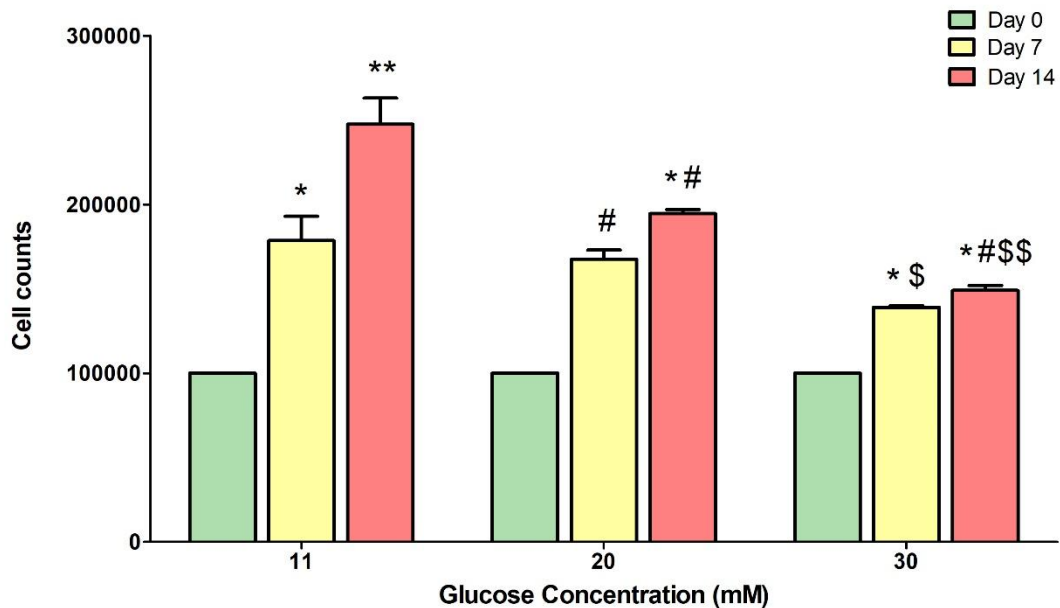


**Figure 3. 22: Effect of Glucose on Keratinocyte Count.** Cell counts were monitored at multiple glucose concentrations (11, 20 and 30mM) for a span of 14 days. There were significant increases when compared to the corresponding day 0 counts (\* $P < 0.05$ , \*\* $P < 0.001$  determined by t-tests;  $n = 3$ ), 11mM controls (# $P < 0.05$  determined by t-tests;  $n = 3$ ) and 20mM controls (\$ $P < 0.05$ , \$\$ $P < 0.001$  determined by t-tests;  $n = 3$ ). Columns and error bars indicate the cell counts per 100,000 keratinocytes  $\pm$  the standard error of the mean (SEM) in all cases.

The keratinocyte counts significantly increased in keratinocytes cultured in all media ( $P = 0.05$ ) on day 7 and day 14 ( $P = 0.005$  11mM,  $P = 0.017$  20mM and  $P = 0.039$  30mM) when compared to day 0. There were significant decreases in 20mM DMEM ( $P = 0.039$ ) and 30mM DMEM ( $P = 0.012$ ) on day 14 when compared to 11mM DMEM. There was also a significant decrease seen in 30mM DMEM on day 7 ( $P = 0.003$ ) and day 14 ( $P = 0.004$ ) when compared to the 20mM DMEM

#### 3.4.4.4 Effect of Glucose on Keratinocyte Appearance

Images of keratinocytes at 11mM and 30mM glucose were taken with a Leica microscope (40x magnification) on day 14 (Figure 3.23).

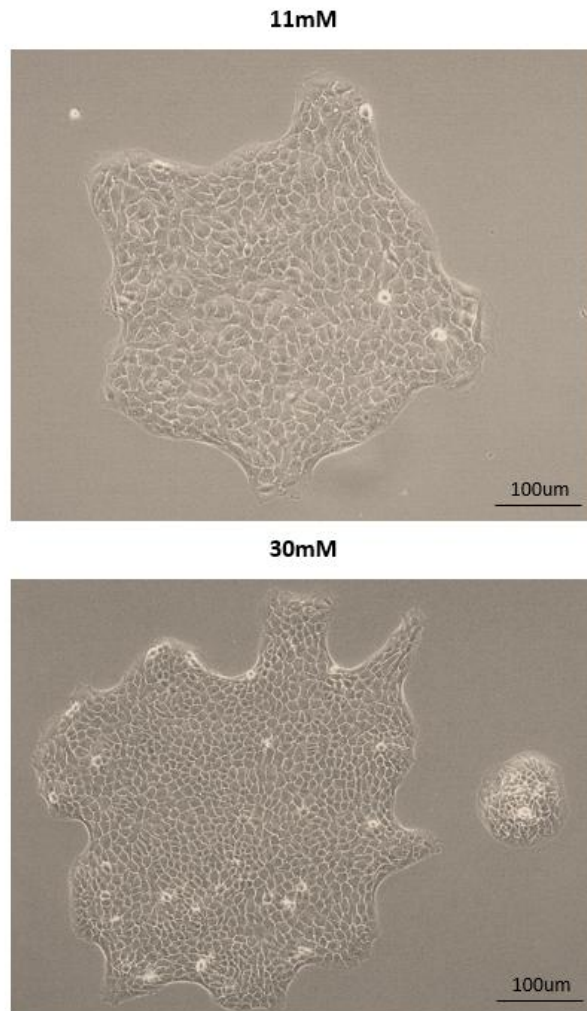


**Figure 3. 23: Effect of Glucose on Keratinocyte Appearance.** HACATs were cultured at 11 and 30mM and incubated for 14 days. Pictures were captured on day 14 at 40x magnification. The 11mM HACATs were seen to form monolayered clusters whereas the 30mM group were very tightly packed with some multilayered clusters.

On day 14 keratinocytes cultured in 11mM DMEM formed small monolayered clusters whereas keratinocytes cultured in 30mM DMEM formed larger tightly packed clusters, and, in some areas, multilayered clusters were seen. It was also noted that the DMEM medium at 30mM had turned yellow. This indicates the cells in this group were proliferating at a faster rate than the 11mM and were producing more waste products resulting in the medium colour change.

### 3.4.5 Effect of Glucose on Cellular Metabolism

#### 3.4.5.1 Fibroblast Metabolism

Fibroblasts (HDFs) were cultured at a density of  $1 \times 10^5$  cells/ml in DMEM supplemented with 11, 20 or 30mM glucose and incubated at 37°C and 5% CO<sub>2</sub> for 24 hours. After the incubation, the cells were analysed by an Agilent seahorse analyser to measure fibroblast oxygen consumption rate (OCR), extracellular acidification rate (ECAR) and real-time ATP production.

The results were displayed in three sections, pre-antibiotic (P/A), post oligomycin (O) and post-[rotenone + antimycin A] (RA). Statistical analysis was performed on the mean OCR measurements from the three timepoints in each section for each glucose concentration (Figure 3.24A). There were significant differences in P/A OCR seen between HDFs cultured at 20 and 30mM ( $P = 0.001$ ) compared to control HDFs cultured at 11mM glucose, and between HDFs cultured at 30mM ( $P = 0.006$ ) and those cultured at 20mM glucose. In section O, significant differences were seen between HDFs cultured at 30mM and control HDFs cultured at 11mM ( $P = 0.053$ ), and between HDFs cultured at 30mM and those cultured at 20mM glucose ( $P = 0.04$ ). In the final RA section, there were significant differences seen between HDFs cultured at 20mM ( $P = 0.021$ ) or 30mM ( $P = 0.022$ ) and control HDFs cultured at 11mM glucose, and between HDFs cultured at 30mM ( $P = 0.026$ ) and those cultures at 20mM glucose.

Statistical analysis was performed on the mean ECAR measurements from the three timepoints in each section for each glucose concentration (Figure 3.24B). There were significant differences seen in P/A ECAR between HDFs cultured at 20mM ( $P = 0.042$ ) and 30mM ( $P = 0.002$ ) compared to control HDFs cultured at 11mM glucose, and between HDFs cultured at 30mM ( $P = 0.018$ ) and those cultured at 20mM glucose. In section O significant differences in ECAR were seen between HDFs cultured at 20mM ( $P = 0.000$ ) or 30mM ( $P = 0.003$ ) and control HDFs cultured at 11mM glucose, and between HDFs cultured at 30mM ( $P = 0.019$ ) and those cultured at 20mM glucose. In section RA there were significant differences seen between HDFs cultured at 20mM ( $P = 0.001$ ) or 30mM ( $P = 0.004$ ) and control HDFs cultured at 11mM glucose.

As glucose levels increased ATP production decreased, with HDFs switching to mainly mitochondrial respiration (mitoATP) rather than ATP production via the glycolysis

pathway (glycoATP) (Figure 3.24C). At 11mM the total ATP production was 184 pmol/min/ $1 \times 10^5$  fibroblasts with 63% of the energy produced by mitoATP and 37% by glycoATP. This reduced by 21.4 pmol/min/ $1 \times 10^5$  fibroblasts at 20mM, with a mitoATP:glycoATP percentage ratio of 67%:33%. Total ATP production then reduced by a further 64.4 pmol/min/ $1 \times 10^5$  fibroblasts at 30mM, with a mitoATP:glycoATP percentage ratio of 75%:25%.

There was a significant decrease in mitoATP production by HDFs cultured at 30mM compared to control HDFs cultured at 11mM ( $P = 0.033$ ) or those cultured at 20mM glucose ( $P = 0.005$ ). There were significant decreases in glycoATP production by HDFs cultured at 20mM ( $P = 0.041$ ) or 30mM ( $P = 0.004$ ) compared to control HDFs cultured at 11mM glucose. There was also a significant decrease in glycoATP production by HDFs cultured at 30mM ( $P = 0.033$ ) compared to those cultured at 20mM glucose.

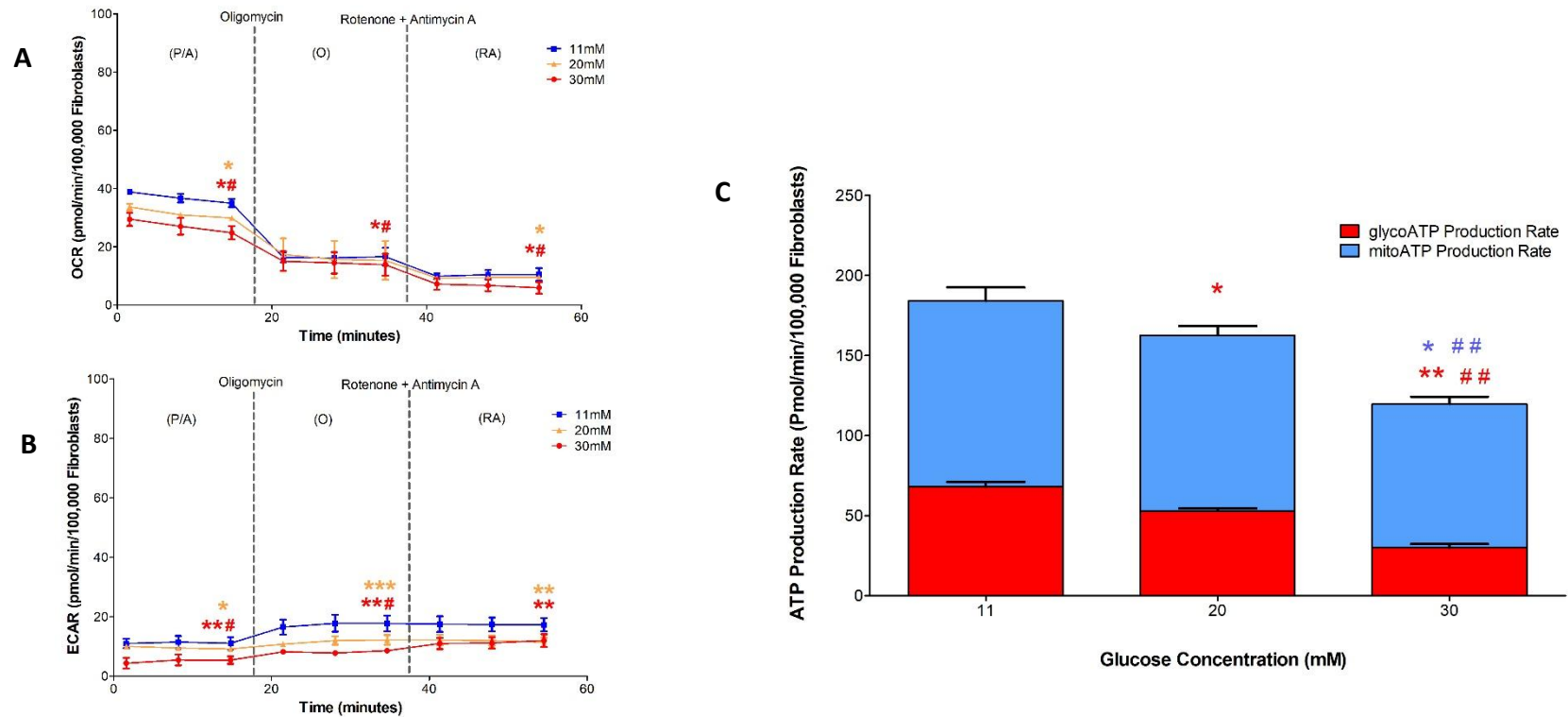


**Figure 3. 24: Fibroblast Cellular Metabolism.** The OCR, ECAR and Real time ATP production of HDFs was analysed via seahorse analysis. There was a significant decrease in OCR (A) (\* $P < 0.05$  determined by t-tests;  $n = 3$ ) as the glucose concentration increased when compared to HDFs cultured at 11mM. Significant differences (#  $P < 0.05$  determined by t-tests;  $n = 3$ ) were also detected between HDFs cultured at 30mM and those cultured at 20mM glucose. There was a significant increase (\* $P < 0.05$ ; \*\*  $P < 0.01$ , \*\*\*  $P < 0.001$  determined by t-tests;  $n = 3$ ) in ECAR (B) as the glucose increased when compared with HDFs cultured at 11mM. Significant differences were also detected (#  $P < 0.05$ , ##  $P < 0.01$  determined by t-tests;  $n = 3$ ) between HDFs cultured at 30mM and those cultured at 20mM glucose. There was a significant decrease (\* $P < 0.05$  and \*\*  $P < 0.01$  determined by t-tests;  $n = 3$ ) in ATP production (C) as glucose concentration increased when compared with HDFs cultured at 11mM. A significant decrease in ATP production was also detected between HDFs cultured at 30mM and those cultured at 20mM glucose (##  $P < 0.01$  determined by t-tests;  $n = 3$ ). Timepoints and error bars indicate the OCR and ECAR, columns and error bars indicate the ATP production rate (pmol/min/100,000 Fibroblasts)  $\pm$  the standard error of the mean (SEM) in all cases.

### 3.4.5.2 Keratinocyte Metabolism

Keratinocytes (HACAT) were cultured at a density of  $1 \times 10^5$  cells/ml in DMEM supplemented with 11, 20 or 30mM glucose and incubated at 37°C and 5% CO<sub>2</sub> for 24 hours. After the incubation, the cells were analysed by an Agilent seahorse analyser to measure fibroblast oxygen consumption rate (OCR), extracellular acidification rate (ECAR) and real-time ATP production.

Statistical analysis was performed on the mean OCR measurements from the three timepoints in each section for each glucose concentration (Figure 3.25A). There were significant differences in P/A OCR seen between HACATs cultured at 20 and 30mM ( $P < 0.01$ ) and control HACATs cultured at 11mM glucose, and between HACATs cultured at 30mM ( $P = 0.05$ ) and those cultured at 20mM glucose. In section O, significant differences were seen between HACATs cultured at 20mM and 30mM compared to control HACATs cultured at 11mM ( $P < 0.01$ ), and between HACATs cultured at 30mM and those cultured at 20mM glucose ( $P = 0.006$ ). In the final RA section, there were significant differences seen between HACATs cultured at 20mM ( $P = 0.001$ ) or 30mM ( $P = 0.000$ ) and control HACATs cultured at 11mM glucose, and between HACATs cultured at 30mM ( $P = 0.002$ ) and those cultures at 20mM glucose.

There were significant differences seen in P/A ECAR between HACATs cultured at 20mM ( $P = 0.001$ ) and 30mM ( $P = 0.008$ ) compared to control HACATs cultured at 11mM glucose (Figure 3.25B). In section O significant differences in ECAR were seen between HACATs cultured at 20mM ( $P = 0.000$ ) or 30mM ( $P = 0.003$ ) and control HACATs cultured at 11mM glucose, and between HACATs cultured at 30mM ( $P = 0.041$ ) and those cultured at 20mM glucose. In section RA there were significant differences seen between HACATs cultured at 20mM ( $P = 0.03$ ) or 30mM ( $P = 0.001$ ) and control HDFs cultured at 11mM glucose, and between HACATs cultured at 30mM ( $P = 0.001$ ) and those cultured at 20mM glucose.

As glucose levels increased ATP production increased, with HACATs switching to mainly glycolysis pathway (glycoATP) rather than ATP production via mitochondrial respiration (mitoATP) (Figure 3.25C). At 11mM the total ATP production was 451 pmol/min/ $1 \times 10^5$  keratinocytes with 61% of the energy produced by mitoATP and 39% by glycoATP. This increased by 66.7 pmol/min/ $1 \times 10^5$  keratinocytes at 20mM, with a mitoATP:glycoATP percentage ratio of 43%:57%. Total ATP production then increased by a further 133.3

pmol/min/ $1 \times 10^5$  keratinocytes at 30mM, with a mitoATP:glycoATP percentage ratio of 36%:64%.

There was a significant decrease in mitoATP production by HACATs cultured at 20mM ( $P = 0.005$ ) and 30mM ( $P = 0.044$ ) compared to control HACATs cultured at 11mM. There were significant increases in glycoATP production by HACATs cultured at 20mM ( $P = 0.002$ ) or 30mM ( $P = 0.001$ ) compared to control HACATs cultured at 11mM glucose. There was also a significant increase in glycoATP production by HACATs cultured at 30mM ( $P = 0.003$ ) compared to those cultured at 20mM glucose.

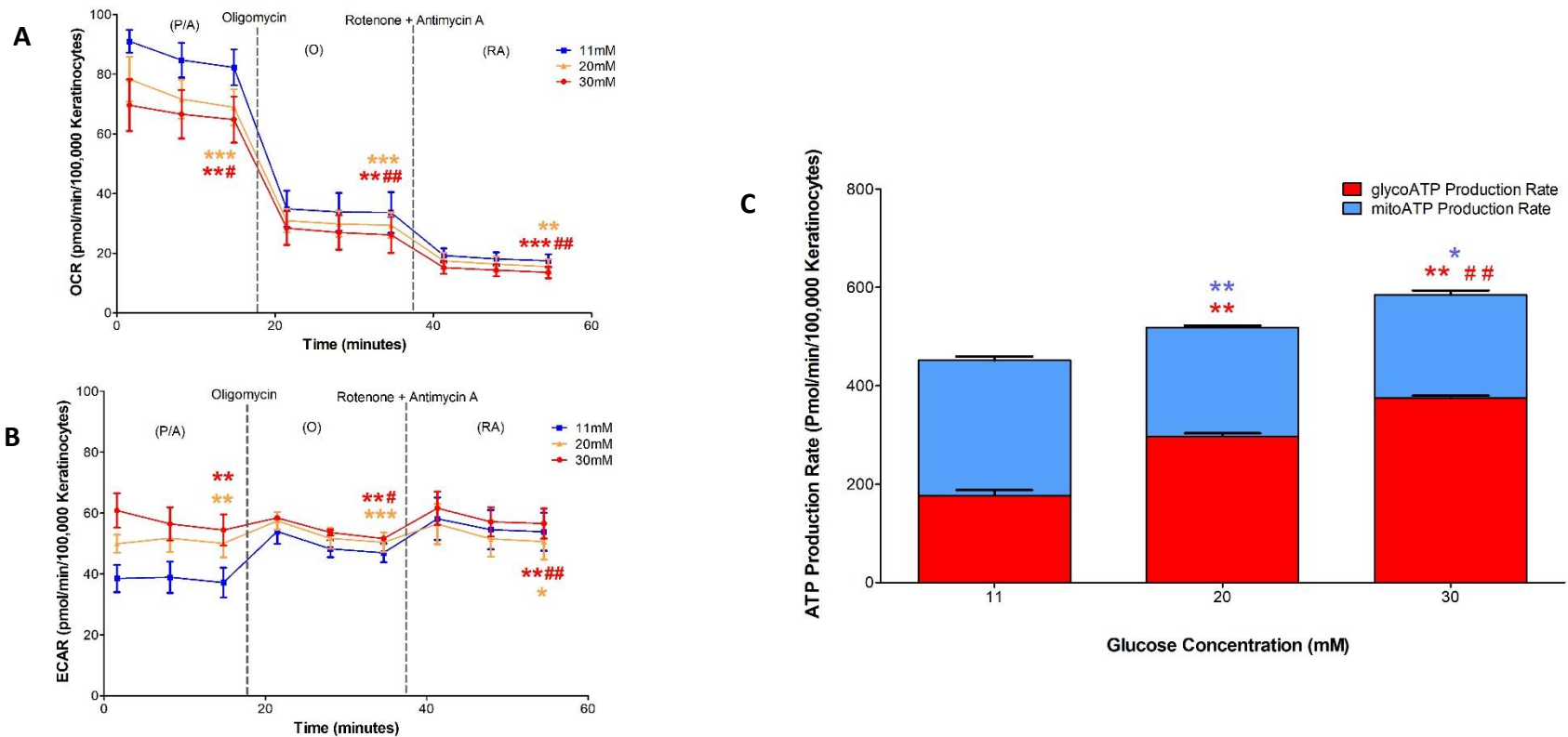


**Figure 3.25: Keratinocyte Cellular Metabolism.** The OCR, ECAR and Real time ATP production of HACATs was analysed via seahorse analysis. There were significant decrease (\*\* $P < 0.01$ , \*\*\* $P < 0.001$ ;  $n = 3$ ) in OCR (A) as the glucose increased when compared to the 11mM control group. Significant differences were seen (#  $P < 0.05$ , ##  $P < 0.01$ ;  $n = 3$ ) when comparisons were made against the 20mM group (A). There was a significant increase (\* $P < 0.05$ ; \*\*  $P < 0.01$ , \*\*\*  $P < 0.001$ ;  $n = 3$ ) in ECAR (B) as the glucose increased when compared to the 11mM control group. Significant differences were seen (#  $P < 0.05$ , ##  $P < 0.01$ ;  $n = 3$ ) when comparisons were made against the 20mM group. There was a significant increase (\* $P < 0.05$  and \*\*  $P < 0.01$ ;  $n = 3$ ) in ATP production (C) as glucose increased when compared to the 11mM control group as well as a significant increase when compared against the 20mM group (##  $P < 0.01$ ;  $n = 3$ ). Timepoints and error bars indicate the OCR and ECAR, columns and error bars indicate the ATP production rate (pmol/min/100,000 Fibroblasts)  $\pm$  the standard error of the mean (SEM) in all cases.

### 3.5 Discussion

This study assessed the effect of hyperglycaemia on differentiation and polarisation of U937 monocytes into M1 macrophages by the detection of CD11b and CD197 cell surface markers. Glucose uptake and utilisation was monitored in multiple cell types (monocytes, macrophages, fibroblasts and keratinocytes) along with the effect on cell counts and viability. Finally, cellular metabolism pathways were also monitored to determine the impact of hyperglycaemia on ATP production by keratinocytes and fibroblasts.

The expression of CD11b was elevated in PMA-differentiated M0 macrophages compared the U937 monocytes cultured at the corresponding glucose concentration. Published data by Serra *et al*, (2012) has confirmed an overall increase in CD11b expression in M0 macrophages compared with monocytes. However, there was a significant concentration-dependent decrease in the expression of CD11b in M0 macrophages as glucose concentration increased (Figure 3.3) indicating that hyperglycaemia impairs the differentiation of U937 monocytes into M0 macrophages. In line with these findings, Serra *et al*, (2012) also showed a significant reduction of CD11b in diabetic mice compared to non-diabetic controls. However, a study by Torres-Castro *et al*, (2016) showed that hyperglycaemia results in higher expression of CD11c in macrophages, so responses may be context-specific. When CD197 expression was analysed (Figure 3.4) there was increased CD197 expression in M0, and particularly M1 macrophages, compared to U937 monocytes. CD197 expression also decreased in M0 macrophages as the concentration of glucose increased, suggesting hyperglycaemia has a tendency to retain U937 cells in a more monocyte-like phenotype by hampering both cell differentiation and polarisation. In contrast, there was concentration-dependent increase in CD197 expression in M1-directed macrophages as the glucose concentration increased, suggesting hyperglycaemia drives enhanced and/or premature M1 polarisation once cells have been stimulated with LPS/IFN- $\gamma$ . It is thought that hyperglycaemia primes macrophages, resulting in increased production of cytokines such as TNF $\alpha$ , IL-1 $\beta$  and IL-6, that are characteristic of a more proinflammatory M1-like phenotype (Pavlou *et al*, 2018; El-Mahmoudy *et al*, 2005; Moganti *et al*, 2017).

Chronic hyperglycaemia induced a statistically higher percentage of damaged or dead macrophages (Figure 3.5). Zhoa *et al*, (2023) also found that elevated glucose results in increased macrophage cell membrane damage by inducing pore formation, particularly following LPS stimulation, which was detected by propidium iodide staining. In concurrence with these findings, macrophages grown in high glucose have shown to illustrate signs of metabolic stress as well increased apoptotic cell death (Rodgers *et al*, 2020).

This study reviewed glucose uptake by monocytes, macrophages, fibroblasts and keratinocytes and its effect on cell counts and viability. Data showed a significant monocyte-mediated decrease in medium glucose levels in all glucose-supplemented RPMI media over a span of 8 days (Figure 3.7) and a corresponding increase in glucose uptake by monocytes as glucose-supplementation increased (Figure 3.8). In terms of monocyte cell counts (Figure 3.9) there was an increase in cell counts after 3 days at the higher glucose concentrations (20 and 30mM) in comparison to lower concentrations. However, by day 8 there was a subsequent decrease in monocyte counts with the lowest readings recorded for monocytes cultured at 30mM. This suggests high glucose may provide an initial boost in cell proliferation but there might be a limit to how much glucose can be used productively by monocytes before they start to undergo oxidative stress and subsequent cell death.

It is known that promotion of TLR expression can result in greater activation of apoptosis and production of proinflammatory cytokines (Zhang *et al*, 2003). It is thought that chronic hyperglycaemia can induce higher TLR expression. A study done by Dasu *et al*, (2008) showed that THP-1 monocytes grown in high glucose (25mM) for 3 days had a significantly higher expression of both TLR2 and TLR4, along with the increased expression of MyD88, IRAK1 and NF- $\kappa$ B. It has also been shown that monocytes grown in hyperglycaemic conditions express higher ROS levels (Gonzalez *et al*, 2012) contributes to monocyte oxidative stress (Krakauer, 2015). The AKT pathway with the assistance of PKC plays an important role in regulating apoptosis and autophagy by stimulating the mammalian target of rapamycin complex 1 (mTORC1) (Volpe *et al*, 2018). The mTORC1 contributes towards normal cell function such as cell growth and proliferation (Saxton and Sabatini, 2017), but hyperglycaemia disrupts this pathway by restricting mTORC1 activation (Krakauer, 2015; Volpe *et al*, 2018).

There was also a macrophage-mediated decrease in medium glucose levels and a corresponding increase in glucose usage observed in macrophages as glucose-supplementation increased. However, the overall/total glucose usage was not as high as that seen in the monocytes, suggesting a higher energy requirement is needed by monocytes compared to differentiated macrophages (Chiu and Bharat, 2016). M1 macrophages in low glucose (11mM) tended to make macrophages form multiple, larger monolayer clusters in comparison to high glucose (30mM) which tended to make macrophages accumulate into small multilayer clusters (Figure 3.14). Hyperglycaemic conditions are known to result in early M1 phenotype polarization resulting in abnormal macrophage morphology and function (Awad *et al*, 2024). Hyperglycaemic conditions have also shown to result in low macrophage cell viability (Ayala *et al*, 2019; Pavlou *et al*, 2018).

The fibroblast-mediated change in medium glucose levels and glucose usage in HDFs was measured over 14 days. Data showed a significant decrease in glucose levels with time in all glucose-supplemented DMEM media over 14 days and a corresponding increase in glucose usage by HDFs as the glucose concentration of media increased. There was also an increase in HDF cell counts by day 14 in all cases, but the increase was reduced as the glucose concentration of the DMEM medium increased. High glucose levels have shown impair both fibroblast cell proliferation and migration (Buranasin *et al*, 2018), possibly due to growth factor resistance and over production of PKC (Hehenberger and Hansson, 1997). It has also been shown that hyperglycaemic conditions results result in low fibroblast cell viability (Buranasin *et al*, 2018).

There were also some visual differences observed in fibroblasts grown at low and high glucose (Figure 3.19). After 14 days of incubation, the fibroblasts in low glucose appeared as long spindle shaped cells in comparison to the high glucose fibroblasts which were visually larger and stellate shaped. There were also a few stellate shapes at low glucose, but these were not as prominent. The large stellate shapes can be associated to the activated form of fibroblasts called myofibroblasts. At pre-diabetic conditions, fibroblasts can be activated by proinflammatory cytokines such as TNF $\alpha$  and ILs (Younesi *et al*, 2024). In the high glucose group, there was an overpopulation of myofibroblasts, and this could indicate that glucose is activating the fibroblasts. Myofibroblasts produce several ILs and MCP-1 at

pre-diabetic conditions (van Caam *et al*, 2016), and increased levels of NF- $\kappa$ B and ILs such as IL-8 under hyperglycaemic conditions (Pang *et al*, 2016).

There was a keratinocyte-mediated decrease in medium glucose levels and a corresponding increase in glucose usage observed in HACAT keratinocytes as glucose-supplementation increased (Figures 3.20 and 3.21). There was an increase in HACAT cell counts over 14 days in all cases but the increase in cell numbers was reduced as the glucose concentration of the DMEM medium increased. This relative decrease in cell counts (Figure 3.22) despite the increased glucose utilisation by HACAT cells suggests glucose is having a damaging effect on keratinocytes. After 14 days of growth in low glucose DMEM, HACAT cells formed small clusters in a monolayer in comparison to HACAT cells cultured in high glucose DMEM which formed densely packed clusters and, in some cases, multilayered clusters. There were also changes observed in the DMEM medium which contained a phenol red indicator. The low glucose DMEM medium did not show any signs of change over the incubation period. However, the high glucose DMEM medium started to turn yellow in colour, indicating an acidic pH which could be due to increased metabolic activity resulting in a high quantity of waste products such as pyruvic acid, lactic acid and CO<sub>2</sub> that play a role in reducing the pH of the cell culture medium (Segeritz and Vallier, 2017). A study conducted by Spravchikov *et al*, (2001) showed that keratinocytes grown in a high concentration of glucose (20mM) appeared in larger tightly packed clusters and that cell proliferation was reduced after 7 days in keratinocytes cultured at 20mM compared to those cultured at 2mM glucose. Another study performed by Terashi *et al*, (2005) also found similar results, with keratinocytes grown in high glucose (12mM) could no longer proliferate after 30 days indicating that hyperglycaemia limits the lifespan of keratinocytes *in vitro*. Keratinocytes grown in high glucose have shown increased NO production (Nakai *et al*, 2003) and increased secretion of proinflammatory cytokines such as IL-8 (Lan *et al*, 2013). Studies have shown that chronic hyperglycaemia can be linked to the inhibition of the p38MAPK pathway and a reduction in human  $\beta$ -3 and  $\beta$ -defensin-2 expression in keratinocytes (Lan *et al*, 2013; Lan *et al*, 2012).

This study also investigated the effect of glucose on the ATP production in both HDFs and HACATs to understand how glucose affects cellular metabolism. The data showed a significant decrease in OCR and ECAR as glucose concentration increased in HDFs. There was

a significant reduction in total ATP production in HDFs as glucose concentration increased, with HDFs producing ATP increasingly through mitochondrial-mediated pathways rather than the glycolytic pathway as glucose levels increased. In relation to HACAT cells there was a significant reduction in OCR and a significant increase in ECAR as the glucose concentration increased. There was also an increase in total ATP production in HACAT keratinocytes as glucose levels increased, with ATP production switching primarily to generation via the glycolytic pathway rather than mitochondrial production in HACAT cells as glucose levels increased. These data showed increased glucose resulted in reduced oxygen consumption rate in both HDFs and HACATs, suggesting cells were not able to function effectively as glucose concentration became elevated. The ECAR values showed a reduction in HDFs but an increase in HACATs as glucose increased, in line with total ATP production levels indicating a reduction in glycoATP in HDF and an increase in glycoATP in HACATs. Studies have shown that high glucose levels result in long term activation of the P2X7 receptor, leading to continuous ATP generation from fibroblasts and subsequent higher rates of cell death (Solini *et al*, 2000). Moreover, high glucose has hypoxic effects on fibroblasts by reducing mitochondrial mass by autophagy and mitophagy (Baracca *et al*, 2013; Zhang *et al*, 2008). High glucose has also shown to elevate ROS which in turn results in mitochondrial dysfunction by cytochrome C release and a decrease in transcription factor A, leading to increased apoptosis via the AKT-IRF3 pathways in keratinocytes (Rizwan *et al*, 2020).

In summary, high glucose levels appeared to have a detrimental effect on multiple cell types in several different ways. This included impaired differentiation and polarisation of macrophages, increased macrophage cell death, reduced cell counts and altered cell morphology in all cell types investigated and dysregulated ATP production in both fibroblasts and keratinocytes. Future work could include investigating how high glucose levels impair metabolic pathways by using molecular inhibitors or neutralising antibodies. This work could also be extended to other cell types involved in the wound healing process, such as endothelial cells and dendritic cells.

## **Chapter 4: The Effect of MGN3 on Monocyte/Macrophage Function**

## 4.1 Introduction

### 4.1.1 *Staphylococcus aureus*

*Staphylococcus aureus* (SA) is a gram-positive bacterium commonly found in the commensal microflora but can become opportunistic, particularly as MRSA in nosocomial infections (Sina *et al*, 2013; Trubiano and Padiglione, 2015). MRSA, 0.5–1.0 $\mu$ m in diameter and coccus-shaped (Harris *et al*, 2002), can form biofilms, which increase survival by storing resources and providing protection from antibiotics and the immune system (Kostakioti *et al*, 2013; Hassan *et al*, 2011). Biofilms complicate wound healing, especially in chronic wounds, causing prolonged inflammation (Attinger and Wolcott, 2012). Studies on bronchial aspirates from critically ill patients show that elevated glucose levels correlate with a higher risk of MRSA infection (Phillips *et al*, 2005). In diabetic foot ulcers (DFUs), MRSA is a common infection (Luo *et al*, 2020), and elevated glucose enhances MRSA biofilm formation (Luo *et al*, 2020; You *et al*, 2014). Glucose fermentation aids MRSA aggregation (Vitko *et al*, 2016) and increasing glucose in culture media directly influences biofilm size (Waldrop *et al*, 2014; Lade *et al*, 2019).

### 4.1.2 *Pseudomonas aeruginosa*

*Pseudomonas aeruginosa* (PA) is a gram-negative bacterium found in commensal microflora (Klockgether and Tümmler, 2017) and can be opportunistic in both hospital and community-acquired infections (Trubiano and Padiglione, 2015). PA is rod-shaped (1–3 $\mu$ m in length, up to 1 $\mu$ m in width) and has a thin peptidoglycan cell wall surrounded by a lipopolysaccharide (LPS) outer membrane, which triggers immune responses (Paterson and Kim, 2009; Fujihara *et al*, 2003). Elevated glucose levels increase PA biofilm formation from clinical isolates, with 2% and 4% glucose significantly enhancing biofilm development without affecting planktonic growth (She *et al*, 2019). Glucose appears to improve bacterial adhesion and upregulate the biofilm matrix (She *et al*, 2019). In contrast, glucose starvation causes PA biofilms to shrink by about 60% and disperse (Huynh *et al*, 2012). Glucose also affects the

appearance of PA biofilms, making them form small "mushroom-like" structures with punctured microcolonies (De Kievit, 2009).

#### 4.1.2.1 Lipopolysaccharides

LPS comprises three main components: O-antigen, core oligosaccharide, and lipid A (Gnauck *et al*, 2016; Zanoni *et al*, 2012) (Figure 4.1). Lipid A anchors LPS to the bacterial outer membrane (Gnauck *et al*, 2016). The core oligosaccharide includes inner and outer regions, linking lipid A to the O-antigen (Gnauck *et al*, 2016; Raetz & Whitfield, 2002). LPS is categorized as smooth (SLPS) or rough (RLPS) (Gnauck *et al*, 2016; Zanoni *et al*, 2012; Bertani & Ruiz, 2002). SLPS includes all three components, while RLPS lacks the O-antigen (Zanoni *et al*, 2012). LOS, often considered a form of RLPS, features a short oligosaccharide chain limited to 10 saccharide units and may represent an analogous LPS subtype (Raetz & Whitfield, 2002; Gnauck *et al*, 2016; Preston *et al*, 1996) (Figure 4.1). SLPS is the wild-type LPS form found in most Gram-negative bacteria, including *P. aeruginosa* (Le Brun *et al*., 2013; Gnauck *et al*, 2016; Zanoni *et al*, 2012). RLPS and LOS results from partial or complete O-antigen loss (Zanoni *et al*, 2012). Both activate TLR4–MD2 pathways but differ in signaling: RLPS triggers MYD88-dependent responses without CD14, whereas SLPS requires CD14 and activates both MYD88-dependent and TRAM–TRIF pathways (Zanoni *et al*, 2012; Jiang *et al*, 2005; Maldonado *et al*, 2016; Godowski, 2005).

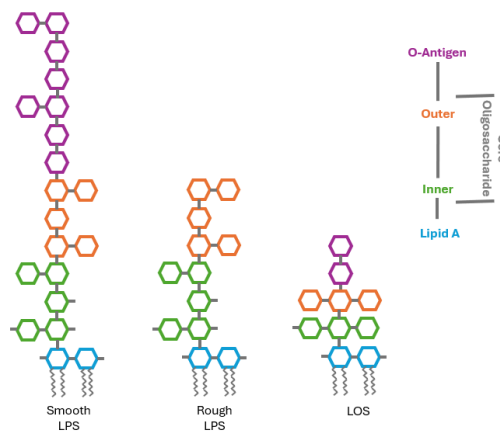


**Figure 4. 1: Schematic illustration of LPS and LOS structure.** LPS consists of Lipid A and a core oligosaccharide, with an O-antigen (smooth LPS) or without an O-antigen (Rough LPS). LOS consists of Lipid A, a core oligosaccharide and a short oligosaccharide extension. Diagram based on information from Gnauck *et al* (2016) and Zanoni *et al* (2012).

#### 4.1.3 Bacterial Biofilms Evade the Immune System

SA biofilms evade immune detection through multiple mechanisms, including shielding from antimicrobial peptides and producing immune-modulating decoys (de Vor *et al*, 2020). Bacteria form biofilms using extracellular polymeric substances (EPS), composed of polysaccharides, extracellular DNA, and lipids, which protect against antimicrobial peptides and conceal PAMPs (Payne & Boles, 2016; Di Martino, 2018; de Vor *et al*, 2020). A key EPS component, polymeric-N-acetyl-glucosamine (PNAG), carries a strong positive charge, enabling it to repel negatively charged peptides like LL-37 (Vuong *et al*, 2004; Riyad & Overhage, 2021). SA can also hijack the host immune system by incorporating host-derived fibrin into the biofilm via coagulase expression (Zapotoczna *et al*, 2015).

Cerca *et al* (2006), showed that IgG penetrates biofilms but binds PNAG within the EPS rather than on the bacterial surface, limiting opsonization and neutrophil-mediated killing. Furthermore, free PNAG can protect planktonic bacteria by sequestering antibodies away from bacterial surfaces (Cerca *et al*, 2006; de Vor *et al*, 2020). Biofilm size also hampers immune clearance. With macrophages averaging  $\sim 14\mu\text{m}$  and neutrophils engulfing particles up to  $10\mu\text{m}$  (Cannon & Swanson, 1992; de Vor *et al*, 2020), they struggle to phagocytose MRSA biofilms, which can reach  $50\text{--}60\mu\text{m}$  after 24 hours (Cheng *et al*, 2021).

#### 4.1.4 Macrophages and Immune Cell Signalling

Monocytes and macrophages are key players in the innate immune system, interacting with fibroblasts and keratinocytes (Ma *et al*, 2019; Correa-Gallegos *et al*, 2021) (Figure 4.2). During injury or infection, classical monocytes are released from the bone marrow via CCR2 signaling (Serbina & Pamer, 2006; Chui & Bharat, 2016). These monocytes secrete MCP-1, a CCR2 ligand, which recruits more monocytes and promotes their differentiation into macrophages (Chui & Bharat, 2016; Nasser *et al*, 2015; Deshmane *et al*, 2009). Macrophages and keratinocytes release  $\text{TGF}\beta 1$ , stimulating fibroblasts to secrete FGF2, which further enhances cytokine production and macrophage recruitment (Plikus *et al*, 2021; Liarte *et al*, 2020; Farooq *et al*, 2021). Macrophages also produce EGF, improving fibroblast migration and contractility (Kim *et al*, 2015).

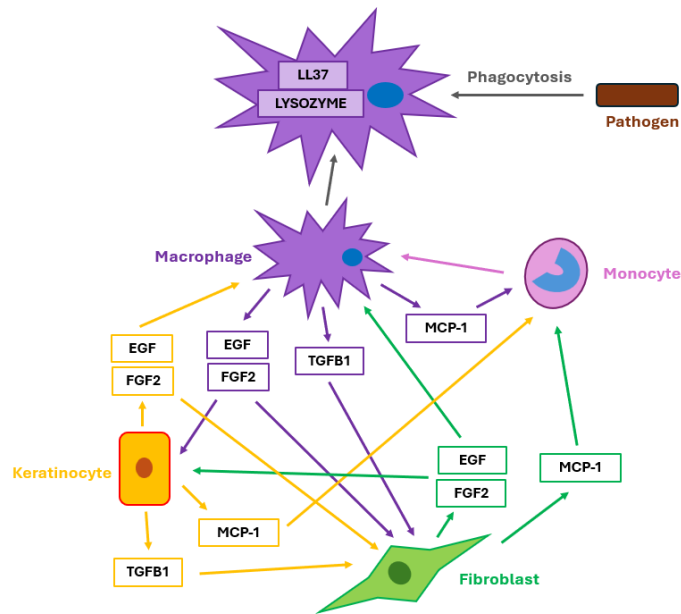


**Figure 4. 2: Macrophage Cell Interactions in the Wound Healing Process.** During the wound healing process monocytes and macrophages secrete chemokines and cytokines which result in the activation and recruitment of additional immune cells. Schematic based on information from Chui and Bharat (2016), Plikus *et al* (2021), Liarte *et al* (2020), Deshmane *et al* (2009), Agier *et al* (2015) and Scheenstra *et al* (2020).

Macrophages, derived from circulating monocytes in response to chemoattractants like MCP-1 and MIPs (Dipietro *et al*, 2001; Maurer & Von Stebut, 2004), are activated by signals such as LPS (Fujihara *et al*, 2003). They play essential roles in both innate and adaptive immunity through phagocytosis and cytokine secretion and are found throughout the body, including the lungs, gut, and bones (Nagl *et al*, 2002; Hirayama *et al*, 2017). During phagocytosis, macrophages detect bacterial chemoattractants via GPCRs, migrate toward pathogens, engulf them, and release hydrolytic enzymes and antimicrobial peptides like LL37 for bacterial lysis (Meena & Kimmel, 2017; Botelho & Grinstein, 2011; Agier *et al*, 2015; Scheenstra *et al*, 2020; Nawaz *et al*, 2022). LL37 also enhances phagocytosis through TLR signalling and promotes cell degranulation (Van Harten *et al*, 2018). Bacterial fragments are then presented on the macrophage surface for further immune processing (Neefjes *et al*, 2011; Unanue *et al*, 2016).

Chronic hyperglycaemia impairs macrophage function, increasing cytokine production and reducing phagocytic activity (Pavlou *et al*, 2018). Diabetic mouse models show elevated inflammatory markers and reduced levels of autophagy-related proteins (LC3b, Beclin-1),

indicating impaired autophagic capacity (Edgar *et al*, 2021; Sousa *et al*, 2023). Grosick *et al* (2018), found that hyperglycaemia primes THP-1 macrophages to produce higher proinflammatory cytokines upon stimulation. This may stem from dysregulation in H3K9 methyltransferase pathways, altering the cells' epigenetic state (Li *et al*, 2016; Raiymbek *et al*, 2020).

#### **4.1.5 The Importance of Toll-like Receptors in the Innate Immune System**

Toll-like receptors (TLRs) are transmembrane proteins essential to the innate immune system, initiating intracellular signalling upon activation (Akira & Sato, 2003) (Figure 4.3). Humans have 10 known TLRs (TLR1–10), and mammals have 13 (Akira & Sato, 2003; Sameer & Nissar, 2021). TLRs are either cell surface-bound (e.g., TLR2, TLR4) or intracellular (e.g., TLR3) (Kraneveld *et al*, 2008; El-Zayat *et al*, 2019). TLR3 responds broadly to stimuli, while TLR2 and TLR4 are more selective (Muzio *et al*, 2000).

TLR2 is activated by lipoproteins like peptidoglycan; TLR4 responds to LPS (Gopalakrishnan & Salgame, 2016; Mukherjee *et al*, 2016; Kaisho & Akira, 2002). Activation of TLR2/4 triggers the MyD88-dependent pathway, recruiting IRAK4, which phosphorylates IRAK1. This activates TRAF6 and TAK1, followed by phosphorylation via TAB1/2 and activation of the IKK complex (IKK $\alpha$ , IKK $\beta$ , and NEMO) (Mukherjee *et al*, 2016; Oeckinghaus *et al*, 2011). IKK then activates NF- $\kappa$ B, leading to proinflammatory cytokine expression such as ILs and TNF $\alpha$  (Lui *et al*, 2017). TAK1 also stimulates MAPK and the transcription factor AP-1 (Oeckinghaus *et al*, 2011; El-Zayat *et al*, 2019).

Additionally, TLR4 activates the TRIF pathway, which further enhances TAK1 and IRF3 activity, promoting cytokine production (Mukherjee *et al*, 2016; Oeckinghaus *et al*, 2011; El-Zayat *et al*, 2019). TLR2 and TLR4 are primarily expressed in phagocytes (e.g., macrophages, dendritic cells) and occasionally in mast cells (Muzio *et al*, 2000; Re & Strominger, 2001; Varadaradjalou *et al*, 2003). Their expression increases in response to bacterial components like LPS and peptidoglycans, supporting their central role in innate immunity (Muzio *et al*, 2000; El-Zayat *et al*, 2019).

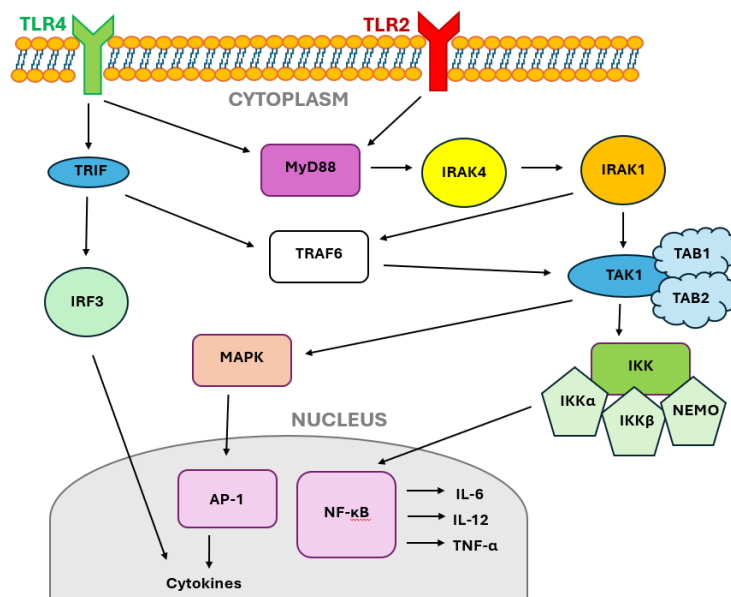


**Figure 4. 3: The signalling pathways of TLR2 and TLR4.** The stimulation of TLR2 and TLR4 results in a cascade of cellular reactions which ultimately result in the production proinflammatory cytokines and chemokines as part of the innate immune response. The cascade includes the activation of MyD88 which recruits IRAK4/IRAK1 and activates TRAF6 and TAK1. The TAK1 complex then undergoes phosphorylation and activates the IKK complex and MAPK resulting in NF- $\kappa$ B and AP-1 activation resulting in cytokine/chemokine production in the nucleus. TLR4 stimulation also results in the TRIF pathway activation which also results cytokine/chemokines. Schematic based on information from Mukherjee *et al*, 2016; Oeckinghaus *et al*, 2011; El-Zayat *et al*, 2019.

#### 4.1.6 Hyperglycaemic Effects on Macrophage Cell Signalling

Hyperglycaemia increases proinflammatory cytokines such as FGF2, MCP-1, and TGF $\beta$ 1 (Hu *et al*, 2018; Shao *et al*, 2017; Wu & Derynck, 2009). Xuan *et al* (2014; 2016), showed it enhances ROS production and inhibits fibroblast migration by repressing FGF2. Diabetic patients also show reduced circulating EGF, possibly due to pancreatic dysfunction suppressing both EGF and insulin (Miettinen *et al*, 2006; Shi *et al*, 2018). High glucose reduces macrophage phagocytosis by downregulating LL37 expression (Montoya-Rosales *et al*, 2016), and phagocytosis of apoptotic  $\beta$ -cells can lead to lysosomal permeabilization, though the mechanism remains unclear (Ward *et al*, 2018).

TLR2 and TLR4 expressions are typically elevated during inflammation, are also upregulated by high glucose (Dasu *et al*, 2008), linked to PKC activation via NADPH oxidase. FFAs further enhance this effect and activate NF- $\kappa$ B (Dasu & Jialal, 2011). Type 1 diabetic patients show significantly higher TLR2/4 protein and mRNA levels (Devaraj *et al*, 2008), and diabetic mice

macrophages exhibit elevated TLR2/4, IL-1, and IL-6, impairing insulin gene expression (Nackiewicz *et al*, 2014). Additionally, TLR-activated monocytes from diabetics produce more IP-10 in high glucose conditions (Devaraj & Jialal, 2009).

#### **4.1.7 Reversing the Hyperglycaemic Effect on Macrophage Cell Signalling**

Obesity and poor diet are key risk factors for diabetes (Egshatyan *et al*, 2016). High-fibre diets can reduce inflammation, particularly in prediabetics (Reynolds *et al*, 2020; Nitzke *et al*, 2024). MGN3, a rice bran-derived fibre, has been shown to reduce inflammation and enhance macrophage phagocytosis under hyperglycaemic conditions (Ghoneum & Jewett, 2000; Ghoneum & Agrawal, 2011, 2014; Ghoneum & Matsuura, 2004; Ghoneum *et al*, 2008). While MGN3 shows promise in improving immune function in diabetics, its direct effects on chemokines like MCP-1 and growth factors such as EGF and FGF2, and their influence on wound-healing immune cells, remain unexplored.

Hyperglycaemia impairs wound healing by prolonging cytokine release, reducing phagocytosis, and causing microvascular damage, leading to peripheral ischaemic neuropathy (McCrimmon *et al*, 2012; Pavlou *et al*, 2018; Falanga, 2005). MGN3 enhances immune function by stimulating M1 macrophages to increase phagocytosis, cytokine, and nitric oxide production (Ghoneum & Matsuura, 2004; Ghoneum *et al*, 2008), and by improving monocyte and neutrophil phagocytosis, promoting monocyte recruitment, and inducing IL-10 from dendritic cells (Govers *et al*, 2020; Bermudez-Brito *et al*, 2015). Prolonged rice bran exposure may induce macrophage activation via the dectin-1 pathway, thereby enhancing innate immune responses (Moerings *et al*, 2022). MGN3 supports immune cell function without directly affecting bacterial growth. It reverses high glucose-induced phagocytic impairment in M0 macrophages and enhances clearance of *MRSA* via TLR4 and dectin-1—effects reduced when TLR4 is blocked (Tan, 2018; Asif, 2020; Shah *et al*, 2023). MGN3 may compete with LPS for TLR4 and dectin-1 binding, likely due to structural similarity, though it activates these receptors less strongly (Li *et al*, 2015; Ghoneum *et al*, 2013; Bowyer *et al*, 2010). While promising, MGN3's effects on immune cells already compromised by hyperglycaemia remain unclear.

## 4.2 Aims and Objectives

### 4.2.1 Aim

To investigate the effect of MGN3 on U937 monocytes and M1 macrophages, including their TLR2/TLR4-mediated phagocytic response to MRSA and PA biofilms under pre-diabetic and hyperglycaemic conditions.

### 4.2.2 Objectives

- To compare the phagocytic function of M1 macrophages cultured at different glucose concentrations on MRSA and PA biofilm clearance.
- To determine the contribution of TLR pathways to MGN3-mediated phagocytosis of bacterial biofilms by U937-derived M1 macrophages under pre-diabetic (11mM glucose) and hyperglycaemic (15, 20, 30mM glucose) conditions using chemical inhibition of TLR2 and TLR4 proteins.
- To compare TLR-mediated phagocytic effects of MGN3 with responses induced by LPS and rice starch (RS) exposure under pre-diabetic and hyperglycaemic conditions.
- Assess the effect of MGN3 on growth factor, chemokine, antimicrobial peptide and antimicrobial enzyme production by M1 macrophages.
- Evaluate the effect of MGN3 on U937 monocyte/macrophage-derived lysozyme activity.
- Assess the influence of supernatants from MGN3-treated M1 macrophages, keratinocytes and fibroblasts on the chemotaxis of U937 monocyte, including chemotactic responses induced by secreted MCP-1.

## 4.3 Methods

### 4.3.1 Generation of M1 macrophages

U937 monocytes were cultured at different glucose concentrations (11, 15, 20 and 30mM) for a minimum of 2 weeks prior to experimental use (see section 2.2.5) and differentiated into M1 macrophages as shown in section 2.2.5.

### 4.3.2 Biofilm Generation

MRSA and PA01 strains were cultured in NB for 3 days at 37 °C with 5% CO<sub>2</sub>, then streaked on NA plates. For experiments, serial dilutions were plated on NA, and a bacterial density of 2×10<sup>4</sup> CFU/mL was used. Bacteria were aliquoted onto membranes and incubated for 24 hours at 37 °C with 5% CO<sub>2</sub> to allow biofilm formation (see section 2.2.7).

### 4.3.3 Host-Pathogen Assay

M1 macrophages were cultured on membranes in varying glucose concentrations (11, 15, 20, 30 mM) and treated for 24 hours with or without RS (2mg/mL), LPS (5mg/mL), and MGN3 (0.5, 1, 2mg/mL). They were then incubated with MRSA biofilms for 1 hour to allow host-pathogen interaction. Bacteria were subsequently plated on NA and incubated for 24 hours before recovery was assessed (see section 2.2.8).

### 4.3.4 ELISAs

ELISAs were used to measure M1 macrophage production of growth factors (EGF, FGF2), the chemokine MCP-1, and the antimicrobial peptide LL37. M1 macrophages (1×10<sup>6</sup> cells/mL) were cultured in low (11mM) or high (30mM) glucose RPMI CM and treated for 24 hours with LPS (5µg/mL), LPS + TLR2i or TLR4i (200µM), MGN3 (2mg/mL), or MGN3 + TLR2i or TLR4i. ELISAs were performed on cell supernatants, except for LL37, which used cell lysates prepared with MPER buffer and normalized via BCA assay (see section 2.2.13.2). Assays followed manufacturer protocols, with absorbance read at 450nm (background subtracted at 570nm) using a FLUOstar Omega plate reader.

#### **4.3.5 Chemotaxis Assay**

M1 macrophages ( $1 \times 10^6$  cells/mL) were cultured in RPMI CM with low (11mM) or high (30mM) glucose. HACAT and HDF cells ( $2 \times 10^5$  cells/mL) were grown in DMEM CM under the same glucose conditions until 80% confluence. All cells were treated for 24 hours with LPS (5  $\mu$ g/mL), LPS + TLR2i or TLR4i (200  $\mu$ M), MGN3 (2 mg/mL), or MGN3 + TLR2i or TLR4i. Supernatants were collected to measure MCP-1 levels via ELISA (n=3). Chemotaxis plates were prepared with supernatants  $\pm$  MCP-1 blocking antibody (1 $\mu$ g/mL; R&D Systems) in lower chambers. After 1 hour at 37 °C, U937 monocytes ( $1 \times 10^6$  cells/mL) were added to upper chambers and incubated for 4 hours. Inserts were removed, and migrated cells in lower chambers were pelleted by centrifugation. Supernatants were discarded, and an MTT assay was performed as described in section 2.2.12, with absorbance read at 570nm and background subtracted at 690nm.

#### **4.3.6 Cathelicidin (LL37) Assay**

Macrophages ( $1 \times 10^6$  cells/mL) were cultured in RPMI CM with low (11mM) or high (30mM) glucose and treated with RS (2mg/mL), LPS (5 $\mu$ g/mL), or MGN3 (2mg/mL) for 24 hours. MRSA and PA broths were prepared as outlined in section 2.2.7. Cells were washed with PBS, and lysates were collected using MPER buffer (section 2.2.13.2). Half the lysates were treated with LL37 blocking antibody (2 $\mu$ g/mL), the other half with antibody dilution buffer (4% BSA). Lysates were incubated at 37 °C for 2 hours, then with MRSA or PA ( $2 \times 10^4$  CFU/mL) for 3 hours. Samples were plated on NA and incubated for 24 hours to assess bacterial recovery.

## 4.4 Results

### 4.4.1 The Direct Effect of MGN3 on MRSA and PA01 Growth

MGN3 did not directly affect MRSA or PA01 growth (Figure 4.4). Statistical analysis showed no significant difference between MGN3-treated and control groups for MRSA ( $P = 0.483$ ) or PA01 ( $P = 0.474$ ), indicating MGN3 did not directly affect bacterial growth.

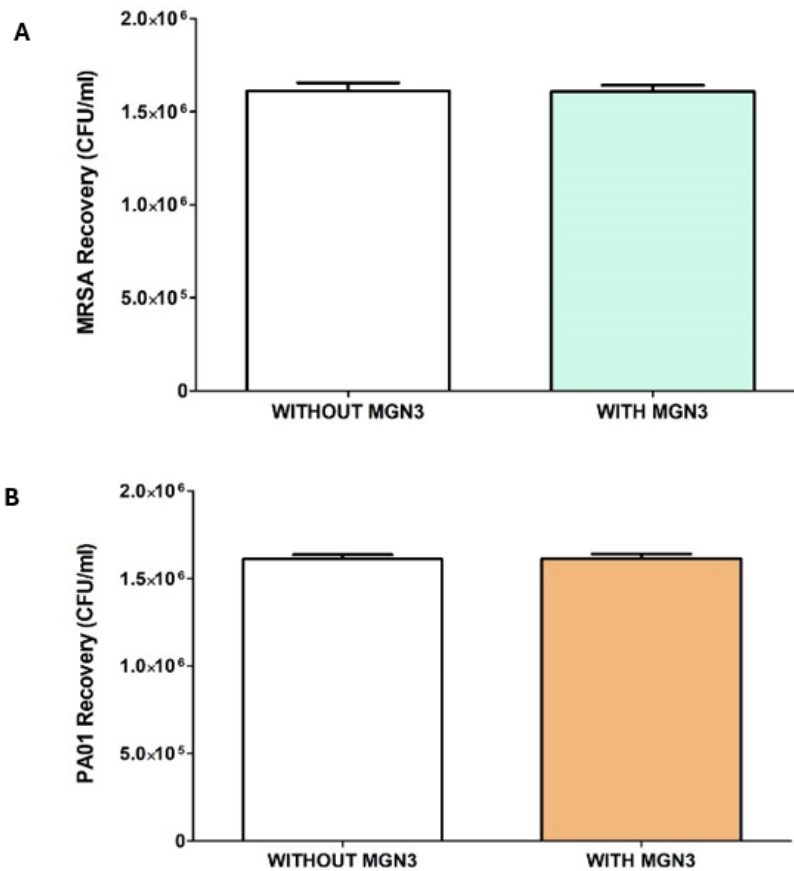


**Figure 4. 4: Direct Effect of MGN3 on MRSA and PA01 Growth.** Mean MRSA (A) and PA01 (B) recovery (CFU/ml) after incubation in 11mM glucose with/without MGN3 treatment for 3 hours. Columns and error bars indicate the mean MRSA recovery (CFU/ml)  $\pm$  the standard error of the mean (SEM) in all cases. No significant differences ( $P > 0.05$  determined by t-tests;  $n = 15$ ) were detected between MRSA/PA01 growth during MGN3 treatment and the corresponding negative control (NC) consisting of MRSA/PA01 grown in the absence of MGN3.

#### 4.4.2 The Effect of Glucose on MRSA and PA01 Growth

MRSA and PA01 recovery increased as glucose concentration increased (Figure 4.5). Statistical analysis showed MRSA and PA01 recovery significantly ( $P < 0.01$ ) increased with increasing glucose concentration compared to the corresponding 11mM.

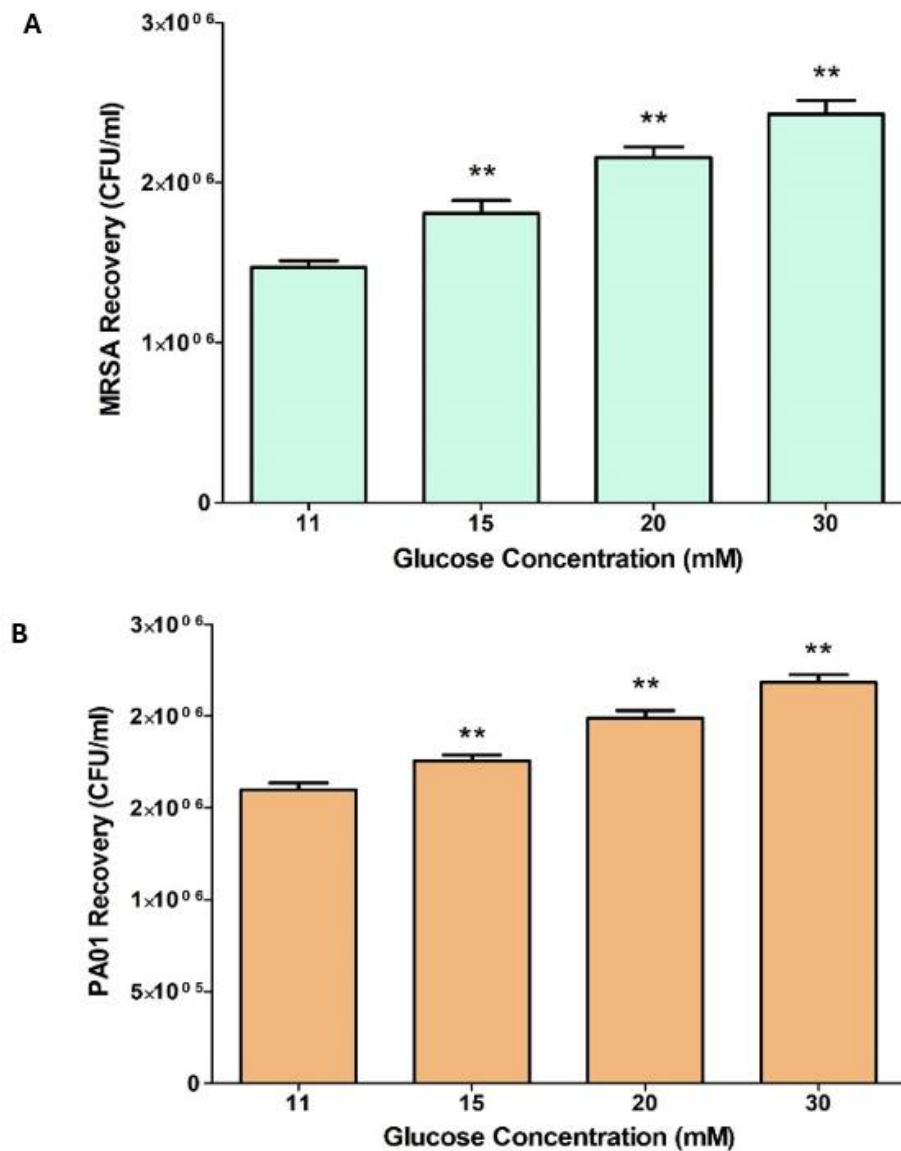


**Figure 4. 5: The Effect of Glucose on MRSA and PA01 Growth.** Mean MRSA (A) and PA01 (B) recovery (CFU/ml) after incubation in different glucose concentrations (11, 15, 20 and 30mM). Columns and error bars indicate the mean MRSA/PA01 recovery (CFU/ml)  $\pm$  the standard error of the mean (SEM) in all cases. Significant differences ( $P < 0.01$  determined by one-way ANOVAs;  $n = 18$ ) were detected in 15, 20 and 30mM glucose groups when compared to the control (11mM) group.

#### 4.4.3 The Effect of MGN3 on Phagocytosis of MRSA Biofilms

MRSA recovery increased with glucose concentration but decreased with LPS or MGN3 treatment. Higher MGN3 doses led to lower MRSA recovery, suggesting enhanced phagocytosis (Figure 4.6).

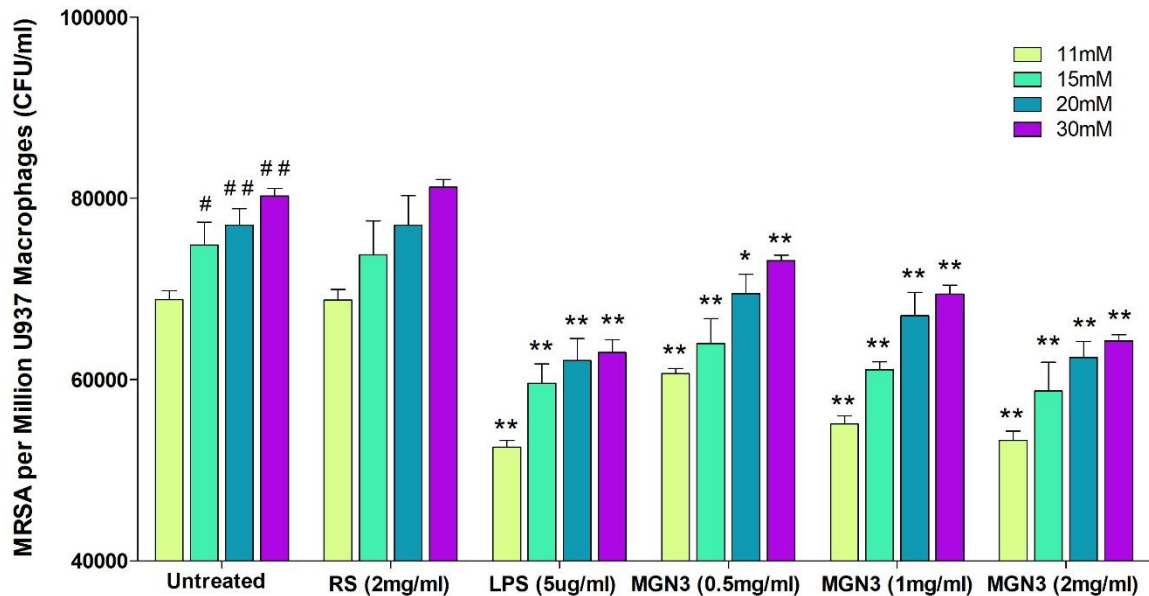


**Figure 4. 6: The Effect of MGN3 on the phagocytosis of MRSA Biofilms.** Mean MRSA recovery (CFU/ml) after incubation of MRSA biofilms with M1 macrophages cultured at different glucose concentrations (11, 15, 20 and 30mM) and treated with or without RS (2mg/ml), LPS (5ug/ml) or MGN3 (0.5, 1, 2mg/ml). Significant differences were seen when comparisons were made against the 11mM Untreated group (#  $P < 0.05$  and ##  $P < 0.01$  determined by one-way ANOVAs) and corresponding untreated groups (\* $P < 0.05$ , \*\*  $P < 0.01$  determined by one-way ANOVAs). Columns and error bars indicate the mean MRSA recovery (CFU/ml)  $\pm$  the standard error of the mean (SEM) in all cases ( $n = 18$ ).

The MRSA recovery significantly increased as glucose levels increased ( $P = 0.035$  15mM RPMI;  $P = 0.001$  20mM RPMI and  $P = 0.000$  30mM RPMI). There was no significant difference ( $P > 0.05$ ) in MRSA recovery between macrophages treated with RS and the corresponding untreated control cultured at the same glucose concentration (11, 15, 20 or 30mM). There was a prominent ( $P < 0.01$ ) reduction in MRSA recovery following incubation of M1 macrophages with LPS compared to untreated M1 macrophages cultured at the same glucose concentration (11, 15, 20 or 30mM). Similarly, there was a significant ( $P < 0.05$ ) reduction in MRSA recovery following incubation of M1 macrophages with the MGN3

treatments (0.5, 1 and 2.0mg/ml) compared to the untreated M1 macrophages cultured at the same glucose concentration (11, 15, 20 or 30mM).

#### 4.4.4 The Effect of MGN3 on Phagocytosis of PA01 Biofilms

PA01 recovery rose with increasing glucose levels but declined following LPS or MGN3 treatment. Reduced PA01 recovery at higher MGN3 doses indicated improved phagocytic activity (Figure 4.7).

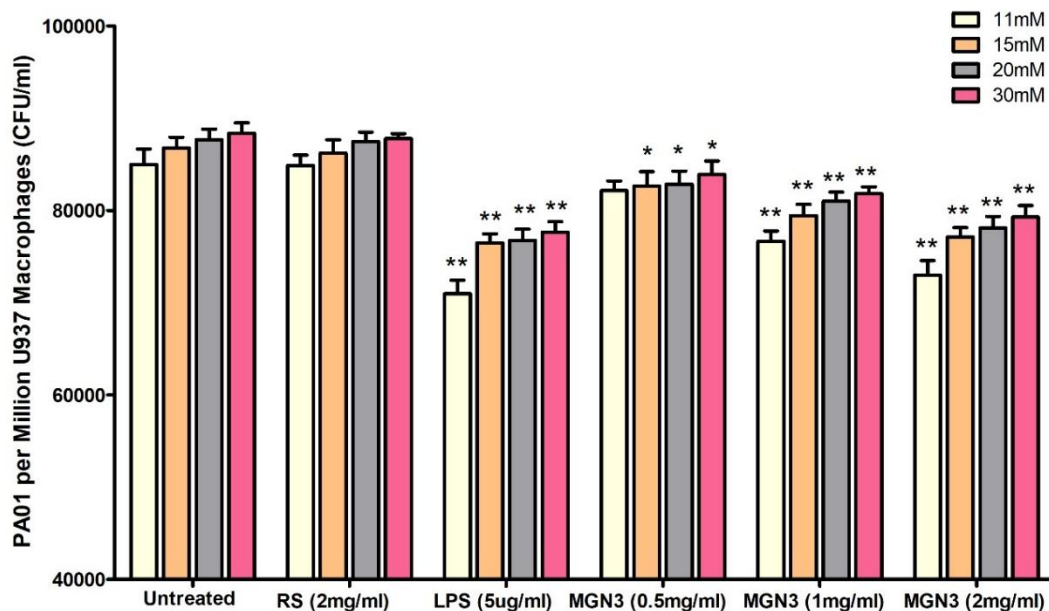


**Figure 4. 7: The Effect of MGN3 on the phagocytosis of PA01 biofilms.** Mean PA01 recovery (CFU/ml) after incubation in different glucose concentrations (11, 15, 20 and 30mM) and treatment with or without RS, with or without LPS and with or without MGN3 at different concentrations (0.5, 1, 2mg/ml). Significant differences were seen between when comparisons between corresponding untreated controls (\* $P < 0.05$  and \*\*  $P < 0.01$  determined by one-way ANOVAs). Columns and error bars indicate the mean MRSA recovery (CFU/ml)  $\pm$  the standard error of the mean (SEM) in all cases ( $n = 18$ ).

There was an increase in PA01 recovery as glucose levels increased, however the data was not significantly different ( $P > 0.05$ ). PA01 recovery significantly decreased following LPS treatments ( $P < 0.01$ ) when compared to corresponding untreated groups. There were significant decreases following 0.5mg/ml ( $P = 0.043$  15mM RPMI;  $P = 0.012$  20mM RPMI and  $P = 0.021$  30mM RPMI), 1mg/ml ( $P < 0.01$  for all cases) and 2mg/ml ( $P < 0.01$  for all cases) MGN3 treatments compared to untreated macrophages at the same glucose concentrations.

#### 4.4.5 The Contribution of TLR Signalling to MGN3-Mediated Phagocytosis of MRSA Biofilms

M1 macrophages treated with LPS or MGN3 had reduced MRSA recovery compared to the 11mM (Figure 4.8A) and 30mM (Figure 4.8B) glycaemic-equivalent untreated control. TLRi increased MRSA recovery compared to the corresponding control without TLRi at both 11 and 30mM glucose.

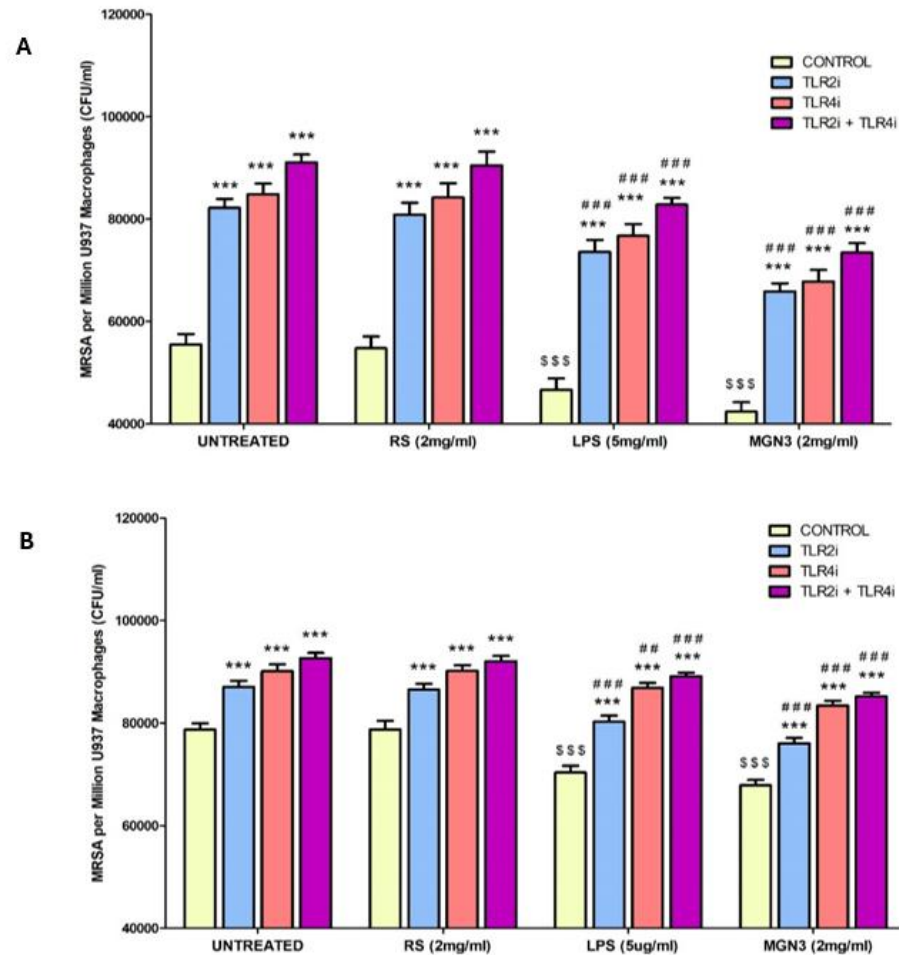


**Figure 4. 8: Contribution of TLR Signalling to MGN3-Mediated Phagocytosis of MRSA Biofilms Under Pre-diabetic and Hyperglycaemic Conditions.** M1 macrophages were cultured at low (A) (11mM) and high (B) (30mM) glucose concentration and treated with or without RS (2mg/ml), LPS (5µg/ml) or MGN3 (2mg/ml), alongside the absence/presence of TLR inhibitors (TLR2i, TLR4i or TLR2i+TLR4i) for 24 hours. Mean MRSA recovery (CFU/ml) was then determined following 1 hour of M1-MRSA interaction. LPS or MGN3, but not RS, treatment significantly (\$\$\$  $P < 0.001$  determined by t-tests;  $n = 12$ ) reduced MRSA recovery compared to the glycaemic-equivalent untreated control. The presence of TLR inhibition (TLRi) significantly increased MRSA recovery compared to the corresponding control lacking TLRi (\*\*\*)  $P < 0.001$  determined by t-tests;  $n = 12$ ). However, treatment of M1 macrophages with LPS or MGN3 in the presence of TLRi still significantly (###  $P < 0.001$  determined by t-tests;  $n = 12$ ) reduced MRSA biofilm recovery compared to untreated M1 macrophages in the presence of TLRi. Columns and error bars indicate the mean MRSA recovery (CFU/ml)  $\pm$  the standard error of the mean (SEM) in all cases.

Treatment of M1 macrophages with LPS or MGN3, but not RS, significantly (\$\$\$ P < 0.001) reduced MRSA recovery compared to the 11mM and 30mM glycaemic-equivalent untreated controls. Moreover, the presence of TLRi significantly increased MRSA recovery compared to the corresponding control lacking TLRi (\*\*\* P < 001) across all treatments, suggesting both the TLR2 and TLR4 pathways are at least in part mediating phagocytic activity in M1 macrophages at both pre-diabetic and hyperglycaemic conditions. The TLRi was partially additive with TLR2i+TLR4i exposure increasing MRSA recovery more than TLR2i or TLR4i alone (11 and 30mM), suggesting each receptor influences phagocytosis independently from the other receptor to some degree.

Neither TLR2 and/or TLR4 inhibition fully negated the observed reduction in MRSA biofilm recovery following MGN3 or LPS treatment of M1 macrophages, suggesting MGN3 and LPS may still be able to influence phagocytosis without the need for TLR2/TLR4 activation.

#### **4.4.6 The Contribution of TLR Signalling to MGN3-Mediated Phagocytosis of PA Biofilms**

M1 macrophages when treated with LPS or MGN3 resulted in reduced PA recovery compared to the 11mM (Figure 4.9A) and 30mM (Figure 4.9B) glycaemic-equivalent untreated control. TLRi increased MRSA recovery compared to the corresponding control without TLRi at both 11 and 30mM glucose.

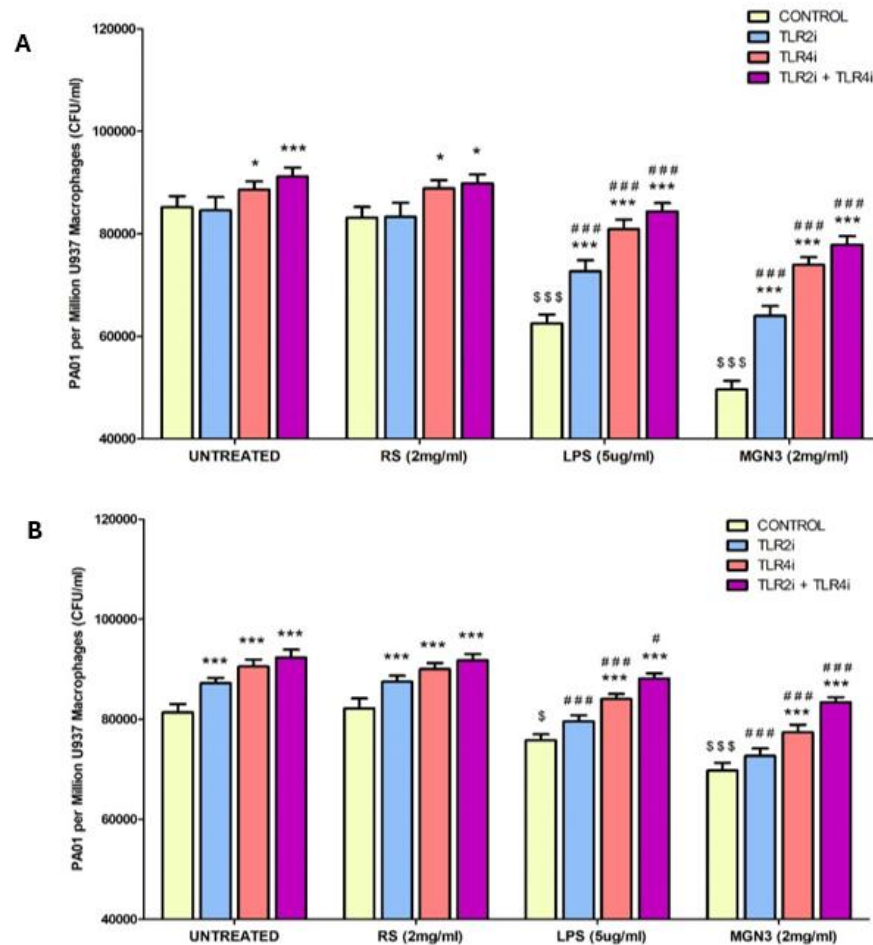


**Figure 4. 9: Contribution of TLR Signaling to MGN3-Mediated Phagocytosis of PA Biofilms Under Pre-diabetic and Hyperglycaemic Conditions** M1 macrophages were cultured at low (A) (11mM) and high (B) (30mM) glucose concentration and treated with or without RS (2mg/ml), LPS (5 $\mu$ g/ml) or MGN3 (2mg/ml), alongside the absence/presence of TLR inhibitors (TLRi: TLR2i, TLR4i or TLR2i+TLR4i) for 24 hours. Mean PA recovery (CFU/ml) was then determined following 1 hour of M1-PA interaction. LPS or MGN, but not RS, treatment significantly (\$\$\$  $P < 0.001$  determined by  $t$ -tests;  $n = 12$ ) reduced PA recovery compared to the glycaemic-equivalent untreated control. The presence of TLR4i inhibition significantly increased PA recovery compared to the corresponding control lacking TLR4i (\*  $P < 0.05$  and \*\*\*  $P < 0.001$  determined by  $t$ -tests;  $n = 12$ ). TLR2i significantly (\*  $P < 0.05$  and \*\*\*  $P < 0.001$  determined by  $t$ -tests;  $n = 12$ ) increased the recovery of PA biofilms only following interaction with LPS/MGN3-treated M1 macrophages. However, treatment of M1 macrophages with LPS or MGN3 in the presence of TLRi still significantly (###  $P < 0.001$  determined by  $t$ -tests;  $n = 12$ ) reduced MRSA biofilm recovery compared to untreated M1 macrophages in the presence of TLRi. Columns and error bars indicate the mean PA recovery (CFU/ml)  $\pm$  the standard error of the mean (SEM) in all cases.

Treatment of M1 macrophages with LPS or MGN, but not MGN, significantly (\$\$\$  $P < 0.001$ ) reduced PA recovery compared to the 11mM and 30mM glycaemic-equivalent untreated controls. Inhibition of TLR4 significantly (\*\*\*  $P < 0.001$ ) increased bacterial recovery under

both pre-diabetic and hyperglycaemic conditions, regardless of whether macrophages were pre-treated with RS, MGN, or LPS. At pre-diabetic conditions, TLR2 inhibition had no significant effect ( $P > 0.05$ ) on PA biofilm recovery following interaction with untreated or RS-treated macrophages, but significantly ( $P < 0.01$ ) increased recovery when macrophages were treated with LPS or MGN3. Conversely, under hyperglycaemic conditions (30mM), TLR2 inhibition significantly ( $P < 0.01$ ) increased PA recovery following interaction with untreated or RS-treated macrophages, while having no significant effect ( $P > 0.05$ ) after LPS or MGN3 treatment. Notably, inhibition of TLR2 and/or TLR4 did not fully negate the reduction in PA biofilm recovery induced by MGN3 or LPS treatment, suggesting these agents may enhance phagocytosis through mechanisms independent of TLR2/TLR4 activation.

#### **4.4.7 Effect of MGN3 on Growth Factor, Chemokine, Antimicrobial Peptide and Antimicrobial Enzyme Production**

Epidermal Growth Factor (EGF), Fibroblast Growth Factor 2 (FGF2) and Monocyte Chemoattractant Protein-1 (MCP-1) levels were measured in the M1 macrophage supernatants, while Cathelicidin (LL37) and lysozyme levels were measured in M1 macrophage cell lysates cultured in low (11mM) or high (30mM) glucose and treated for 24 hours with RS, LPS, or MGN3, with or without TLR2/TLR4 inhibition (see section 4.3.4).

##### **4.4.7.1 Secretion of Epidermal Growth Factor (EGF) by M1 macrophages**

EGF secretion increased under hyperglycaemic conditions in untreated M1 macrophages but was reduced by MGN3 and especially LPS. RS increased EGF under low, but not high, glucose. TLR2/4 inhibition elevated EGF levels under low glucose, including with RS, LPS, or MGN3. Under high glucose, only TLR4 inhibition increased EGF following LPS or MGN3, while TLR2 inhibition had little effect (Figure 4.10).

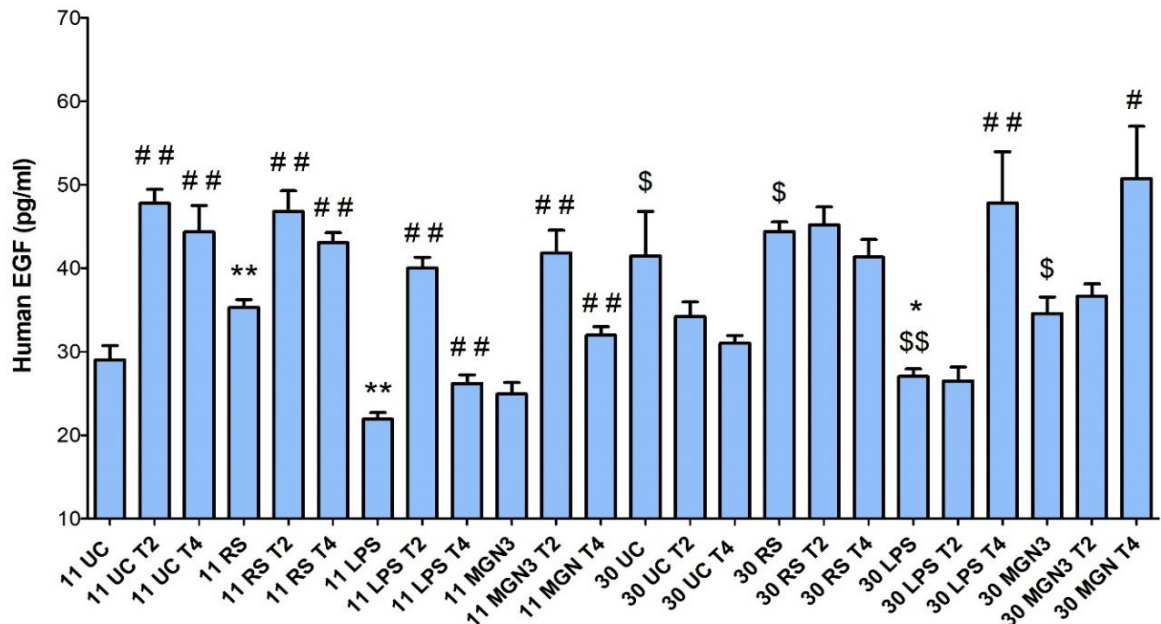


**Figure 4. 10: Secretion of Epidermal Growth Factor (EGF) by M1 macrophages.** EGF levels were measured in the supernatant of M1 macrophages cultured in low (11mM) or high (30mM) glucose and treated with RS, LPS or MGN3 in the presence/absence of TLR2 (T2) or TLR4 (T4) inhibition. There were significant differences between the treatment groups when compared to corresponding UC (\*  $P < 0.05$  and \*\*  $P < 0.01$  determined by t-tests;  $n = 10$ ), corresponding control (#  $P < 0.05$  and ##  $P < 0.01$  determined by t-tests;  $n = 10$ ) and 11mM treatments (without TLRs) (\$  $P < 0.05$  and \$\$  $P < 0.01$  determined by t-tests;  $n = 10$ ). Columns and error bars indicate human EGF levels (pg/ml)  $\pm$  the standard error of the mean (SEM) in all cases.

At high glucose, there were significant increase in EGF for the 30mM UC ( $P = 0.047$ ) compared to the 11mM UC, indicating hyperglycaemia stimulates M1 macrophage production of EGF. Both MGN3 and particularly LPS treatment significantly ( $P < 0.01$ ) impaired EGF production from M1 macrophages compared to the corresponding glycaemic control. Under low glucose conditions, there was a significant increase in EGF following treatment with RS ( $P < 0.01$ ) that was not observed under high glucose conditions.

TLR2/4 inhibition significantly increased ( $P < 0.01$ ) EGF secretion from untreated and RS-treated M1 macrophages under low glucose conditions but not at high glucose conditions when compared with treatments without TLR inhibition. A similar pattern of TLR2 or TLR4 inhibition increasing EGF levels was observed under pre-diabetic (11mM) conditions following treatment with LPS or MGN3. However, under hyperglycaemic (30mM) conditions, only TLR4 inhibition increased EGF levels following treatment of M1 macrophages with LPS or MGN3. In fact, TLR2 inhibition had little effect on M1-derived EGF levels at high glucose levels, regardless of treatment.

#### 4.4.7.2 Secretion of Fibroblast Growth Factor 2 (FGF2) by M1 macrophages

FGF2 was unchanged by high glucose alone. LPS and MGN3 increased FGF2 at high glucose but was reduced relative to untreated controls. RS decreased FGF2 at low glucose only. TLR2 inhibition increased FGF2 with MGN3 at high glucose and with LPS at low glucose. In untreated cells, TLR2 inhibition reduced FGF2 at low glucose, while TLR4 inhibition increased it at high glucose. With RS, both inhibitors raised FGF2 at low glucose; only TLR4 did so at high glucose (Figure 4.11).

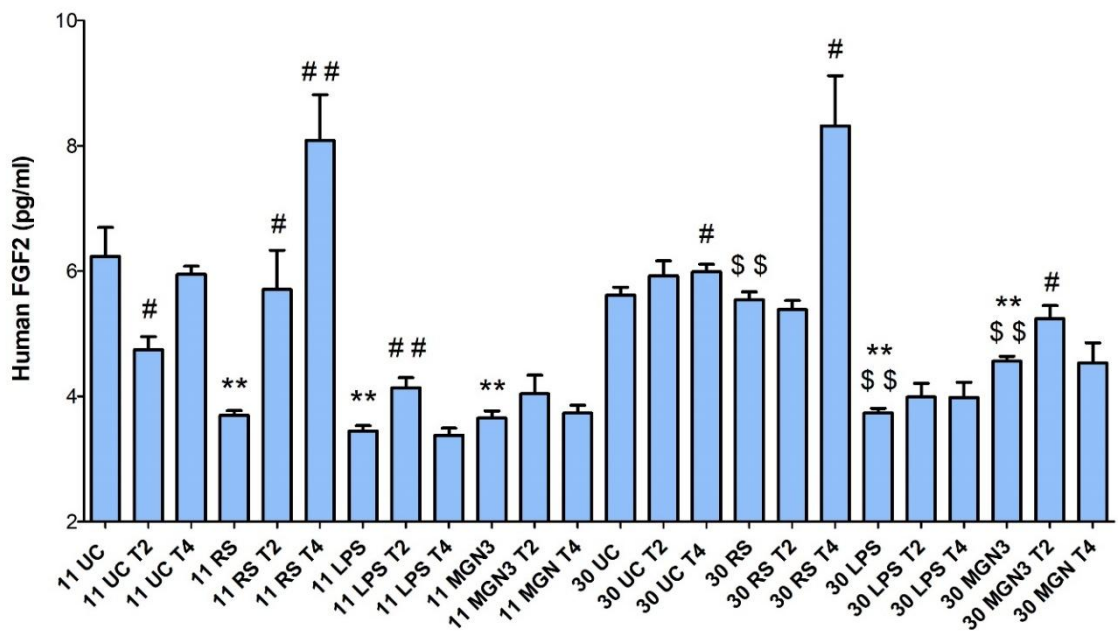


**Figure 4. 11: Secretion of Fibroblast Growth Factor 2 (FGF2) by M1 Macrophages.** FGF2 levels were measured in the supernatant of M1 macrophages cultured in low (11mM) or high (30mM) glucose and treated with RS, LPS or MGN3 in the presence/absence of TLR2 (T2) or TLR4 (T4) inhibition. There were significant differences between the treatment groups when compared to corresponding UC (\*  $P < 0.05$  and \*\*  $P < 0.01$  determined by t-tests;  $n = 8$ ), corresponding control (#  $P < 0.05$  and ##  $P < 0.01$  determined by t-tests;  $n = 8$ ) and 11mM treatments (without TLRs) (\$  $P < 0.05$  and \$\$  $P < 0.01$  determined by t-tests;  $n = 8$ ). Columns and error bars indicate human FGF2 levels (pg/ml)  $\pm$  the standard error of the mean (SEM) in all cases.

Hyperglycaemia (30mM) did not impact FGF levels compared to 11mM. LPS and MGN3 treatments at 30mM significantly increased ( $P < 0.01$ ) FGF2 compared to the 11mM but significantly decreased (in both 11 and 30mM) when compared to the corresponding UC. RS significantly reduced ( $P < 0.01$ ) FGF2 at 11mM but had no impact at 30mM compared to UC. TLRi had no effect on MGN3 responses at 11mM but TLR2i significantly increased ( $P =$

0.014) FGF2 at 30mM compared to MGN3 treatment without TLR2i. In direct contrast, TLRi had no effect on LPS responses at 30mM but TLR2i significantly increased ( $P = 0.003$ ) FGF2 at 11mM compared to LPS treatment without TLR2i. In untreated M1 macrophages, TLR2i significantly decreased ( $P = 0.015$ ) FGF2 at 11mM whereas TLR4i significantly increased ( $P = 0.049$ ) FGF2 at 30mM compared to untreated macrophages without TLR4i. In RS-treated macs, both TLR2i/TLR4i significantly increased ( $P < 0.05$ ) FGF2 at 11mM, whereas only TLR4i increased ( $P = 0.01$ ) FGF2 at 30mM compared to RS treatment without TLR4i.

#### 4.4.7.3 Secretion of Monocyte Chemoattractant Protein-1 (MCP-1) by M1 macrophages

MCP-1 levels were unaffected by high glucose alone. At low glucose, LPS and MGN3 had no effect, while at high glucose, RS, LPS, and MGN3 increased MCP-1 production. TLR inhibition had no impact under low (11mM) conditions, whereas at high (30mM) glucose TLR4 inhibition increased MCP-1 in untreated cells, while TLR2 inhibition reduced it in LPS-treated cells (Figure 4.12).

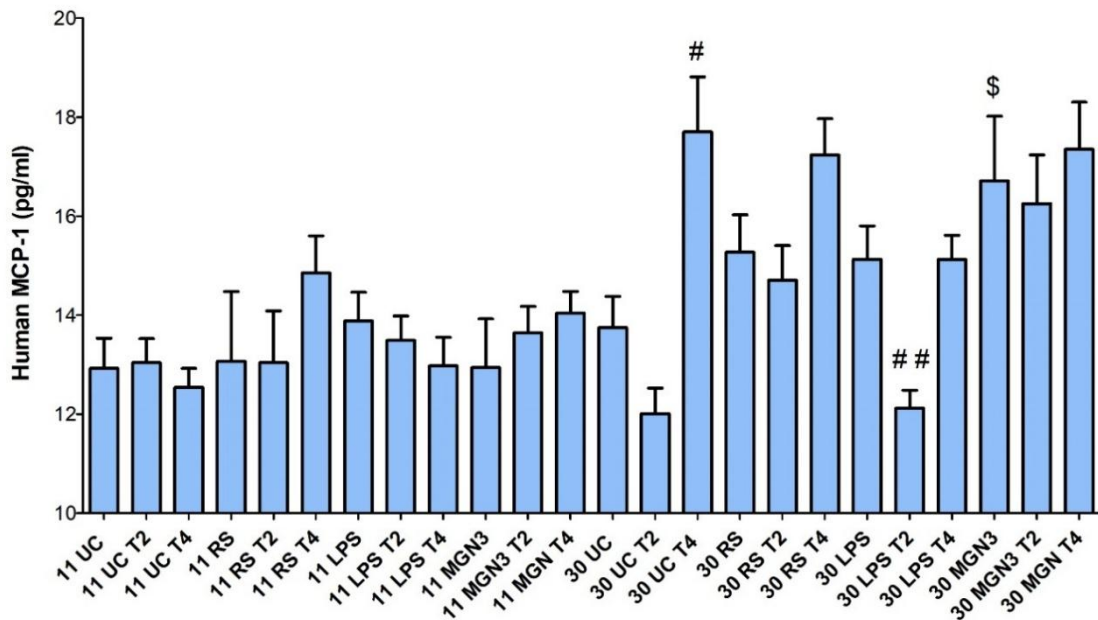


**Figure 4. 12: Secretion of Monocyte Chemoattractant Protein-1 (MCP-1) by M1 Macrophages.** MCP-1 levels were measured in the supernatant of M1 macrophages cultured in low (11mM) or high (30mM) glucose and treated with RS, LPS or MGN3 in the presence/absence of TLR2 (T2) or TLR4 (T4) inhibition. There were significant differences between the treatment groups when compared to corresponding control (#  $P < 0.05$  and ##  $P < 0.01$  determined by t-tests;  $n = 8$ ) and 11mM treatments (without TLRs) (\$  $P < 0.05$  and \$\$  $P < 0.01$  determined by t-tests;  $n = 8$ ). Columns and error bars indicate human MCP-1 levels (pg/ml)  $\pm$  the standard error of the mean (SEM) in all cases.

MCP-1 production did not appear to significantly increase in untreated M1 cells cultured at 30mM compared to those cultured at 11mM, suggesting hyperglycaemia alone was not influencing MCP-1 secretion from M1 macrophages. At low glucose levels LPS and MGN3 did not affect MCP-1 levels but at high glucose levels RS, LPS and MGN3 stimulated MCP-1 production. The TLR inhibitors appeared to have no effect on MCP-1 production under pre-diabetic conditions, and at high glucose inconsistent findings were seen, with TLR4i significantly increasing ( $P = 0.01$ ) MCP-1 production in untreated M1 cells compared to untreated M1s without TLR inhibitors but TLR2i significantly decreased ( $P = 0.003$ ) MCP-1 secretion in LPS-treated M1 macrophages compared to LPS treatment without TLR2i. MGN3 treatment at 30mM significantly increased ( $P = 0.038$ ) MCP-1 production compared to 11mM.

#### 4.4.7.4 Intracellular Cathelicidin (LL37) Levels in M1 Macrophages

High glucose reduced cathelicidin levels in untreated M1 macrophages. LPS increased cathelicidin at both glucose levels, while MGN3 reduced it. At low glucose, TLR2/TLR4 inhibition decreased cathelicidin in untreated and MGN3-treated cells, whereas at high glucose, inhibition increased cathelicidin production (Figure 4.13).

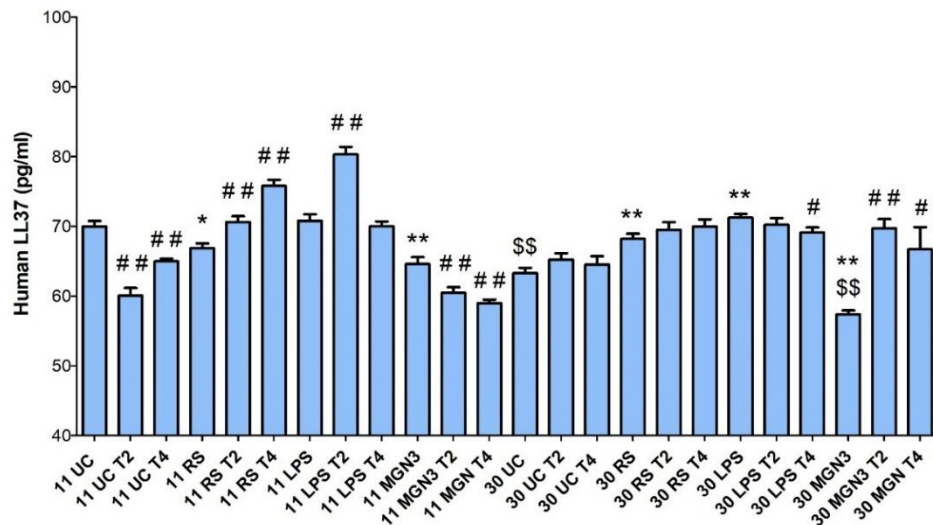


**Figure 4. 13: Secretion of Cathelicidin (LL37) by M1 Macrophages Lysates.** LL37 levels were measured in the supernatant of M1 macrophages cultured in low (11mM) or high (30mM) glucose and treated with RS, LPS or MGN3 in the presence/absence of TLR2 (T2) or TLR4 (T4) inhibition. There were significant differences between the treatment groups when compared to corresponding UC (\*  $P < 0.05$  and \*\*  $P < 0.01$  determined by t-tests;  $n = 9$ ), corresponding control (#  $P < 0.05$  and ##  $P < 0.01$  determined by t-tests;  $n = 9$ ) and 11mM treatments (without TLRs) (\$\$  $P < 0.01$  determined by t-tests;  $n = 9$ ). Columns and error bars indicate human LL37 levels (pg/ml)  $\pm$  the standard error of the mean (SEM) in all cases.

At high glucose conditions, there was a decrease in cathelicidin ( $P < 0.01$ ) in the 30mM UC when compared to the 11mM UC, suggesting hyperglycaemia impairs cathelicidin generation in M1 macrophages. At both glucose levels, LPS stimulated cathelicidin production ( $P < 0.01$ ) whereas MGN3 reduced LL37 production ( $P < 0.01$ ) compared to the UC. At low glucose, TLR2/TLR4 inhibition reduced cathelicidin production in untreated and MGN3-treated M1 macrophages, whereas at high glucose TLR2/TLR4 inhibition increased cathelicidin production.

#### 4.4.7.5 Intracellular Lysozyme Levels in M1 Macrophages

At low glucose, LPS and MGN3 strongly increased lysozyme production, with smaller increases at high glucose. TLR2/4 inhibition reduced lysozyme levels in MGN3-treated macrophages at both glucose levels, and in LPS-treated cells only at low glucose. In untreated and RS-treated cells at low glucose, TLR2 inhibition increased lysozyme, while TLR4 inhibition decreased it. No effects were observed at high glucose (Figure 4.14).

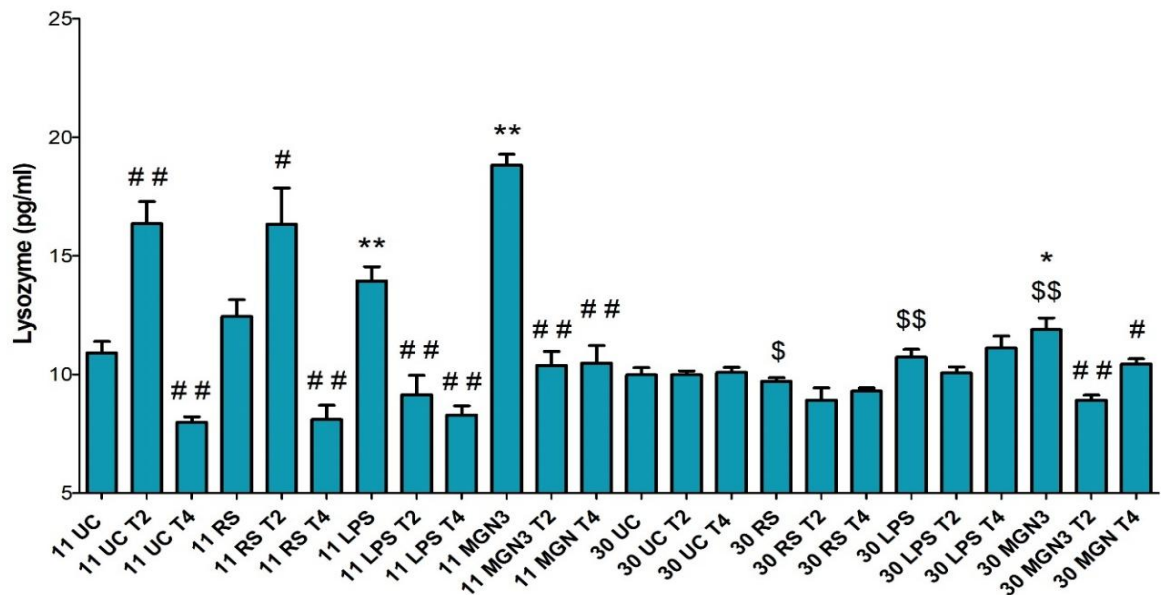


**Figure 4. 14: Intracellular levels of Lysozymes in M1 Macrophages.** Lysozyme levels were measured in the supernatant of M1 macrophages cultured in low (11mM) or high (30mM) glucose and treated with RS, LPS or MGN3 in the presence/absence of TLR2 (T2) or TLR4 (T4) inhibition. There were significant differences between the treatment groups when compared to corresponding UC (\*  $P < 0.05$  and \*\*  $P < 0.01$  determined by t-tests;  $n = 6$ ), corresponding control (#  $P < 0.05$  and ##  $P < 0.01$  determined by t-tests;  $n = 6$ ) and 11mM treatments (without TLRs) (\$\$  $P < 0.01$  determined by t-tests;  $n = 6$ ). Columns and error bars indicate Lysozyme levels (pg/ml)  $\pm$  the standard error of the mean (SEM) in all cases.

At low glucose levels there were very large increases ( $P < 0.01$ ) in lysozyme production in both LPS and MGN3-treated M1 macrophages compared to the UC. At high glucose smaller increases in lysozyme production were observed in M1 macrophages treated with LPS ( $P = 0.002$ ) or MGN3 ( $P = 0.01$ ) compared to the UC. At both low and high glucose conditions, TLR2/4 inhibition significantly decreased lysozyme production in M1 macrophages treated with MGN3 compared to M1 cells treated MGN3 in the absence of TLR inhibition. A similar reduction in lysozyme production was seen for LPS following TLR2/4 inhibition, but only at low glucose conditions. In contrast, an increase in lysozyme production was seen following TLR2 inhibition and a decrease was seen following TLR4 inhibition in untreated and RS-treated M1 macrophages at low (but not high) glucose levels compared to without TLR inhibition.

#### **4.4.8 Chemotaxis Activity of U937 Monocytes in Response to Macrophage, Keratinocyte and Fibroblast-Derived Supernatant**

Supernatant derived from untreated M1 macrophages (Figure 4.15A), keratinocytes (Figure 4.15B) or fibroblasts (Figure 4.15C) cultured under high (30mM) glucose reduced U937 monocyte chemotaxis, and this was reversed by MCP-1 inhibition. TLR2 inhibition of untreated M1 macrophages, keratinocytes or fibroblasts cultured at high glucose increased monocyte chemotaxis compared to corresponding untreated cells in the absence of TLR2 inhibition, while TLR effects were minimal on supernatant derived from corresponding untreated cells cultured at low glucose. Supernatants from LPS and MGN3-treated macrophages or fibroblasts had little impact on monocyte chemotaxis, whereas MGN3 treatment of keratinocytes cultured at high glucose reduced monocyte chemotaxis. Supernatant from TLR4 inhibition of LPS-stimulated M1 macrophages, keratinocytes or fibroblasts cultured at low (11mM) glucose reduced monocyte chemotaxis. Similarly, supernatant from TLR4 inhibition of MGN3-stimulated M1 macrophages or keratinocytes cultured at high (30mM) glucose reduced monocyte chemotaxis.

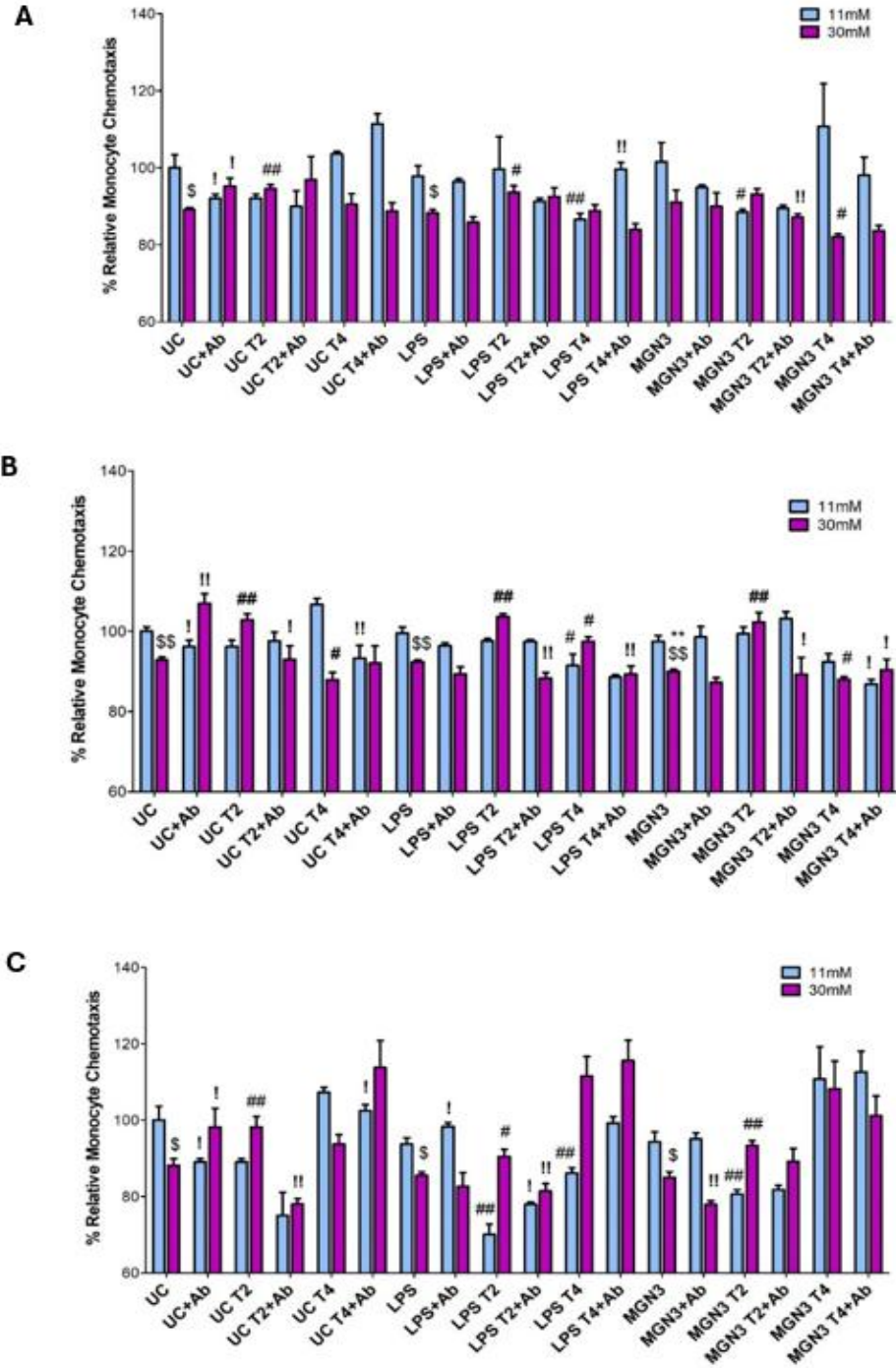


**Figure 4. 15: The Effect of Macrophage, Keratinocyte and Fibroblast Supernatant on U937 Monocyte Chemotaxis.** Supernatant from M1 macrophages (A), keratinocytes (B) or fibroblasts (C) cultured in low (11mM) or high (30mM) glucose and treated with LPS or MGN3 in the presence/absence of TLR2 (T2) or TLR4 (T4) inhibition and MCP-1 blocking antibody (+Ab), was evaluated on monocyte chemotaxis. There were significant differences between the treatment groups when compared to the corresponding 11mM treatments (\$  $P < 0.05$  and \$\$  $P < 0.01$  determined by t-tests;  $n = 8$ ), UC (\*\*  $P < 0.01$  determined by t-tests;  $n = 8$ ), treatment lacking TLR inhibition (#  $P < 0.05$  and ##  $P < 0.01$  determined by t-tests;  $n = 8$ ) or treatment lacking Ab (!  $P < 0.05$  and !!  $P < 0.01$  determined by t-tests;  $n = 8$ ). Columns and error bars indicate % Relative Monocyte Chemotaxis  $\pm$  the standard error of the mean (SEM) in all cases.

U937 monocyte chemotaxis was significantly reduced by supernatants from M1 macrophages cultured at hyperglycaemic conditions compared to pre-diabetic conditions ( $P = 0.015$ ; 89.2% vs. 100%) (Figure 4.15A). This inhibition was reversed by MCP-1 inhibition ( $P = 0.04$ ; 94.5% at 30mM vs. 92% at 11mM), suggesting MCP-1 promotes chemotaxis at 11mM but inhibits it at 30mM. TLRi had no effect at 11mM, but TLR2i significantly increased chemotaxis at 30mM ( $P < 0.01$ ) when compared to 30mM UC group without TLR2i. MCP-1 inhibition reduced chemotaxis at 11mM ( $P = 0.027$ ) and increased it at 30mM ( $P = 0.04$ ), reinforcing its dual role depending on glucose levels. MGN3/LPS-treated M1 macrophage supernatants had no significant effect on chemotaxis at either glucose level. However, at 11mM, TLR4i with LPS and TLR2i with MGN3 both reduced chemotaxis ( $P < 0.05$ ) compared to the corresponding treatments without TLRi. At 30mM, TLR2i increased ( $P = 0.019$ ) and TLR4i decreased ( $P = 0.024$ ) chemotaxis compared to the corresponding treatments without TLRi. These findings indicate LPS acts via TLR4 at 11mM and TLR2 at 30mM, while MGN3 acts through TLR2 at 11mM and TLR4 at 30mM.

U937 monocyte chemotaxis was significantly reduced by supernatants from keratinocytes cultured at hyperglycaemic compared to pre-diabetic conditions ( $P < 0.01$ ; 92.9% vs. 100%) (Figure 4.15B). This was reversed following MCP-1 inhibition ( $P < 0.01$ ; 106.9% vs. 96.2%), suggesting MCP-1 promotes chemotaxis at 11mM but inhibits it at 30mM. MCP-1 inhibition reduced chemotaxis at 11mM ( $P = 0.038$ ) and increased it at 30mM ( $P < 0.01$ ), confirming this dual role. TLRi had no effect at 11mM, but at 30mM, TLR2i increased ( $P < 0.01$ ) and TLR4i inhibition decreased ( $P = 0.021$ ) chemotaxis compared to the corresponding UC without TLRi. MGN3/LPS-treated keratinocyte supernatants at 11mM had no significant effect, but MGN3 at 30mM significantly reduced chemotaxis ( $P < 0.01$ ) compared to the 30mM UC. At 11mM, TLR4i with LPS reduced chemotaxis ( $P = 0.031$ ) compared to 11mM UC. At 30mM, LPS-treated supernatants with TLR2i or TLR4i significantly increased chemotaxis ( $P < 0.05$ ) compared LPS treatment without TLRi. MGN3-treated supernatants at 30mM showed increased chemotaxis with TLR2i ( $P < 0.01$ ) and decreased chemotaxis with TLR4i ( $P = 0.044$ ) compared to MGN3 treatment without TLRi. These results suggest that under hyperglycaemia, MCP-1 inhibits monocyte chemotaxis, and that TLR2/4

modulate MGN3 and LPS responses in a glucose-dependent manner—LPS via TLR4 (11mM) and TLR2/4 (30mM); MGN3 via TLR2 (11mM) and TLR4 (30mM).

U937 monocyte chemotaxis was significantly reduced by supernatants from fibroblasts cultured at hyperglycaemic conditions compared to pre-diabetic conditions ( $P = 0.016$ ; 88.1% vs. 100%). This was reversed following MCP-1 inhibition ( $P = 0.042$ ; 98.2% vs. 89%), suggesting MCP-1 promotes chemotaxis at 11mM but inhibits it at 30mM. MCP-1 inhibition reduced chemotaxis at 11mM ( $P = 0.021$ ) and increased it at 30mM ( $P = 0.042$ ) compared to chemotaxis without MCP-1 inhibition, consistently indicating a dual role. TLRi had no effect at 11mM, but TLR2i significantly increased chemotaxis at 30mM ( $P = 0.005$ ) compared to 30mM UC without TLRi. MGN3/LPS-treated fibroblast supernatants had no significant effect on chemotaxis at either glucose level. However, at 11mM, TLR2i and TLR4i with LPS, and TLR2i with MGN3, significantly reduced chemotaxis ( $P < 0.01$ ) compared to the corresponding treatments without TLRi. At 30mM, TLR2i significantly increased chemotaxis in both LPS and MGN3-treated groups ( $P < 0.05$ ) compared to the corresponding treatments without TLRi. These findings suggest that fibroblast-derived MCP-1 enhances chemotaxis under normoglycaemia but inhibits it under hyperglycaemia, and that TLR2 modulates responses to LPS and MGN3, especially under high glucose conditions.

#### **4.4.9 Antimicrobial Activity of Cathelicidin (LL37) from M1 Cell Lysates**

M1 macrophages cultured in low or high glucose were treated for 24 hours with RS, LPS, or MGN3. Cell lysates were incubated with or without cathelicidin (LL37) blocking antibody for 2 hours, then exposed to MRSA or PA01 ( $2 \times 10^4$  CFU/ml) for 3 hours at 37 °C. Bacterial recovery was assessed after 24-hour incubation on agar plates (see section 4.3.6).

##### **4.4.9.1 The Antibacterial Effect of Cathelicidin (LL37) from M1 Cell Lysates against MRSA**

M1 cell lysates reduced MRSA recovery, particularly in the presence of LPS, with the cathelicidin blocking antibody (AB) partly reversing the antibacterial response of cell lysates (Figure 4.16).

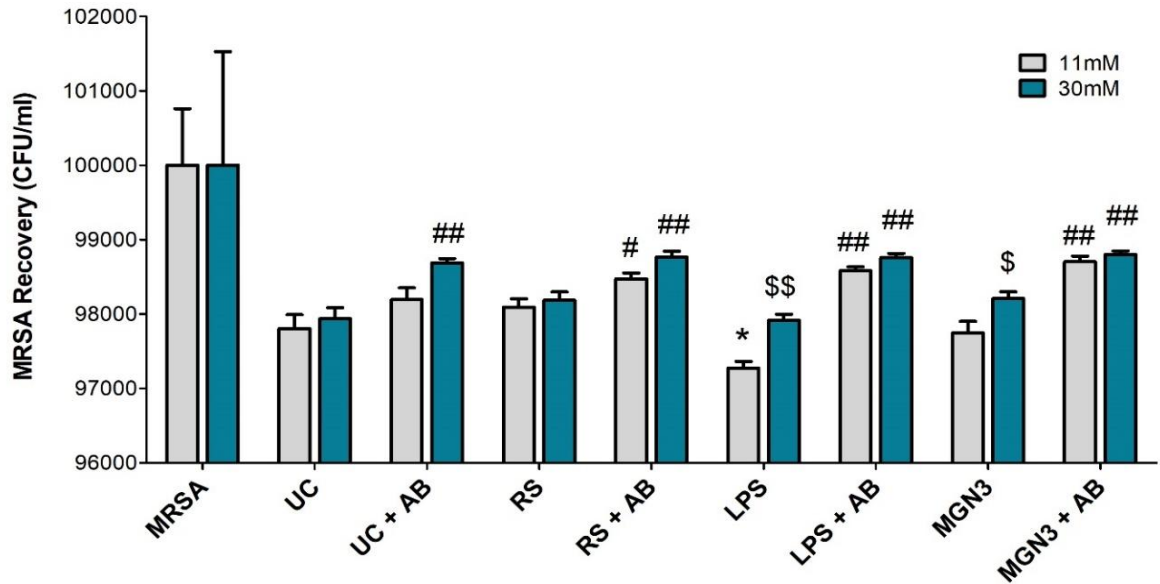


**Figure 4. 16: The Antibacterial Effect of Cathelicidin (LL37) from M1 Cell Lysates against MRSA .** Mean MRSA recovery (CFU/ml) after incubation of M1 macrophages in 11mM and 30mM glucose, and treatment with RS (2mg/ml), LPS (5ug/ml) or MGN3 (2mg/ml) in the presence or absence of a cathelicidin blocking antibody (AB). Significant differences were seen between the groups when comparisons were made against the corresponding 11mM treatment (\$  $P < 0.05$  and \$\$  $P < 0.01$  determined by t-tests;  $n = 10$ ), UC (\*  $P < 0.05$  determined by t-tests;  $n = 10$ ) and treatment lacking AB (#  $P < 0.05$  and ##  $P < 0.01$  determined by t-tests;  $n = 10$ ). Columns and error bars indicate the mean MRSA recovery (CFU/ml)  $\pm$  the standard error of the mean (SEM) in all cases.

The results showed a significant ( $P < 0.01$ ) antibacterial activity of all M1 cell lysates against MRSA, indicating the lysate constituents had substantial antibacterial activity under both pre-diabetic and hyperglycaemic conditions. The addition of cathelicidin blocking antibody (+AB) to M1 cell lysates significantly ( $P < 0.01$ ) increased bacterial recoveries across all treatments, suggesting cathelicidin was a major antibacterial constituent of the isolated M1 cell lysates. MGN3 treatment failed to enhance the antibacterial activity, suggesting the enhanced phagocytic activity against MRSA observed earlier in this chapter following MGN3 stimulation of M1 macrophages must require other mechanisms or factors beyond just the antibacterial activities of M1 intracellular constituents.

#### 4.4.9.2 The Antibacterial Effect of Cathelicidin (LL37) from M1 Cell Lysates Against PA

M1 cell lysates suppressed PA01 growth, again partly via cathelicidin (Figure 4.17).

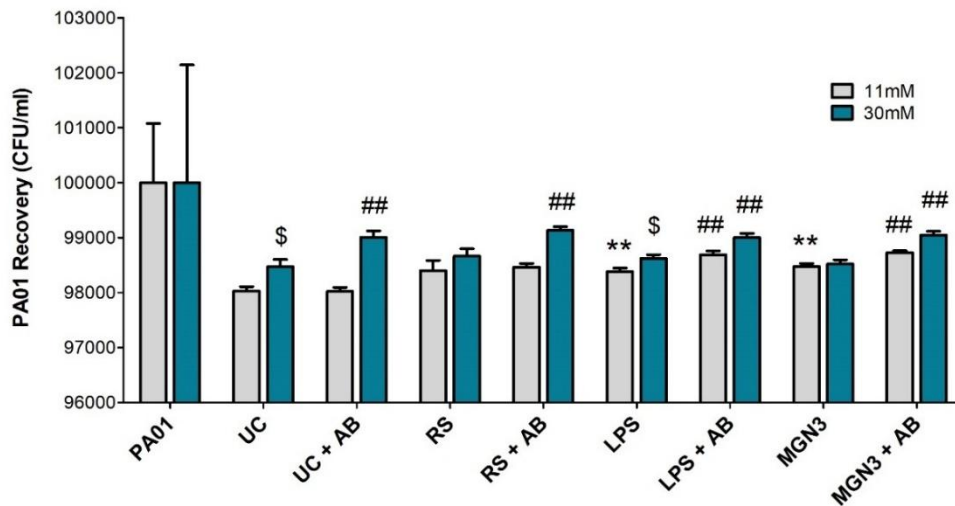


**Figure 4. 17: The Antibacterial Effect of Cathelicidin (LL37) from M1 Cell Lysates Against PA01.** Mean PA01 recovery (CFU/ml) after incubation of M1 macrophages in 11mM and 30mM glucose, and treatment with RS (2mg/ml), LPS (5ug/ml) or MGN3 (2mg/ml) in the presence or absence of a cathelicidin blocking antibody (AB). Significant differences were seen between the groups when comparisons were made against the corresponding 11mM treatment (\$  $P < 0.05$  determined by t-tests;  $n = 10$ ), UC (\*\*  $P < 0.01$  determined by t-tests;  $n = 10$ ) and Ab groups (##  $P < 0.01$  determined by t-tests;  $n = 10$ ). Columns and error bars indicate the mean PA01 recovery (CFU/ml)  $\pm$  the standard error of the mean (SEM) in all cases.

The results showed a significant ( $P < 0.01$ ) antibacterial activity of all M1 cell lysates against PA01, indicating the lysate constituents had substantial antibacterial activity under both pre-diabetic and hyperglycaemic conditions. The addition of cathelicidin blocking antibody (+AB) to M1 cell lysates significantly ( $P < 0.01$ ) increased bacterial recoveries across all treatments, suggesting cathelicidin was a major antibacterial constituent of the isolated M1 cell lysates but unlikely to be the only antibacterial mediator present. Collectively these findings suggest that M1 cell lysates had direct antibacterial activity against PA01, with cathelicidin appearing to be at least one of the major constituents present in the lysates. LPS and MGN3 treatment failed to enhance the antibacterial activity, suggesting the enhanced phagocytic activity against PA01 observed earlier in this Chapter following MGN3 and LPS stimulation of M1 macrophages must require other (additional) mechanisms or factors beyond just the antibacterial activities of M1 intracellular constituents.

## 4.5 Discussion

This study examined how MGN3 influences monocyte/macrophage function including chemotaxis, phagocytosis and the production of growth factors, chemokines, antimicrobial peptides and antimicrobial enzymes under varying glucose levels.

The direct effect of MGN3 on bacterial biofilm formation was tested to understand if MGN3 could directly influence bacterial growth in any way. Data indicated MGN3 had no direct effect on MRSA ( $P = 0.965$ ) or PA ( $P = 0.949$ ) bacterial biofilm growth (Figures 2 and 5), suggesting MGN3 does not have any antimicrobial or bacteriostatic activities, nor any stimulatory effects on biofilm formation. This confirmed that changes in bacterial recovery following treatment of macrophages with MGN3 were due to macrophage-mediated changes in phagocytosis rather than any direct of MGN3 on biofilm growth.

Investigations showed that hyperglycaemia increased bacterial biofilm formation, and this is supported by several published findings (Lu *et al*, 2020; Vitko *et al*, 2016; She *et al*, 2019; Huynh *et al*, 2012). Data showed a significant increase in bacterial recovery when MRSA and PA biofilms were exposed to 20mM or 30mM glucose compared to recovery levels observed following exposure to 11mM glucose. This suggests that the bacteria are using glucose as a possible energy source, leading to increased bacterial biofilm growth (Vitko *et al*, 2016; de Oliveira *et al*, 2021). A clinical study has shown patients with glucose detected in bronchial aspirates were significantly more likely to develop MRSA infections than patients without detectable glucose (Phillips *et al*, 2005). Given MRSA and PA are common pathogens isolated from DFUs (Luo *et al*, 2020; Kifelew *et al*, 2024), these findings suggest both these wound pathogens are likely to thrive and benefit from *in vivo* uncontrolled hyperglycaemic conditions in diabetic patients. It has been shown that high glucose increases the strength of MRSA biofilms (Luo *et al*, 2020; You *et al*, 2014). Moreover, MRSA growth was found to increase in the presence of glucose compared to other monosaccharides (e.g. fructose) or disaccharides (e.g. sucrose) (Luo *et al*, 2020). The fermentation of glucose also assists in the aggregation of MRSA which promotes biofilm formation (Vitko *et al*, 2016; Luo *et al*, 2019). She *et al*, (2019) showed PA biofilms taken from clinical isolates results in larger biofilms when grown in high glucose medium. Interestingly, the authors did not see an increase in

planktonic PA bacterial growth with elevated glucose levels and concluded that elevated glucose levels lead to increased biofilm formation indirectly by promoting bacterial adhesion rather than directly inducing bacterial proliferation itself.

The data showed as glucose levels increased the phagocytic ability of macrophages was reduced, resulting in increased bacterial recovery (both MRSA and PA01). This was due to hyperglycaemia impairing the phagocytic ability of macrophages. Other studies done using macrophages isolated from diabetic patients have also shown phagocytosis is impaired during hyperglycaemic conditions (Pavlou *et al*, 2018; Sousa *et al*, 2023; Lecube *et al*, 2011).

Moreover, the data indicated that as glucose concentration increased bacterial recovery increased, suggesting hyperglycaemia was impairing the phagocytic activity of the M1 macrophages. In line with these findings, Pavlou *et al*, (2018) showed that long term exposure to high glucose led to enhanced proinflammatory cytokine (TNF $\alpha$ ) expression but reduced NO production and phagocytosis in LPS/INF $\gamma$  polarized human bone marrow-derived M1 macrophages. Megawati *et al*, 2022 also showed macrophages grown in high glucose (35mM) medium had significantly higher TNF $\alpha$  levels when exposed to high levels of LPS (2 $\mu$ g/ml). This supporting evidence closely mirrors *in vivo* findings observed in diabetic patients that are showing elevated TNF $\alpha$  but impaired phagocytosis and NO production (Xu *et al*, 2013; Tessari *et al*, 2010). The idea that hyperglycaemia results in elevated proinflammatory cytokines is further supported by Grosick *et al*, (2018) and it has been suggested this may be attributed to abnormalities within the H3K9 methyltransferase mechanistic pathways, which would disturb the epigenetic state within the immune cells (Li *et al*, 2016; Raiymbek *et al*, 2020).

The findings showed a reduction in MRSA and PA recovery from biofilms following interaction with M1 macrophages treated with either LPS or 2.0mg/ml MGN3 compared with corresponding untreated controls, indicative of enhanced host-pathogen engagement and subsequent phagocytosis of bacteria. Given the structural similarities between LPS and MGN3 (Fadel *et al*, 2018; Ogawa *et al*, 2005), these findings open the possibility that MGN3 and LPS may (in part) act through the same pathways to stimulate phagocytosis. Indeed, it has been shown (Asif, 2020; Tan, 2018) that MGN3 competes with LPS for the TLR4 receptor

on the surface of macrophages. Moreover, hyperglycaemia has been shown to induce TLR4 expression in LPS/IFN- $\gamma$  polarized M1 macrophages (Pavlou *et al*, 2018).

Generally, published literature shows that MGN3 has a positive effect on macrophage function under hyperglycaemic conditions, particularly in relation to phagocytosis. MGN3 significantly reversed the hyperglycaemia-induced impairment of phagocytic function of resting M0 macrophages (Asif, 2020). Ghoneum *et al*, 2008 demonstrated that MGN3 therapy significantly boosted the phagocytosis of *E. coli* by both monocytes and neutrophils obtained from human peripheral blood. It has been demonstrated that prolonged exposure to rice brans can teach monocyte-derived macrophages to deliver a more efficient immune response through dectin-1 pathway stimulation (Moerings *et al*, 2022).

However, this is the first investigation to confirm the effect of MGN3 on the clearance of bacterial biofilms by M1 macrophage under hyperglycaemic conditions. There are multiple different ways this work could be expanded and explored further in the future. For example, the host-pathogen interaction period can be extended beyond 1 hour in future experiments and a wider MGN3 exposure period could be investigated to determine optimal treatment timings for each wound pathogen. Similarly, a range of biofilm densities could be investigated along with multi-species biofilms to model DFU infections more closely. The use of additional biofilm disrupters (e.g. surfactants such as poloxamers) could provide synergistic effects by breaking up dense biofilm formations and allowing greater penetration of MGN3-treated M1 macrophages into the infection site.

Currently the Ashworth laboratory at Manchester Metropolitan University is undergoing some promising (currently unpublished) *ex vivo* work exploring the effect of MGN3 on phagocytic activity of macrophages derived from the peripheral blood of DFU patients. The idea is to determine whether the findings of this study can be replicated by evaluating the influence of MGN3 on the clearance of clinical wound pathogens by corresponding blood-derived macrophages obtained from the same DFU patient at the time of infection (Ashworth, *personal communication*).

There was a direct correlation between exposure of M1 macrophages to high glucose levels and an increase in bacterial recovery of both MRSA and PA01 biofilms following 1 hour of

M1-MRSA/PA interaction. These findings are indicative of impaired M1 phagocytic function given that only the M1 macrophages were pre-exposed to chronic hyperglycaemia prior to host-pathogen interaction in these sets of experiments. However, in an *in vivo* DFU environment, both macrophages and wound bacteria could be exposed to chronic hyperglycaemia, leading not only to a detrimental effect on phagocytic activity of macrophages but also increased bacterial colonisation and/or biofilm formation (in line with the direct effect of glucose on biofilm formation found in section 4.4.2). Indeed, a combination of bacterial growth and impaired phagocytic function has been reported to make diabetic wounds difficult to treat (Baig *et al*, 2022).

It was again noted that both LPS and MGN3 treatment significantly reduced MRSA and PA bacterial recovery, indicative of enhanced phagocytosis, following prolonged exposure of M1 macrophages to 11mM or 30mM glucose. Lui *et al*, (2001) showed that LPS stimulation of macrophages from diabetic mice increases TLR2/4 expression which could potentially promote phagocytosis by providing greater TLR availability. Given previous projects carried out in the Ashworth laboratory (Tan, 2018; Asif, 2020) have shown that MGN3 competes with LPS for TLR4 and dectin-1 receptors in simple planktonic bacterial wound infection models, this project aimed to expand the understanding of potential mechanistic signalling pathways through which MGN3 may act by investigating TLR2 and TLR4 signalling in more complex biofilm wound infection models.

For the gram-positive MRSA biofilm, inhibition of TLR2 and particularly TLR4 significantly increased bacterial recovery under pre-diabetic or hyperglycaemic conditions, regardless of whether M1 macrophages were exogenously treated or not with RS/MGN3/LPS prior to bacterial interaction. Furthermore, combined TLR2+TLR4 inhibition led to a partially additive effect. Collectively, these findings suggest that activation of TLR2 and TLR4 signalling inherently influences the phagocytic activity of M1 macrophages against MRSA, possibly through the binding of microbial-derived ligands (Takeda *et al*, 2003), or even endogenous ligands (Yu *et al*, 2010) secreted by M1 macrophages. Indeed, the TLRs are somewhat promiscuous in nature and can be activated by multiple ligands (Takeda *et al*, 2003). Moreover, TLRs can work in concert with each other, forming homodimers or heterodimers to recognise different pathogens and induce subsequent immune responses

(Colleselli *et al*, 2023; Farhat *et al*, 2008). For example, TLR4 homodimers are induced after exposure to LPS from Gram-negative bacteria whereas TLR2 often forms heterodimers with TLR1 or TLR6 that recognize distinct bacterial-derived products (Colleselli *et al*, 2023). It has also been shown that Gram-positive and Gram-negative bacteria can activate different TLR2 dimers (Farhat *et al*, 2008).

For the Gram-negative PA biofilm, inhibition of TLR4 significantly increased bacterial recovery, indicative of enhanced phagocytosis, under pre-diabetic or hyperglycaemic conditions, and this response was observed regardless of whether M1 macrophages were exogenously treated with or without RS/MGN3/LPS prior to bacterial interaction. However, the involvement of TLR2 in M1-mediated phagocytosis of PA biofilms was less prominent and more nuanced than for MRSA biofilm clearance. This may not be surprising given LPS derived from Gram-negative bacteria like PA is typically recognised by TLR4 (Ciesielska *et al*, 2021). There was no significant ( $P > 0.05$ ) evidence of TLR2 inhibition altering the recovery of PA biofilms following interaction with untreated M1 macrophages cultured under pre-diabetic conditions, whereas TLR2 inhibition significantly ( $P < 0.01$ ) increased PA biofilm recovery following interaction with untreated M1 macrophages cultured under hyperglycaemic conditions. Intriguingly, in contrast there was no significant ( $P > 0.05$ ) effect of TLR2 inhibition on the phagocytosis of PA by LPS/MGN3-treated M1 macrophages cultured under hyperglycaemic conditions but TLR2 inhibition significantly ( $P < 0.01$ ) reduced the phagocytosis of PA biofilms by LPS/MGN3-treated M1 macrophages cultured under pre-diabetic conditions. Collectively these findings suggest a pathogen-specific glycaemic switch of some kind may be operating on TLR2 activation in response to Gram-negative PA biofilms that was not seen in response to Gram-positive MRSA.

Neither TLR2 and/or TLR4 inhibition fully negated the observed reduction in MRSA or PA biofilm recovery following MGN3 or LPS treatment of M1 macrophages, suggesting MGN3 and LPS may still be able to influence the phagocytosis without the need for TLR2/TLR4 activation. LPS is a known ligand for TLR4 (Ciesielska *et al*, 2021) but there is emerging evidence that LPS can become cytosolic and activate the non-canonical inflammasome without any participation from TLR4 (Ciesielska *et al*, 2021). LPS can enter the cytosol inside phagosomes, or by binding to high mobility group box 1 (HMGB1) and subsequent

internalisation of HMGB1–LPS complexes within endosomes through the receptor for advanced glycation end-products (RAGE) (Mazgaen and Gurung, 2020). Once LPS is delivered into the cytosol, human caspase-4/-5 senses LPS and induces non-canonical NLRP3 inflammasome activation (Mazgaen and Gurung, 2020). The inflammasome promotes phagosome maturation, leading to enhanced antimicrobial activity that induces bacterial killing (Rathinam and Fitzgerald, 2016). LPS exposure leads to NLRP3 inflammasome activation and maturation of phagosomes containing Gram-negative or Gram-positive bacteria, demonstrating antibacterial activity against phagosome cargo regardless of their Gram-staining cell wall properties (Rathinam and Fitzgerald, 2016). Thus, given the structural similarity between MGN3 and LPS (Fadel *et al*, 2018), MGN3 might also promote bacterial clearance by activating TLR-independent mechanisms such as the non-canonical inflammasome but further investigations would be required to confirm this.

In the future, this experimental work could be expanded to investigate a wider range of TLR receptors or explore some of TLR-independent pathways that may mediate the effects of MGN3. Other phagocytic cells such as neutrophils could also be investigated in future work to compare with M1 macrophages used in this project. The study should also be repeated using other macrophage cell lines as well as *ex vivo* primary macrophages to confirm these findings are not just unique to U937-derived macrophages.

In terms of growth factors, hyperglycaemia significantly increased EGF secretion by M1 macrophages. A study done by Fukuda *et al*, (1997) found that high glucose conditions increased heparin-binding epidermal growth factor (HB-EGF) expression in mice. In contrast, hyperglycaemia (30mM) had no effect on FGF2 levels secreted by M1 macrophages compared to those cultured under pre-diabetic conditions. Another study found an increase in FGF2 mRNA linked to hyperglycaemia in diabetic mice (Teshima-Kondo *et al*, 2004) but that investigation was carried out in fibroblasts. Beyond expression levels, glycation of FGF2 resulting from hyperglycaemia has been shown to change the structural conformation of FGF2 in diabetic mice (Facchiaiano *et al*, 2006). A previous study also suggested that glycation reduces the ability of FGF2 to bind to the tyrosine kinase receptor which in turn reduces mitogenesis (Duraisamy *et al*, 2001).

EGF and FGF secretion from M1 macrophages cultured under both low and high glucose concentration was decreased by MGN3 and LPS treatment. RS unexpectedly increased EGF but decreased FGF2 secretion from M1 macrophages cultured at 11mM but no effects were seen at 30mM glucose. The observed reduction in macrophage-derived EGF and FGF secretion by MGN3 and LPS may potentially reduce excessive inflammation associated with hyperglycaemia. Under normal conditions EGF stimulates macrophage proliferation, which may lead to an excessive inflammatory response (Lu *et al*, 2014). Other studies have shown the selective deletion of EGF receptors (EGFR) on macrophages can influence inflammatory cytokine production, activation of the EGFR can mediate cytokine production as well as mediating anti-inflammatory cytokine feedback (Lu *et al*, 2014; Shang *et al*, 2020; Zhao *et al*, 2016). FGF2 has been shown to promote inflammatory cell recruitment by enhancing endothelial adhesion molecule expression (Zittermann and Issekutz, 2006). FGF2 also assists in angiogenesis and tissue repair in addition to promoting inflammation (Bikfalvi *et al*, 1997; Shen *et al*, 2024; Presta *et al*, 2009).

TLR2/4 inhibition significantly increased EGF secretion from untreated and RS-treated M1 macrophages under low glucose conditions but not at high glucose conditions. As reported previously the TLRs are somewhat promiscuous in nature and can be activated by multiple endogenous-derived ligands (Takeda *et al*, 2003), so the observed responses to TLR inhibition in untreated cells is not unexpected. A similar pattern of TLR2 or TLR4 inhibition leading to increased EGF levels was observed under pre-diabetic conditions following treatment with LPS or MGN3. However, under hyperglycaemic conditions, only TLR4 inhibition increased EGF levels following treatment of M1 macrophages with LPS or MGN3. In fact, TLR2 inhibition had little effect on M1-derived EGF levels at high glucose levels, regardless of treatment. These findings suggest TLR4 may play a part in mediating MGN3-induced EGF production by M1 macrophages under hyperglycaemic conditions since an equivalent response to TLR4 inhibition was not seen in untreated macrophages or M1 cells receiving other treatments. Increased EGFR signalling has been linked with increased TLR4 expression in macrophages through downstream signalling molecules such as Rab5a (Tang *et al*, 2020). The EGFR can also be activated either direct ligand interactions or ligands of TLR4 such as LPS (Lu *et al*, 2014).

In untreated M1 macrophages, TLR2 inhibition decreased FGF secretion at 11mM whereas TLR4 inhibition increased FGF secretion at 30mM. TLR inhibition had no effect on MGN3-mediated FGF2 secretion when M1 macrophages were cultured at 11mM but TLR2 inhibition increased FGF2 levels produced by M1 macrophages at 30mM. In direct contrast, TLR inhibition had no effect on LPS-mediated FGF2 secretion from M1 macrophages at 30mM but TLR2 inhibition increased FGF2 levels produced by M1 macrophages cultured at 11mM. In RS-treated M1 cells, both TLR2/4 inhibition increased FGF2 secretion at 11mM, whereas only TLR4 inhibition increased FGF2 levels produced at 30mM. These differential responses to TLR inhibition suggest the TLRs may play a role in macrophage-mediated production of FGF2, with TLR2 appearing to be more influential on MGN3-mediated production of FGF2 under hyperglycaemic conditions and LPS-mediated production of FGF2 under pre-diabetic conditions. There is limited research to suggest TLR2 and FGF2 production directly, however, it has been members of FGF family can act through TLR2/4 (Marega *et al*, 2021).

MGN3 has been shown to reduce inflammation by mitigating the inflammatory response induced by hyperglycaemia, thus highlighting the beneficial properties of MGN3 for the management of chronic inflammation in diabetes (Ghoneum *et al*, 2008). Hyperglycaemia is known to sensitize macrophages into increasing production of proinflammatory mediators which can lead to pronounced inflammation but impaired phagocytosis (Pavlou *et al*, 2018). In this study, there was a non-significant increase in MCP-1 production from M1 macrophages cultured at 30mM compared to levels seen in M1 macrophages cultured at 11mM, suggesting hyperglycaemia alone was not influencing MCP-1 secretion from M1 macrophages. At low glucose levels, LPS and MGN3 did not affect MCP-1 levels but at high glucose levels RS, LPS and MGN3 stimulated MCP-1 production. The TLR inhibitors appeared to have no effect on MCP-1 production under pre-diabetic conditions, and at high glucose inconsistent findings were seen, with TLR4 inhibition increasing MCP-1 production in untreated M1 cells but TLR2 inhibition decreasing MCP-1 secretion in LPS-treated M1 macrophages. These findings somewhat contradict with the wider literature indicating hyperglycaemia significantly increases the expression and secretion of MCP-1 in macrophages due to the activation of pro-inflammatory pathways (Xu *et al*, 2016). A study

by Mine *et al*, (2006) found a significant increase in serum MCP-1 in diabetic patients compared to non-diabetics. This is thought to be related to oxidative stress caused by hyperglycaemia in macrophages leading to an increase in ROS, which in return has shown to activate signalling pathways (such as NF- $\kappa$ B), thereby enhancing MCP-1 expression (Yang *et al*, 2009). The increased MCP-1 levels in response to hyperglycaemia can attract more monocytes to sites of inflammation, exacerbating chronic inflammatory conditions often seen in diabetes (Grewal *et al*, 1997). High glucose can also influence macrophage polarization, driving them towards a more pro-inflammatory phenotype that further increases MCP-1 secretion (Nio *et al*, 2012; Du *et al*, 2021). Considering the literature, it is possible the ELISA was insufficiently sensitive to detect the glycaemic change in MCP-1 levels based on the macrophage numbers used for the cell lysates so further investigations would be required to further validate these findings, using higher cell densities or more sensitive detection methods such as flow cytometry.

This study also looked at whether MCP-1 may be implicated in the influence of MGN3 on the chemotaxis of U937 monocytes. This was done by exposing U937 monocytes to cell supernatants from MGN3-treated M1 macrophages, keratinocytes or fibroblasts. The chemotaxis of U937 monocytes exposed to the supernatant of untreated M1 macrophages cultured under hyperglycaemic conditions was significantly inhibited compared to U937 monocytes exposed to supernatants collected from untreated M1 macrophages cultured at pre-diabetic conditions. The addition of a blocking antibody against MCP-1 significantly reversed this inhibition of U937 monocyte chemotaxis, increasing chemotaxis levels back toward those seen following exposure to supernatants collected from untreated M1 macrophages cultured at pre-diabetic conditions. The findings suggest high glucose levels have a detrimental effect on monocyte chemotaxis and that macrophage-derived MCP-1 might unexpectedly inhibit U937 monocyte chemotaxis under hyperglycaemic conditions yet promote U937 monocyte chemotaxis under pre-diabetic conditions.

Neither TLR2 or TLR4 inhibition significantly mediated the chemotaxis of U937 monocytes exposed to the supernatant of untreated M1 macrophages cultured under pre-diabetic thereby excluding TLR signalling in mediating secretions from untreated M1 macrophages. However, the addition of a blocking antibody against MCP-1 significantly reduced the

chemotaxis of U937 monocytes exposed to the supernatant of untreated M1 macrophages cultured under pre-diabetic conditions, suggesting that the antibody was preventing the positive chemotactic effects of MCP-1 present in the 11mM-derived supernatant. In direct contrast, the MCP-1 blocking antibody significantly increased the chemotaxis of U937 monocytes exposed to the supernatant of untreated M1 macrophages cultured under hyperglycaemic conditions, suggesting a glycaemic switch occurs whereby MCP-1 has negative chemotactic effect when present in 30mM-derived supernatant. This observation of the MCP-1 blocking antibody decreasing and increasing the chemotaxis of U937 monocytes following exposure to 11mM and 30mM-derived supernatants respectively was relatively consistent across the experimental findings and potentially highlights a dual nature of MCP-1 that has not been previously identified.

There was no evidence to suggest that the supernatants from MGN3/LPS-treated M1 macrophages cultured at either 11mM or 30mM influenced the subsequent chemotaxis of U937 monocytes compared to the corresponding untreated glycaemic control (UC). Similarly, neither TLR2 or TLR4 inhibition significantly mediated the chemotaxis of U937 monocytes exposed to the supernatant of MGN3/LPS-treated M1 macrophages cultured under pre-diabetic or hyperglycaemia conditions. These findings suggest that neither LPS nor MGN-3 were substantially influencing supernatant levels of macrophage-derived MCP-1 at the cell densities tested.

Exposure of U937 monocytes to supernatants from keratinocytes cultured under hyperglycaemic conditions significantly reduced their chemotaxis ( $P < 0.01$ ; % Relative Chemotaxis = 92.9% at 30mM vs. 100.0% at 11mM) compared to monocytes exposed to supernatants from untreated keratinocytes cultured under pre-diabetic conditions (11mM). The inhibition of chemotaxis was significantly reversed ( $P < 0.01$ ) by the addition of an anti-MCP-1 antibody, restoring chemotaxis levels (% Relative Chemotaxis = 106.9% at 30mM vs. 96.2% at 11mM) to those seen in monocytes exposed to supernatants from keratinocytes cultured at pre-diabetic conditions. These results indicate that high glucose levels impair monocyte chemotaxis, and that MCP-1 derived from keratinocytes may inhibit U937 monocyte chemotaxis under hyperglycaemic conditions while promoting it under pre-diabetic conditions.

Inhibition of TLR2 or TLR4 did not significantly ( $P > 0.05$ ) affect the chemotaxis of U937 monocytes exposed to supernatants from untreated keratinocytes cultured under pre-diabetic conditions. However, under hyperglycaemic conditions, TLR2 inhibition led to a significant increase ( $P < 0.01$ ) in chemotaxis, while TLR4 inhibition caused a significant decrease ( $P = 0.021$ ). The addition of an MCP-1 blocking antibody significantly ( $P = 0.038$ ) reduced the chemotaxis of U937 monocytes exposed to supernatants from untreated keratinocytes cultured under pre-diabetic conditions, indicating the antibody was blocking the chemotactic effects of MCP-1 in the 11mM supernatant. In contrast, the MCP-1 blocking antibody significantly ( $P < 0.01$ ) increased the chemotaxis of U937 monocytes exposed to supernatants from keratinocytes cultured under hyperglycaemic conditions. This pattern, where the antibody decreased chemotaxis in response to 11mM-derived supernatants and increased it in response to 30mM-derived supernatants, was consistently observed across the experiments. There was no evidence to suggest that the supernatants from MGN3/LPS-treated keratinocytes cultured at 11mM significantly ( $P > 0.05$ ) influenced chemotaxis. However, at 30mM MGN3 treated keratinocyte supernatant significantly reduced ( $P < 0.01$ ) the subsequent chemotaxis of U937 monocytes compared to the corresponding UC. At 11mM TLR4 inhibition with LPS treatment significantly reduced ( $P = 0.031$ ) monocyte chemotaxis. At 30mM both TLR2/4 inhibition resulted in significant increased ( $P < 0.05$ ) chemotaxis following LPS treated supernatant and TLR2 inhibition significantly increased ( $P < 0.01$ ) and TLR4 inhibition significantly reduced ( $P = 0.044$ ) chemotaxis following MGN3 treated supernatant. These findings suggest that LPS was influenced by TLR4 at 11mM and both TLR4 and TLR2 at 30mM, and MGN-3 by TLR2 at 11mM and TLR4 at 30mM.

The chemotaxis of U937 monocytes exposed to supernatants from fibroblasts cultured under hyperglycaemic (30mM glucose) conditions was significantly reduced ( $P = 0.016$ ; % Relative Chemotaxis = 88.1% at 30mM vs. 100.0% at 11mM) compared to monocytes exposed to supernatants from untreated fibroblasts cultured under pre-diabetic conditions. The addition of an MCP-1 blocking antibody significantly ( $P = 0.042$ ) reversed this inhibition, restoring chemotaxis levels (% Relative Chemotaxis = 98.2% at 30mM vs. 89% at 11mM) closer to those seen with supernatants from fibroblasts cultured under pre-diabetic conditions. These results suggest that high glucose levels impair monocyte chemotaxis and

that fibroblast-derived MCP-1 may unexpectedly inhibit U937 monocyte chemotaxis under hyperglycaemic conditions while promoting it under pre-diabetic conditions.

TLR2/4 inhibition did not significantly ( $P > 0.05$ ) affect the chemotaxis of U937 monocytes exposed to supernatants from untreated fibroblasts cultured under pre-diabetic conditions. However, under hyperglycaemic conditions, TLR2 inhibition resulted in a significant increase ( $P = 0.005$ ) in chemotaxis. The addition of an MCP-1 blocking antibody significantly ( $P = 0.021$ ) reduced the chemotaxis of U937 monocytes exposed to supernatants from untreated fibroblasts cultured under pre-diabetic conditions, indicating that the antibody blocked the chemotactic effects of MCP-1 in the 11mM supernatant. In contrast, the MCP-1 blocking antibody significantly ( $P = 0.042$ ) increased chemotaxis in monocytes exposed to supernatants from fibroblasts cultured under hyperglycaemic conditions. This pattern—where the antibody reduced chemotaxis in response to 11mM supernatants and increased it with 30mM supernatants—was consistent across experiments. No significant ( $P > 0.05$ ) effects on chemotaxis were observed with supernatants from MGN3/LPS-treated fibroblasts cultured at either 11mM or 30mM glucose. At 11mM, TLR2/4 inhibition with LPS treatment, and TLR2 inhibition with MGN3 treatment, significantly reduced ( $P < 0.01$ ) monocyte chemotaxis. At 30mM, TLR2 inhibition significantly increased ( $P < 0.05$ ) chemotaxis following LPS and MGN3-treated supernatants.

Further experiments may be needed using higher M1 cell densities to provide a more concentrated supernatant before conclusively excluding a role for MGN3 and LPS in regulation of monocyte chemotaxis by macrophage-derived, keratinocyte-derived and fibroblast-derived MCP-1.

Immune cells (macrophages, keratinocytes and fibroblasts) cultured in hyperglycaemic conditions have shown to express increased levels of MCP-1 (Grosick *et al*, 2018; Fang *et al*, 2023; Shanmugam *et al*, 2003). These elevated MCP-1 are beneficial in a sense because of the recruitment of monocytes however studies have shown over expression of MCP-1 can lead to early priming of monocytes into macrophages which can exacerbate inflammatory cytokine production in diabetic patients (Kraakman *et al*, 2014; Cucak *et al*, 2014) with a

study even showing MCP-1 primed macrophages have higher cytotoxic tendencies (Wang *et al*, 2014).

Under hyperglycaemic conditions, macrophages can become activated and secrete higher levels of pro-inflammatory cytokines, which can stimulate keratinocytes and fibroblasts to produce MCP-1 (Xu *et al*, 2016). This creates a positive feedback loop, enhancing MCP-1 production. Keratinocytes and fibroblasts can release various cytokines (such as IL-1 $\beta$ , IL-6, and TNF- $\alpha$ ) in response to hyperglycaemia which can further activate macrophages, leading to increased MCP-1 expression and secretion, which may then attract more monocytes to a wound (Wood *et al*, 2014). Hyperglycaemia can alter the composition and properties of the ECM, thereby affecting the interactions between cells and influencing signalling pathways involved in MCP-1 production (Macarie *et al*, 2018). Moreover, direct cell-cell interactions and signalling pathways (like those mediated by gap junctions or receptor-ligand interactions) can facilitate communication between macrophages, keratinocytes, and fibroblasts, enhancing MCP-1 production in response to hyperglycaemic stress (Yadav *et al*, 2010; Pezhman *et al*, 2021; Tiwari *et al*, 2010). Thus, the combined effect of hyperglycaemia and the interactions between macrophages, keratinocytes, and fibroblasts in diabetic patients may create a chronic inflammatory environment by promoting MCP-1 production and monocyte recruitment. This sustained inflammation may ultimately initiate tissue breakdown and promote the formation of a DFU (Monaghan *et al*, 2023).

This study also investigated two potent intracellular antimicrobial mediators produced by M1 macrophages, lysozyme and cathelicidin (LL37). It has been shown that long-term exposure of human and murine macrophages to high glucose levels leads to a reduction in lysosomal proteolytic and lipase activities (Moheimani *et al*, 2012). Hyperglycaemia can destabilize lysosomes and induce alterations in the protein expression and regulation of lysozymes (Sims-Robinson *et al*, 2016). At low glucose levels there were very large increases ( $P < 0.01$ ) in lysozyme production by M1 macrophages following treatment with LPS or MGN3. At high glucose conditions smaller increases in lysozyme production were still observed in M1 macrophages treated with LPS or MGN3. This increase in MGN3-induced intracellular store of lysozyme is likely to promote enhanced bacterial elimination by M1 macrophages since lysozyme is a potent antimicrobial enzyme (Khorshidian *et al*, 2022).

At both low and high glucose conditions, TLR2/4 inhibition decreased lysozyme production in M1 macrophages treated with MGN3. A similar reduction in lysozyme production by M1 cells was seen for LPS following TLR2/4 inhibition, but only at low glucose conditions. In contrast, an increase in lysozyme production was seen following TLR2 inhibition and a decrease was seen following TLR4 inhibition in untreated and RS-treated M1 macrophages at low (but not high) glucose levels. These differential responses to TLR inhibition suggest the TLRs may play a role in macrophage-mediated production of lysozyme, with both TLR2 and TLR4 appearing to be influential in MGN3-mediated production of lysozyme.

At high glucose culture conditions, there was a decrease in cathelicidin production in untreated M1 macrophages compared to levels generated in untreated M1 cells under pre-diabetic conditions, suggesting hyperglycaemia impairs cathelicidin generation in M1 macrophages. At both glucose levels, LPS stimulated cathelicidin production from M1 macrophages whereas MGN3 reduced LL37 production, indicating LPS and MGN3 induce opposing responses in relation to cathelicidin generation. At low glucose, TLR2/TLR4 inhibition reduced cathelicidin production in untreated and MGN3-treated M1 macrophages, whereas TLR2/TLR4 inhibition increased cathelicidin production in MGN3-treated M1 cells under hyperglycaemic conditions. These findings indicate the TLR2 and TLR4 signalling pathways can differentially modulate the MGN3-mediated generation of cathelicidin from M1 macrophages.

The observed reduction in cathelicidin production by MGN3 is likely to decrease the ability of M1 macrophages to kill bacteria as effectively, since LL37 is a potent antimicrobial peptide (Sancho-Vaello *et al*, 2020). However, a moderate suppression of LL37 production by MGN3 may dampen inflammation since cathelicidin is known to delay neutrophil cell death which can lead to sustained inflammation (Minns *et al*, 2021). Cathelicidin can also invoke inflammation by enabling the binding of self, non-coding RNA to cell surface scavenger receptors on macrophages and keratinocytes (Takahashi *et al*, 2018).

Hyperglycaemia can affect LL37 production through multiple mechanisms including through the elevation of pro-inflammatory cytokines such as TNF- $\alpha$  and IL-6, which may enhance LL37 expression in macrophages as part of the immune response (Uribe-Querol and Rosales,

2022; Hao *et al*, 2023). The oxidative stress induced by hyperglycaemia can influence transcription factors that regulate LL37 expression (Shi *et al*, 2024; Xi *et al*, 2024). Research on cathelicidin specifically in the context of hyperglycaemia is limited, but these mechanisms suggest that hyperglycaemia influences LL-37 production indirectly through inflammatory and metabolic pathways. In contrast, MGN3 exhibits antioxidant properties, which can help mitigate oxidative stress caused by high glucose levels (Ooi *et al*, 2018). Further studies are needed in this area to clarify the relationships in more detail.

Finally, this study also looked at whether MGN3 treatment of M1 macrophages can affect the cathelicidin-associated antimicrobial activity of M1 cell lysates against MRSA and PA01 under hyperglycaemic conditions. The results showed a significant ( $P < 0.001$ ) antibacterial activity of all M1 cell lysates against MRSA and PA01, indicating the lysate constituents had substantial antibacterial activity at both pre-diabetic and hyperglycaemic conditions. The addition of cathelicidin blocking antibody to M1 cell lysates increased bacterial recoveries across all treatments, suggesting cathelicidin was a major antibacterial constituent of the isolated M1 cell lysates but unlikely to be the only antibacterial mediator present. Cathelicidin (LL37) is known to have a broad antibacterial activity against both Gram-positive and Gram-negative bacteria (Ridyard and Overhage, 2021).

There was an additional reduction in MRSA recovery after exposure of MRSA to cell lysates from LPS- and MGN3-treated M1 macrophages cultured at both 11mM and 30mM, indicating enhanced MRSA killing compared to exposure of MRSA to cell lysates from untreated or RS-treated M1 macrophages. In contrast, the only further reduction in PA01 recovery was observed following exposure of PA01 to cell lysates from MGN3-treated M1 macrophages cultured at 30mM glucose when compared to exposure of PA01 to cell lysates from corresponding untreated M1 macrophages. This enhanced antimicrobial activity of M1-derived cell lysates against PA01 was not observed for any other treatments at 30mM glucose. Furthermore, none of the treatments applied to M1 macrophages cultured at 11mM enhanced the antibacterial activity of cell lysates against PA01 beyond that observed with the untreated control.

Collectively these findings suggest that M1 cell lysates had direct antibacterial activity against both MRSA and PA01, with cathelicidin appearing to be at least one of the major constituents. Both MGN3 and LPS treatment of M1 macrophages could enhance this antibacterial activity against MRSA further under both pre-diabetic and hyperglycaemic conditions. This suggests the enhanced phagocytic activity against MRSA observed in section 4.4.3 following MGN3 and LPS stimulation of M1 macrophages may be in part due to the antibacterial activities of M1 intracellular constituents, of which cathelicidin appears to be one of the major active constituents. LPS treatment failed to further enhance the antibacterial activity against PA01 beyond that seen in the untreated control, and MGN3 treatment only provided additional enhancement of antibacterial activity against PA01 under hyperglycaemic conditions, suggesting the enhanced phagocytic activity against PA01 observed in section 4.4.4 following MGN3 and LPS stimulation of M1 macrophages must require other mechanisms or factors beyond just the antibacterial activities of M1 intracellular constituents.

In conclusion, this study demonstrated that 2.0mg/ml MGN3 consistently enhanced the phagocytosis of MRSA and PA biofilms by U937-derived M1 macrophages, reversing the suppressive effects of hyperglycaemia. These findings suggest MGN3 holds therapeutic potential for improving immune function in DFU infections. MGN3 appeared to act similarly to LPS, enhancing biofilm clearance through TLR2 and TLR4 pathways, though additional mechanisms are likely involved. More widely, MGN3 has shown to impact a range of monocyte and U937-derived M1 macrophage functions under pre-diabetic and hyperglycaemic conditions including growth factors, antimicrobial peptide and antimicrobial enzyme production. The findings of this Chapter should be explored further to build on the growing body of evidence indicating MGN3-based treatments might lead to therapeutic benefits on wound healing processes in patients with a DFU. Future work could expand on the data presented in this chapter by detangling the intricacies of the TLR signalling pathways in mediating the activities of MGN3 and providing a deeper interrogation of the complex interactions of monocytes/macrophages with other cell types involved in cutaneous wound healing.

# **Chapter 5: The Effect of MGN3 on Fibroblast and Keratinocyte-Mediated Wound Repair under Hyperglycaemic Conditions**

## 5.1 Introduction

### 5.1.1 The Importance of Fibroblasts and Keratinocytes in Wound Healing

Fibroblasts are essential to wound healing, particularly during the proliferative and remodelling phases (Cialdai *et al.*, 2022). Following injury, macrophage-released cytokines (e.g., IL-1, IL-6, IL-8, IL-12, TNF- $\alpha$ ) recruit and activate fibroblasts (Duque & Descoteaux, 2014; Koh & DiPietro, 2011). In turn, fibroblasts secrete additional cytokines, facilitating immune cell recruitment (Bautista-Hernández *et al.*, 2017; Talbott *et al.*, 2022). Dermal fibrocytes are also drawn to wounds by PDGF, TGF- $\beta$ , and FGF (Thulabandu *et al.*, 2018; Schultz & Wysocki, 2009). During proliferation, fibroblasts produce MMPs to degrade damaged matrix, which is replaced by new ECM composed of collagen and fibronectin, supporting cell adhesion and differentiation (Landen *et al.*, 2016; Xue & Jackson, 2015). In response to TGF- $\beta$ , fibroblasts may differentiate into myofibroblasts, which express  $\alpha$ -smooth muscle actin and contract to remodel the ECM (Porter, 2007; Knodler *et al.*, 2023).

Keratinocytes, the primary cells of the epidermis, play key roles in all stages of wound healing—from initiating inflammation to driving re-epithelialization (Kirfel & Herzog, 2004; Raja *et al.*, 2007). Injury triggers inflammatory responses and shifts keratin expression: K5 and K14 dominate under normal conditions, while K6, K16, and K17 increase during regeneration (Wilson *et al.*, 1992; Romashin *et al.*, 2024). Effective wound closure depends on keratinocyte migration, proliferation, and differentiation; disruptions in this process can lead to chronic wounds (Pastar *et al.*, 2014).

### 5.1.2 The Effect of Glucose on Fibroblast and Keratinocyte Function

Hyperglycaemia impairs fibroblast function which in turn negatively affects wound healing. Pang *et al.*, (2016) found that high glucose increases NF- $\kappa$ B pathway activity while reducing its inhibitor Bay11-7082 in dermal fibroblasts. Hyperglycaemia also suppresses bFGF-regulated JNK phosphorylation, essential for cell migration. Xuan *et al.*, (2014) showed delayed fibroblast migration and increased ROS production under 30mM glucose in diabetic

mice. These effects are linked to disruptions in the PI3K-Rac1-JNK pathway, which is critical for fibroblast migration (Xuan *et al*, 2016).

Hyperglycaemia also impairs keratinocyte migration, proliferation, and differentiation. Lan *et al*, (2008) showed reduced keratinocyte proliferation and mobility after five days of high glucose exposure, linked to lower p125FAK levels. Spravchikov *et al*, (2001) also reported altered GLUT1 expression and increased Ca<sup>2+</sup>-induced differentiation under high glucose conditions.

### **5.1.3 The Effect of MGN3 on Fibroblast and Keratinocyte Function**

MGN3 is known to have positive effects on a range of immune cells such as neutrophils, NK cells, macrophages and dendritic cells. Studies have shown MGN3 has enhanced NK cell activity against cancerous cells (Ghoneum, 1998), modulates TNF- $\alpha$ , IFN- $\gamma$ , IL and NO production (Ghoneum and Jewett, 2000; Ghoneum and Agrawal, 2011; Ghoneum and Agrawal, 2014) and increases the macrophage phagocytic ability (Ghoneum and Matsuura, 2004; Ghoneum *et al*, 2008). However, there is little research done to show the effects of MGN3 on fibroblast cell function both at pre-diabetic and hyperglycaemic conditions.

It is understood under hyperglycaemic conditions keratinocyte cell migration and proliferation is impaired which results in chronic wounds such DFUs in diabetic patients. A way of improving this impairment is by using dietary fibres such as MGN3 to potentially increase keratinocyte function in particular, migration and proliferation at the site if injury. MGN3 has had positive effects on several immune cells in previous studies. Examples of these include improved phagocytic ability of macrophages and neutrophils, improved NK cell function against cancerous cells and the reduction of proinflammatory cytokine markers (Ghoneum and Jewett, 2000; Ghoneum and Agrawal, 2011; Ghoneum and Matsuura, 2004; Ghoneum *et al*, 2008). These studies show MGN3 has a positive effect on a range of immune cells however, the effect of MGN3 on keratinocyte cell migration and proliferation has not yet been investigated. This project evaluated the effects on MGN3 on keratinocyte function under hyperglycaemic conditions.

## 5.2 Aims and Objectives

### 5.2.1 Aim

To investigate the effect of MGN3 on an *in vitro* fibroblast and keratinocyte models of wound closure under hyperglycaemic conditions.

### 5.2.2 Objectives

- To use human dermal fibroblasts (HDF) and human keratinocytes (HACAT) cultured under a range of glucose concentrations (11, 20 and 30mM) in wound healing assays to establish an *in vitro* fibroblast model of wound closure.
- To evaluate the effect of both hyperglycaemia (20 and 30mM glucose) and MGN3 on gap ('wound') closure in the *in vitro* fibroblast and keratinocyte models of wound closure.
- To determine the involvement of TLR2 and/or TLR4 in mediating the responses of fibroblasts and keratinocytes in the wound closure model.
- To differentiate between the effects of hyperglycaemia and MGN3 on fibroblast and keratinocyte cell proliferation and migration using specific inhibitors (mitomycin C and cytochalasin D) of these cellular processes.

## 5.3 Methods

### 5.3.1 Cell Culture

Fibroblasts and keratinocytes were seeded at a density of  $5 \times 10^4$  cells/ml in multiple glucose concentrations (11, 20 and 30mM) in DMEM CM in cell-exclusion culture inserts (2 well culture-inserts, Ibidi). Fibroblasts were incubated at 37°C and 5% CO<sub>2</sub> for 4 days and keratinocytes for 3 days.

### 5.3.2 Wound Healing Assay

After removing cell-exclusion inserts, a 500µm gap ("wound") was created in fibroblast /keratinocyte monolayers. Cells were washed and treated with/without LPS (5µg/mL) or MGN3 (2 mg/mL). Additional treatments included TLR2 (200µM) or TLR4 (200µM) inhibitors, and/or cytochalasin D (10 g/mL, to block cell migration) following 2-hour pre-treatment with/without mitomycin C (20µg/mL, to block cell proliferation) as shown in section 2.2.9. Fibroblasts were imaged every 45 minutes for 60 hours and keratinocytes every 1 hour for 24 hours using a Holomonitor live-cell imaging system. Wound closure was quantified from 12 images per well.

To optimize mitomycin C (MC) concentration for inhibiting cell proliferation, fibroblasts and keratinocytes were seeded at  $5 \times 10^4$  cells/mL in 24-well plates and incubated at 37 °C with 5% CO<sub>2</sub> until 50% confluence. After discarding supernatants, cells were treated with varying MC concentrations (2, 5, 10, 20 µg/mL) for 2 hours. Cells were then washed and initial counts taken (n=3) using trypan blue (see section 2.2.2). Fibroblasts and keratinocytes were then incubated for a further 72 hours with fibroblast cell counts taken after 24, 48 and 72 hours and keratinocytes after 24 hours. The % inhibition of cell proliferation in MC-exposed fibroblasts (+MC) compared the negative control (NC) lacking MC exposure at time T (24, 48 and 72 hours) was calculated for each MC concentration using the equations:

$$\% \text{ Inhibition of Cell Proliferation} = (CP_{NC} - CP_{+MC}) / CP_{NC} * 100$$

.....where Cell Proliferation (CP) = Cell Count [at time T] - Initial Cell Count

## 5.4 Results

### 5.4.1 Effect of Glucose on Fibroblast 'Wound' Closure

The results showed as the glucose concentration increased there was a reduction in the % 'wound' closure. After 60 hours the % 'wound' closure was as follows; 85% closure at 11mM, 69% at 20mM and 55% at 30mM glucose (Figure 5.1).

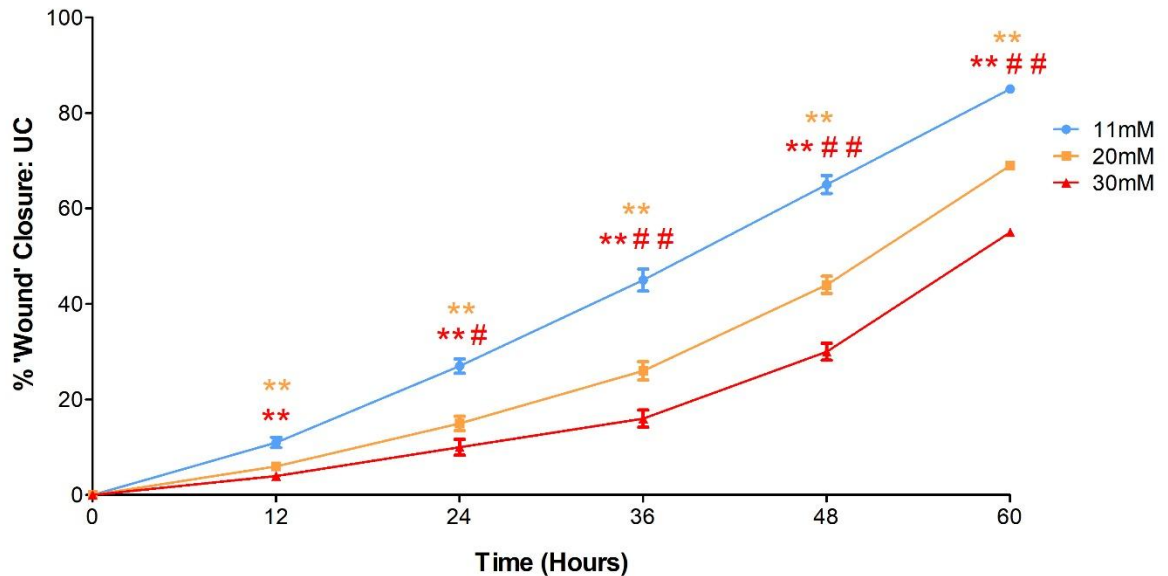
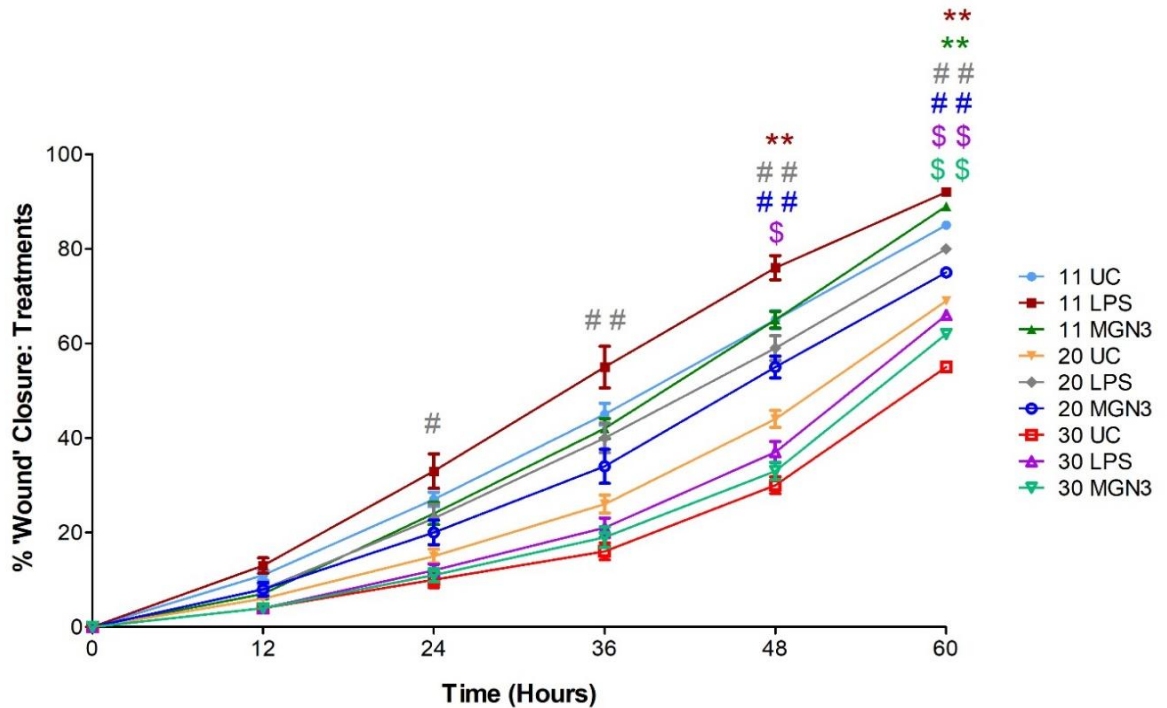


**Figure 5. 1: Effect of Glucose on % Fibroblast 'Wound' Closure.** The % wound closure was calculated based on Holomonitor images captured from HDF wound models cultured at different glucose concentrations (11, 20 and 30mM) over a period of 60 hours. Significant increases in wound closure were observed in fibroblasts cultured at 20mM and 30mM glucose compared to those cultured at 11mM (\*  $P < 0.05$  and \*\*  $P < 0.01$  determined by t-tests;  $n = 12$ ), fibroblasts cultured at 30mM glucose compared to those cultured at 20mM glucose (#  $P < 0.05$  and ##  $P < 0.01$  determined by t-tests;  $n = 12$ ). Lines and error bars indicate the wound area %  $\pm$  the standard error of the mean (SEM) in all cases.

Statistical analysis using two tailed t-tests showed there was significant decreases ( $P < 0.01$ ) in wound closure when fibroblasts were cultured at 20mM or 30mM compared to those cultured at 11mM glucose. There were also significant decreases in wound closure when the fibroblasts were cultured at 30mM after 12 hours ( $P = 0.028$ ) and 36 hours onwards ( $P < 0.01$ ) when compared to fibroblasts grown under 20mM glucose conditions.

### 5.4.2 Effect of MGN3 on Fibroblast 'Wound' Closure

The results showed as the glucose concentration wound closure was slower. The fibroblasts treated with LPS closed the gap faster than other treatment groups. MGN3 treated fibroblasts initially had a slower start compared to untreated and LPS groups however, after 36 hours there was a surge in wound closure (Figure 5. 2).



TIME (hrs)	11U	11LPS	11MGN3	20U	20LPS	20MGN3	30U	30LPS	30MGN3
0	0	0	0	0	0	0	0	0	0
12	11	13	7	6	8	8	4	4	4
24	27	33	24	15	23	20	10	12	11
36	45	55	42	26	40	34	16	21	19
48	65	76	65	44	59	55	30	37	33
60	85	92	89	69	80	75	55	66	62

**Figure 5. 2: Effect of MGN3 on % Fibroblast 'Wound' Closure.** The % wound closure was calculated based on Holomonitor images captured over a period of 60 hours following treatment of HDF wound models cultured at different glucose concentrations (11, 20 and 30mM) with/without MGN3 or LPS. Significant increases in wound closure were observed compared to corresponding untreated controls (11UC: \*  $P < 0.05$  and \*\*  $P < 0.01$ , 20UC: #  $P < 0.05$  and ##  $P < 0.01$ , 30UC: \$  $P < 0.05$  and \$\$  $P < 0.01$  determined by t-tests;  $n = 12$ ). Lines and error bars indicate the wound area (%)  $\pm$  the standard error of the mean (SEM) in all cases. Table shows the % wound closure after treatment at different timepoints.

After the 60-hour time period fibroblasts cultured in 11mM glucose had covered 85% or more of the wound area (11UC – 85%, 11LPS – 92%, 11MGN3 – 89%), fibroblasts cultured in 15mM glucose had covered 69% or more of the wound area (20UC – 69%, 20LPS – 80%, 20MGN3 – 75%) and fibroblasts cultured in 30mM glucose had covered 55% or more of the wound area (30UC – 55%, 30LPS – 66%, 30MGN3 – 62%) (See Figure 5. 3).

Statistical analysis using t-tests showed there was significant differences between the corresponding controls at different glucose concentrations. At 11mM glucose there were significant decreases in wound closure seen at 48 hours onwards ( $P < 0.01$ ) for the LPS treated fibroblasts and MGN3 treated fibroblasts after 60 hours ( $P < 0.001$ ) when compared to untreated fibroblasts. At 20mM there were significant decreases in wound closure seen at 24 hours ( $P = 0.02$ ) and 36 hours onwards ( $P < 0.01$ ) for the LPS treated fibroblasts and MGN3 treated fibroblasts at 48 hours onwards ( $P < 0.01$ ) when compared to UC. There were also significant decreases in wound closure seen in the 30mM groups at 48 hours ( $P = 0.024$ ) and both LPS treated fibroblasts and MGN3 treated fibroblasts after 60 hours ( $P < 0.001$ ) when compared to the UC.

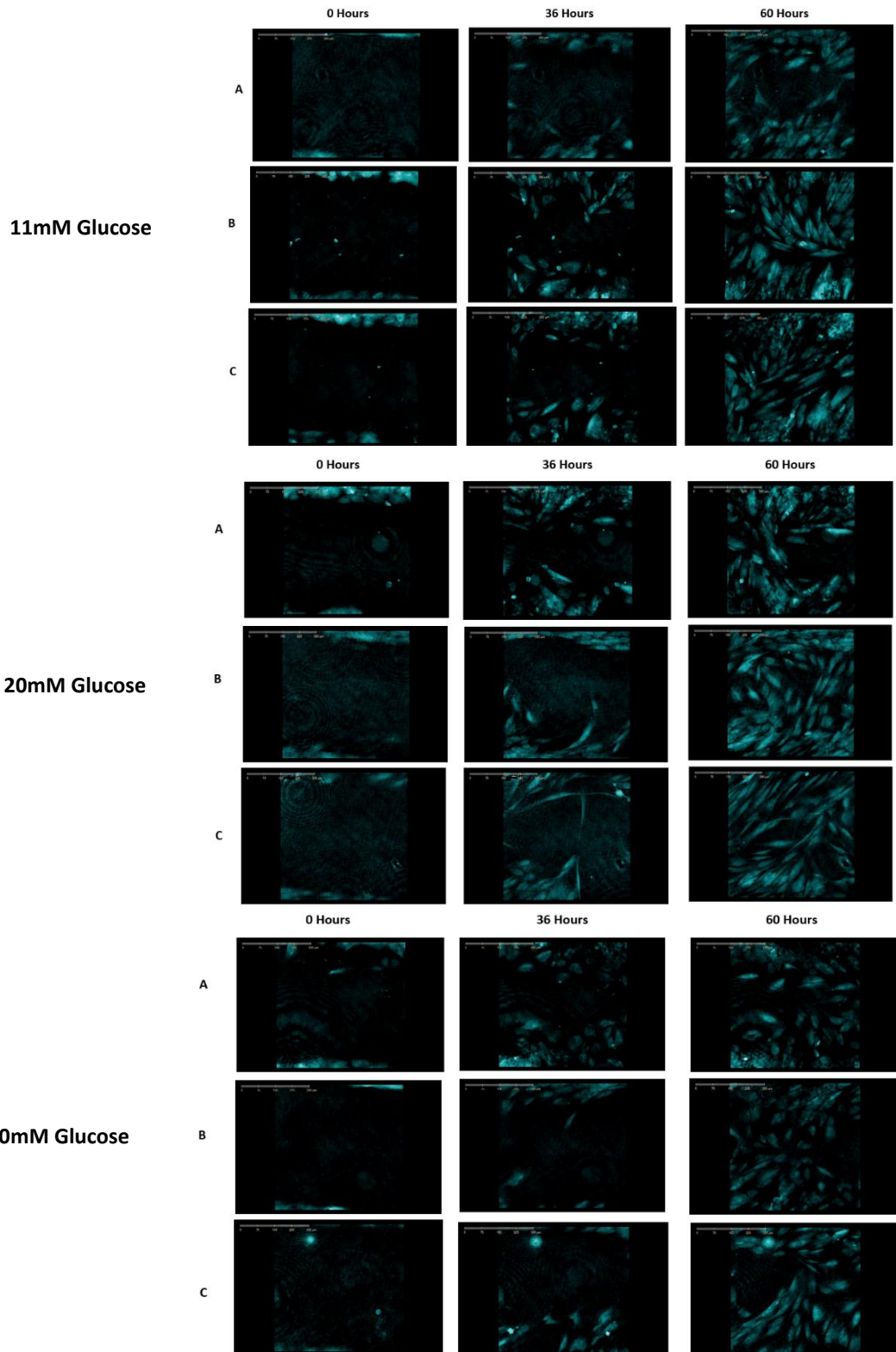
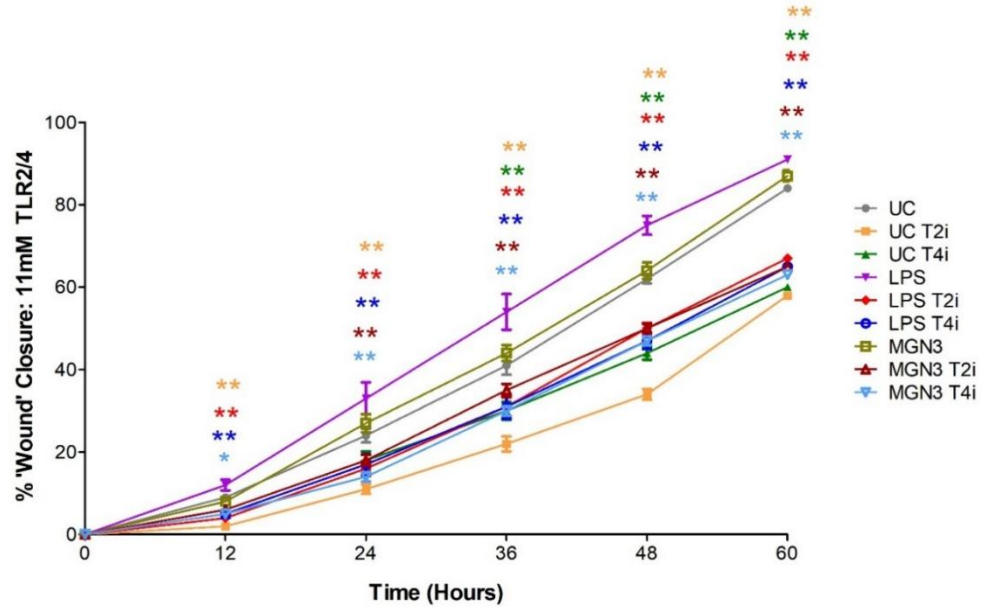


**Figure 5. 3: The Effect of MGN3 on Fibroblast ‘Wound’ Closure at Different Glucose Levels.** HDFs were cultured with 11, 20 and 30mM glucose, treated with LPS or MGN3 and incubated for 60 hours on a Holomonitor microscope. Images shown represent different time points (0, 36 and 60 hours). Panel A show untreated fibroblasts, Panel B are fibroblasts treated with LPS (5ug/ml) and Panel C shows fibroblasts treated with MGN3 (2mg/ml).

### 5.4.3 Effect of TLR inhibition on MGN3-Mediated Fibroblast 'Wound' Closure

#### 5.4.3.1 Effect of TLR inhibition on MGN3\_Mediated Fibroblast 'Wound' Closure at Pre-diabetic (11mM Glucose) Culture Conditions

The results showed TLR2/4 inhibition reduced the ability of the fibroblasts cultured at 11mM glucose to undergo wound closure in all cases (See Figures 5.4, and 5.5) compared to corresponding treatments lacking TLR inhibition.



TIME (hrs)	UC	UC T2i	UC T4i	LPS	LPS T2i	LPS T4i	MGN3	MGN3 T2i	MGN3 T4i
0	0	0	0	0	0	0	0	0	0
12	9	2	6	12	4	5	8	6	5
24	24	11	18	33	16	17	27	18	14
36	41	22	30	54	31	31	44	35	30
48	62	34	44	75	50	47	64	50	47
60	84	58	60	91	67	65	87	65	63

**Figure 5. 4: Effect of TLR inhibition on MGN3-Mediated Fibroblast 'Wound' Closure under 11mM Culture Conditions.** The area % change in wound closure was calculated based on Holomonitor images captured over a period of 60 hours following treatment of HDF wound models cultured at pre-diabetic (11mM glucose) with/without MGN3 (MGN) or LPS in the presence/absence of TLR2 (T2i) or TLR4 (T4i) inhibition. Significant decreases were seen in % wound closure compared to corresponding treatments lacking TLR inhibition (\*  $P < 0.05$  and \*\*  $P < 0.01$  determined by t-tests;  $n = 12$ ). UC = untreated control. Lines and error bars indicate the wound area %  $\pm$  the standard error of the mean (SEM) in all cases. Table shows the % wound closure after treatment at different timepoints.

Statistical analysis by independent two tailed t-tests indicated significant differences between groups. There were significant decreases in wound closure seen at all time points ( $P < 0.001$ ) in TLR2 inhibited untreated fibroblasts and TLR4 inhibited untreated fibroblasts ( $P < 0.01$ ) at 36 hours onwards compared to untreated fibroblasts without TLRi. There were

significant decreases in wound closure seen in TLR2/4 inhibited LPS treated fibroblast ( $P < 0.01$ ) at all time points compared to LPS treatment without TLRI. There were also significant decreases in wound closure seen at 24 hours onwards ( $P < 0.01$ ) in the TLR2 inhibited MGN3 treated fibroblasts and a decrease in TLR4 inhibited MGN3 treated fibroblasts at 12 hours ( $P = 0.013$ ) and 24 hours onwards ( $P < 0.01$ ) compared to MGN3 treatment without TLRI.

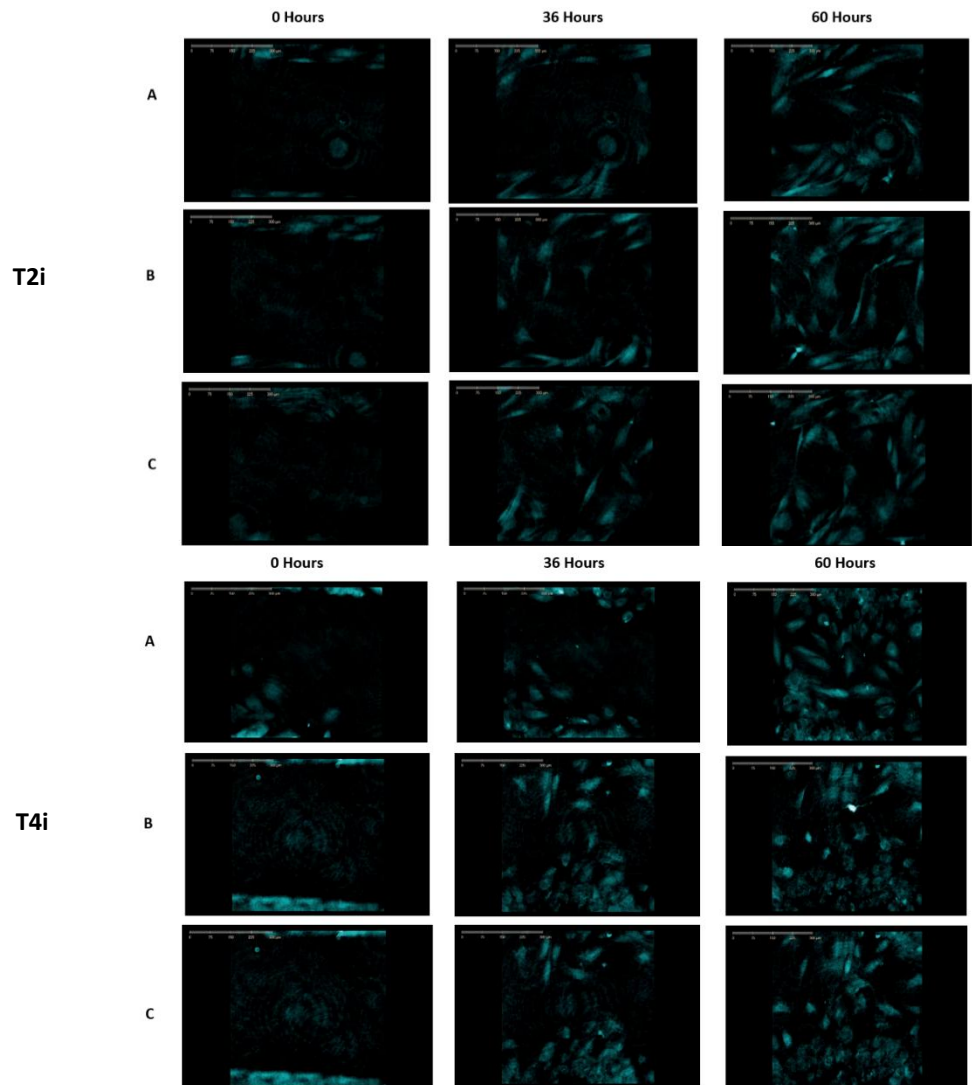
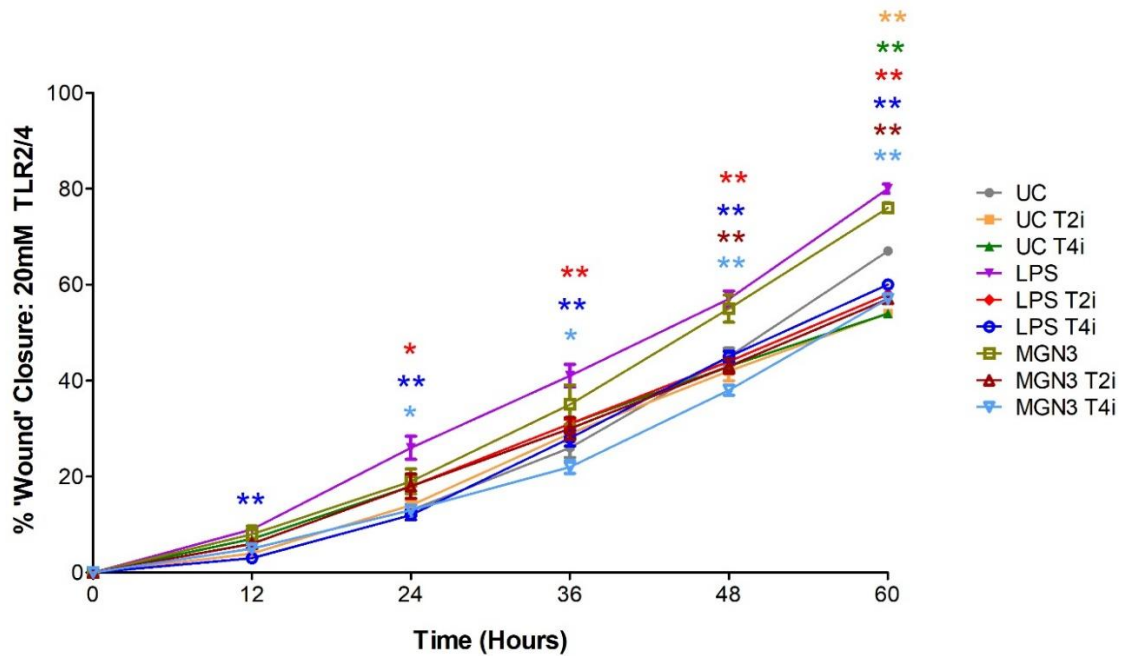


**Figure 5. 5: The Effect of MGN3 on Fibroblast ‘Wound’ Closure at 11mM Glucose after TLR2 and TLR4 Inhibition.** HDFs were cultured with 11mM glucose, treated with LPS (5ug/ml) or MGN3 (2mg/ml) and TLR2 (T2i) or TLR4 (T4i) inhibition and incubated for 60 hours on a Holomonitor microscope. Images shown represent different time points (0, 36 and 60 hours). Panel A show untreated fibroblasts and T2i or T4i, Panel B are fibroblasts treated with LPS and T2i or T4i and Panel C shows fibroblasts treated with MGN3 and T2i or T4i.

### 5.4.3.2 Effect of TLR inhibition on MGN3-Mediated Fibroblast 'Wound' Closure under Hyperglycaemic (20mM Glucose) Culture Conditions

The results showed TLR2/4 inhibition reduced the ability of the fibroblasts cultured at 20mM glucose to undergo wound closure in all cases (Figures 5.6 and 5.7) compared to corresponding treatments lacking TLR inhibition.



TIME (hrs)	UC	UC T2i	UC T4i	LPS	LPS T2i	LPS T4i	MGN3	MGN3 T2i	MGN3 T4i
0	0	0	0	0	0	0	0	0	0
12	5	4	7	9	6	3	8	6	5
24	13	14	18	26	18	12	19	18	13
36	26	29	31	41	31	28	35	30	22
48	45	42	43	57	44	45	55	43	38
60	67	54	54	80	58	60	76	57	57

**Figure 5. 6: Effect of TLR inhibition on MGN3-Mediated Fibroblast 'Wound' Closure under 20mM Culture Conditions.** The area % change in wound closure was calculated based on Holomonitor images captured over a period of 60 hours following treatment of HDF wound models cultured under hyperglycaemic (20mM glucose) with/without MGN3 (MGN) or LPS in the presence/absence of TLR2 (T2i) or TLR4 (T4i) inhibition. Significant decreases were seen in % wound closure compared to corresponding treatments lacking TLR inhibition (\*  $P < 0.05$  and \*\*  $P < 0.01$  determined by t-tests;  $n = 12$ ). UC = untreated control. Lines and error bars indicate the wound area %  $\pm$  the standard error of the mean (SEM) in all cases. Table shows the % wound closure after treatment at different timepoints.

Statistical analysis by independent two tailed t-tests indicated significant differences between the groups. There were significant decreases in wound closure seen after 60 hours ( $P < 0.001$ ) in both TLR2/4 inhibited untreated fibroblasts compared to UC without TLRi. There was a decrease in TLR2 inhibited LPS treated ( $P = 0.013$ ) at 24 hours and 36 hours

onwards ( $P < 0.001$ ) and significant decreases in TLR4 inhibited LPS treated fibroblasts at all time points ( $P < 0.001$ ) compared to LPS treatment without TLRi. There were also significant decreases in wound closure in TLR2 inhibited MGN3 treated fibroblasts at 48 hours onwards ( $P < 0.01$ ) and TLR4 inhibited MGN3 treated fibroblasts at 24 ( $P = 0.037$ ), 36 ( $P = 0.014$ ) and 48 hours onwards ( $P < 0.001$ ) compared to MGN3 treatment without TLRi.

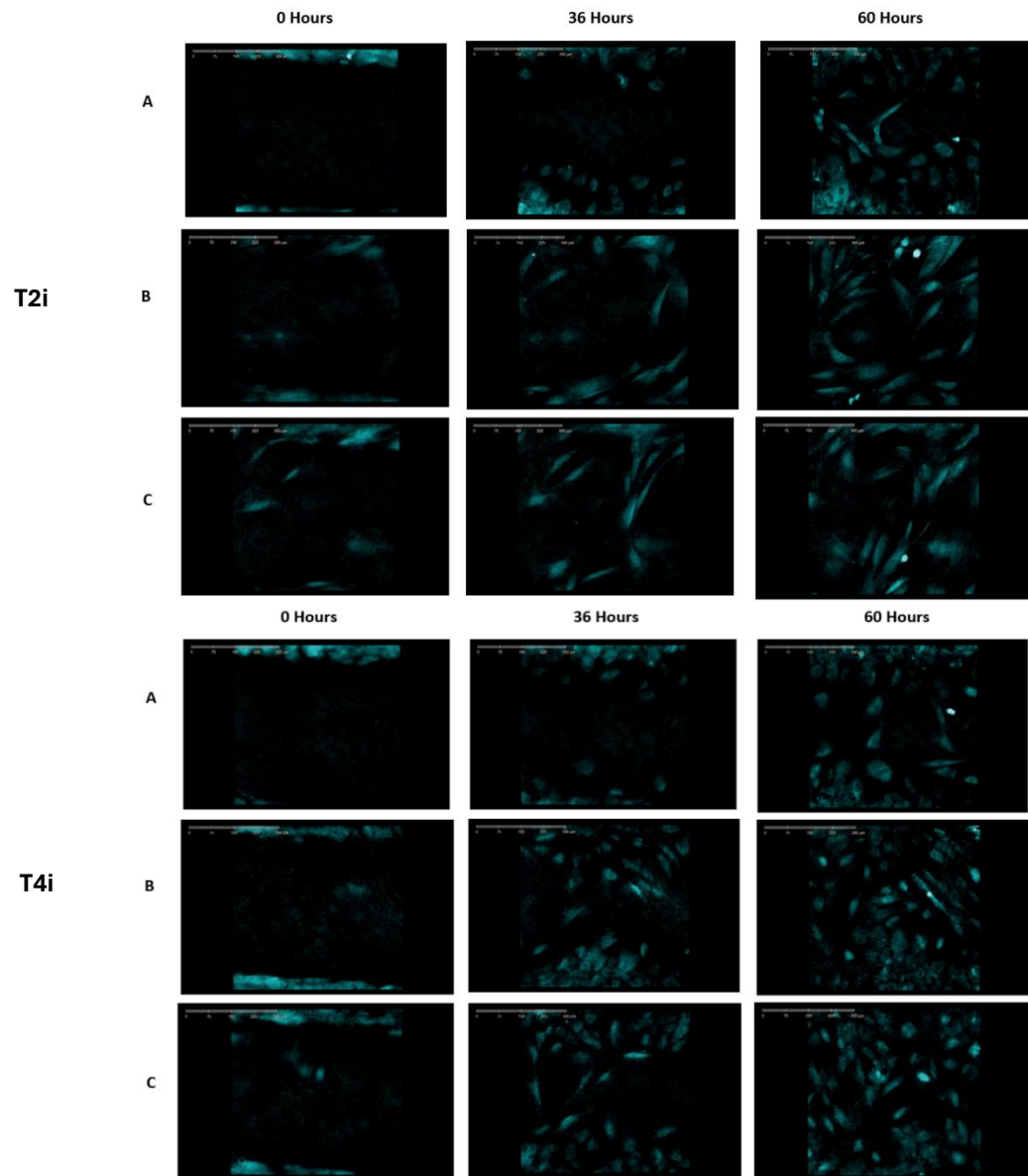


**Figure 5. 7: The Effect of MGN3 on Fibroblast ‘Wound’ Closure at 20mM Glucose after TLR2 and TLR4 Inhibition.** HDFs were cultured with 20mM glucose, treated with LPS (5ug/ml) or MGN3 (2mg/ml) and TLR2 (T2i) or TLR4 (T4i) inhibition and incubated for 60 hours on a Holomonitor microscope. Images shown represent different time points (0, 36 and 60 hours). Panel A show untreated fibroblasts and T2i or T4i, Panel B are fibroblasts treated with LPS and T2i or T4i and Panel C shows fibroblasts treated with MGN3 and T2i or T4i.

### 5.4.3.3 Effect of TLR inhibition on MGN3-Mediated Fibroblast 'Wound' Closure under Hyperglycaemic (30mM Glucose) Culture Conditions

The results showed TLR2/4 inhibition reduced the ability of the fibroblasts cultured at 30mM glucose to undergo wound closure in all cases (Figures 5.8 and 5.9) compared to corresponding treatments lacking TLR inhibition.

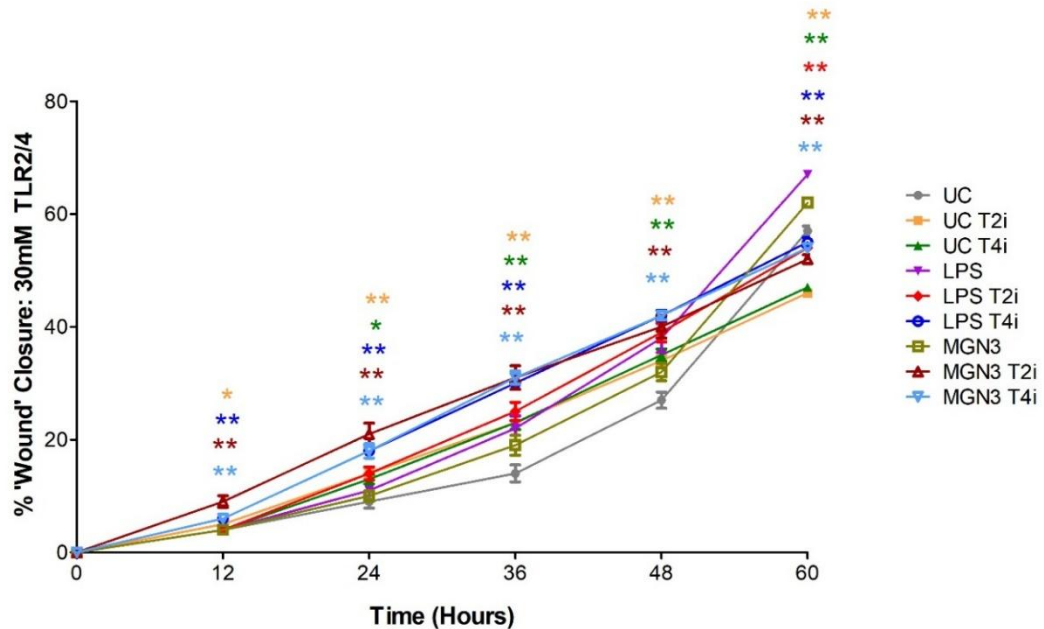


**Figure 5. 8: Effect of TLR inhibition on MGN3-Mediated Fibroblast 'Wound' Closure under 30mM Culture Conditions.** The area % change in wound closure was calculated based on Holomonitor images captured over a period of 60 hours following treatment of HDF wound models cultured under hyperglycaemic (30mM glucose) with/without MGN3 (MGN) or LPS in the presence/absence of TLR2 (T2i) or TLR4 (T4i) inhibition. Significant decreases were seen in % wound closure compared to corresponding treatments lacking TLR inhibition (\*  $P < 0.05$  and \*\*  $P < 0.01$  determined by t-tests;  $n = 12$ ). UC = untreated control. Lines and error bars indicate the wound area %  $\pm$  the standard error of the mean (SEM) in all cases. Table shows the % wound closure after treatment at different timepoints. Table shows the % wound closure after treatment at different timepoints.

Statistical analysis by independent two tailed t-tests indicated significant differences between the groups. There were significant decreases wound closure in the TLR2 inhibited untreated fibroblasts after 12 hours ( $P = 0.037$ ) and 24 hours onwards ( $P < 0.01$ ), and the TLR4 inhibited untreated fibroblasts after 24 hours ( $P = 0.011$ ) and 36 hours onwards ( $P < 0.001$ ) compared to untreated fibroblast without TLRi. There were decreases in TLR2

inhibited LPS treated fibroblasts after 60 hours ( $P < 0.001$ ) and in the TLR4 inhibited LPS treated fibroblasts ( $P < 0.01$ ) at all time points apart from 48 hours compared to LPS treatment without TLRI. There were also significant decreases in wound closure in TLR2/4 inhibited MGN3 treated fibroblasts ( $P < 0.01$ ) at all time points compared to MGN3 treatment without TLRI.

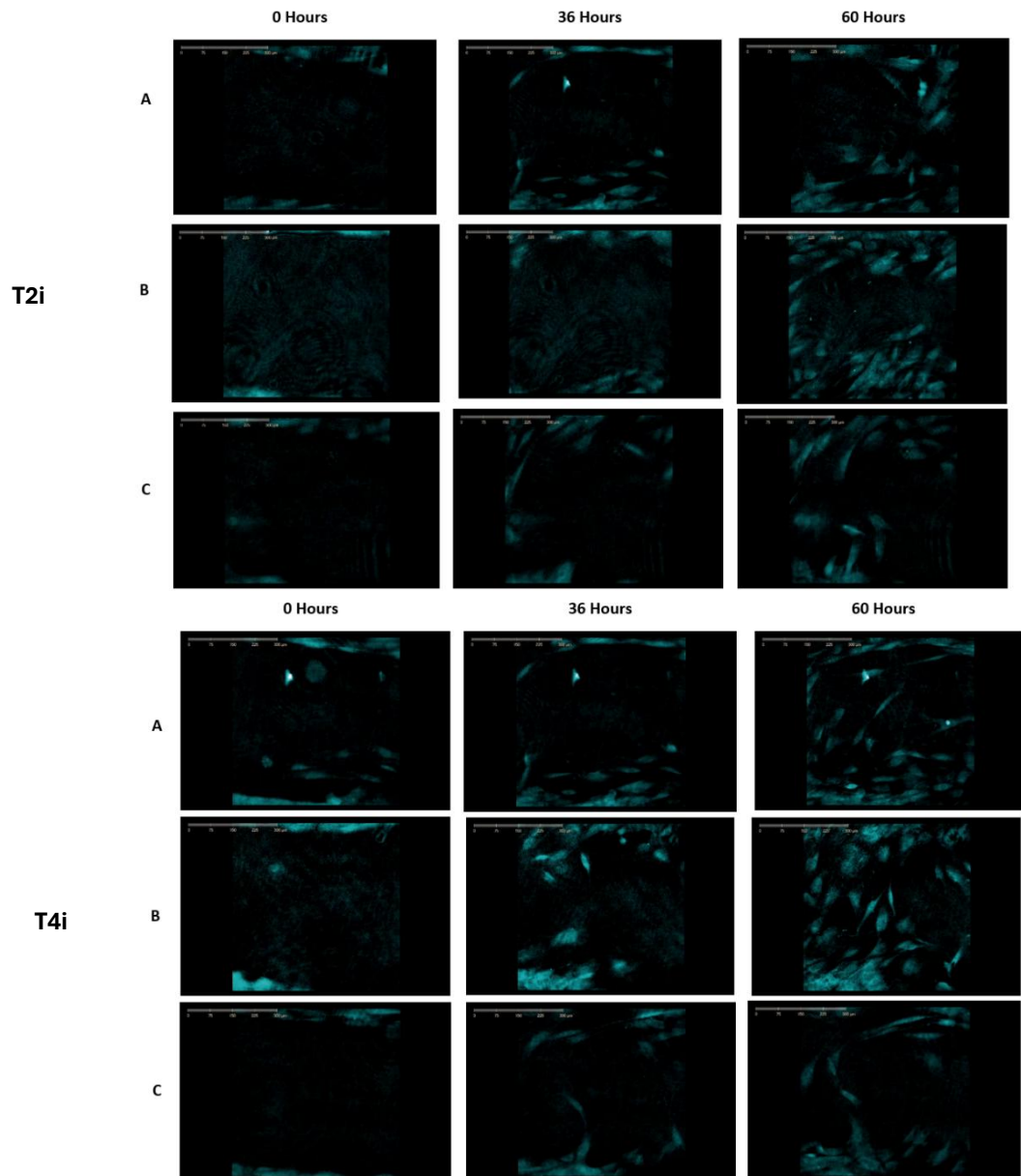


**Figure 5. 9: The Effect of MGN3 on Fibroblast ‘Wound’ Closure at 30mM Glucose after TLR2 and TLR4 Inhibition.** HDFs were cultured with 30mM glucose, treated with LPS (5ug/ml) or MGN3 (2mg/ml) and TLR2 (T2i) or TLR4 (T4i) inhibition and incubated for 60 hours on a Holomonitor microscope. Images shown represent different time points (0, 36 and 60 hours). Panel A show untreated fibroblasts and T2i or T4i, Panel B are fibroblasts treated with LPS and T2i or T4i and Panel C shows fibroblasts treated with MGN3 and T2i or T4i.

#### **5.4.4 Contribution of Cell Proliferation and Migration on MGN3-Mediated Fibroblast 'Wound' Closure**

##### **5.4.4.1 The Effect Mitomycin C on Fibroblast Proliferation**

HDFs were seeded at  $5 \times 10^4$  cells/ml at multiple glucose concentrations (11, 20, and 30mM) in DMEM CM and incubated at 37°C and 5% CO<sub>2</sub> until 50% confluent. Cells were then incubated with/without mitomycin C (MC) at different concentrations (2, 5, 10, 20ug/ml) for 2 hours before taking initial cell counts (time T=0). Fibroblasts were then washed in DMEM CM and cell counts taken again after incubated for time T = 24, 48 and 72 hours (37°C, 5% CO<sub>2</sub>). Cell proliferation (CP) was then determined in the negative control (NC) lacking MC exposure and in fibroblasts exposed to MC at T hours using the equation described in the methods (section 5.3.2). The % inhibition of fibroblast proliferation (Figure 5. 10) caused by exposure to MC compared to the NC was then calculated using the equation in the methods (section 5.3.2). The purpose of this investigation was to determine which concentration of MC inhibited proliferation of fibroblasts by 90% or more over the equivalent time period of the wound closure assay (60 hours) so this concentration could be used to efficiently block fibroblast proliferation in subsequent experiments.

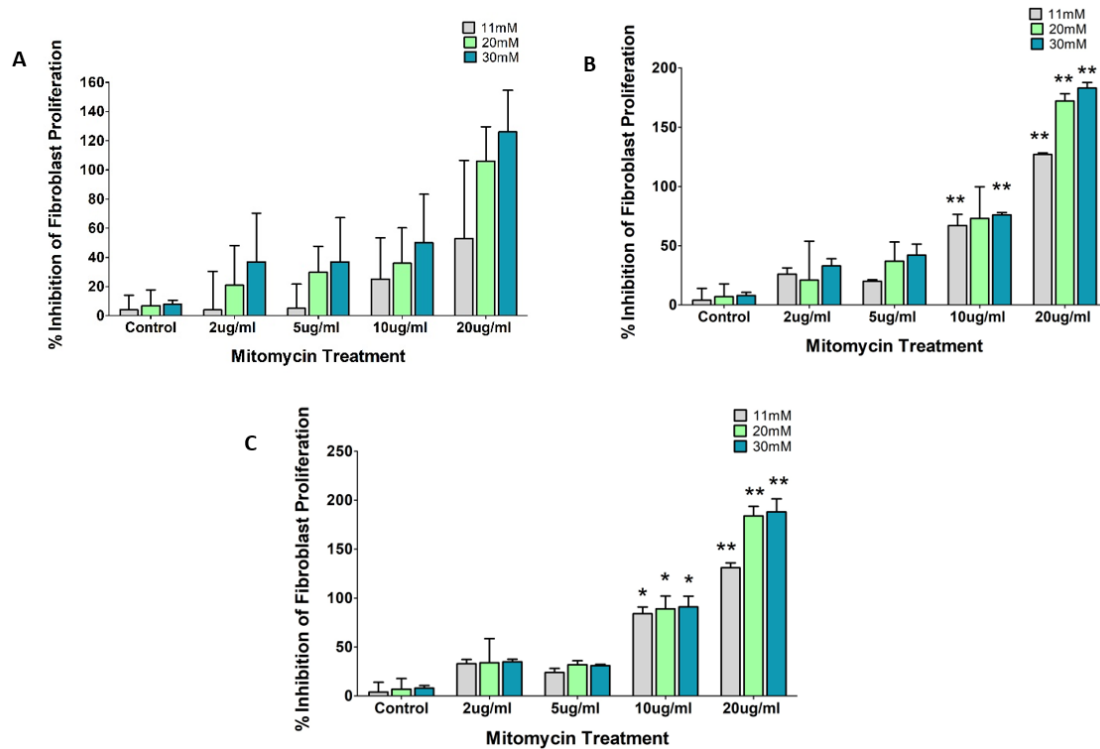


**Figure 5.10: Evaluation of Fibroblast proliferation inhibition following mitomycin C treatment.** HDFs were grown in multiple glucose concentrations (11, 20 and 30mM) and treated with mitomycin (MC) at different concentrations (2, 5, 10 and 20ug/ml) to evaluate cell proliferation. Graph A shows % inhibition following MC after 24 hours, graph B after 48 hours and graph C after 72 hours. Significant increases were seen between the groups when comparisons were made against the corresponding glycaemic untreated control (UC) (\*  $P < 0.05$  and \*\*  $P < 0.01$  determined by t-tests;  $n = 6$ ). Columns and error bars indicate % Inhibition  $\pm$  the standard error of the mean (SEM) in all cases.

After 24 hours MC treatment (Figure 5.10A) fibroblast proliferation was inhibited by 53% in the highest MC treatment (20ug/ml) in fibroblasts cultured in 11mM glucose. The fibroblast proliferation was inhibited by 25% in the 10ug/ml MC group and up to 5% in the lowest MC treatment groups (2 and 5ug/ml). Fibroblast proliferation in the fibroblasts cultured at 20mM glucose was inhibited by 106% and 126% in the fibroblast cultured at 30mM glucose. This is a sharp increase in comparison to fibroblasts treated with 10ug MC at 20mM glucose where 36% of fibroblast proliferation was inhibited and fibroblasts cultured at 30mM where 50% of fibroblast proliferation was inhibited. These results indicate that treatment with 10ug/ml MC steadily inhibited fibroblast inhibition after 24 hours at pre-diabetic (11mM) and hyperglycaemic (20 and 30mM) conditions. Alternatively, treatment with 20ug/ml MC

resulted in 53% fibroblast proliferation at pre-diabetic conditions but greatly inhibited (>100%) fibroblast proliferation at hyperglycaemic conditions.

After 48 hours of MC treatment (Figure 5.10B) fibroblast proliferation ( $P < 0.01$ ) was significantly inhibited in fibroblasts cultured at 11mM glucose (127% inhibition), in fibroblasts cultured at 20mM (172% inhibition) and in fibroblast cultured at 30mM (183% inhibition) compared to the control group. After treatment with 10ug MC fibroblast proliferation was also significantly ( $P < 0.01$ ) inhibited in fibroblasts cultured at 11mM glucose (67% inhibition), in fibroblasts cultured at 20mM (73% inhibition) and in fibroblast cultured at 30mM (76% inhibition) compared to the control group. There were no significant changes ( $P > 0.05$ ) in fibroblast proliferation inhibition seen in the low MC concentration groups (2 and 5ug/ml) at pre-diabetic and hyperglycaemic conditions when compared to corresponding UC. These results suggest treatment with 10ug/ml MC steadily inhibited fibroblast inhibition (>70%) after 48 hours at pre-diabetic (11mM) and hyperglycaemic (20 and 30mM) conditions, but treatment with 20ug/ml MC greatly inhibited (>100%) fibroblast proliferation at both pre-diabetic and hyperglycaemic conditions.

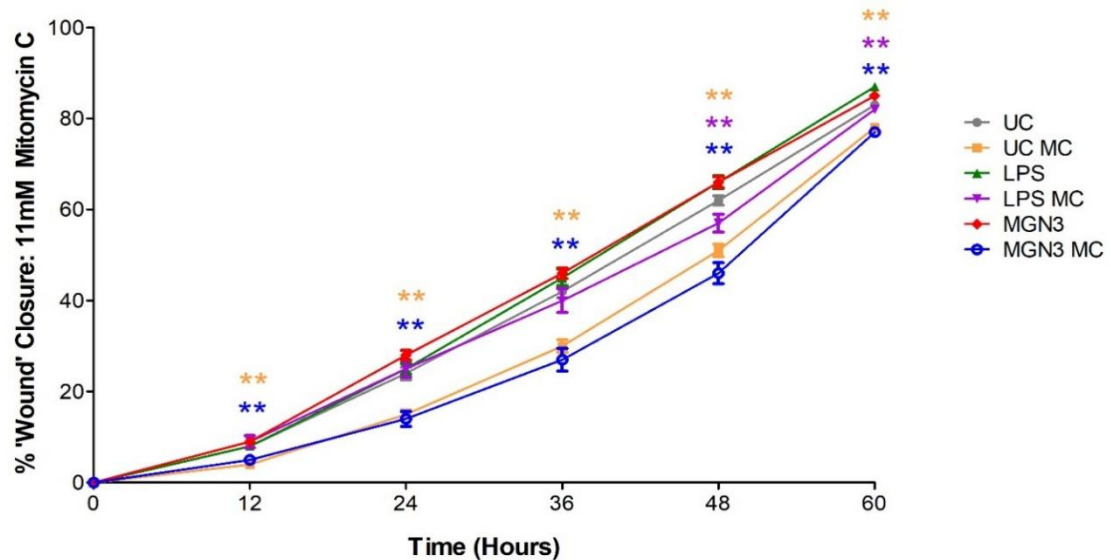
After 72 hours of MC treatment (Figure 5.10C) fibroblast proliferation was significantly ( $P < 0.01$ ) inhibited in fibroblast cultured at 11mM glucose (131% inhibition), in fibroblasts cultured at 20mM (184% inhibition) and in fibroblast cultured at 30mM (188% inhibition), following treatment with 20ug/ml MC compared to the control group. After treatment with 10ug MC fibroblast proliferation was also significantly ( $P < 0.05$ ) inhibited in fibroblasts cultured at 11mM glucose (85% inhibition), in fibroblasts cultured at 20mM (89% inhibition) and in fibroblast cultured at 30mM (91% inhibition) compared to the control group. There were no significant changes ( $P > 0.05$ ) in fibroblast proliferation inhibition seen in the low MC concentration groups (2 and 5ug/ml) at 11m and 20mM glucose, but significant ( $P < 0.01$ ) decreases were seen at 30Mm when comparisons when made against the corresponding controls.

Overall, these results indicate treatment with MC (at 10ug/ml) over 72 hours resulted in a gradual inhibition (>85%) of fibroblast proliferation compared to 20ug/ml MC treatment which resulted in a rapid increase (>100%) in the inhibition of fibroblast proliferation after

24 hours in hyperglycaemic (20 and 30mM) conditions, and pre-diabetic (11mM) conditions after 48 hours. For this reason, it was decided that MC treatment at a concentration of 20ug/ml was best suited in subsequent experiments because it completely and promptly blocked fibroblast proliferation across all glycaemic conditions.

#### 5.4.4.2 The Effect of Mitomycin C on Fibroblast ‘Wound’ Closure at 11mM Glucose

Despite blocking cell proliferation with MC, which did reduce the % wound closure relative to corresponding treatments without MC (Figure 5.12), the wound closure still proceeded relatively closely to that observed in the absence of MC (particularly at T = 12 and 60 hours) (See Figure 5.11) suggesting cell migration (rather than cell proliferation) was probably having a greater influence on driving fibroblast-mediated wound closure.



TIME (hrs)	UC	UC MC	LPS	LPS MC	MGN3	MGN3 MC
0	0	0	0	0	0	0
12	8	4	8	9	9	5
24	24	15	25	25	28	14
36	42	30	45	40	46	27
48	62	51	66	57	66	46
60	83	78	87	82	85	77

**Figure 5. 11: % ‘Wound’ Closure in HDFs at 11mM glucose after MGN3 treatment and mitomycin C treatment.** The % ‘wound’ closure was calculated in HDF at 11mM after LPS, MGN3 and Mitomycin C (MC) treatments for a span of 60 hours. Significant decreases were observed when comparisons were made between treatments in the presence of MC compared against corresponding treatments lacking MC. (\*\*  $P < 0.01$  determined by t-tests;  $n = 12$ ). Lines and error bars indicate the wound area %  $\pm$  the standard error of the mean (SEM) in all cases. Table shows the % wound closure after treatment at different timepoints.

Statistical analysis by independent t-tests showed there was a significant decrease in wound closure in the untreated fibroblasts in the presence of MC and MGN3-treated fibroblasts in the presence of MC ( $P < 0.01$ ) for all time points when compared to corresponding treatment groups. There was also a decrease in LPS treated fibroblasts in the presence of MC ( $P < 0.01$ ) from 48 hours onwards, when comparisons were made against the corresponding LPS treated fibroblasts lacking MC.

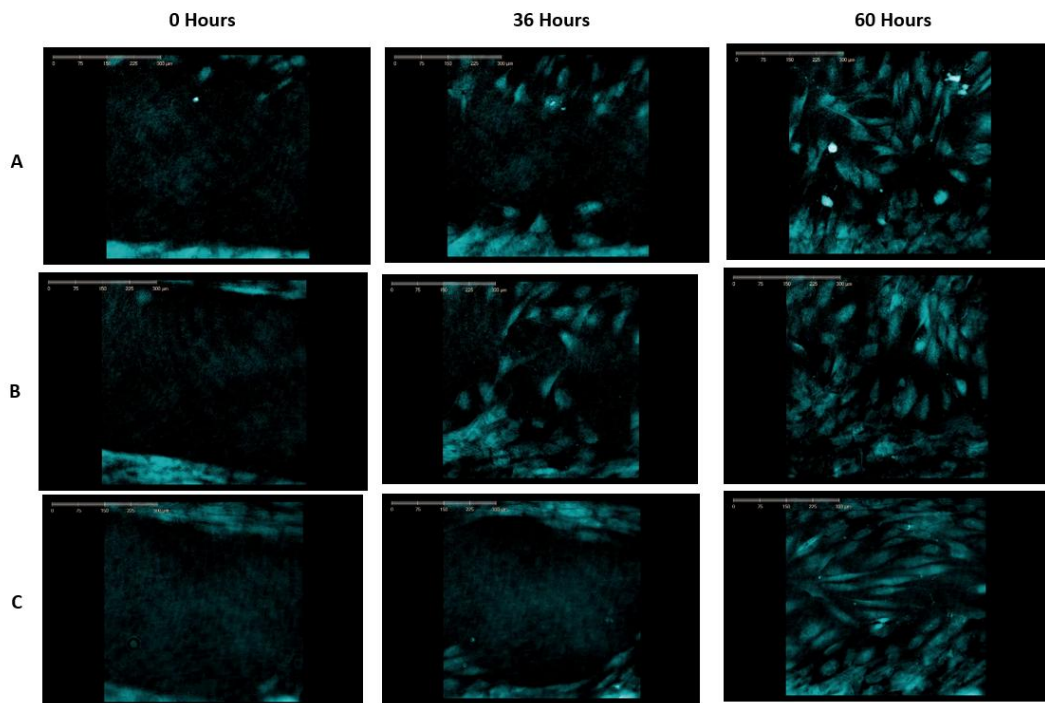
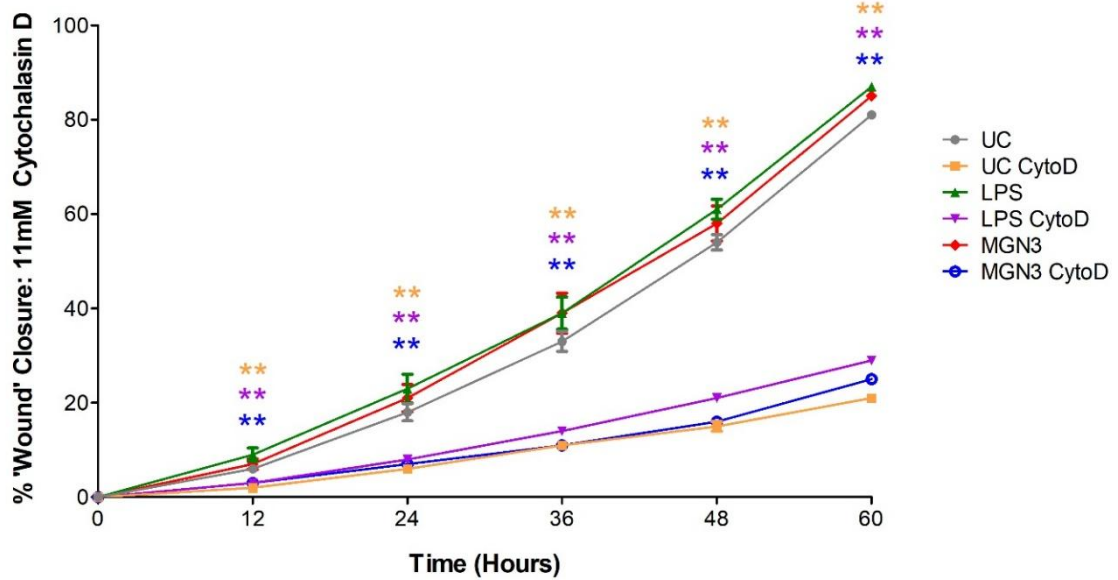


**Figure 5. 12: The Effect of Mitomycin C on Fibroblast ‘Wound’ Closure at 11mM Glucose.** HDFs were cultured with 11mM glucose, treated with LPS (5ug/ml) or MGN3 (2mg/ml) and Mitomycin C (MC) and incubated for 60 hours on a Holomonitor microscope. Images shown represent different time points (0, 36 and 60 hours). Panel A show untreated fibroblasts + MC, Panel B are fibroblasts treated with LPS + MC and Panel C shows fibroblasts treated with MGN3 + MC.

### 5.4.4.3 The Effect of Cytochalasin D on Fibroblast 'Wound' Closure at 11mM

There was a substantial significant ( $P < 0.01$ ) reduction in % wound closure following inhibition of cell migration due exposure to Cytochalasin D (Figures 5.13 and 5.14) compared to corresponding treatments lacking Cytochalasin D exposure (Figure 5.3), with the % wound closure failing to reach above 30% across the 60-hour observation period. These findings align with those in section 5.4.4.2 and confirm that wound closure was principally occurring through fibroblast migration rather than cell proliferation in both untreated and MGN3/LPS-treated fibroblasts.



TIME (hrs)	UC	UC CytoD	LPS	LPS CytoD	MGN3	MGN3 CytoD
0	0	0	0	0	0	0
12	6	2	9	3	7	3
24	18	6	23	8	21	7
36	33	11	39	14	39	11
48	54	15	61	21	58	16
60	81	21	87	29	85	25

**Figure 5. 13: % 'Wound' closure in HDFs at 11mM glucose after MGN3 and Cytochalasin D treatment.** The % 'wound' closure was calculated in HDF at 11mM glucose following LPS or MGN3 and Cytochalasin D (CytoD) treatments. Significant decreases were observed when comparisons were made between treatments in the presence of CytoD compared against corresponding treatments lacking CytoD (\*\*  $P < 0.01$  determined by t-tests;  $n = 12$ ). Lines and error bars indicate the wound area %  $\pm$  the standard error of the mean (SEM) in all cases. Table shows the % wound closure after treatment at different timepoints.

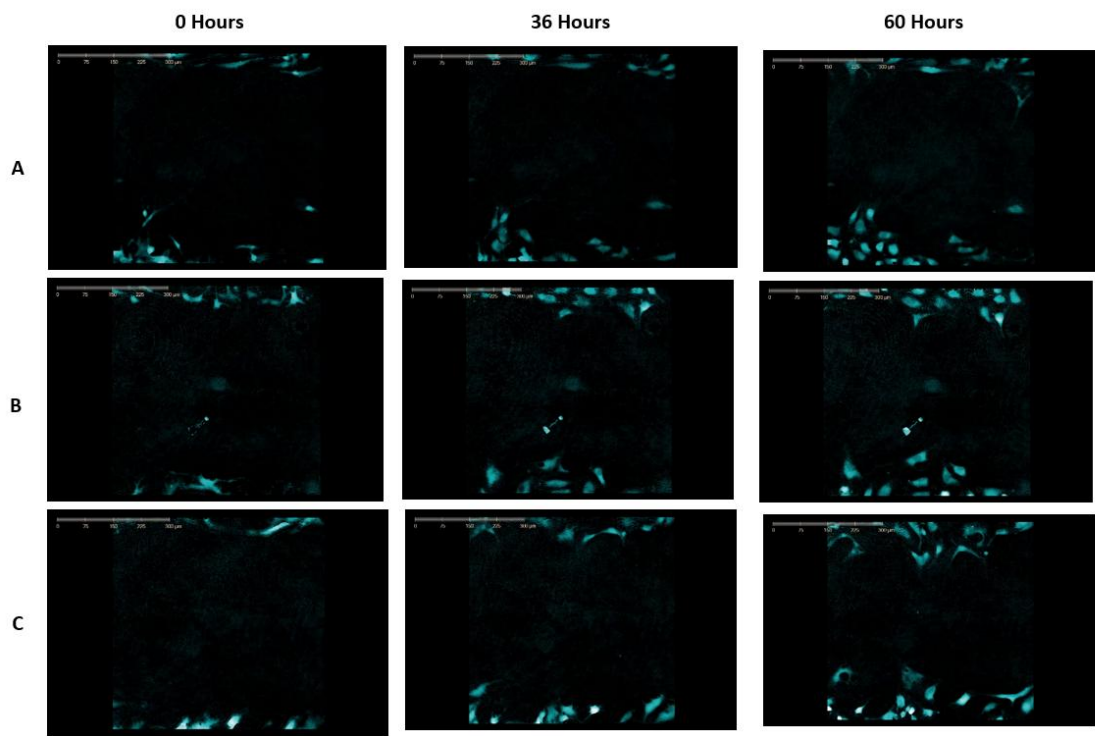
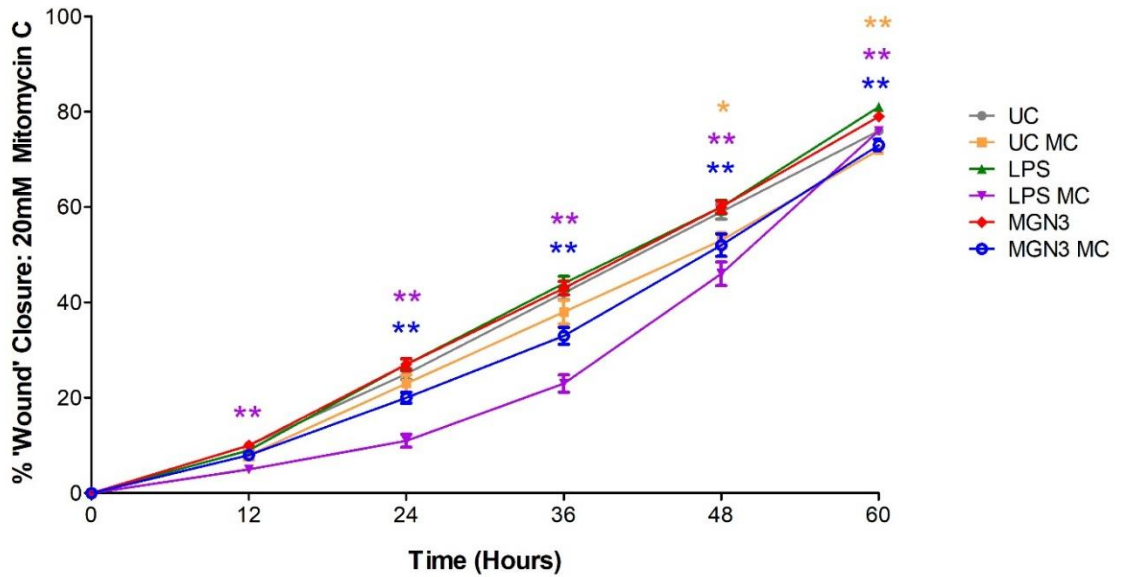


**Figure 5. 14: The Effect of Cytochalasin D on Fibroblast 'Wound' Closure after at 11mM Glucose.** HDFs were cultured with 11mM glucose, treated with LPS (5ug/ml) or MGN3 (2mg/ml) and Cytochalasin D (CytoD) and incubated for 60 hours on a Holomonitor microscope. Images shown represent different time points (0, 36 and 60 hours). Panel A show untreated fibroblasts + CytoD, Panel B are fibroblasts treated with LPS + CytoD and Panel C shows fibroblasts treated with MGN3 + CytoD.

#### 5.4.4.4 The Effect of Mitomycin C on Fibroblast 'Wound' Closure at 20mM glucose

Despite blocking cell proliferation with MC, which did reduce the % wound closure relative to corresponding treatments without MC (Figure 7.21), the wound closure still proceeded relatively closely to that observed in the absence of MC (particularly at T = 12 and 60 hours) suggesting cell migration (rather than cell proliferation) was probably having a greater influence on driving fibroblast-mediated wound closure (Figure 5.15).



TIME (hrs)	UC	UC MC	LPS	LPS MC	MGN3	MGN3 MC
0	0	0	0	0	0	0
12	10	8	9	5	10	8
24	25	23	27	11	27	20
36	42	38	44	23	43	33
48	59	53	60	46	60	52
60	76	72	81	76	79	73

**Figure 5. 15: % 'Wound' closure in HDFs at 20mM glucose after MGN3 treatment and mitomycin C treatment.** The % 'wound' closure was calculated in HDF at 11mM after LPS, MGN3 and MC treatments for a span of 60 hours. Significant decreases were observed when comparisons were made between treatments in the presence of MC compared against corresponding treatments lacking MC (\* P < 0.05 and \*\* P < 0.01 determined by t-tests; n = 12). Lines and error bars indicate the wound area % ± the standard error of the mean (SEM) in all cases. Table shows the % wound closure after treatment at different timepoints.

Statistical analysis by independent t-tests showed there was a significant decrease in wound closure in the untreated fibroblasts in the presence of MC at 48 ( $P = 0.023$ ) and 60 hours ( $P < 0.01$ ) compared to untreated fibroblasts lacking MC. There were significant decreases in wound closure at all timepoints ( $P < 0.01$ ) in LPS treated fibroblasts in the presence of MC and decreases in wound closure in MGN3 treated fibroblasts in the presence of MC from 24 hours onwards ( $P < 0.01$ ) compared to corresponding treatments lacking MC .

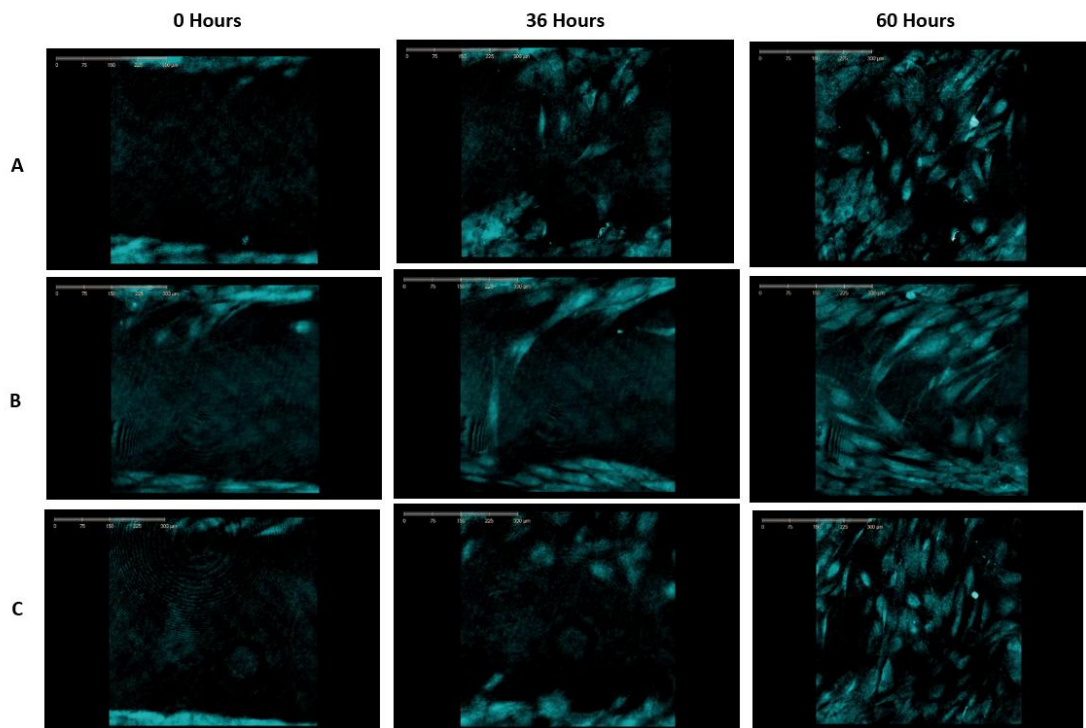
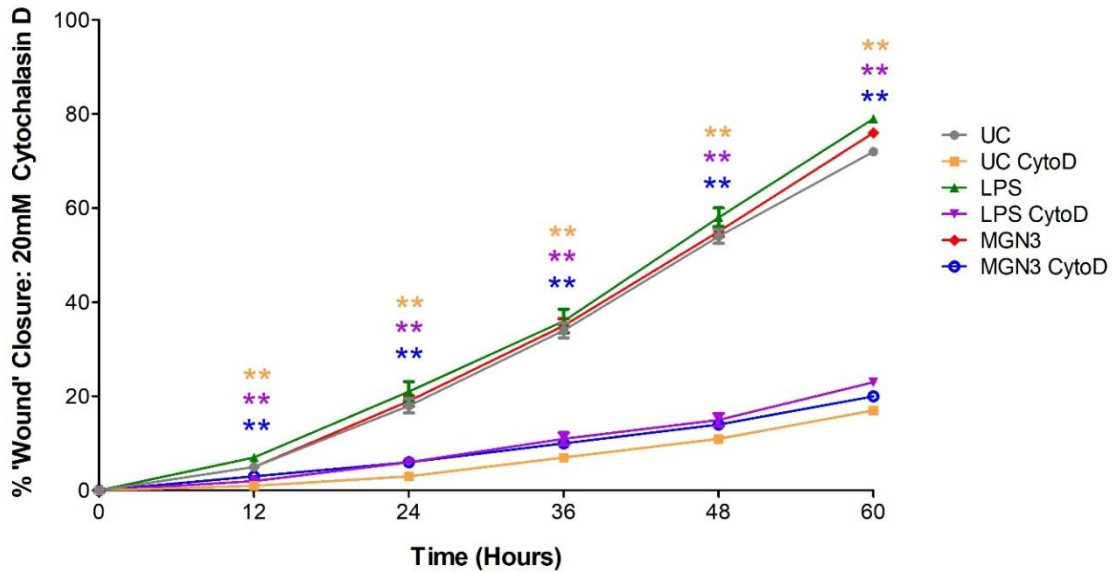


**Figure 5. 16: The Effect of MGN3 on Fibroblast ‘Wound’ Closure after Mitomycin C treatment at 20mM Glucose.** HDFs were cultured with 20mM glucose, treated with LPS (5ug/ml) or MGN3 (2mg/ml) and Mitomycin C (MC) and incubated for 60 hours on a Holomonitor microscope. Images shown represent different time points (0, 36 and 60 hours). Panel A show untreated fibroblasts + MC, Panel B are fibroblasts treated with LPS + MC and Panel C shows fibroblasts treated with MGN3 + MC.

#### 5.4.4.5 The Effect of Cytochalasin D on Fibroblast 'Wound' Closure at 20mM

A significant reduction ( $P < 0.01$ ) in % wound closure percentage was observed after inhibiting cell migration with Cytochalasin D (Figures 5.17 and 5.18), compared to treatments without Cytochalasin D (Figure 5.4). Wound closure did not exceed 25% over the 60-hour observation period. These results are consistent with those in Section 7.4.4.5, further confirming that fibroblast migration, rather than cell proliferation, was primarily responsible for wound closure in both untreated and MGN3/LPS-treated fibroblasts.



TIME (hrs)	UC	UC CytoD	LPS	LPS CytoD	MGN3	MGN3 CytoD
0	0	0	0	0	0	0
12	5	1	7	2	5	3
24	18	3	21	6	19	6
36	34	7	36	11	35	10
48	54	11	58	15	55	14
60	72	17	79	23	76	20

**Figure 5. 17: % 'Wound' closure in HDFs at 20mM glucose after MGN3 and Cytochalasin D treatment.** The % 'wound' closure was calculated in HDF at 20mM glucose following LPS, MGN3 and Cytochalasin D (CytoD) treatments. Significant increases were observed when comparisons were made between treatments in the presence of CytoD compared against corresponding treatments lacking CytoD (\*\*  $P < 0.01$  determined by t-tests;  $n = 12$ ). Lines and error bars indicate the wound area %  $\pm$  the standard error of the mean (SEM) in all cases. Table shows the % wound closure after treatment at different timepoints.

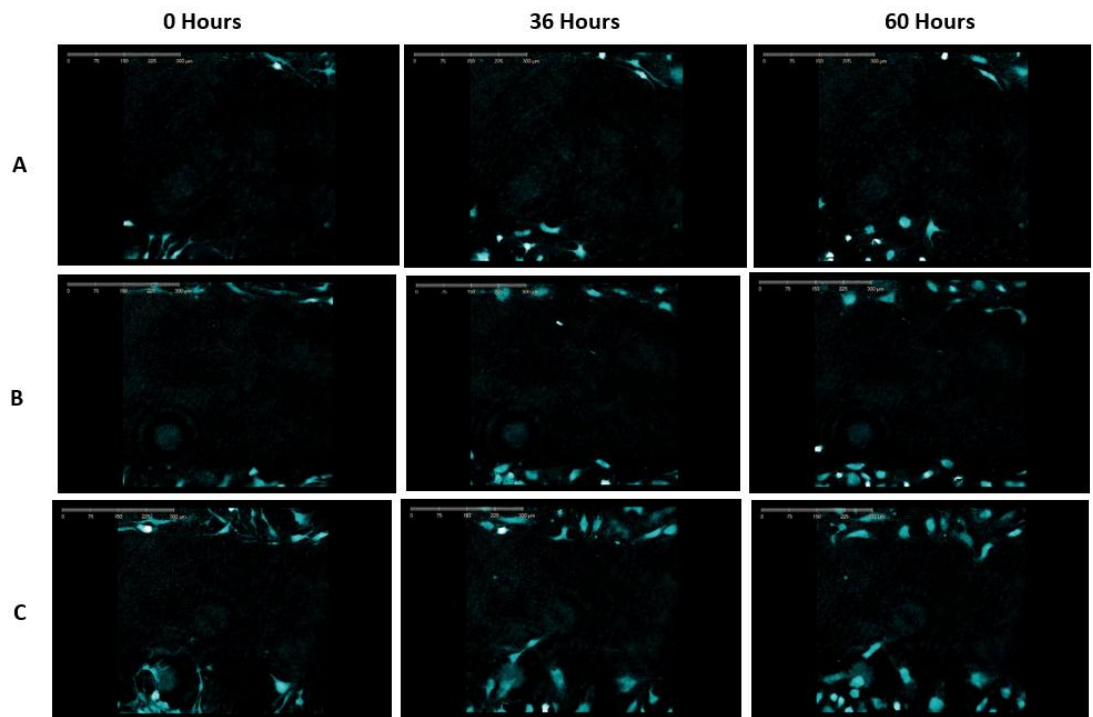
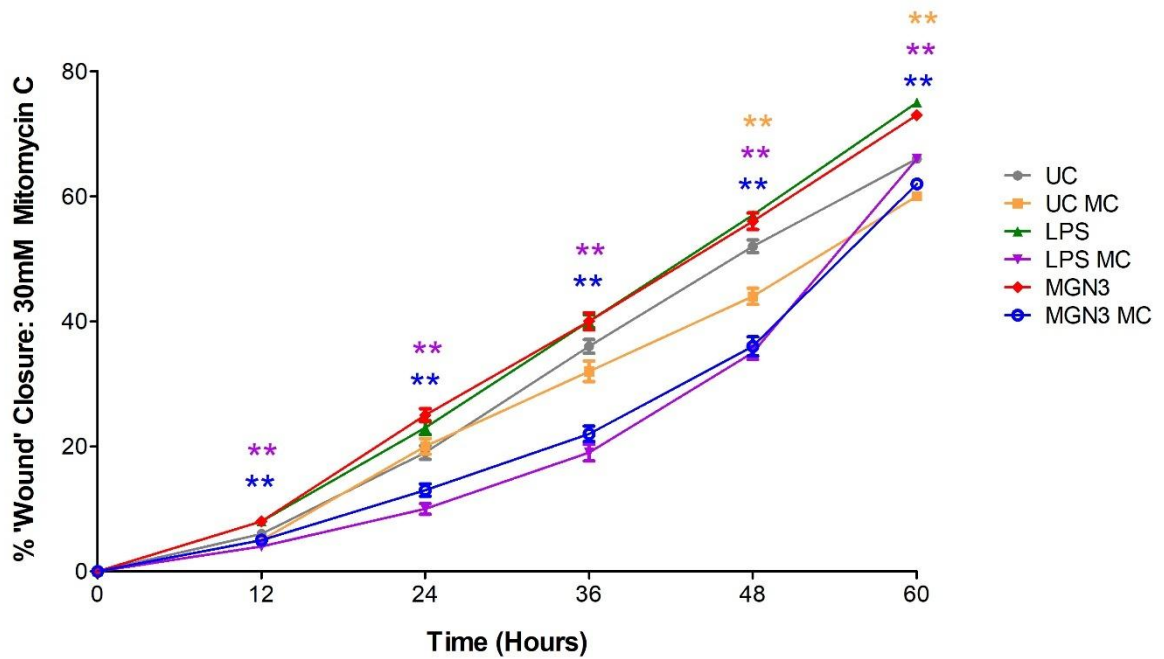


**Figure 5. 18: The Effect of Cytochalasin D on Fibroblast ‘Wound’ Closure after at 11mM Glucose.** HDFs were cultured with 11mM glucose, treated with LPS (5ug/ml) or MGN3 (2mg/ml) and Cytochalasin D (CytoD) and incubated for 60 hours on a Holomonitor microscope. Images shown represent different time points (0, 36 and 60 hours). Panel A show untreated fibroblasts + CytoD, Panel B are fibroblasts treated with LPS + CytoD and Panel C shows fibroblasts treated with MGN3 + CytoD.

#### 5.4.4.6 The Effect of Mitomycin C on Fibroblast 'Wound' Closure at 30mM glucose

Despite blocking cell proliferation with MC, which did reduce the % wound closure relative to corresponding treatments without MC (Figures 5.19 and 5.20), the wound closure still proceeded relatively closely to that observed in the absence of MC (particularly at T = 12 and 60 hours) suggesting cell migration (rather than cell proliferation) was most likely having a greater influence on driving fibroblast-mediated wound closure at 30mM glucose.



TIME (hrs)	UC	UC MC	LPS	LPS MC	MGN3	MGN3 MC
0	0	0	0	0	0	0
12	6	5	8	4	8	5
24	19	20	23	10	25	13
36	36	32	40	19	40	22
48	52	44	57	35	56	36
60	66	60	75	66	73	62

**Figure 5. 19: % 'Wound' Closure in HDFs at 30mM glucose after MGN3 treatment and Mitomycin C treatment.** The % 'wound' closure was calculated in HDF at 11mM after LPS, MGN3 and MC treatments for a span of 60 hours. Significant decreases were observed when comparisons were made between treatments in the presence of MC compared against corresponding treatments lacking MC (\*\*  $P < 0.01$  determined by  $t$ -tests;  $n = 12$ ). Lines and error bars indicate the wound area %  $\pm$  the standard error of the mean (SEM) in all cases. Table shows the % wound closure after treatment at different timepoints.

Statistical analysis by independent t-tests showed there was a significant decrease ( $P = 0.023$ ) in wound closure in the untreated fibroblasts in the presence of MC at 48 and 60 hours compared to untreated fibroblasts lacking MC. There were significant decreases in wound closure at all timepoints ( $P < 0.01$ ) in the MGN3/LPS treated fibroblasts in the presence of MC compared to corresponding treatments lacking MC.

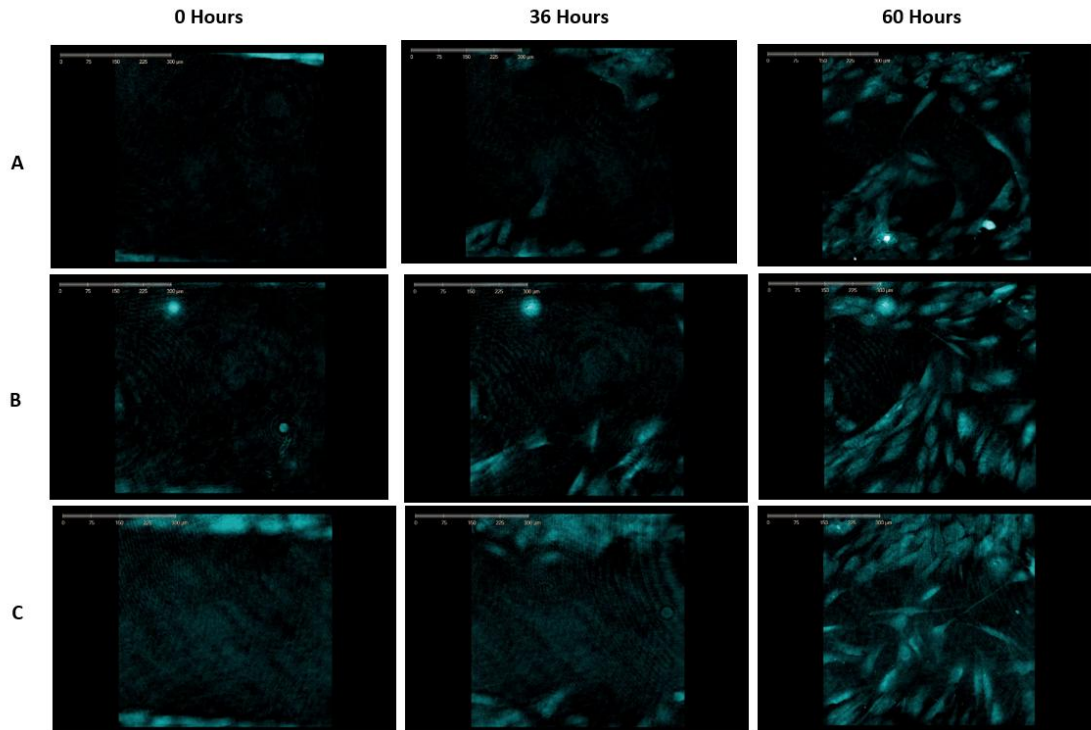
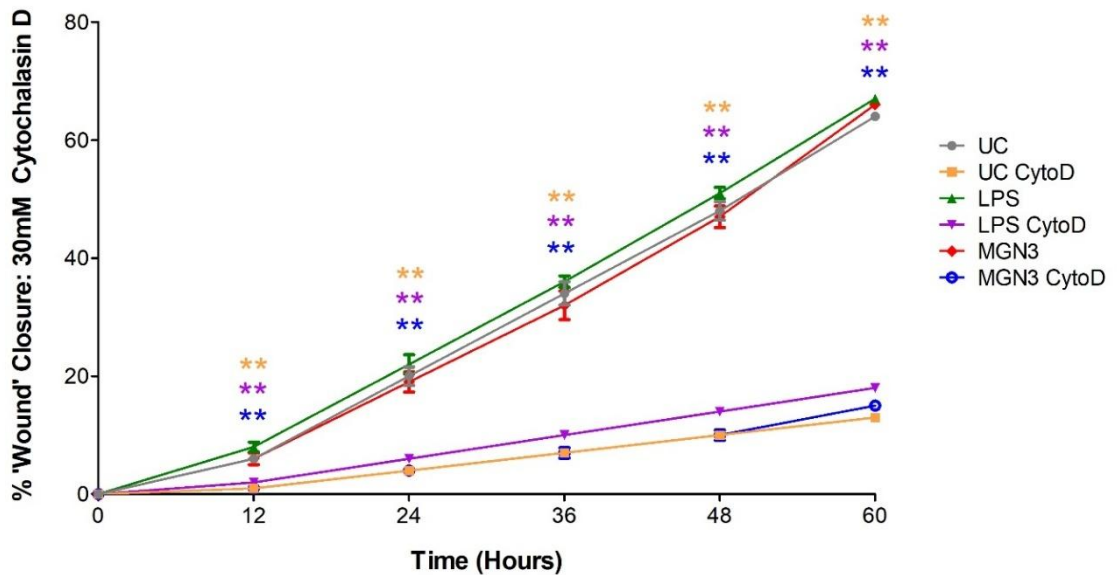


**Figure 5. 20: The Effect of MGN3 on Fibroblast 'Wound' Closure after Mitomycin C treatment at 30mM Glucose.** HDFs were cultured with 30mM glucose, treated with LPS (5ug/ml) or MGN3 (2mg/ml) and Mitomycin C (MC) and incubated for 60 hours on a Holomonitor microscope. Images shown represent different time points (0, 36 and 60 hours). Panel A show untreated fibroblasts + MC, Panel B are fibroblasts treated with LPS + MC and Panel C shows fibroblasts treated with MGN3 + MC.

#### 5.4.4.7 The Effect of Cytochalasin D on Fibroblast 'Wound' Closure at 30mM

A significant reduction ( $P < 0.01$ ) in % wound closure percentage was observed after inhibiting cell migration with Cytochalasin D (Figures 5.21 and 5.22), compared to treatments without Cytochalasin D (Figure 5.5). Wound closure did not exceed 20% over the 60-hour observation period. These results are consistent with those in Section 5.4.4.6, further confirming that fibroblast migration, rather than cell proliferation, was primarily responsible for wound closure in both untreated and MGN3/LPS-treated fibroblast.



TIME (hrs)	UC	UC CytoD	LPS	LPS CytoD	MGN3	MGN3 CytoD
0	0	0	0	0	0	0
12	6	1	8	2	6	1
24	20	4	22	6	19	4
36	34	7	36	10	32	7
48	48	10	51	14	47	10
60	64	13	67	18	66	15

**Figure 5. 21: % 'Wound' closure in HDFs at 30mM glucose after MGN3 and CytoD treatment.** The % 'wound' closure was calculated in HDF at 11mM glucose following LPS, MGN3 and CytoD treatments. Significant increases were observed when comparisons were made between treatments in the presence of CytoD compared against corresponding treatments lacking CytoD (\*\*  $P < 0.01$  determined by t-tests;  $n = 12$ ). Lines and error bars indicate the wound area %  $\pm$  the standard error of the mean (SEM) in all cases. Table shows the % wound closure after treatment at different timepoints.

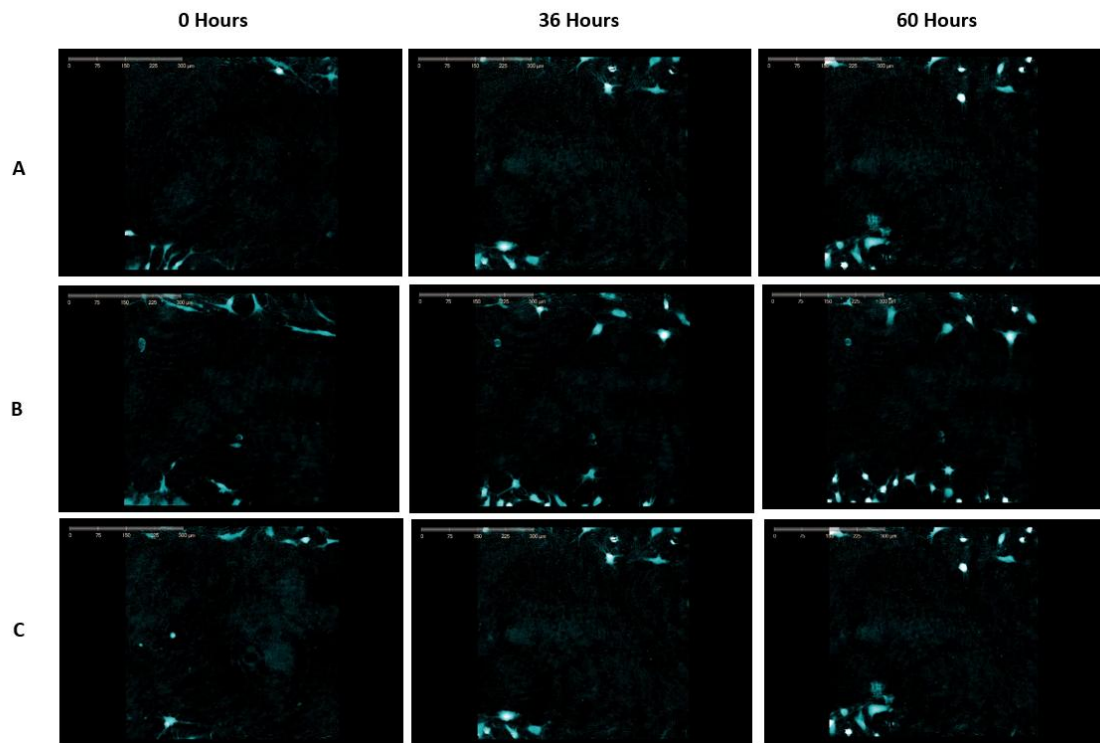


**Figure 5. 22: The Effect of Cytochalasin D on Fibroblast ‘Wound’ Closure after at 30mM Glucose.** HDFs were cultured with 30mM glucose, treated with LPS (5ug/ml) or MGN3 (2mg/ml) and Cytochalasin D (CytoD) and incubated for 60 hours on a Holomonitor microscope. Images shown represent different time points (0, 36 and 60 hours). Panel A show untreated fibroblasts + CytoD, Panel B are fibroblasts treated with LPS + CytoD and Panel C shows fibroblasts treated with MGN3 + CytoD.

#### 5.4.8 The Effect of Glucose on Keratinocyte 'Wound' Closure

The results showed as the glucose concentration increased there was a reduction in the % 'wound' closure after 24 hours (Figure 5. 23).

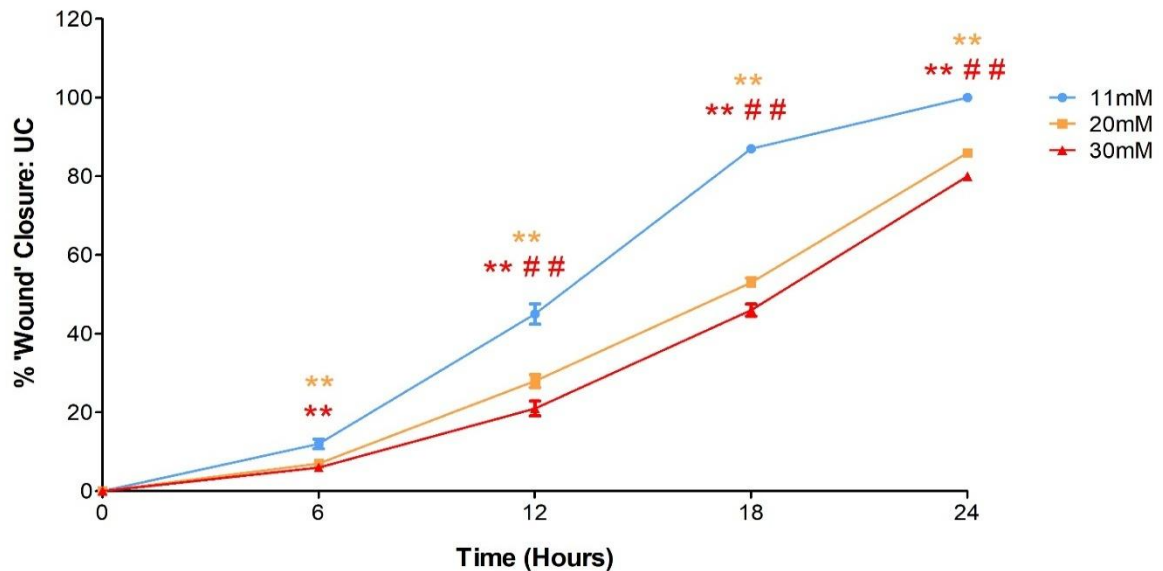


**Figure 5. 23: The Effect of glucose on Keratinocyte % 'Wound' closure.** The area % change was calculated in HACATs at different glucose concentrations (11, 20 and 30mM) for a span of 24 hours. Significant decreases were observed when comparisons were made against the 11UC (\*\*  $P < 0.01$  determined by t-tests;  $n = 12$ ) and 20UC groups (##  $P < 0.01$  determined by t-tests;  $n = 12$ ) Lines and error bars indicate the wound area %  $\pm$  the standard error of the mean (SEM) in all cases.

Statistical analysis using two tailed t-tests showed there was significant decreases ( $P < 0.01$ ) in wound closure in keratinocytes cultured at 20mM and 30mM glucose when compared to the keratinocytes cultured at 11mM glucose. There was also significant decrease ( $P < 0.01$ ) in wound closure in keratinocytes cultured at 30mM glucose after 12 hours onwards when compared to keratinocytes cultured at 20mM glucose.

### 5.4.9 Effect of MGN3 on Keratinocyte 'Wound' Closure

After 24-hour time period keratinocytes cultured in 11mM glucose had fully closed in untreated and MGN3/LPS treated keratinocytes. Keratinocytes cultured in 20mM glucose had covered 86% or more of the wound area (20UC – 86%, 20LPS – 93%, 20MGN3 – 90%) and keratinocytes cultured in 30mM glucose had covered 80% or more of the wound area (30UC – 80%, 30LPS – 86%, 30MGN3 – 83%) (See Figures 5. 24 and 5.25).

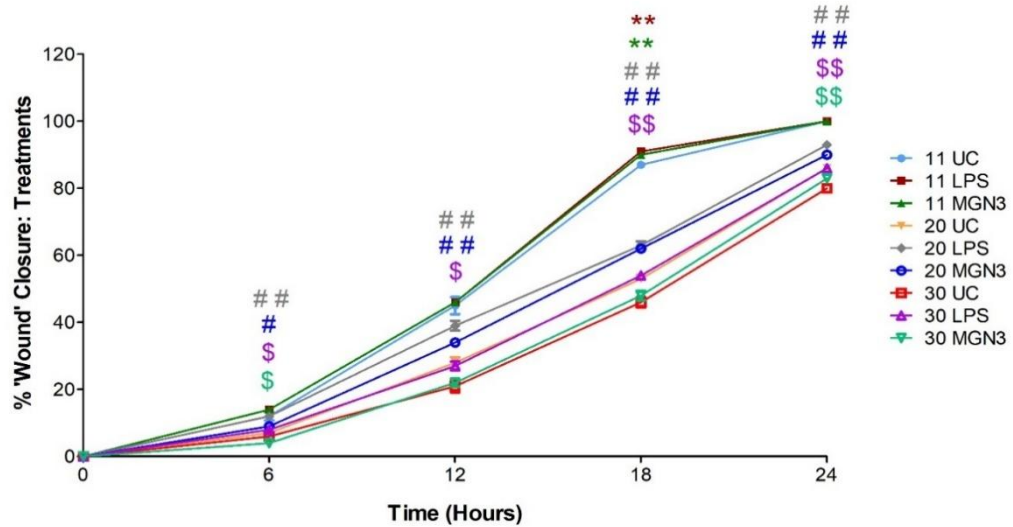


**Figure 5. 24: Effect of MGN3 on Keratinocyte % 'Wound' Closure.** The area % change was calculated in HACATs at different glucose concentrations (11, 20 and 30mM) and treatments (LPS and MGN3) for a span of 24 hours. Significant increases were observed when comparisons were made against the corresponding untreated controls (11UC \*\*  $P < 0.01$ , 20UC #  $P < 0.05$  and ##  $P < 0.01$ , 30UC \$  $P < 0.05$  and \$\$  $P < 0.01$  determined by t-tests;  $n = 12$ ). Lines and error bars indicate the wound area %  $\pm$  the standard error of the mean (SEM) in all cases. Table shows the % wound closure after treatment at different timepoints.

At 18 hours there was a significant increase ( $P < 0.01$ ) in wound closure in the MGN3/LPS treated keratinocytes compare to the corresponding glycaemic controls. At 20mM glucose the wound closure was significantly ( $P < 0.01$ ) increased at all timepoints in LPS treated keratinocytes compared to untreated keratinocytes cultured at 20mM glucose. The wound closure also significantly ( $P < 0.05$ ) at 6 hours and 12 hours onwards ( $P < 0.01$ ) in MGN3 treated keratinocytes compared to untreated keratinocytes at 20mM glucose. At 30mM glucose the wound closure in LPS treated keratinocytes was significantly ( $P < 0.05$ ) increased

at timepoints and significantly ( $P = 0.001$ ) at 24 hours compared to untreated keratinocytes at 30mM glucose.

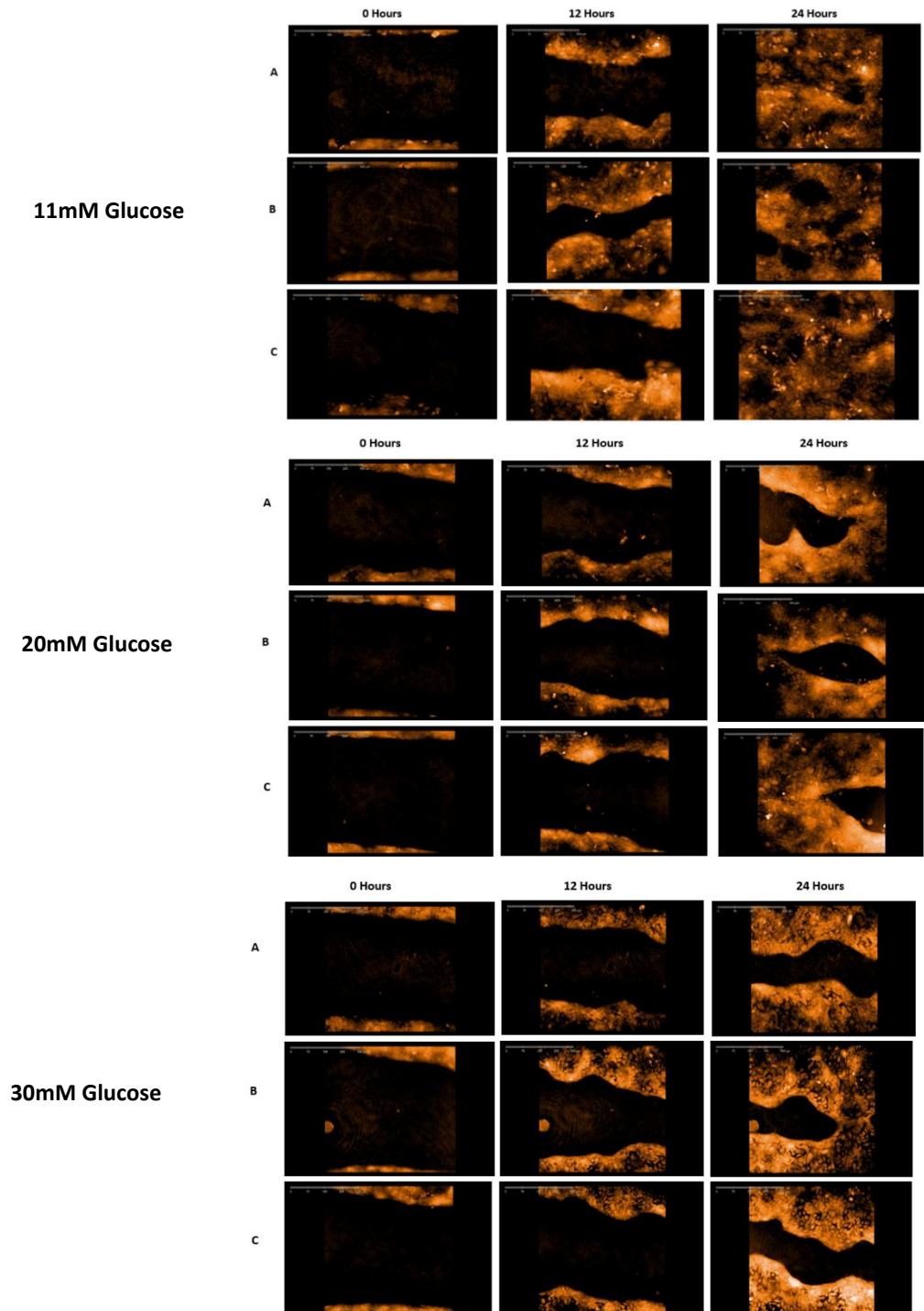
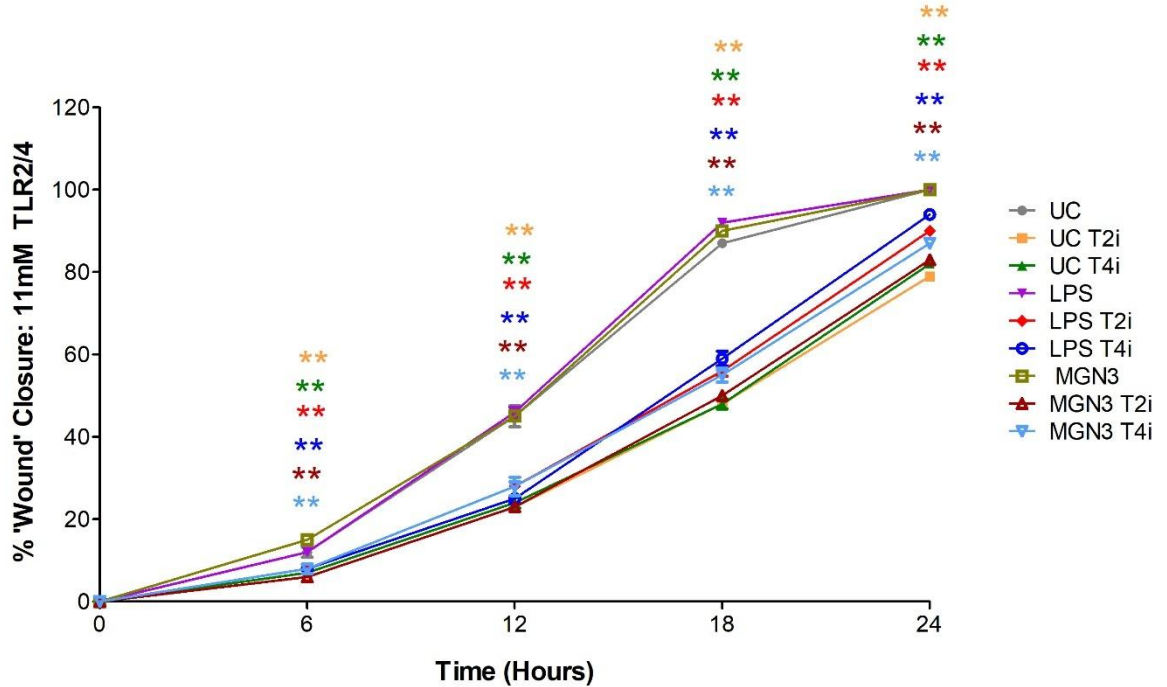


**Figure 5. 25: The Effect of MGN3 on Keratinocyte ‘Wound’ Closure at Different Glucose Levels.** HACATs were cultured with 11, 20 and 30mM glucose, treated with LPS or MGN3 and incubated for 24 hours on a Holomonitor microscope. Images shown represent different time points (0, 12 and 24 hours). Panel A show untreated fibroblasts, Panel B are fibroblasts treated with LPS (5ug/ml) and Panel C shows fibroblasts treated with MGN3 (2mg/ml).

### 5.4.10 Effect of TLR inhibition on MGN3-Mediated Fibroblast 'Wound' Closure

#### 5.4.10.1 The Effect of MGN3 with TLR inhibition on Keratinocyte 'Wound' Closure at 11mM glucose

The results showed TLR2/4 inhibition reduced the ability of the fibroblasts cultured at 11mM glucose to undergo wound closure in all cases (See Figures 5. 26 and 5. 27) compared to corresponding treatments lacking TLR inhibition.



Time (hours)	UC	UC T2	UC T4	LPS	LPS T2	LPS T4	MGN3	MGN3 T2	MGN3 T4
6	12	6	7	12	8	8	15	6	8
12	45	23	24	46	28	25	45	23	28
18	87	48	48	92	56	59	90	50	55
24	100	79	82	100	90	94	100	83	87

**Figure 5. 26: Effect of TLR inhibition on MGN3-Mediated Keratinocyte 'Wound' Closure under 11mM Culture Conditions.** The area % change in wound closure was calculated based on Holomonitor images captured over a period of 24 hours following treatment of HACAT wound models cultured at pre-diabetic (11mM glucose) with/without MGN3 (MGN) or LPS in the presence/absence of TLR2 (T2i) or TLR4 (T4i) inhibition. Significant decreases were seen in % wound closure compared to corresponding treatments lacking TLR inhibition (\*  $P < 0.05$  and \*\*  $P < 0.01$  determined by t-tests;  $n = 12$ ). UC = untreated control. Lines and error bars indicate the wound area %  $\pm$  the standard error of the mean (SEM) in all cases. Table shows the % wound closure after treatment at different timepoints.

Statistical analysis by independent two tailed t-tests indicated significant differences between groups. There were significant decreases in wound closure ( $P < 0.01$ ) at all timepoints in TLR2/4 untreated and MGN3/LPS treated keratinocytes when compared to untreated and MGN3/LPS treated keratinocytes without TLR2/4 inhibition.

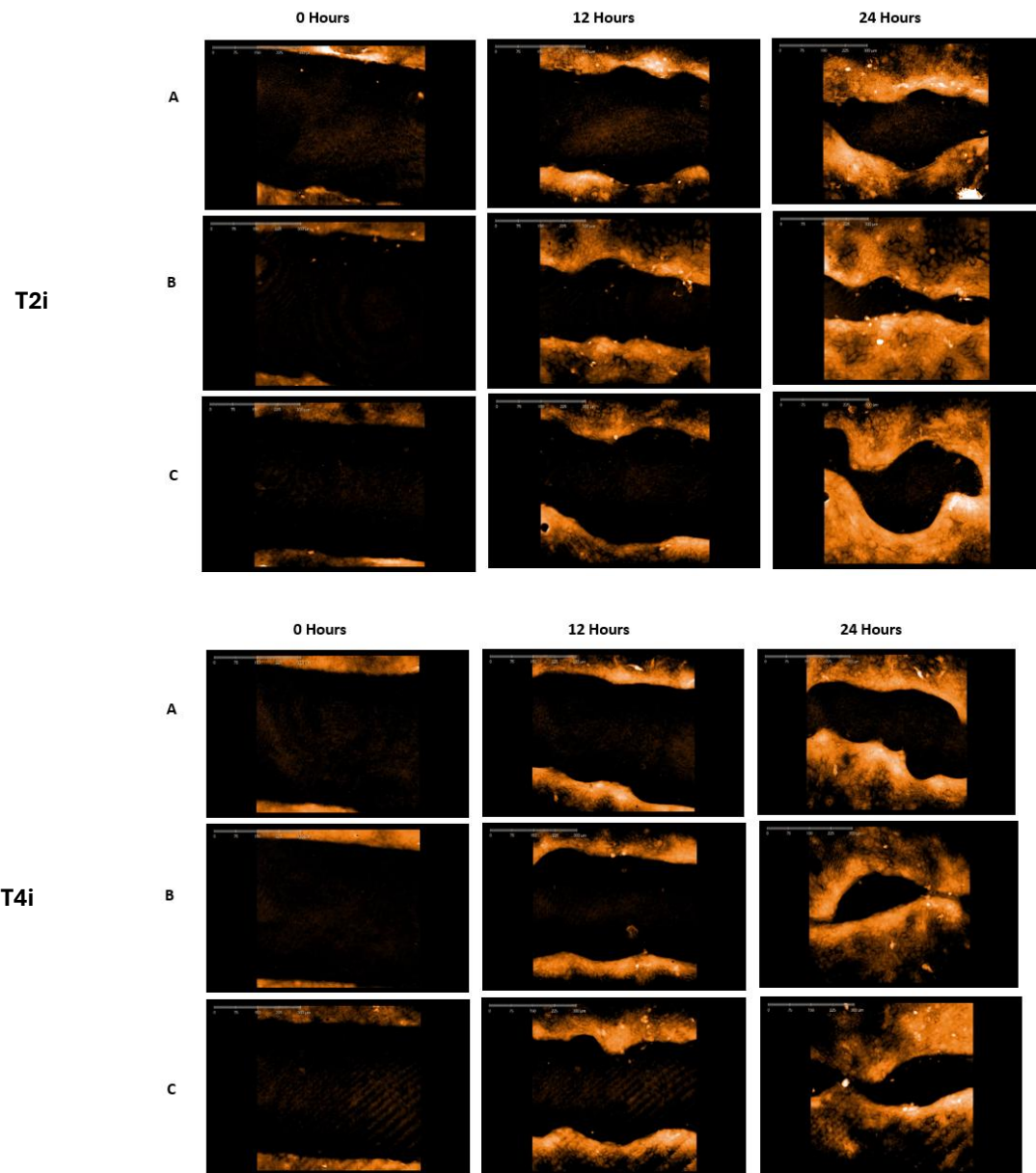


**Figure 5. 27: The Effect of MGN3 on Keratinocyte ‘Wound’ Closure at 11mM Glucose after TLR2 and TLR4 Inhibition.** HACATs were cultured with 11mM glucose, treated with LPS (5ug/ml) or MGN3 (2mg/ml) and TLR2 (T2i) or TLR4 (T4i) inhibition and incubated for 24 hours on a Holomonitor microscope. Images shown represent different time points (0, 12 and 24 hours). Panel A show untreated keratinocytes and T2i or T4i, Panel B are keratinocytes treated with LPS and T2i or T4i and Panel C shows keratinocytes treated with MGN3 and T2i or T4i.

### 5.4.10.2 The Effect of MGN3 with TLR inhibition on Fibroblast 'Wound' Closure at 20mM glucose

The results showed TLR2/4 inhibition reduced the ability of the keratinocytes cultured at 20mM glucose to undergo wound closure in all cases (Figures 5.28 and 5.29) compared to corresponding treatments lacking TLR inhibition.

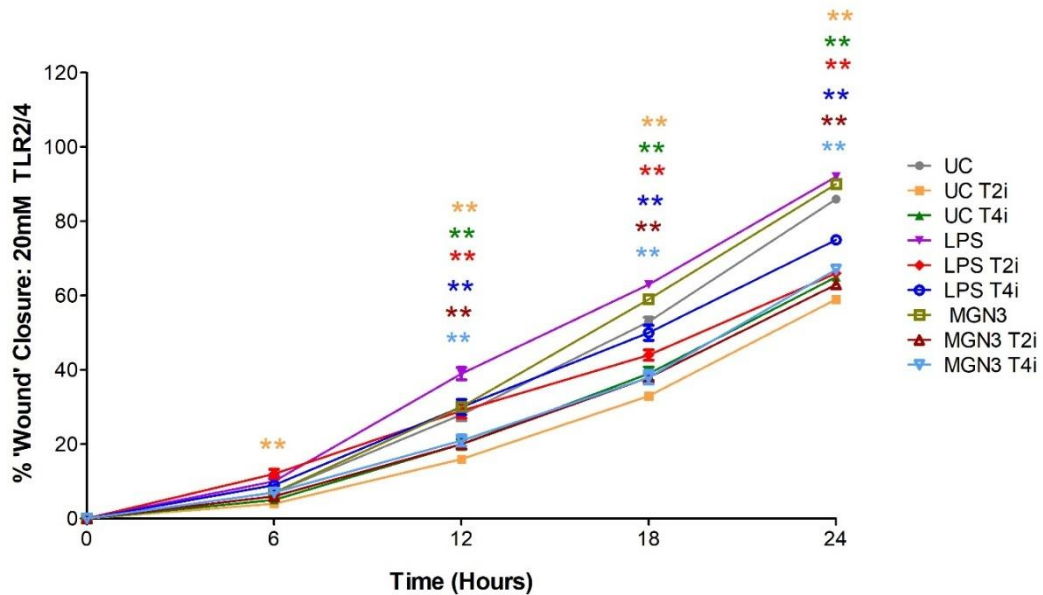


**Figure 5. 28: Effect of TLR inhibition on MGN3-Mediated Keratinocyte 'Wound' Closure under 20mM Culture Conditions.** The area % change in wound closure was calculated based on Holomonitor images captured over a period of 24 hours following treatment of HACAT wound models cultured under hyperglycaemic (20mM glucose) with/without MGN3 or LPS in the presence/absence of TLR2 (T2i) or TLR4 (T4i) inhibition. Significant decreases were seen in % wound closure compared to corresponding treatments lacking TLR inhibition (\*  $P < 0.05$  and \*\*  $P < 0.01$  determined by t-tests;  $n = 12$ ). UC = untreated control. Lines and error bars indicate the wound area %  $\pm$  the standard error of the mean (SEM) in all cases. Table shows the % wound closure after treatment at different timepoints.

Statistical analysis by independent two tailed t-tests indicated significant differences between the groups. There were significant ( $P < 0.01$ ) decreases in wound closure in untreated keratinocytes with TLR2 inhibition at all time points and untreated keratinocytes with TLR4 inhibition at 12 hours onwards compared to untreated keratinocytes without TLRi. There were also significant decreases ( $P < 0.01$ ) in MGN3/LPS treated keratinocytes

with TLR2/4 inhibition from 12 hours onwards compared to corresponding treatments without TLRi.

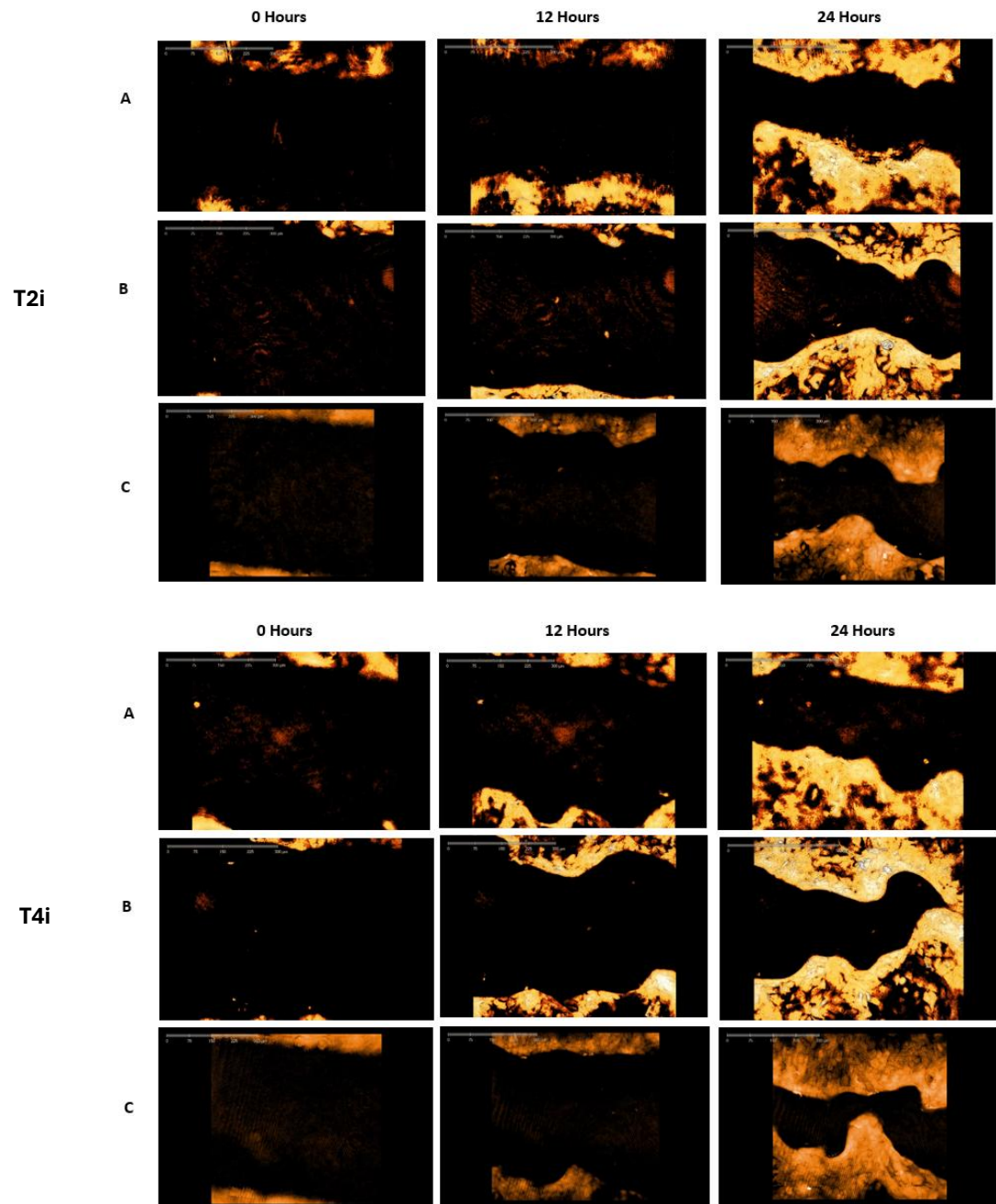
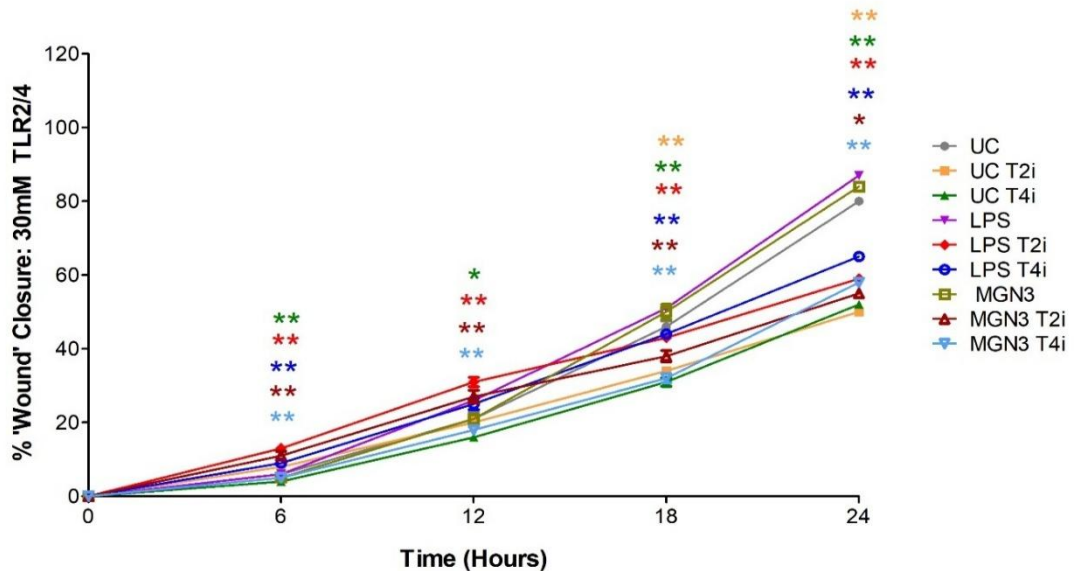


**Figure 5. 29: The Effect of MGN3 on Keratinocyte ‘Wound’ Closure at 20mM Glucose after TLR2 and TLR4 Inhibition.** HACATs were cultured with 20mM glucose, treated with LPS (5ug/ml) or MGN3 (2mg/ml) and TLR2 (T2i) or TLR4 (T4i) inhibition and incubated for 24 hours on a Holomonitor microscope. Images shown represent different time points (0, 12 and 24 hours). Panel A show untreated keratinocytes and T2 or T4ii, Panel B are keratinocytes treated with LPS and T2i or T4ii and Panel C shows keratinocytes treated with MGN3 and T2 or T4ii.

### 5.4.10.3 The Effect of MGN3 with TLR inhibition on Keratinocyte 'Wound' Closure at 30mM glucose

The results showed TLR2/4 inhibition reduced the ability of the fibroblasts cultured at 20mM glucose to undergo wound closure in all cases (Figures 5.30 and 5.31) compared to corresponding treatments lacking TLR inhibition.



Time (hours)	UC	UC T2	UC T4	LPS	LPS T2	LPS T4	MGN3	MGN3 T2	MGN3 T4
6	6	8	4	6	13	9	5	11	5
12	21	20	16	26	31	25	21	27	18
18	46	34	31	51	43	44	50	38	32
24	80	50	52	87	59	65	84	55	58

**Figure 5. 30: Effect of TLR inhibition on MGN3-Mediated Keratinocyte 'Wound' Closure under 30mM Culture Conditions.** The area % change in wound closure was calculated based on Holomonitor images captured over a period of 24 hours following treatment of HACAT wound models cultured under hyperglycaemic (30mM glucose) with/without MGN3 or LPS in the presence/absence of TLR2 (T2i) or TLR4 (T4i) inhibition. Significant decreases were seen in % wound closure compared to corresponding treatments lacking TLR inhibition (\*  $P < 0.05$  and \*\*  $P < 0.01$  determined by t-tests;  $n = 12$ ). UC = untreated control. Lines and error bars indicate the wound area %  $\pm$  the standard error of the mean (SEM) in all cases. Table shows the % wound closure after treatment at different timepoints.

Statistical analysis by independent two tailed t-tests indicated significant differences between the groups. There were significant ( $P < 0.01$ ) decreases in wound closure in untreated keratinocytes with TLR2 inhibition from 18 hours onwards and in untreated keratinocytes with TLR4 inhibition at all time points compared to untreated keratinocytes without TLRi. There were significant decreases in wound closure in LPS treated keratinocytes with TLR2 inhibition ( $P < 0.01$ ) all time points and LPS treated keratinocytes with TLR4

inhibition at 6 hours ( $P = 0.009$ ) and 18 hours onwards ( $P < 0.01$ ) compared to LPS treated keratinocytes without TLRI. There were also significant decreases ( $P < 0.01$ ) in wound closure in MGN3 treated keratinocytes with TLR2/4 at all timepoints compared to MGN3 keratinocytes without TLRI.

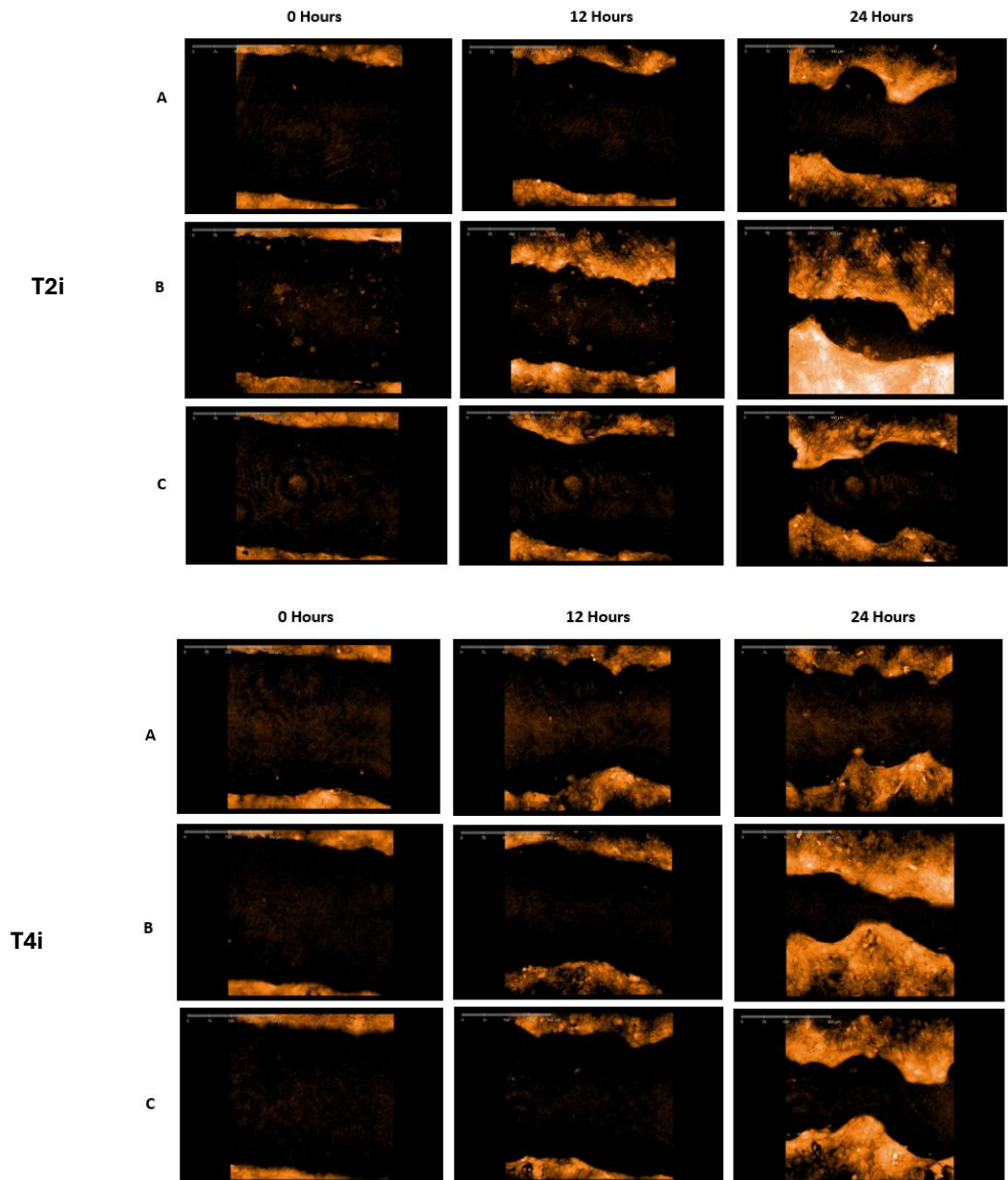


**Figure 5. 31: The Effect of MGN3 on Keratinocyte ‘Wound’ Closure at 30mM Glucose after TLR2 and TLR4 Inhibition.** HACATs were cultured with 30mM glucose, treated with LPS (5ug/ml) or MGN3 (2mg/ml) and TLR2 (T2i) or TLR4 (T4i) inhibition and incubated for 24 hours on a Holomonitor microscope. Images shown represent different time points (0, 12 and 24 hours). Panel A show untreated keratinocytes and T2i or T4i, Panel B are keratinocytes treated with LPS and T2i or T4i and Panel C shows keratinocytes treated with MGN3 and T2i or T4i.

## 5.4.11 Contribution of Cell Proliferation and Migration on MGN3-Mediated Keratinocyte 'Wound' Closure

### 5.4.11.1 The Effect Mitomycin on Cell Proliferation

After 24 hours of mitomycin C (MC) treatment (Figure 8.15) keratinocyte proliferation was inhibited by >90% in all glucose concentrations (96% inhibition at 11mM; 94% inhibition at 20mM; 90% inhibition at 30mM glucose) (Figure 5.32).

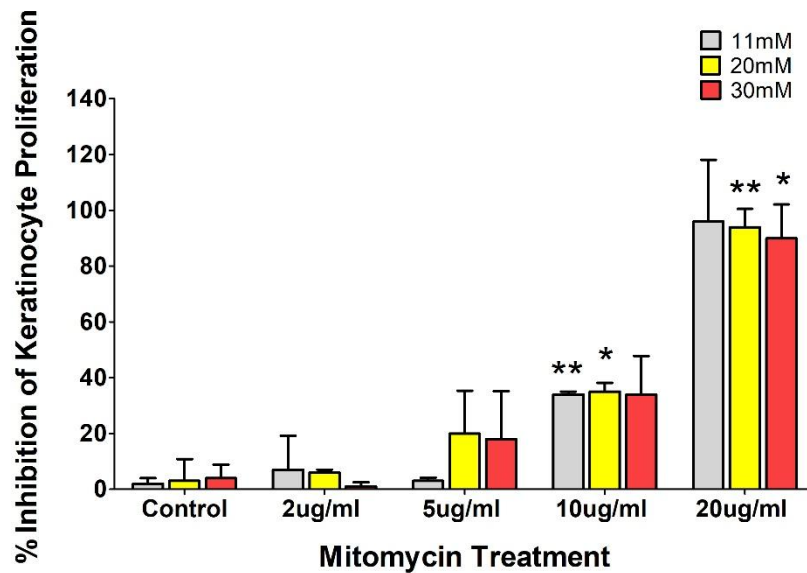


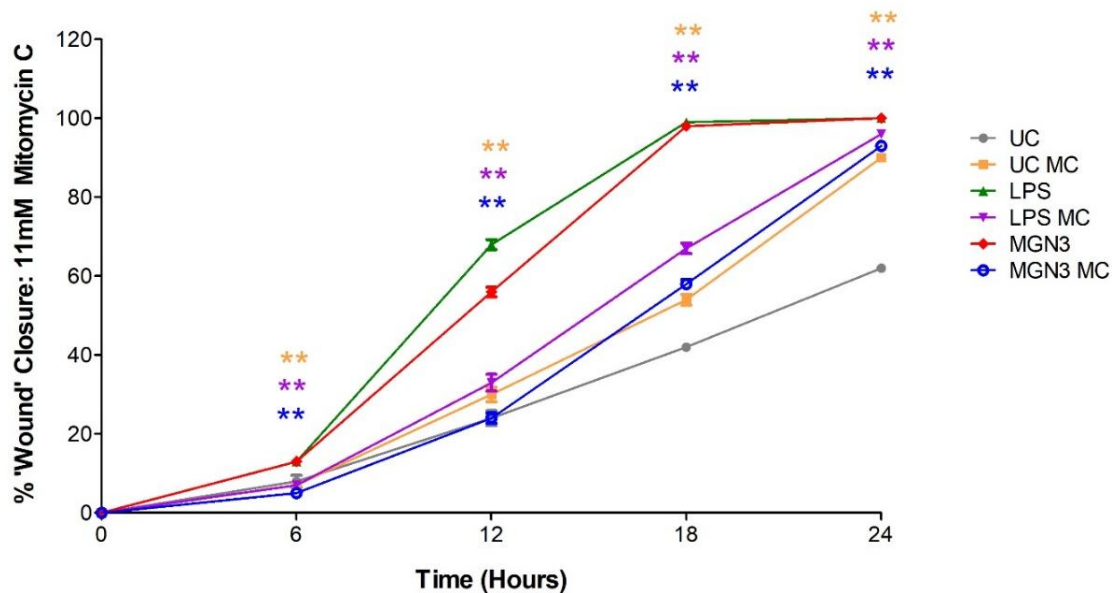
**Figure 5. 32: Evaluation of keratinocyte proliferation following mitomycin C treatment.** HACATs were grown in multiple glucose concentrations (11, 20 and 30mM) and treated with mitomycin (MC) at different concentrations (2, 5, 10 and 20ug/ml) to evaluate cell proliferation after 24 hours. Significant increases were seen between the groups when comparisons were made against the corresponding glycaemic untreated control (UC) (\*  $P < 0.05$  and \*\*  $P < 0.01$  determined by t-tests;  $n = 6$ ). Columns and error bars indicate % Inhibition  $\pm$  the standard error of the mean (SEM) in all cases.

At 11mM glucose, there was a significant ( $P < 0.01$ ) increase in % inhibition with 10ug MC treatment compared to the corresponding control group. There was an increase in % inhibition when the highest MC (20ug) treatment was used compared to 10ug MC treatment (34% inhibition 10ug MC; 96% inhibition 20ug MC) however the data was not significantly different ( $P > 0.05$ ). At 20mM glucose there were significant increases in % inhibition when keratinocytes were treated with 10ug MC ( $P = 0.028$ ) and 20ug MC ( $P = 0.002$ ) compared to the corresponding control group. At 30mM glucose there was a significant increase ( $P = 0.015$ ) in % inhibition in keratinocytes treated with 20ug MC treatment compared to the

corresponding control group. These results indicate MC treatment at 20ug/ml inhibited keratinocyte proliferation by >90% at pre-diabetic (11mM) and hyperglycaemic (20 and 30mM) conditions. It was decided that MC treatment at 20ug/ml would be best suited to inhibit keratinocyte proliferation in the wound healing (closure) assay.

#### 5.4.11.2 The Effect of Mitomycin C on Keratinocyte ‘Wound’ Closure at 11mM glucose

Despite blocking cell proliferation with MC, which did reduce the % wound closure relative to corresponding treatments without MC (Figures 5.33 and 5.34), the wound closure still proceeded relatively closely to that observed in the absence of MC (particularly at T = 24 hours) suggesting cell migration (rather than cell proliferation) was probably having a greater influence on driving keratinocyte-mediated wound closure.



TIME (hrs)	UC	UC MC	LPS	LPS MC	MGN3	MGN3 MC
0	0	0	0	0	0	0
6	13	7	13	7	13	5
12	48	30	68	33	56	24
18	94	54	99	67	98	58
24	100	90	100	96	100	93

**Figure 5. 33: % ‘Wound’ Closure in HACATs at 11mM glucose after MGN3 treatment and mitomycin C treatment.** The % ‘wound’ closure was calculated in HACAT at 11mM after LPS, MGN3 and MC treatments for a span of 24 hours. Significant decreases were observed when comparisons were made between treatments in the presence of MC compared against corresponding treatments lacking MC. (\*\* P < 0.01 determined by t-tests; n = 12). Lines and error bars indicate the wound area % ± the standard error of the mean (SEM) in all cases. The table represents % ‘wound’ closure at different time points. Table shows the % wound closure after treatment at different timepoints.

Statistical analysis by independent t-tests showed there was a significant decrease in wound closure in the untreated keratinocytes in the presence of mitomycin C (MC) and MGN3/LPS treated keratinocytes in the presence of MC ( $P < 0.01$ ) for all time points when comparisons were made against the corresponding treatments lacking MC.

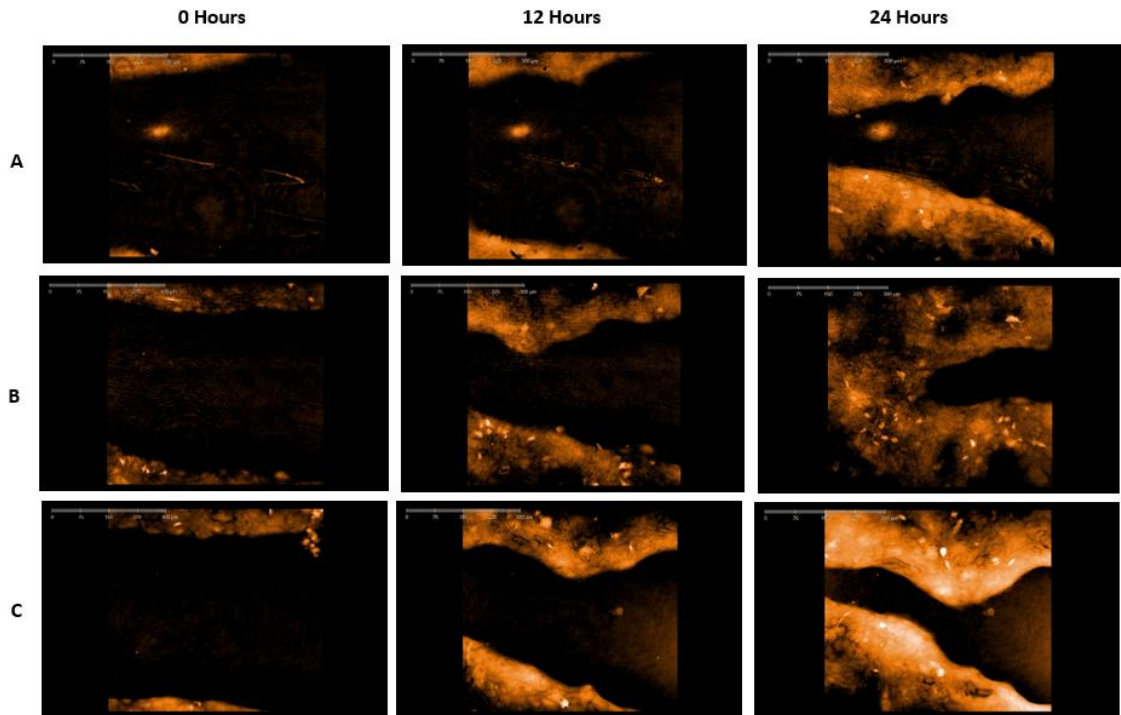


**Figure 5. 34: The Effect of Mitomycin C on Keratinocyte 'Wound' Closure at 11mM Glucose.** HACATs were cultured with 11mM glucose, treated with LPS (5ug/ml) or MGN3 (2mg/ml) and Mitomycin C (MC) and incubated for 24 hours on a Holomonitor microscope. Images shown represent different time points (0, 12 and 24 hours). Panel A show untreated keratinocytes + MC, Panel B are keratinocytes treated with LPS + MC and Panel C shows keratinocytes treated with MGN3 + MC.

### 5.4.11.3 The Effect of Cytochalasin D on Keratinocyte 'Wound' Closure at 11mM

There was a substantial significant ( $P < 0.01$ ) reduction in % wound closure following inhibition of cell migration due exposure to Cytochalasin D (Figures 5.35 and 5.36) compared to corresponding treatments lacking Cytochalasin D exposure, with the % wound closure failing to reach above 30% across the 24-hour observation period. These findings align with those in section 5.4.11.2 and confirm that wound closure was principally occurring through keratinocyte migration rather than cell proliferation in both untreated and MGN3/LPS-treated keratinocytes.

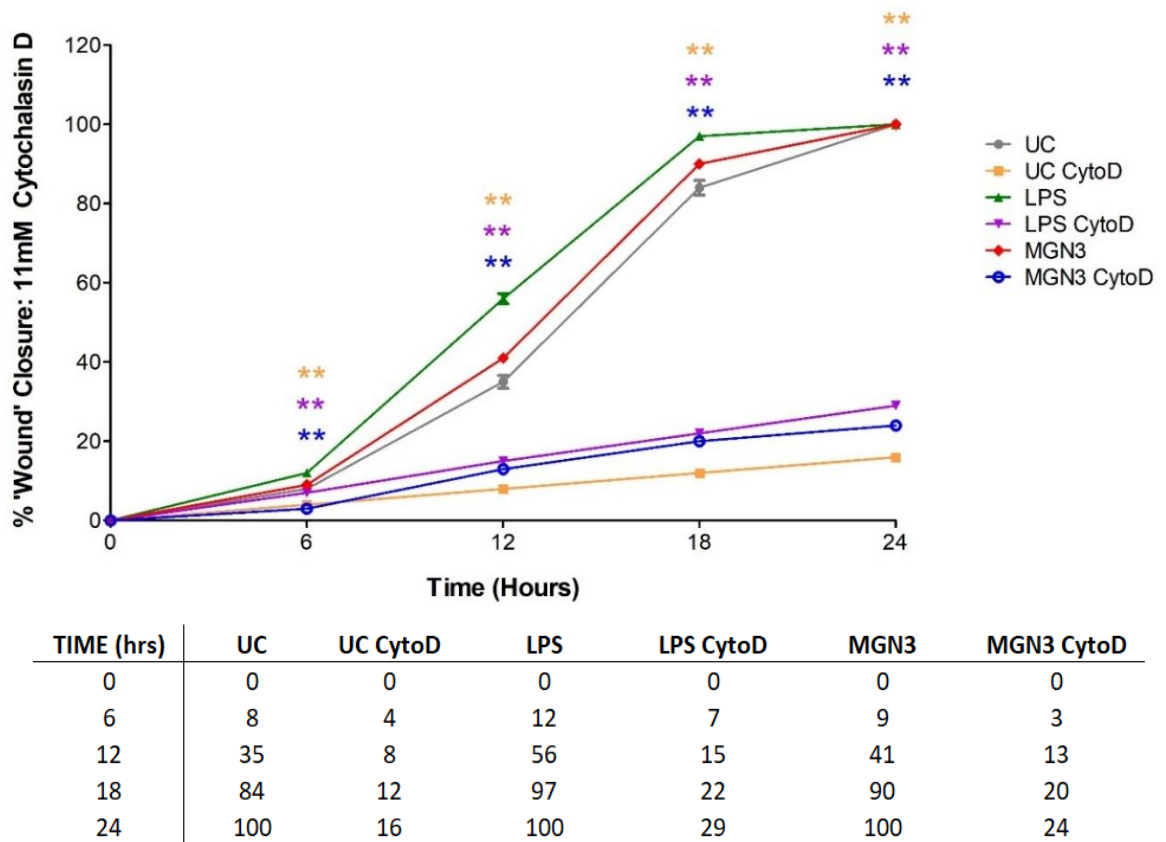


**Figure 5. 35: % 'Wound' closure in HACATs at 11mM glucose after MGN3 and CytoD treatment.** The % 'wound' closure was calculated in HACAT at 11mM glucose following LPS or MGN3 and Cytochalasin D (CytoD) treatments. Significant decreases were observed when comparisons were made between treatments in the presence of CytoD compared against corresponding treatments lacking CytoD (\*\*  $P < 0.01$  determined by t-tests;  $n = 12$ ). Lines and error bars indicate the wound area %  $\pm$  the standard error of the mean (SEM) in all cases. The table represents % 'wound' closure at different time points. Table shows the % wound closure after treatment at different timepoints.

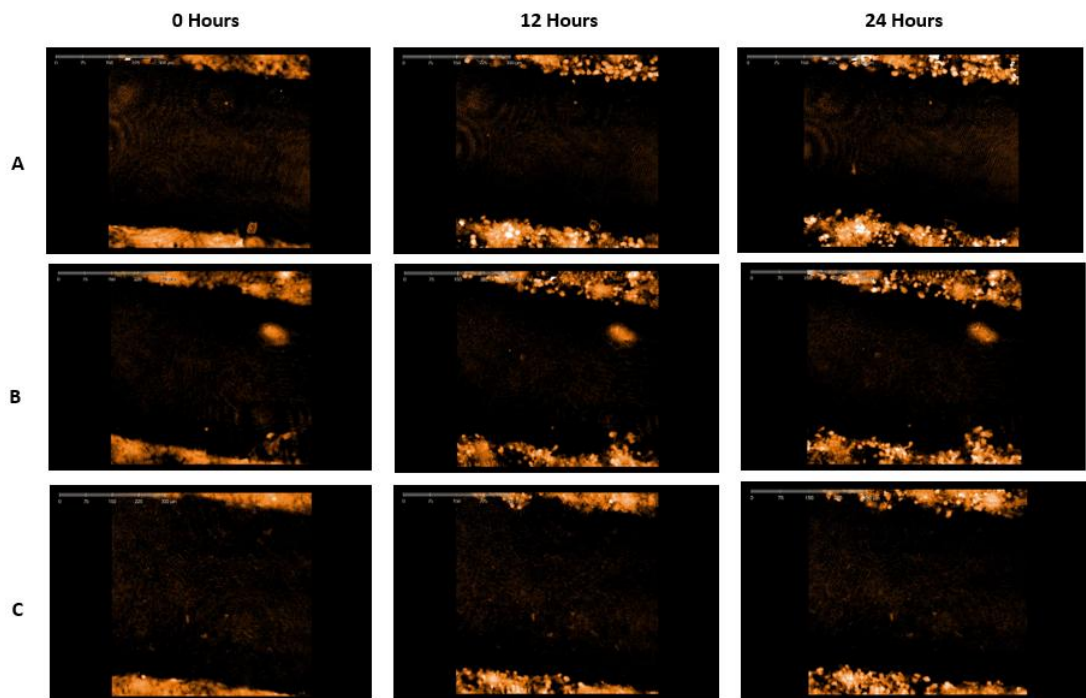
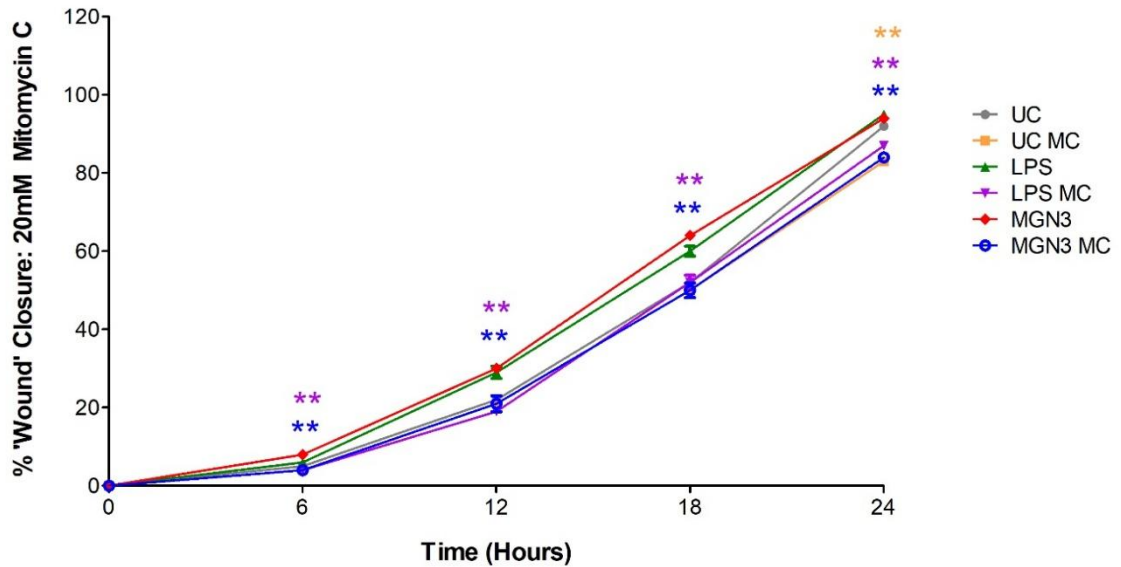


**Figure 5. 36: The Effect of Cytochalasin D on Keratinocyte 'Wound' Closure after at 11mM Glucose.** HACATs were cultured with 11mM glucose, treated with LPS (5ug/ml) or MGN3 (2mg/ml) and Cytochalasin D (CytoD) and incubated for 24 hours on a Holomonitor microscope. Images shown represent different time points (0, 12 and 24 hours). Panel A show untreated keratinocytes + CytoD, Panel B are keratinocytes treated with LPS + CytoD and Panel C shows keratinocytes treated with MGN3 + CytoD.

#### 5.4.11.4 The Effect of Mitomycin C on Keratinocyte 'Wound' Closure at 20mM glucose

Despite blocking cell proliferation with MC, which did reduce the % wound closure relative to corresponding treatments without MC (Figures 5.37 and 5.38), the wound closure still proceeded relatively closely to that observed in the absence of MC (particularly at T = 24 hours) suggesting cell migration (rather than cell proliferation) was probably having a greater influence on driving keratinocyte-mediated wound closure.



TIME (hrs)	UC	UC MC	LPS	LPS MC	MGN3	MGN3 MC
0	0	0	0	0	0	0
6	5	4	6	4	8	4
12	22	21	29	19	30	21
18	52	50	60	52	64	50
24	92	83	95	87	94	84

**Figure 5. 37: % 'Wound' closure in HACATs at 20mM glucose after MGN3 treatment and Mitomycin C treatment.** The % 'wound' closure was calculated in HACAT at 20mM after LPS or MGN3 and Mitomycin C (MC) treatments for a span of 24 hours. Significant decreases were observed when comparisons were made between treatments in the presence of MC compared against corresponding treatments lacking MC (\*\* P < 0.01 determined by t-tests; n = 12). Lines and error bars indicate the wound area %  $\pm$  the standard error of the mean (SEM) in all cases. The table represents % 'wound' closure at different time points. Table shows the % wound closure after treatment at different timepoints.

MC treatments restricted cell proliferation in all cases at 20mM glucose compared to the controls. Statistical analysis by independent t-tests showed there were significant increases in the LPS group ( $P < 0.01$ ) after 12 onwards and MGN3 group ( $P < 0.01$ ) at all time points when compared to the UC. There were significant decreases in the UC MITO group at 24 hours and both LPS and MGN3 MITO groups ( $P < 0.01$ ) at all time points when compared to the corresponding controls. There was also a significant increase in the LPS MITO group at 24 hours ( $P < 0.01$ ) when compared to the UC MITO group.

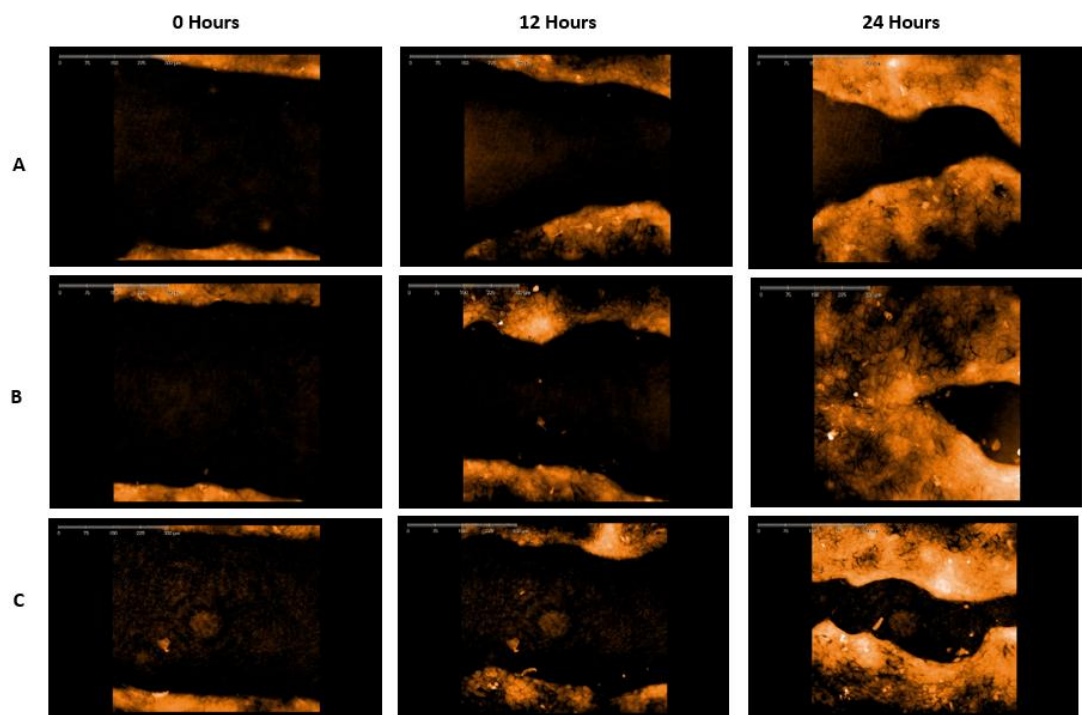
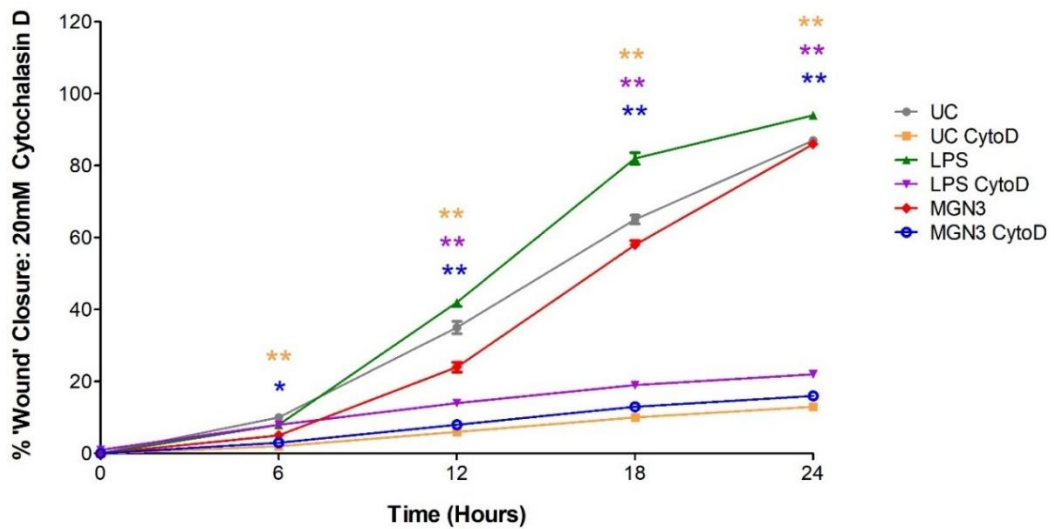


**Figure 5. 38: The Effect of Mitomycin C on Keratinocyte ‘Wound’ Closure at 20mM Glucose.** HACATs were cultured with 20mM glucose, treated with LPS (5ug/ml) or MGN3 (2mg/ml) and Mitomycin C (MC) and incubated for 24 hours on a Holomonitor microscope. Images shown represent different time points (0, 12 and 24 hours). Panel A show untreated keratinocytes + MC, Panel B are keratinocytes treated with LPS + MC and Panel C shows keratinocytes treated with MGN3 + MC.

#### 5.4.11.5 The Effect of Cytochalasin D on Keratinocyte ‘Wound’ Closure at 20mM

There was a substantial significant ( $P < 0.01$ ) reduction in % wound closure following inhibition of cell migration due exposure to Cytochalasin D (Figures 5.39 and 5.40) compared to corresponding treatments lacking Cytochalasin D exposure, with the % wound closure failing to reach above 22% across the 24-hour observation period. These findings align with those in section 5.4.11.4 and confirm that wound closure was principally occurring through keratinocyte migration rather than cell proliferation in both untreated and MGN3/LPS-treated keratinocytes.



TIME (hrs)	UC	UC CytoD	LPS	LPS CytoD	MGN3	MGN3 CytoD
0	0	0	0	1	0	0
6	10	2	8	8	5	3
12	35	6	42	14	24	8
18	65	10	82	19	58	13
24	87	13	94	22	86	16

**Figure 5. 39: % ‘Wound’ closure in HDFs at 20mM glucose after MGN3 and CytoD treatment.** The % ‘wound’ closure was calculated in HDF at 11mM glucose following LPS or MGN3 and Cytochalasin D (CytoD) treatments. Significant decreases were observed when comparisons were made between treatments in the presence of CytoD compared against corresponding treatments lacking CytoD (\*  $P < 0.05$  and \*\*  $P < 0.01$  determined by t-tests;  $n = 12$ ). Lines and error bars indicate the wound area %  $\pm$  the standard error of the mean (SEM) in all cases. The table represents % ‘wound’ closure at different time points. Table shows the % wound closure after treatment at different timepoints.

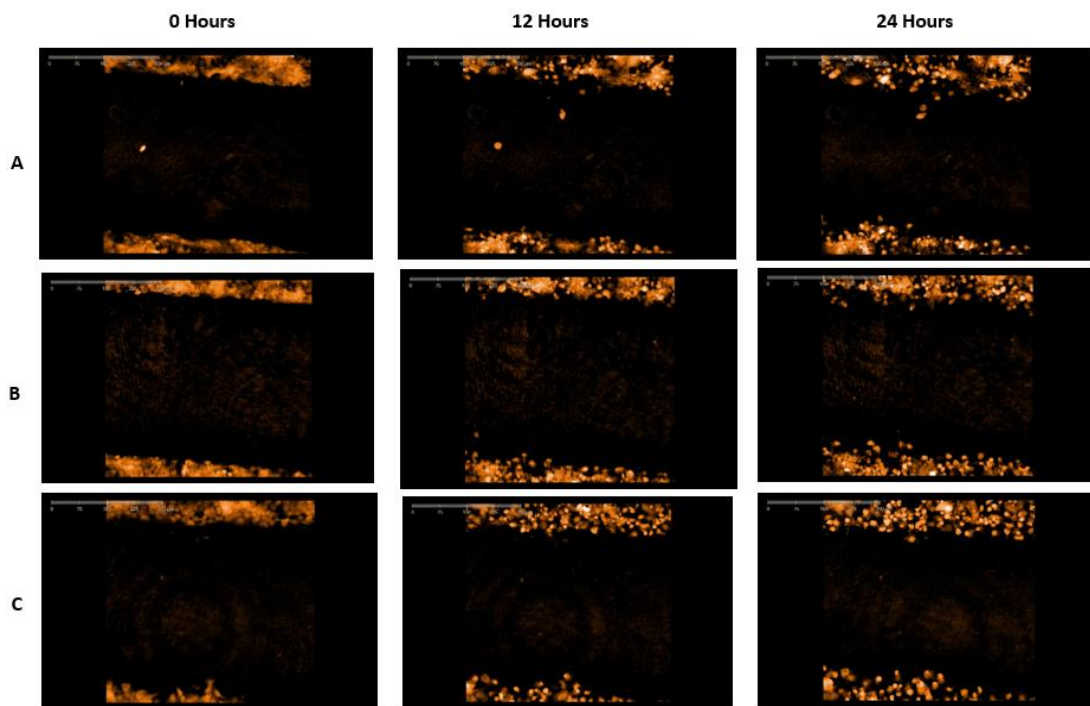
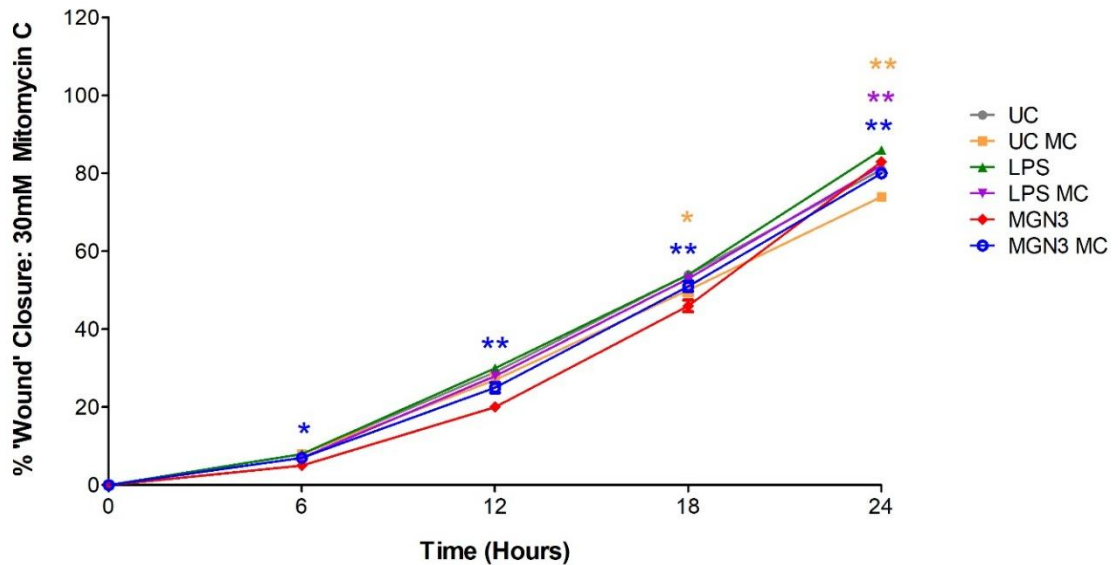


**Figure 5. 40: The Effect of Cytochalasin D on Keratinocyte 'Wound' Closure after at 20mM Glucose.** HACATs were cultured with 11mM glucose, treated with LPS (5ug/ml) or MGN3 (2mg/ml) and Cytochalasin D (CytoD) and incubated for 24 hours on a Holomonitor microscope. Images shown represent different time points (0, 12 and 24 hours). Panel A show untreated keratinocytes + CytoD, Panel B are keratinocytes treated with LPS + CytoD and Panel C shows keratinocytes treated with MGN3 + CytoD.

#### 5.4.11.6 The Effect of Mitomycin C on Keratinocyte ‘Wound’ Closure at 30mM glucose

Despite blocking cell proliferation with MC, which did reduce the % wound closure relative to corresponding treatments without MC (Figures 5.41 and 5.42), the wound closure still proceeded relatively closely to that observed in the absence of MC (particularly at T = 24 hours) suggesting cell migration (rather than cell proliferation) was probably having a greater influence on driving keratinocyte-mediated wound closure.



TIME (hrs)	UC	UC MC	LPS	LPS MC	MGN3	MGN3 MC
0	0	0	0	0	0	0
6	8	8	8	7	5	7
12	29	27	30	28	20	25
18	54	50	54	53	46	51
24	81	74	86	82	83	80

**Figure 5. 41: % ‘Wound’ Closure in HACATs at 30mM glucose after MGN3 treatment and mitomycin C treatment.** The % ‘wound’ closure was calculated in HACAT at 30mM after LPS, MGN3 and MC treatments for a span of 24 hours. Significant decreases were observed when comparisons were made between treatments in the presence of MC compared against corresponding treatments lacking MC (\*  $P < 0.05$  and \*\*  $P < 0.01$  determined by t-tests;  $n = 12$ ). Lines and error bars indicate the wound area %  $\pm$  the standard error of the mean (SEM) in all cases. The table represents % ‘wound’ closure at different time points. Table shows the % wound closure after treatment at different timepoints.

Statistical analysis by independent t-tests showed there was a significant decrease in wound closure in the untreated keratinocytes in the presence of MC at 18 hours ( $P = 0.016$ ) and 24 hours ( $P < 0.001$ ) compared to untreated keratinocytes lacking MC. There was a significant decrease in wound closure in the LPS treated keratinocytes in the presence of MC at 24 hours ( $P < 0.001$ ) and significant decreases in wound closure in the MGN3 treated keratinocytes in the presence of mitomycin C (MC) at 6 hours ( $P = 0.024$ ) and 12 hours onwards ( $P < 0.01$ ) compared to treatments lacking MC.

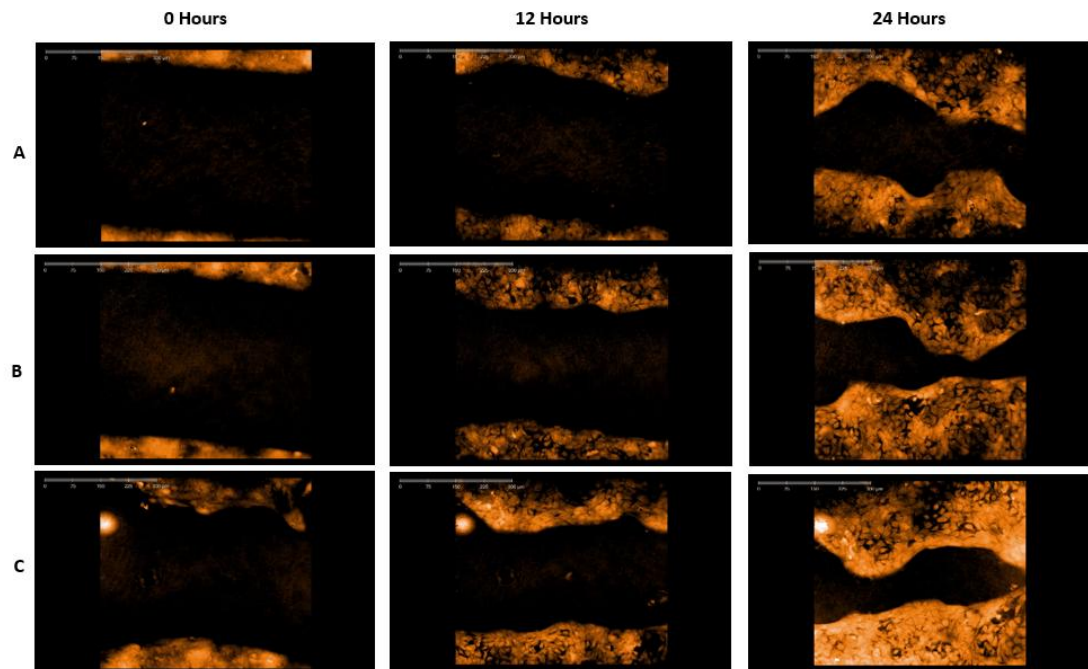
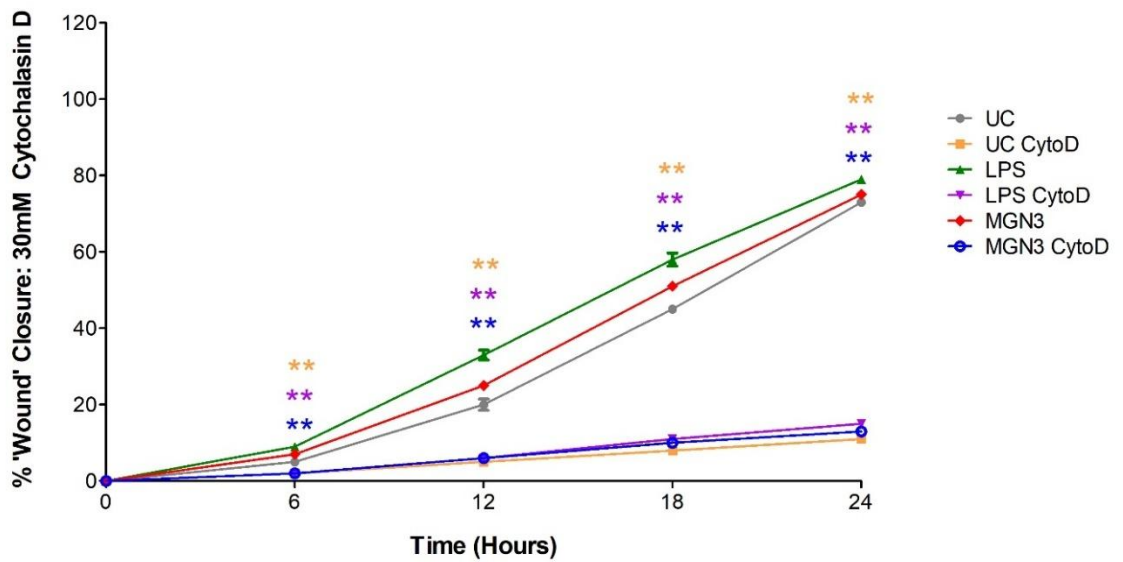


**Figure 5.42: The Effect of Mitomycin C on Keratinocyte ‘Wound’ Closure at 30mM Glucose.** HACATs were cultured with 30mM glucose, treated with LPS (5ug/ml) or MGN3 (2mg/ml) and Mitomycin C (MC) and incubated for 24 hours on a Holomonitor microscope. Images shown represent different time points (0, 12 and 24 hours). Panel A show untreated keratinocytes + MC, Panel B are keratinocytes treated with LPS + MC and Panel C shows keratinocytes treated with MGN3 + MC.

#### 5.4.11.7 The Effect of Cytochalasin D on Keratinocyte 'Wound' Closure at 30mM

There was a substantial significant ( $P < 0.01$ ) reduction in % wound closure following inhibition of cell migration due exposure to Cytochalasin D (Figures 5.43 and 5.44) compared to corresponding treatments lacking Cytochalasin D exposure, with the % wound closure failing to reach above 15% across the 24-hour observation period. These findings align with those in section 5.4.11.6 and confirm that wound closure was principally occurring through keratinocyte migration rather than cell proliferation in both untreated and MGN3/LPS-treated keratinocytes.



TIME (hrs)	UC	UC CytoD	LPS	LPS CytoD	MGN3	MGN3 CytoD
0	0	0	0	0	0	0
6	5	2	9	2	7	2
12	20	5	33	6	25	6
18	45	8	58	11	51	10
24	73	11	79	15	75	13

**Figure 5. 43: % 'Wound' closure in HACATs at 30mM glucose after MGN3 and CytoD treatment.** The % 'wound' closure was calculated in HACAT at 30mM glucose following LPS or MGN3 and Cytochalasin D (CytoD) treatments. Significant decreases were observed when comparisons were made between treatments in the presence of CytoD compared against corresponding treatments lacking CytoD (\*\*  $P < 0.01$  determined by  $t$ -tests;  $n = 12$ ). Lines and error bars indicate the wound area %  $\pm$  the standard error of the mean (SEM) in all cases. The table represents % 'wound' closure at different time points. Table shows the % wound closure after treatment at different timepoints.

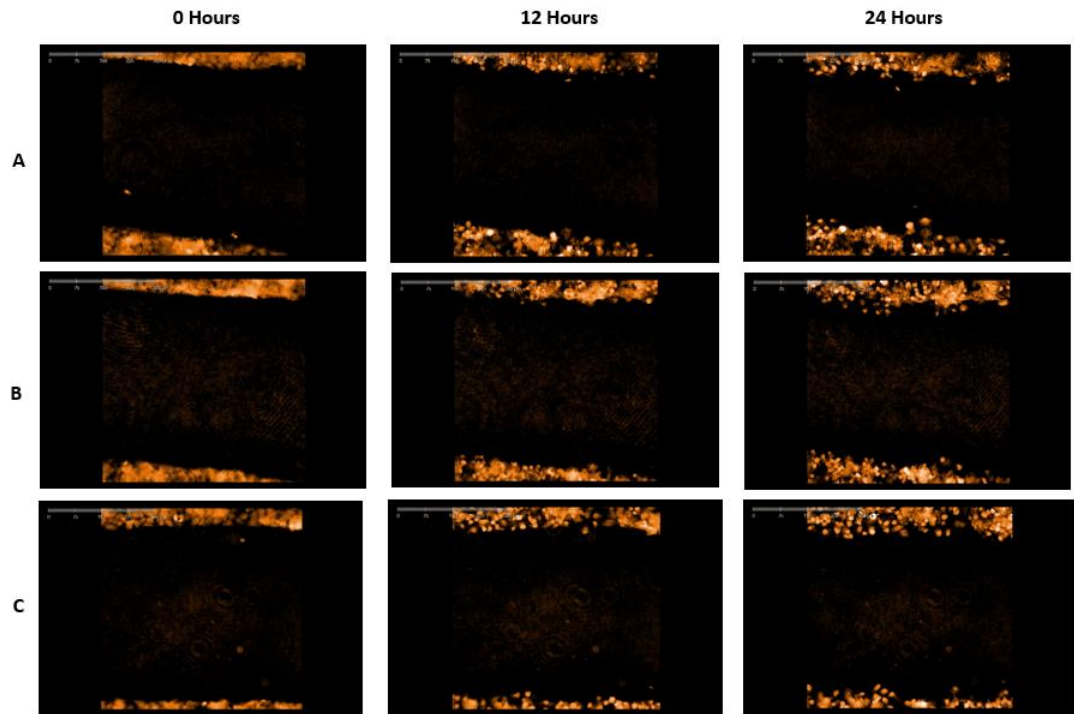


**Figure 5. 44: The Effect of Cytochalasin D on Keratinocyte ‘Wound’ Closure after at 30mM Glucose.** HACATs were cultured with 30mM glucose, treated with LPS (5ug/ml) or MGN3 (2mg/ml) and Cytochalasin D (CytoD) and incubated for 24 hours on a Holomonitor microscope. Images shown represent different time points (0, 12 and 24 hours). Panel A show untreated keratinocytes + CytoD, Panel B are keratinocytes treated with LPS + CytoD and Panel C shows keratinocytes treated with MGN3 + CytoD.

## 5.5 Discussion

The aim of this study was to evaluate how MGN3 can influence wound closure by dermal fibroblasts and keratinocytes under hyperglycaemic conditions. The study showed high glucose had a negative impact on HDF and HACAT-mediated wound closure. As glucose increased the % 'wound' closure decreased, indicating glucose has inhibitory effects on fibroblast proliferation and/or migration.

The results showed hyperglycaemic conditions significantly ( $P < 0.01$ ) reduced % 'wound' closure. To distinguish between the influence of cell proliferation and cell migration in this study, mitomycin C was used to disrupt cell proliferation and cytochalasin D was used to inhibit cell migration. Mitomycin C is effective in preventing cell proliferation because of its ability to suppress DNA synthesis via alkylating DNA strands (Basu *et al*, 1993). Cytochalasin D, on the other hand, inhibits cell migration by binding to actin filaments, rendering them obsolete (Shoji *et al*, 2012). By using these specific inhibitors of cell proliferation and migration, this study indicated the inhibition of wound closure was predominantly due to impaired cell migration. These findings are supported by evidence in the literature showing glucose at 30mM delays fibroblast cell migration in diabetic mice (Xuan *et al*, 2014). This hyperglycaemia-induced impairment of fibroblast migration is linked to elevated ROS production and repression of JNK phosphorylation (Xuan *et al*, 2018; Lamers *et al*, 2011). JNK along with PI3-Kinase-Rac1 pathways play essential roles in cell migration (Xuan *et al*, 2016). It is known that diabetic patients have elevated levels 3-deoxyglucosone (3DG), a precursor of AGEs, which results in a buildup of AGEs on matrix collagen as patients get older (Loughlin and Artlett, 2009). It has been shown that fibroblasts have a higher affinity for 3DG-treated collagen but in doing so their ability to migrate across wounds is greatly suppressed (Loughlin and Artlett, 2009). A study by Hehenberger *et al*, (2019) investigated fibroblast function in fibroblast extracted from diabetic wounds in comparison to normal dermal fibroblasts. It was concluded fibroblast proliferation was greatly inhibited in fibroblasts taken from diabetic patients. A similar study found associated this reduced fibroblast proliferation to increased oxidative stress resulting from hyperglycaemia (Buranasin *et al*, 2018).

The results showed LPS and MGN3 treatment increased % wound closure at both pre-diabetic and hyperglycaemic levels of glucose. Again, the use of inhibitors of cell proliferation and migration confirmed the stimulation of wound closure by MGN3 was mediated predominantly through increased fibroblast migration, rather than increased cell proliferation. There are very few studies investigating the impact of MGN3 on fibroblast function in relation to wound healing. Most studies focus on the influence of MGN3 treatments on immune cells, ranging from macrophages to dendritic cells (Ghoneum and Jewett, 2000; Ghoneum and Agrawal, 2011; Ghoneum and Agrawal, 2014). Thus, these findings expand the overall picture of the potential influence of MGN3 on different stages of wound healing, confirming its actions are not limited to just modulating inflammatory cells.

A previous study done by Asif (2020) showed MGN3 competes with LPS for TLR4 binding in inflammatory cells. It is also known TLR2 and TLR4 can form dimers and that ligand binding can activate the similar intracellular pathways (Takeda *et al*, 2003). Thus, this study investigated whether the effects of LPS/MGN3 on fibroblast-driven wound closure was mediated by TLR2 and/or TLR4. This study showed that inhibition of TLR2 or TLR4 receptors significantly reduced % wound closure in untreated cells at all glucose concentrations, suggesting endogenous-derived ligands are likely to exist (Yu *et al*, 2010) that are acting through TLR2/TLR4 to promote fibroblast migration. Inhibition of TLR2/4 along with treatment of LPS or MGN3 also reduced the % wound closure but no more so than the reduction seen in untreated fibroblasts, suggesting MGN3 and LPS are likely to be promoting fibroblast migration through alternative mechanisms other than TLR2/4.

This study also showed high glucose had a negative impact on HACAT-mediated wound closure. Other studies have also found hyperglycaemia results in impaired keratinocyte migration as well as proliferation (Raja *et al.*, 2007; Pastar *et al.*, 2014). A study by Lan *et al.* (2008) showed high glucose restricts keratinocyte proliferation and motility over a span of 5 days. The authors also found a connection between low P125FAK signalling in diabetic patients and impaired keratinocyte migration (Lan *et al.*, 2008).

The data showed LPS and MGN3 treatment increased % wound closure at both pre-diabetic and hyperglycaemic levels of glucose. Again, the use of inhibitors of cell proliferation and migration confirmed the stimulation of wound closure by LPS/MGN3 was mediated predominantly through increased fibroblast migration, rather than increased cell proliferation. There is little research on the effects of MGN3 in keratinocyte motility however, the general mechanisms of MGN3 can be applied to understand how it may enhance keratinocyte migration. Some ways in which MGN3 could potentially increase keratinocyte motility include dampened inflammation, enhanced growth factor signalling, improved cell to cell interactions, reduced oxidative stress, enhanced activation of cell signalling pathways (MAPK and PI3K) and more efficient regulation of cytoskeleton dynamics. Chronic inflammation associated with diabetic conditions can impair keratinocyte motility (Mansoub, 2021). MGN3 is known to have anti-inflammatory properties which help in the reduction of pro-inflammatory cytokines such as TNF- $\alpha$  and IL-6 (Ghoneum *et al*, 2008), which would increase keratinocyte motility at the wound site. MGN3 has shown to stimulate growth factors, such as EGF, that are important for keratinocyte motility (Ooi *et al*, 2023).

Under hyperglycaemic conditions cell adhesion such as integrins can be comprised, leading to suppressed keratinocyte migration (Li *et al*, 2019). MGN3 could help to restore integrin expression in keratinocytes as it already shown to increase integrins in T-cells (Weeks *et al*, 2008). Focal adhesion kinase (FAK) is also involved in cell migration by regulating the attachment of cells to the extracellular matrix. A study by Phurisom *et al*, (2021) has suggested that MGN3 may activate signalling pathways that enhance FAK activity, thus supporting keratinocyte migration and wound closure. Hyperglycaemia is known to lead to oxidative stress which damages keratinocytes and restricts their motility (Rizwan *et al*, 2020). MGN3 is known to have antioxidant properties which allow the neutralization of free radicals which provides additional protection for keratinocytes and enhances their motility (Noaman *et al*, 2008). MGN3 has been shown to activate the MAPK and PI3K pathways (Tan, 2018; Zhang *et al*, 2020) which are important in numerous cellular processes including F-actin dynamics and motility (Vazquez-Victorio *et al*, 2016).

Thus, this study investigated whether the effects of LPS/MGN3 on keratinocyte-driven wound closure was mediated by TLR2 and/or TLR4. This study showed that inhibition of TLR2 or TLR4 receptors significantly reduced % wound closure in untreated cells at all glucose concentrations, suggesting endogenous-derived ligands are likely to exist (Yu *et al*, 2010) that are acting through TLR2/TLR4 to promote keratinocyte migration. Inhibition of TLR2/TLR4 along with treatment of LPS or MGN3 also reduced the % wound closure but no more so than the reduction seen in untreated keratinocytes, suggesting MGN3 and LPS are likely to be promoting keratinocyte migration through alternative mechanisms other than TLR2/TLR4.

In conclusion, this study has shown hyperglycaemia had a detrimental effect on both fibroblast and keratinocyte-mediated wound closure that is driven by impaired cell migration rather than reduced cell proliferation. MGN3 and LPS had a positive effect on wound closure by stimulating fibroblast and keratinocyte cell motility under both pre-diabetic and hyperglycaemic conditions. This study may have important implications for wound healing in diabetic patients, suggesting further investigations are warranted to determine whether MGN3 might stimulate wound closure in DFUs by promoting fibroblast migration. The potential of MGN3 to stimulate wound closure *in vivo* could be compared to conventional wound therapies in human trials by applying MGN3 to debrided DFUs within specialized hydrogel dressings that can deliver MGN3 directly to fibroblasts in the wound bed.

# **Chapter 6: The Effect of MGN3 on Fibroblast and Keratinocyte Cell Function**

## 6.1 Introduction

### 6.1.1 Immune Cell Signalling with Fibroblasts and Keratinocytes

Fibroblasts play key roles in the proliferative and remodelling phases of wound healing through interactions with macrophages, monocytes, and keratinocytes (Cialdai et al., 2022). These cell-to-cell interactions are simplified in Figure 6.1. Fibroblasts produce enzymes like MMP-1 to break down collagen (Pardo & Selman, 2005) and secrete COL-1 to support ECM formation (Chen et al., 2021). TGF $\beta$ 1 from macrophages and keratinocytes induces fibroblast differentiation into myofibroblasts, enhancing collagen production (Plikus et al., 2021; Knoedler et al., 2023). TGF $\beta$ 1 also promotes FGF2 release, stimulating cell growth and macrophage recruitment (Strutz et al., 2001; Farooq et al., 2021). Growth factors like EGF and KGF further activate fibroblasts and immune cell recruitment (Canady et al., 2013). EGF enhances fibroblast migration, contraction, VEGF production, and angiogenesis, partly through MAPK/AP-1 pathways (Kim et al., 2015; Yu et al., 2012; Kajanne et al., 2007). Fibroblasts also secrete chemokines like MCP-1/CCL2, attracting monocytes and NK cells (Deshmane et al., 2009).

Keratinocytes, the primary cells of the epidermis, form a multilayered epithelium held together by ECM components, adhesive proteins, desmosomes, and hemidesmosomes (Kirfel & Herzog, 2004; Raja et al., 2007). They play a central role in wound healing by initiating inflammation and driving re-epithelialisation through migration, proliferation, and differentiation (Barker et al., 1991; Raja et al., 2007; Pastar et al., 2014). Injury disrupts keratinocytes, triggering inflammatory responses (Piipponen et al., 2020). Keratin expression shifts depending on cell state: K5 and K14 are dominant under normal conditions for filament stability, while K6, K16, and K17 are upregulated during injury for regeneration (Wilson et al., 1992; Romashin et al., 2024). Keratinocytes also interact with immune cells and fibroblasts via cytokines (see Figure 6.1). During injury, they secrete TGF $\beta$ 1 and FGF2 to activate fibroblasts, which in turn produce FGF2 for cell growth and macrophage recruitment (Plikus et al., 2021; Shirakata, 2010; Strutz et al., 2001; Farooq et al., 2021). NRF2, regulated by Keap1, governs keratinocyte-macrophage communication via the

NRF2/MCP-1/EGF axis; disruption of this pathway is linked to impaired diabetic wound healing (Villarreal-Ponce et al., 2020; Saha et al., 2020; Deshmane et al., 2009; Kansanen et al., 2013; Soares et al., 2016). Additionally, keratinocytes produce antimicrobial peptides such as LL37 and BD2, which contribute to innate immunity by targeting negatively charged bacterial membranes (Afshar & Gallo, 2013).

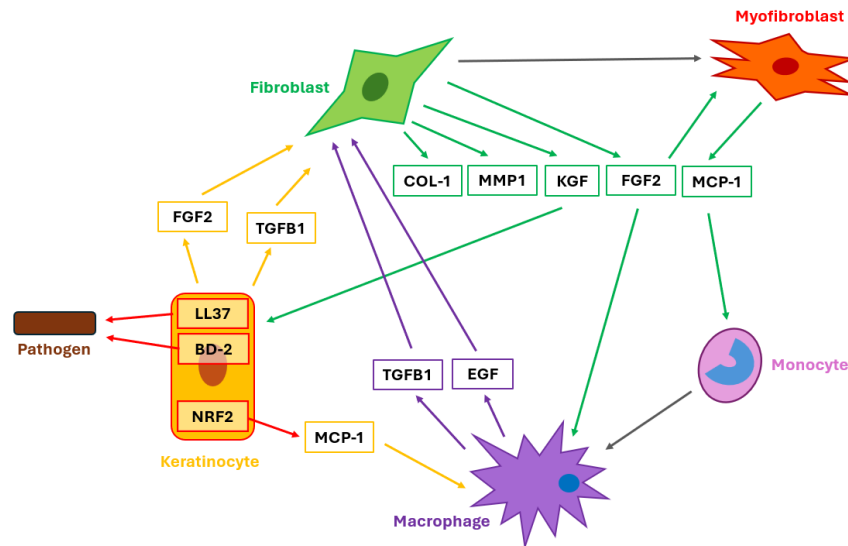


**Figure 6. 1 Fibroblast and Keratinocyte Cell Interactions Involved in Wound Healing.** During the wound healing process fibroblasts, keratinocytes and other immune cells secrete growth factors and cytokines which result in the activation and recruitment of additional immune cells. Schematic based on information from Plikus et al (2021), Liarte et al (2020), Strutz et al (2001), Farooq et al (2021), Canady et al (2013), Deshmane et al (2009) and Villarreal-ponce et al (2020), Afshar and Gallo (2013).

### 6.1.2 The Hyperglycaemic Effects on Fibroblasts and Keratinocytes

Hyperglycaemia can have detrimental effects on cell function greatly impacting wound healing. Studies have shown that high glucose levels increase collagen production, which has been linked to diabetic neuropathy (Tang et al., 2007; Ha et al., 1997; Ighodaro & Adeosun, 2018; Tuleta & Frangogiannis, 2021). Hyperglycaemia activates NF- $\kappa$ B, leading to elevated cytokine expression, including MMP-1, which degrades COL-1 and triggers compensatory collagen production (Suryavanshi & Kulkarni, 2017; Soydas et al., 2018). Hyperglycaemia also increases proinflammatory cytokines such as FGF2 and MCP-1 (Shao et al., 2017; Hu et al., 2018), while suppressing FGF2-mediated JNK phosphorylation, impairing fibroblast migration and increasing ROS (Xuan et al., 2014; Xuan et al., 2016).

Additionally, it induces cell hypertrophy and overexpression of TGF $\beta$ 1 and ECM components (Wu & Derynck, 2009).

Hyperglycaemia impairs keratinocyte migration, proliferation, and differentiation (Raja et al., 2007; Pastar et al., 2014). Lan et al. (2008) reported reduced keratinocyte mobility and proliferation after 5 days of high glucose exposure, while Spravchikov et al. (2001) found altered GLUT1 expression and increased Ca<sup>2+</sup>-induced differentiation under similar conditions. Impaired migration has been linked to decreased p125FAK in diabetic patients (Lan et al., 2008). Hyperglycaemia also reduces BD2 expression by inhibiting pSTAT-1 signaling in keratinocytes (Lan et al., 2012), and diabetic wound healing is further compromised by reduced LL37 activity (Piipponen et al., 2020). LL37 treatment has been shown to enhance autophagy and keratinocyte migration, promoting healing in diabetic mice (Xi et al., 2024). Oxidative stress from hyperglycaemia disrupts the NRF2-Keap1 pathway, contributing to prolonged inflammation (Kaussikaa et al., 2024; Braun et al., 2002). Since NRF2 regulates MCP-1, its deficiency impairs keratinocyte-driven immune signaling (Villarreal-Ponce et al., 2020). Additionally, hyperglycaemia is associated with elevated TGF $\beta$ 1 and reduced FGF2 expression in diabetic patients (Long et al., 2016; Brizeno et al., 2016).

### **6.1.3 Reversing the Hyperglycaemic Effect on Fibroblasts and Keratinocytes**

Diet is a known risk factor for diabetes, and increasing dietary fibre intake has been shown to reduce inflammation and lower glycaemic index in prediabetics (Egshatyan et al., 2016; Reynolds et al., 2020; Nitzke et al., 2024). MGN3, a rice bran-derived fibre, has demonstrated anti-inflammatory effects, modulation of cytokine production, and improved phagocytic activity of macrophages, neutrophils, and NK cells under at pre-diabetic and hyperglycaemic conditions (Ghoneum & Jewett, 2000; Ghoneum & Agrawal, 2011, 2014; Ghoneum & Matsuura, 2004; Ghoneum et al., 2008; Koike et al., 2000). However, its impact on fibroblasts and keratinocytes remains unexplored.

Efforts to reverse hyperglycaemia include targeting insulin levels. Rapamycin has been shown to increase bioactive insulin in epidermal keratinocytes (Tian et al., 2008), though it

does not directly address impaired wound healing. Given the role of diet in diabetes, lifestyle interventions—such as diet and exercise—may help improve diabetic wound healing (Walker et al., 2010). While MGN3 has proven benefits across various immune cells, its potential to restore keratinocyte function and counteract hyperglycaemia-induced damage is largely unknown. If effective, its water solubility makes it a promising candidate for use in hydrogels for direct wound application in diabetic foot ulcers (Koike et al., 2000).

## 6.2 Aims and Objectives

### 6.2.1 Aim

To investigate the effect of MGN3 on fibroblast and keratinocyte cell activities at pre-diabetic and hyperglycaemic culture conditions.

### 6.2.2 Objectives

- To evaluate the effect of MGN3 on fibroblast and keratinocyte proliferation and viability at low and high glucose levels.
- To evaluate the effect of MGN3 on fibroblast and keratinocyte cellular metabolism.
- To assess the effect of MGN3 on matrix (collagen-1), growth factor (EGF, FGF2, KGF, TGF $\beta$ 1) and inflammatory cytokine (MCP-1) secretion by dermal fibroblasts.
- To assess the effect of MGN3 on growth factor (EGF, FGF2 and TGF $\beta$ 1), transcription factor (NRF2) and antibacterial peptide production (LL37 and BD2) by keratinocytes.
- To visualize the influence of MGN3 on matrix (collagen-1) and inflammatory cytokine (MCP-1) production by fibroblasts and antibacterial peptide (LL37) expression by keratinocytes.
- To interrogate the influence of MGN3-induced M1 macrophage-, keratinocyte- and fibroblast-derived EGF and FGF2 secretion on subsequent fibroblast and keratinocyte proliferation.
- To determine the effect of MGN3 treatment on keratinocyte-derived antimicrobial peptide (BD2 and LL37) bactericidal activity.
- To determine the effect of MGN3 treatment on NRF2 protein expression and downstream MCP-1 levels in keratinocytes following NRF2 inhibition.

## 6.3 Methods

### 6.3.1 MTT Assay

HDFs and HACATs were seeded at  $1 \times 10^5$  cells/mL and cultured for 24hrs in low (11 mM) or high (30 mM) glucose. The cells were then treated with RS, LPS or MGN3. After washing with DMEM CM, MTT solution was added for 3 hours. MTT solution was removed, and MTT solvent was added for 10mins to dissolve the formazan crystals. Absorbance was measured at 570nm using a FLUOstar Omega microplate reader to assess viability relative to untreated controls (see section 2.2.12 for more details).

### 6.3.2 Seahorse Analysis

HDFs and HACATs were seeded at  $1 \times 10^5$  cells/mL in low glucose for 24hrs. Cells were then treated with treatments and TLR inhibitors, for an additional 24hrs. For Seahorse analysis, sensor cartridges were hydrated and incubated overnight at 37 °C without CO<sub>2</sub>. On the assay day, Seahorse assay medium and reagents—oligomycin (O) and rotenone/antimycin A (RA)—were prepared according to the manufacturer's instructions. Cellular metabolism was assessed by measuring oxygen consumption rate (OCR), extracellular acidification rate (ECAR), and ATP production (see section 2.2.10 for more details).

### 6.3.3 ELISAs

HDFs were seeded at  $5 \times 10^4$  cells/mL in low or high glucose DMEM CM and incubated for 48hrs. Cells were then treated with treatments and TLR inhibitors for 24hrs. Supernatants were collected and analysed by ELISA for COL-1, FGF2, EGF, KGF, MCP-1, MMP-1, and TGF- $\beta$ 1. HACATs were seeded at  $1 \times 10^5$  cells/mL under the same conditions and treated identically. Supernatants were analysed for EGF, FGF2, MCP-1, TGF- $\beta$ 1, NRF2, and intracellular LL-37) and BD-2 by ELISA per manufacturer instructions (see section 2.2.13.2 for more details).

#### **6.3.4 Thunder Microscopy**

HDFs ( $1 \times 10^4$  cells/mL) and HACATs ( $5 \times 10^4$  cells/mL) were seeded on microscope coverslips in low (11 mM) or high (30mM) glucose DMEM CM and incubated (72hrs for HDFs; 48hrs for HACATs). Cells were then treated treatments and TLR inhibitors for 24hrs. Cells were imaged for fluorescence intensity of specific markers using a Leica THUNDER Imager Tissue microscope at 60 $\times$  magnification. COL-1 and TGF $\beta$ 1 were assessed in HDFs, while LL-37 and TGF $\beta$ 1 were assessed in HACATs. Fluorescence intensity was quantified using ImageJ software (see section 2.2.13.1 for more details).

#### **6.3.5 Functional Protein Assays**

HDFs, HACATs and M1 macrophages were cultured at low and high glucose in DMEM CM at  $1 \times 10^5$  cells/ml for 48hrs. Cells were treated with treatments and TLR inhibitors for 24hrs. The HDFs were incubated for 1hr in the presence/absence of anti-EGF or anti-FGF2 antibody before treatment with the stored HDF, HACAT or M1 supernatants for 24hrs. After the incubation, cell counts were taken using the trypan blue method described previously in section 2.2.2 . The MTT assay was performed as described in section 6.3.1 and absorbance was measure at 570nm (see sections 2.2.14.4 and 2.2.14.5 for more details).

#### **6.3.6 Antimicrobial Peptide Assays**

HACATs were cultured at  $2 \times 10^5$  cells/mL in RPMI CM with 11 or 30mM glucose until 80% confluence, then treated with LPS or and MGN3 for 24hrs. Cell lysates were prepared and incubated for 2 hours with/without BD2 or LL37 blocking antibody. Bacteria were then added for 3 hours. And samples were plated and incubated for 24 hours to quantify bacterial recovery via CFU count (see sections 2.2.14.1 and 2.2.14.2 for more details).

#### **6.3.7 NRF2 Assay**

HACATs were cultured at  $2 \times 10^5$  cells/mL in 11 or 30mM glucose for 24hrs. An NRF2 inhibitor was added to half the cells for 1hr, followed by treatment with LPS or MGN3  $\pm$  NRF2i for

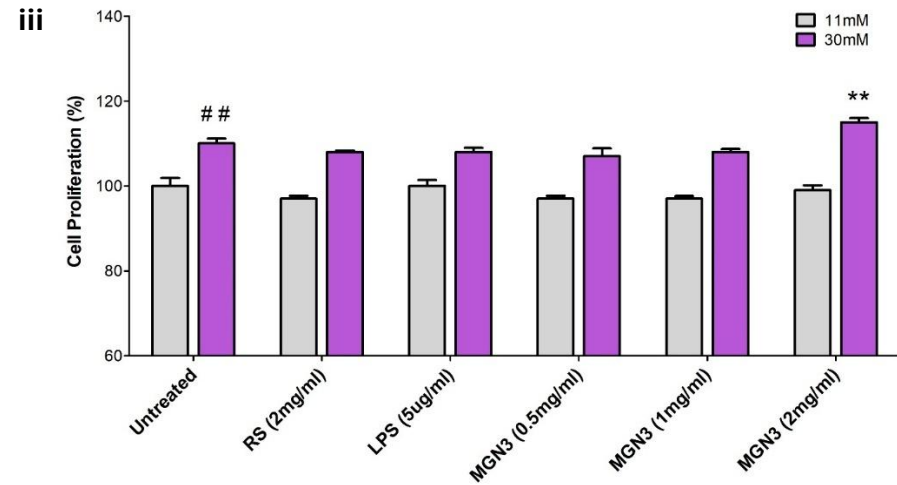
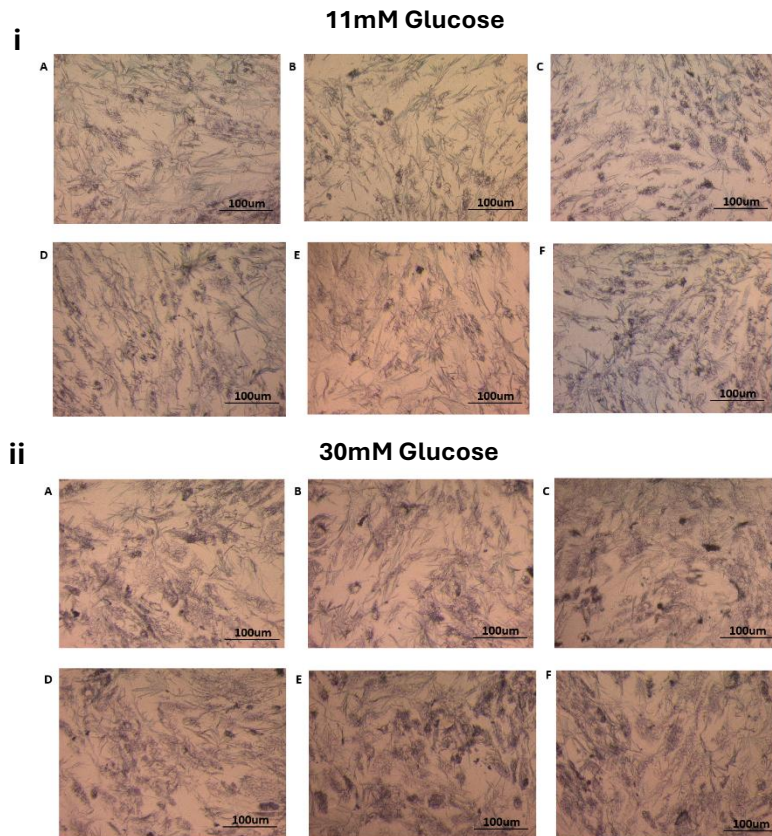
24hrs. NRF2 production was analysed via flow cytometer and secreted levels of MCP-1 following NRF2 inhibition was measured by ELISA (see section 2.2.14.7 for more details).

## 6.4 Results

### 6.4.1 The Effect of MGN3 on HDF Cell Viability and Proliferation

After MTT solution was added to fibroblasts cultured at 11 and 30mM and following treatments (RS, LPS or MGN3) there was an abundance of formazan crystal formation indicating a high viability of cells (Figure 6.2i and ii).

At 30mM there was an increase in fibroblast proliferation in all cases compared to 11mM glucose (Figure 6.2iii). Hyperglycaemia significantly ( $##$ ;  $P < 0.01$ ) increased HDF proliferation but had no significant effect ( $P > 0.05$ ) on cell viability when compared to untreated fibroblasts cultured at pre-diabetic conditions. MGN3 significantly ( $P < 0.01$ ) increased fibroblast proliferation (115.4%) compared to corresponding untreated fibroblasts (109.6%) cultured under hyperglycaemic conditions. No other treatments except 2mg/ml MGN3 under hyperglycaemic conditions significantly influenced fibroblast proliferation. Furthermore, cytotoxicity results (Figure 6.2iv) illustrated all treatments induced low ( $< 3.5\%$ ) cytotoxicity to the fibroblasts, with no significant ( $P > 0.05$ ) detrimental effects on cell viability detected following any of the treatments.



**iv** **MTT HDF % cytotoxicity**

	11mm	30mm
Untreated	0.000	0.000
RS	3.443	0.000
LPS	0.000	0.000
0.5mg/ml MGN3	2.651	0.000
1mg/ml MGN3	2.983	0.000
2mg/ml MGN3	1.057	0.000

**Figure 6. 2: The Effect of MGN3 on HDF Proliferation.** HDF proliferation was measured in fibroblasts cultured in low (11mM) or high (30mM) glucose following treatment with RS (2mg/ml), LPS (5ug/ml) or MGN3 (0.5, 1 and 2mg/ml) for 24 hours. After treatment MTT solution was added and the cells (cultured at 11; i and 30mM glucose ; ii) were incubated for 3 hours to allow for crystal formation prior to image capture. Panel A is the untreated control (UC), B is RS, C is LPS, and panels D, E and F are MGN3 treatments at 0.5 1 and 2mg/ml respectively. All images were taken with a Zeiss microscope at 40x magnification. The cell proliferation significantly increased (iii) in the 30mM untreated control (UC) compared to the 11mM UC (##  $P < 0.01$  determined by t-tests;  $n = 24$ ). Fibroblast proliferation was also significantly increased when fibroblasts cultured at 30mM were treated with 2 mg/ml MGN3 compared to the corresponding glycaemic untreated control (\*\*  $P < 0.01$  determined by t-tests;  $n = 24$ ). Columns and error bars indicate the % HDF proliferation relative to the 11mM UC  $\pm$  the standard error of the mean (SEM) in all cases. The cytotoxicity of treatments including MGN3 was evaluated as part of the MTT analysis at pre-diabetic (11) and hyperglycaemic (30mM) conditions (iv). All cytotoxicity values were  $< 3.5\%$ , indicating all treatment including MGN3 had no appreciable cytotoxic effects on HDFs.

## 6.4.2 The Effect of MGN3 on Fibroblast Cellular Metabolism

### 6.4.2.1 Fibroblast Metabolism at Low Glucose Following TLR inhibition

TLR2 inhibition (T2i) significantly increased OCR in untreated fibroblasts after oligomycin (post O:  $P = 0.004$ ) and rotenone/antimycin A (post RA:  $P = 0.015$ ). TLR4 inhibition (T4i) significantly elevated OCR at all timepoints ( $P < 0.01$ ) compared to controls without TLR inhibition (Figure 6.3A). In LPS-treated fibroblasts, T2i significantly increased OCR post O and post RA ( $P < 0.01$ ), while T4i increased OCR only post O ( $P = 0.016$ ). In MGN3-treated fibroblasts, T2i elevated OCR post O ( $P = 0.004$ ), and T4i significantly increased OCR at all timepoints ( $P < 0.05$ ) compared to LPS treatments without TLRi. Both T2i and T4i significantly increased ECAR in untreated and LPS-treated fibroblasts at all timepoints ( $P < 0.01$ ; Figure 6.3B) compared to LPS treatments without TLRi. In MGN3-treated fibroblasts, T2i increased ECAR during P/A ( $P = 0.014$ ) and post-antibiotics ( $P < 0.01$ ), while T4i inhibition increased OCR at all timepoints ( $P < 0.01$ ) compared to MGN3 treatments without TLRi.

LPS treatment led to a small but significant increase in total ATP production ( $P < 0.05$ ; Fig. 6.3C), with 63% derived from glycolysis compared to 36% in the UC group. MGN3 treatment caused a substantial reduction in total ATP production compared to both UC and LPS groups, with HDFs primarily using the mitoATP pathway (58%), similar to UC (64%). However, mitoATP significantly decreased following LPS ( $P = 0.039$ ) and MGN3 ( $P = 0.03$ ) treatments. TLR inhibition increased total ATP production, mainly via glycoATP, in both LPS- and MGN3-treated groups (Fig. 6.3C). In UC fibroblasts, mitoATP accounted for 64% of ATP, but this dropped significantly with T2i (4%;  $P = 0.015$ ) and T4i (12%;  $P = 0.02$ ), while glycoATP significantly increased ( $P = 0.018$  and  $P = 0.004$ , respectively). Following LPS, mitoATP fell from 37% to 8% with T2i ( $P = 0.022$ ) and 6% with T4i ( $P = 0.084$ ), with a corresponding glycoATP increase ( $P = 0.041$  and  $P < 0.001$ ). Similarly, after MGN3, mitoATP decreased from 58% to 12% with T2i ( $P = 0.018$ ) and 8% with T4i ( $P = 0.043$ ), while glycoATP significantly rose ( $P = 0.041$  and  $P = 0.006$ ). Collectively, these findings showed the TLR2 and TLR4 pathways can regulate ATP production in a similar manner in untreated as well as LPS/MGN3-treated fibroblasts. This suggests the effects of MGN3 and LPS on ATP

production in fibroblasts cultured at pre-diabetic conditions are mediated by mechanisms other than the TLR2/TLR4 pathways.

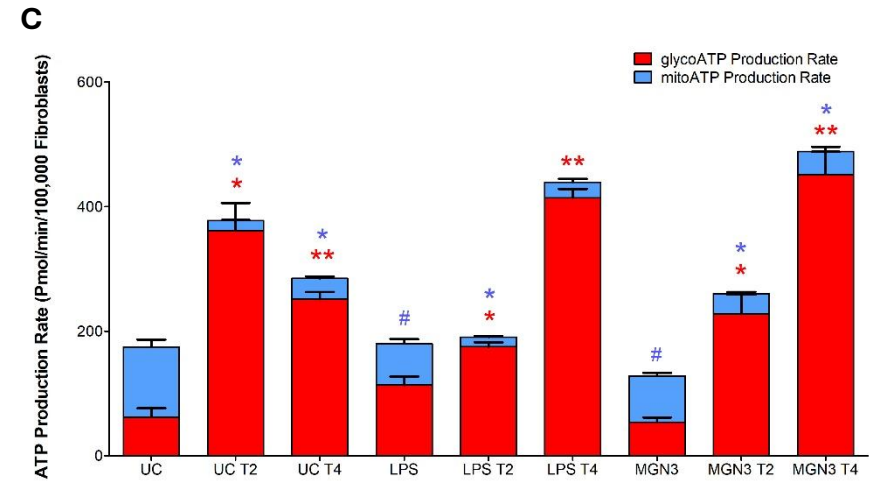
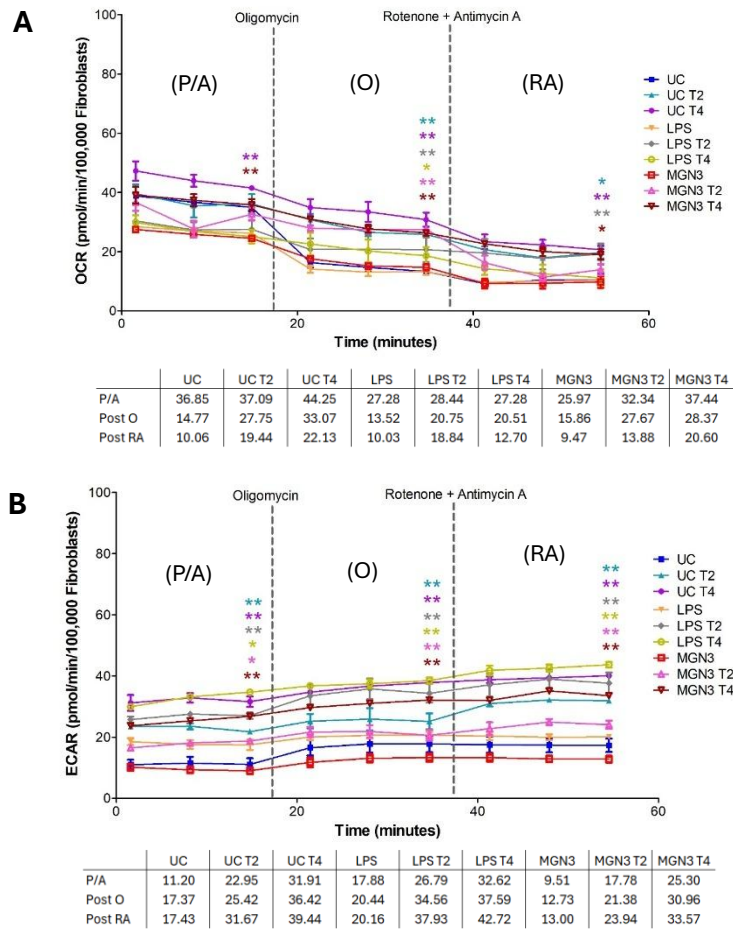


**Figure 6. 3: Fibroblast Cellular Metabolism at Low Glucose Following TLR Inhibition.** The OCR, ECAR and Real time ATP production of HDFs was analysed via seahorse analysis. There were significant differences (\* $P < 0.05$  and \*\* $P < 0.01$  determined by *t*-tests;  $n = 3$ ) in OCR (A), ECAR (B) and in ATP production (C) were observed between treatments with TLR2 (T2) and TLR4 (T4) inhibition and corresponding treatments without TLR inhibition. There was also a significant decrease (#  $P < 0.05$  determined by *t*-tests;  $n = 3$ ) in mitoATP production (C) in the LPS and MGN3 groups compared to the UC group. Timepoints and error bars indicate the OCR and ECAR, columns and error bars indicate the ATP production rate (pmol/min/100,000 Fibroblasts)  $\pm$  the standard error of the mean (SEM) in all cases. The tables indicate the average OCR and ECAR values at pre-antibiotic (P/A), post Oligomycin (O) and post Rotenone+Antimycin A (RA) exposure.

#### 6.4.2.2 Fibroblast Metabolism at High Glucose Following TLR Inhibition

There were significant increases ( $P < 0.01$ ) in OCR (Figure 6.4A) and ECAR (Figure 6.4B) for LPS and MGN3 treatments following TLR inhibition at all timepoints compared to corresponding treatments lacking TLR inhibition. Similarly, T2i and T4i significantly increased ( $P < 0.01$ ) OCR and ECAR levels in untreated fibroblasts at all timepoints compared to untreated fibroblasts lacking TLR inhibition.

There was a decrease in the total ATP production (Figure 6.4C) following treatment of fibroblasts with LPS or MGN3 compared to the UC group under hyperglycaemic conditions. Following LPS treatment there was a 50% split between ATP produced by mitoATP and glycoATP, whereas in the UC group 73% of ATP was produced via the mitoATP pathway. Following treatment of fibroblasts with MGN3 mitoATP production was 62%. There was a significant decrease in mitoATP production in fibroblasts treated with LPS or MGN3 ( $P = 0.029$  and  $P = 0.015$  respectively) when compared to the UC. There was a significant increase in total ATP production (Figure 6.6C), notably glycoATP, following TLR inhibition in untreated and treated fibroblasts cultured under hyperglycaemic conditions. In UC fibroblasts, 73% of ATP production was via the mitoATP pathway whereas this was substantially reduced following T2i (9%;  $P = 0.001$ ) or T4i (12%;  $P = 0.022$ ). Similarly, 50% of ATP was produced via mitoATP following treatment with LPS but this was substantially reduced with T2i (3%;  $P = 0.015$ ) or T4i (9%;  $P = 0.38$ ). Similarly, 62% of ATP was produced via mitoATP pathways following MGN3 treatment but this was significantly reduced to 14% ( $P = 0.12$ ) with T2i and 20% ( $P = 0.885$ ) with T4i. In contrast, T2i and T4i in untreated fibroblasts significantly increased glycoATP ( $P = 0.003$  and  $P = 0.016$  respectively) compared to untreated fibroblasts lacking TLR inhibition. Similarly, T2i and T4i also significantly increased glycoATP in LPS-treated ( $P < 0.01$ ) and MGN3-treated ( $P = 0.000$  and  $P = 0.024$  respectively) fibroblasts compared to corresponding fibroblasts lacking TLR inhibition.

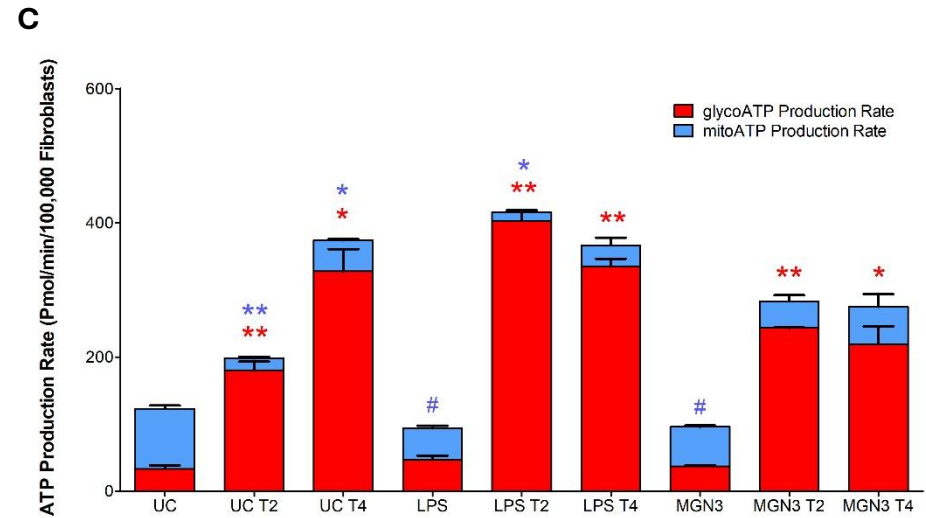
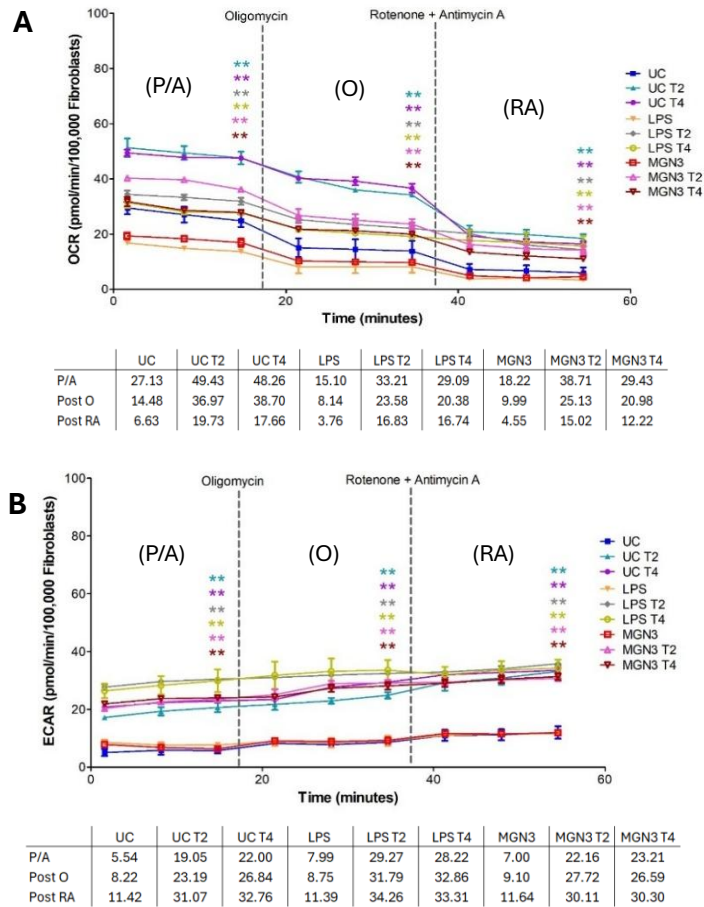


**Figure 6. 4: Fibroblast Cellular Metabolism at High Glucose following TLR inhibition.** The OCR, ECAR and Real time ATP production of HDFs was analysed via seahorse analysis. There were significant differences in OCR (A), ECAR (B) and ATP production (C) (\* $P < 0.05$  and \*\* $P < 0.01$  determined by t-tests;  $n = 3$ ) between treatments with TLR2 (T2i) and TLR4 (T4i) inhibition and corresponding treatments without TLR inhibition. There was also a significant decrease (#  $P < 0.05$  determined by t-tests;  $n = 3$ ) in mitoATP production (C) in the LPS and MGN3 groups compared to the UC group. Timepoints and error bars indicate the OCR and ECAR, columns and error bars indicate the ATP production rate (pmol/min/100,000 Fibroblasts)  $\pm$  the standard error of the mean (SEM) in all cases. The tables indicate the OCR and ECAR values at pre-antibiotic (P/A), post Oligomycin (O) and post Rotenone+Antimycin A (RA) exposure.

### 6.4.3 Effect of MGN3 on Matrix, Growth Factor and Inflammatory Cytokine Secretion by Human Dermal Fibroblasts (HDFs)

#### 6.4.3.1 Secretion of Collagen-1 levels from HDFs

Hyperglycaemia significantly ( $P = 0.039$ ) inhibited collagen-1 secretion in untreated fibroblasts compared with fibroblasts cultured at pre-diabetic conditions (Figure 6.5). MGN3/LPS-treated fibroblasts secreted significantly ( $P < 0.01$ ) increased amounts of COL-1 at 11mM and particularly at 30mM compared to untreated cells, with significantly higher levels ( $P < 0.01$ ) produced at 30mM compared to 11mM. At 11mM, TLRi significantly decreased ( $P < 0.01$ ) COL-1 secretion in untreated fibroblasts but TLRi had no significant impact ( $P > 0.05$ ) at 30mM in untreated fibroblasts compared to corresponding untreated fibroblasts without TLRi. There was also significantly ( $P < 0.05$ ) decrease in COL-1 secretion when fibroblasts were treated with MGN3/LPS and TLRi at both 11mM and 30mM glucose compared to treatments without TLRi. These findings suggest TLR2 and TLR4 mediate MGN3/LPS-induced collagen secretion under hyperglycaemic conditions but not at pre-diabetic conditions.

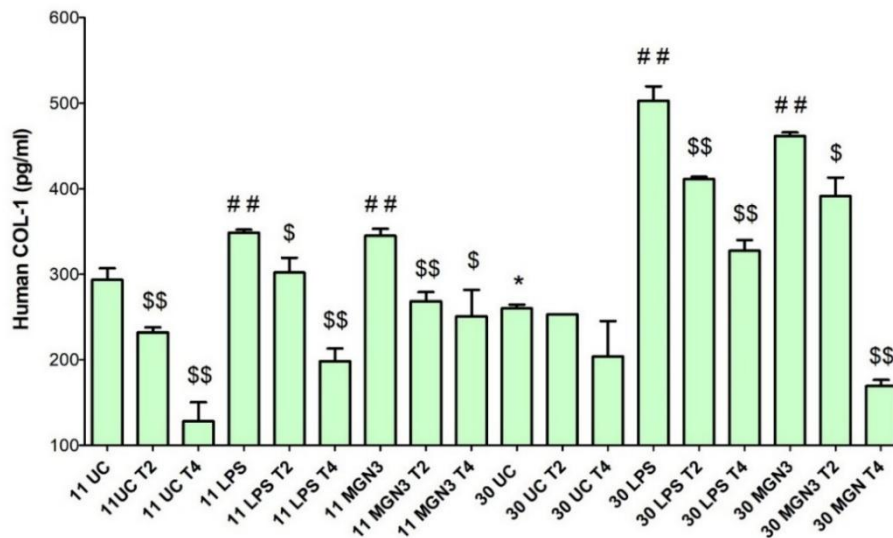


**Figure 6. 5: Secretion of Collagen-1 (COL-1) by Fibroblasts.** COL-1 levels were measured in the supernatant from fibroblasts cultured in low (11mM) or high (30mM) glucose following treatment with LPS or MGN3 in the presence/absence of TLR2 (T2) or TLR4 (T4) inhibition. There was a significant decrease in COL-1 in untreated control (UC) fibroblasts cultured at 30mM compared to UC fibroblasts cultured at 11mM glucose (\*  $P < 0.05$  determined by t-tests;  $n = 10$ ). There were significant increases in COL-1 between fibroblasts treated with LPS or MGN3 and the corresponding glycaemic UC (##  $P < 0.01$  determined by t-tests;  $n = 10$ ). There were significant decreases in COL-1 between fibroblasts in the presence of TLR inhibitors and corresponding fibroblasts lacking TLR inhibition (\$  $P < 0.05$  and \$\$  $P < 0.01$  determined by t-tests;  $n = 10$ ). Columns and error bars indicate human COL-1 levels (pg/ml)  $\pm$  the standard error of the mean (SEM) in all cases.

### 6.4.3.2 Secretion of Epidermal Growth Factor from HDFs

EGF secretion was significantly reduced ( $P < 0.001$ ) in untreated fibroblasts cultured in hyperglycaemic conditions compared to pre-diabetic conditions (Figure 6.6). MGN3/LPS-treated fibroblasts secreted significantly ( $P < 0.01$ ) increased EGF levels at both 11mM and 30mM glucose, but with significantly greater secretion at 11mM compared to 30mM ( $P < 0.05$ ). TLR2 inhibition significantly increased ( $P < 0.01$ ) EGF production in untreated fibroblasts at 11mM, whereas TLRi increased EGF secretion from untreated fibroblasts at 30mM glucose compared to untreated fibroblasts without TLRi. TLR2 inhibition significantly increased ( $P = 0.001$ ) EGF in LPS-treated fibroblasts at 11mM, whereas TLRi had no significant effect ( $P > 0.05$ ) on LPS-treated fibroblasts at 30mM glucose conditions compared to LPS treatment without TLRi, Although TLR2 inhibition had no effect ( $P > 0.05$ ) on MGN3-treated fibroblasts at either glycaemic condition, TLR4 inhibition significantly ( $P < 0.01$ ) reduced EGF secretion from MGN3-treated cells at 11mM and 30mM glucose compared to MGN3 treatment without TLRi,. These findings suggest EGF secretion from fibroblasts was mediated by MGN3 at least in part through TLR4 at pre-diabetic and hyperglycaemic conditions.

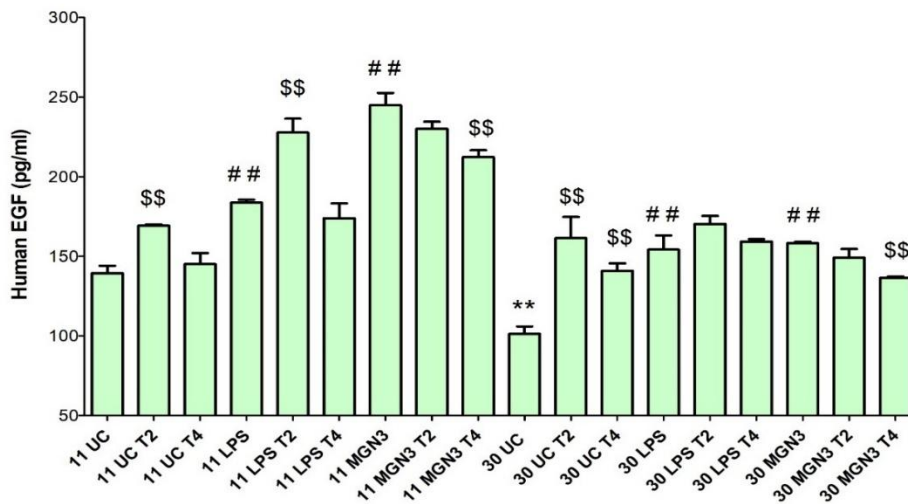


**Figure 6. 6: Secretion of Epidermal Growth Factor (EGF) by Fibroblasts.** EGF levels were measured in the supernatant of fibroblasts cultured in low (11mM) or high (30mM) glucose and treated with LPS or MGN3 in the presence/absence of TLR2 (T2) or TLR4 (T4) inhibition. There was a significant decrease in EGF in untreated control (UC) fibroblasts cultured at 30mM compared to UC fibroblasts cultured at 11mM glucose (\*  $P < 0.05$  and \*\*  $P < 0.01$  determined by t-tests;  $n = 8$ ). There were significant increases in EGF between fibroblasts treated with LPS or MGN3 and the corresponding glycaemic UC (##  $P < 0.01$  determined by t-tests;  $n = 8$ ). There were significant differences in EGF between fibroblasts in the presence of TLR inhibitors and corresponding fibroblasts lacking TLR inhibition (\$\$  $P < 0.01$  determined by t-tests;  $n = 8$ ). Columns and error bars indicate human EGF levels (pg/ml)  $\pm$  the standard error of the mean (SEM) in all cases.

### 6.4.3.3 Fibroblast Growth Factor-2 Secretion from HDFs

Hyperglycaemia significantly ( $P < 0.01$ ) increased fibroblast FGF2 secretion compared to pre-diabetic conditions (Figure 6.7). TLRi significantly increased ( $P < 0.01$ ) FGF2 secretion by untreated fibroblasts cultured at both 11mM and 30mM glucose compared to untreated fibroblasts lacking TLR inhibition. FGF2 production was significantly ( $P = 0.029$ ) inhibited by LPS at 11mM but was significantly increased ( $P < 0.01$ ) by LPS treatment at 30mM compared to the correspond UC. TLRi inhibition also significantly increased ( $P < 0.01$ ) FGF2 production in LPS-treated fibroblasts at both 11mM and 30mM glucose compared to LPS-treated fibroblasts without TLRi,. MGN3 had no significant ( $P > 0.05$ ) effect on FGF2 secretion from fibroblasts compared to untreated fibroblasts cultured at the same glycaemic concentration. TLR2 inhibition significantly increased ( $P < 0.01$ ) FGF2 production by MGN3-treated fibroblasts at 11mM and 30mM glucose, in a similar manner to the pattern of responses observed in untreated fibroblasts. TLR4 inhibition had no significant effect on MGN3-treated fibroblasts cultured at 11mM but significantly reduced ( $P < 0.05$ ) FGF2 production at 30mM glucose compared to MGN3-treated fibroblasts without TLRi,

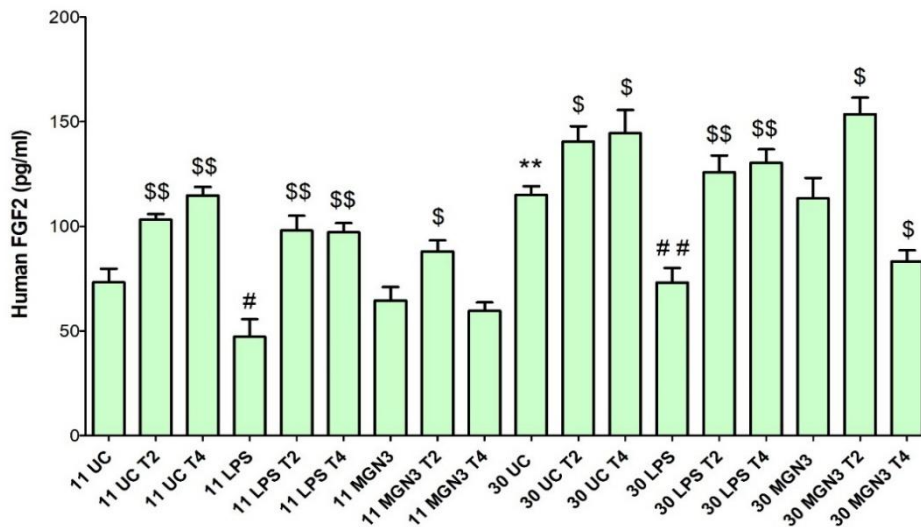


**Figure 6. 7: Secretion of Fibroblast Growth Factor 2 (FGF2) by Fibroblasts.** FGF2 levels were measured in the supernatant of fibroblasts cultured in low (11mM) or high (30mM) glucose and treated with LPS or MGN3 in the presence/absence of TLR2 (T2) or TLR4 (T4) inhibition. There was a significant increase in FGF2 in untreated control (UC) fibroblasts cultured at 30mM compared to UC fibroblasts cultured at 11mM glucose (\*\*  $P < 0.01$  determined by t-tests;  $n = 8$ ). There were significant decreases in COL-1 between fibroblasts treated with LPS or MGN3 and the corresponding glycaemic UC (#  $P < 0.05$  and ##  $P < 0.01$  determined by t-tests;  $n = 8$ ). There were significant differences in FGF2 between fibroblasts in the presence of TLR inhibitors and corresponding fibroblasts lacking TLR inhibition (\$  $P < 0.05$  and \$\$  $P < 0.01$  determined by t-tests;  $n = 8$ ). Columns and error bars indicate human FGF2 levels (pg/ml)  $\pm$  the standard error of the mean (SEM) in all cases.

#### 6.4.3.4 Monocyte Chemoattractant Protein-1 Secretion from HDFs

MCP-1 secretion was significantly ( $P < 0.01$ ) increased from fibroblasts cultured in hyperglycaemic conditions compared to pre-diabetic conditions (Figure 6.8). MGN3 significantly reduced ( $P < 0.01$ ) MCP-1 secretion in fibroblasts cultured at 30mM compared to corresponding glycaemic untreated fibroblasts but had no effect ( $P > 0.05$ ) on MCP-1 secretion at 11mM. LPS had no significant effect on MCP-1 secretion from fibroblasts cultured under 11mM or 30mM glucose compared to corresponding glycaemic UC fibroblasts. TLR2 inhibition significantly ( $P < 0.01$ ) increased MCP-1 production in untreated and LPS-treated fibroblasts cultured at 11mM whereas both TLR inhibition significantly ( $P < 0.01$ ) reduced MCP-1 production from untreated and LPS-treated fibroblasts cultured at 30mM glucose in comparison to corresponding treatments without TLRi. There was no significant ( $P > 0.05$ ) effect on MGN3-mediated MCP-1 production from fibroblasts cultured at 11mM or 30mM glucose following TLRi in comparison MGN3 treatment without TLRi. These results indicate MGN3 treatment reduced MCP-1 secretion from fibroblasts cultured at 30mM but not at 11mM glucose. Moreover, TLR2/TLR4 influenced MCP-1 secretion in untreated fibroblasts, but neither TLR2 nor TLR4 influenced the MGN3-mediated inhibition of MCP-1 secretion.

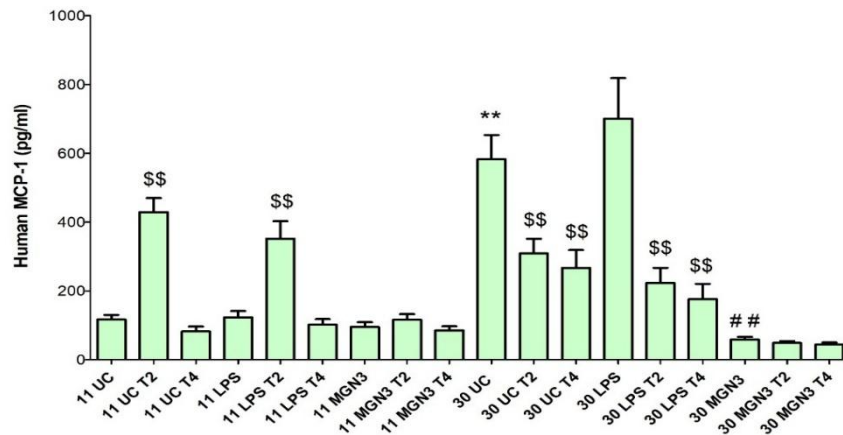


**Figure 6. 8: Secretion of Monocyte Chemoattractant Protein-1 (MCP-1) by Fibroblasts.** MCP-1 levels were measured in the supernatant of fibroblasts cultured in low (11mM) or high (30mM) glucose and treated with LPS or MGN3 in the presence/absence of TLR2 (T2) or TLR4 (T4) inhibition. There was a significant increase in MCP-1 in untreated control (UC) fibroblasts cultured at 30mM compared to UC fibroblasts cultured at 11mM glucose (\*\*  $P < 0.01$  determined by *t*-tests;  $n = 6$ ). There were significant differences in MCP-1 between fibroblasts treated with LPS or MGN3 and the corresponding glycaemic UC (##  $P < 0.01$  determined by *t*-tests;  $n = 6$ ). There were significant differences in MCP-1 between fibroblasts in the presence of TLR inhibitors and corresponding fibroblasts lacking TLR inhibition (\$\$  $P < 0.01$  determined by *t*-tests;  $n = 6$ ). Columns and error bars indicate human MCP-1 levels (pg/ml)  $\pm$  the standard error of the mean (SEM) in all cases.

#### 6.4.3.5 Matrix Metalloproteinase-1 Secretion from HDFs

Hyperglycaemia significantly increased ( $P < 0.01$ ) MMP-1 secretion from fibroblasts compared to fibroblasts cultured at pre-diabetic conditions (Figure 6.9). LPS-treated fibroblasts secreted significantly higher ( $P < 0.01$ ) MMP-1 than corresponding fibroblasts cultured at the same glucose concentration. MGN3-treated fibroblasts cultured at 30mM (but not 11mM) secreted significantly higher ( $P < 0.01$ ) MMP-1 than corresponding fibroblasts cultured at the same glucose concentration. TLRi significantly increased ( $P < 0.01$ ) MMP-1 production in untreated fibroblasts at 11mM glucose, whereas only TLR2 inhibition significantly increased ( $P < 0.001$ ) MMP-1 production in untreated fibroblasts at 30mM compared to corresponding untreated fibroblasts. TLR4 inhibition significantly decreased ( $P < 0.01$ ) MMP-1 production by MGN3/LPS-treated fibroblasts cultured at 11mM compared MGN3/LPS-treated fibroblasts without TLRi. In contrast, both TLR2 and TLR4 inhibition significantly increased ( $P < 0.05$ ) MMP-1 production from MGN3/LPS-treated fibroblasts cultured at 30mM glucose compared to MGN3/LPS-treated fibroblasts without TLRi. These results indicate that TLR4 at least in part influences MGN3/LPS-mediated MMP-1 secretion from fibroblasts.

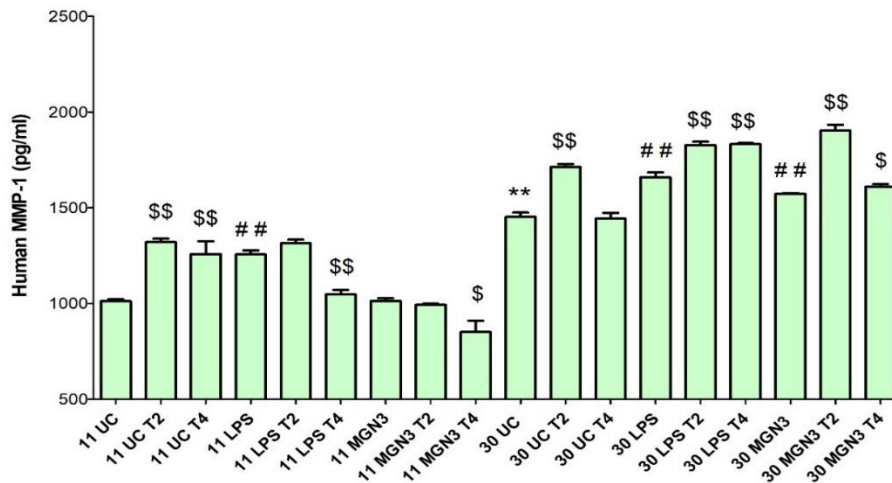


**Figure 6. 9: Secretion of Matrix Metalloproteinase-1 (MMP-1) by Fibroblasts.** MMP-1 levels were measured in the supernatant of fibroblasts cultured in low (11mM) or high (30mM) glucose and treated with LPS or MGN3 in the presence/absence of TLR2 (T2) or TLR4 (T4) inhibition. There was a significant decrease in MMP-1 in untreated control (UC) fibroblasts cultured at 30mM compared to UC fibroblasts cultured at 11mM glucose (\*\*  $P < 0.01$  determined by t-tests;  $n = 10$ ). There were significant increases in MMP-1 between fibroblasts treated with LPS or MGN3 and the corresponding glycaemic UC (##  $P < 0.01$  determined by t-tests;  $n = 10$ ). There were significant differences in MMP-1 between fibroblasts in the presence of TLR inhibitors and corresponding fibroblasts lacking TLR inhibition (\$  $P < 0.05$  and \$\$  $P < 0.01$  determined by t-tests;  $n = 10$ ). Columns and error bars indicate human MMP-1 levels (pg/ml)  $\pm$  the standard error of the mean (SEM) in all cases.

#### 6.4.3.6 Transforming Growth Factor beta 1 Secretion from HDFs

TGFβ1 expression was significantly higher ( $P < 0.01$ ) in untreated fibroblasts under hyperglycaemic vs. pre-diabetic conditions (Figure 6.10). MGN3/LPS-treated fibroblasts secreted significantly more TGFβ1 at 30mM ( $P < 0.01$ ) compared to untreated fibroblasts but showed no significant change at 11mM ( $P > 0.05$ ) glucose. TLR4 inhibition (not TLR2) significantly reduced TGFβ1 in untreated fibroblasts ( $P < 0.01$ ), especially at 30mM glucose compared to untreated fibroblasts without TLRi. In LPS-treated fibroblasts, TLR4 (not TLR2) inhibition also reduced TGFβ1 at both 11mM and 30mM ( $P < 0.05$ ) glucose compared to LPS treated fibroblasts without TLRi. In MGN3-treated fibroblasts, TLRi reduced TGFβ1 at 11mM glucose ( $P < 0.01$ ), while only TLR4 inhibition was effective at 30mM glucose ( $P < 0.001$ ) in comparison to MGN3 treatments without TLRi. These results show TGFβ1 secretion is TLR4-dependent at both glucose levels, but TLR4 does not explain the MGN3-induced increase at 30mM glucose. TLR2 influenced TGFβ1 only in MGN3-treated fibroblasts at 11mM glucose.

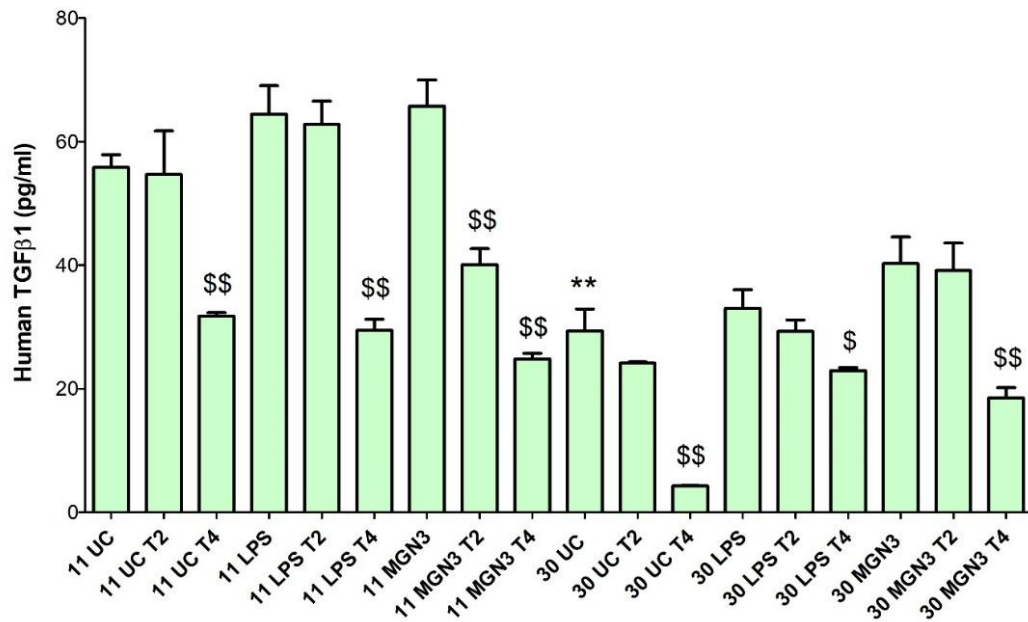


**Figure 6. 10: Secretion of Transforming Growth Factor beta 1 (TGFβ1) by Fibroblasts.** TGFβ1 levels were measured in the supernatant of fibroblasts cultured in low (11mM) or high (30mM) glucose and treated with LPS or MGN3 in the presence/absence of TLR2 (T2) or TLR4 (T4) inhibition. There was a significant decrease in TGFβ1 in untreated control (UC) fibroblasts cultured at 30mM compared to UC fibroblasts cultured at 11mM glucose (\*\*  $P < 0.01$  determined by t-tests;  $n = 8$ ). There were significant increases in TGFβ1 between fibroblasts treated with LPS or MGN3 and the corresponding glycaemic UC (\$  $P < 0.05$  and \$\$  $P < 0.01$  determined by t-tests;  $n = 8$ ). There were significant decreases in TGFβ1 between fibroblasts in the presence of TLR inhibitors and corresponding fibroblasts lacking TLR inhibition. Columns and error bars indicate human TGFβ1-1 levels (pg/ml)  $\pm$  the standard error of the mean (SEM) in all cases.

### 6.4.3.7 Keratinocyte Growth Factor Secretion from HDFs

Hyperglycaemia significantly reduced ( $P = 0.000$ ) KGF secretion from untreated fibroblasts compared to pre-diabetic conditions (Figure 6.11). MGN3 also significantly decreased KGF secretion at 11mM ( $P < 0.01$ ) but increased it at 30mM conditions ( $P < 0.01$ ) whereas LPS significantly stimulated KGF secretion at 30 mM ( $P < 0.05$ ) but had no effect at 11mM ( $P > 0.05$ ) in comparison to the corresponding UC. TLR4 inhibition (not TLR2) reduced KGF secretion at 11mM ( $P = 0.005$ ), while both TLR2 and TLR4 inhibition increased it at 30 mM ( $P < 0.01$ ) in untreated fibroblasts compared to untreated fibroblast without TLRi. Neither TLR2 nor TLR4 inhibition affected KGF levels from LPS-treated fibroblasts ( $P > 0.05$ ), but both significantly reduced MGN3-induced KGF secretion at 11 mM ( $P < 0.01$ ), with no effect at 30mM in comparison to the corresponding treatments without TLRi. Thus, TLR2/4 modulate MGN3-mediated KGF secretion specifically at pre-diabetic conditions.

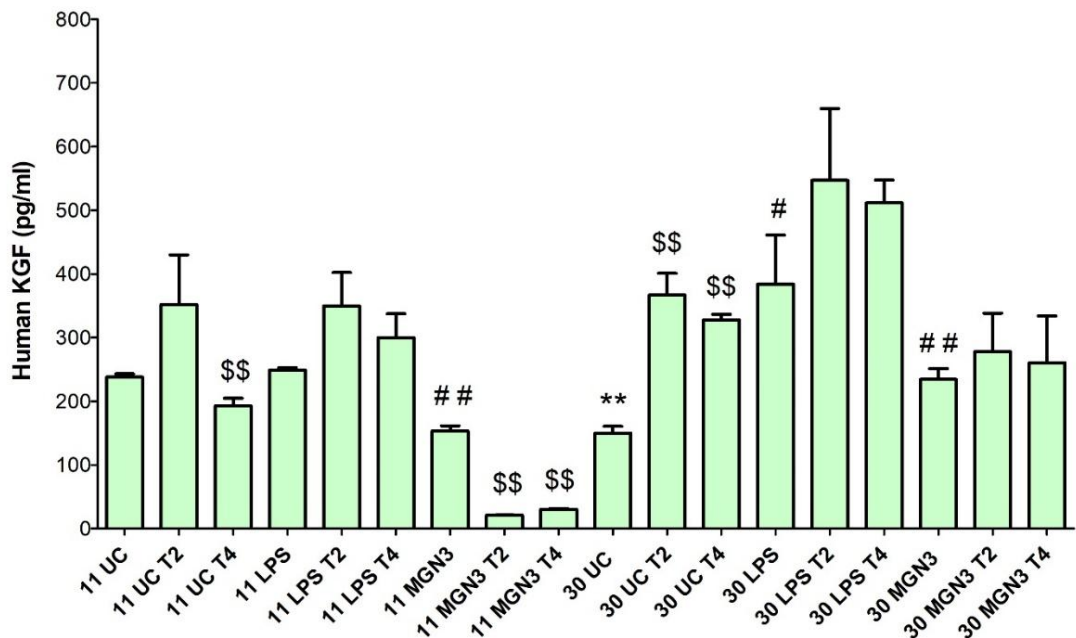


**Figure 6. 11: Secretion of Keratinocyte Growth Factor (KGF) by Fibroblasts.** KGF levels were measured in the supernatant of fibroblasts cultured in low (11mM) or high (30mM) glucose and treated with LPS or MGN3 in the presence/absence of TLR2 (T2) or TLR4 (T4) inhibition. There was a significant decrease in KGF in untreated control (UC) fibroblasts cultured at 30mM compared to UC fibroblasts cultured at 11mM glucose (\*\*  $P < 0.01$  determined by t-tests;  $n = 10$ ). There were significant differences in KGF between fibroblasts treated with LPS or MGN3 and the corresponding glycaemic UC (#  $P < 0.05$  and ##  $P < 0.01$  determined by t-tests;  $n = 10$ ). There were significant differences in KGF between fibroblasts in the presence of TLR inhibitors and corresponding fibroblasts lacking TLR inhibition (\$\$  $P < 0.01$  determined by t-tests;  $n = 10$ ). Columns and error bars indicate human KGF levels (pg/ml)  $\pm$  the standard error of the mean (SEM) in all cases.

#### **6.4.4 Effect of MGN3 on Matrix, Growth Factor and Inflammatory Cytokine Protein Expression in Human Dermal Fibroblasts (HDFs)**

##### **6.4.4.1 COL-1 Protein Expression in HDFs**

Hyperglycaemia had no effect on COL-1 expression in untreated fibroblasts (Figures 6.12i and 6.12ii). At 11mM glucose, mean fluorescence intensity (MFI) increased in LPS/MGN3-treated fibroblasts compared to control group (Figure 6.12iii). At 30mM, no changes in MFI were observed in MGN3/LPS-treated fibroblasts compare their glycaemic control group.

There was no significant difference ( $P>0.05$ ) observed in MFI of COL-1 levels in untreated fibroblasts cultured at 30mM glucose compared to untreated fibroblasts cultured at 11mM glucose. At 11mM there was a significant increase in MFI in LPS treated fibroblasts (MFI = 2.2;  $P=0.045$ ) and MGN3 treated fibroblasts (MFI=2.91;  $P<0.01$ ) compared to untreated fibroblasts (MFI = 1). The addition of TLR2 inhibitor significantly increased ( $P<0.05$ ) MFI in LPS treated fibroblasts compared to LPS treatment without TLR2 inhibition. The addition of TLR4 inhibitor significantly increased MFI in untreated fibroblasts ( $P<0.05$ ) and significantly decreased ( $P<0.01$ ) COL-1 MFI in MGN3 /LPS treated fibroblasts in comparison to corresponding treatments without TLR4 inhibition. At 30mM there were no significant differences ( $P>0.05$ ) seen in MGN3/LPS treated fibroblasts compared to the UC. There were also no significant differences seen ( $P>0.05$ ) following TLR inhibition. These results TLR4 influences COL-1 expression in untreated and MGN3/LPS treated fibroblasts at pre-diabetic conditions.

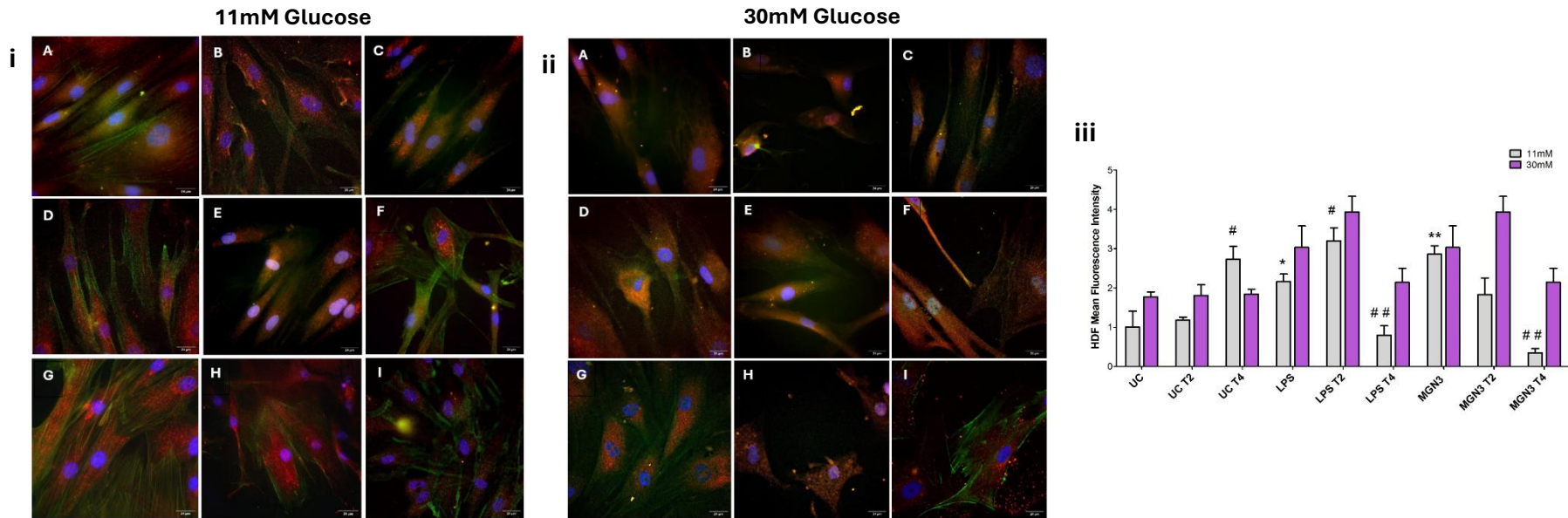


**Figure 6. 12: COL-1 Protein Expression in HDFs at Low and High Glucose.** The expression of COL-1 in HDFs cultured at Low (11mM) (i) and High (30mM) (ii) glucose was captured using thunder microscopy. MFI of COL-1 expression (iii) was measured in fibroblasts following treatments (with LPS and MGN3) and TLR2 (T2) and TLR4 (T4) inhibition. The different cell components were identified using fluorescent stains; red indicated COL-1 expression, green identified f-actin using phalloidin and blue represented the nucleus using DAPI. Fibroblasts received different treatments; Panel A = UC, panel B = UC + T2, panel C = UC + T4, panel D = LPS, panel E = LPS + T2, panel F = LPS + T4, panel G = MGN3, panel H = MGN3 + T2 and panel I = MGN3 + T4. Images were captured at 60x magnification. There were significant increases MFI in MGN3/LPS treated fibroblasts when compared to the corresponding glycaemic untreated control (UC) (\*  $P < 0.05$  and \*\*  $P < 0.01$  determined by t-tests;  $n = 5$ ). There were significant differences in MFI between fibroblasts in the presence of TLR inhibitors and corresponding fibroblasts lacking TLR inhibition (#  $P < 0.05$  and ##  $P < 0.01$  determined by t-tests;  $n = 5$ ). Columns and error bars indicate HDF MFI  $\pm$  the standard error of the mean (SEM) in all cases.

#### 6.4.4.2 TGFβ1 Protein Expression in HDFs

Hyperglycaemia reduced TGFβ1 expression in untreated fibroblasts compared to fibroblasts cultured at prediabetic (11mM) conditions (Figures 6.13i and 6.13ii). At prediabetic conditions, LPS increased TGFβ1 expression, which was reduced by TLR4 inhibition. TGFβ1 expression was slightly increased in MGN3-treated fibroblasts and then decreased following TLR inhibition. Under hyperglycaemia, MGN3/LPS treatments elevated TGFβ1 expression and reversed by TLR4 inhibition.

Hyperglycaemia significant inhibited ( $P<0.01$ ) effect on the mean fluorescence intensity (MFI) of TGFβ1 levels in untreated fibroblasts (Figure 6.13iii). At prediabetic conditions there was a significant increase ( $P=0.042$ ) in MFI in LPS treated fibroblasts compared to untreated fibroblasts. The addition of TLR4 inhibitor significantly decreased ( $P=0.022$ ) MFI in LPS treated fibroblasts. TLR2/4 inhibition resulted in significant ( $P<0.01$ ) decreases in MFI in MGN3 treated fibroblasts compared to MGN3 treated fibroblasts without TLRi. At 30mM glucose there significant ( $P<0.01$ ) increases in MFI in MGN3/LPS treated fibroblasts compared to the untreated fibroblasts. the addition of TLR2 inhibitor resulted in a significant ( $P<0.01$ ) decrease in MFI in untreated fibroblast. In MGN3/LPS treated fibroblasts there were significant ( $P<0.01$ ) decreases in MFI when TLR4 inhibitor was added. These results LPS influences TGFβ1 expression in fibroblast through TLR4 at pre-diabetic and hyperglycaemic conditions.

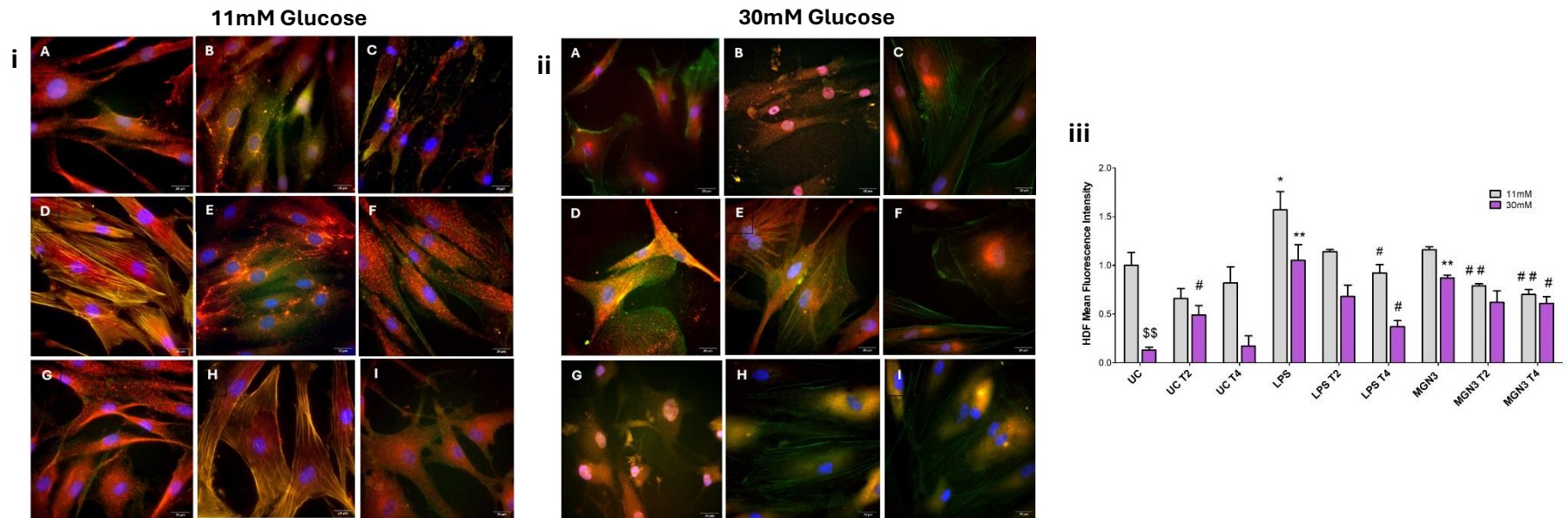


**Figure 6. 13: TGF $\beta$ 1 Expression in HDFs at Low and High Glucose.** The TGF $\beta$ 1 expression in HDFs cultured at Low (11mM) (i) and High (30mM) (ii) glucose was captured using thunder microscopy. MFI of TGF $\beta$ 1 expression (iii) was measured in fibroblasts following treatments (with LPS and MGN3) and TLR2 (T2) and TLR4 (T4) inhibition. The different cell components were identified using fluorescent stains; red indicated TGF $\beta$ 1 expression, green identified f-actin using phalloidin and blue represented the nucleus using DAPI. Fibroblasts received different treatments; Panel A = UC, panel B = UC + T2, panel C = UC + T4, panel D = LPS, panel E = LPS + T2, panel F = LPS + T4, panel G = MGN3, panel H = MGN3 + T2 and panel I = MGN3 + T4. Images were captured at 60x magnification. There was a significant decrease in MFI in untreated control (UC) fibroblasts cultured at 30mM compared to UC fibroblasts cultured at 11mM glucose (\$\$  $P < 0.01$  determined by t-tests;  $n = 5$ ). There were significant differences in MFI in LPS and MGN3 treated fibroblast when compared to the corresponding glycaemic untreated control (UC) (\*  $P < 0.05$  and \*\*  $P < 0.01$  determined by t-tests;  $n = 5$ ). There were significant differences in MFI between fibroblasts in the presence of TLR inhibitors and corresponding fibroblasts lacking TLR inhibition (#  $P < 0.05$  and ##  $P < 0.01$  determined by t-tests;  $n = 5$ ). Columns and error bars indicate HDF MFI  $\pm$  the standard error of the mean (SEM) in all cases.

## **6.4.5 Influence of MGN3-Induced M1 Macrophage-, Keratinocyte- and Fibroblast-Derived EGF and FGF2 Secretion on Fibroblast Proliferation**

### **6.4.5.1 Influence of MGN3-Induced EGF Secretion on Fibroblast Proliferation**

HDF proliferation was significantly reduced by supernatants from fibroblasts cultured at hyperglycaemic conditions compared to pre-diabetic conditions ( $P = 0.02$ ; 88.9% vs. 100%) (Figure 6.14A). EGF inhibition had no significant effect at 30mM (84.8%) but significantly reduced proliferation at 11mM ( $P < 0.05$ ), suggesting higher EGF presence at pre-diabetic conditions. TLR2/4 inhibition significantly reduced HDF proliferation at 11mM ( $P < 0.01$ ), with TLR4 inhibition also reducing proliferation at 30mM ( $P < 0.01$ ) compared to untreated fibroblasts without TLRi. Supernatants from MGN3/LPS-treated fibroblasts significantly decreased HDF proliferation at 11mM and increased it at 30mM ( $P < 0.05$ ) in comparison to treatments compared to the correspond untreated controls. EGF inhibition further reduced proliferation at 11mM ( $P < 0.01$ ), indicating EGF involvement at pre-diabetic conditions. TLR2/4 inhibition in LPS-treated fibroblasts at 11mM increased HDF proliferation, whereas TLR4 inhibition at 30mM decreased it ( $P < 0.05$ ) compared to corresponding LPS treated fibroblast without TLRi. In MGN3-treated fibroblasts, TLR2/4 inhibition at both glucose levels significantly reduced HDF proliferation ( $P < 0.05$ ) compared to corresponding MGN3 treated fibroblast without TLRi. These results suggest TLR2/4 mediate LPS responses at 11mM and MGN3 responses at both glucose levels, with inhibition producing effects opposite to untreated controls.

HDF proliferation was significantly reduced by supernatants from keratinocytes cultured at hyperglycaemic conditions compared to pre-diabetic conditions ( $P = 0.003$ ; 67.8% vs. 100%) (Figure 6.14B). EGF inhibition had no effect at 30mM but further reduced proliferation at 11mM ( $P < 0.01$ ; 70.1%), suggesting higher EGF levels in supernatants from keratinocytes cultured at pre-diabetic conditions. TLR2/4 inhibition significantly reduced HDF proliferation in response to supernatants from untreated keratinocytes at 11mM ( $P < 0.05$ ) but had no effect at 30mM compared to corresponding untreated keratinocytes without TLRi. Supernatants from MGN3/LPS-treated keratinocytes at 11mM reduced HDF proliferation ( $P < 0.05$ ), while those at 30mM had no effect compared to corresponding UC. EGF blockade

significantly decreased proliferation only with 11mM MGN3-treated supernatants ( $P = 0.005$ ), suggesting limited EGF involvement. TLR4 (not TLR2) inhibition further reduced proliferation with 11mM MGN3-treated supernatants; LPS effects were unaffected by TLR inhibition. Overall, MGN3/LPS-treated keratinocytes likely secrete factors that inhibit HDF proliferation, but EGF is unlikely to be a key mediator.

HDF proliferation was significantly reduced by supernatants from macrophages cultured at hyperglycaemic compared to pre-diabetic conditions ( $P = 0.038$ ; 83.7% vs. 100%) (Figure 6.14C). EGF inhibition had no significant effect, with similar proliferation levels observed (83.9% vs. 100%). These findings suggest high glucose impairs fibroblast proliferation, but macrophage-derived EGF is not the primary mediator. TLR2 inhibition significantly reduced fibroblast proliferation in response to supernatants from untreated macrophages at 11mM ( $P = 0.01$ ), but neither TLR2 nor TLR4 inhibition had effects at 30mM in comparison to untreated macrophages without TLRi. EGF inhibition significantly reduced proliferation at 11mM ( $P = 0.042$ ), indicating EGF's positive role at pre-diabetic conditions, but had no effect at 30mM. Interestingly, EGF inhibition increased proliferation in response to LPS-treated 11mM supernatants ( $P < 0.01$ ) but had no effect on MGN3/LPS-treated 30mM supernatants. MGN3-treated macrophage supernatants significantly reduced fibroblast proliferation ( $P < 0.05$ ), though MGN3/LPS-treated 30mM supernatants showed no significant effect. At 30mM, TLR2 inhibition significantly decreased proliferation in response to MGN3-treated supernatants ( $P = 0.007$ ) compared to MGN3 treated macrophages without TLRi, suggesting TLR2 involvement under hyperglycaemia.

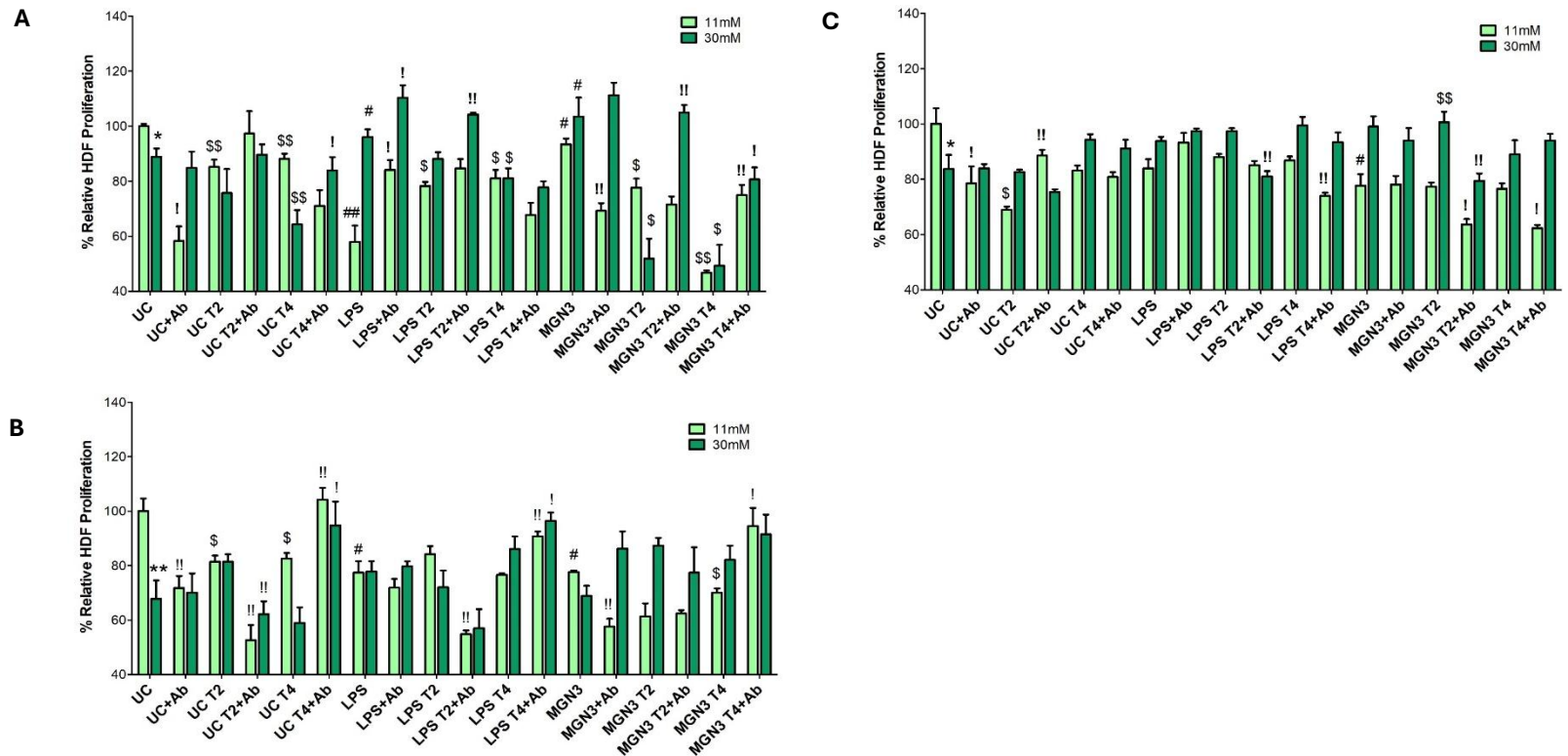


**Figure 6. 14: Influence of MGN3-Induced EGF Secretion on Fibroblast Proliferation.** The supernatants from fibroblasts, keratinocyte and macrophages cultured in low (11mM) or high (30mM) glucose was collected following treatment with/without LPS or MGN3, in the presence/absence of TLR2 (T2) or TLR4 (T4) inhibitors to evaluate fibroblast-derived (A), keratinocyte-derived (B) and macrophage-derived (C) EGF on fibroblast proliferation. Separate HDFs pre-incubated with/without EGF blocking antibody (Ab) were treated with the supernatants to determine the effect on HDF proliferation. There was a significant reduction in HDF proliferation following exposure to supernatant from the 30mM untreated control (UC) compared with the 11mM UC (\*  $P < 0.05$  and \*\*  $P < 0.01$  determined by t-tests;  $n = 4$ ). There were significant differences in HDF proliferation following exposure to MGN3/LPS-derived supernatant compared with the corresponding glycaemic UC (#  $P < 0.05$  and ##  $P < 0.01$  determined by t-test;  $n = 4$ ). There were also significant differences in HDF proliferation following exposure to supernatant derived from untreated/treated fibroblasts in the presence of TLR inhibition and supernatants from corresponding treatments lacking TLR inhibition (\$  $P < 0.05$  and \$\$  $P < 0.01$  determined by t-tests;  $n = 4$ ). There were differences in HDF proliferation following exposure to supernatants in the presence of blocking Ab and corresponding supernatants in the absence of Ab (!  $P < 0.05$  and !!  $P < 0.01$  determined by t-tests;  $n = 4$ ). Columns and error bars indicate % HDF Proliferation  $\pm$  the standard error of the mean (SEM) relative to levels observed in the 11mM UC.

#### 6.4.5.2 Influence of MGN3-Induced FGF2 Secretion on Fibroblast Proliferation

HDF proliferation was significantly reduced by supernatants from fibroblasts cultured at hyperglycaemic conditions compared to pre-diabetic conditions ( $P = 0.038$ ; 85.1% vs. 100%) (Figure 6.15A). FGF2 inhibition had no significant effect, though proliferation slightly increased at 30mM (93.7%). This suggests high glucose impairs proliferation, but fibroblast-derived FGF2 is not a key inhibitor. TLR2/4 inhibition had no effect at 11mM, but TLR4 inhibition significantly increased proliferation at 30mM ( $P < 0.01$ ) compared to untreated fibroblasts without TLRi. FGF2 inhibition significantly increased proliferation at 11mM ( $P = 0.001$ ) but had no effect at 30mM, indicating a role for FGF2 at pre-diabetic conditions but not hyperglycaemic conditions. FGF2 inhibition also increased proliferation with LPS-treated 11mM supernatants ( $P = 0.013$ ) but had no effect on MGN3/LPS-treated 30mM supernatants. MGN3/LPS-treated fibroblast supernatants at 11mM significantly reduced proliferation overall ( $P < 0.05$ ), though 30mM supernatants had no significant impact compared to the corresponding untreated fibroblasts. At 11mM, TLRi with LPS increased proliferation ( $P < 0.05$ ), while TLRi with MGN3 reduced it ( $P < 0.05$ ) in comparison to corresponding treatments without TLRi. No significant TLR effects were seen at 30mM. These results suggest LPS and MGN3 influence proliferation via TLR2/4 at 11mM.

HDF proliferation was reduced by supernatants from keratinocytes cultured at hyperglycaemic conditions but not significantly ( $P = 0.102$ ; 70.4% vs. 100% at 11mM) (Figure 6.15B). FGF2 inhibition had no significant effect ( $P > 0.05$ ), suggesting keratinocyte-derived FGF2 does not regulate fibroblast proliferation under either glucose condition. TLR inhibition also had no significant impact at 11mM or 30mM. Proliferation increased with MGN3-treated 30mM supernatants. At 11mM, TLR4 inhibition with LPS significantly reduced proliferation ( $P = 0.044$ ), while at 30mM, TLR2 inhibition plus FGF2 inhibition significantly increased it ( $P = 0.009$ ), though the mechanism is unclear. These results suggest LPS effects may be mediated by TLR4 at 11mM.

HDF proliferation slightly increased with supernatants from macrophages cultured at hyperglycaemic conditions but not significantly ( $P = 0.278$ ; 103.5% vs. 100% at 11mM) (Figure 6.15C). FGF2 inhibition at 30mM significantly enhanced proliferation ( $P = 0.025$ ;

164.4%), suggesting macrophage-derived FGF2 may limit proliferation under hyperglycaemia. No significant effects were seen with TLR inhibition at 11mM, but TLR2 inhibition at 30mM significantly increased proliferation ( $P < 0.01$ ) when comparison were made against the corresponding untreated macrophages. FGF2 inhibition had no effect at 11mM, indicating FGF2 is not involved at pre-diabetic conditions. MGN3-treated 11mM supernatants increased proliferation ( $P = 0.021$ ) in comparison to the UC, with further enhancement when combined with FGF2 inhibition ( $P = 0.01$ ). TLR inhibition had no effect on MGN3/LPS supernatants at 11mM, but TLR2 inhibition significantly reduced proliferation with MGN3-treated supernatants at 30mM ( $P = 0.001$ ) compared to corresponding treatments without TLRi, indicating TLR2 involvement under hyperglycaemia.

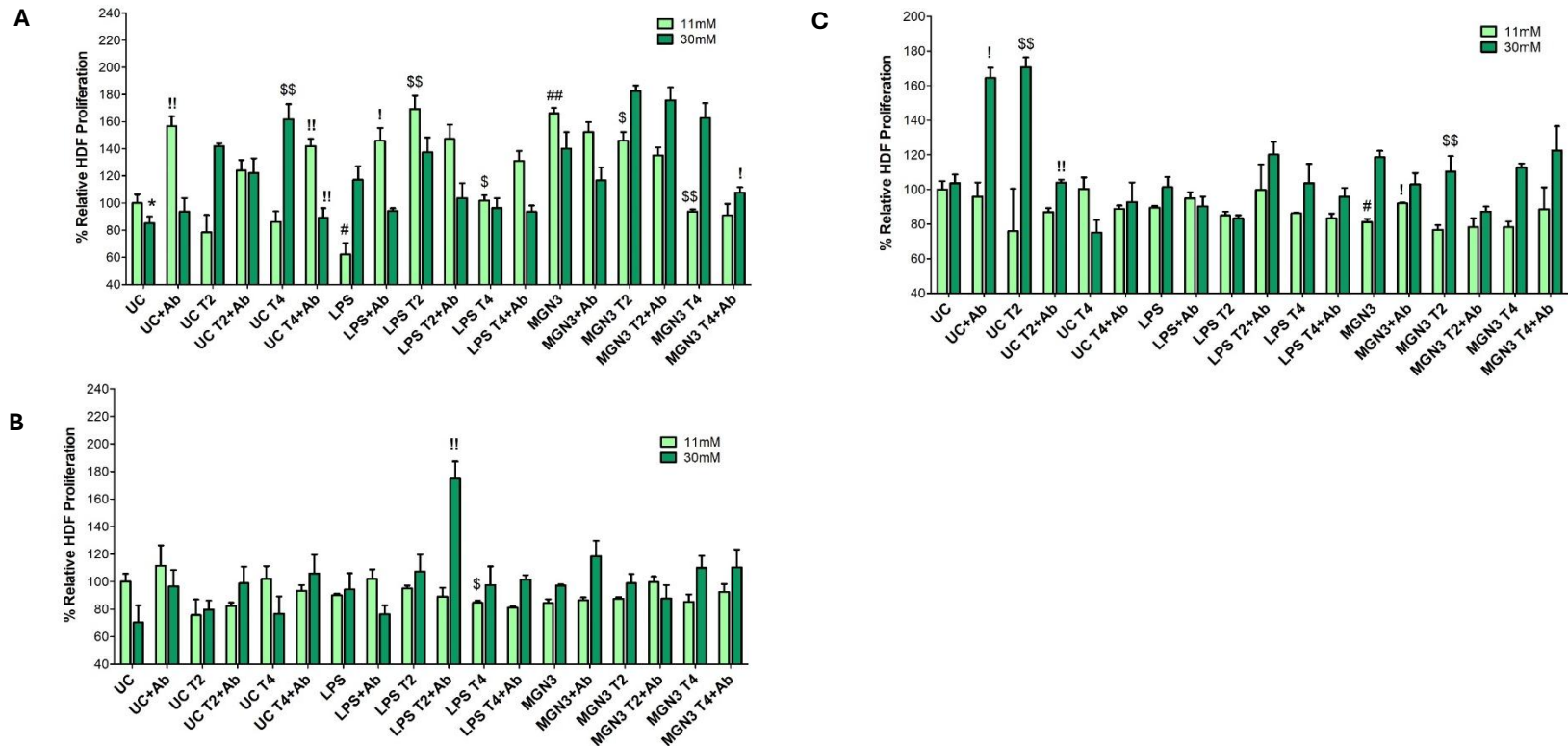
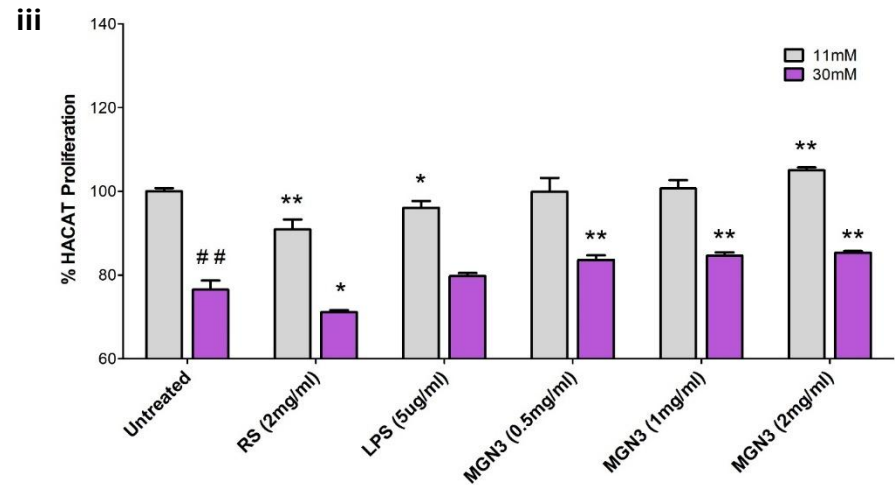
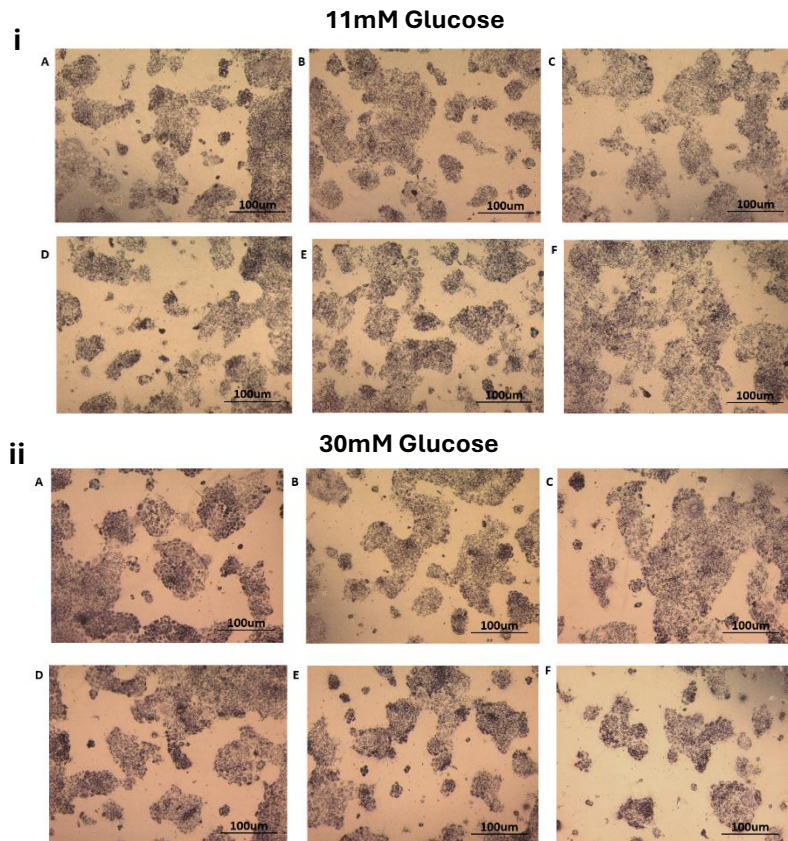


**Figure 6. 15: Influence of MGN3-Induced FGF2 Secretion on Fibroblast Proliferation.** The supernatants from fibroblasts, keratinocyte and macrophages cultured in low (11mM) or high (30mM) glucose was collected following treatment with/without LPS or MGN3, in the presence/absence of TLR2 (T2) or TLR4 (T4) inhibitors to evaluate fibroblast-derived (A), keratinocyte-derived (B) and macrophage-derived (C) FGF2 on fibroblast proliferation. Separate HDFs pre-incubated with/without FGF2 blocking antibody (Ab) were treated with the supernatants to determine the effect on HDF proliferation. There was a significant reduction in HDF proliferation following exposure to supernatant from the 30mM untreated control (UC) compared with the 11mM UC (\*  $P < 0.05$  determined by t-tests;  $n = 4$ ). There were significant differences in HDF proliferation following exposure to MGN3/LPS-derived supernatant compared with the corresponding glycaemic UC (#  $P < 0.05$  and ##  $P < 0.01$  determined by t-test;  $n = 4$ ). There were also significant differences in HDF proliferation following exposure to supernatant derived from untreated/treated fibroblasts in the presence of TLR inhibition and supernatants from corresponding treatments lacking TLR inhibition (§  $P < 0.05$  and §§  $P < 0.01$  determined by t-tests;  $n = 4$ ). There were differences in HDF proliferation following exposure to supernatants in the presence of blocking Ab and corresponding supernatants in the absence of Ab (!  $P < 0.05$  and !!  $P < 0.01$  determined by t-tests;  $n = 4$ ). Columns and error bars indicate % HDF Proliferation  $\pm$  the standard error of the mean (SEM) relative to levels observed in the 11mM UC.

#### 6.4.6 The Effect of MGN3 on HACAT Cell Viability and Proliferation

After MTT solution was added to keratinocytes cultured at 11 and 30mM and following treatments (RS, LPS or MGN3) there was an abundance of formazan crystal formation indicating a high viability of cells (Figure 6.16i and 6.16ii).

Hyperglycaemia significantly ( $P < 0.01$ ) decreased keratinocyte proliferation when compared to keratinocytes grown at pre-diabetic conditions (76.5% at 30mM vs 100.0% at 11mM) (Figure 6.16iii). Under 11mM glycaemic conditions, keratinocyte proliferation was significantly ( $P < 0.05$ ) inhibited following treatment with LPS/RS compared to the untreated control. However, there was a significant increase ( $P < 0.01$ ) in keratinocyte proliferation in MGN3-treated (2mg/ml) keratinocytes cultured at 11mM and MGN3-treated (0.5, 1.0 and 2.0mg/ml) keratinocytes cultured at 30mM compared to the glycaemic controls. At 30mM, keratinocyte proliferation was significantly inhibited ( $P = 0.024$ ) in RS-treated keratinocytes compared to untreated keratinocytes. LPS did not significantly influence ( $P > 0.05$ ) keratinocyte proliferation under hyperglycaemic conditions. These results indicate that hyperglycaemia restricts keratinocyte proliferation whereas MGN3 could reverse this detrimental effect to some extent. Also, MGN3 was not shown to have any cytotoxic effects on keratinocyte proliferation at pre-diabetic or hyperglycaemic conditions (Figure 6.16iv).



**iv**

**% HACAT Cytotoxicity**

	11mM	30mM
Untreated	0.000	0.000
RS	0.000	0.000
LPS	0.000	0.000
0.5mg MGN3	0.000	0.000
1mg MGN3	0.000	0.000
2mg MGN3	0.000	0.000

**Figure 6. 16: The Effect of MGN3 on HACAT Proliferation.** HACAT proliferation was measured in keratinocytes cultured in low (11mM) or high (30mM) glucose following treatment with RS (2mg/ml), LPS (5ug/ml) or MGN3 (0.5, 1 and 2mg/ml) for 24 hours. After treatment MTT solution was added and the cells (cultured at 11; i and 30mM glucose ; ii) were incubated for 3 hours to allow for crystal formation prior to image capture. Panel A is the untreated control (UC), B is RS, C is LPS, and panels D, E and F are MGN3 treatments at 0.5 1 and 2mg/ml respectively. All images were taken with a Zeiss microscope at 40x magnification. The cell proliferation significantly decreased (iii) in the 30mM untreated control (UC) compared to the 11mM UC (##  $P < 0.01$  determined by t-tests;  $n = 24$ ). There were also significant differences in keratinocyte proliferation when comparisons were made against the corresponding glycaemic (UC) control (\*  $P < 0.05$  and \*\*  $P < 0.01$  determined by t-tests;  $n = 24$ ). Columns and error bars indicate the % HACAT proliferation relative to the 11mM UC  $\pm$  the standard error of the mean (SEM) in all cases. The cytotoxicity of treatments including MGN3 was evaluated as part of the MTT analysis at pre-diabetic (11) and hyperglycaemic (30mM) conditions (iv). All cytotoxicity values were 0%, indicating all treatment including MGN3 had no appreciable cytotoxic effects on HACATs.

## 6.4.7 The Effect of MGN3 on Keratinocyte Cellular Metabolism

### 6.4.7.1 Keratinocyte Metabolism at Low Glucose Following TLR Inhibition

TLR2 inhibition significantly decreased ( $P < 0.01$ ) OCR levels (Figure 6.17A) in untreated keratinocytes at all timepoints and TLR4 inhibition also significantly decreased OCR levels in untreated keratinocytes in the P/A ( $P = 0.033$ ) period and post O ( $P < 0.001$ ) but then significantly ( $P < 0.01$ ) increased again post RA compared to untreated keratinocytes without TLR inhibition. TLR2 inhibition significantly ( $P < 0.05$ ) reduced OCR in LPS-treated keratinocytes at all timepoints and TLR4 significantly increased ( $P < 0.01$ ) compared to LPS treated keratinocytes without TLR inhibition. TLR2/4 inhibition significantly ( $P < 0.01$ ) reduced OCR in MGN3-treated keratinocytes during the P/A period and post O compared to MGN3 treated keratinocytes without TLR inhibition. TLR4 inhibition also significantly ( $P < 0.01$ ) increased OCR in MGN3-treated keratinocytes post RA compared to MGN3 treated keratinocytes without TLR inhibition. TLR inhibition significantly decreased ( $P < 0.01$ ) ECAR levels (Figure 6.17B) in untreated and LPS treated keratinocytes at all timepoints compared to untreated and LPS treated keratinocytes without TLR inhibition. TLR2 inhibition significantly ( $P < 0.01$ ) reduced ECAR in MGN3-treated keratinocytes post RA whereas TLR4 inhibition significantly ( $P < 0.01$ ) inhibited ECAR in MGN3-treated keratinocytes at all timepoints compared to MGN3 treated keratinocytes without TLR inhibition.

Total ATP production increased in LPS/MGN3-treated keratinocytes compared to untreated controls (UC) (Figure 6.17C). In UC and LPS-treated groups, 82% of ATP was glycolytic, while in MGN3-treated cells, glycolytic ATP dropped to 60%, with a significant rise in mitoATP ( $P = 0.003$ ). TLR2/4 inhibition reduced total ATP in all groups. In untreated keratinocytes, ATP levels fell to 607 and 636pmol (vs. UC: 837pmol), with glycolytic ATP increasing to 91% (TLR2) and 94% (TLR4). LPS-treated keratinocytes showed marked ATP reduction after TLR inhibition (369 and 119pmol vs. 1010pmol), and glycolytic ATP rose to 95% (T2) from 80%. MGN3-treated keratinocytes also showed reduced ATP with TLR2 (532pmol) and TLR4 (477pmol) inhibition (vs. 937pmol), with glycolytic ATP increasing to 85% and 94%, respectively (vs. 60%). TLR2/4 inhibition significantly decreased mitoATP in UC ( $P = 0.018$ ;  $P = 0.002$ ) and in MGN3-treated keratinocytes ( $P < 0.01$ ) compared to MGN3 treated

keratinocytes without TLR inhibition. Both TLR2/4 inhibition suppressed glycoATP and mitoATP in LPS-treated cells ( $P < 0.05$ ), and TLR4 inhibition significantly reduced glycoATP in MGN3-treated cells ( $P = 0.019$ ) compared to corresponding treatments without TLR inhibition.

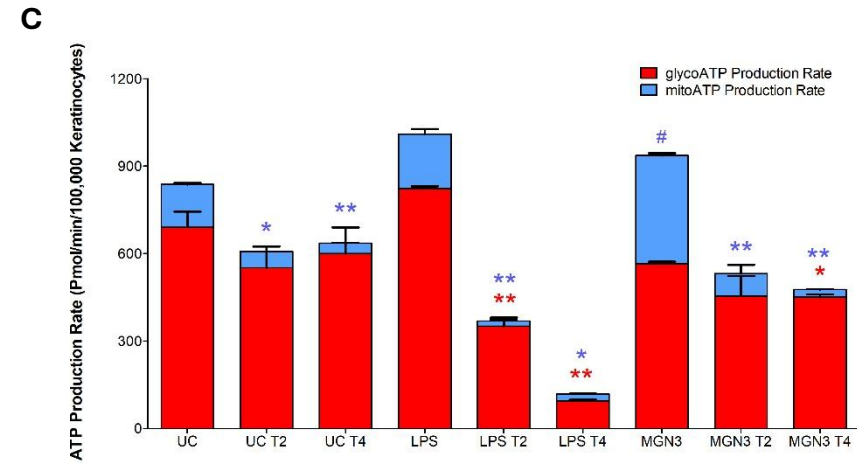
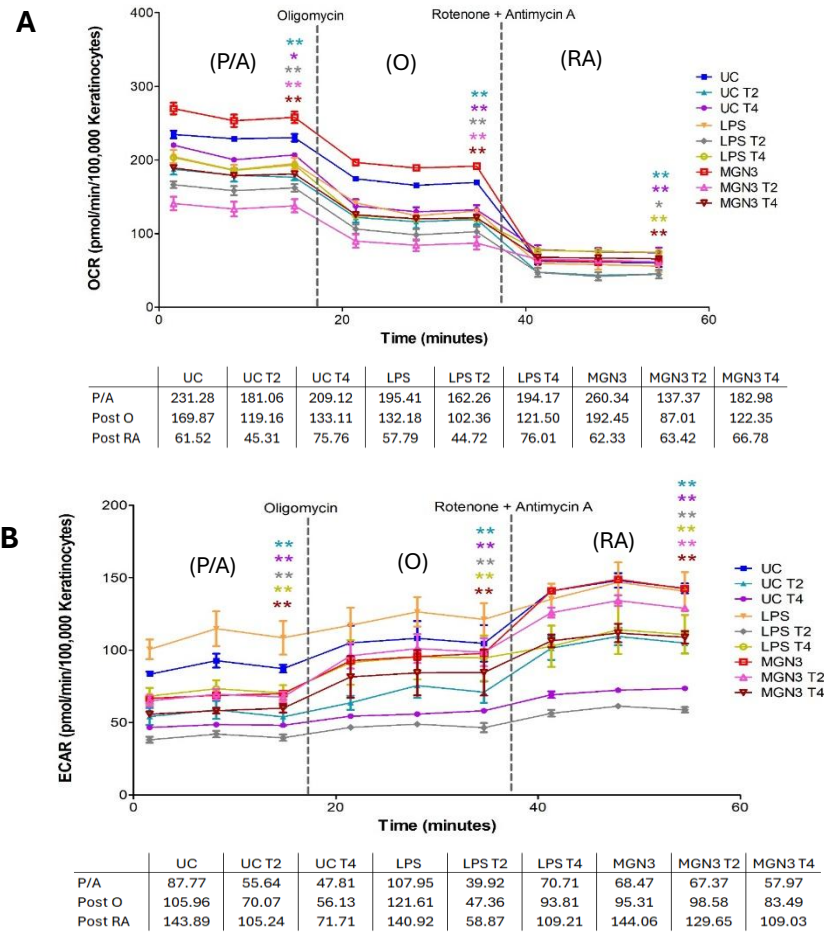


**Figure 6. 17: Keratinocyte Cellular Metabolism at Low Glucose Following TLR Inhibition.** The OCR, ECAR and Real time ATP production of HACATs was analysed via seahorse analysis. There were significant differences ( $*P < 0.05$  and  $**P < 0.01$  determined by t-tests;  $n = 3$ ) in OCR (A), ECAR (B) and in ATP production (C) were observed between treatments with TLR2 (T2) and TLR4 (T4) inhibition and corresponding treatments without TLR inhibition. There was a significant increase ( $\# P < 0.05$  determined by t-tests;  $n = 3$ ) in mitoATP production (C) in the MGN3 group compared to the UC group. Timepoints and error bars indicate the OCR and ECAR, columns and error bars indicate the ATP production rate (pmol/min/100,000 Keratinocytes)  $\pm$  the standard error of the mean (SEM) in all cases. The tables indicate the average OCR and ECAR values at pre-antibiotic (P/A), post Oligomycin (O) and post Rotenone+Antimycin A (RA) exposure.

#### 6.4.7.2 Keratinocyte Metabolism at High Glucose Following TLR Inhibition

TLR2/4 inhibition significantly increased ( $P < 0.05$ ) the OCR (Figure 6.18A) in untreated keratinocytes at all timepoints compared to untreated keratinocytes without TLR inhibition. TLR2/4 inhibition significantly ( $P < 0.01$ ) increased the OCR in LPS treated keratinocytes at post O and RA compared to LPS treated keratinocytes without TLR inhibition. TLR2 inhibition significantly increased ( $P < 0.01$ ) the OCR in MGN3 treated keratinocytes at all timepoints compared to MGN3 treated keratinocytes without TLR2 inhibition. TLR4 inhibition significantly increased ( $P < 0.01$ ) the OCR in MGN3 treated keratinocytes at P/A and post RA compared to MGN3 treated keratinocytes without TLR4 inhibition. TLR2/4 inhibition significantly ( $P < 0.05$ ) inhibited ECAR (Figure 6.18B) in untreated keratinocytes compared to untreated keratinocytes without TLR inhibition. TLR2 inhibition significantly ( $P = 0.022$ ) inhibited ECAR post O and TLR4 significantly ( $P < 0.01$ ) ECAR at all timepoints in LPS treated keratinocytes compared to LPS treated keratinocytes without TLR inhibition. TLR2 inhibition significantly ( $P = 0.018$ ) inhibited ECAR post O and TLR4 significantly ( $P < 0.05$ ) ECAR at all timepoints in MGN3 treated keratinocytes compared to MGN3 treated keratinocytes without TLR inhibition.

Total ATP decreased in LPS-treated keratinocytes and slightly increased in MGN3-treated cells compared to untreated controls (UC). Glycolytic ATP was 82% in UC, 63% in LPS-treated, and 74% in MGN3-treated cells. Both LPS and MGN3 treatments significantly increased mitoATP ( $P = 0.003$  and  $P = 0.031$ ), while glycoATP significantly decreased in LPS-treated cells compared to untreated keratinocytes. TLR inhibition reduced total ATP in all groups. In UC, TLR4 inhibition lowered ATP to 658pmol (vs. 793pmol), while increasing glycoATP to 96–99% (vs. 82%). In LPS-treated cells, TLR2 inhibition decreased ATP (489pmol) and raised glycolytic ATP to 98%; TLR4 inhibition increased ATP (729pmol) and glycolytic ATP to 68% (vs. 63%). In MGN3-treated cells, ATP increased with TLR2 inhibition (887pmol) and decreased with TLR4 inhibition (641pmol) vs. untreated MGN3 (819pmol). TLR2/4 inhibition significantly reduced mitoATP in UC ( $P < 0.01$ ) and in LPS-treated cells ( $P < 0.05$ ), with TLR4 inhibition also significantly increasing glycoATP ( $P = 0.007$ ) compared to corresponding treatments without TLR inhibition. In MGN3-treated cells, TLR2 inhibition significantly

increased mitoATP ( $P = 0.014$ ), while TLR4 inhibition significantly decreased it ( $P = 0.002$ ) compared to MGN3 treated keratinocytes without TLR inhibition.

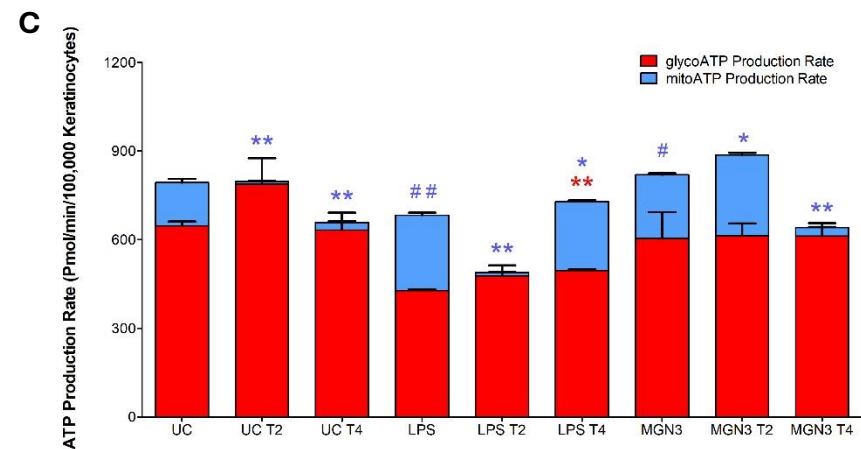
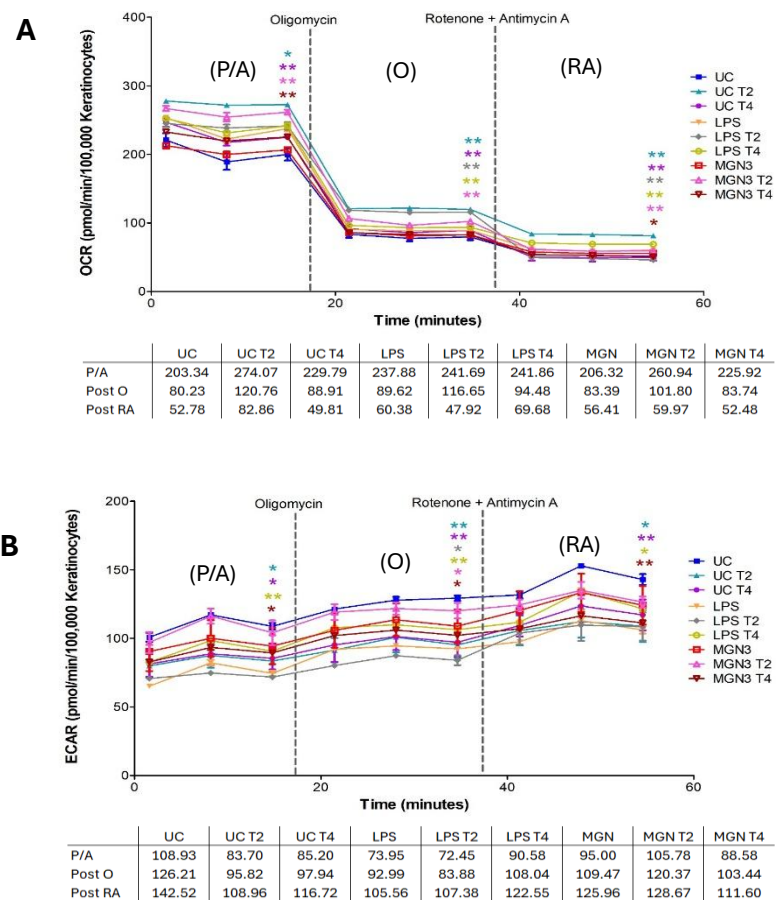


**Figure 6. 18: Keratinocyte Cellular Metabolism at High Glucose Following TLR Inhibition.** The OCR, ECAR and Real time ATP production of HACATs was analysed via seahorse analysis. There were significant differences ( $*P < 0.05$  and  $**P < 0.01$  determined by t-tests;  $n = 3$ ) in OCR (A), ECAR (B) and in ATP production (C) were observed between treatments with TLR2 (T2) and TLR4 (T4) inhibition and corresponding treatments without TLR inhibition. There were also significant increases ( $\# P < 0.05$  and  $\#\# P < 0.01$  determined by t-tests;  $n = 3$ ) in mitoATP production (C) in the LPS and MGN3 groups compared to the UC group. Timepoints and error bars indicate the OCR and ECAR, columns and error bars indicate the ATP production rate (pmol/min/100,000 Keratinocytes)  $\pm$  the standard error of the mean (SEM) in all cases. The tables indicate the average OCR and ECAR values at pre-antibiotic (P/A), post Oligomycin (O) and post Rotenone+Antimycin A (RA) exposure.

## 6.4.8 Effect of MGN3 on Growth Factor, Transcription Factor and Antimicrobial Peptide Production by HACAT Cells

### 6.4.8.1 Secretion of Epidermal Growth Factor from HACATs

Hyperglycaemia significantly increased EGF production in untreated keratinocytes compared to pre-diabetic conditions (Figure 6.19). LPS significantly elevated EGF at 11mM glucose ( $P = 0.000$ ) compared to the UC. TLR2 inhibition significantly increased EGF in untreated ( $P = 0.000$ ) and MGN3-treated ( $P = 0.007$ ) keratinocytes at 11mM compared to corresponding treatments without TLR inhibition. At 30mM glucose, TLR2 inhibition reduced EGF in LPS-treated cells ( $P = 0.018$ ), while both TLR2 and TLR4 inhibition significantly decreased EGF in MGN3-treated keratinocytes ( $P < 0.05$ ) compared to corresponding treatments without TLR inhibition. These findings suggest LPS-driven EGF secretion is TLR2-dependent, and MGN3-mediated EGF production involves both TLR2 and TLR4 under hyperglycaemic conditions.

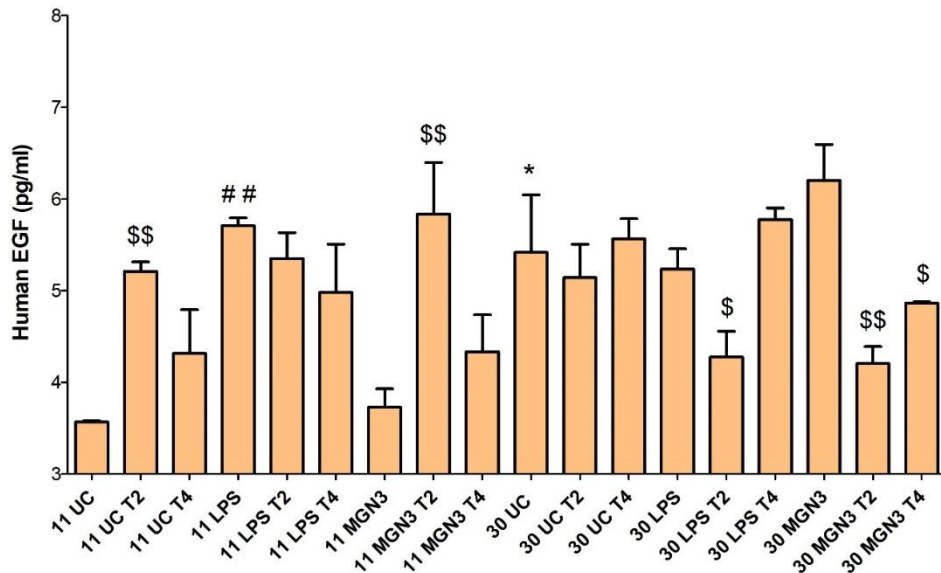


**Figure 6. 19: Secretion of Epidermal Growth Factor (EGF) by Keratinocytes.** EGF levels were measured in the supernatant keratinocytes cultured in low (11mM) or high (30mM) glucose and treated with LPS or MGN3 in the presence/absence of TLR2 (T2) or TLR4 (T4) inhibition. There was a significant decrease in EGF in untreated control (UC) keratinocytes cultured at 30mM compared to UC keratinocytes cultured at 11mM glucose (\*  $P < 0.05$  determined by t-tests;  $n = 8$ ). There was a significant increase in EGF between keratinocytes treated with LPS at 11mM the corresponding UC keratinocytes (##  $P < 0.01$  determined by t-tests;  $n = 8$ ). There were significant differences in EGF between keratinocytes in the presence of TLR inhibitors and corresponding keratinocytes lacking TLR inhibition (\$  $P < 0.05$  and \$\$  $P < 0.01$  determined by t-tests;  $n = 8$ ). Columns and error bars indicate human EGF levels (pg/ml)  $\pm$  the standard error of the mean (SEM) in all cases.

#### 6.4.8.2 Secretion of Fibroblast Growth Factor 2 by HACATs

Hyperglycaemia significantly ( $P < 0.001$ ) decreased FGF2 production in untreated keratinocytes compared to pre-diabetic conditions (Figure 6.20). MGN3/LPS-treated keratinocytes secreted significantly ( $P < 0.05$ ) increased FGF2 at both pre-diabetic and hyperglycaemic conditions compared to the corresponding untreated keratinocytes. TLR2/4 inhibition significantly ( $P < 0.01$ ) inhibited FGF2 production in untreated and LPS/MGN3-treated keratinocytes at both pre-diabetic and hyperglycaemic conditions compared to corresponding treatments without TLR inhibition, with no distinct differences noted between untreated and MGN3/LPS-treated keratinocytes.

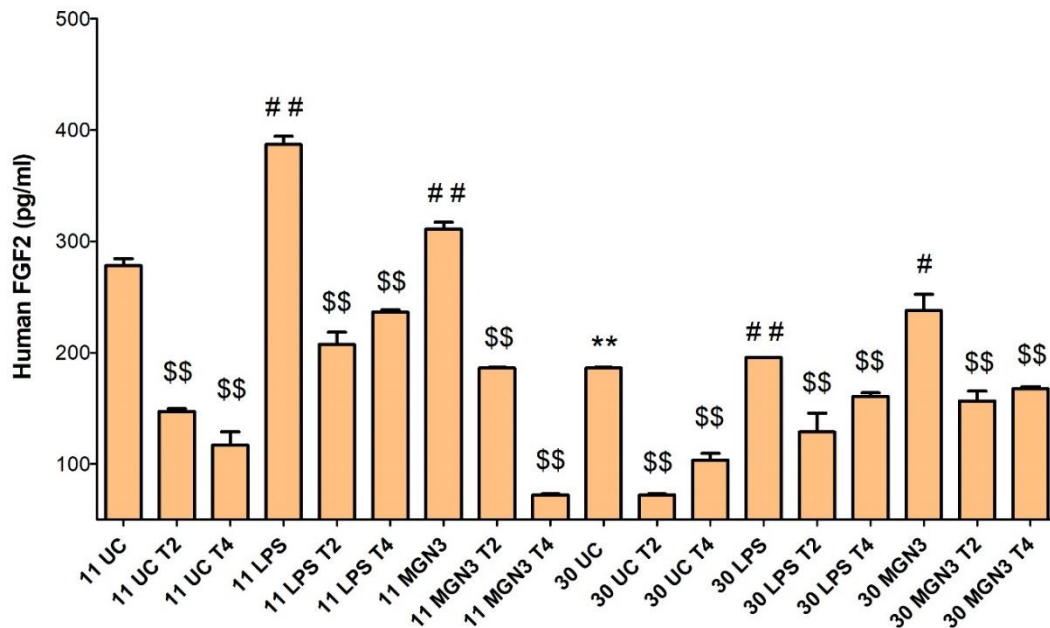


**Figure 6. 20: Secretion of Fibroblast Growth Factor 2 (FGF2) by Keratinocytes.** FGF2 levels were measured in the supernatant keratinocytes cultured in low (11mM) or high (30mM) glucose and treated with LPS or MGN3 in the presence/absence of TLR2 (T2) or TLR4 (T4) inhibition. There was a significant decrease in FGF2 in untreated control (UC) keratinocytes cultured at 30mM compared to UC keratinocytes cultured at 11mM glucose (\*\*  $P < 0.01$  determined by t-tests;  $n = 8$ ). There were significant increases in FGF2 between keratinocytes treated with LPS or MGN3 at 11mM the corresponding UC keratinocytes (#  $P < 0.05$  and ##  $P < 0.01$  determined by t-tests;  $n = 8$ ). There were significant differences in FGF2 between keratinocytes in the presence of TLR inhibitors and corresponding keratinocytes lacking TLR inhibition (\$  $P < 0.05$  and \$\$  $P < 0.01$  determined by t-tests;  $n = 8$ ). Columns and error bars indicate human FGF2 levels (pg/ml)  $\pm$  the standard error of the mean (SEM) in all cases.

### 6.4.8.3 Secretion of Transforming Growth Factor Beta 1 by HACATs

Hyperglycaemia did not significantly ( $P < 0.05$ ) effect TGF $\beta$ 1 secretion from untreated keratinocytes compared to pre-diabetic conditions (Figure 6.21). TLR2/4 inhibition significantly decreased ( $P < 0.001$ ) TGF $\beta$ 1 secretion from untreated keratinocytes cultured under 11mM glucose conditions, and TLR2 inhibition again significantly ( $P < 0.001$ ) decreased TGF $\beta$ 1 levels under 30mM glucose conditions compared to untreated keratinocytes without TLR inhibition. Although MGN3 (but not LPS) significantly reduced TGF $\beta$ 1 secretion at 11mM conditions, neither LPS nor MGN3 influenced TGF $\beta$ 1 secretion under 30mM conditions compared to corresponding UC. TLR inhibition did not significantly ( $P > 0.05$ ) effect TGF $\beta$ 1 secretion from MGN3/LPS-treated keratinocytes under 11mM conditions. In contrast, TLR inhibition significantly ( $P < 0.05$ ) inhibited TGF $\beta$ 1 secretion from MGN3/LPS-treated keratinocytes at 30mM conditions compared to corresponding treatments without TLR inhibition. These results suggested MGN3/LPS-mediated TGF $\beta$ 1 secretion from keratinocytes is influenced by TLR4 at hyperglycaemic conditions but not at pre-diabetic conditions.

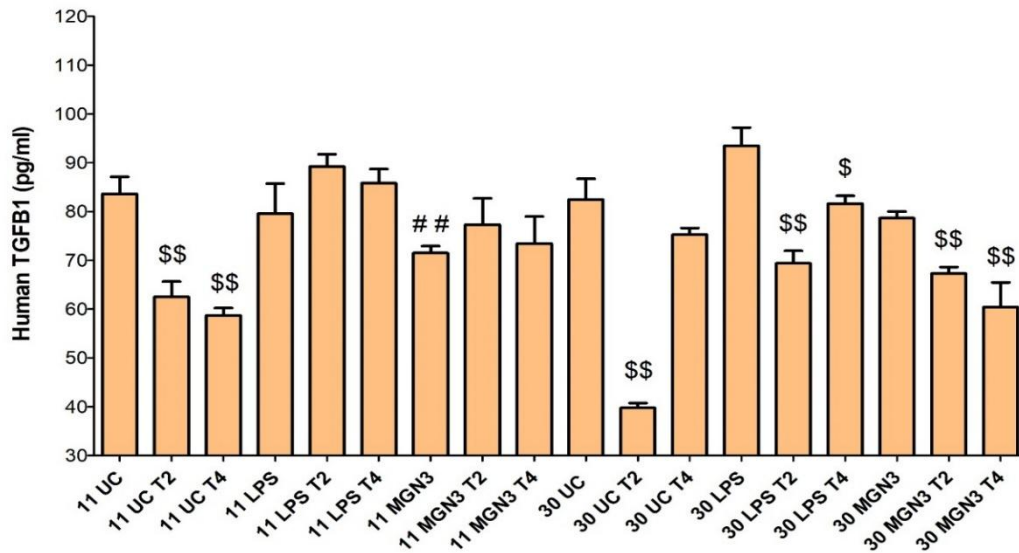


**Figure 6. 21: Secretion of Transforming Growth Factor beta 1 (TGF $\beta$ 1) by Keratinocytes.** TGF $\beta$ 1 levels were measured in the supernatant keratinocytes cultured in low (11mM) or high (30mM) glucose and treated with LPS or MGN3 in the presence/absence of TLR2 (T2) or TLR4 (T4) inhibition. There were significant decreases in TGF $\beta$ 1 between keratinocytes treated with MGN3 at 11mM the corresponding UC keratinocytes (# $P < 0.05$  determined by t-tests;  $n = 15$ ). There were significant differences in TGF $\beta$ 1 between keratinocytes in the presence of TLR inhibitors and corresponding keratinocytes lacking TLR inhibition (\$ $P < 0.05$  and \$\$ $P < 0.01$  determined by t-tests;  $n = 15$ ). Columns and error bars indicate human TGF $\beta$ 1 levels (pg/ml)  $\pm$  the standard error of the mean (SEM) in all cases.

#### 6.4.8.4 Secretion of Nuclear Factor Erythroid 2–related Factor 2 by HACATs

Hyperglycaemia significantly ( $P = 0.035$ ) increased NRF2 secretion from untreated keratinocytes compare to pre-diabetic conditions (Figure 6.22). MGN3-treated keratinocytes secreted significantly ( $P = 0.005$ ) higher levels of NRF2 compared to untreated keratinocytes when cultured at 11mM. In contrast, MGN3-treated (but not LPS-treated) keratinocytes secreted substantially ( $P = 0.001$ ) lower levels of NRF2 than untreated keratinocytes at 30mM conditions. TLR2 inhibition significantly ( $P = 0.012$ ) decreased NRF2 secretion from untreated keratinocytes at 11mM conditions whereas at 30mM conditions both TLR2 and TLR4 significantly ( $P < 0.05$ ) inhibited NRF2 secretion compared to untreated keratinocytes without TLR inhibition. At 11mM conditions, TLR4 (but not TLR2) inhibition significantly ( $P = 0.002$ ) decreased NRF2 in LPS-treated keratinocytes whereas TLR inhibition had no significant influence on NRF2 secretion from MGN3-treated keratinocytes compared to corresponding treatments without TLR inhibition. Both TLR2 and TLR4 significantly ( $P < 0.05$ ) inhibited NRF2 in MGN3/LPS-treated keratinocytes at 30mM conditions compared to corresponding treatments without TLR inhibition.

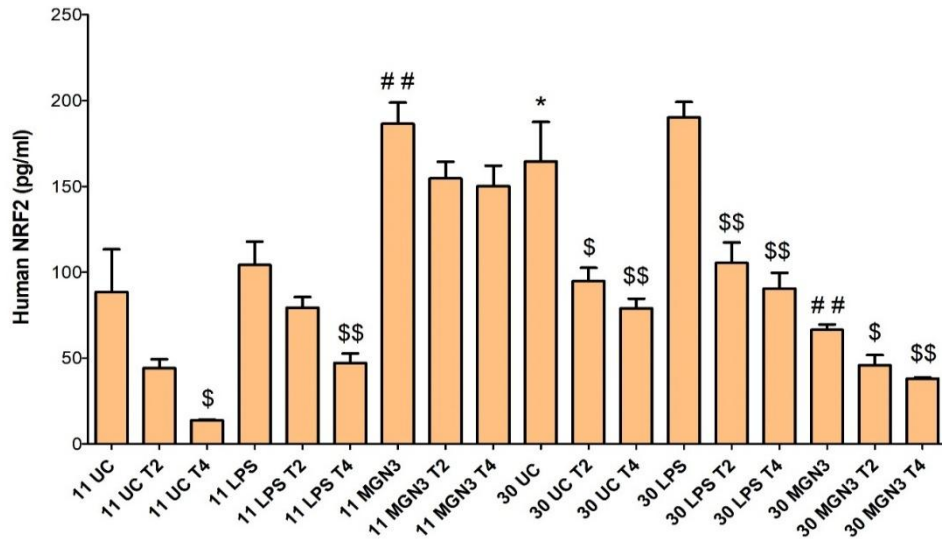


**Figure 6. 22: Secretion of Nuclear factor erythroid 2-related factor 2 (NRF2) by Keratinocytes.** NRF2 levels were measured in the supernatant keratinocytes cultured in low (11mM) or high (30mM) glucose and treated with LPS or MGN3 in the presence/absence of TLR2 (T2) or TLR4 (T4) inhibition. There was a significant increase in NRF2 in untreated control (UC) keratinocytes cultured at 30mM compared to UC keratinocytes cultured at 11mM glucose (\*  $P < 0.05$  determined by t-tests;  $n = 12$ ). There were significant differences in NRF2 between keratinocytes treated with MGN3 and the corresponding UC keratinocytes (##  $P < 0.01$  determined by t-tests;  $n = 12$ ). There were significant differences in NRF2 between keratinocytes in the presence of TLR inhibitors and corresponding keratinocytes lacking TLR inhibition (\$  $P < 0.05$  and \$\$  $P < 0.01$  determined by t-tests;  $n = 12$ ). Columns and error bars indicate human NRF2 levels (pg/ml)  $\pm$  the standard error of the mean (SEM) in all cases.

#### 6.4.8.5 Intracellular Nuclear Factor Erythroid 2–related Factor 2 Protein Expression in HACATs

Hyperglycaemia significantly ( $P = 0.004$ ) increased intracellular NRF2 expression compared to untreated keratinocytes at pre-diabetic conditions (Figure 6.23). At 11mM and 30mM conditions MGN3/LPS-treated keratinocytes expressed significantly ( $P < 0.01$ ) higher levels of NRF2 protein compared to corresponding glycaemic untreated keratinocytes. TLR2/4 inhibition significantly decreased NRF2 expression in untreated and MGN3/LPS-treated keratinocytes cultured at 11mM ( $P < 0.05$ ) and 30mM conditions ( $P < 0.01$ ) compared to corresponding treatments without TLR inhibition. These results suggest MGN3/LPS-mediated intracellular NRF2 production was not appreciably influenced by TLR2/4 above that observed in untreated keratinocytes at either pre-diabetic or hyperglycaemic conditions.

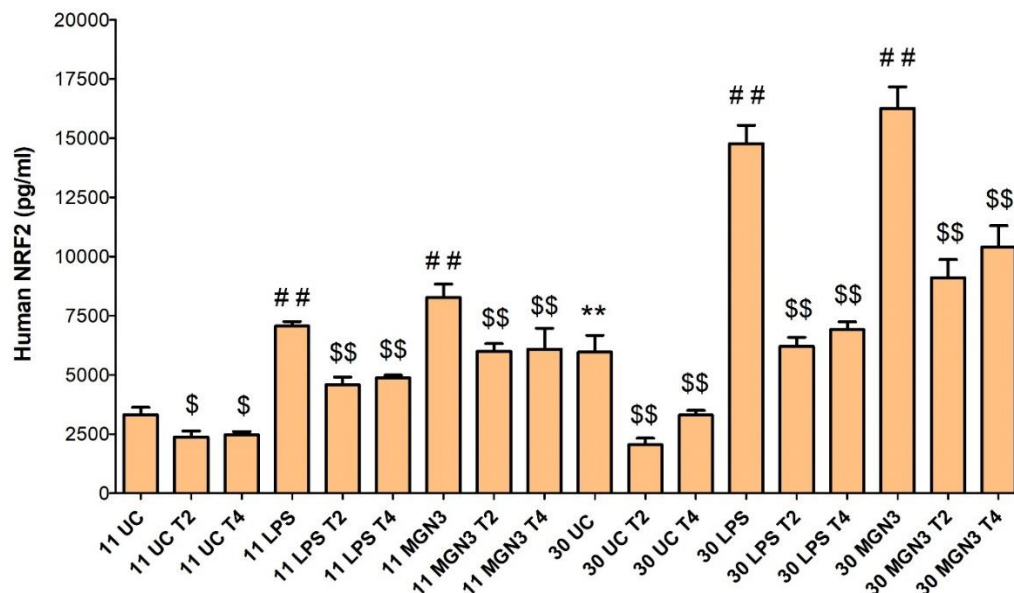


**Figure 6. 23: Intracellular Nuclear Factor Erythroid 2–related Factor 2 Protein Expression in HACATs.** NRF2 levels were measured in keratinocytes lysates which had been cultured in low (11mM) or high (30mM) glucose and treated with LPS or MGN3 in the presence/absence of TLR2 (T2) or TLR4 (T4) inhibition. There was a significant increase in NRF2 in untreated control (UC) keratinocytes cultured at 30mM compared to UC keratinocytes cultured at 11mM glucose (\*\*  $P < 0.01$  determined by t-tests;  $n = 12$ ). There were significant increases in NRF2 between keratinocytes treated with LPS or MGN3 and the corresponding UC keratinocytes (##  $P < 0.01$  determined by t-tests;  $n = 12$ ). There were significant differences in NRF2 between keratinocytes in the presence of TLR inhibitors and corresponding keratinocytes lacking TLR inhibition (\$  $P < 0.05$  and \$ \$  $P < 0.01$  determined by t-tests;  $n = 12$ ). Columns and error bars indicate human NRF2 levels (pg/ml)  $\pm$  the standard error of the mean (SEM) in all cases.

#### 6.4.8.6 Intracellular Cathelicidin Peptide Expression in HACATs

Hyperglycaemia significantly reduced LL37 production ( $P < 0.001$ ) in untreated keratinocytes compared to pre-diabetic conditions (Figure 6.24). MGN3 and LPS significantly increased LL37 at 11mM glucose ( $P < 0.01$ ) but had no effect at 30mM glucose compared to corresponding untreated keratinocytes. TLR4 inhibition (not TLR2) significantly decreased LL37 in untreated cells at 11mM ( $P = 0.002$ ), while neither had an effect at 30mM ( $P > 0.05$ ) compared to untreated keratinocytes without TLR inhibition. TLR2/4 inhibition significantly reduced LL37 in LPS-treated keratinocytes at both glucose levels ( $P < 0.01$ ) compared to LPS treated keratinocytes without TLR inhibition. In MGN3-treated cells, both inhibitors reduced LL37 at 11 mM ( $P < 0.01$ ), but only TLR4 inhibition had an effect at 30 mM ( $P = 0.011$ ) compared to MGN3 treated keratinocytes without TLR inhibition. These results indicate that LL37 induction by LPS and MGN3 is TLR2-dependent at 11 mM, while under hyperglycaemia, TLR4 plays a more dominant role in modulating LL37 expression.

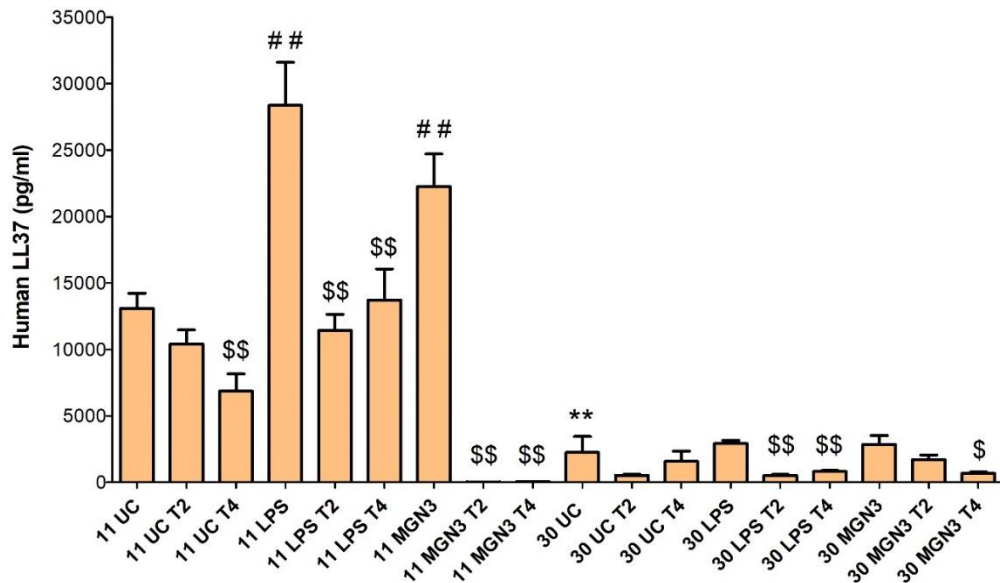


**Figure 6. 24: Intracellular Cathelicidin Peptide Expression in HACATs.** Cathelicidin (LL37) peptide levels were measured in keratinocytes lysates which had been cultured in low (11mM) or high (30mM) glucose and treated with LPS or MGN3 in the presence/absence of TLR2 (T2) or TLR4 (T4) inhibition. There was a significant decrease in LL37 in untreated control (UC) keratinocytes cultured at 30mM compared to UC keratinocytes cultured at 11mM glucose (\*\* $P < 0.01$  determined by t-tests;  $n = 10$ ). There were significant increases in NRF2 between keratinocytes treated with LPS or MGN3 at 11mM and the corresponding UC keratinocytes (## $P < 0.01$  determined by t-tests;  $n = 10$ ). There were significant differences in NRF2 between keratinocytes in the presence of TLR inhibitors and corresponding keratinocytes lacking TLR inhibition (\$  $P < 0.05$  and \$\$  $P < 0.01$  determined by t-tests;  $n = 10$ ). Columns and error bars indicate human LL37 levels (pg/ml)  $\pm$  the standard error of the mean (SEM) in all cases.

#### 6.4.8.7 Intracellular Beta Defensin 2 Peptide Expression in HACATs

Hyperglycaemia substantially ( $P = 0.022$ ) decreased BD2 production in untreated keratinocytes compared to those cultured at pre-diabetic conditions (Figure 6.25). LPS-treated keratinocytes significantly increased the expression of BD2 peptide ( $P < 0.001$ ) at 11mM conditions compared to corresponding untreated keratinocytes. LPS/MGN3-treated keratinocytes cultured at 30mM glucose expressed significantly ( $P < 0.01$ ) higher BD2 peptide levels than corresponding untreated keratinocytes. TLR2/4 inhibition significantly ( $P < 0.01$ ) decreased BD2 in untreated keratinocytes at 11mM and 30mM conditions compared to corresponding untreated keratinocytes without TLR inhibition. TLR2/4 inhibition also significantly ( $P < 0.01$ ) decreased BD2 in MGN3/LPS-treated keratinocytes cultured at 11 and 30mM conditions compared to corresponding treatments without TLR inhibition. These results indicate BD2 production is influenced by TLR2/4 at pre-diabetic and hyperglycaemic conditions in both untreated and MGN3/LPS-treated keratinocytes.

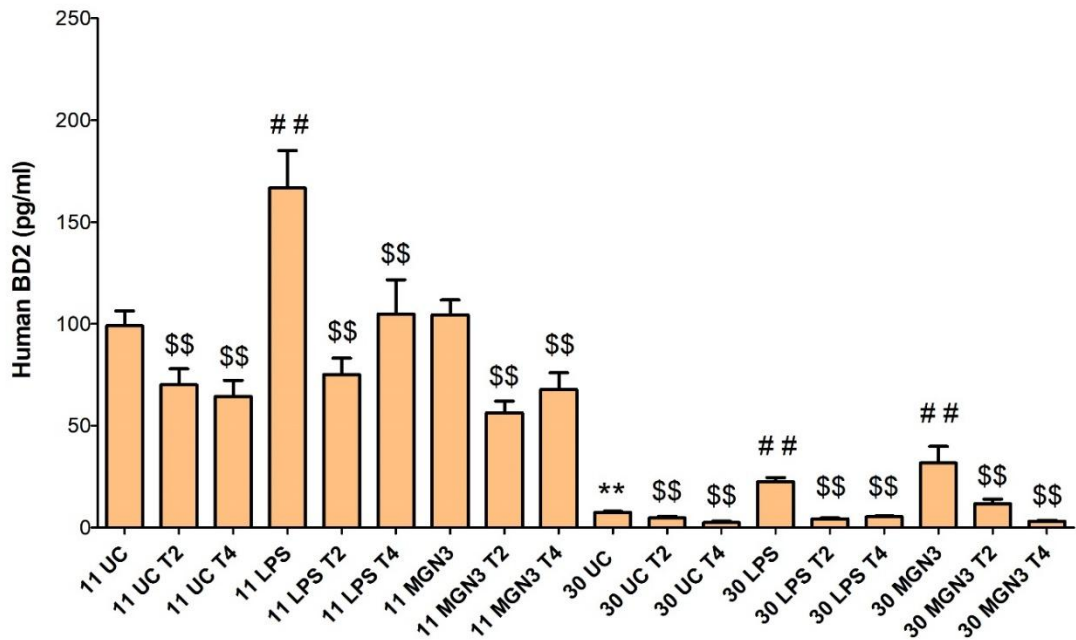


**Figure 6. 25: Intracellular Beta Defensin 2 Peptide Expression in HACATs.** BD2 peptide levels were measured in keratinocyte lysates cultured in low (11mM) or high (30mM) glucose and treated with LPS or MGN3 in the presence/absence of TLR2 (T2) or TLR4 (T4) inhibition. There was a significant decrease in BD2 in untreated control (UC) keratinocytes cultured at 30mM compared to UC keratinocytes cultured at 11mM glucose (\*\*  $P < 0.01$  determined by t-tests;  $n = 15$ ). There were significant increases in BD2 between keratinocytes treated with LPS or MGN3 and the corresponding UC keratinocytes (##  $P < 0.01$  determined by t-tests;  $n = 15$ ). There were significant differences in NRF2 between keratinocytes in the presence of TLR inhibitors and corresponding keratinocytes lacking TLR inhibition (\$\$  $P < 0.01$  determined by t-tests;  $n = 15$ ). Columns and error bars indicate human BD2 levels (pg/ml)  $\pm$  the standard error of the mean (SEM) in all cases.

## **6.4.9 Effect of MGN3 on Intracellular TGFβ1 Protein and Cathelicidin Peptide Expression in HACAT Cells**

### **6.4.9.1 Intracellular TGFβ1 Expression in HACATs**

TGFβ1 MFI was not affected by hyperglycaemia in untreated keratinocytes compared to pre-diabetic conditions (Figure 6.36i and 6.26ii). MGN3 reduced MFI at 11mM, while LPS increased it at 30mM compared to corresponding untreated keratinocytes. TLR2 inhibition reduced MFI in untreated cells at both glucose levels and in LPS-treated cells at 11mM compared to corresponding treatments without TLR inhibition. No changes were seen with MGN3 at 11mM or with MGN3/LPS at 30mM.

Hyperglycaemia did not significantly ( $P>0.05$ ) influence the MFI of TGFβ1 in untreated keratinocytes compared to pre-diabetic conditions (Figure 6.26iii). At 11mM conditions MFI was significantly ( $P<0.01$ ) reduced in MGN3 treated keratinocytes compared to untreated keratinocytes at 11mM. At 30mM conditions MFI was significantly ( $P<0.01$ ) increased in LPS treated keratinocytes compared to untreated keratinocytes at 30mM. The addition of TLR2 inhibitor to untreated keratinocytes significantly ( $P<0.01$ ) inhibited MFI at 11mM and 30mM conditions compared to corresponding untreated keratinocytes without TLR inhibition. At 11mM there was also a significant ( $P=0.043$ ) decrease in MFI in LPS treated keratinocytes following TLR2 inhibition compared to LPS treated keratinocytes at 11mM. There were no significant differences ( $P>0.05$ ) seen in MGN3 treated keratinocytes at 11mM conditions or MGN3/LPS treated keratinocytes at 30mM conditions compared to corresponding untreated keratinocytes. These results suggest LPS influences TGFβ1 expression in keratinocytes at pre-diabetic conditions but not hyperglycaemic conditions and MGN3 does not seem to influence TGFβ1 expression at both glucose conditions.

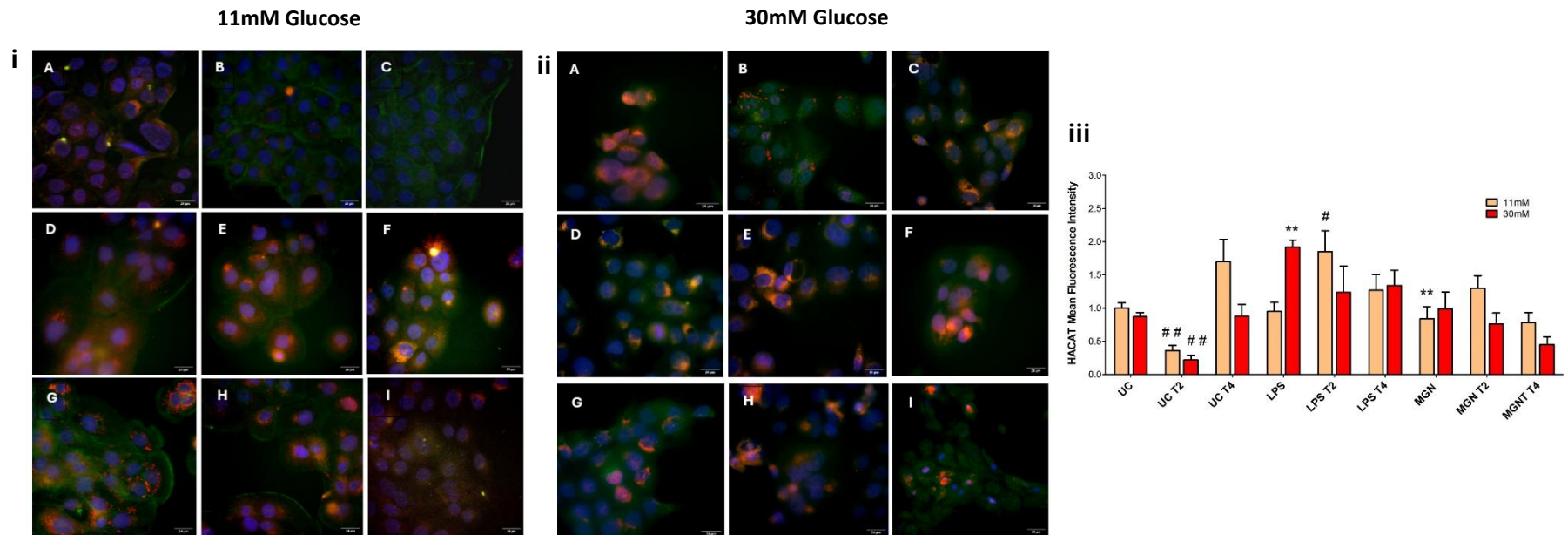


**Figure 6. 26 TGFβ1 Expression in HACATs at Low and High Glucose.** The TGFβ1 expression in HACATs cultured at Low (11mM) (i) and High (30mM) (ii) glucose was captured using thunder microscopy. MFI of TGFβ1 expression (iii) was measured in keratinocytes following treatments (with LPS and MGN3) and TLR2 (T2) and TLR4 (T4) inhibition. The different cell components were identified using fluorescent stains; red indicated TGFβ1 expression, green identified f-actin using phalloidin and blue represented the nucleus using DAPI. Fibroblasts received different treatments; Panel A = UC, panel B = UC + T2, panel C = UC + T4, panel D = LPS, panel E = LPS + T2, panel F = LPS + T4, panel G = MGN3, panel H = MGN3 + T2 and panel I = MGN3 + T4. Images were captured at 60x magnification. There were significant differences in MGN3/LPS treated keratinocytes when compared to the corresponding glycaemic untreated control (UC) (\*\* P < 0.01 determined by t-tests; n = 5). There were significant differences in MFI between keratinocytes in the presence of TLR inhibitors and corresponding keratinocytes lacking TLR inhibition (# P < 0.05 and ## P < 0.01 determined by t-tests; n = 5). Columns and error bars indicate HACAT MFI ± the standard error of the mean (SEM) in all cases.

#### 6.4.9.2 Cathelicidin (LL37) Expression in HACATs

LL37 expression was unaffected by hyperglycaemia compared to pre-diabetic conditions (Figures 6.27i and 6.27ii). LL37 expression increased following MGN3/LPS treatment at 11mM and 30mM compared to glycaemic untreated keratinocytes. At 11mM, TLR2 inhibition reduced LL37 in LPS-treated cells, and both TLR2 and TLR4 inhibition reduced it in MGN3-treated cells compared to corresponding treatments without TLR inhibition. At 30mM, TLR inhibition had no effect with LPS but reduced LL37 in MGN3-treated cells compared corresponding treatments without TLR inhibition.

Hyperglycaemia did not significantly affect ( $P>0.05$ ) MFI of LL37 in untreated keratinocytes compared to pre-diabetic conditions (Figure 6.27iii). There was no evidence to suggest MGN3/LPS treated keratinocytes significantly ( $P>0.05$ ) effected LL37 expression in comparison to untreated keratinocytes at 11mM and 30mM conditions. TLR inhibition did not affect ( $P>0.05$ ) MFI in untreated keratinocytes at 11mM and 30mM conditions in comparison to untreated keratinocytes without TLR inhibition. At 11mM MFI was significantly ( $P=0.024$ ) inhibited in LPS treated keratinocytes following TLR2 inhibition compared to LPS treated keratinocytes without TLR inhibition. Also, at 11mM TLR inhibition resulted in significantly ( $P<0.01$ ) reduced MFI in MGN3 treated keratinocytes compared to MGN3 treated keratinocytes without TLR inhibition. At 30mM conditions TLR inhibition did not affect ( $P>0.05$ ) MFI in LPS treated keratinocytes however there were significant reductions ( $P<0.05$ ) in MFI in MGN3 treated keratinocytes following TLR inhibition compared to corresponding treatments without TLR inhibition. These results suggest LPS influences LL37 expression in keratinocytes at pre-diabetic conditions (but not hyperglycaemic conditions) and MGN3 influences LL37 expression through both TLR2 and TLR4 at pre-diabetic and hyperglycaemic conditions.

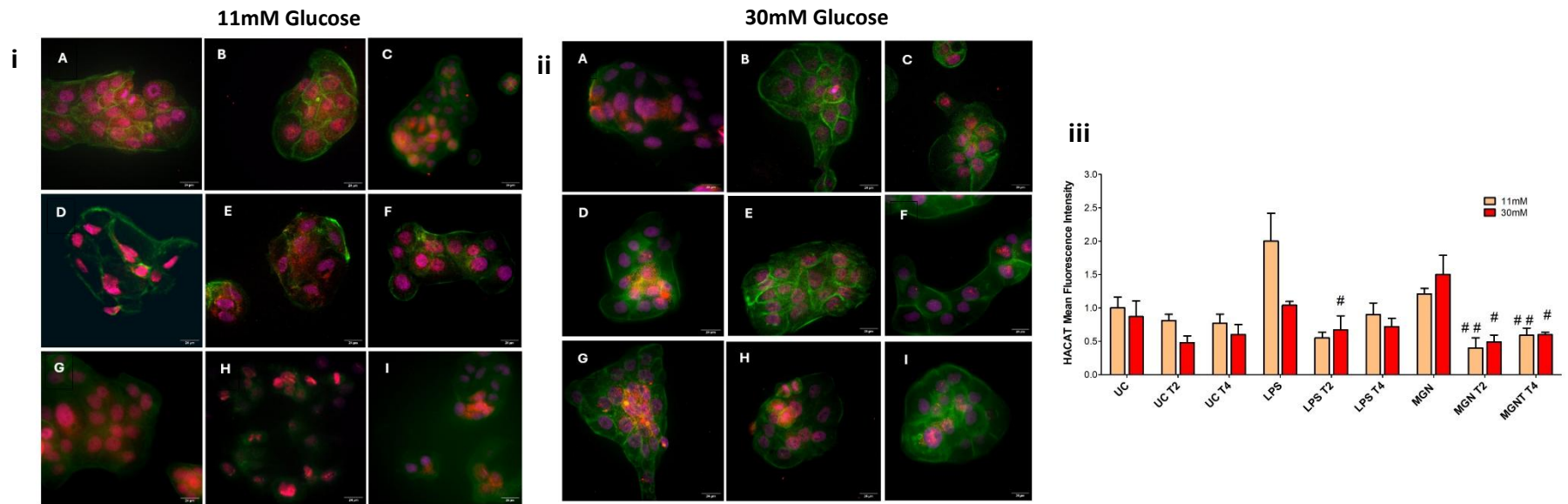


**Figure 6. 27: LL37 Expression in HACATs at Low and High Glucose.** The LL37 expression in HACATs cultured at Low (11mM) (i) and High (30mM) (ii) glucose was captured using thunder microscopy. MFI of LL37 expression (iii) was measured in keratinocytes following treatments (with LPS and MGN3) and TLR2 (T2) and TLR4 (T4) inhibition. The different cell components were identified using fluorescent stains; red indicated TGFβ1 expression, green identified f-actin using phalloidin and blue represented the nucleus using DAPI. Fibroblasts received different treatments; Panel A = UC, panel B = UC + T2, panel C = UC + T4, panel D = LPS, panel E = LPS + T2, panel F = LPS + T4, panel G = MGN3, panel H = MGN3 + T2 and panel I = MGN3 + T4. Images were captured at 60x magnification. There were significant differences in MFI between keratinocytes in the presence of TLR inhibitors and corresponding keratinocytes lacking TLR inhibition (#  $P < 0.05$  and ##  $P < 0.01$  determined by t-tests;  $n = 5$ ). Columns and error bars indicate HACAT MFI  $\pm$  the standard error of the mean (SEM) in all cases.

#### **6.4.10 Influence of MGN3-Induced Keratinocyte-, Fibroblast- and M1 Macrophage-Derived EGF and FGF2 Secretion on Keratinocyte Proliferation**

##### **6.4.10.1 Influence of MGN3-Induced EGF Secretion on Keratinocyte Proliferation**

Keratinocyte proliferation did not significantly change ( $P = 0.34$ ; 106.6% at 30 mM vs. 100.0% at 11 mM) when exposed to supernatant from untreated keratinocytes cultured at 30mM compared to 11mM conditions (Figure 6.28A). EGF inhibition significantly reduced proliferation at both glucose levels ( $P = 0.003$ ) compared to untreated keratinocytes without EGF inhibition, confirming EGF presence in both supernatants. TLR2/4 inhibition significantly decreased ( $P < 0.05$ ) keratinocyte proliferation in response to supernatants from untreated keratinocytes at both glucose concentrations compared to untreated keratinocytes without TLR inhibition. Proliferation significantly increased ( $P < 0.01$ ) when exposed to supernatants from MGN3/LPS-treated keratinocytes at 11mM conditions but significantly decreased ( $P < 0.001$ ) at 30mM conditions compared to correspond untreated keratinocytes. EGF inhibition significantly reduced proliferation ( $P < 0.01$ ) in response to MGN3/LPS-treated supernatants at 11 mM and LPS-treated supernatants at 30mM compared to corresponding treatments without EGF inhibition. TLR2/4 inhibition reduced proliferation ( $P < 0.01$ ) in response to MGN3/LPS-treated supernatants at 11mM, and LPS-treated (but not MGN3-treated) supernatants at 30 mM ( $P < 0.05$ ) compared to corresponding treatments without EGF inhibition. Overall, MGN3 treatment increased keratinocyte proliferation at pre-diabetic conditions but decreased proliferation at hyperglycaemic conditions.

Keratinocyte proliferation was significantly inhibited ( $P = 0.000$ ; 16.2% at 30mM vs. 100.0% at 11mM) when exposed to supernatant from fibroblasts cultured at 30mM compared to 11mM conditions (Figure 6.28B). EGF inhibition had no significant effect ( $P > 0.05$ ) under 30mM, but significantly reduced proliferation at 11mM ( $P = 0.033$ ) compared to corresponding untreated fibroblasts without EGF inhibition, indicating EGF's proliferative role at pre-diabetic conditions. TLR4 inhibition in untreated fibroblast supernatant significantly reduced keratinocyte proliferation at 11mM conditions ( $P = 0.001$ ) but had no effect at 30mM conditions ( $P > 0.05$ ) compared to corresponding untreated fibroblast

supernatant without TLR inhibition. TLR2 inhibition significantly increased proliferation ( $P < 0.05$ ) in LPS-treated fibroblast supernatant at 11mM compared to LPS-treated supernatant without TLR inhibition, suggesting TLR2 involvement at pre-diabetic conditions. Supernatant from LPS-treated fibroblasts decreased keratinocyte proliferation ( $P = 0.019$ ), while MGN3/LPS treatment had no significant effect on keratinocyte proliferation at 30 mM ( $P > 0.05$ ) compared to corresponding untreated fibroblast supernatant. However, MGN3/LPS-treated fibroblast supernatant significantly reduced keratinocyte proliferation at 30mM compared to 11mM conditions ( $P < 0.01$ ). EGF inhibition had no significant effect on keratinocyte proliferation with MGN3/LPS-treated supernatants at either glucose level ( $P > 0.05$ ) compared to corresponding treatments without EGF inhibition. TLR inhibition had no significant effect ( $P > 0.05$ ) on keratinocyte proliferation under hyperglycaemia compared to corresponding treatments without TLR inhibition. These findings indicate high glucose impairs keratinocyte proliferation via fibroblast-derived EGF secretion as well as via TLR2 involvement at pre-diabetic conditions.

Keratinocyte proliferation was significantly reduced ( $P = 0.000$ ; 45.1% at 30 mM vs. 100.0% at 11 mM) when exposed to supernatants from macrophages cultured under hyperglycaemic conditions compared to pre-diabetic conditions (Figure 6.28C), suggesting high glucose impairs M1 macrophage-mediated support of keratinocyte growth. EGF inhibition significantly reduced proliferation at both 11mM ( $P = 0.000$ ) and 30mM ( $P = 0.011$ ) compared to corresponding untreated macrophage supernatant without EGF inhibition, confirming EGF's presence in macrophage supernatants. TLR2 inhibition at 11mM ( $P = 0.000$ ), and both TLR2/4 inhibition at 30mM ( $P < 0.05$ ) compared to corresponding untreated macrophage supernatant without TLR inhibition, significantly decreased proliferation. MGN3-treated macrophage supernatants significantly increased keratinocyte proliferation at 11mM ( $P < 0.01$ ), while MGN3/LPS-treated supernatants significantly decreased proliferation at both 11mM and 30mM conditions ( $P < 0.01$ ) compared to corresponding untreated macrophage supernatant. EGF inhibition further reduced proliferation with MGN3-treated supernatants ( $P = 0.002$ ) compared to MGN3-treated supernatant without EGF inhibition. TLR2 inhibition with LPS increased keratinocyte proliferation at 11mM ( $P = 0.023$ ) but decreased proliferation at 30mM conditions ( $P =$

0.000) compared to LPS treated supernatant without TLR inhibition. TLR4 inhibition with MGN3 treatment increased proliferation at 30mM (P = 0.003) compared to MGN3 treated supernatant without TLR inhibition. In summary, MGN3 enhanced keratinocyte proliferation at pre-diabetic conditions but suppressed it under hyperglycaemia.

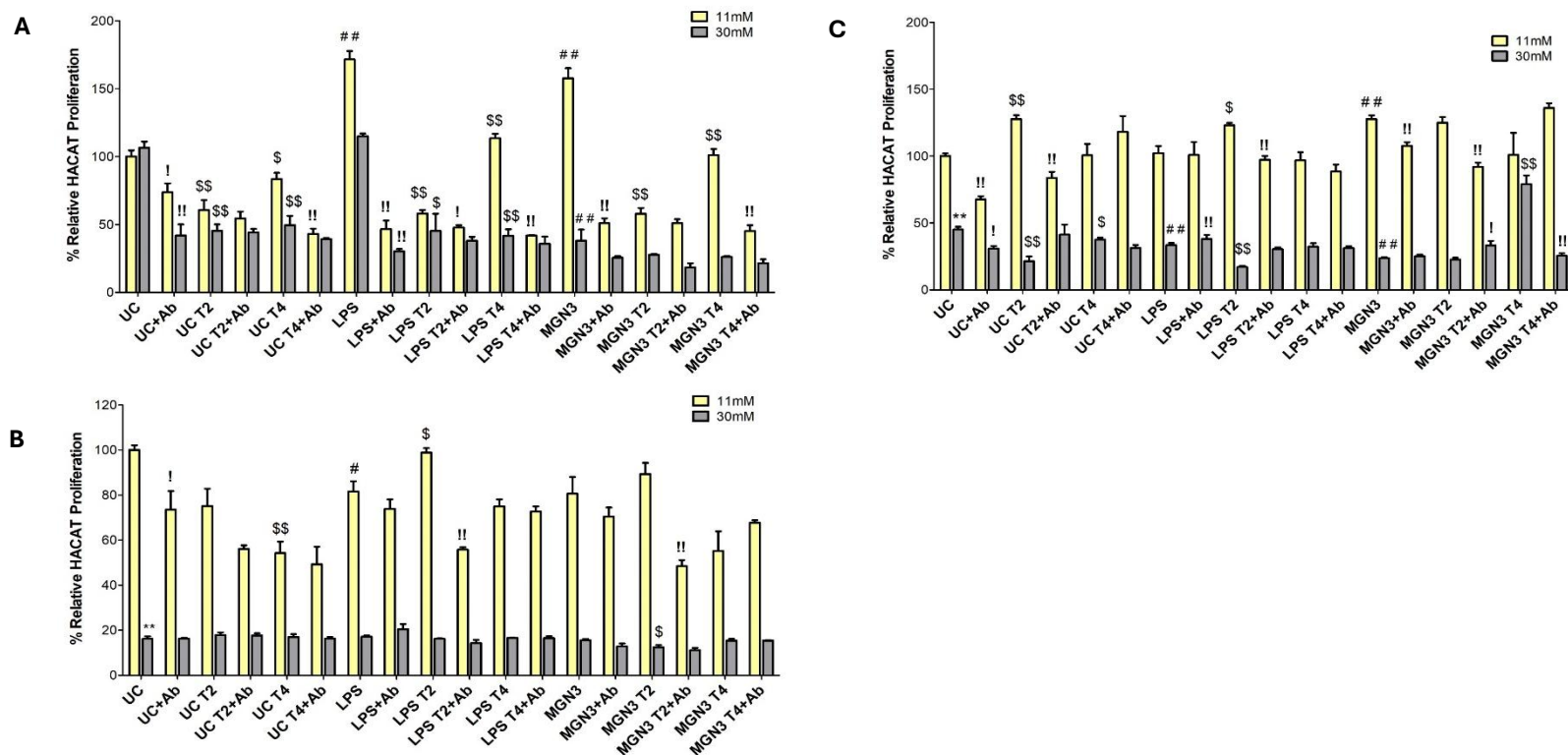


**Figure 6. 28: : Influence of MGN3-Induced EGF Secretion on Keratinocyte Proliferation.** The supernatants from keratinocytes, fibroblasts and macrophages cultured in low (11mM) or high (30mM) glucose was collected following treatment with/without LPS or MGN3, in the presence/absence of TLR2 (T2) or TLR4 (T4) inhibitors to evaluate keratinocyte-derived (A), fibroblast-derived (B) and macrophage-derived (C) EGF on keratinocyte proliferation. Separate HACATs pre-incubated with/without EGF blocking antibody (Ab) were treated with the supernatants to determine the effect on HACAT proliferation. There were significant reductions in HACAT proliferation following exposure to supernatant from the 30mM untreated control (UC) compared with the 11mM UC (\*\*  $P < 0.01$  determined by t-tests;  $n = 4$ ). There were significant differences in HACAT proliferation following exposure to MGN3/LPS-derived supernatant compared with the corresponding glycaemic UC (#  $P < 0.05$  and ##  $P < 0.01$  determined by t-test;  $n = 4$ ). There were significant differences in HACAT proliferation following exposure to supernatant derived from untreated/treated keratinocytes in the presence of TLR inhibition and supernatants from corresponding treatments lacking TLR inhibition ( $\$ P < 0.05$  and  $$$ P < 0.01$  determined by t-tests;  $n = 4$ ). There were differences in HACAT proliferation following exposure to supernatants in the presence of blocking Ab and corresponding supernatants in the absence of Ab (!  $P < 0.05$  and !!  $P < 0.01$  determined by t-tests;  $n = 4$ ). Columns and error bars indicate % HACAT Proliferation  $\pm$  the standard error of the mean (SEM) relative to levels observed in the 11mM UC.

#### 6.4.10.2 Influence of MGN3-Induced FGF2 Secretion on Keratinocyte Proliferation

Keratinocyte proliferation was significantly inhibited ( $P = 0.022$ ; 76.1% vs. 100%) when exposed to supernatant from untreated keratinocytes cultured under hyperglycaemic conditions compared to pre-diabetic conditions (Figure 6.29A), indicating a detrimental effect of high glucose. Supernatant from untreated keratinocytes cultured with TLR2/4 inhibitors at 11mM conditions significantly increased proliferation ( $P < 0.01$ ), while no effect was observed at 30mM conditions ( $P > 0.05$ ) compared to untreated keratinocytes without TLR inhibition. Supernatants from MGN3/LPS-treated keratinocytes significantly increased proliferation under both glucose conditions ( $P < 0.05$ ) compared corresponding untreated keratinocytes. FGF2 inhibition had no significant effect at 11mM ( $P > 0.05$ ) but significantly reduced proliferation at 30mM ( $P < 0.05$ ) compared to untreated keratinocytes without FGF2 inhibition, indicating FGF2 involvement only at hyperglycaemic conditions. Supernatants from LPS-treated keratinocytes at 11mM with TLR inhibition significantly reduced proliferation ( $P = 0.022$  and  $P = 0.036$ , respectively) compared to LPS-treated keratinocytes without TLR inhibition. Similarly, MGN3-treated keratinocyte supernatants with TLR2/4 inhibition at both glucose conditions significantly reduced proliferation ( $P < 0.05$ ) compared to MGN3-treated keratinocytes without TLR inhibition. These findings suggest TLR2/4 modulate responses differently in LPS/MGN3-treated versus untreated keratinocytes under hyperglycaemic conditions. While LPS/MGN3 treatment promotes keratinocyte proliferation, FGF2 is not the sole mediator, as its inhibition did not consistently reduce proliferation.

Keratinocyte proliferation was significantly reduced ( $P = 0.002$ ; 74.6% vs. 100%) when exposed to supernatant from fibroblasts cultured under hyperglycaemic conditions compared to pre-diabetic conditions (Figure 6.29B), indicating hyperglycaemia impairs fibroblast-mediated FGF2 secretion and thus restricting keratinocyte proliferation. FGF2 inhibition significantly increased proliferation at 30mM glucose ( $P = 0.002$ ; 116.4%) compared to untreated fibroblasts supernatant without FGF2 inhibition, suggesting that FGF2 may inhibit keratinocyte proliferation under hyperglycaemic conditions. This indicated fibroblast derived FGF2 alone does not mediate keratinocyte proliferation. TLR2/4 inhibition did not significantly impact keratinocyte proliferation at either glucose condition ( $P > 0.05$ )

compared to untreated fibroblast supernatant without TLR inhibition. Supernatants from LPS/MGN3-treated fibroblasts significantly reduced keratinocyte proliferation at 11mM ( $P < 0.05$ ), and MGN3-treated fibroblasts also reduced proliferation at 30mM conditions ( $P = 0.031$ ) compared to corresponding treatments without TLR inhibition. However, FGF2 inhibition reversed this effect, significantly increasing proliferation at both 11mM ( $P < 0.05$ ) and 30mM ( $P = 0.008$ ) compared to corresponding treatments without FGF2 inhibition, suggesting fibroblast-derived FGF2 may contribute to MGN3/LPS-induced inhibition. TLR4 inhibition with LPS treatment significantly increased proliferation at 11mM ( $P = 0.003$ ), but not at 30mM conditions compared to LPS treated supernatant without TLR inhibition, suggesting glucose level influences TLR4-mediated effects. Overall, high glucose impairs fibroblast-mediated keratinocyte proliferation, FGF2 playing context-dependent roles.

Keratinocyte proliferation was significantly reduced when exposed to supernatant from macrophages cultured in hyperglycaemic conditions compared to pre-diabetic conditions ( $P = 0.024$ ; 74.4% vs. 100.0%) (Figure 6.29C). FGF2 inhibition significantly increased keratinocyte proliferation at 30mM ( $P = 0.026$ ; 104.9% vs. 100.0%) compared to untreated macrophage supernatant without FGF2 inhibition, indicating that macrophage derived FGF2 is not solely responsible for the observed inhibition. TLR inhibition had no significant effect ( $P > 0.05$ ) under either glucose condition compared untreated supernatant without TLR inhibition. At 11mM glucose, supernatant from MGN3-treated macrophages significantly decreased keratinocyte proliferation ( $P = 0.007$ ), while MGN3/LPS-treated supernatants had no effect at 30mM condition ( $P > 0.05$ ) compared to corresponding untreated supernatant. However, MGN3 supernatant at 30mM glucose caused a significant decrease in proliferation compared to 11mM ( $P = 0.023$ ). FGF2 inhibition significantly increased proliferation in response to MGN3 supernatant at 11mM ( $P = 0.007$ ) compared to MGN3 supernatant without FGF2 inhibition. TLR2/4 inhibition in MGN3/LPS-treated macrophages did not significantly affect proliferation under either glucose condition ( $P > 0.05$ ) compared to corresponding treatments without TLR inhibition.

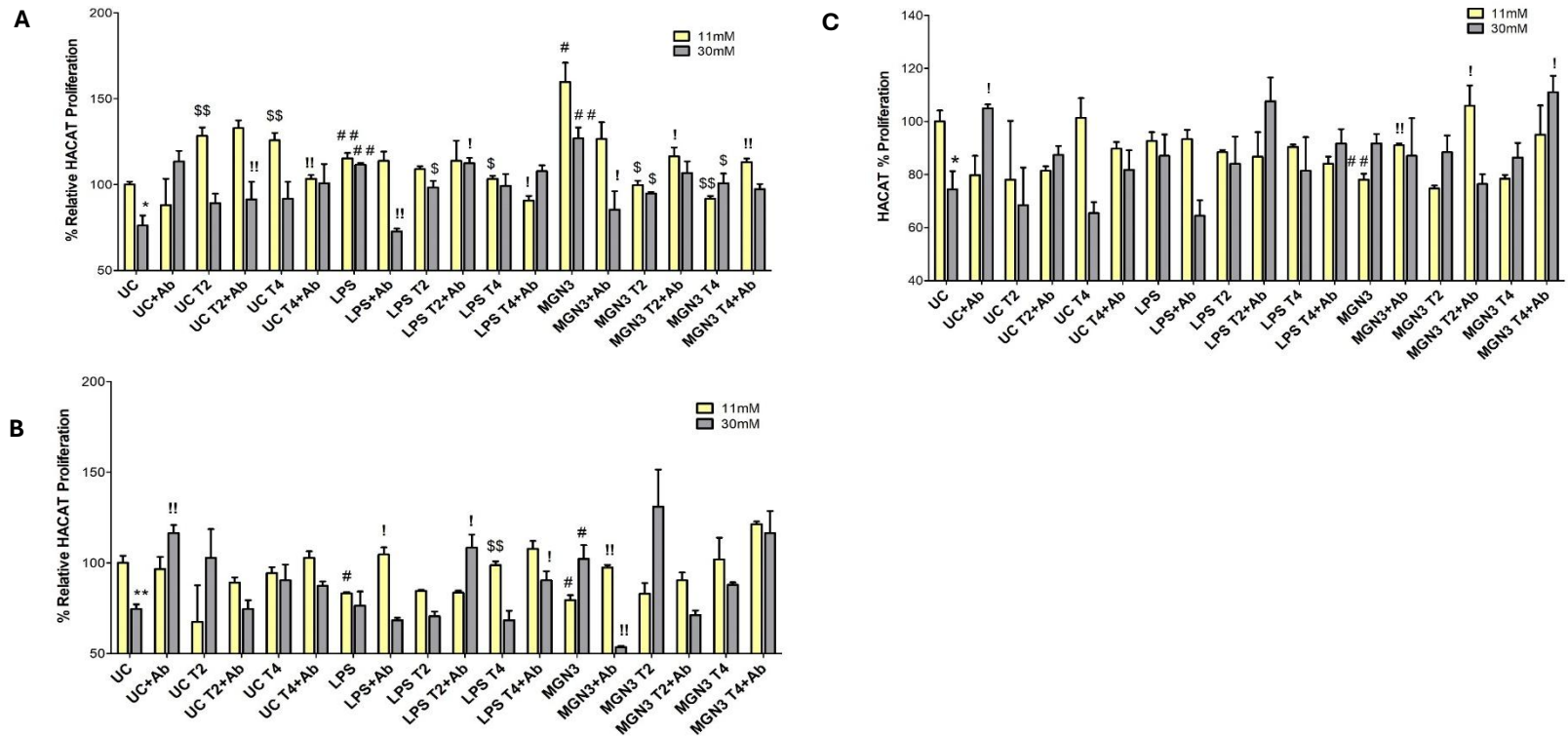


**Figure 6. 29: Influence of MGN3-Induced FGF2 Secretion on Keratinocyte Proliferation.** The supernatants from keratinocytes, fibroblasts and macrophages cultured in low (11mM) or high (30mM) glucose was collected following treatment with/without LPS or MGN3, in the presence/absence of TLR2 (T2) or TLR4 (T4) inhibitors to evaluate keratinocyte-derived (A), fibroblast-derived (B) and macrophage-derived (C) FGF2 on keratinocyte proliferation. Separate HACATs pre-incubated with/without FGF2 blocking antibody (Ab) were treated with the supernatants to determine the effect on HACAT proliferation. There were significant reductions in HACAT proliferation following exposure to supernatant from the 30mM untreated control (UC) compared with the 11mM UC (\*  $P < 0.05$  and \*\*  $P < 0.01$  determined by t-tests;  $n = 4$ ). There were significant differences in HACAT proliferation following exposure to MGN3/LPS-derived supernatant compared with the corresponding glycaemic UC (#  $P < 0.05$  and ##  $P < 0.01$  determined by t-test;  $n = 4$ ). There were significant differences in HACAT proliferation following exposure to supernatant derived from untreated/treated keratinocytes in the presence of TLR inhibition and supernatants from corresponding treatments lacking TLR inhibition (\$  $P < 0.05$  and \$\$  $P < 0.01$  determined by t-tests;  $n = 4$ ). There were differences in HACAT proliferation following exposure to supernatants in the presence of blocking Ab and corresponding supernatants in the absence of Ab (!  $P < 0.05$  and !!  $P < 0.01$  determined by t-tests;  $n = 4$ ). Columns and error bars indicate % HACAT Proliferation  $\pm$  the standard error of the mean (SEM) relative to levels observed in the 11mM UC.

## 6.4.11 Effect of Keratinocyte-Derived Antimicrobial Peptides on Bactericidal Activity

### 6.4.11.1 Effect of Keratinocyte-Derived BD2 Peptide on MRSA and PAO1 Killing

Hyperglycaemic conditions significantly increased MRSA and PAO1 recovery compared to pre-diabetic controls ( $P < 0.01$ ) (Figure 6.30), indicating reduced bactericidal activity. BD2 inhibition significantly increased recovery at 11mM ( $P < 0.01$ ), but not 30mM compared to untreated keratinocytes without BD2 inhibition, suggesting BD2 is present in 11mM lysates and not under hyperglycaemia. LPS/MGN3 treatment significantly reduced MRSA and PAO1 recovery under both glucose conditions ( $P < 0.01$ ) compared to the glycaemic UC, indicating enhanced bactericidal activity. BD2 inhibition increased MRSA recovery ( $P < 0.01$ ) in untreated lysates, confirming BD2 involvement, while PAO1 recovery was unaffected ( $P > 0.05$ ) in comparisons to untreated keratinocytes without BD2 inhibition, suggesting BD2 plays a limited role against PAO1 killing.

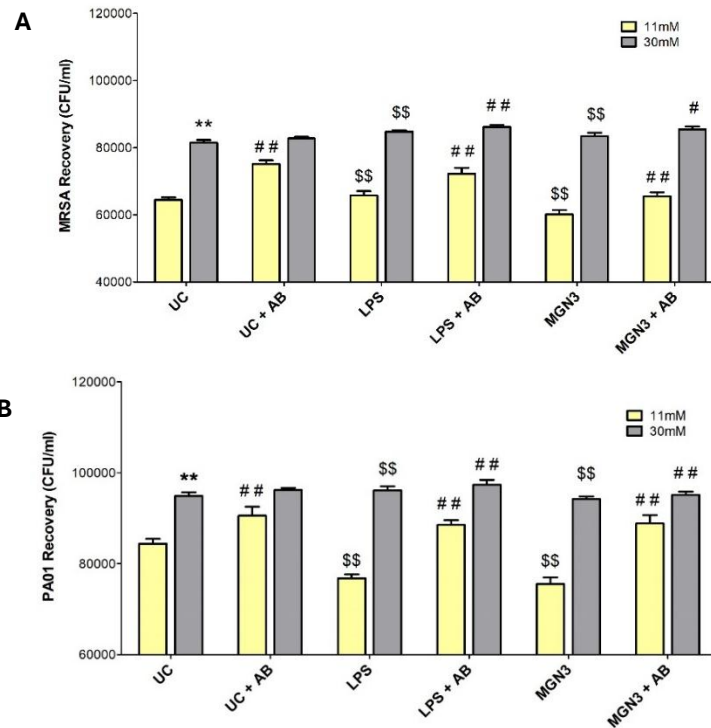


**Figure 6.30: Effect of Keratinocyte-Derived BD2 Peptide on MRSA and PAO1 Killing.** MRSA (A) and PAO1 (B) recovery (CFU/ml) after incubation in 11mM and 30mM glucose, and treatments with LPS (+/- BD2 antibody) and MGN3 (+/- BD2 antibody). Significant differences were seen between the 30mM glucose untreated control (UC) and the 11mM glucose UC (\*\*  $P < 0.01$  determined by t-tests;  $n = 10$ ), between LPS/MGN3 treatments and corresponding glycaemic UC (\$\$  $P < 0.01$  determined by t-tests;  $n = 10$ ), and between samples exposed to BD2 blocking antibody (Ab) and those without Ab (##  $P < 0.01$  determined by t-tests;  $n = 10$ ). Columns and error bars indicate the bacterial recovery (CFU/ml)  $\pm$  the standard error of the mean (SEM) in all cases.

#### 6.4.11.2 Effect of Keratinocyte-Derived LL37 Peptide on MRSA and PAO1 Killing

Hyperglycaemic conditions significantly increased MRSA and PAO1 recovery compared to pre-diabetic controls ( $P < 0.01$ ) (Figure 6.31), indicating reduced bactericidal activity. LL37 inhibition significantly increased both MRSA and PAO1 recovery of at 11mM conditions (MRSA:  $P = 0.016$ ; PAO1:  $P < 0.01$ ) compared to untreated keratinocytes without LL37 inhibition, suggesting LL37 presence in 11mM but not 30mM lysates. LPS/MGN3 treatment significantly reduced MRSA and PAO1 recovery under both glucose conditions ( $P < 0.01$ ) compared to untreated keratinocytes, indicating enhanced bactericidal activity. LL37 inhibition significantly increased bacterial recovery in MGN3/LPS-treated lysates ( $P < 0.01$ ) compared to corresponding treatments without LL37 inhibition, confirming LL37 production under both conditions post-treatment.

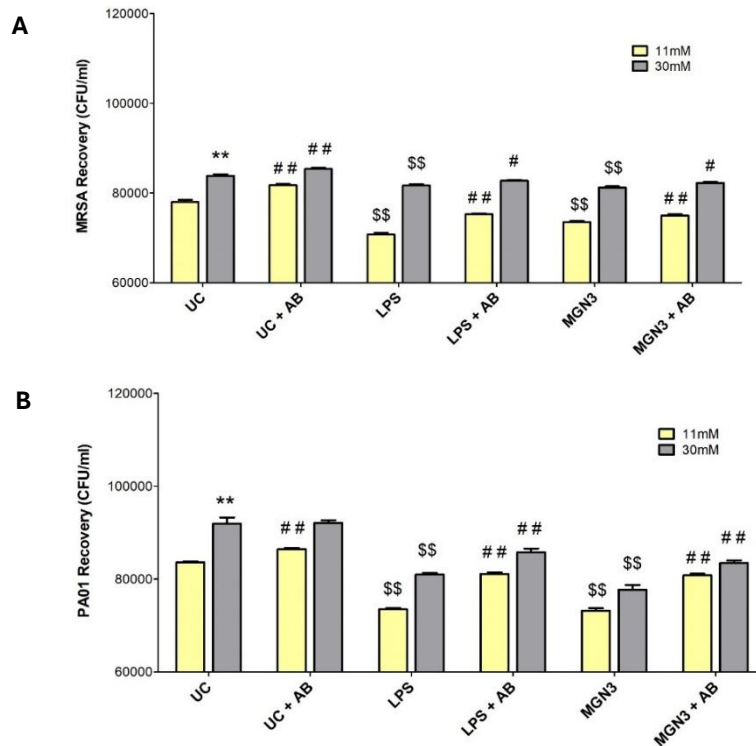


**Figure 6. 31: Effect of Keratinocyte-Derived LL37 Peptide on MRSA and PAO1 Killing.** MRSA (A) and PAO1 (B) recovery (CFU/ml) after incubation in 11mM and 30mM glucose, and treatments with LPS (+/- LL37 antibody) and MGN3 (+/- LL37 antibody). Significant differences were seen between the 30mM glucose untreated control (UC) and the 11mM glucose UC (\*\*  $P < 0.01$  determined by t-tests;  $n = 10$ ), between LPS/MGN3 treatments and corresponding glycaemic UC (\$\$  $P < 0.01$  determined by t-tests;  $n = 10$ ), and between samples exposed to LL37 blocking antibody (Ab) and those without Ab (#  $P < 0.05$  and ##  $P < 0.01$  determined by t-tests;  $n = 10$ ). Columns and error bars indicate the bacterial recovery (CFU/ml)  $\pm$  the standard error of the mean (SEM) in all cases.

## 6.4.12 Effect of MGN3 on NRF2 Protein Expression in HACATs

### 6.4.12.1 NRF2 Expression in Keratinocytes

Hyperglycaemia significantly increased ( $P < 0.01$ ) NRF2 expression in untreated keratinocytes compared to untreated keratinocytes cultured at pre-diabetic conditions (Figure 6.32). Compared to the corresponding UC, NRF2 expression was significantly ( $P < 0.01$ ) increased in MGN3/LPS-treated keratinocytes cultured at 11mM. However, only LPS significantly ( $P < 0.05$ ) increased NRF2 expression at 30mM conditions, with MGN3 having no effect ( $P > 0.05$ ) on NRF2 levels in comparison to untreated keratinocytes. These results suggest that LPS stimulates NRF2 expression at both 11mM and 30mM conditions, whereas MGN3 only promotes NRF2 expression at 11mM conditions. Exposure of keratinocytes to the NRF2 inhibitor (NRF2i) significantly reduced ( $P < 0.01$ ) NRF2 expression in MGN3/LPS-treated cells and UC keratinocytes cultured at 11mM conditions compared to corresponding treatments without NRF2i. At 30mM NRF2i with LPS significantly decreased ( $P < 0.01$ ) and NRF2i with MGN3 increased ( $P < 0.01$ ) NRF2 expression compared to corresponding treatments without NRF2i.

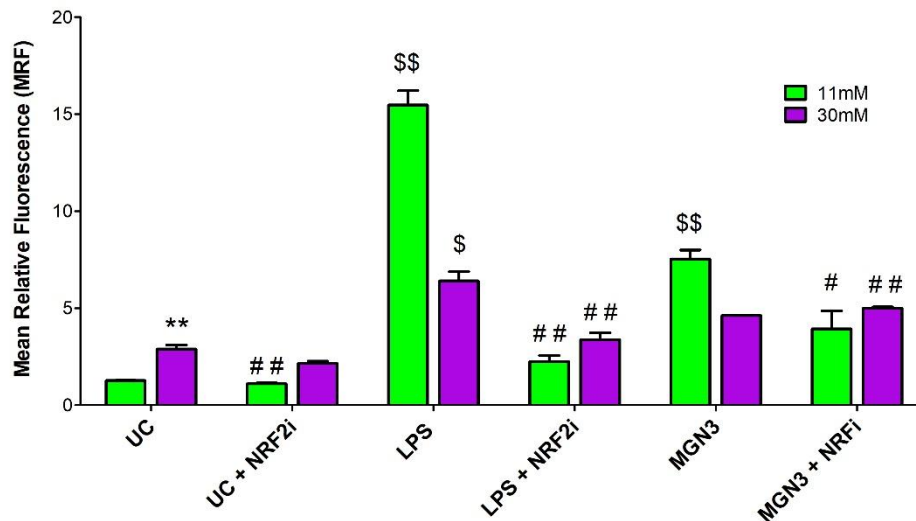


**Figure 6. 32: The Effect of MGN3 on NRF2 Expression in Keratinocytes.** NRF2 expression in keratinocytes after treatments with LPS (5ug/ml) or MGN3 (2mg/ml) at pre-diabetic (11mM) and hyperglycaemic (30mM) conditions. MGN3 and LPS increased expression of NRF2 compared to the UC. The mean relative fluorescence (MRF) of NRF2 was substantially increased in untreated control keratinocytes cultured at 30mM compared to those cultured at 11mM (\*\*  $P < 0.01$ ). There were significant differences in NRF2 expression seen between MGN3/LPS treatments and the corresponding UC (\$  $P < 0.05$ ; \$\$  $P < 0.01$ ;  $n = 10$ ). There were significant differences in NRF2 expression seen between samples exposed to NRF2 inhibitor (NRF2i) and corresponding samples lacking NRF2i (#  $P < 0.05$ ; ##  $P < 0.01$ ;  $n = 10$ ). MRF values are relative to levels detected in the UC (MRF = 1). Columns and error bars indicate the MRF  $\pm$  standard error of the mean (SEM) in all cases.

#### 6.4.12.2 Secretion of MCP-1 from Keratinocytes after NRF2 Inhibition

Hyperglycaemia did not significantly affect ( $P > 0.05$ ) secreted MCP-1 levels in untreated keratinocytes compared to untreated keratinocytes cultured at pre-diabetic conditions (Figure 6.33). NRF2i significantly ( $P < 0.01$ ) reduced MCP-1 levels in untreated keratinocytes at both 11mM and 30mM conditions compared to untreated keratinocytes without NRF2i. There were significant increases in MCP-1 levels following MGN3 (but not LPS) treatment of keratinocytes at 11mM ( $P < 0.001$ ) and 30mM ( $P = 0.01$ ) conditions compared to the corresponding glycaemic UC. NRF2i significantly ( $P > 0.05$ ) inhibited MCP-1 levels in MGN3/LPS treated keratinocytes at both 11mM and 30mM conditions compared to corresponding treatments lacking NRF2i. These results suggest NRF2 in part mediates MCP-1 production in keratinocytes cultured at pre-diabetic and hyperglycaemic conditions and that MGN3 influences keratinocyte secretion of MCP-1 production in keratinocytes more so than LPS or glycaemic levels (given they had no effect on MCP-1 secretion).

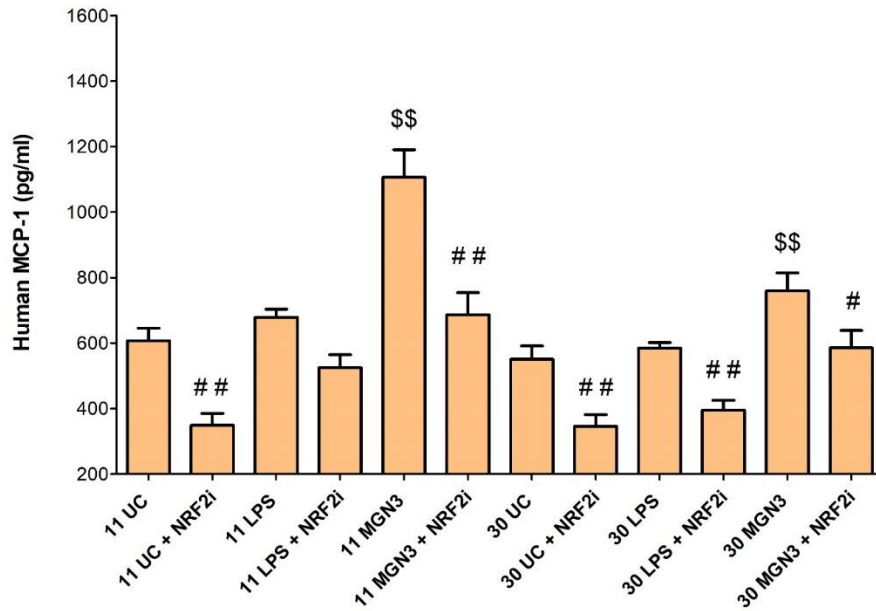


**Figure 6. 33: Secretion of MCP-1 from Keratinocytes after NRF2 Inhibition.** MCP-1 levels were measured in the supernatant keratinocytes cultured in low (11mM) or high (30mM) glucose and treated with LPS or MGN3 in the presence/absence of NRF2 inhibition (NRF2i). There were significant differences in MCP-1 levels observed between supernatant from LPS/MGN3-treated keratinocytes and corresponding supernatant from untreated control (UC) keratinocytes ( $$$ P < 0.01$ ;  $n = 8$ ). There were significant reductions in MCP-1 following the addition of NRF2i to treated and UC keratinocytes compared to corresponding supernatant samples lacking NRF2 inhibition ( $# P < 0.05$  and  $## P < 0.01$ ;  $n = 8$ ). Columns and error bars indicate human MCP-1 levels (pg/ml)  $\pm$  the standard error of the mean (SEM) in all cases.

## 6.5 Discussion

This study examined the effects of MGN3 on fibroblast and keratinocyte functions at pre-diabetic and hyperglycaemic conditions. MGN3 was non-cytotoxic to fibroblasts and significantly enhanced proliferation at 2mg/ml under hyperglycaemia. In keratinocytes, MGN3's effects on proliferation and cytotoxicity were assessed via MTT assay, while metabolism was evaluated by real-time ATP production (Seahorse). ELISA and Thunder microscopy were used to measure production of growth factors (EGF, FGF2, TGF $\beta$ 1), antimicrobial peptides (LL37, BD2), and NRF2 under hyperglycaemia. BD2/LL37 bactericidal activity was tested against MRSA and PA01. NRF2 expression was analysed by flow cytometry, and MCP-1 secretion assessed following NRF2 inhibition.

These results are in line with other studies showing MGN3 promotes enhanced cell function including stimulating NK cell activity against cancer cells (Ooi *et al*, 2018), increasing the phagocytic ability of macrophages (Ghoneum *et al*, 2008) and promoting cytokine production in dendritic cells with an associated increase in IFN  $\gamma$  (Ghoneum and Agrawal, 2011). A comprehensive review was carried out by Ooi *et al*, (2018) to assess the effectiveness of MGN3 as a complementary therapy alongside cancer treatment. After reviewing over thirty articles, they found no evidence of any adverse events therefore concluded MGN3 is safe to use. Also, Elsaid *et al* (2018), found MGN3 did not have any toxic effects on participants who ingested MGN3 for 30 days to assess NK cell activity. MGN3 has also shown to increase proliferation in T and B cells when taken daily as a part a cancer treatment study (Ghoneum and Brown, 1999).

This study assessed the impact of TLR2/4 inhibition on fibroblast metabolism and collagen production. TLR inhibition increased total ATP production across all conditions, primarily through enhanced glycolysis (glycoATP), with limited mitochondrial ATP (mitoATP), consistent with previous findings that TLR inhibition shifts metabolism toward glycolysis (Krawczyk *et al*, 2010). This may relate to structural similarities with TIRAP, which recruits MyD88—known to promote TLR-dependent glycolysis (Tan & Kagan, 2019; Chen *et al*, 2020). Under hyperglycaemia, untreated fibroblasts showed significantly reduced COL-1 secretion and expression. In contrast, MGN3/LPS-treated fibroblasts exhibited increased

intracellular and secreted COL-1 under both glycaemic conditions. This aligns with prior studies showing hyperglycaemia enhances COL-1 synthesis via ERK1/2 activation (Han *et al*, 1999; Tang *et al*, 2007), a key MAPK pathway involved in fibroblast function (Kong *et al*, 2019; Cargnello & Roux, 2011). This study further found TLR2/4 mediate MGN3/LPS-induced COL-1 secretion under 30mM, but not 11mM conditions. Hyperglycaemia increases TLR4 activation and MyD88 complex formation, promoting COL-1 production (Portou *et al*, 2020; Wang *et al*, 2020), while MyD88 inhibition reduces MAPK signalling and collagen output (Luo *et al*, 2022).

EGF secretion was significantly reduced ( $P < 0.001$ ) in untreated fibroblasts at 30mM compared to 11mM conditions. MGN3/LPS increased EGF at both glucose levels, more so at 11mM. TLR2 inhibition increased EGF in untreated and LPS-treated fibroblasts at 11mM, while dual TLR2/4 inhibition elevated EGF under hyperglycaemia. In MGN3-treated cells, TLR2 inhibition had no effect, but TLR4 inhibition significantly reduced EGF ( $P < 0.01$ ), indicating MGN3-induced EGF secretion is TLR4-dependent. EGF suppression under hyperglycaemia may involve impaired JNK signalling and reduced EGF sensitivity (Xuan *et al*, 2014; Hehenberger & Hansson, 1997). FGF2 secretion increased under hyperglycaemia ( $P < 0.01$ ) and was further enhanced by TLR2/4 inhibition in untreated fibroblasts at both glucose levels. LPS reduced FGF2 at 11mM but increased it at 30mM conditions, with TLR inhibition reversing this. In MGN3-treated fibroblasts, TLR2 inhibition raised FGF2, while TLR4 inhibition reduced it under hyperglycaemia, contrary to the response in untreated cells. MGN3 alone did not alter FGF2, but with TLR4 inhibition, FGF2 declined at 30mM conditions. Elevated FGF2 in diabetes is linked to PKC- $\beta$ 1 and JNK suppression with increased ROS (Vasko *et al*, 2009; Xuan *et al*, 2014; Xuan *et al*, 2016).

MCP-1 secretion was significantly higher ( $P < 0.01$ ) in fibroblasts at 30 mM compared to 11mM conditions. MGN3 significantly reduced MCP-1 at 30mM but had no effect at 11mM. TLR2 inhibition increased MCP-1 at 11mM, while combined TLR2/4 inhibition reduced MCP-1 at 30mM conditions in untreated and LPS-treated fibroblasts. TLR inhibition did not affect MGN3-mediated MCP-1 suppression. These results suggest MGN3 downregulates MCP-1 under hyperglycaemia independently of TLR2/4. Hyperglycaemia likely increases MCP-1 via oxidative stress and p38 MAPK activation (Yu *et al*, 2006; Takashi *et al*, 2003).

Hyperglycaemia and both LPS and MGN3 treatment increased MMP-1 secretion ( $P < 0.01$ ). TLR2/4 inhibition enhanced MMP-1 in untreated fibroblasts at 11 mM, while only TLR2 inhibition did so at 30mM conditions. TLR4 inhibition reduced MMP-1 in MGN3/LPS-treated fibroblasts at 11mM but increased it at 30mM, suggesting TLR4 partially regulates MGN3/LPS-induced MMP-1. This may contribute to collagen turnover at hyperglycaemia (Suryavanshi & Kulkarni, 2017). Despite increased MMP-1 levels, collagen production remained high with MGN3, indicating net collagen maintenance. TGF $\beta$ 1 secretion was significantly higher at 30mM compared to 11mM ( $P < 0.01$ ). MGN3/LPS further elevated TGF $\beta$ 1. TLR4 inhibition reduced TGF $\beta$ 1 in untreated and LPS-treated fibroblasts, especially at 30mM. In MGN3-treated fibroblasts, TLR2/4 inhibition reduced TGF $\beta$ 1 at 11 mM, while only TLR4 inhibition did so at 30mM. These findings indicate TLR4 is central to TGF $\beta$ 1 regulation, but not solely responsible for MGN3-mediated induction. TGF $\beta$ 1 increases COL-1 via ROS under hyperglycaemia (Iglesias-De la Cruz *et al*, 2002). Hyperglycaemia significantly reduced KGF secretion ( $P < 0.001$ ). MGN3 reduced KGF at 11mM but increased it at 30mM. TLR4 inhibition reduced KGF in untreated fibroblasts at 11 mM; both TLR2 and TLR4 inhibition increased KGF under 30mM. TLR inhibition had no effect on KGF in LPS-treated cells but reduced KGF in MGN3-treated fibroblasts at 11mM. This data suggests TLRs modulate KGF secretion in a glucose-dependent and MGN3-specific manner. Reduced KGF under hyperglycaemia may impair wound healing (Marti *et al*, 2004).

This study examined how EGF and FGF2 from fibroblast, keratinocyte, and macrophage supernatants influence HDF proliferation at pre-diabetic and hyperglycaemic conditions. HDF proliferation significantly declined ( $P < 0.05$ ) with supernatants from untreated fibroblasts at 30mM glucose. EGF inhibition reduced proliferation only in 11mM supernatants, indicating lower EGF activity at hyperglycaemia. TLR2/4 inhibition increased proliferation at 11mM but TLR4 inhibition reduced it at 30mM, showing glucose-dependent TLR effects. MGN3/LPS-treated fibroblast supernatants decreased proliferation at 11mM but increased it at 30mM. TLR2/4 inhibition boosted proliferation in LPS-treated fibroblasts at 11mM but reduced it at 30mM. TLR2/4 inhibition in MGN3-treated fibroblasts suppressed proliferation at both glucose levels, suggesting TLR signalling mediates MGN3's pro-proliferative effects. These findings align with Mendoza-Mari *et al* (2022), who showed

TLR2/4 inhibition suppressed EGF expression in LPS-treated diabetic fibroblasts. Previous studies also report impaired fibroblast responsiveness to growth factors like EGF and IGF-1 under hyperglycaemia due to ROS and altered EGFR/PI3K/AKT signalling (Xu *et al*, 2009; Hehenberger & Hansson, 1997; Loots *et al*, 2002; Xu *et al*, 2018).

Fibroblast proliferation was significantly reduced by supernatants from keratinocytes cultured at hyperglycaemic conditions (67.8% at 30 mM vs. 100% at 11 mM glucose;  $P = 0.003$ ). EGF inhibition had no effect at 30mM but significantly inhibited proliferation at 11mM (70.1% vs. 100%;  $P < 0.01$ ), suggesting higher EGF levels at 11mM conditions. Reduced EGF in hyperglycaemia may stem from impaired keratinocyte proliferation (Terashi *et al*, 2005). TLR2/4 inhibition decreased fibroblast proliferation with supernatants from untreated keratinocytes at 11mM ( $P < 0.05$ ), but not at 30mM conditions. Supernatants from MGN3/LPS-treated keratinocytes reduced proliferation at 11mM ( $P < 0.05$ ), but not at 30mM. EGF and TLR4 inhibition further reduced proliferation with MGN3-treated supernatants at 11mM ( $P \leq 0.005$ ). LPS-treated keratinocyte effects were unaffected by TLR inhibition at either glucose level, possibly due to structural similarities between LPS and MGN3 (Fadel *et al*, 2018; Ogawa *et al*, 2005).

Fibroblast proliferation was significantly reduced by macrophage supernatants under hyperglycaemic conditions (83.7% at 30mM vs. 100% at 11mM;  $P = 0.038$ ). EGF blocking antibody had no effect at 30mM but significantly reduced proliferation at 11mM ( $P = 0.042$ ), indicating EGF's role only at pre-diabetic conditions. TLR2 inhibition decreased proliferation at 11mM ( $P = 0.01$ ) but not at 30mM. MGN3-treated macrophage supernatants reduced proliferation ( $P < 0.05$ ), while LPS-treated supernatants increased proliferation when combined with EGF inhibition at 11mM ( $P < 0.01$ ). Neither EGF nor TLR inhibition affected proliferation at hyperglycaemia, suggesting other mechanisms mediate inhibition at high glucose.

Fibroblast proliferation was significantly inhibited by supernatants from fibroblasts cultured at 30mM versus 11mM conditions. FGF2 inhibition did not significantly affect proliferation at 30mM but significantly increased proliferation at 11mM ( $P = 0.001$ ), suggesting impaired FGF2 signalling and glycosylated FGF2 production in hyperglycaemia (Gedaj *et al*, 2024;

Facchiano *et al*, 2006). TLR inhibition had no effect at 11mM but TLR4 inhibition significantly increased proliferation at 30mM ( $P < 0.01$ ). LPS and MGN3 effects on proliferation were modulated by TLR2/4 at 11mM, with inhibition increasing proliferation under LPS but reducing it under MGN3 treatment; no effects were seen at 30mM. FGF2 inhibition increased proliferation with LPS-treated 11mM supernatants ( $P = 0.013$ ) but not with MGN3/LPS-treated 30mM supernatants. These findings indicate hyperglycaemia impairs fibroblast proliferation independently of FGF2 inhibition, while TLR2/4 modulate responses to LPS and MGN3 at pre-diabetic conditions (Rahimi *et al*, 2005; Akhtar *et al*, 2021).

Fibroblast proliferation was inhibited by keratinocyte supernatants at 30mM, but not significantly versus 11mM conditions. Other studies have shown hyperglycaemia reduces keratinocyte proliferation and FGF2 levels (Terashi *et al*, 2005; Ortega *et al*, 1998). FGF2 inhibition did not significantly affect proliferation ( $P > 0.05$ ), suggesting keratinocyte-derived FGF2 has minimal impact. Neither TLR2 nor TLR4 inhibition altered proliferation under either glucose condition. MGN3-treated supernatants at 30mM increased proliferation. At 11mM, TLR4 inhibition with LPS reduced proliferation ( $P = 0.044$ ), while at 30mM, TLR2 inhibition plus FGF2 inhibition increased proliferation with LPS-treated supernatants ( $P = 0.009$ ). These data indicate high glucose does not impair fibroblast proliferation and that LPS effects are modulated by TLR4 at pre-diabetic conditions, linked to ERK1/2-mediated FGF2 regulation (Saha *et al*, 2015; Chen *et al*, 2019).

Fibroblast proliferation slightly increased with macrophage supernatants at hyperglycaemia but not significantly versus pre-diabetic conditions. FGF2 inhibition significantly boosted proliferation ( $P = 0.025$ ), especially under hyperglycaemia. TLR2 inhibition increased proliferation at 30mM ( $P < 0.01$ ) but had no effect at 11mM. FGF2 inhibition had no effect at 11mM, indicating macrophage-derived FGF2's limited role at low glucose. MGN3-treated supernatants increased proliferation at 11mM ( $P = 0.021$ ), further enhanced by FGF2 blockade ( $P = 0.01$ ). At 30mM, TLR2 inhibition reduced proliferation with MGN3 supernatants ( $P = 0.001$ ), suggesting high glucose promotes fibroblast proliferation via macrophage-derived FGF2 and that MGN3 effects involve TLR2 under hyperglycaemia.

These findings partly contrast with earlier results showing MGN3 enhanced proliferation and EGF/FGF2 production, suggesting the MTT assay may lack sensitivity for supernatant effects. To improve detection, repeating experiments with higher cell densities to produce more concentrated supernatants is recommended. Future studies could use direct co-culture of fibroblasts with treated cells to better mimic in vivo conditions and allow exploration of varied treatments and exposure times.

This study assessed MGN3's impact on keratinocyte metabolism after TLR2 and TLR4 inhibition. At pre-diabetic conditions, OCR and total ATP production decreased following TLR2/TLR4 inhibition compared to controls. Conversely, hyperglycaemic conditions led to increased OCR but decreased mitoATP after TLR2 inhibition in the LPS group and TLR4 inhibition in UC and MGN3 groups. Previous research shows TLR2/4 inhibition shifts metabolism from mitoATP to glycoATP, likely due to TIRAP-like proteins blocking TLRs and MyD88 activation promoting glycolysis. Elevated glucose availability may further drive this metabolic shift. MGN3 treatment has also been shown to reduce cellular oxidative stress.

This study examined MGN3's effects on growth factors and antimicrobial peptides (EGF, FGF2, TGF $\beta$ 1, NRF2, LL37, BD2) in keratinocytes under hyperglycaemic conditions. Hyperglycaemia significantly increased EGF in untreated cells versus pre-diabetic. At 11mM, LPS but not MGN3, increased EGF; at 30mM, both LPS and MGN3 raised EGF, with MGN3 having a stronger effect. LPS-driven EGF production was mainly TLR4-dependent, while MGN3's effect involved both TLR2 and TLR4 under hyperglycaemic conditions. LPS influences EGF production in keratinocytes primarily through TLR4-mediated inflammatory signalling (Müller-Decker *et al*, 2005; Kim *et al*, 2018; De *et al*, 2015).

Hyperglycaemia significantly decreased ( $P < 0.01$ ) fibroblast FGF2 secretion versus pre-diabetic conditions. Both LPS and MGN3 increased FGF2 production at both glucose levels, with no distinct TLR2 or TLR4 influence on FGF2 among treated or untreated keratinocytes. LPS-stimulated FGF2 elevation, especially under hyperglycaemia, aligns with prior studies (Peng *et al*, 2024; Piipponen *et al*, 2020; Petit *et al*, 2022). TGF $\beta$ 1 secretion was unaffected by hyperglycaemia ( $P > 0.05$ ) in untreated cells. MGN3 (not LPS) significantly reduced TGF $\beta$ 1 at pre-diabetic conditions, but neither altered TGF $\beta$ 1 under hyperglycaemia. Since elevated

TGF $\beta$ 1 impairs keratinocyte proliferation and wound healing via NF- $\kappa$ B inflammatory pathways (Coffey *et al*, 1988; Pietenpol *et al*, 1990; Hogan *et al*, 2013; Luo *et al*, 2017), MGN3's reduction at pre-diabetic conditions may promote proliferation and reduce inflammation. Hyperglycaemia significantly increased NRF2 secretion (P=0.035) in untreated keratinocytes compared to pre-diabetic conditions. MGN3 elevated NRF2 secretion at pre-diabetic conditions but decreased it under hyperglycaemia; LPS had no effect. Recent work suggests extracellular vesicles mediate NRF2 delivery between cells (Gai *et al*, 2024). Both MGN3 and LPS increased intracellular NRF2 protein at both glucose levels. NRF2 protects against oxidative stress and inflammation (Gęgotek & Skrzydlewska, 2015; He *et al*, 2020). NRF2 deficiency in diabetic mice causes prolonged inflammation and reduced MCP-1 expression, impairing monocyte recruitment (Braun *et al*, 2002; Villarreal-Ponce *et al*, 2020). Hyperglycaemia substantially reduced LL37 production in untreated keratinocytes compared to pre-diabetic conditions. At 11mM, LPS and MGN3 increased LL37, and MGN3 also raised BD2 levels; under hyperglycaemia, MGN3 increased BD2 only. LL37 and BD2 are potent antimicrobial peptides (Ramos *et al*, 2011; Afshar & Gallo, 2013), with LL37 linked to improved wound healing via autophagy activation (Piipponen *et al*, 2020; Xi *et al*, 2024) and BD2 effective against PA in ischemia (Casal *et al*, 2019). These increases are likely to enhance keratinocyte antimicrobial activity.

In summary, MGN3 enhanced EGF and FGF2 secretion and increased LL37 and BD2 production in keratinocytes under hyperglycaemic conditions. At pre-diabetic conditions, MGN3 reduced TGF $\beta$ 1 secretion, which may suppress NF- $\kappa$ B-mediated inflammation and promote keratinocyte proliferation—key factors in improving wound healing (Coffey *et al*, 1988; Pietenpol *et al*, 1990; Hogan *et al*, 2013; Luo *et al*, 2017).

This study assessed the impact of MGN3-induced EGF and FGF2 secretion from fibroblasts, keratinocytes, and M1 macrophages on HACAT proliferation at pre-diabetic and hyperglycaemic conditions. Keratinocyte proliferation increased with supernatant from MGN3/LPS-treated keratinocytes at 11mM but decreased with MGN3-treated supernatant at 30mM conditions. EGF inhibition significantly (P = 0.003) reduced proliferation at both glucose levels, confirming EGF's presence. These findings align with Xie *et al* (2024), who reported LPS-stimulated keratinocytes showed reduced proliferation.

Keratinocyte proliferation was not significantly increased ( $P = 0.34$ ) in response to supernatant from untreated cells under hyperglycaemic compared to pre-diabetic conditions (106.6% vs. 100.0%). EGF inhibition significantly reduced proliferation at both glucose levels ( $P = 0.003$ ), confirming EGF presence. Similar findings were reported by Shirakata *et al* (2005), who observed reduced HB-EGF and proliferation under hyperglycaemia. TLR2/4 inhibition significantly reduced ( $P < 0.05$ ) proliferation in response to supernatants from untreated keratinocytes under both glucose conditions. Proliferation significantly increased ( $P < 0.01$ ) when exposed to MGN3/LPS-treated supernatants at 11mM but decreased ( $P < 0.001$ ) with MGN3-treated supernatants at 30mM conditions. EGF inhibition significantly reduced proliferation ( $P < 0.01$ ) in response to MGN3/LPS-treated supernatants at 11mM and LPS-treated supernatants at 30mM conditions. TLR2/4 inhibition of MGN3/LPS-treated keratinocytes at 11mM significantly reduced proliferation ( $P < 0.01$ ). At 30mM, only LPS-treated supernatants with TLR2/4 inhibition significantly reduced proliferation ( $P < 0.05$ ). These results support previous findings that LPS promotes keratinocyte proliferation via TLR4 (Müller-Decker *et al*, 2005; Kim *et al*, 2018; Preciado *et al*, 2005).

Keratinocyte proliferation was significantly inhibited ( $P = 0.000$ ; 16.2% vs. 100%) by supernatants from fibroblasts cultured at hyperglycaemia compared to pre-diabetic conditions. This is consistent with studies linking hyperglycaemia to reduced EGF and impaired proliferation (Terash *et al*, 2014; Hu *et al*, 2016). EGF-blocking antibody had no significant effect ( $P > 0.05$ ), suggesting glucose, not EGF, drives this inhibition. At 11mM, TLR4 inhibition significantly reduced proliferation ( $P = 0.001$ ) in response to fibroblast supernatant, and EGF inhibition also lowered proliferation ( $P = 0.033$ ), indicating EGF's involvement. Neither treatment affected proliferation under hyperglycaemia ( $P > 0.05$ ). Supernatant from LPS-treated fibroblasts significantly reduced fibroblast proliferation ( $P = 0.019$ ), but MGN3/LPS supernatants had no effect. However, MGN3/LPS supernatants from fibroblasts at 30mM significantly reduced keratinocyte proliferation ( $P < 0.01$ ) compared to 11mM conditions. EGF inhibition had no impact in this context ( $P > 0.05$ ). TLR2 inhibition significantly increased ( $P < 0.05$ ) keratinocyte proliferation in LPS-treated cells at pre-diabetic conditions, but TLR2/4 inhibition had no effect under hyperglycaemia ( $P > 0.05$ ),

suggesting TLR2's role is more prominent in low-glucose conditions. This contrasts with studies showing LPS acts via both TLR2 and TLR4 (Loryman & Mansbridge, 2008).

Keratinocyte proliferation was significantly reduced ( $P = 0.000$ ; 45.1% vs. 100%) when exposed to supernatants from macrophages cultured under hyperglycaemic compared to pre-diabetic conditions, suggesting high glucose impairs macrophage-mediated support of keratinocyte growth. This may result from reduced EGF secretion due to altered inflammatory signalling and oxidative stress (Krzyszczuk *et al*, 2018), leading to lower NRF2 in keratinocytes and impaired proliferation (Villarreal-Ponce *et al*, 2020). EGF inhibition significantly reduced proliferation under both glucose conditions ( $P = 0.000$  and  $P = 0.011$ ), confirming EGF's role. TLR2 inhibition significantly decreased proliferation at 11mM ( $P = 0.000$ ), while both TLR2 and TLR4 inhibition reduced it 30mM conditions ( $P < 0.05$ ). MGN3-treated macrophage supernatants significantly increased keratinocyte proliferation at 11mM ( $P < 0.01$ ), whereas MGN3/LPS-treated supernatants decreased it at both 11mM and 30mM ( $P < 0.01$ ). EGF inhibition also reduced proliferation in MGN3-treated conditions ( $P = 0.002$ ). TLR2 inhibition with LPS increased proliferation at 11mM ( $P = 0.023$ ) but decreased it at 30mM ( $P = 0.000$ ). TLR4 inhibition with MGN3 increased proliferation at 30mM ( $P = 0.003$ ). Overall, MGN3-treated macrophages promoted keratinocyte proliferation at pre-diabetic conditions but inhibited proliferation at hyperglycaemic conditions.

Keratinocyte proliferation was significantly reduced ( $P = 0.022$ ; 76.1% vs. 100%) when exposed to supernatants from untreated keratinocytes cultured under hyperglycaemic conditions compared to pre-diabetic conditions, indicating high glucose impairs proliferation—likely due to increased ROS, reduced FGF2, or AGE formation (Wang & Grave, 2020; Shirakata *et al*, 2005; Tian *et al*, 2012). At 11mM, TLR2/4 inhibition significantly increased keratinocyte proliferation ( $P < 0.01$ ), but had no effect at 30mM ( $P > 0.05$ ). Supernatants from MGN3/LPS-treated keratinocytes significantly enhanced proliferation at both glucose levels ( $P < 0.05$ ). FGF2 inhibition had no effect at 11mM but significantly reduced proliferation at 30mM ( $P < 0.05$ ), suggesting FGF2 plays a larger role under hyperglycaemia. TLR4 and TLR2 inhibition of LPS-treated keratinocytes at 11mM conditions significantly reduced proliferation ( $P = 0.022$  and  $P = 0.036$ , respectively). Similarly, TLR2/4 inhibition of MGN3-treated keratinocytes reduced proliferation at both glucose levels ( $P <$

0.05). These findings suggest LPS and MGN3 modulate keratinocyte proliferation through TLR2/4 pathways differently under hyperglycaemia, and factors beyond FGF2 likely drive the proliferative effects of MGN3/LPS-treated supernatants.

Keratinocyte proliferation was significantly reduced ( $P = 0.002$ ; 74.6% vs. 100%) when exposed to supernatants from fibroblasts cultured under hyperglycaemic conditions compared to pre-diabetic conditions, indicating that hyperglycaemia impairs fibroblast-mediated keratinocyte proliferation. Unexpectedly, FGF2 inhibition increased proliferation at 30mM ( $P = 0.002$ ; 116.4%), suggesting factors other than FGF2 may drive suppression. TLR2/4 inhibition had no significant effect ( $P > 0.05$ ) on proliferation with untreated fibroblast supernatants at either glucose level. Supernatants from MGN3/LPS-treated fibroblasts significantly reduced keratinocyte proliferation at 11 mM ( $P < 0.05$ ), and MGN3-treated fibroblasts did so at 30 mM ( $P = 0.031$ ). Blocking FGF2 significantly restored proliferation in both cases ( $P < 0.05$  at 11 mM;  $P = 0.008$  at 30 mM), suggesting FGF2 contributes to suppression in treated conditions. At 11mM, TLR4 inhibition with LPS significantly increased keratinocyte proliferation ( $P = 0.003$ ), but had no effect under hyperglycaemia—supporting TLR4's role in LPS-mediated signalling (Peng *et al*, 2024; Kurat *et al*, 2008).

Keratinocyte proliferation was significantly reduced ( $P = 0.024$ ; 74.4% vs. 100%) when exposed to supernatants from macrophages cultured under hyperglycaemic conditions compared to pre-diabetic conditions, suggesting high glucose impairs macrophage-mediated support. FGF2 reduction due to oxidative stress and altered signalling may contribute (Krzyszczuk *et al*, 2018), disrupting keratinocyte–macrophage crosstalk and lowering NRF2 in keratinocytes (Villarreal-Ponce *et al*, 2020). FGF2 inhibition significantly increased proliferation at 30 mM ( $P = 0.026$ ; 104.9%) but had no effect at 11 mM ( $P > 0.05$ ), indicating FGF2 partially mediates suppression under hyperglycaemia. TLR2/4 inhibition had no significant effect ( $P > 0.05$ ) on proliferation in supernatants from untreated macrophages at either glucose level. Supernatants from MGN3-treated macrophages significantly reduced keratinocyte proliferation at 11 mM ( $P = 0.007$ ) and at 30 mM compared to 11 mM ( $P = 0.023$ ), while MGN3/LPS had no effect at 30mM conditions. FGF2 inhibition significantly restored proliferation in MGN3-treated conditions at 11mM ( $P = 0.007$ ). TLR2/4 inhibition

in MGN3/LPS-treated macrophages had no significant impact at either glucose level ( $P > 0.05$ ).

Other research has shown chronic hyperglycaemia inhibits keratinocyte proliferation, though the underlying mechanisms remain unclear (Terashi *et al*, 2005). Normally, proliferation is driven by EGF via MAPK/PI3K/STAT pathways and by FGF2, which supports Rac activation and lamellipodia formation (Ai *et al*, 2017; Seeger & Paller, 2015). However, high glucose ( $> 12.5$  mM) rapidly glycosylates FGF2, reducing its activity (Facchiano *et al*, 2006), while hyperglycaemia also impairs EGF signalling via Akt, disrupting wound healing (Xu *et al*, 2009). Additionally, hyperglycaemia reduces HB-EGF production (Shirakata *et al*, 2005), with contributing factors including oxidative stress, EGF suppression, and AGE accumulation (Wang & Grave, 2020; Tian *et al*, 2012). LPS may further regulate keratinocyte proliferation by modulating FGF2/NRF2 through TLR4 (Peng *et al*, 2024; Kurat *et al*, 2008).

Hyperglycaemic conditions significantly increased MRSA and PA01 recovery ( $P < 0.01$ ), indicating reduced antimicrobial activity. Supernatants from MGN3- and LPS-treated keratinocytes at 11mM and 30mM conditions decreased bacterial recovery. Blocking LL37 or BD2 reversed this effect, suggesting MGN3/LPS enhances intracellular killing of MRSA and PA01 via increased LL37 and BD2 production. Hyperglycaemia is known to suppress antimicrobial peptides in keratinocytes (Kim *et al*, 2018), including BD2 (Lan *et al*, 2012; Kareem & Mohammed, 2024; Cruz Díaz *et al*, 2015) and LL37 (Hu *et al*, 2016). A clinical trial demonstrated improved healing of infected diabetic foot ulcers with topical LL37, supporting its reduced expression in diabetes (Miranda *et al*, 2023).

This study examined MGN3's effect on NRF2/MCP-1 signalling in keratinocytes at pre-diabetic and hyperglycaemic conditions. Hyperglycaemia increased NRF2 expression in untreated keratinocytes. MGN3/LPS treatment raised NRF2 at 11mM, but at 30mM, only LPS increased NRF2; MGN3 had no effect. NRF2 inhibition reduced NRF2 levels in MGN3/LPS-treated and untreated keratinocytes at 11mM conditions, suggesting NRF2 may self-regulate via a feedback loop (Villareal-Ponce *et al*, 2020; Dodson *et al*, 2022). MCP-1 production in untreated keratinocytes was unaffected by hyperglycaemia. MGN3 significantly increased MCP-1 under both glucose conditions ( $P < 0.01$ ). NRF2 inhibition

significantly reduced MCP-1 levels in untreated and MGN3/LPS-treated keratinocytes at both pre-diabetic and hyperglycaemic conditions, confirming NRF2's role. These results show MGN3 stimulates MCP-1 production via NRF2, consistent with research linking NRF2 activation to MCP-1 secretion, which promotes macrophage EGF release and keratinocyte proliferation (Villarreal-Ponce *et al*, 2020). NRF2 activation by oxidative stress triggers transcription factors (AP-1, NF- $\kappa$ B, STAT3) that induce MCP-1 release (Süntar *et al*, 2021; Schmidt *et al*, 2019; Sim *et al*, 2022; Merecz-Sadowska *et al*, 2021). Future studies could co-culture keratinocytes with macrophages to confirm MGN3-induced MCP-1 stimulates macrophage EGF via NRF2.

In conclusion, this study shows MGN3 enhances keratinocyte ATP production under hyperglycaemia, stimulates key growth factors (EGF, FGF2), and inhibits TGF $\beta$ 1. It promotes MCP-1 secretion via NRF2 and boosts antimicrobial peptides (LL37, especially BD2), increasing bactericidal activity against MRSA and PA01. MGN3 also raises collagen-1, growth factors (EGF, TGF $\beta$ 1), and MMP-1 while reducing MCP-1 in fibroblasts under hyperglycaemia. Overall, MGN3 may improve wound repair by enhancing fibroblast proliferation, modulating metabolism to reduce oxidative stress, increasing growth factors, and lowering inflammation in hyperglycaemic conditions.

# **Chapter 7: Discussion and Future Work**

## 7.1 Discussion

Diabetes mellitus (DM) is a prevalent chronic condition characterized by high blood glucose levels, or hyperglycaemia (Chait and Bornfeldt, 2009; Shaw et al, 2010). The chronic nature of DM is primarily due to persistent hyperglycaemia (Chait and Bornfeldt, 2009), which is believed to result from inadequate or insufficient insulin production (McCrimmon *et al*, 2012). The condition leads to chronic inflammation and excessive production of pro-inflammatory cytokines, which impair bacterial clearance and hinder wound healing (McCrimmon *et al*, 2012; Idriss and Naismith, 2000; Anas *et al*, 2010). Chronic wounds often arise from compromised wound healing, particularly during the inflammatory phase (Frykberg and Banks, 2015). Diabetic foot ulcers (DFUs) are a prime example of chronic wounds. They typically result from diabetic neuropathy, where patients may not feel the initial foot injury. Prolonged pressure can then cause tissue ischemia, necrosis, and inflammation, which rapidly lead to DFUs (Doupis *et al*, 2009; Boulton *et al*, 2020). DFUs are marked by significant inflammation and prolonged tissue ischemia (Alavi *et al*, 2014) and are often colonized by opportunistic bacteria. If untreated, they are prone to infection (Ogba *et al*, 2019; Percival *et al*, 2018; Piri *et al*, 2013).

The dietary fibre MGN3 has been shown to positively affect the immune system, from activating various immune cell types (Ghoneum and Agrawal, 2011) to reducing immunosenescence (Elsaid *et al*, 2018). Clinical trials involving MGN3 indicate its ability to enhance NK cell activity (Elsaid *et al*, 2018) and improve cognitive function in older adults (Elsaid *et al*, 2020). MGN3 has also been found to stimulate peripheral lymphocytes to boost interleukin-2 (IL-2) production (Giese *et al*, 2008) while reducing levels of pro-inflammatory cytokines (Ali *et al*, 2012). Further evidence from *in vivo* studies supports these findings, showing that MGN3 enhances the phagocytic function of M0 macrophages (Asif, 2020; Tan, 2018). Asif (2020) demonstrated that MGN3 promotes bacterial clearance *in vitro* and significantly ( $P < 0.05$ ) reversed impaired phagocytic function caused by elevated glucose levels. In an earlier study, Tan (2018) found that MGN3 increased macrophage-mediated phagocytosis of MRSA through its action on TLR-4 and dectin-1 receptors. Additionally, MGN3 was shown to enhance the phagocytosis of yeast by murine macrophages (Ghoneum

and Matsuura, 2004) and *Escherichia coli* by human monocytes and neutrophils (Ghoneum *et al*, 2008).

MGN3 exhibits several properties that suggest it could be an effective topical treatment for wound management, particularly due to its positive impact on various immune cells. Already widely used as a dietary supplement (Elsaid *et al*, 2018), MGN3 has a well-established safety profile (Ghoneum *et al*, 2013). Additionally, it is highly soluble in water (Kamiya *et al*, 2014), which makes it easily compatible with hydrogels commonly used in aqueous topical wound dressings (Uraloğlu *et al*, 2014). However, to date, the potential of MGN3 as a topical treatment for promoting wound healing and/or combating bacterial infections in chronic wounds has not been explored. Furthermore, there is limited research on how MGN3 affects fibroblast and keratinocyte function, especially under hyperglycaemic conditions and in the context of chronic wounds.

This project aimed to evaluate the effect of MGN3 on the cellular function and activities of several cell types typically involved in the wound healing process (monocytes/macrophages, fibroblasts and keratinocytes) under hyperglycaemic conditions. The first step was to appreciate how hyperglycaemia with or without treatment with MGN3 alters key processes such as cellular metabolism, cell differentiation and the phagocytic capacity of macrophages. The project then assessed the impact of hyperglycaemia and MGN3 treatment on fibroblast and keratinocyte proliferation and migration. Moreover, the effect of hyperglycaemia and MGN3 treatment on the expression and/or secretion of key mediators of immune responses and wound repair were investigated including growth factor (EGF, FGF2, TGFβ1, KGF), chemokine (MCP-1), antimicrobial peptide (cathelicidin and BD2) and transcription factor (NRF2) assessments. Finally, crosstalk between different cell types was extensively investigated in relation to the above mediators to build an initial picture of the potential cell interactions, receptors and signalling pathways through which MGN3 might act to modulate the immune and wound healing processes in response to hyperglycaemia.

Hyperglycaemic conditions impaired macrophage differentiation, detected by a significant decrease in CD11b expression in M0 macrophages (Figure 3. 3). However, hyperglycaemia

subsequently promoted polarisation of macrophages toward an inflammatory M1-like phenotype, detected by a significant increase in CD197 expression (Figure 3. 4). The results indicate glucose inhibited the differentiation of U937 monocytes to M0 macrophages but then stimulated the polarisation of those macrophages toward a more proinflammatory M1 macrophage phenotype. Other studies have shown hyperglycaemia leads to increased CD11b expression in both human monocytes (Torres-Castro *et al*, 2016) and monocytes from diabetic mice (Sierra *et al*, 2012). Other studies have also suggested hyperglycaemia can prime macrophages to become more proinflammatory, resulting in elevated TNF $\alpha$ , IL-1 $\beta$  and IL-6 cytokine secretion (Pavlou *et al*, 2018; El-Mahmoudy *et al*, 2005; Moganti *et al*, 2017). Chronic hyperglycaemia also resulted in a statistically higher percentage of damaged or dead macrophages (Figure 3. 5). Elevated glucose has been shown to increase macrophage cell membrane damage, which was detected by propidium iodide staining, through increased pore formation and especially after LPS treatment (Zhoa *et al*, 2023). Additionally, macrophages grown under hyperglycaemic conditions display signs of metabolic stress and increased apoptotic cell death (Rodgers *et al*, 2020).

This study examined glucose utilisation and its effects on proliferation and cell death in monocytes, macrophages, fibroblasts, and keratinocytes at initial glucose concentrations of 11, 15, 20, and 30mM. Over 8 days, significant glucose depletion indicated active uptake across all cell types. Glucose utilisation per cell increased with glucose concentration, especially in monocytes, suggesting heightened ATP generation under hyperglycaemia. Monocyte proliferation increased until day 3 but declined at 20 and 30 mM by day 8, indicating glucose toxicity and potential cell damage, reflected in morphological changes. There was a similar trend seen in macrophages except glucose utilisation was appreciably reduced compared to monocytes, and viable macrophage counts were higher at day 8 at hyperglycaemic conditions (>15mM glucose) starting conditions compared to pre-diabetic conditions, consistent with reports that monocytes have higher metabolic demands during differentiation (Chui & Bharat, 2016).

A limitation of this study was the extended culture of cells (7 or 14 days) without medium replacement during the glucose utilisation assay. This allowed the measurement of glucose over a set timeframe (7 or 14 days). While this approach preserved the glucose dynamics

within the culture medium, it may have introduced some confounding variables. It is important to note that the 'extended culture' was only implemented in the glucose utilisation assay and the cells cultured for this assay were not used for any downstream analyses (e.g. measurements of migration, proliferation, phagocytosis, cytokines, growth factors etc.) in this study. All cell types cultured for other assays in this PhD project followed the standard cell culture procedure of regular medium changes every 2 days (as indicated in section 2.2.2) as thus the findings of all other assays are not affected by this potential issue. Over time, nutrient depletion, pH shifts, and the accumulation of metabolic by-products in spent medium could negatively affect cell viability, function, and gene expression profiles. This may influence observed cellular responses independently of experimental treatments, particularly under stress conditions like hyperglycaemia. Moreover, prolonged exposure to high glucose without fresh medium changes could exacerbate oxidative stress or alter signalling dynamics, potentially amplifying or masking treatment effects. To mitigate this potential issue to some degree, cell densities were set low for the glucose utilisation assay to minimise the amount of detrimental confounding factors present in the spent medium. Nonetheless, the findings of the glucose utilisation assay should only be considered as tentative approximations beyond the first 2 or 3 days given confounding factors might be influencing cell glucose utilisation at later time points. Although this approach was necessary for continuous measurement of glucose utilisation over an extended culture period, future glucose utilisation assays could consider alternative methods to avoid factors accumulating that might impact cell health. For example, timed medium collection and replenishment could be adopted by generating fresh medium of differing glucose concentrations that exactly match the glucose levels observed at the point of replenishment. Unfortunately, such medium does not commercially exist and would require complicated, bespoke medium creation by removing glucose from commercial medium (11mM) using an enzyme such as glucose oxidase to create medium with glucose levels lower than 11mM. However, this is not without complications since the enzyme then needs neutralizing without damaging other medium components and the reaction also creates hydrogen peroxide (that can damage cellular structures) so the hydrogen peroxide then needs removing using another enzyme such as catalase before supplementing with the

desired concentration of glucose. This complicated process of generating bespoke glucose-supplemented media was considered for adoption in this PhD project but deemed overly complex on balance given the increased risk of bacterial contamination due to medium manipulation, together with the fact it was only required for a single complementary assay within this project, with no bearing on other experimental data presented throughout the thesis.

Glucose utilisation by fibroblasts and keratinocytes over 14 days showed significant depletion by day 8, indicating active metabolism. Under hyperglycaemic conditions, glucose uptake increased, but cell proliferation declined in both cell types. Hyperglycaemia impairs fibroblast proliferation and migration, likely due to growth factor resistance and PKC overproduction (Hehenberger & Hansson, 1997; Buranasin *et al*, 2018). Hyperglycaemia also appeared to induce a myofibroblast-like phenotype, associated with elevated NF- $\kappa$ B signalling and IL-8 production (Pang *et al*, 2016; van Caam *et al*, 2018; Haas *et al*, 2021). Keratinocytes under high glucose similarly increased pro-inflammatory cytokine and nitric oxide production (Nakai *et al*, 2003; Lan *et al*, 2013) and showed reduced  $\beta$ -defensin expression via p38MAPK inhibition (Lan *et al*, 2012; Lan *et al*, 2013). Chronic hyperglycaemia is linked to decreased viability across multiple cell types, including macrophages, fibroblasts, and keratinocytes (Ayala *et al.*, 2019; Pavlou *et al*, 2018; Rizwan *et al*, 2020).

After confirming glucose uptake, its effect on metabolism was assessed in fibroblasts (HDFs) and keratinocytes (HACATs). In HDFs, increasing glucose led to reduced oxygen consumption rate (OCR), extracellular acidification rate (ECAR), and total ATP production, with a metabolic shift toward mitochondrial ATP over glycolysis. In contrast, HACATs showed decreased OCR but increased ECAR and ATP production, relying predominantly on glycolysis at 30mM glucose. These results indicate hyperglycaemia impairs mitochondrial function in both cell types but promotes glycolytic metabolism in keratinocytes. Hyperglycaemia can impair fibroblast function by inducing autophagy and mitophagy, reducing mitochondrial mass and promoting hypoxia-like effects (Zhang *et al*, 2008; Baracca *et al*, 2013). It also triggers prolonged P2X7 activation in fibroblasts, causing ATP depletion and cell death (Solini *et al*, 2000). In keratinocytes, hyperglycaemia increases ROS, decreases mitochondrial transcription factor A, and promotes apoptosis via AKT–IRF3 signalling (Rizwan *et al*, 2020).

The phagocytic capacity of M1 macrophages to clear MRSA and PA biofilms under hyperglycaemia and MGN3 treatment was assessed using TLR2/TLR4 inhibitors to determine if MGN3 acts via TLR signalling. Prior to phagocytosis assays, the direct effects of varying glucose levels (11, 15, 20, and 30 mM) and MGN3 treatment on MRSA and PA biofilms were tested. Results showed that MGN3 had no direct antimicrobial effect, confirming that any changes in subsequent bacterial clearance were due to macrophage activity rather than direct action of MGN3 on biofilms.

Hyperglycaemia has been shown to enhance bacterial biofilm formation and growth (Lu *et al*, 2020; Vitko *et al*, 2016; She *et al*, 2019; Huynh *et al*, 2012). In this study, direct exposure of MRSA and PA biofilms to 20mM or 30mM glucose significantly increased bacterial recovery compared to 11mM, supporting clinical findings that glucose in bronchial aspirates correlates with higher MRSA colonisation risk (Phillips *et al*, 2005). As MRSA and PA are common in diabetic foot ulcers (DFUs) (Luo *et al*, 2020), these results highlight how uncontrolled hyperglycaemia may promote their persistence. Glucose specifically enhances MRSA biofilm structure and growth more than other sugars (Luo *et al*, 2020; You *et al*, 2014), likely via fermentation-driven aggregation (Vitko *et al*, 2016; Luo *et al*, 2019). She *et al*, (2019) further showed that hyperglycaemic levels increase PA biofilm size without boosting planktonic growth, suggesting enhanced adhesion rather than proliferation. Bacterial recovery increased under hyperglycaemic conditions, suggesting hyperglycaemia impairs the phagocytic activity of M1 macrophages. Supporting these findings, Pavlou *et al*, (2018) demonstrated that prolonged exposure to high glucose reduces phagocytosis in LPS/INF $\gamma$ -polarized human bone marrow-derived M1 macrophages. These results also align with *in vivo* observations in diabetic patients, who exhibit impaired phagocytosis (Berbudi *et al*, 2020; Xu *et al*, 2013; Tessari *et al*, 2010).

Hyperglycaemia promotes bacterial biofilm formation (Lu *et al*, 2020; Vitko *et al*, 2016; She *et al*, 2019; Huynh *et al*, 2012). In this study, MRSA and PA biofilms exposed to 20 and 30mM glucose showed significantly higher bacterial recovery than at 11mM, aligning with clinical data linking airway glucose to increased MRSA colonisation (Phillips *et al*, 2005). As common DFU pathogens (Luo *et al*, 2020), MRSA and PA may thrive under poor glycaemic control. Glucose uniquely enhances MRSA biofilm formation over other sugars (Luo *et al*, 2020; You

*et al*, 2014), likely via fermentation-driven aggregation (Vitko *et al*, 2016; Luo *et al*, 2019). High glucose also increases PA biofilm size without affecting planktonic growth, suggesting enhanced adhesion (She *et al*, 2019). LPS activation in diabetic mouse macrophages upregulates TLR2 and TLR4, potentially enhancing phagocytosis via increased receptor availability (Lui *et al*, 2001). Building on previous work showing MGN3 competes with LPS for TLR4 and dectin-1 binding in planktonic models (Tan, 2018; Asif, 2020), this study investigated whether MGN3 modulates TLR2/4 signalling in biofilm-based wound infection models.

Inhibition of TLR2—and especially TLR4—significantly increased MRSA biofilm recovery under both pre-diabetic and hyperglycaemic conditions, regardless of M1 macrophage pretreatment (RS/MGN3/LPS). Dual inhibition had a partially additive effect, indicating that TLR2/4 signalling is critical for macrophage-mediated clearance, possibly via microbial or endogenous ligands (Takeda *et al*, 2003; Yu *et al*, 2010). TLRs are promiscuous receptors activated by diverse ligands and can form homo- or heterodimers to broaden pathogen recognition (Colleselli *et al*, 2023; Farhat *et al*, 2008). For example, TLR4 typically detects LPS as a homodimer, while TLR2 partners with TLR1 or TLR6 to detect distinct bacterial-derived products (Colleselli *et al*, 2023).

TLR4 inhibition significantly increased PA biofilm recovery under both pre-diabetic and hyperglycaemic conditions, regardless of M1 macrophage pretreatment, highlighting its key role in phagocytosis—consistent with recognition by TLR4 of Gram-negative LPS (Ciesielska *et al*, 2021). In contrast, TLR2 played a less consistent role. Under pre-diabetic conditions, TLR2 inhibition had no effect in untreated M1 macrophages ( $P > 0.05$ ) but increased biofilm recovery under hyperglycaemia ( $P < 0.01$ ). Interestingly, in LPS/MGN3-treated M1 macrophages, TLR2 inhibition reduced phagocytosis under pre-diabetic conditions ( $P < 0.01$ ) but had no effect under hyperglycaemia. These results suggest a glycaemia-dependent shift in TLR2 signalling in response to PA, a pattern not observed with MRSA. Inhibition of TLR2 and/or TLR4 did not fully block the MGN3- or LPS-induced reduction in MRSA and PA biofilm recovery, suggesting TLR-independent mechanisms may also enhance phagocytosis. While LPS is a known TLR4 ligand (Ciesielska *et al*, 2021), it can also enter the cytosol—via phagosomes or HMGB1–RAGE complexes—and activate the non-canonical NLRP3

inflammasome through caspase-4/5, promoting phagosome maturation and bacterial killing (Mazgaeen & Gurung, 2020; Rathinam & Fitzgerald, 2016). This pathway enhances clearance of both Gram-negative and Gram-positive bacteria. Given its structural similarity to LPS (Fadel *et al*, 2018), MGN3 may similarly activate TLR-independent inflammasome pathways, though further investigation is needed.

Fibroblast- and keratinocyte-mediated wound closure was assessed under hyperglycaemia and MGN3 treatment using TLR2/4 inhibitors to explore TLR involvement. Hyperglycaemia impaired fibroblast-driven closure, suggesting reduced migration and/or proliferation, while MGN3 enhanced closure, especially at high glucose levels. TLR2/4 inhibition significantly reduced closure across all glucose conditions. Using mitomycin C and cytochalasin D, results indicated MGN3 primarily promoted fibroblast migration rather than proliferation. These findings align with previous studies showing hyperglycaemia inhibits fibroblast migration. For example, glucose concentrations of 30mM have been shown to delay fibroblast cell migration in diabetic mice (Xuan *et al*, 2014). This effect has been linked to hyperglycaemia-induced increases in reactive oxygen species (ROS) production and inhibition of JNK phosphorylation. The JNK and PI3-Kinase-Rac1 pathways are crucial for cell migration, as highlighted by Xuan *et al*, (2016). Additionally, diabetic patients typically have elevated levels of 3-deoxyglucosone (3DG), a precursor to advanced glycation end-products (AGEs), which leads to the accumulation of AGEs on collagen as patients age (Loughlin and Artlett, 2009). It has been shown that fibroblasts exhibit a higher affinity for 3DG-treated collagen, but this results in a significant reduction in their ability to migrate across wounds (Loughlin and Artlett, 2009).

Keratinocyte wound closure was similarly impaired by hyperglycaemia but enhanced by MGN3 at 11mM and 30mM glucose. Cytochalasin D significantly reduced this closure, while mitomycin C had less effect, indicating MGN3 primarily promotes keratinocyte migration, with a minor role for proliferation. Previous studies also show hyperglycaemia impairs keratinocyte migration and proliferation (Raja *et al*, 2007; Pastar *et al*, 2014). Lan *et al*, (2008) linked hyperglycaemia-induced keratinocyte motility loss to reduced P125FAK signalling. Hyperglycaemia also impairs integrin-mediated adhesion, further hindering migration (Li *et al*, 2019). MGN3 may restore integrin expression, as seen in T-cells (Weeks

*et al*, 2008) and activate FAK pathways to promote keratinocyte migration and wound healing (Phurisom *et al*, 2021). Hyperglycaemia-induced oxidative stress damages keratinocytes, but MGN3's antioxidant effects protect them and support motility (Rizwan *et al*, 2020; Noaman *et al*, 2008). Additionally, MGN3 activates MAPK and PI3K pathways, essential for F-actin dynamics and cell movement (Tan, 2018; Zhang *et al*, 2020; Vazquez-Victorio *et al*, 2016).

This study investigated the effects of MGN3 on U937 monocytes and M1 macrophages at pre-diabetic and hyperglycaemic conditions, with implications for wound healing in diabetic patients with DFUs. Hyperglycaemia increased EGF secretion from M1 macrophages, aligning with findings by Fukuda *et al* (1997), who observed elevated HB-EGF expression in hyperglycaemic mice. However, FGF2 secretion remained unchanged, despite previous reports of increased FGF2 mRNA (Teshima-Kondo *et al*, 2004) and altered FGF2 structure via glycation (Facchiano *et al*, 2006). Glycation also impairs FGF2 receptor binding, reducing mitogenic activity (Duraisamy *et al*, 2001). MGN3 combined with LPS reduced both EGF and FGF2 secretion in M1 macrophages under low and high glucose. Conversely, RS increased EGF and decreased FGF2 secretion at 11mM glucose but had no effect at 30mM. These changes suggest MGN3 may help reduce inflammation in hyperglycaemia. EGF promotes macrophage proliferation, potentially intensifying inflammation (Lu *et al*, 2014). EGFR signalling regulates cytokine production and feedback (Lu *et al*, 2014; Zhao *et al*, 2016; Shang *et al*, 2020). FGF2 enhances inflammatory cell recruitment via endothelial adhesion molecules (Zittermann & Issekutz, 2006) but also supports angiogenesis and tissue repair (Bikfalvi *et al*, 1997; Presta *et al*, 2009; Shen *et al*, 2024).

TLR inhibition increased EGF secretion in untreated and RS-treated M1 macrophages at low glucose (11mM) but had no effect at high glucose (30mM). This aligns with TLR-mediated activation by various endogenous ligands (Takeda *et al*, 2003). Similarly, at 11mM TLR inhibition increased EGF levels following LPS or MGN3 treatment. However, at 30mM, only TLR4 inhibition elevated EGF after LPS or MGN3, suggesting TLR4 mediates LPS/MGN3-induced EGF production in high glucose. TLR4's link to EGFR signalling via Rab5a supports this finding (Tang *et al*, 2020), and EGFR can be activated directly or via TLR4 ligands like LPS (Lu *et al*, 2014).

TLR2 inhibition reduced FGF2 secretion in untreated cells at 11mM, while TLR4 inhibition increased it at 30mM conditions. In MGN3-treated cells, TLR inhibition had no effect at 11mM, but TLR2 inhibition increased FGF2 at 30mM glucose. With LPS, TLR2 inhibition increased FGF2 only at 11mM glycaemic level. In RS-treated cells, both TLR2 and TLR4 inhibition increased FGF2 at 11 mM glucose conditions, while only TLR4 inhibition had an effect at 30mM. These findings suggest TLR2 influences MGN3-induced FGF2 under hyperglycaemia and LPS-induced FGF2 under euglycemia. Though direct links between TLR2 and FGF2 are limited, some FGF family members may signal through TLR2/4 (Marega *et al*, 2021).

In this study, the secretion of chemokine MCP-1 from macrophage was investigated. Hyperglycaemia (30mM) had no significant effect on MCP-1 in untreated M1 macrophages. However, RS, LPS and MGN3 treatments elevated MCP-1 secretion under hyperglycaemic conditions. This contrasts with studies showing hyperglycaemia alone increases MCP-1 via oxidative stress and NF- $\kappa$ B activation (Xu *et al*, 2016; Yang *et al*, 2009). Diabetic patients also show higher serum MCP-1 (Mine *et al*, 2006), likely due to ROS-induced activation of proinflammatory pathways. Elevated MCP-1 levels in response to hyperglycaemia are thought to recruit more monocytes to sites of inflammation, exacerbating the chronic inflammation commonly seen in diabetes (Grewal *et al*, 1997). Additionally, high glucose can alter macrophage polarization, pushing them towards a more pro-inflammatory phenotype, which further promotes MCP-1 secretion (Nio *et al*, 2012; Du *et al*, 2021). Given the current findings, it is possible that the ELISA used in this study was not sensitive enough to detect some changes in MCP-1 levels due to the macrophage densities used to generate the cell lysates. Therefore, further studies using higher cell densities or more sensitive techniques, such as flow cytometry, are needed to confirm these results.

MCP-1 inhibition reduced U937 monocyte chemotaxis in supernatants from untreated M1 macrophages at 11mM but increased chemotaxis at 30mM conditions, suggesting a glucose-dependent, dual role of MCP-1 in chemotaxis. Supernatants from MGN3- or LPS-treated M1 macrophages had no significant effect on chemotaxis at either glucose level, nor did TLR2 or TLR4 inhibition, indicating limited MCP-1 modulation at the tested cell densities. Supernatants from untreated keratinocytes or fibroblasts cultured in 30mM glucose

reduced monocyte chemotaxis compared to 11mM glucose, an effect reversed by MCP-1 blocking, suggesting hyperglycaemia actively induces MCP-1 secretion from these cell types. Under hyperglycaemia, TLR2 inhibition increased chemotaxis, while TLR4 inhibition decreased it, with responses varying by treatment. Notably, MGN3-treated keratinocyte supernatants (at 30mM) significantly reduced chemotaxis; fibroblast supernatants had no such effect. These results highlight the central role of MGN3 in chemotaxis, with TLR2/4 contributions influenced by glucose levels and cell type.

Macrophages, keratinocytes, and fibroblasts produce elevated MCP-1 under hyperglycaemic conditions (Grosick *et al*, 2018; Fang *et al*, 2023; Shanmugam *et al*, 2003). While MCP-1 aids monocyte recruitment, its overexpression can prematurely prime monocytes, promoting macrophage differentiation and excessive cytokine production in diabetes (Kraakman *et al*, 2014; Cuca *et al*, 2014). MCP-1-primed macrophages also show increased cytotoxicity (Wang *et al*, 2014). Hyperglycaemia induces macrophages to release pro-inflammatory cytokines, which stimulate keratinocytes and fibroblasts to further produce MCP-1, forming a positive feedback loop (Xu *et al*, 2016). This also leads to the release of IL-1 $\beta$ , IL-6, and TNF- $\alpha$ , enhancing MCP-1 expression and monocyte recruitment (Wood *et al*, 2014). Additionally, hyperglycaemia alters fibroblast-derived ECM, impacting MCP-1 signalling (Macarie *et al*, 2018), while direct cell-cell interactions also amplify MCP-1 production (Yadav *et al*, 2010; Pezhman *et al*, 2021; Tiwari *et al*, 2010). Altogether, these processes create a chronic inflammatory environment, promoting sustained MCP-1 overproduction and monocyte recruitment, contributing to tissue damage and diabetic foot ulcer formation (Monaghan *et al*, 2023).

This study examined two key antimicrobial mediators, lysozyme and cathelicidin (LL37), in M1 macrophages. Hyperglycaemia is known to impair lysosomal activity and lysozyme regulation (Moheimani *et al*, 2012; Sims-Robinson *et al*, 2016). However, no significant difference in lysozyme levels was found between untreated macrophages at pre-diabetic and hyperglycaemic conditions. At 11mM glucose, LPS and MGN3 significantly increased lysozyme production ( $P < 0.01$ ); at 30mM glucose, MGN3 still induced a smaller but significant increase. Given the potent antimicrobial action of lysozyme, this suggests MGN3 may enhance bacterial clearance (Khorshidian *et al*, 2022). TLR2/4 inhibition reduced

MGN3-induced lysozyme at both glucose levels. LPS-induced lysozyme was similarly reduced by TLR inhibition, but only at 11mM. In untreated and RS-treated cells at low glucose, TLR2 inhibition increased lysozyme activity, while TLR4 inhibition decreased it, highlighting a regulatory role for TLRs in lysozyme production.

Under hyperglycaemic conditions, LL37 production decreased in untreated M1 macrophages, indicating impaired antimicrobial response. LPS increased LL37 under high glucose, while MGN3 reduced it, showing opposing effects. TLR2/TLR4 inhibition reduced LL37 production at low glucose but increased it under high glucose in MGN3-treated macrophages, suggesting glucose-dependent modulation of MGN3 effects via TLR pathways. MGN3-induced LL37 suppression may impair bacterial killing (Sancho-Vaello *et al*, 2020) but could help limit inflammation, as LL37 delays neutrophil death (Minns *et al*, 2021) and promotes inflammation by enhancing RNA-scavenger receptor interactions (Takahashi *et al*, 2018). Hyperglycaemia may influence LL37 via elevated cytokines like TNF- $\alpha$  and IL-6 (Uribe-Querol & Rosales, 2022; Hao *et al*, 2023) and oxidative stress affecting LL37-regulating transcription factors (Shi *et al*, 2024; Xi *et al*, 2024). MGN3's antioxidant properties (Ooi *et al*, 2018) may counteract these effects. Further studies are needed to explore these relationships in greater detail.

This study assessed whether MGN3 treatment affected the cathelicidin-associated antimicrobial activity of M1 macrophage lysates against MRSA and PA01 under hyperglycaemia. LL37 has broad antibacterial activity (Ridyard & Overhage, 2021). All M1-derived lysates showed significant antibacterial effects ( $P < 0.001$ ) against both strains at pre-diabetic and hyperglycaemic conditions, indicating potent antimicrobial activity. However, MGN3-treated supernatants did not significantly alter bacterial recovery compared to controls, suggesting MGN3 did not enhance MRSA killing. This aligns with earlier findings that MGN3 reduces LL37 production (see previous paragraph). Adding a cathelicidin-blocking antibody increased bacterial recovery in all treatments under hyperglycaemia, confirming LL37 contributes to antibacterial activity, though other antimicrobial components are also likely involved.

This study found that MGN3 was non-toxic to fibroblasts and promoted their proliferation, particularly under hyperglycaemic conditions—aligning with previous research showing MGN3 enhances cell function in NK cells, macrophages, and dendritic cells. Specifically, it stimulates NK activity against cancer cells (Ooi *et al*, 2018), boosts macrophage phagocytosis (Ghoneum *et al*, 2008), and increases dendritic cell cytokine output, including IFN- $\gamma$  (Ghoneum & Agrawal, 2011).

At hyperglycaemic conditions, untreated fibroblasts showed reduced total ATP compared to keratinocytes at pre-diabetic conditions. Both LPS and MGN3 treatments further decreased ATP levels as glucose increased. At 11mM glucose, LPS-treated fibroblasts had the highest ATP production; MGN3-treated cells had the lowest. Glycolysis contributed to 63% of ATP in LPS-treated cells, compared to 32% in MGN3-treated and 36% in the UC group. At 30mM glucose, untreated fibroblasts had the highest ATP, with MGN3 and LPS yielding similar, lower levels. Mitochondrial ATP accounted for over 70% in controls, versus 62% (MGN3) and 50% (LPS). Consistent with Solini *et al* (2000), hyperglycaemia-induced ATP may trigger fibroblast hypertrophy, increased fibronectin, IL-6, and apoptosis via P2X7 receptor activation. TLR2/4 inhibition increased OCR, ECAR, and ATP in all groups, shifting ATP production from mitochondrial to glycolytic pathways, most likely due to TIRAP-mimicking effects enhancing MYD88-mediated glycolysis (Chen *et al*, 2020).

This study found that high glucose significantly reduced COL-1 secretion in untreated fibroblasts, consistent with previous findings linking hyperglycaemia to increased MMPs and AGEs (Argyropoulo *et al*, 2016; Andreea *et al*, 2008). In contrast, MGN3 and LPS treatments enhanced COL-1 secretion at both pre-diabetic and hyperglycaemic conditions, suggesting MGN3 may support ECM restoration in diabetic wounds. Hyperglycaemia is known to elevate MMP-1 and TGF $\beta$ 1, leading to collagen degradation, fibroblast hypertrophy, and reduced ECM production (Suryavanshi & Kulkarni, 2017; Vasko *et al*, 2009; Xuan *et al*, 2014, 2016; Wu & Derynck, 2009).

This project examined fibroblast proliferation following exposure to EGF and FGF2 in supernatants from fibroblasts, keratinocytes or M1 macrophages cultured under euglycemic or hyperglycaemic conditions.

Fibroblast proliferation was reduced when exposed to supernatants from fibroblasts, keratinocytes, or M1 macrophages cultured at hyperglycaemic versus pre-diabetic conditions. EGF inhibition further decreased proliferation only at 11mM, indicating EGF presence at low glucose levels. MGN3/LPS-treated fibroblast supernatants decreased fibroblast proliferation at 11mM but increased it at 30mM. TLR2/4 inhibition in MGN3-treated fibroblasts reduced fibroblast proliferation at both glucose levels, confirming TLR-dependent effects. Similarly, MGN3-treated keratinocyte supernatants reduced fibroblast proliferation only at 11 mM, with TLR2/4 inhibition decreasing it further, suggesting MGN3 acts via TLR2/4 at 11mM and via TLR4 at 30mM glycaemic conditions. M1 macrophage supernatants at 30mM conditions also suppressed fibroblast proliferation and EGF inhibition reduced proliferation only at 11mM. TLR2 inhibition at 11mM and MGN3 treatment under both glucose conditions decreased fibroblast proliferation, though MGN3 had no effect under hyperglycaemia unless combined with TLR2 inhibition. Overall, hyperglycaemia impaired EGF secretion and fibroblast proliferation, with the effect of MGN3 being TLR-dependent and varying with glucose level and cell type.

Fibroblast proliferation was reduced by supernatants obtained from fibroblasts cultured under hyperglycaemia. TLR4 inhibition increased fibroblast proliferation, but TLR4-inhibited supernatants from fibroblasts reduced proliferation of untreated fibroblasts whereas TLR2 inhibition had no such effect. MGN3-treated fibroblasts (at both glucose levels) produced supernatants that increased fibroblast proliferation, that was unaffected by FGF2 inhibition. MGN3/LPS-treated keratinocyte supernatants had no significant effect on fibroblast proliferation, and FGF2 inhibition had no impact, indicating low FGF2 secretion in keratinocyte supernatants. MGN3-treated macrophages reduced fibroblast proliferation at 11mM glucose, while TLR2 inhibition (in both untreated and MGN3-treated macrophages) increased fibroblast proliferation. Again, FGF2 inhibition had no effect, suggesting minimal contribution from FGF2 in macrophage supernatants.

Hyperglycaemia impairs wound healing by disrupting EGFR–PI3K/AKT signalling, likely via increased ROS (Xu *et al*, 2009). Fibroblasts exposed to high glucose become resistant to growth factors like IGF-I and EGF, reducing proliferation (Hehenberger & Hansson, 1997). Similar resistance has been observed in fibroblasts from diabetic ulcers, showing reduced

responsiveness to IGF-I, EGF, FGF2 and PDGF (Loots *et al*, 2002; Xu *et al*, 2018). Diabetic fibroblasts overexpress FGF2 mRNA and protein, linked to PKC- $\beta$ 1 upregulation (Vasko *et al*, 2009). Hyperglycaemia also increases glycated, less biologically active FGF2 (Gedaj *et al*, 2024; Facchiano *et al*, 2006). Inflammatory stimuli like LPS upregulate FGF2 via TLR2/4 activation in fibroblasts and keratinocytes (Rahimi *et al*, 2005; Akhtar *et al*, 2021; Saha *et al*, 2015), potentially through ERK1/2 signalling (Chen *et al*, 2019).

This study found that MGN3 reduced total ATP production in keratinocytes as glucose levels increased. At pre-diabetic conditions, untreated and LPS-treated cells relied heavily on glycolysis (82%), while MGN3-treated cells used it less (60%). Under hyperglycaemia, glycolytic activity increased in MGN3-treated cells (74%) compared to LPS-treated cells (63%), likely due to oxidative stress and impaired mitochondrial ATP production. Hyperglycaemia has been linked to mitochondrial dysfunction and increased ROS in keratinocytes, leading to TFAM depletion, mtDNA damage, and activation of ERK1/2–PI3K/Akt–IRF3 pathways (Rizwan *et al*, 2020; Rizwan *et al*, 2023), driving a shift from oxidative phosphorylation to glycolysis (Moura *et al*, 2019). TLR2/4 inhibition decreased OCR at 11mM in all groups, but increased OCR at 30mM conditions. Total ATP decreased with TLR inhibition at 11mM and, to a lesser extent, at 30mM, particularly following TLR2 inhibition of LPS-treated cells and TLR4 inhibition of untreated or MGN3-treated cells. TLR inhibition has been shown to shift metabolism from mitoATP to glycoATP (Krawczyk *et al*, 2010), potentially due to TIRAP-mediated MyD88 recruitment (Chen *et al*, 2020; Tan & Kagan, 2019). Hyperglycaemia may further promote this shift further towards glycoATP (Chou *et al*, 2022).

This study investigated MGN3's effect on keratinocyte production of growth factors (EGF, FGF2, TGF $\beta$ 1), NRF2, and antimicrobial peptides (LL37, BD2) under hyperglycaemic conditions. Hyperglycaemia increased EGF secretion in untreated keratinocytes compared to pre-diabetic conditions. EGF was upregulated by LPS at 11mM glucose and by both LPS and MGN3 under at 30mM glycaemic conditions, with MGN3 showing a stronger effect. LPS acted via TLR2, while MGN3 acted via both TLR2 and TLR4, as blocking these receptors reduced EGF secretion. Hyperglycaemia reduced FGF2 secretion in untreated cells. Both LPS

and MGN3 increased FGF2 at both glucose levels via TLR2 and TLR4. Inhibition of either TLR reduced FGF2 in all conditions, with no major difference between treatments.

Other studies have also indicated that LPS affects FGF2 signalling through TLR4 (Peng *et al*, 2024; Kurata *et al*, 2008). EGF production in keratinocytes stimulated with LPS has also shown to be mediated through TLR4 signalling (Müller-Decker *et al*, 2005; Kim *et al*, 2018; De *et al*, 2015). Under hyperglycaemic conditions, there is a reduction in keratinocyte-derived HB-EGF, which impairs keratinocyte proliferation (Shirakata *et al*, 2005). This decreased proliferation in hyperglycaemia is associated with several factors, including increased ROS levels due to oxidative stress, lowered EGF synthesis, and the buildup of AGEs (Wang and Grave, 2020; Shirakata *et al*, 2005; Tian *et al*, 2012).

Hyperglycaemia did not significantly affect TGFβ1 secretion in untreated keratinocytes. MGN3/LPS treatment reduced TGFβ1 at 11mM glucose; at 30mM, LPS increased TGFβ1 while MGN3 decreased it. TLR inhibition lowered TGFβ1 in both groups at 30mM. Reduced TGFβ1 from MGN3 may aid healing, as high TGFβ1 impairs keratinocyte proliferation and delays wound repair by activating inflammatory NF-kB pathways (Coffey *et al*, 1988; Pietenpol *et al*, 1990; Hogan *et al*, 2013; Luo *et al*, 2017). Hyperglycaemia increased intracellular and extracellular NRF2 in untreated keratinocytes. MGN3 raised NRF2 secretion at 11mM but reduced it at 30mM conditions. TLR inhibition had minimal impact on NRF2 beyond untreated levels. Intracellular NRF2 increased after MGN3 or LPS treatment at both glucose levels, independent of TLR2/4 (Braun *et al*, 2002; Villarreal-Ponce *et al*, 2020). LL37 and BD2 increased in keratinocyte lysates after LPS and MGN3 at 11mM glucose, with smaller rises at 30mM. Reduced LL37 activity is linked to poor wound healing in diabetes (Piipponen *et al*, 2020). LL37 promotes healing via autophagy activation (Xi *et al*, 2024), and BD2 aids clearance of PA in ischemic wounds (Casal *et al*, 2019).

In summary, these findings suggest that MGN3 stimulates the production of keratinocyte-derived EGF, FGF2, NRF2, LL37, and BD2 under hyperglycaemic conditions, while reducing the secretion of TGFβ1. Other studies have shown that hyperglycaemia disrupts growth factor and cytokine signalling pathways in keratinocytes (Raja *et al*., 2007; Pastar *et al*.,

2014). Another study by Braun *et al*, (2002) found NRF2 levels were reduced under hyperglycaemic conditions resulting in prolonged inflammation.

This project examined keratinocyte proliferation following exposure to EGF and FGF2 in supernatants from keratinocytes, fibroblasts or M1 macrophages cultured under euglycemic or hyperglycaemic conditions. Keratinocyte supernatants at hyperglycaemic conditions had no significant effect on keratinocyte proliferation. However, adding an EGF-blocking antibody reduced keratinocyte proliferation under both glucose conditions, confirming the presence of EGF. Supernatants from MGN3/LPS-treated keratinocytes (11mM) increased keratinocyte proliferation, while MGN3 alone (30mM) decreased it. TLR2/4 inhibition had no notable additional effect on keratinocyte proliferation. Keratinocyte proliferation was reduced by fibroblast-derived supernatants at 30mM compared to 11mM conditions. EGF inhibition reduced keratinocyte proliferation only following exposure to supernatants from 11mM-cultured fibroblasts, indicating a possible loss of EGF at 30mM conditions. MGN3-treated fibroblast-derived supernatants did not alter keratinocyte proliferation, potentially suggesting limited EGF induction. Macrophage-derived supernatants at 30mM glucose suppressed keratinocyte proliferation. Whilst TLR2 inhibition reduced keratinocyte proliferation following exposure to supernatants from 11mM-exposed macrophages, both TLR2 and TLR4 inhibition suppressed keratinocyte proliferation when exposed to supernatants from macrophages cultured under hyperglycaemia. EGF inhibition reduced keratinocyte proliferation at both glucose conditions, confirming presence of EGF in macrophage supernatants. MGN3-treated macrophage supernatants (at 11mM) increased keratinocyte proliferation, which was reversed by EGF inhibition. In contrast, MGN3/LPS-treated macrophage supernatants (at 30mM) decreased keratinocyte proliferation. TLR4 inhibition in these MGN3-treated macrophages restored keratinocyte proliferation, suggesting TLR4 modulates MGN3-driven secretory responses under hyperglycaemia.

Supernatants from Keratinocyte cultured at 30mM glucose reduced keratinocyte proliferation compared to those derived from 11mM conditions. FGF2 inhibition had no effect, indicating little involvement from FGF2. TLR2/4 inhibition in untreated keratinocytes increased keratinocyte proliferation at 11mM glucose only. MGN3/LPS-treated keratinocyte-derived supernatants enhanced Keratinocyte proliferation at both glucose

levels, whilst FGF2 inhibition reduced this effect at 30mM, suggesting appreciable FGF2 presence under hyperglycaemia. TLR2/4 inhibition of MGN3-treated keratinocytes reduced Keratinocyte proliferation, highlighting a TLR2-dependent response distinct from untreated cells. Supernatants from fibroblasts cultured at 30mM inhibited keratinocyte proliferation. MGN3-treated fibroblast-derived supernatants decreased keratinocyte proliferation at 11 mM but increased it at 30mM glycaemic conditions. FGF2 inhibition reduced Keratinocyte proliferation only with hyperglycaemic MGN3-treated fibroblast supernatants, indicating induced secretion of FGF2 under hyperglycaemia. TLR2/4 inhibition had no further effect on the proliferative properties of fibroblast-derived supernatants. Supernatants from macrophages cultured at 30mM reduced keratinocyte proliferation. MGN3-treated macrophage-derived supernatants decreased keratinocyte proliferation at 11mM glucose but had no effect at 30mM. FGF2 blockade had no impact on keratinocyte proliferation, suggesting FGF2 secretion from macrophages was not a contributing factor. TLR2/4 inhibition in macrophages also had no effect on keratinocyte proliferation at either glucose level.

Other studies have demonstrated that chronic hyperglycaemia inhibits keratinocyte proliferation (Terashi *et al*, 2005), although the underlying mechanisms for this effect remain unclear. Research by Facchiano *et al* (2006), found that FGF2 exposed to high glucose (>12.5mM) becomes glycated in as little as 30 minutes, significantly reducing its effectiveness on cells like keratinocytes. Hyperglycaemia has also been shown to impair EGF signalling via disrupted Akt activation, which contributes to delayed wound healing in diabetic patients (Xu *et al*, 2009).

The effect of MGN3 on the bactericidal activity of keratinocytes cultured euglycemic and hyperglycaemic conditions was measured against MRSA and PA in relation to antimicrobial peptide (BD2 and LL37) production. The recovery of MRSA and PA01 increased following exposure to cell lysate from keratinocytes cultured under hyperglycaemic conditions, indicating hyperglycaemia was inhibiting the bactericidal activity of keratinocytes. The addition of BD2 blocking antibody to lysates from untreated keratinocytes cultured under euglycemic conditions increased bacterial recovery further, confirming BD2 was present in appreciable amounts in the lysates of untreated keratinocytes cultured under euglycemic

(but not hyperglycaemic) conditions. The addition of LL37 blocking antibody to lysates from untreated keratinocytes cultured at pre-diabetic conditions increased bacterial recovery further, confirming LL37 was present in appreciable amounts in the lysates of untreated keratinocytes cultured at pre-diabetic conditions. The addition of LL37 blocking antibody to lysates from untreated keratinocytes cultured under hyperglycaemic conditions increased MRSA (but not PA) recovery further, confirming LL37 was sufficiently present in the lysates of untreated keratinocytes cultured under hyperglycaemic conditions to influence MRSA (but not PA). MRSA and PA recovery was significantly reduced following exposure to lysates from keratinocytes treated with MGN3 or LPS at pre-diabetic or hyperglycaemic conditions, suggesting MGN3 and LPS induced additional bactericidal activity against MRSA and PA in keratinocyte lysates. The addition of BD2 blocking antibody increased MRSA and PA recovery following exposure to lysates from keratinocytes treated with MGN3/LPS under euglycemic or hyperglycaemic conditions. Similarly, the addition of LL37 blocking antibody increased MRSA and PA recovery following exposure to lysates from keratinocytes treated with MGN3/LPS at pre-diabetic or hyperglycaemic conditions. These findings indicated both BD2 and LL37 peptide production were present in appreciable amounts in the supernatants of keratinocytes treated with MGN3 or LPS at both pre-diabetic and hyperglycaemic conditions.

Hyperglycaemia has been associated with reduced antimicrobial peptide activity in keratinocytes. Studies have demonstrated that impaired wound healing in diabetic patients can result from a suppression of BD2 expression due to hyperglycaemic conditions (Lan *et al*, 2012; Kareem and Mohammed, 2024; Cruz Díaz *et al*, 2015). Additionally, hyperglycaemia has been shown to suppress the activity of cathelicidin in keratinocytes (Hu *et al*, 2016). A randomized double-blind study showed the healing of diabetic foot ulcers with mild infection improved when LL37 cream was applied, suggesting LL37 expression is suppressed in diabetic patients under hyperglycaemic conditions (Miranda *et al*, 2023).

Lastly, this project examined the influence of MGN3 on NRF2 expression and activation in keratinocytes cultured at pre-diabetic and hyperglycaemic conditions, and subsequent NRF2-mediated MCP-1 secretion from keratinocytes. NRF2 expression was substantially increased by hyperglycaemia in untreated keratinocytes when compared to untreated

keratinocytes cultured at pre-diabetic conditions. In contrast, NRF2 expression was only increased in MGN3/LPS-treated keratinocytes cultured at pre-diabetic conditions. Hyperglycaemia did not significantly affect MCP-1 secretion from untreated keratinocytes. However, MGN3 treatment increased MCP-1 secretion from keratinocytes at both pre-diabetic and hyperglycaemic conditions. NRF2 inhibition reduced MCP-1 secretion from untreated and MGN3-treated keratinocytes at both glucose conditions, indicating MCP-1 production was at least in part regulated by NRF2 at both pre-diabetic and hyperglycaemic conditions. These findings suggest that NRF2 plays a key role in regulating MGN3 activities in keratinocytes at both pre-diabetic and hyperglycaemic conditions. Previous research has shown that NRF2 activation is linked to MCP-1 expression in keratinocytes, forming a crosstalk loop with macrophages that then secrete EGF in response to MCP-1 stimulation (Villarreal-Ponce *et al*, 2020). This activation is triggered by oxidative stress, which leads to NRF2 binding to antioxidant response elements (AREs) and activating other transcription factors (such as AP-1, NF- $\kappa$ B, STAT3), ultimately resulting in the release of MCP-1 from keratinocytes (Süntar *et al*, 2021; Schmidt *et al*, 2019; Sim *et al*, 2022; Merez-Sadowska *et al*, 2021).

## 7.2 Future Work

This study opens up several potential avenues for further exploration into the impact of MGN3 on wound healing. One area for investigation could be the effect of MGN3 on other immune cells that were not evaluated in this study. For instance, examining how MGN3 influences endothelial cells, which play a crucial role in wound repair, could provide valuable insights. Additionally, the impact of MGN3 on cell interactions and crosstalk could be explored by developing co-culture systems or 3D in vitro wound models. Animal studies, such as using diabetic mouse models, could help visualize MGN3's effect on wound healing in vivo. Microarray analysis could be employed to identify genes regulated by MGN3, while mechanistic studies could involve knockout cells, animal models, or gene silencing techniques like small interfering RNAs (siRNAs), microRNAs (miRNAs), or CRISPR gene editing to further dissect the underlying pathways. A potential direction for future research

could involve investigating the effect of MGN3 in other cell lines and on *ex vivo* cells derived from diabetic patients (e.g. immune cells) to determine if key findings of this project can be replicated. If some or all the findings can be successfully replicated, this could form a body of evidence to open the door for MGN3 as a potential topical treatment for impaired healing and/or infected wounds in diabetic patients, potentially in the form of wound dressings where MGN3 could be incorporated into hydrogels given its water-soluble nature.

### 7.3 Conclusion

This thesis has demonstrated that elevated glucose levels exert multifaceted detrimental effects on critical cell types involved in wound healing. Specifically, chronic hyperglycaemia impairs macrophage differentiation and phagocytic function, disrupts cellular metabolism and cell cycle dynamics, and hinders fibroblast and keratinocyte activity, each of which plays a vital role in the wound repair cascade (see Figure 7.1).

Importantly, this work has shown that MGN3 can counteract many of these dysfunctions. MGN3 significantly improved fibroblast and keratinocyte metabolism by enhancing mitochondrial respiration, particularly under hyperglycaemic conditions. It also promoted cell proliferation and growth factor production in fibroblasts and keratinocytes, enhanced epidermal and dermal wound closure primarily via increased migration, and upregulated collagen-1 production in fibroblasts regardless of glucose concentration. Furthermore, MGN3 attenuated hyperglycaemia-induced overproduction of TGF $\beta$ 1 by keratinocytes while simultaneously increasing macrophage-derived MCP-1, supporting better coordination between immune and tissue-resident cells during wound healing.

Crucially, MGN3 restored macrophage antimicrobial function under hyperglycaemic stress. A 24-hour exposure to MGN3 enhanced M1 macrophage phagocytosis of MRSA and PA biofilms and stimulated secretion of antimicrobial mediators including lysozyme, LL37, and BD2. These effects directly address the impaired immune clearance seen in DFUs and provide strong preclinical justification for further therapeutic exploration.

Mechanistically, MGN3 exerted its effects at least partly through TLR2 and TLR4 signalling pathways, which were shown to be critical in mediating enhanced phagocytosis, improved

fibroblast and keratinocyte metabolism, and increased migratory activity. In addition, MGN3 upregulated the anti-inflammatory transcription factor NRF2, both in terms of protein expression at pre-diabetic conditions and functional activity across both glycaemic environments, highlighting its potential to modulate redox balance and inflammation in diabetic wounds.

The wider implications of this research could be significant for diabetic patients with infected or non-infected diabetic foot ulcers (DFUs), as MGN3 may offer a novel therapeutic approach to enhance wound healing and modulate immune responses, potentially improving clinical outcomes and reducing complications associated with chronic wounds in diabetes. As a wound healing and immune-regulating therapy, MGN3 could provide a promising adjunct or alternative to current treatments, addressing both the underlying inflammation and impaired healing often seen in diabetic patients.

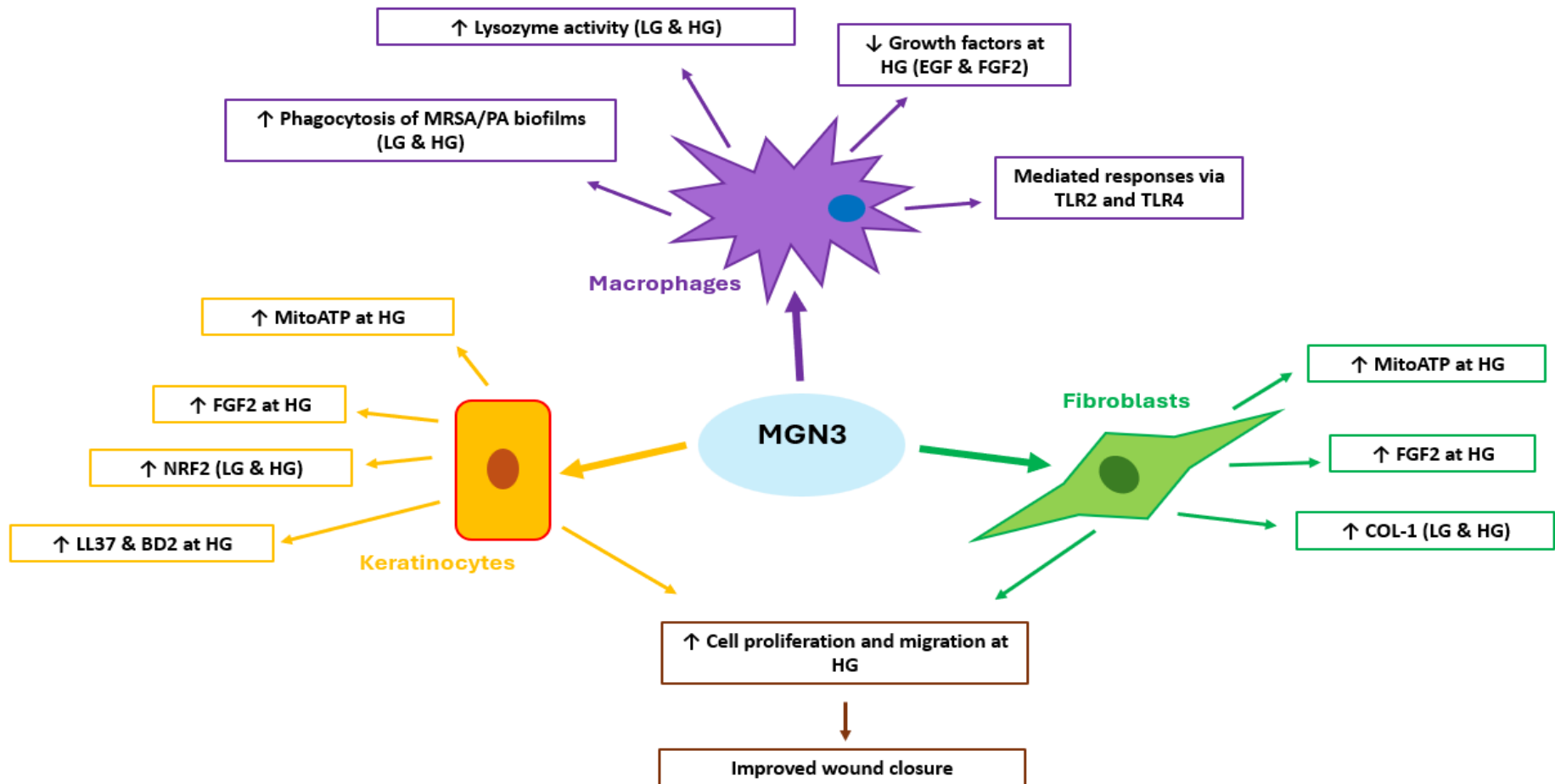


**Figure 7. 1: The Effects of MGN3 on different cell types involved in wound healing.** The overview of the effects of MGN3 on macrophage, fibroblast and keratinocyte cell function at low glucose (LG) and high glucose (HG) conditions.

## **Chapter 8: References**

- Adam, J., Ramracheya, R., Chibalina, M.V., Ternette, N., Hamilton, A., Tarasov, A.I., Zhang, Q., Rebelato, E., Rorsman, N.J., Martín-del-Río, R. and Lewis, A., 2017. Fumarate hydratase deletion in pancreatic  $\beta$  cells leads to progressive diabetes. *Cell Reports*, 20(13), pp.3135-3148.
- Adeva-Andany, M.M., González-Lucán, M., Donapetry-García, C., Fernández-Fernández, C. and Ameneiros-Rodríguez, E., 2016. Glycogen metabolism in humans. *BBA clinical*, 5, pp.85-100.
- Afshar, M. and Gallo, R.L., 2013. Innate immune defense system of the skin. *Veterinary dermatology*, 24(1), pp.32-e9.
- Agier, J., Efenberger, M. and Brzezińska-Błaszczyk, E., 2015. Cathelicidin impact on inflammatory cells. *Central European Journal of Immunology*, 40(2), pp.225-235.
- Ai, G., Shao, X., Meng, M., Song, L., Qiu, J., Wu, Y., Zhou, J., Cheng, J. and Tong, X., 2017. Epidermal growth factor promotes proliferation and maintains multipotency of continuous cultured adipose stem cells via activating STAT signal pathway in vitro. *Medicine*, 96(30), p.e7607.
- Akhtar, R., Tahir, H., Stewart, E., Wei, R., Mohammed, I. and Amoaku, W.M., 2021. Toll-like receptor signalling pathways regulate hypoxic stress induced fibroblast growth factor but not vascular endothelial growth factor-A in human microvascular endothelial cells. *International Journal of Translational Medicine*, 1(1), pp.25-38.
- Akira, S. and Sato, S., 2003. Toll-like receptors and their signaling mechanisms. *Scandinavian journal of infectious diseases*, 35(9), pp.555-562.
- Andreea, S.I., Marieta, C. and Anca, D., 2008. AGEs and glucose levels modulate type I and III procollagen mRNA synthesis in dermal fibroblasts cells culture. *Experimental Diabetes Research*, 2008.
- Antonetti, D.A., Reynet, C. and Kahn, C.R., 1995. Increased expression of mitochondrial-encoded genes in skeletal muscle of humans with diabetes mellitus. *The Journal of clinical investigation*, 95(3), pp.1383-1388.
- Argyropoulos, A.J., Robichaud, P., Balimunkwe, R.M., Fisher, G.J., Hammerberg, C., Yan, Y. and Quan, T., 2016. Alterations of dermal connective tissue collagen in diabetes: molecular basis of aged-appearing skin. *PloS one*, 11(4), p.e0153806.
- Arneth, B., Arneth, R. and Shams, M., 2019. Metabolomics of type 1 and type 2 diabetes. *International journal of molecular sciences*, 20(10), p.2467.
- Asif, M.S., 2020. *The Effects of Dietary Fibres on Inflammatory Processes under Hyperglycaemic Conditions* (Doctoral dissertation, Manchester Metropolitan University).
- Asif, M.S., Tan, S., El Mohtadi, M. and Ashworth, J., 2023. Biobran (MGN-3) acts through toll-like receptor-4 (TRL-4) and reverses the detrimental effects of hyperglycaemia on phagocytosis.
- Awad, A.S., You, H., Gao, T., Cooper, T.K., Nedospasov, S.A., Vacher, J., Wilkinson, P.F., Farrell, F.X. and Reeves, W.B., 2015. Macrophage-derived tumor necrosis factor- $\alpha$  mediates diabetic renal injury. *Kidney international*, 88(4), pp.722-733.
- Awad, K., Kakkola, L. and Julkunen, I., 2024. High Glucose Increases Lactate and Induces the Transforming Growth Factor Beta-Smad 1/5 Atherogenic Pathway in Primary Human Macrophages. *Biomedicines*, 12(7), p.1575.
- Ayala, T.S., Tessaro, F.H.G., Jannuzzi, G.P., Bella, L.M., Ferreira, K.S. and Martins, J.O., 2019. High glucose environments interfere with bone marrow-derived macrophage inflammatory mediator release, the TLR4 pathway and glucose metabolism. *Scientific reports*, 9(1), p.11447.

- Baig, M.S., Banu, A., Zehravi, M., Rana, R., Burle, S.S., Khan, S.L., Islam, F., Siddiqui, F.A., Massoud, E.E.S., Rahman, M.H. and Cavalu, S., 2022. An overview of diabetic foot ulcers and associated problems with special emphasis on treatments with antimicrobials. *Life*, 12(7), p.1054.
- Baracca, A., Sgarbi, G., Padula, A. and Solaini, G., 2013. Glucose plays a main role in human fibroblasts adaptation to hypoxia. *The international journal of biochemistry & cell biology*, 45(7), pp.1356-1365.
- Barker, J.N., Griffiths, C.E., Nickoloff, B.J., Mitra, R.S. and Dixit, V.M., 1991. Keratinocytes as initiators of inflammation. *The Lancet*, 337(8735), pp.211-214.
- Basu, A.K., Hanrahan, C.J., Malia, S.A., Kumar, S., Bizanek, R. and Tomasz, M., 1993. Effect of site specifically located mitomycin C-DNA monoadducts on in vitro DNA synthesis by DNA polymerases. *Biochemistry*, 32(18), pp.4708-4718.
- Bautista-Hernández, L.A., Gómez-Olivares, J.L., Buentello-Volante, B. and Bautista-de Lucio, V.M., 2017. Fibroblasts: the unknown sentinels eliciting immune responses against microorganisms. *European Journal of Microbiology and Immunology*, 7(3), pp.151-157.
- Beckman, K.B. and Ames, B.N., 1998. The free radical theory of aging matures. *Physiological reviews*.
- Bermudez-Brito, M., Sahasrabudhe, N.M., Rösch, C., Schols, H.A., Faas, M.M. and de Vos, P., 2015. The impact of dietary fibers on dendritic cell responses in vitro is dependent on the differential effects of the fibers on intestinal epithelial cells. *Molecular nutrition & food research*, 59(4), pp.698-710.
- Bertani, B. and Ruiz, N., 2018. Function and biogenesis of lipopolysaccharides. *Ecosal plus*, 8(1), pp.10-1128.
- Bikfalvi, A., Klein, S., Pintucci, G. and Rifkin, D.B., 1997. Biological roles of fibroblast growth factor-2. *Endocrine reviews*, 18(1), pp.26-45.
- Botelho, R.J. and Grinstein, S., 2011. Phagocytosis. *Current Biology*, 21(14), pp.R533-R538.
- Bowyer, A., Baardsnes, J., Ajamian, E., Zhang, L. and Cygler, M., 2011. Characterization of interactions between LPS transport proteins of the Lpt system. *Biochemical and biophysical research communications*, 404(4), pp.1093-1098.
- Braun, S., Hanselmann, C., Gassmann, M.G., auf dem Keller, U., Born-Berclaz, C., Chan, K., Kan, Y.W. and Werner, S., 2002. Nrf2 transcription factor, a novel target of keratinocyte growth factor action which regulates gene expression and inflammation in the healing skin wound. *Molecular and cellular biology*.
- Brereton, M.F., Rohm, M., Shimomura, K., Holland, C., Tornovsky-Babeay, S., Dadon, D., Iberl, M., Chibalina, M.V., Lee, S., Glaser, B. and Dor, Y., 2016. Hyperglycaemia induces metabolic dysfunction and glycogen accumulation in pancreatic  $\beta$ -cells. *Nature communications*, 7(1), p.13496.
- Brizeno, L.A.C., Assreuy, A.M.S., Alves, A.P.N., Sousa, F.B., Silva, P.G.D.B., de Sousa, S.C.O.M., Lascane, N.A., Evangelista, J.S.A.M. and Mota, M.R.L., 2016. Delayed healing of oral mucosa in a diabetic rat model: Implication of TNF- $\alpha$ , IL-1 $\beta$  and FGF-2. *Life sciences*, 155, pp.36-47.
- Brun, T., Li, N., Jourdain, A.A., Gaudet, P., Duhamel, D., Meyer, J., Bosco, D. and Maechler, P., 2015. Diabetogenic milieus induce specific changes in mitochondrial transcriptome and differentiation of human pancreatic islets. *Human molecular genetics*, 24(18), pp.5270-5284.

- Buranasin, P., Mizutani, K., Iwasaki, K., Pawaputanon Na Mahasarakham, C., Kido, D., Takeda, K. and Izumi, Y., 2018. High glucose-induced oxidative stress impairs proliferation and migration of human gingival fibroblasts. *PLoS one*, 13(8), p.e0201855.
- Canady, J., Arndt, S., Karrer, S. and Bosserhoff, A.K., 2013. Increased KGF expression promotes fibroblast activation in a double paracrine manner resulting in cutaneous fibrosis. *Journal of Investigative Dermatology*, 133(3), pp.647-657.
- Cannon, G.J. and Swanson, J.A., 1992. The macrophage capacity for phagocytosis. *Journal of cell science*, 101(4), pp.907-913.
- Cargnello, M. and Roux, P.P., 2011. Activation and function of the MAPKs and their substrates, the MAPK-activated protein kinases. *Microbiology and molecular biology reviews*, 75(1), pp.50-83.
- Casal, D., Iria, I., Ramalho, J.S., Alves, S., Mota-Silva, E., Mascarenhas-Lemos, L., Pontinha, C., Guadalupe-Cabral, M., Ferreira-Silva, J., Ferraz-Oliveira, M. and Vassilenko, V., 2019. BD-2 and BD-3 increase skin flap survival in a model of ischemia and *Pseudomonas aeruginosa* infection. *Scientific Reports*, 9(1), p.7854.
- Cerca, N., Jefferson, K.K., Oliveira, R., Pier, G.B. and Azeredo, J., 2006. Comparative antibody-mediated phagocytosis of *Staphylococcus epidermidis* cells grown in a biofilm or in the planktonic state. *Infection and immunity*, 74(8), pp.4849-4855.
- Chen, C., Ko, Y., Delannoy, M., Ludtke, S.J., Chiu, W. and Pedersen, P.L., 2004. Mitochondrial ATP synthasome: three-dimensional structure by electron microscopy of the ATP synthase in complex formation with carriers for Pi and ADP/ATP. *Journal of Biological Chemistry*, 279(30), pp.31761-31768.
- Chen, C., Ma, X., Yang, C., Nie, W., Zhang, J., Li, H., Rong, P., Yi, S. and Wang, W., 2018. Hypoxia potentiates LPS-induced inflammatory response and increases cell death by promoting NLRP3 inflammasome activation in pancreatic  $\beta$  cells. *Biochemical and biophysical research communications*, 495(4), pp.2512-2518.
- Chen, L., Zheng, L., Chen, P. and Liang, G., 2020. Myeloid differentiation primary response protein 88 (MyD88): the central hub of TLR/IL-1R signaling. *Journal of medicinal chemistry*, 63(22), pp.13316-13329.
- Chen, L.C., Shibu, M.A., Liu, C.J., Han, C.K., Ju, D.T., Chen, P.Y., Viswanadha, V.P., Lai, C.H., Kuo, W.W. and Huang, C.Y., 2019. ERK1/2 mediates the lipopolysaccharide-induced upregulation of FGF-2, uPA, MMP-2, MMP-9 and cellular migration in cardiac fibroblasts. *Chemico-Biological Interactions*, 306, pp.62-69.
- Chen, Y., Yang, S., Lovisa, S., Ambrose, C.G., McAndrews, K.M., Sugimoto, H. and Kalluri, R., 2021. Type-I collagen produced by distinct fibroblast lineages reveals specific function during embryogenesis and Osteogenesis Imperfecta. *Nature communications*, 12(1), p.7199.
- Cheng, T., Torres, N.S., Chen, P., Srinivasan, A., Cardona, S., Lee, G.C., Leung, K.P., Lopez-Ribot, J.L. and Ramasubramanian, A.K., 2021. A facile high-throughput model of surface-independent *Staphylococcus aureus* biofilms by spontaneous aggregation. *MSphere*, 6(2), pp.10-1128.
- Chiu, S. and Bharat, A., 2016. Role of monocytes and macrophages in regulating immune response following lung transplantation. *Current opinion in organ transplantation*, 21(3), pp.239-245.
- Chou, W.C., Rampanelli, E., Li, X. and Ting, J.P.Y., 2022. Impact of intracellular innate immune receptors on immunometabolism. *Cellular & molecular immunology*, 19(3), pp.337-351.

- Cialdai, F., Risaliti, C. and Monici, M., 2022. Role of fibroblasts in wound healing and tissue remodeling on Earth and in space. *Frontiers in bioengineering and biotechnology*, 10, p.958381.
- Ciesielska, A., Matyjek, M. and Kwiatkowska, K., 2021. TLR4 and CD14 trafficking and its influence on LPS-induced pro-inflammatory signaling. *Cellular and molecular life sciences*, 78, pp.1233-1261.
- Coffey Jr, R.J., Bascom, C.C., Sipes, N.J., Graves-Deal, R., Weissman, B.E. and Moses, H.L., 1988. Selective inhibition of growth-related gene expression in murine keratinocytes by transforming growth factor  $\beta$ . *Molecular and cellular biology*, 8(8), pp.3088-3093.
- Colleselli, K., Stierschneider, A. and Wiesner, C., 2023. An update on toll-like receptor 2, its function and dimerization in pro-and anti-inflammatory processes. *International Journal of Molecular Sciences*, 24(15), p.12464.
- Cong, L.N., Chen, H., Li, Y., Zhou, L., McGibbon, M.A., Taylor, S.I. and Quon, M.J., 1997. Physiological role of Akt in insulin-stimulated translocation of GLUT4 in transfected rat adipose cells. *Molecular endocrinology*, 11(13), pp.1881-1890.
- Coordt, M.C., Ruhe, R.C. and McDonald, R.B., 1995. Aging and insulin secretion. *Proceedings of the Society for Experimental Biology and Medicine*, 209(3), pp.213-222.
- Correa-Gallegos, D., Jiang, D. and Rinkevich, Y., 2021. Fibroblasts as confederates of the immune system. *Immunological reviews*, 302(1), pp.147-162.
- Cruz Díaz, L.A., Flores Miramontes, M.G., Chávez Hurtado, P., Allen, K., Gonzalez Ávila, M. and Prado Montes de Oca, E., 2015. Ascorbic Acid, Ultraviolet C Rays, and Glucose but not Hyperthermia Are Elicitors of Human  $\beta$ -Defensin 1 mRNA in Normal Keratinocytes. *BioMed Research International*, 2015(1), p.714580.
- Cucak, H., Grunnet, L.G. and Rosendahl, A., 2014. Accumulation of M1-like macrophages in type 2 diabetic islets is followed by a systemic shift in macrophage polarization. *Journal of leukocyte biology*, 95(1), pp.149-160.
- Dan'shina, P.V., Schmalhausen, E.V., Arutiunov, D.Y., Pleten', A.P. and Muronetz, V.I., 2003. Acceleration of glycolysis in the presence of the non-phosphorylating and the oxidized phosphorylating glyceraldehyde-3-phosphate dehydrogenases. *Biochemistry (Moscow)*, 68, pp.593-600.
- Dasu, M.R. and Jialal, I., 2011. Free fatty acids in the presence of high glucose amplify monocyte inflammation via Toll-like receptors. *American journal of physiology-endocrinology and metabolism*, 300(1), pp.E145-E154.
- Dasu, M.R., Devaraj, S., Zhao, L., Hwang, D.H. and Jialal, I., 2008. High glucose induces toll-like receptor expression in human monocytes: mechanism of activation. *Diabetes*, 57(11), pp.3090-3098.
- Davies, K.M., Strauss, M., Daum, B., Kief, J.H., Osiewacz, H.D., Rycovska, A., Zickermann, V. and Kühlbrandt, W., 2011. Macromolecular organization of ATP synthase and complex I in whole mitochondria. *Proceedings of the National Academy of Sciences*, 108(34), pp.14121-14126.
- De Kievit, T.R., 2009. Quorum sensing in *Pseudomonas aeruginosa* biofilms. *Environmental microbiology*, 11(2), pp.279-288.
- de Oliveira, R.D., Novello, V., da Silva, L.F., Gomez, J.G.C. and Le Roux, G.A.C., 2021. Glucose metabolism in *Pseudomonas aeruginosa* is cyclic when producing Polyhydroxyalkanoates and Rhamnolipids. *Journal of Biotechnology*, 342, pp.54-63.

- de Vor, L., Rooijackers, S.H. and van Strijp, J.A., 2020. Staphylococci evade the innate immune response by disarming neutrophils and forming biofilms. *FEBS letters*, 594(16), pp.2556-2569.
- De, S., Zhou, H., DeSantis, D., Croniger, C.M., Li, X. and Stark, G.R., 2015. Erlotinib protects against LPS-induced endotoxicity because TLR4 needs EGFR to signal. *Proceedings of the National Academy of Sciences*, 112(31), pp.9680-9685.
- Peng, B., Dai, Q., Liu, X. and Jiang, S., 2024. Fraxin alleviates oral lichen planus by suppressing OCT3-mediated activation of FGF2/NF- $\kappa$ B pathway. *Naunyn-Schmiedeberg's Archives of Pharmacology*, pp.1-17.
- Deshmane, S.L., Kremlev, S., Amini, S. and Sawaya, B.E., 2009. Monocyte chemoattractant protein-1 (MCP-1): an overview. *Journal of interferon & cytokine research*, 29(6), pp.313-326.
- Devaraj, S. and Jialal, I., 2009. Increased secretion of IP-10 from monocytes under hyperglycemia is via the TLR2 and TLR4 pathway. *Cytokine*, 47(1), pp.6-10.
- Devaraj, S., Dasu, M.R., Rockwood, J., Winter, W., Griffen, S.C. and Jialal, I., 2008. Increased toll-like receptor (TLR) 2 and TLR4 expression in monocytes from patients with type 1 diabetes: further evidence of a proinflammatory state. *The journal of clinical endocrinology & metabolism*, 93(2), pp.578-583.
- Di Martino, P., 2018. Extracellular polymeric substances, a key element in understanding biofilm phenotype. *AIMS microbiology*, 4(2), p.274.
- Dipietro, L.A., Reintjes, M.G., Low, Q.E.H., Levi, B. and Gamelli, R.L., 2001. Modulation of macrophage recruitment into wounds by monocyte chemoattractant protein-1. *Wound Repair and Regeneration*, 9(1), pp.28-33.
- Dodson, M., Shakya, A., Anandhan, A., Chen, J., Garcia, J.G. and Zhang, D.D., 2022. NRF2 and diabetes: the good, the bad, and the complex. *Diabetes*, 71(12), pp.2463-2476.
- Du, Q., Fu, Y.X., Shu, A.M., Lv, X., Chen, Y.P., Gao, Y.Y., Chen, J., Wang, W., Lv, G.H., Lu, J.F. and Xu, H.Q., 2021. Loganin alleviates macrophage infiltration and activation by inhibiting the MCP-1/CCR2 axis in diabetic nephropathy. *Life sciences*, 272, p.118808.
- Duberley, K.E., Heales, S.J.R., Abramov, A.Y., Chalasani, A., Land, J.M., Rahman, S. and Hargreaves, I.P., 2014. Effect of Coenzyme Q10 supplementation on mitochondrial electron transport chain activity and mitochondrial oxidative stress in Coenzyme Q10 deficient human neuronal cells. *The international journal of biochemistry & cell biology*, 50, pp.60-63.
- Duque, G.A., and Descoteaux, A., 2014. Macrophage cytokines: involvement in immunity and infectious diseases. *Frontiers in immunology*, 5, p.491.
- Duraisamy, Y., Slevin, M., Smith, N., Bailey, J., Zweit, J., Smith, C., Ahmed, N. and Gaffney, J., 2001. Effect of glycation on basic fibroblast growth factor induced angiogenesis and activation of associated signal transduction pathways in vascular endothelial cells: possible relevance to wound healing in diabetes. *Angiogenesis*, 4, pp.277-288.
- Edgar, L., Akbar, N., Braithwaite, A.T., Krausgruber, T., Gallart-Ayala, H., Bailey, J., Corbin, A.L., Khojraty, T.E., Chai, J.T., Alkhalil, M. and Rendeiro, A.F., 2021. Hyperglycemia induces trained immunity in macrophages and their precursors and promotes atherosclerosis. *Circulation*, 144(12), pp.961-982.
- Egshatyan, L., Kashtanova, D., Popenko, A., Tkacheva, O., Tyakht, A., Alexeev, D., Karamnova, N., Kostyukova, E., Babenko, V., Vakhitova, M. and Boytsov, S., 2016. Gut microbiota and diet in patients with different glucose tolerance. *Endocrine Connections*, 5(1), pp.1-9.
- Eliasson, L., Abdulkader, F., Braun, M., Galvanovskis, J., Hoppa, M.B. and Rorsman, P., 2008. Novel aspects of the molecular mechanisms controlling insulin secretion. *The Journal of physiology*, 586(14), pp.3313-3324.

- Elliott, S.S., Keim, N.L., Stern, J.S., Teff, K. and Havel, P.J., 2002. Fructose, weight gain, and the insulin resistance syndrome. *The American journal of clinical nutrition*, 76(5), pp.911-922.
- El-Mahmoudy, A., Shimizu, Y., Shiina, T., Matsuyama, H., Nikami, H. and Takewaki, T., 2005. Macrophage-derived cytokine and nitric oxide profiles in type I and type II diabetes mellitus: effect of thymoquinone. *Acta Diabetologica*, 42, pp.23-30.
- Elsaid, A.F., Shaheen, M. and Ghoneum, M., 2018. Biobran/MGN-3, an arabinoxylan rice bran, enhances NK cell activity in geriatric subjects: A randomized, double-blind, placebo-controlled clinical trial. *Experimental and therapeutic medicine*, 15(3), pp.2313-2320.
- El-Zayat, S.R., Sibaii, H. and Manna, F.A., 2019. Toll-like receptors activation, signaling, and targeting: an overview. *Bulletin of the National Research Centre*, 43(1), pp.1-12.
- Epelman, S., Lavine, K.J. and Randolph, G.J., 2014. Origin and functions of tissue macrophages. *Immunity*, 41(1), pp.21-35.
- Facchiano, F., D'Arcangelo, D., Russo, K., Fogliano, V., Mennella, C., Ragone, R., Zambruno, G., Carbone, V., Ribatti, D., Peschle, C. and Capogrossi, M.C., 2006. Glycated fibroblast growth factor-2 is quickly produced in vitro upon low-millimolar glucose treatment and detected in vivo in diabetic mice. *Molecular endocrinology*, 20(11), pp.2806-2818.
- Fadel, A., Plunkett, A., Li, W., Ranneh, Y., Tessu Gyamfi, V.E., Salmon, Y., Nyaranga, R.R. and Ashworth, J., 2018. Arabinoxylans from rice bran and wheat immunomodulatory potentials: a review article. *Nutrition & Food Science*, 48(1), pp.97-110.
- Falanga, V., 2005. Wound healing and its impairment in the diabetic foot. *The Lancet*, 366(9498), pp.1736-1743.
- Fang, W.C. and Lan, C.C.E., 2023. The epidermal keratinocyte as a therapeutic target for management of diabetic wounds. *International Journal of Molecular Sciences*, 24(5), p.4290.
- Farhat, K., Riekenberg, S., Heine, H., Debarry, J., Lang, R., Mages, J., Buwitt-Beckmann, U., Röschmann, K., Jung, G., Wiesmüller, K.H. and Ulmer, A.J., 2008. Heterodimerization of TLR2 with TLR1 or TLR6 expands the ligand spectrum but does not lead to differential signaling. *Journal of Leucocyte Biology*, 83(3), pp.692-701.
- Farooq, M., Khan, A.W., Kim, M.S. and Choi, S., 2021. The role of fibroblast growth factor (FGF) signaling in tissue repair and regeneration. *Cells*, 10(11), p.3242.
- Fujihara, M., Muroi, M., Tanamoto, K.I., Suzuki, T., Azuma, H. and Ikeda, H., 2003. Molecular mechanisms of macrophage activation and deactivation by lipopolysaccharide: roles of the receptor complex. *Pharmacology & therapeutics*, 100(2), pp.171-194.
- Fukuda, K., Kawata, S., Inui, Y., Higashiyama, S., Matsuda, Y., Igura, T., Tamura, S., Taniguchi, N. and Matsuzawa, Y., 1997. High concentration of glucose increases mitogenic responsiveness to heparin-binding epidermal growth factor-like growth factor in rat vascular smooth muscle cells. *Arteriosclerosis, thrombosis, and vascular biology*, 17(10), pp.1962-1968.
- Fukushi, A., Kim, H.D., Chang, Y.C. and Kim, C.H., 2022. Revisited metabolic control and reprogramming cancers by means of the warburg effect in tumor cells. *International journal of molecular sciences*, 23(17), p.10037.
- Gai, C., Li, T., Zhao, Y., Cheng, Y., Song, Y., Luo, Q., Liu, D. and Wang, Z., 2024. Mesenchymal stromal cells deliver H2S-enhanced Nrf2 via extracellular vesicles to mediate mitochondrial homeostasis for repairing hypoxia-ischemia brain damage. *Free Radical Biology and Medicine*, 225, pp.528-545.

- Gasmi, A., Peana, M., Arshad, M., Butnariu, M., Menzel, A. and Bjørklund, G., 2021. Krebs cycle: activators, inhibitors and their roles in the modulation of carcinogenesis. *Archives of Toxicology*, 95(4), pp.1161-1178.
- Gędaj, A., Gregorczyk, P., Żukowska, D., Chorążewska, A., Ciura, K., Kalka, M., Porębska, N. and Opaliński, Ł., 2024. Glycosylation of FGF/FGFR: an underrated sweet code regulating cellular signaling programs. *Cytokine & Growth Factor Reviews*.
- Gęgotek, A. and Skrzydlewska, E., 2015. The role of transcription factor Nrf2 in skin cells metabolism. *Archives of Dermatological Research*, 307, pp.385-396.
- Genova, J., Zheliaskova, A. and Mitov, M.D., 2007. Monosaccharides (fructose, glucose) and disaccharides (sucrose, trehalose) influence the elasticity of SOPC membranes. *Journal of optoelectronics and advanced materials*, 9(2), p.427.
- Ghoneum, M. and Agrawal, S., 2011. Activation of human monocyte-derived dendritic cells in vitro by the biological response modifier arabinoxylan rice bran (MGN-3/Biobran). *International journal of immunopathology and pharmacology*, 24(4), pp.941-948.
- Ghoneum, M. and Agrawal, S., 2014. MGN-3/Biobran enhances generation of cytotoxic CD8+ T cells via upregulation of DEC-205 expression on dendritic cells. *International journal of immunopathology and pharmacology*, 27(4), pp.523-530.
- Ghoneum, M. and Brown, J., 1999. NK immunorestitution of cancer patients by MGN-3, a modified arabinoxylan rice bran (study of 32 patients followed for up to 4 years). *Anti-aging medical therapeutics*, 3, pp.217-226.
- Ghoneum, M. and Jewett, A., 2000. Production of tumor necrosis factor-alpha and interferon-gamma from human peripheral blood lymphocytes by MGN-3, a modified arabinoxylan from rice bran, and its synergy with interleukin-2 in vitro. *Cancer detection and prevention*, 24(4), pp.314-324.
- Ghoneum, M. and Matsuura, M., 2004. Augmentation of macrophage phagocytosis by modified arabinoxylan rice bran (MGN-3/biobran). *International journal of immunopathology and pharmacology*, 17(3), pp.283-292.
- Ghoneum, M., 1998. Enhancement of human natural killer cell activity by modified arabinoxylane from rice bran (MGN-3). *International Journal of Immunotherapy*, 14(2), pp.89-99
- Ghoneum, M., Badr El-Din, N. K., Abdel Fattah, S. M. and Tolentino, L., 2013. Arabinoxylan rice bran (MGN-3/Biobran) provides protection against whole-body irradiation in mice via restoration of hematopoietic tissues. *Journal of Radiation Research*, 54(3) pp. 419-429
- Ghoneum, M., Matsuura, M. and Gollapudp, S., 2008. Modified arabinoxylan rice bran (MGN-3/Biobran) enhances intracellular killing of microbes by human phagocytic cells in vitro. *International journal of immunopathology and pharmacology*, 21(1), pp.87-95.
- Ghoneum, M.H. and El Sayed, N.S., 2021. Protective Effect of Biobran/MGN-3 against Sporadic Alzheimer's Disease Mouse Model: Possible Role of Oxidative Stress and Apoptotic Pathways. *Oxidative Medicine and Cellular Longevity*, 2021(1), p.8845064.
- Gnaiger, E., 2023. Complex II ambiguities—FADH2 in the electron transfer system. *Journal of Biological Chemistry*, p.105470.
- Gnauck, A., Lentle, R.G. and Kruger, M.C., 2016. The characteristics and function of bacterial lipopolysaccharides and their endotoxic potential in humans. *International reviews of immunology*, 35(3), pp.189-218.

- Godowski, P.J., 2005. A smooth operator for LPS responses. *Nature immunology*, 6(6), pp.544-546.
- Gonzalez, Y., Herrera, M.T., Soldevila, G., Garcia-Garcia, L., Fabián, G., Pérez-Armendariz, E.M., Bobadilla, K., Guzmán-Beltrán, S., Sada, E. and Torres, M., 2012. High glucose concentrations induce TNF- $\alpha$  production through the down-regulation of CD33 in primary human monocytes. *BMC immunology*, 13, pp.1-14.
- Gopalakrishnan, A. and Salgame, P., 2016. Toll-like receptor 2 in host defense against *Mycobacterium tuberculosis*: to be or not to be—that is the question. *Current Opinion in Immunology*, 42, pp.76-82.
- Govers, C., Tang, Y., Stolte, E.H., Wichers, H.J. and Mes, J.J., 2020. Wheat-derived arabinoxylans reduced M2-macrophage functional activity, but enhanced monocyte-recruitment capacity. *Food & Function*, 11(8), pp.7073-7083.
- Grewal, I.S., Rutledge, B.J., Fiorillo, J.A., Gu, L., Gladue, R.P., Flavell, R.A. and Rollins, B.J., 1997. Transgenic monocyte chemoattractant protein-1 (MCP-1) in pancreatic islets produces monocyte-rich insulinitis without diabetes: abrogation by a second transgene expressing systemic MCP-1. *Journal of immunology (Baltimore, Md.: 1950)*, 159(1), pp.401-408.
- Grosick, R., Alvarado-Vazquez, P.A., Messersmith, A.R. and Romero-Sandoval, E.A., 2018. High glucose induces a priming effect in macrophages and exacerbates the production of pro-inflammatory cytokines after a challenge. *Journal of pain research*, pp.1769-1778.
- Ha, S.W., Seo, Y.K., Kim, J.G., Kim, I.S., Sohn, K.Y., Lee, B.H. and Kim, B.W., 1997. Effect of high glucose on synthesis and gene expression of collagen and fibronectin in cultured vascular smooth muscle cells. *Experimental & Molecular Medicine*, 29(1), pp.59-64.
- Haas, M.R., Nguyen, D.V. and Shook, B.A., 2021. Recovery of altered diabetic myofibroblast heterogeneity and gene expression are associated with CD301b+ macrophages. *Biomedicines*, 9(12), p.1752.
- Hamed, S., Ullmann, Y., Egozi, D., Daod, E., Hellou, E., Ashkar, M., Gilhar, A. and Teot, L., 2011. Fibronectin potentiates topical erythropoietin-induced wound repair in diabetic mice. *Journal of investigative dermatology*, 131(6), pp.1365-1374.
- Han, D.C., Isono, M., Hoffman, B.B. and Ziyadeh, F.N., 1999. High glucose stimulates proliferation and collagen type I synthesis in renal cortical fibroblasts: mediation by autocrine activation of TGF- $\beta$ . *Journal of the American Society of Nephrology*, 10(9), pp.1891-1899.
- Han, H.S., Kang, G., Kim, J.S., Choi, B.H. and Koo, S.H., 2016. Regulation of glucose metabolism from a liver-centric perspective. *Experimental & molecular medicine*, 48(3), pp.e218-e218.
- Hansen, L., Fjordvang, H., Rasmussen, S.K., Vestergaard, H., Echwald, S.M., Hansen, T., Alessi, D., Shenolikar, S., Saltiel, A.R., Barbetti, F. and Pedersen, O., 1999. Mutational analysis of the coding regions of the genes encoding protein kinase B-alpha and -beta, phosphoinositide-dependent protein kinase-1, phosphatase targeting to glycogen, protein phosphatase inhibitor-1, and glycogenin: lessons from a search for genetic variability of the insulin-stimulated glycogen synthesis pathway of skeletal muscle in NIDDM patients. *Diabetes*, 48(2), pp.403-407.
- Hao, Z., Liu, G., Ren, L., Liu, J., Liu, C., Yang, T., Wu, X., Zhang, X., Yang, L., Xia, J. and Li, W., 2023. A self-healing multifunctional hydrogel system accelerates diabetic wound healing through orchestrating immunoinflammatory microenvironment. *ACS Applied Materials & Interfaces*, 15(16), pp.19847-19862.
- He, F., Ru, X. and Wen, T., 2020. NRF2, a transcription factor for stress response and beyond. *International journal of molecular sciences*, 21(13), p.4777.

- Hehenberger, K. and Hansson, A., 1997. High glucose-induced growth factor resistance in human fibroblasts can be reversed by antioxidants and protein kinase C-inhibitors. *Cell Biochemistry and Function: Cellular biochemistry and its modulation by active agents or disease*, 15(3), pp.197-201.
- Hehenberger, K., Heilborn, J.D., Brismar, K. and Hansson, A., 1998. Inhibited proliferation of fibroblasts derived from chronic diabetic wounds and normal dermal fibroblasts treated with high glucose is associated with increased formation of L-lactate. *Wound repair and regeneration*, 6(2), pp.135-141.
- Herman, M.A. and Birnbaum, M.J., 2021. Molecular aspects of fructose metabolism and metabolic disease. *Cell metabolism*, 33(12), pp.2329-2354.
- Heyrovska, R., 2014. Atomic Structures of Glucose, Fructose and Sucrose and Explanation of Anomeric Carbon. *bioRxiv*, p.002022.
- Hirayama, D., Iida, T. and Nakase, H., 2017. The phagocytic function of macrophage-enforcing innate immunity and tissue homeostasis. *International journal of molecular sciences*, 19(1), p.92.
- Hogan, K.A., Ravindran, A., Podolsky, M.A. and Glick, A.B., 2013. The TGF $\beta$ 1 pathway is required for NF $\kappa$ B dependent gene expression in mouse keratinocytes. *Cytokine*, 64(3), pp.652-659.
- Hu, R., Xia, C.Q., Butfiloski, E. and Clare-Salzler, M., 2018. Effect of high glucose on cytokine production by human peripheral blood immune cells and type I interferon signaling in monocytes: Implications for the role of hyperglycemia in the diabetes inflammatory process and host defense against infection. *Clinical immunology*, 195, pp.139-148.
- Hu, S.C.S. and Lan, C.C.E., 2016. High-glucose environment disturbs the physiologic functions of keratinocytes: focusing on diabetic wound healing. *Journal of Dermatological Science*, 84(2), pp.121-127.
- Huynh, T.T., McDougald, D., Klebensberger, J., Al Qarni, B., Barraud, N., Rice, S.A., Kjelleberg, S. and Schleheck, D., 2012. Glucose starvation-induced dispersal of *Pseudomonas aeruginosa* biofilms is cAMP and energy dependent.
- Hwang, S.J., Kim, S.H., Seo, W.Y., Jeong, Y., Shin, M.C., Ryu, D., Lee, S.B., Choi, Y.J. and Kim, K., 2021. Effects of human collagen  $\alpha$ -1 type I-derived proteins on collagen synthesis and elastin production in human dermal fibroblasts. *BMB reports*, 54(6), p.329.
- Iacobazzi, V. and Infantino, V., 2014. Citrate—new functions for an old metabolite. *biological chemistry*, 395(4), pp.387-399.
- Ighodaro, O. and Adeosun, A., 2018. Vascular complications in diabetes mellitus. *kidney*, 4, pp.16-19.
- Iglesias-De la Cruz, M.C., Ziyadeh, F.N., Isono, M., Kouahou, M., Han, D.C., Kalluri, R., Mundel, P. and Chen, S., 2002. Effects of high glucose and TGF- $\beta$ 1 on the expression of collagen IV and vascular endothelial growth factor in mouse podocytes. *Kidney international*, 62(3), pp.901-913.
- Iwaisako, K., Brenner, D.A. and Kisseleva, T., 2012. What's new in liver fibrosis? The origin of myofibroblasts in liver fibrosis. *Journal of gastroenterology and hepatology*, 27, pp.65-68.
- Jiang, X., Guo, X., Xu, X., Teng, M., Huang, C., Zhang, D., Zhang, Q., Zhang, J. and Huang, Y., 2014. Hypoxia regulates CD9-mediated keratinocyte migration via the P38/MAPK pathway. *Scientific reports*, 4(1), p.6304.
- Jiang, Z., Georgel, P., Du, X., Shamel, L., Sovath, S., Mudd, S., Huber, M., Kalis, C., Keck, S., Galanos, C. and Freudenberg, M., 2005. CD14 is required for MyD88-independent LPS signaling. *Nature immunology*, 6(6), pp.565-570.

- Kadomoto, S., Izumi, K. and Mizokami, A., 2021. Macrophage polarity and disease control. *International Journal of Molecular Sciences*, 23(1), p.144.
- Kaisho, T. and Akira, S., 2002. Toll-like receptors as adjuvant receptors. *Biochimica et Biophysica Acta (BBA)-Molecular Cell Research*, 1589(1), pp.1-13.
- Kajanne, R., Miettinen, P., Mehlem, A., Leivonen, S.K., Birrer, M., Foschi, M., Kähäri, V.M. and Leppä, S., 2007. EGF-R regulates MMP function in fibroblasts through MAPK and AP-1 pathways. *Journal of cellular physiology*, 212(2), pp.489-497.
- Kansanen, E., Kuosmanen, S.M., Leinonen, H. and Levonen, A.L., 2013. The Keap1-Nrf2 pathway: Mechanisms of activation and dysregulation in cancer. *Redox biology*, 1(1), pp.45-49.
- Kareem, H.I.A. and Mohammed, S.H., 2024. The Significance of Measuring Human Beta Defensin-2 in Patients with Diabetic Foot Ulcer. *Al-Rafidain Journal of Medical Sciences (ISSN 2789-3219)*, 6(2), pp.70-75.
- Kaussikaa, S., Prasad, M.K. and Ramkumar, K.M., 2024. Nrf2 Activation in Keratinocytes: A Central Role in Diabetes-Associated Wound Healing. *Experimental Dermatology*, 33(10), p.e15189.
- Kennett, E. and Kuchel, P., 2003. Redox reactions and electron transfer across the red cell membrane. *IUBMB life*, 55(7), pp.375-385.
- Khorshidian, N., Khanniri, E., Koushki, M.R., Sohrabvandi, S. and Yousefi, M., 2022. An overview of antimicrobial activity of lysozyme and its functionality in cheese. *Frontiers in nutrition*, 9, p.833618.
- Kifelew, L.G., Warner, M.S., Morales, S., Gordon, D.L., Thomas, N., Mitchell, J.G. and Speck, P.G., 2024. Lytic activity of phages against bacterial pathogens infecting diabetic foot ulcers. *Scientific Reports*, 14(1), p.3515.
- Kim, D., Kim, S.Y., Mun, S.K., Rhee, S. and Kim, B.J., 2015. Epidermal growth factor improves the migration and contractility of aged fibroblasts cultured on 3D collagen matrices. *International Journal of Molecular Medicine*, 35(4), pp.1017-1025.
- Kim, J.H., Yoon, N.Y., Kim, D.H., Jung, M., Jun, M., Park, H.Y., Chung, C.H., Lee, K., Kim, S., Park, C.S. and Liu, K.H., 2018. Impaired permeability and antimicrobial barriers in type 2 diabetes skin are linked to increased serum levels of advanced glycation end-product. *Experimental dermatology*, 27(8), pp.815-823.
- Villarreal-Ponce, A., Tiruneh, M.W., Lee, J., Guerrero-Juarez, C.F., Kuhn, J., David, J.A., Dammeyer, K., Mc Kell, R., Kwong, J., Rabbani, P.S. and Nie, Q., 2020. Keratinocyte-macrophage crosstalk by the Nrf2/Ccl2/EGF signaling axis orchestrates tissue repair. *Cell reports*, 33(8).
- Kim, J.M., Choo, J.E., Lee, H.J., Kim, K.N. and Chang, S.E., 2018. Epidermal growth factor attenuated the expression of inflammatory cytokines in human epidermal keratinocyte exposed to *Propionibacterium acnes*. *Annals of dermatology*, 30(1), pp.54-63.
- Kirfel, G. and Herzog, V., 2004. Migration of epidermal keratinocytes: mechanisms, regulation, and biological significance. *Protoplasma*, 223, pp.67-78.
- Knoedler, S., Broichhausen, S., Guo, R., Dai, R., Knoedler, L., Kauke-Navarro, M., Diatta, F., Pomahac, B., Machens, H.G., Jiang, D. and Rinkevich, Y., 2023. Fibroblasts—The cellular choreographers of wound healing. *Frontiers in Immunology*, 14, p.1233800.
- Koh, T.J. and DiPietro, L.A., 2011. Inflammation and wound healing: the role of the macrophage. *Expert reviews in molecular medicine*, 13, p.e23.
- Koike, J., Masada, M. and Maeda, H., 2000. Scavenging activity of MGN-3 (arabinoxylane from rice bran) with natural killer cell activity on free radicals. *Biotherapy*, 14(5), pp.493-495.

- Kong, T., Liu, M., Ji, B., Bai, B., Cheng, B. and Wang, C., 2019. Role of the extracellular signal-regulated kinase 1/2 signaling pathway in ischemia-reperfusion injury. *Frontiers in physiology*, 10, p.1038.
- Korla, K., Vadlakonda, L. and Mitra, C.K., 2015. Kinetic simulation of malate-aspartate and citrate-pyruvate shuttles in association with Krebs cycle. *Journal of Biomolecular Structure and Dynamics*, 33(11), pp.2390-2403.
- Koulmanda, M., Bhasin, M., Awdeh, Z., Qipo, A., Fan, Z., Hanidziar, D., Putheti, P., Shi, H., Cszuadia, E., Libermann, T.A. and Strom, T.B., 2012. The role of TNF- $\alpha$  in mice with type 1-and 2-diabetes. *PLoS One*, 7(5), p.e33254.
- Kraakman, M.J., Murphy, A.J., Jandeleit-Dahm, K. and Kammoun, H.L., 2014. Macrophage polarization in obesity and type 2 diabetes: weighing down our understanding of macrophage function?. *Frontiers in immunology*, 5, p.470.
- Krakauer, T., 2015. Inflammasome, mTORC1 activation, and metabolic derangement contribute to the susceptibility of diabetics to infections. *Medical Hypotheses*, 85(6), pp.997-1001.
- Kraneveld, A.D., Rijniere, A., Nijkamp, F.P. and Garssen, J., 2008. Neuro-immune interactions in inflammatory bowel disease and irritable bowel syndrome: future therapeutic targets. *European journal of pharmacology*, 585(2-3), pp.361-374.
- Krawczyk, C.M., Holowka, T., Sun, J., Blagih, J., Amiel, E., DeBerardinis, R.J., Cross, J.R., Jung, E., Thompson, C.B., Jones, R.G. and Pearce, E.J., 2010. Toll-like receptor-induced changes in glycolytic metabolism regulate dendritic cell activation. *Blood, The Journal of the American Society of Hematology*, 115(23), pp.4742-4749.
- Kruse, C.R., Singh, M., Sørensen, J.A., Eriksson, E. and Nuutila, K., 2016. The effect of local hyperglycemia on skin cells in vitro and on wound healing in euglycemic rats. *journal of surgical research*, 206(2), pp.418-426.
- Krzyszczuk, P., Schloss, R., Palmer, A. and Berthiaume, F., 2018. The role of macrophages in acute and chronic wound healing and interventions to promote pro-wound healing phenotypes. *Frontiers in physiology*, 9, p.419.
- Lade, H., Park, J.H., Chung, S.H., Kim, I.H., Kim, J.M., Joo, H.S. and Kim, J.S., 2019. Biofilm formation by *Staphylococcus aureus* clinical isolates is differentially affected by glucose and sodium chloride supplemented culture media. *Journal of clinical medicine*, 8(11), p.1853.
- Lamers, M.L., Almeida, M.E., Vicente-Manzanares, M., Horwitz, A.F. and Santos, M.F., 2011. High glucose-mediated oxidative stress impairs cell migration. *PLoS one*, 6(8), p.e22865.
- Lan, C.C., Liu, I.H., Fang, A.H., Wen, C.H. and Wu, C.S., 2008. Hyperglycaemic conditions decrease cultured keratinocyte mobility: implications for impaired wound healing in patients with diabetes. *British Journal of Dermatology*, 159(5), pp.1103-1115.
- Lan, C.C., Wu, C.S., Huang, S.M., Kuo, H.Y., Wu, I.H., Liang, C.W. and Chen, G.S., 2012. High-glucose environment reduces human  $\beta$ -defensin-2 expression in human keratinocytes: implications for poor diabetic wound healing. *British Journal of Dermatology*, 166(6), pp.1221-1229.
- Lan, C.C.E., Wu, C.S., Huang, S.M., Kuo, H.Y., Wu, I.H., Wen, C.H., Chai, C.Y., Fang, A.H. and Chen, G.S., 2011. High-glucose environment inhibits p38MAPK signaling and reduces human  $\beta$ -3 expression in keratinocytes. *Molecular Medicine*, 17, pp.771-779.
- Lan, C.C.E., Wu, C.S., Huang, S.M., Wu, I.H. and Chen, G.S., 2013. High-glucose environment enhanced oxidative stress and increased interleukin-8 secretion from keratinocytes: new insights into impaired diabetic wound healing. *Diabetes*, 62(7), pp.2530-2538.

- Landén, N.X., Li, D. and Ståhle, M., 2016. Transition from inflammation to proliferation: a critical step during wound healing. *Cellular and Molecular Life Sciences*, 73, pp.3861-3885.
- Lankatillake, C., Huynh, T. and Dias, D.A., 2019. Understanding glycaemic control and current approaches for screening antidiabetic natural products from evidence-based medicinal plants. *Plant Methods*, 15(1), p.105.
- Larsson, N.G., Wang, J., Wilhelmsson, H., Oldfors, A., Rustin, P., Lewandoski, M., Barsh, G.S. and Clayton, D.A., 1998. Mitochondrial transcription factor A is necessary for mtDNA maintenance and embryogenesis in mice. *Nature genetics*, 18(3), pp.231-236.
- Laville, M. and Nazare, J.A., 2009. Diabetes, insulin resistance and sugars. *Obesity reviews*, 10, pp.24-33.
- Le Brun, A.P., Clifton, L.A., Halbert, C.E., Lin, B., Meron, M., Holden, P.J., Lakey, J.H. and Holt, S.A., 2013. Structural characterization of a model gram-negative bacterial surface using lipopolysaccharides from rough strains of *Escherichia coli*. *Biomacromolecules*, 14(6), pp.2014-2022.
- Lecube, A., Pachón, G., Petriz, J., Hernández, C. and Simó, R., 2011. Phagocytic activity is impaired in type 2 diabetes mellitus and increases after metabolic improvement. *PLoS one*, 6(8), p.e23366.
- Lee, E.G., Luckett-Chastain, L.R., Calhoun, K.N., Frempah, B., Bastian, A. and Gallucci, R.M., 2019. Interleukin 6 function in the skin and isolated keratinocytes is modulated by hyperglycemia. *Journal of immunology research*, 2019(1), p.5087847.
- Lee, H.K., Song, J.H., Shin, C.S., Park, D.J., Park, K.S., Lee, K.U. and Koh, C.S., 1998. Decreased mitochondrial DNA content in peripheral blood precedes the development of non-insulin-dependent diabetes mellitus. *Diabetes research and clinical practice*, 42(3), pp.161-167.
- Li, L., Zhang, J., Zhang, Q., Zhang, D., Xiang, F., Jia, J., Wei, P., Zhang, J., Hu, J. and Huang, Y., 2019. High glucose suppresses keratinocyte migration through the inhibition of p38 MAPK/autophagy pathway. *Frontiers in physiology*, 10, p.24.
- Li, M.F., Zhang, R., Li, T.T., Chen, M.Y., Li, L.X., Lu, J.X. and Jia, W.P., 2016. High glucose increases the expression of inflammatory cytokine genes in macrophages through H3K9 methyltransferase mechanism. *Journal of Interferon & Cytokine Research*, 36(1), pp.48-61.
- Li, W., Zhang, S. and Smith, C. 2015. The molecular structure features-immune stimulatory activity of arabinoxylans derived from the pentosan fraction of wheat flour. *Journal of Cereal Science*, 62 pp. 81-86
- Liarte, S., Bernabé-García, Á. and Nicolás, F.J., 2020. Role of TGF- $\beta$  in skin chronic wounds: a keratinocyte perspective. *Cells*, 9(2), p.306.
- Long, M., Rojo de la Vega, M., Wen, Q., Bharara, M., Jiang, T., Zhang, R., Zhou, S., Wong, P.K., Wondrak, G.T., Zheng, H. and Zhang, D.D., 2016. An essential role of NRF2 in diabetic wound healing. *Diabetes*, 65(3), pp.780-793.
- Loots, M.A., Kenter, S.B., Au, F.L., Van Galen, W.J.M., Middelkoop, E., Bos, J.D. and Mekkes, J.R., 2002. Fibroblasts derived from chronic diabetic ulcers differ in their response to stimulation with EGF, IGF-I, bFGF and PDGF-AB compared to controls. *European journal of cell biology*, 81(3), pp.153-160.
- Loryman, C. and Mansbridge, J., 2008. Inhibition of keratinocyte migration by lipopolysaccharide. *Wound repair and regeneration*, 16(1), pp.45-51.

- Loughlin, D.T. and Artlett, C.M., 2009. 3-Deoxyglucosone-collagen alters human dermal fibroblast migration and adhesion: implications for impaired wound healing in patients with diabetes. *Wound repair and regeneration*, 17(5), pp.739-749.
- Lu, N., Wang, L., Cao, H., Liu, L., Van Kaer, L., Washington, M.K., Rosen, M.J., Dubé, P.E., Wilson, K.T., Ren, X. and Hao, X., 2014. Activation of the epidermal growth factor receptor in macrophages regulates cytokine production and experimental colitis. *The Journal of Immunology*, 192(3), pp.1013-1023.
- Luo, K., 2017. Signaling cross talk between TGF- $\beta$ /Smad and other signaling pathways. *Cold Spring Harbor perspectives in biology*, 9(1), p.a022137.
- Luo, W., Wu, G., Chen, X., Zhang, Q., Zou, C., Wang, J., Liu, J., Chattipakorn, N., Wang, Y. and Liang, G., 2022. Blockage of MyD88 in cardiomyocytes alleviates cardiac inflammation and cardiomyopathy in experimental diabetic mice. *Biochemical Pharmacology*, 206, p.115292.
- Luo, Z., Chen, M., Chen, T., She, P. and Wu, Y., 2019. Lactic acid produced by glycolysis contributed to *Staphylococcus aureus* aggregation induced by glucose. *Current Microbiology*, 76, pp.607-612.
- Luo, Z., Chen, Z., Zhu, Z., Hao, Y., Feng, J., Luo, Q., Zhang, Z., Yang, X., Hu, J., Liang, W. and Ding, G., 2022. Angiotensin II induces podocyte metabolic reprogramming from glycolysis to glycerol-3-phosphate biosynthesis. *Cellular Signalling*, 99, p.110443.
- Luo, Z., Yue, S., Chen, T., She, P., Wu, Y. and Wu, Y., 2020. Reduced growth of *Staphylococcus aureus* under high glucose conditions is associated with decreased pentaglycine expression. *Frontiers in microbiology*, 11, p.537290.
- Lushchak, O.V., Piroddi, M., Galli, F. and Lushchak, V.I., 2014. Aconitase post-translational modification as a key in linkage between Krebs cycle, iron homeostasis, redox signaling, and metabolism of reactive oxygen species. *Redox Report*, 19(1), pp.8-15.
- Ma, W.T., Gao, F., Gu, K. and Chen, D.K., 2019. The role of monocytes and macrophages in autoimmune diseases: a comprehensive review. *Frontiers in immunology*, 10, p.1140.
- Macarie, R.D., Vadana, M., Ciortan, L., Tucureanu, M.M., Ciobanu, A., Vinereanu, D., Manduteanu, I., Simionescu, M. and Butoi, E., 2018. The expression of MMP-1 and MMP-9 is up-regulated by smooth muscle cells after their cross-talk with macrophages in high glucose conditions. *Journal of cellular and molecular medicine*, 22(9), pp.4366-4376.
- Maechler, P. and Wollheim, C.B., 2001. Mitochondrial function in normal and diabetic  $\beta$ -cells. *Nature*, 414(6865), pp.807-812.
- Maechler, P., Jornot, L. and Wollheim, C.B., 1999. Hydrogen peroxide alters mitochondrial activation and insulin secretion in pancreatic beta cells. *Journal of Biological Chemistry*, 274(39), pp.27905-27913.
- Magatti, M., Vertua, E., De Munari, S., Caro, M., Caruso, M., Silini, A., Delgado, M. and Parolini, O., 2017. Human amnion favours tissue repair by inducing the M1-to-M2 switch and enhancing M2 macrophage features. *Journal of tissue engineering and regenerative medicine*, 11(10), pp.2895-2911.
- Mahoney, D.E., Hiebert, J.B., Thimmesch, A., Pierce, J.T., Vacek, J.L., Clancy, R.L., Sauer, A.J. and Pierce, J.D., 2018. Understanding D-ribose and mitochondrial function. *Advances in bioscience and clinical medicine*, 6(1), p.1.

- Maione, A.G., Smith, A., Kashpur, O., Yanez, V., Knight, E., Mooney, D.J., Veves, A., Tomic-Canic, M. and Garlick, J.A., 2016. Altered ECM deposition by diabetic foot ulcer-derived fibroblasts implicates fibronectin in chronic wound repair. *Wound repair and regeneration*, 24(4), pp.630-643.
- Maldonado, R.F., Sá-Correia, I. and Valvano, M.A., 2016. Lipopolysaccharide modification in Gram-negative bacteria during chronic infection. *FEMS microbiology reviews*, 40(4), pp.480-493.
- Manna, P. and Jain, S.K., 2013. PIP3 but not PIP2 increases GLUT4 surface expression and glucose metabolism mediated by AKT/PKC $\zeta$ / $\lambda$  phosphorylation in 3T3L1 adipocytes. *Molecular and cellular biochemistry*, 381, pp.291-299.
- Mansoub, N.H., 2021. The role of keratinocyte function on the defected diabetic wound healing. *International journal of burns and trauma*, 11(6), p.430.
- Marega, M., Chen, C. and Bellusci, S., 2021. Cross-talk between inflammation and fibroblast growth factor 10 during organogenesis and pathogenesis: lessons learnt from the lung and other organs. *Frontiers in Cell and Developmental Biology*, 9, p.656883.
- Marti, G., Ferguson, M., Wang, J., Byrnes, C., Dieb, R., Qaiser, R., Bonde, P., Duncan, M.D. and Harmon, J.W., 2004. Electroporative transfection with KGF-1 DNA improves wound healing in a diabetic mouse model. *Gene therapy*, 11(24), pp.1780-1785.
- Maurer, M. and Von Stebut, E., 2004. Macrophage inflammatory protein-1. *The international journal of biochemistry & cell biology*, 36(10), pp.1882-1886.
- Mazgaean, L. and Gurung, P., 2020. Recent advances in lipopolysaccharide recognition systems. *International journal of molecular sciences*, 21(2), p.379.
- McAnulty, R.J., 2007. Fibroblasts and myofibroblasts: their source, function and role in disease. *The international journal of biochemistry & cell biology*, 39(4), pp.666-671.
- McCrimmon, R.J., Ryan, C.M. and Frier, B.M., 2012. Diabetes and cognitive dysfunction. *The Lancet*, 379(9833), pp.2291-2299.
- McWhorter, F.Y., Davis, C.T. and Liu, W.F., 2015. Physical and mechanical regulation of macrophage phenotype and function. *Cellular and Molecular Life Sciences*, 72(7), pp.1303-1316.
- Meena, N.P. and Kimmel, A.R., 2017. Chemotactic network responses to live bacteria show independence of phagocytosis from chemoreceptor sensing. *Elife*, 6, p.e24627.
- Megawati, E.R., Meutia, N. and Lubis, L.D., 2022. The effect of hyperglycaemia on the macrophages in the cell culture. *Folia Morphologica*, 81(2), pp.387-393.
- Merecz-Sadowska, A., Sitarek, P., Zajdel, K., Kucharska, E., Kowalczyk, T. and Zajdel, R., 2021. The modulatory influence of plant-derived compounds on human keratinocyte function. *International Journal of Molecular Sciences*, 22(22), p.12488.
- Michikawa, Y., Mazzucchelli, F., Bresolin, N., Scarlato, G. and Attardi, G., 1999. Aging-dependent large accumulation of point mutations in the human mtDNA control region for replication. *Science*, 286(5440), pp.774-779.
- Miettinen, P.J., Ustinov, J., Ormio, P., Gao, R., Palgi, J., Hakonen, E., Juntti-Berggren, L., Berggren, P.O. and Otonkoski, T., 2006. Downregulation of EGF receptor signaling in pancreatic islets causes diabetes due to impaired postnatal  $\beta$ -cell growth. *Diabetes*, 55(12), pp.3299-3308.
- Mine, S., Okada, Y., Tanikawa, T., Kawahara, C., Tabata, T. and Tanaka, Y., 2006. Increased expression levels of monocyte CCR2 and monocyte chemoattractant protein-1 in patients with diabetes mellitus. *Biochemical and biophysical research communications*, 344(3), pp.780-785.

- Minns, D., Smith, K.J., Alessandrini, V., Hardisty, G., Melrose, L., Jackson-Jones, L., MacDonald, A.S., Davidson, D.J. and Gwyer Findlay, E., 2021. The neutrophil antimicrobial peptide cathelicidin promotes Th17 differentiation. *Nature communications*, 12(1), p.1285.
- Miranda, E., Bramono, K., Yunir, E., Reksodiputro, M.H., Suwarsa, O., Rengganis, I., Harahap, A.R., Subekti, D., Suwanto, S., Hayun, H. and Bardosono, S., 2023. Efficacy of LL-37 cream in enhancing healing of diabetic foot ulcer: A randomized double-blind controlled trial. *Archives of dermatological research*, 315(9), pp.2623-2633.
- Moerings, B.G., van Bergenhenegouwen, J., Furber, M., Abbring, S., Schols, H.A., Witkamp, R.F., Govers, C. and Mes, J.J., 2022. Dectin-1b activation by arabinoxylans induces trained immunity in human monocyte-derived macrophages. *International Journal of Biological Macromolecules*, 209, pp.942-950.
- Moganti, K., Li, F., Schmuttermaier, C., Riemann, S., Klüter, H., Gratchev, A., Harmsen, M.C. and Kzhyshkowska, J., 2017. Hyperglycemia induces mixed M1/M2 cytokine profile in primary human monocyte-derived macrophages. *Immunobiology*, 222(10), pp.952-959.
- Moheimani, F., Kim, C.H., Rahmanto, A.S., van Reyk, D.M. and Davies, M.J., 2012. Inhibition of lysosomal function in macrophages incubated with elevated glucose concentrations: a potential contributory factor in diabetes-associated atherosclerosis. *Atherosclerosis*, 223(1), pp.144-151.
- Monaghan, M.G., Borah, R., Thomsen, C. and Browne, S., 2023. Thou shall not heal: Overcoming the non-healing behaviour of diabetic foot ulcers by engineering the inflammatory microenvironment. *Advanced Drug Delivery Reviews*, p.115120.
- Montoya-Rosales, A., Castro-Garcia, P., Torres-Juarez, F., Enciso-Moreno, J.A. and Rivas-Santiago, B., 2016. Glucose levels affect LL-37 expression in monocyte-derived macrophages altering the Mycobacterium tuberculosis intracellular growth control. *Microbial pathogenesis*, 97, pp.148-153.
- Mukherjee, S., Karmakar, S. and Babu, S.P.S., 2016. TLR2 and TLR4 mediated host immune responses in major infectious diseases: a review. *Brazilian Journal of Infectious Diseases*, 20(2), pp.193-204.
- Müller-Decker, K., Manegold, G., Butz, H., Hinz, D.E., Hüttner, D., Richter, K.H., Tremmel, M., Weißflog, R. and Marks, F., 2005. Inhibition of cell proliferation by bacterial lipopolysaccharides in TLR4-positive epithelial cells: independence of nitric oxide and cytokine release. *Journal of investigative dermatology*, 124(3), pp.553-561.
- Musatov, A. and Robinson, N.C., 2012. Susceptibility of mitochondrial electron-transport complexes to oxidative damage. Focus on cytochrome c oxidase. *Free radical research*, 46(11), pp.1313-1326.
- Muzio, M., Polentarutti, N., Bosisio, D., Kumar, P.M. and Mantovani, A., 2000. Toll-like receptor family and signalling pathway. *Biochemical society transactions*, 28(5), pp.563-566.
- Nackiewicz, D., Dan, M., He, W., Kim, R., Salmi, A., Rützi, S., Westwell-Roper, C., Cunningham, A., Speck, M., Schuster-Klein, C. and Guardiola, B., 2014. TLR2/6 and TLR4-activated macrophages contribute to islet inflammation and impair beta cell insulin gene expression via IL-1 and IL-6. *Diabetologia*, 57, pp.1645-1654.
- Nagl, M., Kacani, L., Müllauer, B., Lemberger, E.M., Stoiber, H., Sprinzl, G.M., Schennach, H. and Dierich, M.P., 2002. Phagocytosis and killing of bacteria by professional phagocytes and dendritic cells. *Clinical and vaccine immunology*, 9(6), pp.1165-1168.

- Nakai, K., Fujii, S., Yamamoto, A., Igarashi, J., Kubota, Y. and Kosaka, H., 2003. Effects of high glucose on NO synthesis in human keratinocyte cell line (HaCaT). *Journal of dermatological science*, 31(3), pp.211-218.
- Nasser, M.W., Elbaz, M., Ahirwar, D.K. and Ganju, R.K., 2015. Conditioning solid tumor microenvironment through inflammatory chemokines and S100 family proteins. *Cancer letters*, 365(1), pp.11-22.
- Nawaz, N., Wen, S., Wang, F., Nawaz, S., Raza, J., Iftikhar, M. and Usman, M., 2022. Lysozyme and its application as antibacterial agent in food industry. *Molecules*, 27(19), p.6305.
- Neefjes, J., Jongsma, M.L., Paul, P. and Bakke, O., 2011. Towards a systems understanding of MHC class I and MHC class II antigen presentation. *Nature reviews immunology*, 11(12), pp.823-836.
- NICE (2024). *When Should I Suspect Type 2 Diabetes in an adult?* [online] NICE. Available at: <https://cks.nice.org.uk/topics/diabetes-type-2/diagnosis/diagnosis-in-adults/>.
- Nio, Y., Yamauchi, T., Iwabu, M., Okada-Iwabu, M., Funata, M., Yamaguchi, M., Ueki, K. and Kadowaki, T., 2012. Monocyte chemoattractant protein-1 (MCP-1) deficiency enhances alternatively activated M2 macrophages and ameliorates insulin resistance and fatty liver in lipotrophic diabetic A-ZIP transgenic mice. *Diabetologia*, 55, pp.3350-3358.
- Nitzke, D., Czereminski, J., Rosa, C., Coghetto, C., Fernandes, S.A. and Carteri, R.B., 2024. Increasing dietary fiber intake for type 2 diabetes mellitus management: A systematic review. *World Journal of Diabetes*, 15(5), p.1001.
- Noaman, E., El-Din, N.K.B., Bibars, M.A., Abou Mossallam, A.A. and Ghoneum, M., 2008. Antioxidant potential by arabinoxylan rice bran, MGN-3/biobran, represents a mechanism for its oncostatic effect against murine solid Ehrlich carcinoma. *Cancer letters*, 268(2), pp.348-359.
- Oeckinghaus, A., Hayden, M.S. and Ghosh, S., 2011. Crosstalk in NF- $\kappa$ B signaling pathways. *Nature immunology*, 12(8), pp.695-708.
- Ogawa, K., Takeuchi, M. and Nakamura, N., 2005. Immunological effects of partially hydrolyzed arabinoxylan from corn husk in mice. *Bioscience, biotechnology, and biochemistry*, 69(1), pp.19-25.
- Omar-Hmeadi, M. and Idevall-Hagren, O., 2021. Insulin granule biogenesis and exocytosis. *Cellular and Molecular Life Sciences*, 78, pp.1957-1970.
- Ooi, S.L., McMullen, D., Golombick, T., Nut, D. and Pak, S.C., 2018. Evidence-based review of BioBran/MGN-3 arabinoxylan compound as a complementary therapy for conventional cancer treatment. *Integrative Cancer Therapies*, 17(2), pp.165-178.
- Ooi, S.L., Micalos, P.S. and Pak, S.C., 2023. Modified Rice bran arabinoxylan by *Lentinus edodes* mycelial enzyme as an Immunocutical for health and aging—a comprehensive literature review. *Molecules*, 28(17), p.6313.
- Orekhov, A.N., Orekhova, V.A., Nikiforov, N.G., Myasoedova, V.A., Grechko, A.V., Romanenko, E.B., Zhang, D. and Chistiakov, D.A., 2019. Monocyte differentiation and macrophage polarization. *Vessel Plus*, 3.
- Ortega, S., Ittmann, M., Tsang, S.H., Ehrlich, M. and Basilico, C., 1998. Neuronal defects and delayed wound healing in mice lacking fibroblast growth factor 2. *Proceedings of the National Academy of Sciences*, 95(10), pp.5672-5677.
- Pang, L., Wang, Y., Zheng, M., Wang, Q., Lin, H., Zhang, L. and Wu, L., 2016. Transcriptomic study of high-glucose effects on human skin fibroblast cells. *Molecular medicine reports*, 13(3), pp.2627-2634.

- Pardo, A. and Selman, M., 2005. MMP-1: the elder of the family. *The international journal of biochemistry & cell biology*, 37(2), pp.283-288.
- Park, J.S., KIM, J.Y., Cho, J.Y., KANG, J.S. and YU, Y.H., 2000. Epidermal Growth Factor (EGF) Antagonizes Transforming Growth Factor (TGF)- $\beta$ 1-Induced Collagen Lattice Contraction by Human Skin Fibroblasts. *Biological and Pharmaceutical Bulletin*, 23(12), pp.1517-1520.
- Pastar, I., Stojadinovic, O. and Tomic-Canic, M., 2008. Role of keratinocytes in healing of chronic wounds. *Surgical technology international*, 17, pp.105-112.
- Pastar, I., Stojadinovic, O., Yin, N.C., Ramirez, H., Nusbaum, A.G., Sawaya, A., Patel, S.B., Khalid, L., Isseroff, R.R. and Tomic-Canic, M., 2014. Epithelialization in wound healing: a comprehensive review. *Advances in wound care*, 3(7), pp.445-464.
- Patergnani, S., Baldassari, F., De Marchi, E., Karkucinska-Wieckowska, A., Wieckowski, M.R. and Pinton, P., 2014. Methods to monitor and compare mitochondrial and glycolytic ATP production. In *Methods in enzymology* (Vol. 542, pp. 313-332). Academic Press.
- Pavlou, S., Lindsay, J., Ingram, R., Xu, H. and Chen, M., 2018. Sustained high glucose exposure sensitizes macrophage responses to cytokine stimuli but reduces their phagocytic activity. *BMC immunology*, 19, pp.1-13.
- Payne, D.E. and Boles, B.R., 2016. Emerging interactions between matrix components during biofilm development. *Current genetics*, 62, pp.137-141.
- Peng, B., Dai, Q., Liu, X. and Jiang, S., 2024. Fraxin alleviates oral lichen planus by suppressing OCT3-mediated activation of FGF2/NF- $\kappa$ B pathway. *Naunyn-Schmiedeberg's Archives of Pharmacology*, pp.1-17.
- Petersen, M.C. and Shulman, G.I., 2018. Mechanisms of insulin action and insulin resistance. *Physiological reviews*.
- Petit, I., Levy, A., Estrach, S., Féral, C.C., Trentin, A.G., Dingli, F., Loew, D., Qu, J., Zhou, H., Théry, C. and Prunier, C., 2022. Fibroblast growth factor-2 bound to specific dermal fibroblast-derived extracellular vesicles is protected from degradation. *Scientific Reports*, 12(1), p.22131.
- Pezhman, L., Tahrani, A. and Chimen, M., 2021. Dysregulation of leukocyte trafficking in type 2 diabetes: mechanisms and potential therapeutic avenues. *Frontiers in cell and developmental biology*, 9, p.624184.
- Philips, B.J., Redman, J., Brennan, A., Wood, D., Holliman, R., Baines, D. and Baker, E.H., 2005. Glucose in bronchial aspirates increases the risk of respiratory MRSA in intubated patients. *Thorax*, 60(9), pp.761-764.
- Piipponen, M., Li, D. and Landén, N.X., 2020. The immune functions of keratinocytes in skin wound healing. *International journal of molecular sciences*, 21(22), p.8790.
- Plikus, M.V., Wang, X., Sinha, S., Forte, E., Thompson, S.M., Herzog, E.L., Driskell, R.R., Rosenthal, N., Biernaskie, J. and Horsley, V., 2021. Fibroblasts: Origins, definitions, and functions in health and disease. *Cell*, 184(15), pp.3852-3872.
- Polonsky, K.S., Sturis, J. and Bell, G.I., 1996. Non-insulin-dependent diabetes mellitus—a genetically programmed failure of the beta cell to compensate for insulin resistance. *New England Journal of Medicine*, 334(12), pp.777-783.
- Porter, S., 2007. The role of the fibroblast in wound contraction and healing. *WOUNDS UK*, 3(1), p.33.

- Portou, M.J., Yu, R., Baker, D., Xu, S., Abraham, D. and Tsui, J., 2020. Hyperglycaemia and ischaemia impair wound healing via toll-like receptor 4 pathway activation in vitro and in an experimental murine model. *European Journal of Vascular and Endovascular Surgery*, 59(1), pp.117-127.
- Preciado, D., Caicedo, E., Jhanjee, R., Silver, R., Harris, G., Juhn, S.K., Choo, D.I. and Ondrey, F., 2005. *Pseudomonas aeruginosa* lipopolysaccharide induction of keratinocyte proliferation, NF- $\kappa$ B, and cyclin D1 is inhibited by indomethacin. *The Journal of Immunology*, 174(5), pp.2964-2973.
- Presta, M., Andrés, G., Leali, D., Dell’Era, P. and Ronca, R., 2009. Inflammatory cells and chemokines sustain FGF2-induced angiogenesis. *European cytokine network*, 20(2), pp.39-50.
- Preston, A., Mandrell, R.E., Gibson, B.W. and Apicella, M.A., 1996. The lipooligosaccharides of pathogenic gram-negative bacteria. *Critical reviews in microbiology*, 22(3), pp.139-180.
- Raetz, Christian RH, and Chris Whitfield. "Lipopolysaccharide endotoxins." *Annual review of biochemistry* 71, no. 1 (2002): 635-700.
- Rahimi, F., Hsu, K., Endoh, Y. and Geczy, C.L., 2005. FGF-2, IL-1 $\beta$  and TGF- $\beta$  regulate fibroblast expression of S100A8. *The FEBS journal*, 272(11), pp.2811-2827.
- Raiymbek, G., An, S., Khurana, N., Gopinath, S., Larkin, A., Biswas, S., Trievel, R.C., Cho, U.S. and Rangunathan, K., 2020. An H3K9 methylation-dependent protein interaction regulates the non-enzymatic functions of a putative histone demethylase. *Elife*, 9, p.e53155.
- Raja, K.S., Garcia, M.S. and Isseroff, R.R., 2007. Wound re-epithelialization: modulating keratinocyte migration in wound healing. *Frontiers in Bioscience-Landmark*, 12(8), pp.2849-2868.
- Ramos, R.R., Domingues, L. and Gama, F.M., 2011. LL37, a human antimicrobial peptide with immunomodulatory properties.
- Rathinam, V.A. and Fitzgerald, K.A., 2016. Inflammasome complexes: emerging mechanisms and effector functions. *Cell*, 165(4), pp.792-800.
- Reynolds, A.N., Akerman, A.P. and Mann, J., 2020. Dietary fibre and whole grains in diabetes management: Systematic review and meta-analyses. *PLoS medicine*, 17(3), p.e1003053.
- Ricci, J.C.D., 2000. ADP modulates the dynamic behavior of the glycolytic pathway of *Escherichia coli*. *Biochemical and Biophysical Research Communications*, 271(1), pp.244-249.
- Ridyard, K.E. and Overhage, J., 2021. The potential of human peptide LL-37 as an antimicrobial and anti-biofilm agent. *Antibiotics*, 10(6), p.650.
- Rizwan, H., Pal, S., Sabnam, S. and Pal, A., 2020. High glucose augments ROS generation regulates mitochondrial dysfunction and apoptosis via stress signalling cascades in keratinocytes. *Life sciences*, 241, p.117148.
- Rogers, L.M., Serezani, C.H., Eastman, A.J., Hasty, A.H., Englund-Ögge, L., Jacobsson, B., Vickers, K.C. and Aronoff, D.M., 2020. Palmitate induces apoptotic cell death and inflammasome activation in human placental macrophages. *Placenta*, 90, pp.45-51.
- Romashin, D.D., Tolstova, T.V., Varshaver, A.M., Kozhin, P.M., Rusanov, A.L. and Luzgina, N.G., 2024. Keratins 6, 16, and 17 in Health and Disease: A Summary of Recent Findings. *Current Issues in Molecular Biology*, 46(8), pp.8627-8641.
- Rorsman, P. and Ashcroft, F.M., 2018. Pancreatic  $\beta$ -cell electrical activity and insulin secretion: of mice and men. *Physiological reviews*, 98(1), pp.117-214.

- Rosenberg, M., Azevedo, N.F. and Ivask, A., 2019. Propidium iodide staining underestimates viability of adherent bacterial cells. *Scientific reports*, 9(1), p.6483.
- Ryan, D.G. and O'Neill, L.A., 2020. Krebs cycle reborn in macrophage immunometabolism. *Annual review of immunology*, 38(1), pp.289-313.
- Saha, S., Buttari, B., Panieri, E., Profumo, E. and Saso, L., 2020. An overview of Nrf2 signaling pathway and its role in inflammation. *Molecules*, 25(22), p.5474.
- Sameer, A.S. and Nissar, S., 2021. Toll-like receptors (TLRs): structure, functions, signaling, and role of their polymorphisms in colorectal cancer susceptibility. *BioMed Research International*, 2021(1), p.1157023.
- Sancho-Vaello, E., Gil-Carton, D., François, P., Bonetti, E.J., Kreir, M., Pothula, K.R., Kleinekathöfer, U. and Zeth, K., 2020. The structure of the antimicrobial human cathelicidin LL-37 shows oligomerization and channel formation in the presence of membrane mimics. *Scientific reports*, 10(1), p.17356.
- Savina, A. and Amigorena, S., 2007. Phagocytosis and antigen presentation in dendritic cells. *Immunological reviews*, 219(1), pp.143-156
- Saxton, R.A. and Sabatini, D.M., 2017. mTOR signaling in growth, metabolism, and disease. *Cell*, 168(6), pp.960-976.
- Sazanov, L.A., 2015. A giant molecular proton pump: structure and mechanism of respiratory complex I. *Nature reviews Molecular cell biology*, 16(6), pp.375-388.
- Scheenstra, M.R., Van Harten, R.M., Veldhuizen, E.J., Haagsman, H.P. and Coorens, M., 2020. Cathelicidins modulate TLR-activation and inflammation. *Frontiers in immunology*, 11, p.1137.
- Schmidt, A., von Woedtke, T., Vollmar, B., Hasse, S. and Bekeschus, S., 2019. Nrf2 signaling and inflammation are key events in physical plasma-spurred wound healing. *Theranostics*, 9(4), p.1066.
- Schultz, G.S. and Wysocki, A., 2009. Interactions between extracellular matrix and growth factors in wound healing. *Wound repair and regeneration*, 17(2), pp.153-162.
- Seeger, M.A. and Paller, A.S., 2015. The roles of growth factors in keratinocyte migration. *Advances in wound care*, 4(4), pp.213-224.
- Seery, C. (2022). *Normal and Diabetic Blood Sugar Level Ranges - Blood Sugar Levels for Diabetes*. [online] Diabetes.co.uk. Available at: [https://www.diabetes.co.uk/diabetes\\_care/blood-sugar-level-ranges.html](https://www.diabetes.co.uk/diabetes_care/blood-sugar-level-ranges.html).
- Segeritz, C.P. and Vallier, L., 2017. Cell culture: Growing cells as model systems in vitro. In *Basic science methods for clinical researchers* (pp. 151-172). Academic Press.
- Segerstolpe, Å., Palasantza, A., Eliasson, P., Andersson, E.M., Andréasson, A.C., Sun, X., Picelli, S., Sabirsh, A., Clausen, M., Bjursell, M.K. and Smith, D.M., 2016. Single-cell transcriptome profiling of human pancreatic islets in health and type 2 diabetes. *Cell metabolism*, 24(4), pp.593-607.
- Seo, M.D., Kang, T.J., Lee, C.H., Lee, A.Y. and Noh, M., 2012. HaCaT keratinocytes and primary epidermal keratinocytes have different transcriptional profiles of cornified envelope-associated genes to T helper cell cytokines. *Biomolecules & therapeutics*, 20(2), p.171.
- Serbina, N.V. and Pamer, E.G., 2006. Monocyte emigration from bone marrow during bacterial infection requires signals mediated by chemokine receptor CCR2. *Nature immunology*, 7(3), pp.311-317.

- Serra, A.M., Waddell, J., Manivannan, A., Xu, H., Cotter, M. and Forrester, J.V., 2012. CD11b+ Bone marrow–derived monocytes are the major leukocyte subset responsible for retinal capillary leukostasis in experimental diabetes in mouse and express high levels of CCR5 in the circulation. *The American journal of pathology*, 181(2), pp.719-727.
- Sesti, G., Federici, M., Hribal, M.L., Lauro, D., Sbraccia, P. and Lauro, R., 2001. Defects of the insulin receptor substrate (IRS) system in human metabolic disorders. *The FASEB Journal*, 15(12), pp.2099-2111.
- Shah, S., El Mohtadi, M. and Ashworth, J., 2023. Biobran (MGN-3) enhances host-pathogen interaction in an in vitro hyperglycaemic model of an infected diabetic foot ulcer via the CD14/TLR-4 pathway.
- Shang, D., Sun, D., Shi, C., Xu, J., Shen, M., Hu, X., Liu, H. and Tu, Z., 2020. Activation of epidermal growth factor receptor signaling mediates cellular senescence induced by certain pro-inflammatory cytokines. *Aging Cell*, 19(5), p.e13145.
- Shanmugam, N., Reddy, M.A., Guha, M. and Natarajan, R., 2003. High glucose-induced expression of proinflammatory cytokine and chemokine genes in monocytic cells. *Diabetes*, 52(5), pp.1256-1264.
- Shao, X., Chen, S., Yang, D., Cao, M., Yao, Y., Wu, Z., Li, N., Shen, N., Li, X., Song, X. and Qian, Y., 2017. FGF2 cooperates with IL-17 to promote autoimmune inflammation. *Scientific reports*, 7(1), p.7024.
- She, P., Wang, Y., Liu, Y., Tan, F., Chen, L., Luo, Z. and Wu, Y., 2019. Effects of exogenous glucose on *Pseudomonas aeruginosa* biofilm formation and antibiotic resistance. *Microbiologyopen*, 8(12), p.e933.
- Shen, L., Li, Y. and Zhao, H., 2024. Fibroblast growth factor signaling in macrophage polarization: impact on health and diseases. *Frontiers in Immunology*, 15, p.1390453.
- Shen, Y., Dinh, H.V., Cruz, E.R., Chen, Z., Bartman, C.R., Xiao, T., Call, C.M., Ryseck, R.P., Pratas, J., Weilandt, D. and Baron, H., 2024. Mitochondrial ATP generation is more proteome efficient than glycolysis. *Nature chemical biology*, pp.1-10.
- Shi, G.J., Shi, G.R., Zhou, J.Y., Zhang, W.J., Gao, C.Y., Jiang, Y.P., Zi, Z.G., Zhao, H.H., Yang, Y. and Yu, J.Q., 2018. Involvement of growth factors in diabetes mellitus and its complications: A general review. *Biomedicine & Pharmacotherapy*, 101, pp.510-527.
- Shi, R., Qiao, J., Sun, Q., Hou, B., Li, B., Zheng, J., Zhang, Z., Peng, Z., Zhou, J., Shen, B. and Deng, J., 2024. Self-assembly of PEG–PPS polymers and LL-37 peptide nanomicelles improves the oxidative microenvironment and promotes angiogenesis to facilitate chronic wound healing. *Bioengineering & Translational Medicine*, 9(2), p.e10619.
- Shirakata, Y., 2010. Regulation of epidermal keratinocytes by growth factors. *Journal of dermatological science*, 59(2), pp.73-80.
- Shirakata, Y., Kimura, R., Nanba, D., Iwamoto, R., Tokumaru, S., Morimoto, C., Yokota, K., Nakamura, M., Sayama, K., Mekada, E. and Higashiyama, S., 2005. Heparin-binding EGF-like growth factor accelerates keratinocyte migration and skin wound healing. *Journal of cell science*, 118(11), pp.2363-2370.
- Shoji, K., Ohashi, K., Sampei, K., Oikawa, M. and Mizuno, K., 2012. Cytochalasin D acts as an inhibitor of the actin–cofilin interaction. *Biochemical and biophysical research communications*, 424(1), pp.52-57.

- Silva, J.P., Köhler, M., Graff, C., Oldfors, A., Magnuson, M.A., Berggren, P.O. and Larsson, N.G., 2000. Impaired insulin secretion and  $\beta$ -cell loss in tissue-specific knockout mice with mitochondrial diabetes. *Nature genetics*, 26(3), pp.336-340.
- Sim, S.L., Kumari, S., Kaur, S. and Khosrotehrani, K., 2022. Macrophages in skin wounds: functions and therapeutic potential. *Biomolecules*, 12(11), p.1659.
- Sims-Robinson, C., Bakeman, A., Rosko, A., Glasser, R. and Feldman, E.L., 2016. The role of oxidized cholesterol in diabetes-induced lysosomal dysfunction in the brain. *Molecular neurobiology*, 53, pp.2287-2296.
- Singer, A.J. and Clark, R.A., 1999. Cutaneous wound healing. *New England journal of medicine*, 341(10), pp.738-746.
- Smogorzewski, M., Galfayan, V. and Massry, S.G., 1998. High glucose concentration causes a rise in  $[Ca^{2+}]_i$  of cardiac myocytes. *Kidney international*, 53(5), pp.1237-1243.
- Soares, M.A., Cohen, O.D., Low, Y.C., Sartor, R.A., Ellison, T., Anil, U., Anzai, L., Chang, J.B., Saadeh, P.B., Rabbani, P.S. and Ceradini, D.J., 2016. Restoration of Nrf2 signaling normalizes the regenerative niche. *Diabetes*, 65(3), pp.633-646.
- Solini, A., Chiozzi, P., Falzoni, S., Morelli, A., Fellin, R. and Di Virgilio, F., 2000. High glucose modulates P2X7 receptor-mediated function in human primary fibroblasts. *Diabetologia*, 43, pp.1248-1256.
- Sousa, E.S., Queiroz, L.A., Guimarães, J.P., Pantoja, K.C., Barros, R.S., Epiphany, S. and Martins, J.O., 2023. The influence of high glucose conditions on macrophages and its effect on the autophagy pathway. *Frontiers in immunology*, 14, p.1130662.
- Soydas, T., Yaprak Sarac, E., Cinar, S., Dogan, S., Solakoglu, S., Tuncdemir, M. and Kanigur Sultuybek, G., 2018. The protective effects of metformin in an in vitro model of aging 3T3 fibroblast under the high glucose conditions. *Journal of physiology and biochemistry*, 74, pp.273-281.
- Spravchikov, N., Sizyakov, G., Gartsbein, M., Accili, D., Tennenbaum, T. and Wertheimer, E., 2001. Glucose effects on skin keratinocytes: implications for diabetes skin complications. *Diabetes*, 50(7), pp.1627-1635.
- Stoffels, J.M., Zhao, C. and Baron, W., 2013. Fibronectin in tissue regeneration: timely disassembly of the scaffold is necessary to complete the build. *Cellular and Molecular Life Sciences*, 70(22), pp.4243-4253.
- Strutz, F., Zeisberg, M., Renziehausen, A., Raschke, B., Becker, V., Van Kooten, C. and Müller, G.A., 2001. TGF- $\beta$ 1 induces proliferation in human renal fibroblasts via induction of basic fibroblast growth factor (FGF-2). *Kidney international*, 59(2), pp.579-592.
- Süntar, I., Çetinkaya, S., Panieri, E., Saha, S., Buttari, B., Profumo, E. and Saso, L., 2021. Regulatory role of Nrf2 signaling pathway in wound healing process. *Molecules*, 26(9), p.2424.
- Suryavanshi, S.V. and Kulkarni, Y.A., 2017. NF- $\kappa$ B: a potential target in the management of vascular complications of diabetes. *Frontiers in pharmacology*, 8, p.798.
- Suzuki, Y., Lanner, C., Kim, J.H., Vilardo, P.G., Zhang, H., Yang, J., Cooper, L.D., Steele, M., Kennedy, A., Bock, C.B. and Scrimgeour, A., 2001. Insulin control of glycogen metabolism in knockout mice lacking the muscle-specific protein phosphatase PP1G/RGL. *Molecular and cellular biology*, 21(8), pp.2683-2694.

- Takahashi, T., Kulkarni, N.N., Lee, E.Y., Zhang, L.J., Wong, G.C. and Gallo, R.L., 2018. Cathelicidin promotes inflammation by enabling binding of self-RNA to cell surface scavenger receptors. *Scientific reports*, 8(1), p.4032
- Takeda, K., Kaisho, T. and Akira, S., 2003. Toll-like receptors. *Annual review of immunology*, 21(1), pp.335-376.
- Talbott, H.E., Mascharak, S., Griffin, M., Wan, D.C. and Longaker, M.T., 2022. Wound healing, fibroblast heterogeneity, and fibrosis. *Cell stem cell*, 29(8), pp.1161-1180.
- Tan, S., 2018. *An investigation of the cellular uptake and mechanisms of action of MGN-3 on inflammatory processes* (Doctoral dissertation, Manchester Metropolitan University).
- Tan, V.P. and Miyamoto, S., 2015. HK2/hexokinase-II integrates glycolysis and autophagy to confer cellular protection. *Autophagy*, 11(6), pp.963-964.
- Tan, Y. and Kagan, J.C., 2019. Innate immune signaling organelles display natural and programmable signaling flexibility. *Cell*, 177(2), pp.384-398.
- Tang, J., Zhou, B., Scott, M.J., Chen, L., Lai, D., Fan, E.K., Li, Y., Wu, Q., Billiar, T.R., Wilson, M.A. and Wang, P., 2020. EGFR signaling augments TLR4 cell surface expression and function in macrophages via regulation of Rab5a activation. *Protein & Cell*, 11(2), pp.144-149.
- Tang, M., Zhang, W., Lin, H., Jiang, H., Dai, H. and Zhang, Y., 2007. High glucose promotes the production of collagen types I and III by cardiac fibroblasts through a pathway dependent on extracellular-signal-regulated kinase 1/2. *Molecular and cellular biochemistry*, 301, pp.109-114.
- Tarique, A.A., Logan, J., Thomas, E., Holt, P.G., Sly, P.D. and Fantino, E., 2015. Phenotypic, functional, and plasticity features of classical and alternatively activated human macrophages. *American journal of respiratory cell and molecular biology*, 53(5), pp.676-688.
- Terashi, H., Izumi, K., Devenci, M., Rhodes, L.M. and Marcelo, C.L., 2005. High glucose inhibits human epidermal keratinocyte proliferation for cellular studies on diabetes mellitus. *International wound journal*, 2(4), pp.298-304.
- TeSlaa, T. and Teitell, M.A., 2014. Techniques to monitor glycolysis. *Methods in enzymology*, 542, pp.91-114.
- Tessari, P., Cecchet, D., Cosma, A., Vettore, M., Coracina, A., Million, R., Iori, E., Puricelli, L., Avogaro, A. and Vedovato, M., 2010. Nitric oxide synthesis is reduced in subjects with type 2 diabetes and nephropathy. *Diabetes*, 59(9), pp.2152-2159.
- Thulabandu, V., Chen, D. and Atit, R.P., 2018. Dermal fibroblast in cutaneous development and healing. *Wiley Interdisciplinary Reviews: Developmental Biology*, 7(2), p.e307.
- Tian, J., Lei, P., Laychock, S.G. and Andreadis, S.T., 2008. Regulated insulin delivery from human epidermal cells reverses hyperglycemia. *Molecular Therapy*, 16(6), pp.1146-1153.
- Tian, M., Lu, S., Niu, Y., Xie, T., Dong, J., Cao, X., Song, F., Jin, S. and Qing, C., 2012. Effects of advanced glycation end-products (AGEs) on skin keratinocytes by nuclear factor-kappa B (NF-κB) activation. *African Journal of Biotechnology*, 11(50), pp.11132-11142.
- Tiedge, M., Lortz, S., Drinkgern, J. and Lenzen, S., 1997. Relation between antioxidant enzyme gene expression and antioxidative defense status of insulin-producing cells. *Diabetes*, 46(11), pp.1733-1742.
- Titov, D.V., Cracan, V., Goodman, R.P., Peng, J., Grabarek, Z. and Mootha, V.K., 2016. Complementation of mitochondrial electron transport chain by manipulation of the NAD<sup>+</sup>/NADH ratio. *Science*, 352(6282), pp.231-235.

- Tiwari, R.L., Singh, V. and Barthwal, M.K., 2008. Macrophages: an elusive yet emerging therapeutic target of atherosclerosis. *Medicinal research reviews*, 28(4), pp.483-544.
- Torres-Castro, I., Arroyo-Camarena, Ú.D., Martínez-Reyes, C.P., Gómez-Arauz, A.Y., Dueñas-Andrade, Y., Hernández-Ruiz, J., Béjar, Y.L., Zaga-Clavellina, V., Morales-Montor, J., Terrazas, L.I. and Kzhyshkowska, J., 2016. Human monocytes and macrophages undergo M1-type inflammatory polarization in response to high levels of glucose. *Immunology letters*, 176, pp.81-89.
- Toschi, E., Camastra, S., Sironi, A.M., Masoni, A., Gastaldelli, A., Mari, A., Ferrannini, E. and Natali, A., 2002. Effect of acute hyperglycemia on insulin secretion in humans. *Diabetes*, 51(suppl\_1), pp.S130-S133.
- Tuleta, I. and Frangogiannis, N.G., 2021. Diabetic fibrosis. *Biochimica et Biophysica Acta (BBA)-Molecular Basis of Disease*, 1867(4), p.166044.
- Uribe-Querol, E. and Rosales, C., 2022. Neutrophils actively contribute to obesity-associated inflammation and pathological complications. *Cells*, 11(12), p.1883.
- van Caam, A., Vonk, M., van den Hoogen, F., van Lent, P. and van der Kraan, P., 2018. Unraveling SSc pathophysiology; the myofibroblast. *Frontiers in immunology*, 9, p.2452.
- Van Harten, R.M., Van Woudenberg, E., Van Dijk, A. and Haagsman, H.P., 2018. Cathelicidins: immunomodulatory antimicrobials. *Vaccines*, 6(3), p.63.
- Vance, J., Santos, A., Sadofsky, L., Morice, A. and Cervantes, J., 2019. Effect of high glucose on human alveolar macrophage phenotype and phagocytosis of mycobacteria. *Lung*, 197, pp.89-94.
- Varadaradjalou, S., Feger, F., Thieblemont, N., Hamouda, N.B., Pleau, J.M., Dy, M. and Arock, M., 2003. Toll-like receptor 2 (TLR2) and TLR4 differentially activate human mast cells. *European journal of immunology*, 33(4), pp.899-906.
- Vasko, R., Koziolk, M., Ikehata, M., Rastaldi, M.P., Jung, K., Schmid, H., Kretzler, M., Müller, G.A. and Strutz, F., 2009. Role of basic fibroblast growth factor (FGF-2) in diabetic nephropathy and mechanisms of its induction by hyperglycemia in human renal fibroblasts. *American Journal of Physiology-Renal Physiology*, 296(6), pp.F1452-F1463.
- Vazquez-Victorio, G., Gonzalez-Espinosa, C., Espinosa-Riquer, Z.P. and Macias-Silva, M., 2016. GPCRs and actin–cytoskeleton dynamics. In *Methods in cell biology* (Vol. 132, pp. 165-188). Academic Press.
- Villarreal-Ponce, A., Tiruneh, M.W., Lee, J., Guerrero-Juarez, C.F., Kuhn, J., David, J.A., Dammeyer, K., Mc Kell, R., Kwong, J., Rabbani, P.S. and Nie, Q., 2020. Keratinocyte-macrophage crosstalk by the Nrf2/Ccl2/EGF signaling axis orchestrates tissue repair. *Cell reports*, 33(8).
- Vitko, N.P., Grosser, M.R., Khatri, D., Lance, T.R. and Richardson, A.R., 2016. Expanded glucose import capability affords *Staphylococcus aureus* optimized glycolytic flux during infection. *MBio*, 7(3), pp.10-1128.
- Volpe, C.M.O., Villar-Delfino, P.H., Dos Anjos, P.M.F. and Nogueira-Machado, J.A., 2018. Cellular death, reactive oxygen species (ROS) and diabetic complications. *Cell death & disease*, 9(2), p.119.
- Vuong, C., Voyich, J.M., Fischer, E.R., Braughton, K.R., Whitney, A.R., DeLeo, F.R. and Otto, M., 2004. Polysaccharide intercellular adhesin (PIA) protects *Staphylococcus epidermidis* against major components of the human innate immune system. *Cellular microbiology*, 6(3), pp.269-275.

- Wager, C.L. and Wormley Jr, F.L., 2014. Classical versus alternative macrophage activation: the Ying and the Yang in host defense against pulmonary fungal infections. *Mucosal immunology*, 7(5), pp.1023-1035.
- Waldrop, R., McLaren, A., Calara, F. and McLemore, R., 2014. Biofilm growth has a threshold response to glucose in vitro. *Clinical Orthopaedics and Related Research*<sup>®</sup>, 472(11), pp.3305-3310.
- Walker, K.Z., O’Dea, K., Gomez, M., Girgis, S. and Colagiuri, R., 2010. Diet and exercise in the prevention of diabetes. *Journal of human nutrition and dietetics*, 23(4), pp.344-352.
- Wang, H., Li, B., Li, A., An, C., Liu, S. and Zhuang, Z., 2024. Integrative Metabolomics, Enzymatic Activity, and Gene Expression Analysis Provide Insights into the Metabolic Profile Differences between the Slow-Twitch Muscle and Fast-Twitch Muscle of *Pseudocaranx dentex*. *International Journal of Molecular Sciences*, 25(11), p.6131.
- Wang, Q., Ren, J., Morgan, S., Liu, Z., Dou, C. and Liu, B., 2014. Monocyte chemoattractant protein-1 (MCP-1) regulates macrophage cytotoxicity in abdominal aortic aneurysm. *PloS one*, 9(3), p.e92053.
- Wang, Y. and Graves, D.T., 2020. Keratinocyte function in normal and diabetic wounds and modulation by FOXO1. *Journal of Diabetes Research*, 2020(1), p.3714704.
- Wang, Z., Cheng, Z.X., Abrams, S.T., Lin, Z.Q., Yates, E.D., Yu, Q., Yu, W.P., Chen, P.S., Toh, C.H. and Wang, G.Z., 2020. Extracellular histones stimulate collagen expression in vitro and promote liver fibrogenesis in a mouse model via the TLR4-MyD88 signaling pathway. *World journal of gastroenterology*, 26(47), p.7513.
- Wang, Z., Zheng, Y., Lai, Z., Hu, X., Wang, L., Wang, X., Li, Z., Gao, M., Yang, Y., Wang, Q. and Li, N., 2024. Effect of monosaccharide composition and proportion on the bioactivity of polysaccharides: A review. *International Journal of Biological Macromolecules*, 254, p.127955.
- Ward, M.G., Li, G. and Hao, M., 2018. Apoptotic  $\beta$ -cells induce macrophage reprogramming under diabetic conditions. *Journal of Biological Chemistry*, 293(42), pp.16160-16173.
- Weeks, B.S., Lee, S.W., Perez, P.P., Brown, K., Chauhan, H. and Tsaava, T., 2008. Natramune and PureWay-C reduce xenobiotic-induced human T-cell  $\alpha$ 5b1 integrin-mediated adhesion to fibronectin. *Med Sci Monit*, 14(12), p.285.
- Werner, S., Krieg, T. and Smola, H., 2007. Keratinocyte–fibroblast interactions in wound healing. *Journal of investigative dermatology*, 127(5), pp.998-1008.
- Wilson, A.K., Coulombe, P.A. and Fuchs, E., 1992. The roles of K5 and K14 head, tail, and R/KLLEGE domains in keratin filament assembly in vitro. *The Journal of cell biology*, 119(2), pp.401-414.
- Wojtowicz, A.M., Oliveira, S., Carlson, M.W., Zawadzka, A., Rousseau, C.F. and Baksh, D., 2014. The importance of both fibroblasts and keratinocytes in a bilayered living cellular construct used in wound healing. *Wound repair and regeneration*, 22(2), pp.246-255.
- Wood, S., Jayaraman, V., Huelsmann, E.J., Bonish, B., Burgad, D., Sivaramakrishnan, G., Qin, S., DiPietro, L.A., Zloza, A., Zhang, C. and Shafikhani, S.H., 2014. Pro-inflammatory chemokine CCL2 (MCP-1) promotes healing in diabetic wounds by restoring the macrophage response. *PloS one*, 9(3), p.e91574.
- Wu, C., Khan, S.A. and Lange, A.J., 2005. Regulation of glycolysis—role of insulin. *Experimental gerontology*, 40(11), pp.894-899.

- Wu, L. and Derynck, R., 2009. Essential role of TGF- $\beta$  signaling in glucose-induced cell hypertrophy. *Developmental cell*, 17(1), pp.35-48.
- Xi, L., Du, J., Xue, W., Shao, K., Jiang, X., Peng, W., Li, W. and Huang, S., 2024. Cathelicidin LL-37 promotes wound healing in diabetic mice by regulating TFEB-dependent autophagy. *Peptides*, 175, p.171183.
- Xiao, W., Wang, R.S., Handy, D.E. and Loscalzo, J., 2018. NAD (H) and NADP (H) redox couples and cellular energy metabolism. *Antioxidants & redox signaling*, 28(3), pp.251-272.
- Xie, Z., Zhou, S., Tang, S., Zhang, Q. and Liu, L., 2024. High glucose combined with lipopolysaccharide stimulation inhibits cell proliferation and migration of human HaCaT keratinocytes by impacting redox homeostasis and activating the polyol pathway. *Molecular Biology Reports*, 51(1), pp.1-11.
- Xu, F., Zhang, C. and Graves, D.T., 2013. Abnormal cell responses and role of TNF- $\alpha$  in impaired diabetic wound healing. *BioMed research international*, 2013(1), p.754802.
- Xu, J., Min, D., Guo, G., Liao, X. and Fu, Z., 2018. Experimental study of epidermal growth factor and acidic fibroblast growth factor in the treatment of diabetic foot wounds. *Experimental and therapeutic medicine*, 15(6), pp.5365-5370.
- Xu, K.P., Li, Y., Ljubimov, A.V. and Yu, F.S.X., 2009. High glucose suppresses epidermal growth factor receptor/phosphatidylinositol 3-kinase/Akt signaling pathway and attenuates corneal epithelial wound healing. *Diabetes*, 58(5), pp.1077-1085.
- Xu, X., Qi, X., Shao, Y., Li, Y., Fu, X., Feng, S. and Wu, Y., 2016. High glucose induced-macrophage activation through TGF- $\beta$ -activated kinase 1 signaling pathway. *Inflammation Research*, 65, pp.655-664.
- Xuan, Y., Chi, L., Tian, H., Cai, W., Sun, C., Wang, T., Zhou, X., Shao, M., Zhu, Y., Niu, C. and Sun, Y., 2016. The activation of the NF- $\kappa$ B-JNK pathway is independent of the PI3K-Rac1-JNK pathway involved in the bFGF-regulated human fibroblast cell migration. *Journal of Dermatological Science*, 82(1), pp.28-37.
- Xuan, Y.H., Huang, B.B., Tian, H.S., Chi, L.S., Duan, Y.M., Wang, X., Zhu, Z.X., Cai, W.H., Zhu, Y.T., Wei, T.M. and Ye, H.B., 2014. High-glucose inhibits human fibroblast cell migration in wound healing via repression of bFGF-regulating JNK phosphorylation. *PloS one*, 9(9), p.e108182.
- Xue, M. and Jackson, C.J., 2015. Extracellular matrix reorganization during wound healing and its impact on abnormal scarring. *Advances in wound care*, 4(3), pp.119-136.
- Yadav, A., Saini, V. and Arora, S., 2010. MCP-1: chemoattractant with a role beyond immunity: a review. *Clinica chimica acta*, 411(21-22), pp.1570-1579.
- Yang, J., Park, Y., Zhang, H., Gao, X., Wilson, E., Zimmer, W., Abbott, L. and Zhang, C., 2009. Role of MCP-1 in tumor necrosis factor- $\alpha$ -induced endothelial dysfunction in type 2 diabetic mice. *American Journal of Physiology-Heart and Circulatory Physiology*, 297(4), pp.H1208-H1216.
- You, Y., Xue, T., Cao, L., Zhao, L., Sun, H. and Sun, B., 2014. *Staphylococcus aureus* glucose-induced biofilm accessory proteins, GbaAB, influence biofilm formation in a PIA-dependent manner. *International Journal of Medical Microbiology*, 304(5-6), pp.603-612.
- Younesi, F.S., Miller, A.E., Barker, T.H., Rossi, F.M. and Hinz, B., 2024. Fibroblast and myofibroblast activation in normal tissue repair and fibrosis. *Nature Reviews Molecular Cell Biology*, pp.1-22.

- Yu, A., Matsuda, Y., Takeda, A., Uchinuma, E. and Kuroyanagi, Y., 2012. Effect of EGF and bFGF on fibroblast proliferation and angiogenic cytokine production from cultured dermal substitutes. *Journal of Biomaterials Science, Polymer Edition*, 23(10), pp.1315-1324.
- Yu, L., Wang, L. and Chen, S., 2010. Endogenous toll-like receptor ligands and their biological significance. *Journal of cellular and molecular medicine*, 14(11), pp.2592-2603.
- Yu, T., Robotham, J.L. and Yoon, Y., 2006. Increased production of reactive oxygen species in hyperglycemic conditions requires dynamic change of mitochondrial morphology. *Proceedings of the National Academy of Sciences*, 103(8), pp.2653-2658.
- Zanoni, I., Bodio, C., Broggi, A., Ostuni, R., Caccia, M., Collini, M., Venkatesh, A., Spreafico, R., Capuano, G. and Granucci, F., 2012. Similarities and differences of innate immune responses elicited by smooth and rough LPS. *Immunology letters*, 142(1-2), pp.41-47.
- Zapotoczna, M., McCarthy, H., Rudkin, J.K., O'Gara, J.P. and O'Neill, E., 2015. An essential role for coagulase in *Staphylococcus aureus* biofilm development reveals new therapeutic possibilities for device-related infections. *The Journal of infectious diseases*, 212(12), pp.1883-1893
- Zhang, B., Zhang, M., Tian, J., Zhang, X., Zhang, D., Li, J. and Yang, L., 2024. Advances in the regulation of radiation-induced apoptosis by polysaccharides: A review. *International Journal of Biological Macromolecules*, p.130173.
- Zhang, H., Bosch-Marce, M., Shimoda, L.A., Tan, Y.S., Baek, J.H., Wesley, J.B., Gonzalez, F.J. and Semenza, G.L., 2008. Mitochondrial autophagy is an HIF-1-dependent adaptive metabolic response to hypoxia. *Journal of Biological Chemistry*, 283(16), pp.10892-10903.
- Zhang, Y. and Bliska, J.B., 2003. Role of Toll-like receptor signaling in the apoptotic response of macrophages to Yersinia infection. *Infection and immunity*, 71(3), pp.1513-1519.
- Zhao, G., Liu, L., Peek, R.M., Hao, X., Polk, D.B., Li, H. and Yan, F., 2016. Activation of epidermal growth factor receptor in macrophages mediates feedback inhibition of M2 polarization and gastrointestinal tumor cell growth. *Journal of Biological Chemistry*, 291(39), pp.20462-20472.
- Zittermann, S.I. and Issekutz, A.C., 2006. Basic fibroblast growth factor (bFGF, FGF-2) potentiates leukocyte recruitment to inflammation by enhancing endothelial adhesion molecule expression. *The American journal of pathology*, 168(3), pp.835-846.